1,2-Diazoles: Versatile Tectons for Metallosupramolecular Assemblies

---

A Thesis Submitted in Partial Fulfilment of the Requirements for the Degree of ***Doctor of Philosophy*** *in* ***Chemistry***

Chris Samuel Hawes

University of Canterbury

2012

Table of Contents

Acknowledgements

First and foremost, I would like to thank my supervisor, Assoc. Prof. Paul Kruger, for his guidance and support throughout my Honours and PhD projects; without his wisdom, encouragement and optimism this work would not have been possible. I must also extend my appreciation to my co-supervisor Chris Fitchett who, as well as generously donating countless hours of his time to impart his considerable expertise in crystallography, both challenged and encouraged me at many crucial moments during the last few years.

During my time at Canterbury I have been privileged to work alongside a fantastic group of people; the Kruger group, and in particular Marky, Alan and Rosanna, have been a constant source of both education and entertainment; David Anderson, who provided a great deal of support throughout my research, but particularly at the very beginning and end of my time here; the Fitchett and Steel groups, who, as well as being an excellent source of borrowed chemicals, have provided years of friendly competition (may you one day graduate to transition metals!); and Jayne Gulbransen, who has helped keep me sane these past 5 years with afternoon teas and beers where appropriate.

I am grateful to the entire academic and general staff of the Chemistry department for providing a productive and enjoyable place to work, but in particular; Dr Marie Fitchett, for her invaluable knowledge and assistance with NMR, UV and Mass Spec., as well as her kind encouragement over the years; Dr Matt Polson, for his willingness to share his wisdom in everything from organic synthesis to X-ray diffraction; Dr Meike Holzenkaempfer, for Mass Spec. and NMR assistance; The organic group and the 'tough love' of their ruthless meetings; Wayne Mackay, Rob McGregor and the department technical staff, for fixing anything I could break; and all those involved in getting the department back on its feet after the earthquakes.

During this project I have received assistance from several of our local and international collaborators, whose time and expertise have been greatly appreciated; Dr Shane Telfer (Massey), for providing X-ray crystallography facilities during our lengthy downtime; Prof. Stuart Batten (Monash), for lending his considerable expertise in coordination polymer network descriptions; Assoc. Prof. Brendan Abrahams and Keith White (Melbourne) for gas sorption experiments.

I wish to acknowledge the University of Canterbury College of Science, for providing a PhD scholarship, and to the Marsden Fund for a PhD scholarship top-up and additional funding, and particularly to the understanding and generosity of both funding sources regarding earthquake extensions. I also wish to acknowledge the NZIC for providing conference travel funding, and Prof. John Blunt, for providing me with part-time work with MarinLit.

And of course, to my wife Niki, for her endless patience, support and encouragement.

Abstract

This study investigates the metallosupramolecular chemistry of functionalised 1,2-diazole ligands, by the preparation and characterisation of a range of first-row transition metal coordination polymers and discrete assemblies. To this end, twenty-six ligands containing 1,2-diazole functionality have been synthesised, twenty-one of which have not previously appeared in the coordination chemistry literature. Utilising these compounds, forty new coordination compounds have been prepared and characterised by single-crystal X-ray crystallography and other analytical techniques, and their solid-state structural features discussed in the search for reproducible new diazole-based synthons for the designed synthesis of new functional materials. Particular attention is paid to the contribution of the second nitrogen atom on the diazole ring, which participates in structure-directing hydrogen bonding interactions, or acts as a synthetic handle to easily append further functionality to the ligand system.

The design of the ligands is separated into two primary categories, representing the different approaches adopted for the synthesis of the metallosupramolecular architectures. The combination of *1H*-pyrazole and carboxylic acid functionality in mixed-ligand assemblies was investigated with the combination of bis-pyrazole and bis-carboxylic acid ligands, and with the preparation of ligands containing both functional groups. This approach was extended to the related heterocyclic species indazole, with all five possible isomers of indazole-carboxylic acid synthesised and used in coordination chemistry for the first time. The *1H*-diazole-carboxylate synthon was employed in the synthesis of fourteen coordination polymers and three discrete assemblies.

Heteroaryl substitution at the 1-position of pyrazole or indazole compounds was employed to generate chelating ligands containing pyridine or benzimidazole functionality, which were used to form nineteen discrete complexes, including dinuclear helicates and metallocycles, and five coordination polymers. The effect of flexibility and distance between coordination sites in bis-bidentate ligand systems was examined, in conjunction with studies into the effect of steric bulk and variation of the electronic nature of the coordinating groups.

While this study is primarily concerned with the solid-state structural chemistry of 1,2-diazole coordination compounds, attention is paid where appropriate to solution-based measurements such as NMR and UV/Visible studies, and the pertinent behaviour of functional materials, such as thermogravimetric analysis for solvated species and gas uptake studies for stable void-containing materials.

Abbreviations

NMR: Nuclear Magnetic Resonance

nOesy: Nuclear Overhauser Effect Spectroscopy

COSY: Correlation Spectroscopy

HSQC: Heteronuclear Single Quantum Coherence

HMBC: Heteronuclear Multiple Bond Correlation

IR: Infrared

MP: Melting Point

UV/Vis: Ultraviolet/Visible

ESMS: Electrospray Mass Spectrometry

MOF: Metal-Organic Framework

TGA: Thermogravimetric Analysis

EF: Edge-to-Face

OFF: Offset Face-to-Face

P4AE: Parallel Fourfold Aryl Embrace

Atom Colour Scheme:

Black: Carbon

White: Hydrogen

Red: Oxygen

Light Blue: Nitrogen

Green: Chlorine, Fluorine

Dark Blue: Cobalt, Copper, Silicon

Orange: Iron

Grey: Nickel, Zinc

Magenta: Manganese

Light Purple: Boron, Cadmium

Yellow: Sulfur

Chapter 1

Introduction

1.1 Preamble and Scope

This study investigates the coordination chemistry of functionalised 1,2-diazole ligands with specific focus on the synthesis of coordination polymers and discrete metallosupramolecular assemblies, with the aim of broadening the understanding of ditopic hetero-substituted pyrazole and indazole compounds and their coordniation behaviour within first-row transition metal complexes. Particular attention is paid to the synthesis of coordination polymer materials and aspects of their solid-state structural chemistry, specifically the impact of the unique geometric and electronic nature of the diazole ring system on the local and extended structure through the action of weak intermolecular forces, primarily hydrogen bonding and π-π interactions.

The study of supramolecular chemistry, which concerns the weak forces between molecules which give rise to larger, self-assembled architectures, is extremely broad in scope, and cannot be suitably condensed below in its entirety; therefore, a brief summary of the origins and basic tenets of supramolecular chemistry, its design principles, and the applications of selected classes of discrete and polymeric metallosupramolecular architectures is provided below, as well as a primer into the necessary heterocyclic and coordination chemistry of pyrazoles and indazoles. Where appropriate, more specific explanations of key concepts are given at the start of pertinent chapters. For a more exhaustive discussion of all aspects of supramolecular chemistry, the reader is directed to any one of a number of excellent texts on the subject.[1-3]

1.2 Supramolecular Chemistry

Supramolecular chemistry is referred to by many definitions, but perhaps the most fitting is that of Lehn, who described the science as "*the designed chemistry of the intermolecular bond"*.[4] While traditional (molecular) chemistry is focused on the chemistry of the covalent bond, and the synthesis and properties of individual molecules, supramolecular chemistry concerns the weaker interactions between molecules, which give rise to polymolecular assemblies.[2] Although the study of self-assembled polymolecular architectures can trace its origins to the early studies of host-guest interactions in biological systems,[5] and was advanced by the studies of hydrogen bonding in the early 20th century,[6, 7] supramolecular chemistry as it is known today originated in the 1960s, with the study of inclusion compounds derived from crown ethers and cryptands, macrocyclic polyethers and polyamines capable of encapsulating a cationic guest (Figure 1.1).[8-10] This work led to the award of

the Nobel Prize in Chemistry for 1987 to Lehn, Cram and Pedersen *"for their development and use of molecules with structure-specific interactions of high selectivity"*. [11]

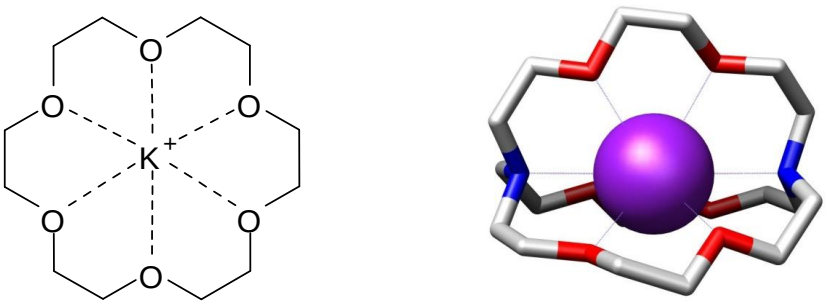

Figure 1.1: (Left) Structure of 18-crown-6, shown coordinating a potassium ion. (Right) Representation of a cryptand with encapsulated potassium ion.[12]

Since the pioneering work of Lehn, Cram and Pedersen, an enormous quantity of research has been published in the field of supramolecular chemistry, making it one of the fastest growing fields of research in modern chemistry.[2] While organic supramolecular host architectures such as calixarenes,[13] cucurbiturils[14] and cyclodextrins[15] continue to garner much attention for their applications in molecular recognition and guest binding, a great deal of attention has since been paid to metallosupramolecular chemistry,[16, 17] in which metal-ligand bonds play a key role in the assembly of polymolecular architectures by directing geometry and connectivity based on the coordination preferences of the metal ion.

1.3 Synthons in Metallosupramolecular Chemistry

A key concept in all forms of supramolecular chemistry is the notion of reversibility. Whereas strong interactions, such as those present in covalent bonds, usually show no spontaneous reversibility, weak interactions are able to rapidly equilibrate to the most thermodynamically favourable state by virtue of the low activation barrier to bond rupture. This property results in the concept of 'self-assembly',[18] where the building blocks of a supramolecular assembly will spontaneously aggregate into the most thermodynamically favourable arrangement, where other kinetically favoured products are short lived. The process of reversing the formation of kinetically favoured products is sometimes referred to as 'error-checking',[2] where the equilibrium process rapidly disassembles and reassembles the architectures, minimising unwanted products. To take full advantage of this process, information can be 'encoded' to ensure thermodynamic favourability of a particular configuration; this information

takes the form of molecular shape, number and nature of interaction sites, receptor geometry *etc.* The *synthons* in supramolecular assemblies are the weak interactions between the building blocks,[19] or *tectons*,[20] which bind the assemblies together. These synthons can take many forms, the presence of which must be controlled in order to sensibly design such assemblies.[21] The most obvious synthon in the 'toolbox' of metallosupramolecular chemistry is the metal-ligand bond; these relatively strong forces define the primary structure of a metallosupramolecular assembly, acting as a type of 'supramolecular glue',[22] and may be controlled by careful choice of the metal ion, taking into account the preferred coordination number, geometry and affinity for different ligand sets, as well as by thoughtful ligand design, controlling the quantity and nature of the metal binding sites and their relative geometries.[23] Some common metal ion geometries are represented in Figure 1.2.

Aside from geometry, a number of other factors must be considered in the choice of metal ions for metallosupramolecular applications. In order to promote the self-assembly process, comparatively labile metal-ligand bonds are required; while some metal-ligand bonds rival covalent bonds in their strength (Table 1.1), a compromise must be made between strength and reversibility, to both maximise the robustness of the resulting framework and to allow the resulting assembly to equilibrate under achievable conditions. Where specific applications are concerned, the redox and photochemical stability of the metal ion must also be considered, to ensure long term stability under the operating conditions. Finally, cost must be considered, especially where applications are envisaged requiring materials in large quantities. For these reasons, the late first row transition metals in their +2 oxidation state are excellent candidates for studies in metallosupramolecular chemistry, achieving a balance of predictable geometries, reversibility of coordination, stability and cost.

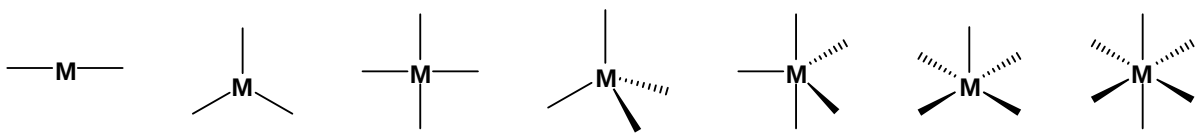

Figure 1.2: Examples of commonly encountered transition metal geometries. From left to right:linear, trigonal planar, square planar, tetrahedral, trigonal bipyramidal, square pyramidal, octahedral.

Aside from the metal-ligand interactions, weaker intermolecular forces must be taken into account in the rational design of metallosupramolecular assemblies. The presence of hydrogen bond donor or acceptor sites often plays a key role in the structural outcomes of supramolecular chemistry,[24] where such species can dictate the secondary structure of a supramolecular assembly, an approach employed in the synthesis of organic supramolecular 'foldamer' species.[25, 26] Hydrogen bonding interactions can be responsible for the formation of many novel extended network structures, with predictable

interactions between known tectons forming the basis for a number of topologically interesting structures (Figure 1.3).[27-29] As well as the common N-H or O-H hydrogen bond donors, in many cases C-H groups can act as hydrogen bond donors, especially where the donor carbon is in an electron-poor environment, imparting a larger electrostatic contribution to the interaction.[30]

Where the tectons are aromatic in nature, π-π stacking interactions are ubiquitous throughout structural chemistry.[31] A wealth of information, both theoretical and observational, has been collected regarding the tendency for π-systems to interact by way of parallel 'stacking' interactions, in which the π-systems of parallel rings partially overlap, typically at interplanar distances of *ca.* 3.4 Å and slightly offset to maximise the electrostatic interaction, with the strongest interactions taking place between π-polarised systems or in alternating π-rich and π-poor systems.[32-34] A number of motifs of π-π interactions have been documented in the metallosupramolecular literature; as well as the common offset face-to-face (OFF) interaction, stabilisation energy is also gained in edge-to-face (EF) interactions (C-H···π interactions), and combinations of the two, such as the parallel fourfold aryl embrace (P4AE) motif, in which two L-shaped aromatic systems, such as those found in triphenylphosphine or phenanthroline complexes, associate with the formation of one OFF interaction and two EF interactions (Figure 1.3).[35-37]

Halogen bonding,[38] argentophilic and other metal-metal attractive forces,[39-41] cation-π interactions[42] and other weak intermolecular forces are also often found in many types of supramolecular assemblies, although the structure directing ability of the weaker interactions in solid state structures can be limited when stronger forces are present.

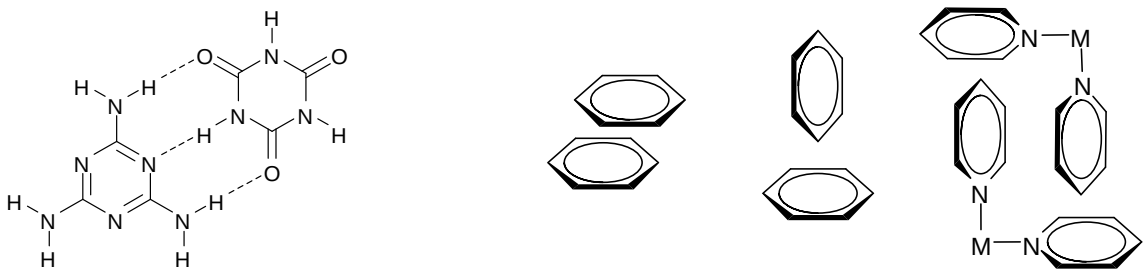

Figure 1.3: (Left) An example of strong hydrogen bonding interactions in the structure of the organic co-crystal melamine cyanurate;[43] (Right) Examples of π-π interactions; from left to right: Offset face-to-face (OFF); Edge-to-face (EF); Metal-templated parallel fourfold aryl embrace (P4AE)

These interactions can be somewhat identified by the distance between the tectons; although caution must be applied,[24] approximate distance ranges and angular constraints can be applied as 'cutoffs', where interactions that fall substantially outside of these ranges are likely to be ascribed to crystal-

packing effects[44] rather than a significant attractive force. A summary of the distances and energies involved in the interactions key to metallosupramolecular chemistry are summarised in Table 1.1.

Interaction Type	Typical Distance Range	Typical Energy Range[a]	Notes
Coordination Bond	~1.8 - 2.5 Å	~50 - 500 kJ mol	Representative for first row M(II) or M(III)
Hydrogen Bond - N, O donors/acceptors	≤ 3.2 Å (D···A)[b]	10 - 30 kJ mol^{-1}	Highly dependent on D-H···A angle (Directional)
Hydrogen Bond - C donor, N, O acceptor	3 - 3.5Å (D···A)	8 - 15 kJ mol^{-1}	Directional
C-H···π interaction	3.5 - 3.8 Å (C···π)	2 - 8 kJ mol^{-1}	Directional
π-π (Offset face-to-face)	3.3 - 3.8 Å (interplanar)	2 - 50 kJ mol^{-1}	Dependent on size and electronic nature of π system

Table 1.1: Summary of relevant parameters for commonly encountered metallosupramolecular interactions.[2, 24, 30, 33, 45-48]

[a]Values for typical systems have been chosen. Particularly strong hydrogen bonds can exhibit bond dissociation enthalpies of over 150 kJ mol^{-1}; the discussion of such systems is outside the scope of this work. [b]Although interactions substantially longer than the sum of the van der Waals radii can still provide electrostatic stabilisation energy, such a distance restraint is sufficient for N or O donors and acceptors for the purposes of this discussion.

1.4 Discrete Assemblies

Following on from the work of Lehn, Cram and Pederson, an enormous volume of research has been carried out into the properties of discrete assemblies of a number of different classes, including helicates,[49, 50] catenanes,[51-53] rotaxanes[54, 55] and knots,[56-58] examples of which are shown in Figure 1.4. Consistently at the forefront of modern discrete supramolecular chemistry, however, has been the notion of host-guest chemistry, in which a host species with an internal cavity of designed shape and size is used to selectively encapsulate a guest in order to enforce certain spatial restraints.[59] In such assemblies, the properties of the metal-ligand bond is particularly useful; as well as the influence on the molecular geometry dictated by the coordination preferences of a metal ion, the reversibility of binding promotes the self-assembly process, allowing for the association and dissociation of the host-guest species.

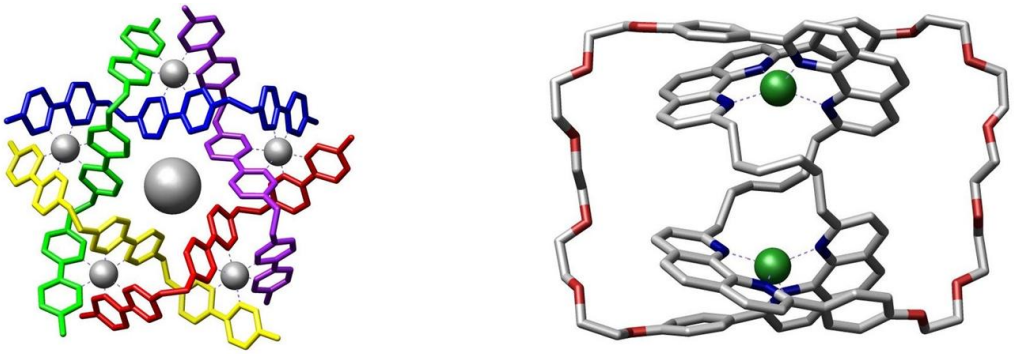

Figure 1.4: (Left) Example of a metal-templated circular helicate[60] reported by Lehn et al. [61] (Right) A molecular trefoil knot[62] reported by Sauvage et al.[63]

As well as their uses as functional materials, there has been significant interest in discrete metallosupramolecular assemblies from the point of view of fundamental synthesis, and specifically the application of synthetic chemistry to the preparation of new structural types.[64] This approach has led to several memorable reports in recent years detailing the rational, systematic synthesis of aesthetically pleasing molecular species such as trefoil knots[63] and borromean rings,[65] and the recent preparation of a pentafoil knot.[66] As well as being visually appealing, the synthesis of such complex species provides a fundamental understanding of the chemical processes involved with catenation and molecular association, knowledge which will prove vital for the preparation of molecular devices containing discrete metallosupramolecular entities in the future.

1.4.1 Applications of Discrete Supramolecular Assemblies

Much of the research conducted to date in the field of discrete supramolecular assemblies is based on host-guest chemistry; that is, the recognition, selective encapsulation and/or reaction, and controlled release of a substrate by a supramolecular host, with each reversible step representing a potential application of the host material.[67-70]

Recognition of a substrate, and the subsequent signalling of a recognition event, represents an important application of discrete supramolecular assemblies.[71, 72] Systems capable of recognising one or more species out of a mixture have been investigated as molecular sensors, especially for biological applications, where compounds of interest may be present in low concentrations in a complex mixture.[73-75] Typically, sensor molecules will incorporate one or more receptor sites, tailored to interact with the substrate *via* supramolecular forces and some manner of signalling mechanism, such

as a chromophore, the colorimetric properties of which are altered upon binding of the desired guest.[76] Indeed, fluorescent sensors based on discrete supramolecular systems have already been implemented in the medical field, as shown in Figure 1.5.

Figure 1.5: OPTI Medical Systems blood gas and electrolyte analyser with casette. This system uses a cavitand-based ion receptor to signal alkali metal concentrations in blood via a change in fluorescence.[77]

Encapsulation of a substrate by a discrete architecture utilising supramolecular forces is a concept dating back to the work of Pedersen regarding encapsulation of alkali metal ions.[8] More recently, substrate encapsulation has been aimed towards delivery of a guest into an otherwise unfavourable environment, for example in phase transfer catalysis[78, 79] or targeted drug delivery.[80] For biological applications such as drug delivery, a biologically benign host molecule is preferred, and as such cyclodextrins and related molecules have seen significant use in this field,[81, 82] including the recent synthesis of an "edible Metal-Organic Framework" by Yaghi, Stoddart and colleagues.[83] The encapsulation process itself can impose a completely different environment on the guest, independent of the nature of the bulk solution. The impact of encapsulation on the behaviour of chemical species has been shown by Nitschke, who recently demonstrated the encapsulation of white phosphorous P_4 by a self-assembled host, imparting air stability to the usually pyrophoric molecule.[84] Encapsulation of a guest can also affect the properties of the host molecule, as demonstrated by Batten *et al*., who recently reported a self-assembled 'nanoball', which displayed guest dependent spin crossover behaviour for the Fe(II) ions present in the host framework.[85] Two examples of metallosupramolecular capsules are shown in Figure 1.6.

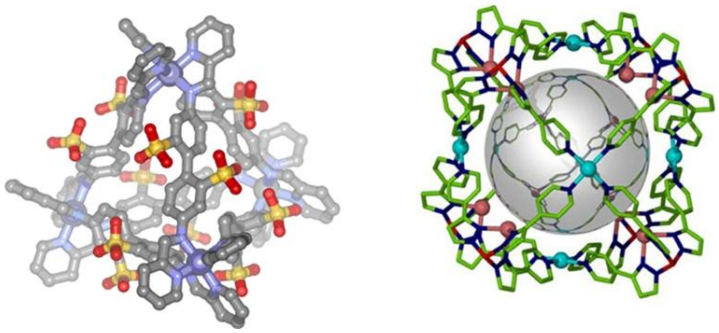

Figure 1.6: (Left) Example of a tetrahedral self-assembled metallocapsule[86] reported by Nitschke.[84] (Right) The self-assembled bimetallic 'nanoball'[87] reported by Batten.[85]

Reactions taking place within supramolecular hosts are often seen as a primary goal of discrete supramolecular chemistry, and can demonstrate the enormous potential for controlling reactivity on a single molecule scale using engineered void spaces.[88] Where reactivity within soluble supramolecular capsules is concerned, there are several key factors to consider in comparison to bulk reactivity.[89] Encapsulating two or more reactants within a host species of commensurate size has the effect of increasing the effective concentrations of the two substrates such that the rate of reaction is often greatly increased at low bulk concentrations, such as may be required to avoid side reactions. Secondly, and most often discussed, is the impact of imposing restrictions on the shape and size of the transition state of any reactions which take place within the capsule. Altering the internal surface of a capsule can have profound consequences on the reactivity of species contained within, such as to favour the formation of a diastereomer or regioisomer which would not otherwise form in the bulk solution. Examples of this selectivity have been displayed by Rebek, for the regioselective synthesis of 1,4-disubstituted triazoles,[90] and by Fujita, in the synthesis of Diels-Alder adducts with regioselectivity not available in bulk solution.[91] Work in this field aims to achieve 'enzyme-like' catalysis,[92] where the geometry of the desired transition state is favoured within the cavity and the product is efficiently removed. Currently, inhibition by competitive encapsulation of the reaction products remains a challenge to be overcome in such systems.[88]

Other methods of promoting reactions within capsules have also been investigated. The capsule walls themselves can participate in photochemical reactions, as seen in the photochemical oxidation of adamantane reported by Fujita in which a radical transfer mechanism from the capsule wall activates the substrate.[93] Host species can also encapsulate traditional catalysts, as demonstrated by Raymond with the encapsulation of an iridium-based C-H bond activation catalyst within a tetrahedral capsule. Where the capsules are inherently chiral and can be resolved, chiral catalysis is possible, as recently demonstrated by Raymond with the resolution of a mechanically stable

homochiral capsule capable of enantioselective catalysis of an Aza-Cope rearrangement.[94] More recently, Fujita reported the formation of monodisperse silica nanoparticles within a metallosupramolecular capsule by lining the internal surface with carbohydrate species and other functional groups.[95]

1.5 Infinite Assemblies

It has been long known that the reaction of a divergent bridging ligand with a metal ion can give rise to a polymeric framework. In fact, Prussian Blue, a polymeric assembly of cyanide-bridged Fe(II) and Fe(III) ions, was the first reported synthetic coordination compound[96, 97] - although its structure was not unambiguously elucidated until much later[98] - and metal-cyanide materials are still providing substantial contributions to modern-day chemistry.[99-101] Despite this rich history, the rational design of hybrid organic-inorganic coordination polymers as we know it today was not described until a landmark paper by Robson in 1990, in which the 'node and spacer' approach to the synthesis of coordination polymers was first alluded.[102] Following this work, intense worldwide attention was focused on the synthesis of coordination polymer materials, largely due to their potential applications in gas storage, separation, sensing and catalysis, all based on the prospect of a stable, porous material with pore shape, size and functionality controllable *via* chemical synthesis, where internal void space can be designed into the structure with careful choice of starting materials.[103-107] Comparisons to zeolite chemistry are apt, where the industrial applications of aluminosilicate and aluminophosphate materials for their porous nature are well-known.[108, 109] The notion of deliberately engineering stable and porous coordination polymers, often referred to as Metal-Organic Frameworks (MOFs), was further developed by several groups, with important works by Yaghi, Kitagawa, Ferey and others in the 1990s and early 2000s bringing the chemistry of MOFs to the forefront of modern science.[110-119] Several well-known MOFs are shown in Figure 1.7.

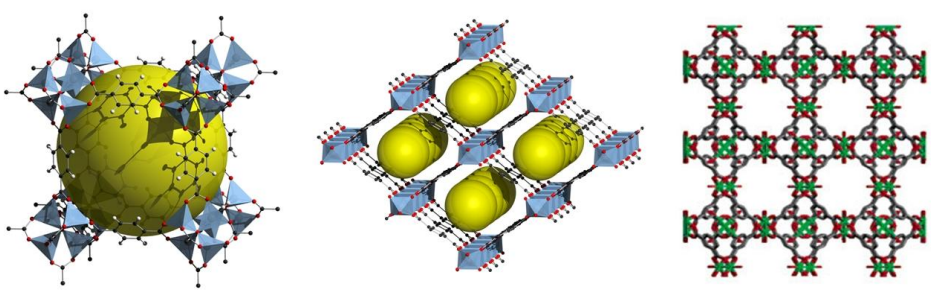

Figure 1.7: Structures of several well-known porous coordination polymer materials[120] From left to right: MOF-5,[111] MIL-53,[113] HKUST-1.[118]

A substantial quantity of research in the field of coordination polymers remains directed towards the synthesis and investigation of new framework materials, utilising new polyfunctional ligands and incorporating the lessons learned from the previous generation of materials in terms of the importance of thermal and chemical robustness, framework flexibility and control of interpenetration and polymorphism and, most importantly, the incorporation of porosity into the framework.[121-128] Recently, the chemistry of porous coordination polymers has further diverged into several sub-categories based on specific applications. Porous coordination networks hold interest as well-defined, monodisperse scaffolds, to carry out fundamental science and to impart specific function.[129] With the advent of robust and reproducible synthetic methods,[110, 130, 131] unprecedented opportunities now exist for the study of a wide variety of processes such as spin switching, negative thermal expansion, guest exchange and catenation occuring within framework materials,[132-137] as well as providing significant new challenges for theoretical and computational chemistry.[138-141] Studies have been carried out investigating practical aspects of the preparation of MOF materials for large scale applications, with investigations into morphology control,[142] the growth of thin films[143, 144] and beaviour under compression[145, 146] emerging in recent years. As has been seen with the discrete supramolecular assemblies described above, catalysis carried out within functional pores also remains an area of intense research in coordination polymer chemistry.[147-149] Chemical modification of the internal surfaces of coordination polymers has also been reported, with work by Cohen and others demonstrating the possibility of chemically grafting functional groups within porous crystalline materials post-synthesis.[150-152] The possibilities of unique photophysical properties from the unprecedented chemical versatility offered by coordination polymer materials has also led to research towards both sensor applications and nonlinear optical properties of such materials.[153-155] Undoubtedly, however, the most often-quoted application of porous coordination polymer materials is in the field of gas separation, storage and delivery.[156-161]

1.5.1 Coordination Polymers for Gas Sorption Applications.

Arguably the most significant challenge facing scientists in the early 21st century is the development of environmentally benign and renewable methods of energy generation, storage and transport.[162] With atmospheric CO_2 levels likely to exceed 400 ppm in the coming years (Figure 1.8), efforts have recently focused on the development of new technologies to severely reduce greenhouse gas emissions while providing affordable alternatives for energy generation.[163] In this area, sorption

materials provide a number of new options, both for alternative energy sources and to retrofit existing technologies.[164]

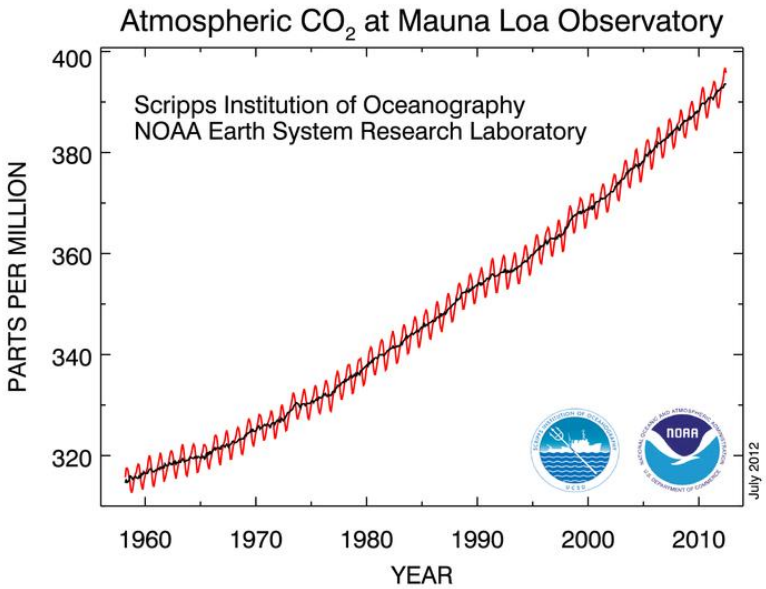

Figure 1.8: Atmospheric CO_2 levels as recorded over a 50 year period at Mauna Loa Observatory, Hawaii.[165]

Where coordination polymers are to be used in gas sorption applications, a number of design factors need to be taken into account. Whereas early coordination polymer research was often focused on preparing materials with the largest possible void spaces, aside from being progressively more difficult to achieve, this strategy must eventually result in materials where the guest molecules experience little to no interaction with the pore walls.[166] It became clear that an ideal sorption material would contain pores of a size sufficiently large to allow the desired guest access to the sorption sites, but sufficiently small to maximise the surface to volume ratio.[161] There has been a growing number of reports of 'breathable' MOFs, where the pore volume of the desorbed material appears negligible, but where a reversible phase transition takes place on gas uptake, changing the nature of the pore walls or offering further sorption sites.[124, 167] Flexibility in the nodes and/or ligand backbone seems crucial in these systems, prompting some research into the use of flexible linkers instead of the traditional rigid aromatic ligands. Of vital importance to practical gas sorption applications is the sorption enthalpy, a measure of the strength of the attractions between the gas molecules and the pore walls. For diatomic gas molecules, such as H_2, these interactions rely on comparatively weak van der Waals forces. Where the adsorbate contains polar bonds or is chemically reactive, as is the case with CO_2, stronger bonds can be formed by hydrogen bonding or a reaction with a suitably reactive site such as an amine

group.[168, 169] Several design features can be incorporated to increase binding enthalpy; the presence of unsaturated metal sites, for example, can provide a much stronger interaction with H_2 molecules.[170] Extended aromatic systems provide good scaffolds for gas sorption, although increasing the breadth of a linker molecule will necessarily reduce the available pore volume.[171, 172] Currently, most MOF-based H_2 sorption materials exhibit binding enthalpies of less than 7 kJ mol^{-1},[157] while simulation suggests an optimum binding enthalpy of ~ 15 kJ mol^{-1} is required to meet viability thresholds; specifically, to raise the working temperature of such sorption devices from 77 K to room temperature, without the release of a large amount of thermal energy on charging.[173]

Recently there has been significant interest from many sectors regarding the utility of gaseous hydrogen as a vehicular fuel source, with the most striking advantages being the zero carbon emission nature of hydrogen combustion, and the abundant supply of hydrogen from water.[174-176] A mass produced vehicle powered either by hydrogen fuel cell technology or a hydrogen internal combustion engine would represent a major milestone in the search for sustainable energy in the 21st century.[175] The major downside of hydrogen as a vehicle fuel is the low volumetric energy density offered by gaseous fuels in general, but especially hydrogen with its extremely low boiling point of 20 Kelvin and low molecular weight. As such, current hydrogen vehicle prototypes rely on either high pressure (typically 350 or 700 atm) or cryogenic storage, both of which raise serious safety concerns preventing mass production. Another downside of current storage technology is the gravimetric energy density limitations, with the benchmark 5 kg of H_2 requiring storage systems weighing in excess of 100 kg. Physisorption systems such as MOFs provide a unique solution to the problem of H_2 storage, in their ability to adsorb gasses at higher volumetric density than empty containers at the same pressure, as a consequence of their extremely high accessible surface areas. Indeed, candidate materials such as MOF-210 (Figure 1.9), with a BET surface area of 6240 m^2g^{-1} can exhibit up to 8% gravimetric H_2 storage under certain conditions (80 bar, 77 K).[177] A significant advantage of MOFs over competing hydrogen storage technology is the rapid recyclability afforded by the physisorption process, where other systems can be limited by sluggish kinetics or the need for off-board recycling of fuel storage materials.[178, 179] The concept of 'spillover', where hydrogen dissociation catalysts are impregnated into the MOF surface, allowing for storage of atomic hydrogen, has shown some promise towards room temperature H_2 storage; however, the mechanism is not yet well understood.[180]

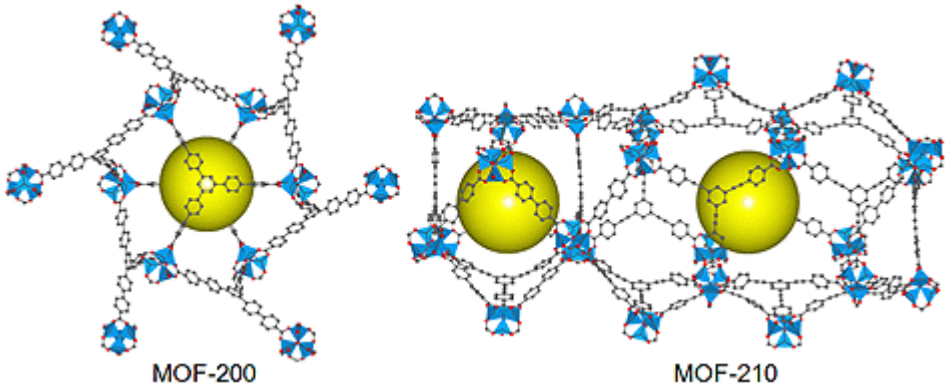

Figure 1.9: High surface area compounds MOF-200 and MOF-210,[177] possible candidates for H_2 storage applications.[181]

Capture of CO_2 from industrial flue gas can currently be achieved by the use of aqueous amine scrubber systems, where CO_2 is fixed chemically, first as the carbamate species, followed by reversible formation of bicarbonate in the presence of H_2O.[182] Employed as a solution of approximately 20-30% by weight, aqueous amine-based carbon capture suffers from poor mass efficiency, with excess water serving to increase the wasted mass of the system, and requiring large amounts of energy (*ca* 25% of the total energy output) to regenerate by a temperature-swing process.[183] Amine systems are also susceptible to poisoning by other flue gas contaminants, such as SO_2. Recently, research has been directed towards the use of porous materials such as MOFs to reversibly capture CO_2.[159, 160] In this field, the unique potential of MOF systems towards internal functionalisation may result in more efficient and reversible CO_2 capture in the future, with current research exploring the potential for post-synthetically grafted alkylamine groups,[184] and the incorporation of unsaturated metal sites to increase sorption enthalpy to levels capable of supporting significant sorption capacities at room temperature. One difficulty arises from the nature of flue gas itself, which is a warm, humid mixture of gasses containing only *ca.* 10% CO_2, requiring highly selective sorption at low partial pressure of CO_2, and excellent stability in the presence of water vapour.[159] Current non-functionalised MOFs with large surface areas may be more suitable in the transport and storage of CO_2 at high pressure, with candidate materials such as MOF-177 showing extremely high capacity for storage of CO_2 when charged from a high pressure stream of the pure gas at low temperature.[185]

1.5.2 Topology

Key to understanding the structure and properties of coordination polymers, as with any network solids,[186] is a thorough description of the three-dimensional structure.[187, 188] Often the underlying connectivity of a network can be obscured by the wide variety of possible ligand and metal coordination modes, especially in densely interconnected three-dimensional structures. The structural diversity displayed in coordination polymers requires the use of nomenclature based on mathematical descriptions of networks, in order to fully describe their connectivity.[189] The mathematical fields of nets and topology have been thoroughly studied, and several aspects of these areas are of relevance to coordination polymer chemistry. It must be stressed that the objective of using such terms to represent a coordination network is to *simplify* the structure by providing a rational description of the complete connectivity of the network, which can be easily related to the real structure.[188] In some instances, a topological description of a network becomes so cumbersome as to be of little practical value, although still necessary as a complete description of the structure. It should be noted that the net approach can be applied to describe any extended network; as well as coordination polymers, hydrogen bonding networks can also benefit from such an analysis. However, such descriptions are most useful for well-defined interactions which can be unambiguously recognised, and become increasingly arbitrary when applied to networks defined by weaker interactions which can overlap with crystal packing forces.

An infinitely repeating, interconnected structure such as a three-dimensional coordination polymer can be described in terms of *nodes* and *links*; a node is a structural feature which is connected to three or more other nodes *via* links. *As such, any structural component within a network which connects to only two others is a link, while any structural component which connects to three or more others is a node*. In the realm of coordination polymer chemistry, the structural components consist of metal ions and ligands, where the connection between nodes and links is the coordination bond. This simple concept is intuitively related to the node and spacer approach discussed by Robson.[102] In a simple coordination polymer, assigning nodes and links is straightforward; for a tetrahedral metal and linear bridging ligand, such as in the case of poly-$[Cd(CN)_2]$, the cyanide ligand, bridging two metal ions, is a link, and the metal ion, being connected through links to four other metal ions, is a node. However, the assignment of nodes is not always straightforward; ligands which link more than two metal ions, such as benzene-1,3,5-tricarboxylate, must also be considered nodes, while metal ions can be considered links when they join only two nodes, either in the cases of 2-coordinate complexes, or due to chelation or the presence of capping ligands. In the case of a simple one-dimensional coordination polymer, where each structural component joins only two others, no nodes are present,

and the analogy to networks is invalid. Although nodes are typically assigned to either metal ions or ligand centroids, other assignments may be necessary in order to provide a sensible structural description. For example, in the structure of MOF-5 and its analogues, each vertex consists of a basic zinc acetate cluster of the formula $[Zn_4O(R\text{-}COO)_6)]$, linked to six adjacent clusters by the aromatic R-group. By one interpretation, each zinc ion must be a node, being connected to three other zinc ions through carboxylate and oxo bridges, and as such, the central μ_4-oxo ligand must also be a node, as must each ligand, which bridges four metal centres. The resulting structural description, although correct, quickly becomes unwieldly, involving three unique nodes of varying connectivity. A simpler representation is arrived at by simply assigning the entire Zn_4O vertex as a node, which transforms the bridging ligands into links (Figure 1.10). Both assignments are correct, but the simpler description is considerably more useful as a representation of the physical structure. Furthermore, it must be noted that in the reduction of a crystal structure to a net, information regarding angles and distances are disregarded; the geometry of a node does not necessarily correspond to the atomic geometry, and no angular information is required, nor is the length of the links taken into account. By this property, any two networks which can be interconverted without the breaking of bonds are considered identical (Figure 1.11)

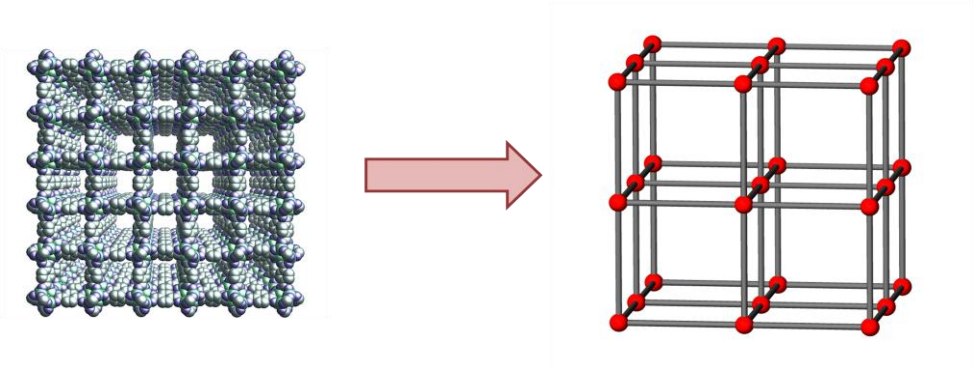

Figure 1.10: Deconstruction from a complete chemical representation of MOF-5[190] into a topological representation, choosing the $[Zn_4O(COO)_6]$ cluster as a node.

Once the nodes and links have been classified, the structure as a whole can be assigned a numerical descriptor, of which several conventions are in common use, with each employing some variation on the node connectivity, and the number of nodes required to complete a *circuit*, that is, how many nodes are passed through to return to the original node. The number of shortest circuits for a node is related to the connectivity by the formula n = (P(P-1))/2, where n is the number of shortest circuits and P is the connectivity. This formula also describes the number of unique angles for a coordination polyhedron. For a four-connected node, a circuit leaving through one link has three unique paths back

to the original node; accounting for these, a circuit departing through any of the remaining three links has two unique paths remaining, leaving only one circuit unaccounted for, for a total of 6 unique circuits. A net in which all of the shortest circuits are of the same length is known as a *uniform* net; in addition, if all nodes are identical, the net is a *uniform platonic* net, and can be described by the symbol (a, b) where a is the length of each circuit, and b is the connectivity of the node. The common diamondoid network meets these criteria, and is given the symbol (6,4). Several two-dimensional networks also meet these criteria, such as the (6,3) network, shown in Figure 1.11. Although the (4,4) network (Figure 1.11) technically contains 6-membered circuits as well as 4-membered, the (4,4) notation is in far more common use in the literature than the more correct description, $(4^4 \cdot 6^2)$.

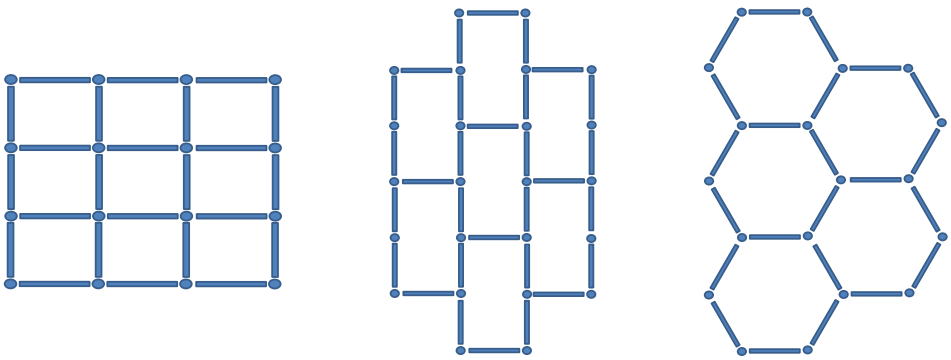

Figure 1.11: Schematic representation of the (4,4) network (left), and representations of two topologically equivalent (6,3) networks (centre and right)

For networks containing more than one type of node, or more than one circuit length, a more thorough analysis is required. Such networks can be described by the use of the point symbol, which takes the form $(A^d \cdot B^e \cdot C^f)$, where A, B and C are the lengths of each circuit, and d, e and f are the number of unique occurrences of each circuit in the structure. For example, the niobium oxide (**nbo**) network (Figure 1.12) contains four 6-membered circuits and two 8-membered circuits per node, and so is given the point symbol $(6^4 \cdot 8^2)$. The connectivity of the node can be derived by the total number of circuits, in this case 6, which describes a four-connected node by the formula n = (P(P-1))/2 described above. In the case of networks with more than one type of node, each node is given its own term in the point symbol, with subscripts denoting the relative quantities of each type of node; for example, the 2-dimensional net described by $(4 \cdot 6^2)_4(6^4 \cdot 10^2)$ is a binodal net, with four 3-connected nodes for every one 4-connected node. A related description can be obtained by the use of the vertex symbol, which is related to the point symbol but takes into account 'shortcuts';[187] however, these symbols can

become cumbersome for some networks, and for the purposes of this discussion, topological assignment will be limited to point symbols and RCSR codes (see below).

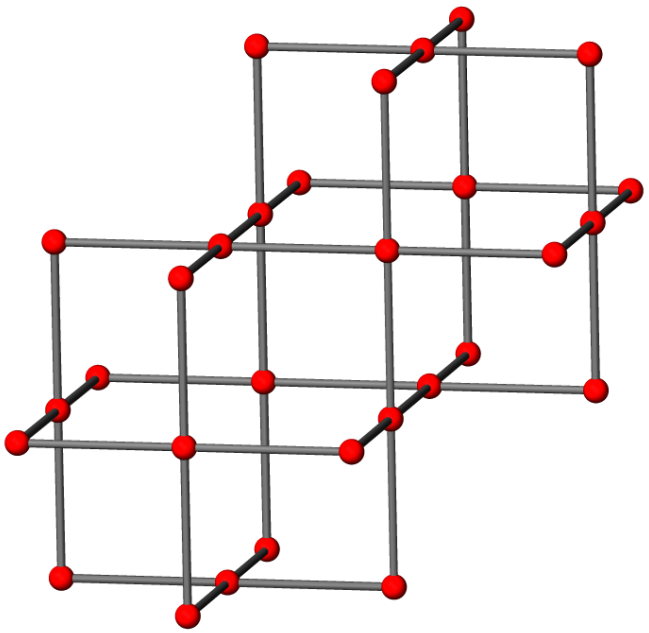

*Figure 1.12: Representation of the 3-dimensional, 4-connected **nbo** network, with point symol ($6^4 \cdot 8^2$).*

One point of note in the symbolic description of nets is a numerical description may apply to more than one network; for example, the related 4-connected networks diamondoid and lonsdaleite, as uniform platonic nets, are both described by the symbol (6,4), and both have the same point symbol (6^6) and vertex symbol $6_2.6_2.6_2.6_2.6_2.6_2$; however, the networks are visibly different; in the diamondoid network, each six-membered ring is in the chair conformation, leading to a network of identical adamantoid cages with four windows each, while lonsdaleite contains six-membered rings in both the chair and boat conformations, leading to a mixture of cages with either 3 or 5 windows (Figure 1.13). As such, an additional means of identification is required to differentiate between such structures; a three dimensional graphical representation, which can often be compared to the structure of a known mineral. The Reticular Chemistry Structural Resource (RCSR),[191] a library of known mineral structures each assigned a unique three-letter code, is routinely used to describe coordination polymer networks, due to the frequent occurrence of a relatively small group of topologies in both minerals and coordination polymers. In this way, diamondoid and lonsdaleite structures can be differentiated by applying their RCSR three-letter codes **dia** and **lon**. Where possible, structural

reports of coordination polymers are almost always accompanied by the appropriate RCSR code, allowing rapid identification of known networks.

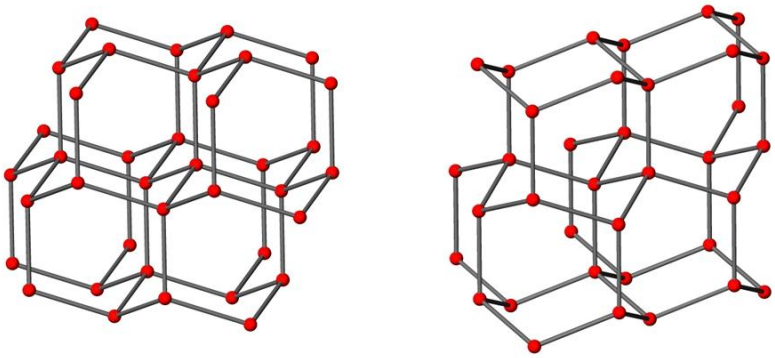

*Figure 1.13: Structures of diamondoid **dia** (left) and lonsdaleite **lon** (right), both of which share the same point and vertex symbols, but are physically different.*

Finally, the notion of interpenetration must be quantified.[188, 192, 193] The mechanical interlocking of two or more networks is commonly observed where the underlying net is a *self-dual* – where placing a node at the centre of each cavity within a network generates a second network of the same topology. The diamondoid network, as one of relatively few examples of naturally self-dual networks, is very commonly observed to be interpenetrated. Interpenetration of non-self dual networks can also observed, but is less common, and is sometimes referred to as "interweaving". Interpenetration is referred to as *n*-fold, where n is the total number of networks; at the time of writing, the greatest degree of interpenetration observed was a 54-fold interpenetrated **srs** network.[194] Champness, Schröder and co-workers recently reported the synthesis of a novel 'partially interpenetrated' network, in which incomplete fragments of an interpenetrating network were observed within a coordination polymer as periodic structural defects.[195] It must be noted that interpenetrated networks are linked in such a way as to prevent their separation without the breaking of bonds, equivalent to the catenation of discrete species, with no (strong) chemical bonds between the two species. The interpenetration of 2-dimensional networks can be further described in terms of dimensionality, where several modes of interpenetration are possible; 2-dimensional networks can interlock to form a denser 2-dimensional sheet with no extension into the perpendicular dimension (2D→2D interpenetration), or the interpenetrating sheets can be inclined with respect to each other, to give an overall 3-dimensional network consisting of interlocked 2-dimensional components (inclined 2D→3D interpenetration). Less common is the possibility of parallel 2-dimensional sheets being interlocked, where the interlocking of more parallel sheets along the perpendicular axis gives rise to a 3-dimensional

structure (parallel 2D→3D interpenetration). An example of twofold interpenetration of the 3-dimensional **dia** network is shown in Figure 1.14.

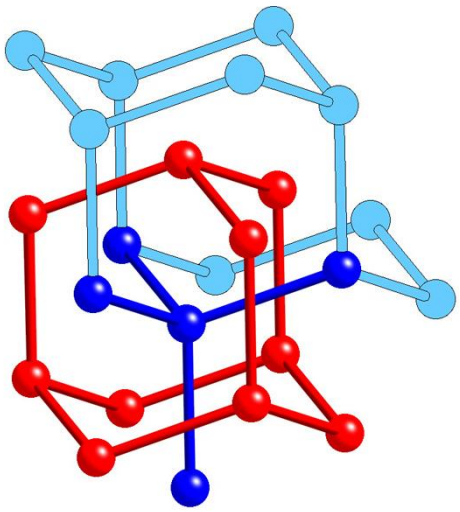

Figure 1.14: Representation of two interpenetrated diamondoid networks,[196] independent networks coloured separately.

1.6 Chemistry of 1,2-diazoles

1.6.1 Properties of Pyrazole and Pyrazole Derivatives

Pyrazole, a 5-membered aromatic heterocycle containing two nitrogen atoms at the 1 and 2 positions, is a relatively well-known member of the nitrogen heterocycle family, and the most common 1,2-diazole.[197, 198] The free compound was first isolated by Knorr and Buchner in the 1880s after investigations on the substituted pyrazolonone analgesic, antipyrine (phenazone).[199] Although not commonly isolated from natural sources, pyrazoles and pyrazolonones currently find widespread use in pharmaceuticals, with numerous examples of biologically active pyrazole-containing molecules such as Celecoxib[200] (Pfizer) and Regadenoson[201] (Astellas). Chemically, the pyrazole ring is a π-excessive heterocycle containing two distinct classes of nitrogen atom in rapid tautomerism.[202] N1 is a pyrrole-like N-H site in which the nitrogen lone pair is donated into the π system, while N2 more closely resembles the nitrogen found on pyridine, although with pKa for the conjugate acid of 2.5, the N2 atom of pyrazole is considerably less basic than that of pyridine (conjugate acid pKa = 5.3). As would be expected, the pyrrole-like N-H group is very weakly acidic, with pKa 14.2, similar to that of imidazole. Extensive studies into the electronic and structural aspects of the tautomerism and

hydrogen bonding associations of pyrazoles and their derivatives have been carried out by Elguero and coworkers.[203-205] Some examples of pyrazole compounds are shown in Figure 1.15.

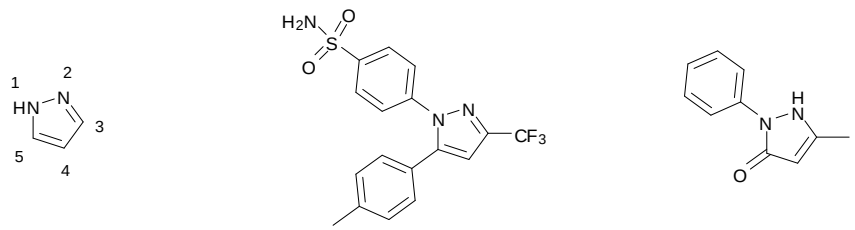

Figure 1.15 (Left) Structure of pyrazole with numbering scheme; (Right) Two pyrazole-based pharmaceuticals, Celecoxib (centre) and Phenazone (right).

1.6.2 Synthesis of Pyrazole Derivatives

A commonly employed method of synthesis for pyrazoles and pyrazole derivatives is by the action of hydrazine, or a 1-alkyl or 1-aryl hydrazine, on a 1,3-dicarbonyl or synthetic equivalent.[197] For example, the reaction of hydrazine with 2,4-pentanedione gives the product 3,5-dimethyl-1*H*-pyrazole in quantitative yield (Figure 1.16).[206] Suitably functionalised 1,3-diketones are therefore often the preferred method for synthesis of 3,5-disubstituted pyrazoles. It should be noted that many 1,3-diketones exist as a mixture of their keto and enol tautomers,[207] depending on the substitution pattern. For the purposes of this and later discussions, any compound with tautomeric contribution from the 1,3-diketone form will be referred to as such, even though in many cases the enol form dominates.

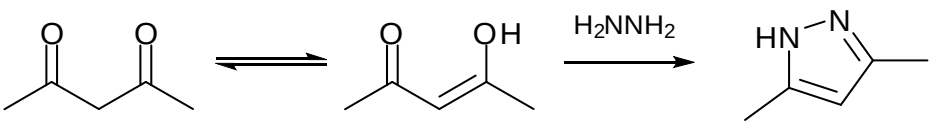

Figure 1.16 Synthesis of 3,5-dimethyl-1H-pyrazole from 2,4-pentanedione showing tautomeric forms of the diketone.

Where the desired product is a 3,5-unsubstituted pyrazole, reactions with hydrazine must take place with suitable dielectrophiles, such as dialdehydes or their synthetic equivalents, diacetals. An example is the synthesis of pyrazole itself by the action of hydrazine on the diacetal 1,1,3,3-tetramethoxypropane.[208] Functionality can be achieved at the 3- and 5-positions by employing other electrophilic starting materials in place of a diketone or dialdehyde, and 1-substituted pyrazoles can be arrived at in one step by employing a substituted hydrazine, as shown in Figure 1.17. Amino functionality in the pyrazole 3-position is the result of inclusion of a nitrile group in the place of a

carbonyl,[209] where as 3-pyrazolononones can be prepared by the action of hydrazine on a β-ketoester or β-ketoacid.[210] As an alternative to hydrazine-based routes, the pyrazole ring can also be formed by a 1,3-dipolar addition of diazoalkanes to alkynes.[211]

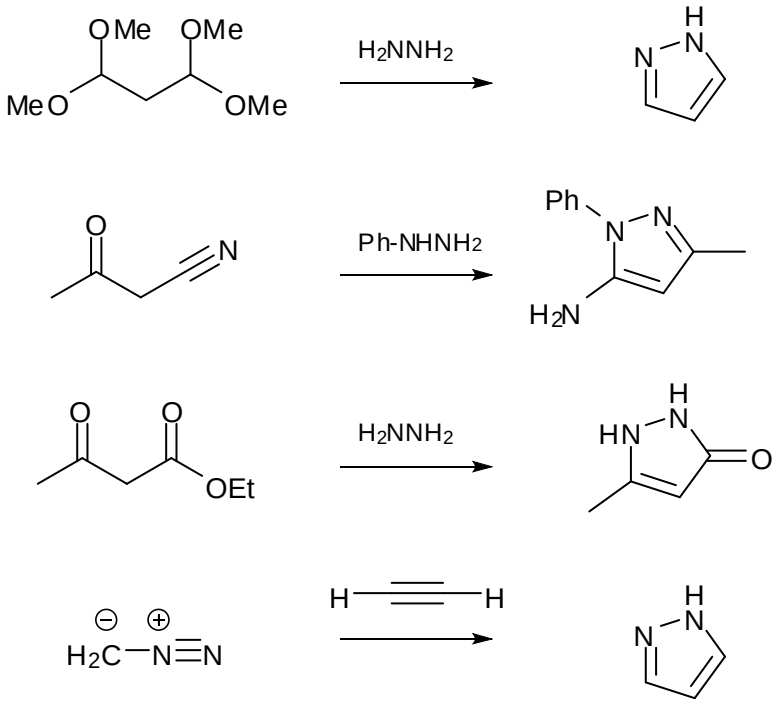

Figure 1.17 Examples of pyrazole syntheses involving ring formation

Once formed, the pyrazole ring can undergo a number of synthetically useful reactions.[198] Pyrazole reacts readily at the N1 position with carbon electrophiles to form N-aryl or N-alkyl pyrazoles. N1 can be protected using a suitable protecting group, allowing substitution on the 5-position *via* lithiation, or allowing substituents to be added to the 4-position *via* electrophilic aromatic substitution, such as formylation with a Vilsmeier-Haack reaction.[197]

1.6.3 Pyrazoles in Coordination Chemistry

Although the synthetic chemistry of pyrazoles traces its origins to medicinal applications, pyrazole and its derivatives have long been utilised in the field of coordination chemistry.[212-215] One reason for the widespread use of pyrazole for these applications is the variety of coordination modes which can be adopted,[216] commonly presented as either monodentate as the neutral compound, *exo*-bidentate as the mono-anionic species, or polydentate chelates following suitable functionalisation (Figure 1.18). Examples have also been reported of metallation at the 4 position, and metallocene-type complexes are known for the cases of suitably substituted rings.

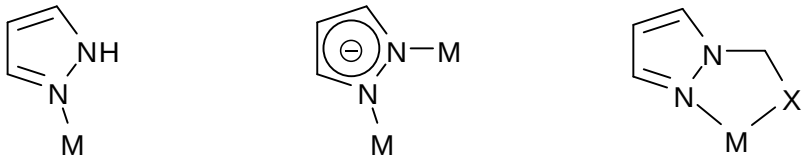

Figure 1.18: Some examples of pyrazole coordination behaviour. From left to right: Monodentate; exo-Bidentate as the pyrazolate anion; Polydentate chelate through functionalisation, where X = N, O etc.

As a neutral monodentate coordinating species, pyrazole behaves as a typical nitrogen donor heterocycle, with weaker ligand field than pyridine owing to poorer π-acceptor character.[217, 218] Upon deprotonation, the resulting pyrazolate anion can engage in an enormous variety of bridging modes, either forming polymeric materials or discrete systems of two or more metal centres.[216] A large variety of pyrazole-containing clusters have been reported; common among them is the $Cu_3O(pz)_3$ cluster (Figure 1.19) in which three Cu(I) or Cu(II) ions are coordinated in a triangular arrangement by three deprotonated pyrazolate anions, with or without a central μ_3-oxo bridge, with the metal ions' coordination requirements being filled by anions or solvent molecules in the remaining positions. Pyrazolate anions are also known to form one-dimensional polymeric structures, bridging tetrahedral divalent metal ions in a zig-zag mode.[219] Owing to the low acidity of the pyrazole N-H group, *exo*-bidentate coordination from the pyrazolate anion tends to give rise to substantially more hydrolytically stable assemblies than the comparable carboxylate equivalents, a key factor in the preparation of porous coordination polymers for gas sorption applications.[159]

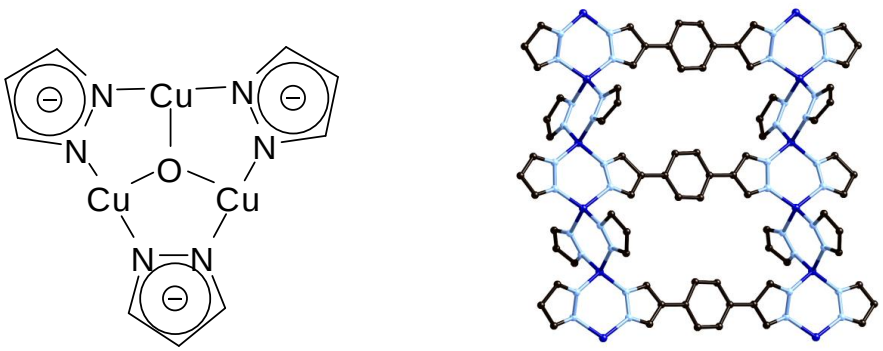

Figure 1.19: (Left) Base structure of $[Cu_3O(pz)_3]$. (Right) Example of polymeric bridging pyrazolate anions in the structure of [Co(1,4-benzenedipyrazolate)] reported by Long et al.[219]

Since the mid 20th century, a wealth of experimental data has been collected on complexes of the polypyrazolylborates,[220-222] a family of polydentate ligands where 2, 3 or 4 pyrazole ligands are bound through N1 to a boron atom, providing both endo- and exo-polydentate coordination environments

with an appropriate metal ion. This approach has been extended to polypyrazolylalkanes, where the reaction of pyrazole with dichloromethane or chloroform yields 1,1′-methylenebispyrazole and 1,1′,1″-methylenetrispyrazole, respectively, both of which have been widely used as ligands.[223] The straightforward functionalisation of pyrazole or its precursors allows a range of other coordinating groups to be included with relative ease, such as the widely-used pyrazole-3,5-dicarboxylic acid,[224-226] readily available from oxidation of the dimethyl precursor. Some examples of common pyrazole-based ligands are shown in Figure 1.20.

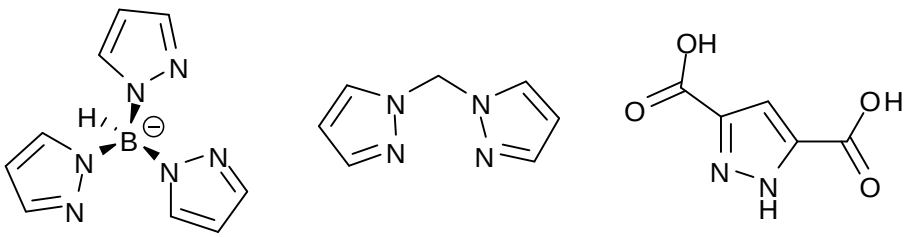

Figure 1.20: Some examples of common pyrazole-based ligands. From left to right: A trispyrazolylborate; 1,1′-methylenebispyrazole; pyrazole-3,5-dicarboxylic acid.

Inevitably, pyrazole-based ligands have appeared in the metallosupramolecular chemistry literature in the last 20 years, with ditopic pyrazole ligands such as 4-(4-pyridyl)-*1H*-pyrazole,[227, 228] 4,4′-*p*-phenylenebispyrazole[229] and 3,3′,5,5′-tetramethyl-4,4′-bipyrazole (Figure 1.21),[230-237] having been employed in coordination polymer synthesis in recent years. However, despite the wealth of experience in pyrazole synthesis derived from over a century of medicinal and coordination chemistry applications, pyrazoles remain a comparatively infrequently used functional group in metallosupramolecular and coordination polymer chemistry, lagging behind structural isomer imidazole, and other heterocyclic compounds such as pyrazine and pyrimidine in the number of publications in the supramolecular literature.[238] In particular, the combination of pyrazole with other functional groups within coordination frameworks is an area requiring further study, given the potential for the interplay of forces between π-electron rich, hydrogen bond donating pyrazole ligands contrasted with electron poor hydrogen bond acceptors such as aromatic carboxylic acids or six-membered heterocycles.

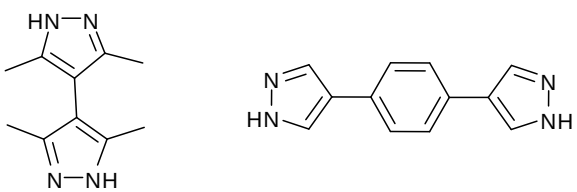

Figure 1.21: Examples of pyrazole ligands used in the MOF literature, 3,3',5,5'-tetramethyl-4,4'-bipyrazole (left) and 4,4'-p-phenylenebispyrazole (right).

1.6.4 Properties of Indazoles

The coordination chemistry of 1,2-diazoles need not be limited to pyrazole itself; indeed, a number of related compounds present similar potential as ligands in the preparation of supramolecular assemblies. Indazole, or benzo[d]pyrazole, is the fused ring derivative of pyrazole in which a benzene ring is fused to the C(4) and C(5) carbons of pyrazole.[197] Similar to pyrazoles, indazoles are most widely known for their pharmaceutical properties, and are employed in a range of medicinal applications, such as 7-nitroindazole (7-NI),[239] used as a nitric oxide synthase inhibitor, and Benzydamine,[240] an anti-inflammatory agent. Some examples of common indazoles are shown in Figure 1.22 below.

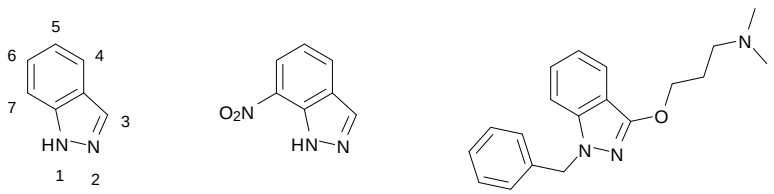

Figure 1.22: Examples of common indazole compounds. From left to right: 1H-indazole with numbering scheme; 7-nitroindazole; Benzydamine

The reactivity of indazole is similar to its parent compound pyrazole, and structural isomer benzimidazole. One notable exception is the annular tautomerism of indazole; for all indazoles the *1H*- and *2H*- arrangements are non-equivalent due to the lower symmetry imposed by the position of the ring junction.[241, 242] As such, derivitisation of the ring nitrogens produces a mixture of 1- and 2-substitution.[243] The six membered ring of indazole is electron rich, and electrophilic aromatic substitution occurs mainly at the 5- position.[197] Synthetically, indazole can be prepared by a number of methods, most of which involve ring closing of the five-membered ring.[244] Phenylhydrazines with carbonyl functional groups in the *ortho* position can be converted to indazoles, and *ortho*-halobenzophenone derivatives can give indazoles by reaction with hydrazine to the intermediate hydrazone followed by ring closure by nucleophilic aromatic substitution. The Jacobson method for indazole synthesis involves nitrosylation of an acetylated *ortho*-alkylaniline followed by thermally initiated C-N bond formation.[245]

The indazole ring system, when suitably functionalised, would be expected to display many unique properties as a ligand in metallosupramolecular chemistry. The unique geometry of the benzodiazole ring system allows access to linker geometries not readily available from the standard 60, 120 and 180° linkers common to six-membered rings. The amenability of the synthetic methods described above to a range of functionalisation opportunities on the phenyl backbone allows a

systematic study of substitution pattern and the effect on the resulting metallosupramolecular architecture following coordination to a suitable metal ion. The diazole moiety of indazole would be expected to display similar electronic characteristics to pyrazole, albeit with some difference in pKa values (pKa 1.3 and 13.9 for neutral compound and conjugate acid, respectively)[197], leading to similar coordination characteristics, while likely remaining protonated under mild conditions to participate in hydrogen bonding interactions. Despite the enormous potential of functionalised indazoles in coordination chemistry, to date there have been no structurally characterised examples of indazole-based ligands acting as linkers in coordination polymers.

1.7 Present Study

The present study aims to exploit the synthetic versatility of the 1,2-diazole family of heterocyclic compounds to generate a range of new ligand species, in order to broaden the knowledge of their metallosupramolecular chemistry. Focus is given to the solid-state structural chemistry of coordination oligomers and polymers formed with first-row transition metals, ascertained primarily from single crystal X-ray crystallograpic data, with the goal of building a library of structures from which to draw conclusions regarding reproducible structural motifs which could be used in the rational design of metallosupramolecular assemblies containing diazole functionality for specific applications. The key feature unique to 1,2-diazole ligands, namely the behaviour of the second nitrogen atom directly adjacent to the donor atom, will form an important aspect of these discussions; either as a source of potentially structure-directing hydrogen bonding in the immediate vicinity of the metal site, or to provide a scaffold for further substitution, giving access to ligand geometries not easily available with other ligand systems.

Chapter 2 details the preparation of a family of coordination polymers of Co(II) in which bis-pyrazole and bis-carboxylate ligands are combined to form a hydrogen bonded ‘secondary building unit’ around the coordination sphere. The influence of flexibility and spacer length on the network topologies are investigated by altering the ligand backbones while maintaining a relatively rigid geometry at the network nodes.

In Chapter 3, two related bis-pyrazole ligands are functionalised by the addition of pyridine groups to the pyrazole 1-positions, giving flexible bis-bidentate ligands which are used to generate several discrete metallosupramolecular architectures, including dinuclear double and triple helicates, as well as a number of coordination polymers. This work is extended in Chapter 4 to include

benzimidazole-substituted pyrazoles, where the ready functionalisation of the benzimidazole ring allows the covalent linking of two pyrazolyl-benzimidazole binding sites in several different ways, giving rise to both discrete and polymeric metallosupramolecular assemblies.

Chapter 5 describes the preparation of indazole-based ligands, where in the first instance pyridine substitution is carried out on indazole itself to test the viability of pyridyl-indazole ligands akin to the pyridyl-pyrazole systems employed in Chapter 3. Attention is then turned to the 5 possible isomers of indazole-carboxylic acid and the synthesis of the first reported indazole-based coordination polymers, including the description of a robust framework capable of carbon dioxide sorption.

Finally, Chapter 6 deals with the synthesis of pyrazole-carboxylate and heteroaryl-pyrazole-carboxylate ligands in order to draw comparisons with results presented in the previous chapters, and extend these systems to explore the coordination potential of 3,5-heterosubstituted pyrazoles containing carboxylate functionalities.

Chapter 7 presents a brief summary of these results, and provides a discussion of future work in these areas.

1.7.1 Methods of Compound Preparation and Data Collection

The following report documents the preparation of a large number of new heterocyclic ligands and their resulting complexes with a range of transition metals. Often, the synthetic procedures used to prepare the ligand species have been adapted from preparations for similar compounds from the organic and medicinal chemistry literature. All organic precursors and ligand molecules have been fully characterised using nuclear magnetic resonance (NMR), electrospray mass spectrometry (ESMS), infrared spectroscopy (IR) and melting point (MP) analyses, as well as single crystal X-ray diffraction where possible.

The metal complexes, both discrete and polymeric, have been prepared using several different techniques. The necessity for X-ray crystallographic analysis to provide full structural information has driven the choice of these synthetic techniques with an emphasis towards the preparation of single crystals in the first instance. Solvothermal techniques are relied upon for the synthesis of most of the coordination polymers discussed, where the reactants are combined in a sealed vessel capable of being heated to generate a high pressure environment, allowing higher temperatures to be reached which promote the self-assembly process by providing more energy to the reactants than is possible at atmospheric pressure. The elevated temperatures also assist in solubility, especially for organic materials containing multiple hydrogen bond donors and acceptors such as *1H*-pyrazole compounds. The remainder of the coordination compounds described in this study were generally prepared by

gentle heating under atmospheric pressure, and utilised standard benchtop evaporation or solvent diffusion crystallisation techniques as discussed in the text.

All metal complexes prepared were initially characterised by single crystal X-ray crystallography, and the structures were analysed to determine the optimum methods of further characterisation. Pertanent to this point, it should be noted that "R-factors" quoted in the text as indications of refinement quality represent the parameter $R_{1(I>2\sigma)}$, as is conventional. In addition, all metal complexes were characterised by infrared spectroscopy and elemental analysis, and, aside from where thermally unstable perchlorate species were present, thermogravimetric analysis was also carried out. It must be noted that by nature, the exact levels of solvation associated with void-containing materials can be difficult to quantify; in all cases, a combination of single crystal X-ray diffraction, elemental analysis and thermogravimetric analysis was used in an attempt to estimate the solvent content of both freshly isolated and air-dried batches of such samples. In some instances, only where the solvent contribution to the crystallographic model was so diffuse as to be impossible to sensibly model, and where such modeling contributed little to the understanding of the compound, the SQUEEZE routine[246] within PLATON was applied to suppress the contribution of the disordered solvent electron density to the framework atoms; in these instances, the calculated electron density was combined with physical measurements to estimate the solvent content. Where appropriate, mass spectrometry, NMR and UV/Visible spectroscopy were also carried out, in an attempt to correlate the solution-phase behaviour with that observed in the solid state.

It should be noted that complete lists of bonding parameters and crystallographic refinement details are not explicity reported within the body of the text; tables of crystallographic refinement information, hydrogen bonding parameters and coordination bond details are presented in Appendices 1-3, tables A1-A29, while all crystallographic data is included as electronic supplementary information in .cif format on the accompanying CD-ROM.

Chapter 2

Pyrazole-Carboxylate Mixed Ligand Systems

2.1 Introduction

Network prediction in the engineering of coordination polymers has been a goal of supramolecular scientists for many years.[105, 247] While some early systems achieved a level of predictability in their topology and structure by utilising simple and well-known building blocks, many coordination polymers reported to date show tendencies towards unexpected topologies and interpenetration modes. Although the goals are fundamentally different, the challenges faced by coordination polymer chemists can be compared to the challenge of predicting X-ray crystal structures for small molecules;[248] while often the geometry of the molecule or fragment in question can be predicted computationally with a fair degree of accuracy, subtle effects such as minor changes in torsion angles or energetically similar modes of intermolecular interaction can have drastic effects on the crystal packing. Recently, several groups have reported success in computational methods to predict possible structures and polymorphs of inorganic and hybrid polymers; however, in general these methods are most effective with well-understood systems, and can involve exhaustive searches of many candidates before arriving at a small number of energy minimised structures.[249, 250]

One approach to address the degree of complexity is to reduce known structural motifs into 'Secondary Building Units' or SBUs. This method is often employed in zeolite chemistry, where a structure is broken down into multi-atom subunits in order to describe its connectivity, and also to allow rational design of new systems.[251] This approach can be compared to the 'node-and-spacer' concept in coordination polymer chemistry.[252] The SBU approach is also a useful tool in coordination polymer synthesis, where clusters or polyhedra known to form under certain conditions are incorporated into new structures.[253] Secondary building units as a basis for the design of porous coordination networks have become increasingly popular, the most obvious example being the $[Zn_4O(RCOO)_6]$ cluster used by Yaghi and colleagues to prepare a series of isoreticular frameworks of varying edge length.[110] In fact, metal-carboxylate clusters are by far the most commonly employed approaches to SBU-based coordination polymer synthesis, with building units like those shown in Figure 2.1 among the most prevalent.

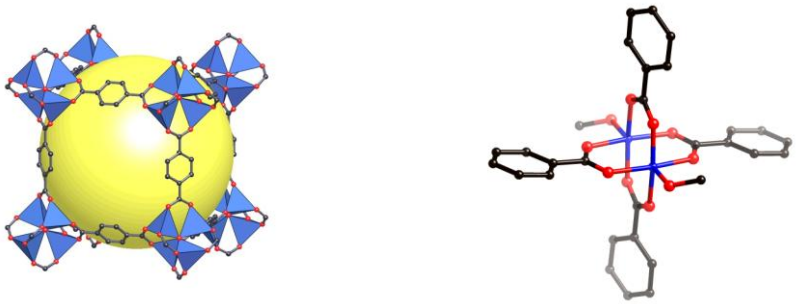

Figure 2.1: (Left) Structure of MOF-5, where zinc atoms within $[Zn_4O(COO)_6]$ vertices are represented as blue tetrahedra; (Right) Generic example of the Cu(II) paddlewheel motif, shown for an aromatic acid with methanol as the axial ligand.

In order to continue to advance the science of structure prediction in inorganic and hybrid solids, more work is needed to identify reproducible secondary building units based on other chemical functionalities. Recently, Mondal and co-workers proposed a pyrazole-carboxylate mixed-ligand coordination motif as a non-cluster secondary building unit for coordination polymers.[254, 255] As shown in Figure 2.2, the basis of this approach is the coordination around a tetrahedral metal ion, in this case Zn(II), of two (3,5-dimethyl-*1H*-pyrazole)-containing moieties and two carboxylate groups, which results in two N-H···O hydrogen bonds forming seven-membered rings around the periphery of the coordination sphere. For the purposes of this study, this subunit will be referred to as $[M(HPz)_2(COO)_2]$, where HPz = any *1H*-3,5-dimethylpyrazole moiety.

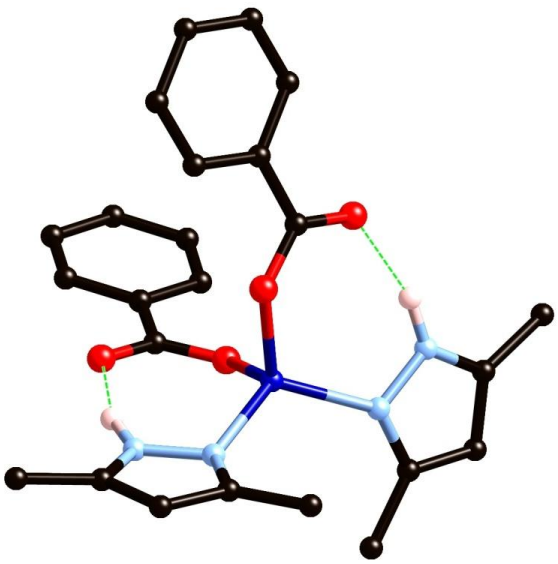

Figure 2.2: Schematic representation of the $[M(HPz)_2(COO)_2]$ secondary building unit showing hydrogen bonding. Here the acid is shown as an aromatic carboxylic acid, though an equivalent structure is known to form with alkyl acids.[254]

Mondal has shown this building unit to be reasonably reproducible under hydrothermal conditions with a range of dicarboxylic acids, forming a series of primarily 1- and 2-dimensional coordination polymers. The pyrazole moiety used in these studies, 4,4′-methylenebis-(3,5-dimethyl-*1H*-pyrazole) **L2.1** (Scheme 2.1), comprises two 3,5-dimethylpyrazole units linked by a methylene spacer through the 4 position, which lends a degree of flexibility to the overall structure. The methyl groups attached to the pyrazole rings at the 3- and 5- positions impose steric hindrance on the coordination sphere, likely enforcing some restriction on the coordination number of the metal, especially in complexes of first row transition metals. In the structures reported by Mondal, however, there are instances of only partial formation of the building unit, where for example a mismatch exists in the number of carboxylate groups present compared to the number of pyrazole groups, resulting in a non-coordinating carboxylic acid group disrupting the local hydrogen bonding. In these cases, although the coordination sphere of the metal was relatively unchanged, where only one or zero hydrogen bonding interactions exist around the periphery of the metal, the added rigidity of the SBU is lost. Where the carboxylic acids are fully rigid, shape and size considerations must be taken into account to ensure a tetrahedral coordination geometry does not inhibit the hydrogen bonding system, as was the case with Mondal's isophthalic acid complex, where the rigid 120° angle between the carboxylate groups prevented both ends from engaging in hydrogen bonding simultaneously. At the other end of the scale, highly flexible alkyl chains containing terminal carboxylic acids, of the formula HOOC-$(CH_2)_n$-COOH, where n = 2-7, reproducibly form the SBU at the metal site with both hydrogen bonding interactions intact; however, the high flexibility of these ligands leads in all but one case to networks of only 1 or 2 dimensions, the exception being the triply-interpenetrated diamondoid network formed with adipic acid (n = 4). From these observations, a number of key points can be extracted for the general use of the $[M(HPz)_2(COO)_2]$ secondary building unit:

- Consistency in the stoichiometry of the functional groups; for example, pendant hydrogen bonding groups are likely to disrupt the SBU formation;
- Rigid linkers should be of commensurate geometry to adopt tetrahedral coordination at each binding site;
- The degree of total flexibility in the overall system should be controlled if robust high dimensionality networks are the desired result.

Previous work in our group showed cobalt(II) behaved in the same way as the zinc salts used by Mondal, with the formation of the **L2.1**/terephthalic acid diamondoid network isostructural to the zinc analogue.[256] In order to further probe the utility of this building unit, studies into the usefulness of

semi-rigid ligands, of shapes complementary to the original **L2.1**, are required. It should be noted that during the course of this study, a compound isostructural to complex **2.20** was reported in the literature by Mondal *et al.*[257]

2.2 Ligand Synthesis

As outlined in section 1.6, the synthesis of 3,5-disubstituted pyrazole compounds can be achieved by utilising a number of synthetic strategies; however, the most common is the action of hydrazine (or a suitably substituted hydrazine-containing compound for 1-substituted pyrazoles) on a β-diketone. For the simplest 3,5-disubstituted pyrazole, 3,5-dimethyl-*1H*-pyrazole, the cyclocondensation reaction of hydrazine with acetylacetone produces the product in quantitative yield. This approach to the synthesis of the pyrazoles themselves was employed for all ligands discussed in this chapter.

*2.2.1 Synthesis of bis-pyrazole ligands **L2.1, L2.2** and **L2.3***

For ligand 4,4′-(methylenebis)-3,5-dimethyl-1H-pyrazole **L2.1** the synthetic route (shown in Scheme 2.1) employed was that of Wilson *et al.*,[258] in which acetylacetone is subjected to a Knöevenagel condensation with formaldehyde to give the crude tetraketone product **2.8** as a viscous yellow oil after stirring at room temperature for seven days. As was the case with many of the α-alkyl-β-diketones employed in this study, the product exists as a mixture of keto- and enol tautomers, in this case giving a mixture of three possible tautomers. This tautomerism caused difficulty with purification for these materials, and as such the general approach was to employ the crude material for the cyclisation step and purify the pyrazole product as required. Cyclocondensation to form **L2.1** with hydrazine hydrate in ethanol then proceeded in good yield. Following this procedure, ligand **L2.1** was prepared from acetylacetone in 2 steps with an overall yield of 57%.

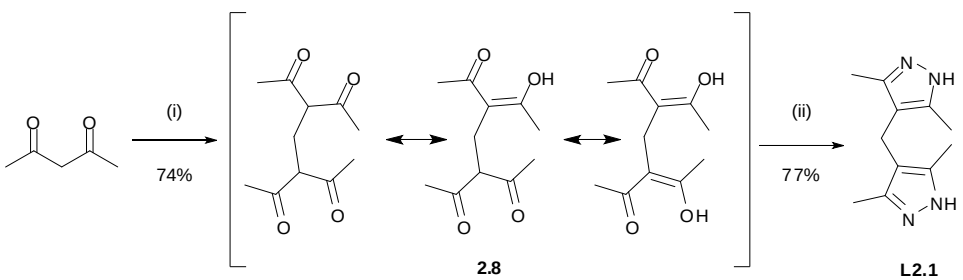

*Scheme 2.1: Synthesis of **L2.1**. Reagents and conditions: (i) CH_2O, RT, 7 days;[258] (ii) $H_2NNH_2{\cdot}H_2O$, EtOH, reflux 6 hr.*

Ligand **L2.1** possesses a flexible methylene linker between the two rigid aromatic rings, and the effect of this spacer was investigated by preparing two other bis-pyrazole ligands in which the degree of flexibility was altered. Ligand α,α′-*p*-xylylenebis-(3,5-dimethyl-*1H*-pyrazol-4-yl) **L2.2** was envisioned as a closely related compound which included still further flexibility by inclusion of a second methylene site between the pyrazole rings, and also included a phenyl spacer to increase the distance between the metal coordination sites. Here, the synthetic route shown in Scheme 2.2 was adapted from that reported by Marquet *et al.*, who employed a radical reaction between anhydrous cobalt(II) acetylacetonate and an alkyl bromide in a melt at 120 °C, to give the corresponding α-alkyl-β-diketone.[259] In this instance, use of α,α′-dibromo-*p*-xylene gave the bis-diketone, which underwent reaction with hydrazine hydrate to give ligand **L2.2** in 28% overall yield. Again, the tautomerism of the bis-diketone made purification difficult, and, as such, the most convenient method of preparing **L2.2** was employing the crude mixture containing the bis-diketone, followed by purification as necessary for the pyrazole product.

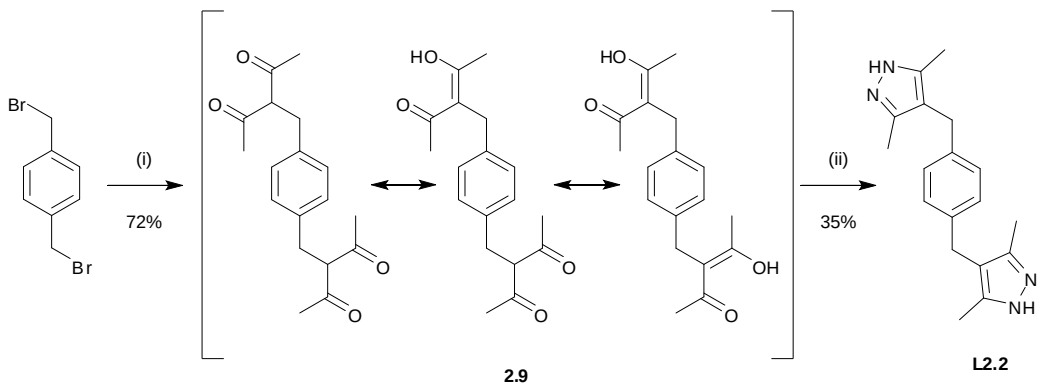

*Scheme 2.2: Synthesis of ligand **L2.2**. Reagents and conditions: (i) $Co(acac)_2$, $CHCl_3$, 120 °C (melt), 30 mins; (ii) $H_2NNH_2 \cdot H_2O$, EtOH, reflux 6 hr.*

The final bis-pyrazole employed in this study, 3,3′,5,5′-tetramethyl-4,4′-bis-*1H*-pyrazole **L2.3**, was prepared as a rigid analogue to **L2.1**, where two 3,5-dimethyl-1H-pyrazole units are directly linked through the 4- position. This compound has been prepared by a number of methods in the literature, typically through the action of I_2 on a slurry of sodium acetylacetonate in dry ether or some modification therein.[260] This method was adopted in order to generate the bulk of the tetraketone **2.10** required, due to its applicability to larger scale preparations (~1g product), despite the low yield. The method of Romero *et al.* was also attempted, in which the tetraketone is prepared by oxidative dimerisation of acetylacetone with ceric ammonium nitrate in methanol at -20 °C, as shown in

Scheme 2.3.[261] Although the yields obtained with this method were similar to those obtained by the previous procedure, the difficulty in scaling the reaction precluded the large scale synthesis of **2.10** by this method. In contrast to tetraketones **2.8** and **2.9**, **2.10** existed primarily as a single tautomer, allowing for simple purification and isolation.

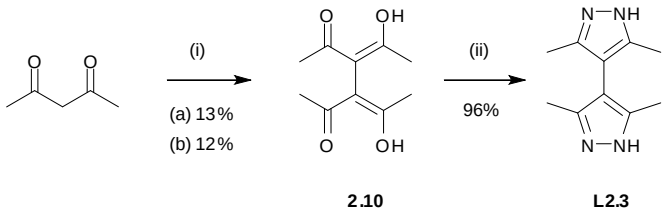

*Scheme 2.3: Synthesis of **L2.3**. Reagents and conditions: (i) (a) CAN, MeOH, -20 °C, 20min,[261] or (b) NaH, I_2, Et_2O, reflux 10 hr;[260] (ii) $H_2NNH_2{\cdot}H_2O$, EtOH, reflux 6 hr.*

*2.2.2 Synthesis of carboxylic acids **H_2L2.4** and **H_2L2.5***

In conjunction with ligands **L2.1-2.3**, dicarboxylic acids **H_2L2.4** and **H_2L2.5** were prepared to act as co-ligands. In both cases, as well as with **HL2.6** and **HL2.7** discussed below, a protected form of the carboxylic acid group is used in all but the last step to avoid unwanted reactivity and to subvert the solubility issues which are typically pervasive in the chemistry of aromatic carboxylic acids. 4,4′-oxybis(benzoic acid) **H_2L2.4** was prepared in two steps in a method similar to that reported by Tesauro *et al*.[262] A mixture of *p*-cyanophenol, *p*-nitrobenzonitrile and anhydrous potassium carbonate was heated in dry DMF to give 4,4′-oxybis(benzonitrile) **2.11**, from which **H_2L2.4** was available in good yield *via* hydrolysis, as outlined in Scheme 2.4.

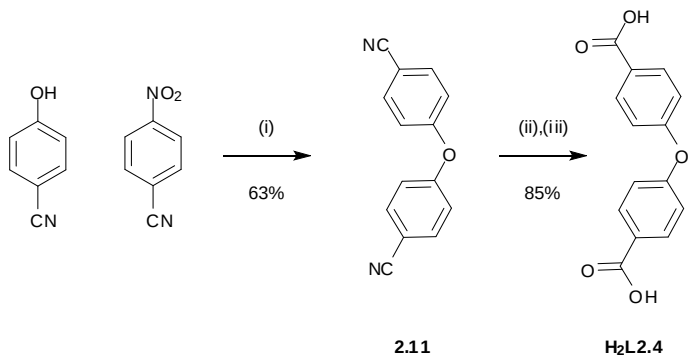

*Scheme 2.4: Synthesis of **H_2L2.4**. Reagents and conditions: (i) K_2CO_3, DMF, Ar, 120 °C, 7 hr, RT 72 hr; (ii) LiOH, THF/H_2O, reflux 48 hr; (iii) HCl/H_2O, RT.*

2,8-dicarboxy-6H,12H-5,11-methanodibenzo[b,f][1,5]diazocine **H_2L2.5** was prepared by the reaction of ethyl-*p*-aminobenzoate with paraformaldehyde in neat trifluoroacetic acid (TFA), following the standard method reported by Sergeyev *et al.* for the synthesis of electron deficient 2,8-disubstituted Tröger's base analogues.[263] This was followed by alkaline hydrolysis in THF/water, as outlined in Scheme 2.5. Neutralisation with dilute hydrochloric acid gave the product **H_2L2.5** as a white powder, in a yield of 53% over two steps.

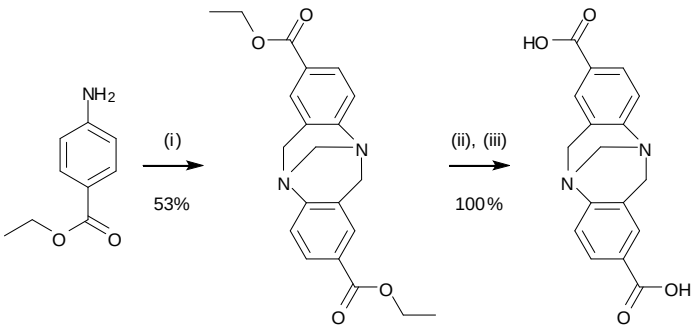

*Scheme 2.5: Synthesis of **H_2L2.5**. Reagents and Conditions: (i) CH_2O, TFA, 48 hrs, RT;[263] (ii)) LiOH, THF/H_2O, reflux 48 hr; (iii) HCl/H_2O*

The acid **H_2L2.5**, having not been reported in the literature in its neutral form, was crystallised solvothermally from acetonitrile to generate single crystals suitable for X-ray diffraction in order to gauge the relevant physical dimensions. The data obtained were solved and the structure model refined in the tetragonal space group $I4_1cd$ (R-factor 4.16%). Unexpectedly, the asymmetric unit of **H_2L2.5**·MeCN contained two halves of unique molecules of **H_2L2.5**, and one molecule of acetonitrile. Crystallographic symmetry operators lead to the existence of two geometrically unique molecules of **H_2L2.5** within the unit cell, each existing as both enantiomeric forms, with a total of 16 molecules of **H_2L2.5** within the unit cell. One such molecule is shown in Figure 2.3. As shown, **H_2L2.5** contains a 'cleft' resulting from the fusion of two unsaturated 6-membered rings, with some rigidity brought about by the high barrier to inversion of the tertiary amines, imposing an interplanar angle of between 80 and 90° on the two phenyl rings in this case. This barrier is the source of chirality in all methylene-bridged Tröger's Base analogues – however, while certain examples have been resolved chromatographically, the presence of weak acids causes protonation of one tertiary amine, leading to racemisation *via* the achiral iminium ion formed by ring opening.[264-266] As such, no attempt was made to resolve **H_2L2.5**, as any zwitterionic character in the carboxylic acid form would lead to rapid racemisation.

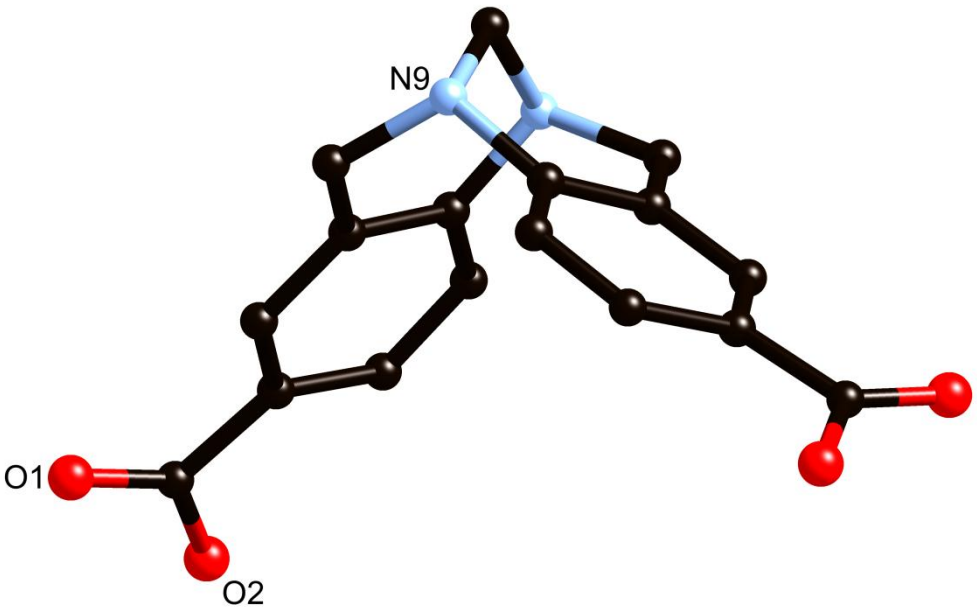

Figure 2.3: Representative structure of ***H_2L2.5*** *with unique heteroatom labelling. Unit A is shown, containing atoms O(1)-C(12) and their symmetry equivalents. Hydrogen atoms, acetonitrile molecule and non-equivalent units of* ***H_2L2.5*** *omitted for clarity.*

Geometrically, the non-equivalent units of **H_2L2.5** are largely identical, but do show several minor differences. The most notable structural differences lie in the cleft and torsion angles of the two units. Unit A, containing atoms O(1)-C(12) and their symmetry equivalents, shows a cleft angle (calculated by the angular offset of the phenyl ring mean planes) of 87.62(10)° and a phenyl-carboxylate torsion angle of 18.4(3)°, while Unit B (O(13)-C(24)) displays a cleft angle of 81.55(10)° and phenyl-carboxylate torsion angle of 14.6(3)°. These differences, while minor in themselves, may play significant roles in determining the three-dimensional structure, as described below.

In the extended structure of **H_2L2.5**·MeCN, each unit of **H_2L2.5** behaves in the same way with respect to intermolecular interactions. The primary interactions observed are hydrogen bonding between carboxylic acids and amines, as shown in Figure 2.4. Crystallographically, the positions of the protons in question could not be unambiguously determined through electron density considerations, and as such were modelled as fully bonded to the oxygen atoms; however, in reality it is expected that these protons will likely be shared with the amine nitrogens. Topologically, the hydrogen bonding arrangement of each molecule allows the assignment of a 4-connected node to each molecule, which connects to two others *via* hydrogen bond donors and two others *via* hydrogen bond acceptors. A logical place to envisage this node is the bridgehead methylene carbon. Adopting this approach it becomes obvious that units A and B (as defined above) and their enantiomers only engage

in hydrogen bonding to identical molecules. As such, there must exist four networks in the structure of **H_2L2.5**·MeCN; networks containing only A, A', B and B', where A' is the enantiomer of A. Perhaps even more interesting is the observation that although the hydrogen bonding parameters for A-A and B-B interactions differ (d(D-A) = 2.729(2) for O(1)-H(1)···N(10), *vs.* 2.798(3) for O(13)-H(13)···N(22)) the inter-nodal distances for all four networks are identical within error. Presumably the differences in cleft angle and phenyl-carboxylate torsion compensate for the differences in hydrogen bonding leading to equality of the overall network dimensions and the resulting high degree of symmetry. When an individual molecule is isolated and its hydrogen bonding network is expanded into 3 dimensions, the quintessential (6,4) diamondoid (**dia**) network is the result, with edge length 10.1970(2) Å. However, inclusion of all 4 **H_2L2.5** units gives rise to a quadruply interpenetrating network, with each single network having very similar geometrical properties. The overall structure is represented in Figure 2.4 below.

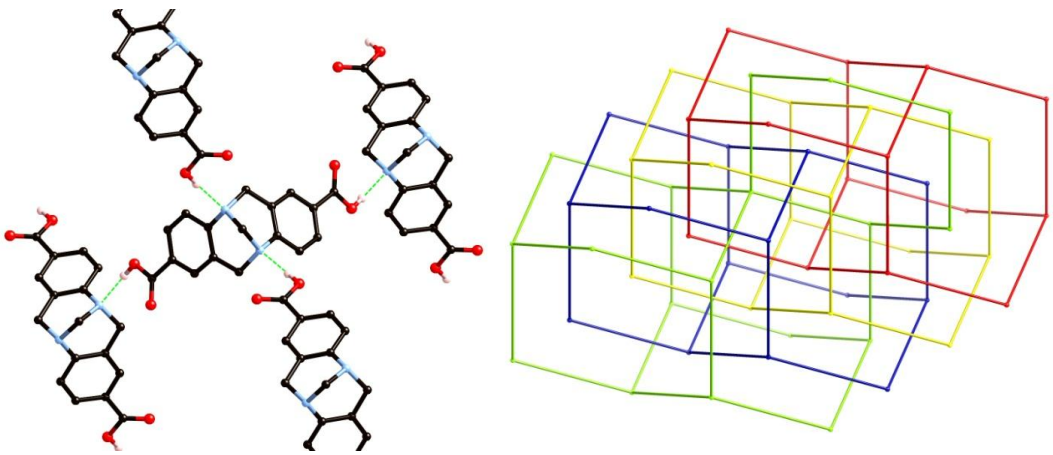

*Figure 2.4: (left) Hydrogen bonding motif in **H_2L2.5**·MeCN, uninvolved hydrogen atoms omitted for clarity; (Right) Interpenetration of four non-equivalent but geometrically identical **H_2L2.5** networks.*

Although the acetonitrile guest molecules do not participate in the hydrogen bonding interactions, their presence in the structure of **H_2L2.5**·MeCN is clear when the structure is viewed along the *c* unit cell axis, as shown in Figure 2.5; the guest molecules are aligned in a one-dimensional channel structure. Perhaps unsurprisingly, the loosely bound nature of the acetonitrile molecules, as well as ready accessibility to the surface *via* these channels, results in rapid loss of guest molecules on drying in air, with accompanying loss of single crystallinity. Indeed, on standing in air the crystals were found to have been reduced to the formula **H_2L2.5**·0.8MeCN by thermogravimetric and microanalyses, with loss of single crystallinity caused by or accompanying the loss of *ca.* 20% of the included guest molecules.

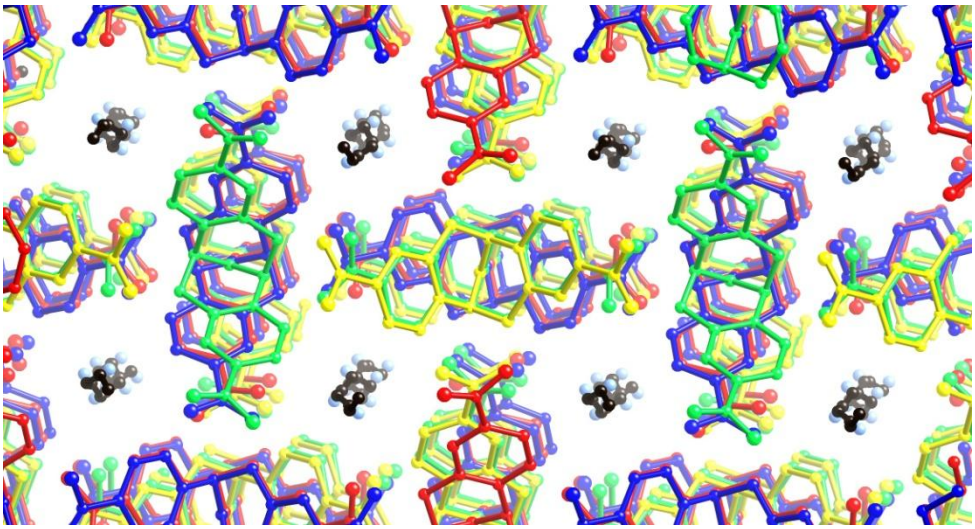

*Figure 2.5: Channel structure of **H_2L2.5**·MeCN viewed along the unique axis. Unique **H_2L2.5** molecules coloured separately. Colour key: Yellow: Unit A; Green: Unit B; Blue: Unit A'; Red: Unit B'. Acetonitrile molecules coloured by element. Hydrogen atoms omitted for clarity.*

Although not a direct influence on the topology of **H_2L2.5**·MeCN, intermolecular π-π interactions are present in the structure, and provide a key insight into the interactions expected to influence the intermolecular behaviour of **H_2L2.5** in the absence of self-complimentary hydrogen bonding. As hinted above in Figure 2.5, the units of **H_2L2.5** can be seen to be arranged in a columnar-type fashion, where all four units take part in 1-dimensional π-π stacking along the unique axis, in the order A-B-A'-B'-A. The nature of these interactions is displayed in Figure 2.6. The utility of these interactions in the preparation of other networks is dubious, however, as the interplanar and point-to-point distances of any two π-systems involved are at least 4.0 Å, indicating that if any attractive interaction is present, it is likely of less utility than simply the complementary shape of the molecules. More likely as an attractive force in this case is the C-H···π interactions of the methylene bridgehead hydrogen atoms with the phenyl ring located above, where the shortest carbon - mean plane distance of 3.700(2)Å, corresponding with a C-H···(centroid) angle of 162.42(12)°, indicate an interaction of moderate strength.[47]

In terms of the utility of **H_2L2.5** in coordination chemistry, it was expected that the carboxylate sites would coordinate preferentially over the tertiary amines. In this instance, **H_2L2.5** can be simplified to a 90 degree linker, where the distance from each binding site to the vertex is approximately 7 Å, and a linear distance between coordination sites of approximately 10 Å. Although the backbone of **H_2L2.5** contains no rotatable bonds, the saturated bridgehead region is expected to

allow a slight tweezer-type motion; indeed, literature examples of Tröger's base analogues show the cleft angle can vary by up to 30° in the solid state depending on substituents.[267]

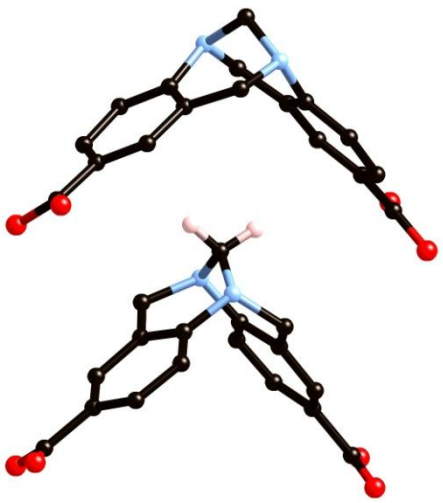

Figure 2.6: Possible π-π and/or C-H---π interactions between representative units of ***H_2L2.5,*** *in this case A and B'. Uninvolved hydrogen atoms omitted for clarity.*

2.2.3 Synthesis of 4-(carboxyphenyl)-3,5-dimethyl-1H-pyrazole ***HL2.6***

Ligand 4-(carboxyphenyl)-3,5-dimethyl-*1H*-pyrazole **HL2.6** was devised as a rigid, single molecule pyrazole-carboxylate ligand in order to generate similar systems to those previously observed, without the need for co-ligands. Synthetically, a number of routes to **HL2.6** could be envisaged, all centred on the formation of the carbon-carbon bond from the 4-position of the pyrazole to the *para* position of the benzoic acid moiety. In this instance, the key step of the synthesis is the cuprous iodide/L-proline catalysed reaction of acetylacetone with an aryl iodide, as suggested by Jiang *et al*.[268] Specifically, ethyl *p*-aminobenzoate was subjected to a diazotisation reaction and reacted *in situ* with potassium iodide to give ethyl *p*-iodobenzoate **2.13**, which was reacted with acetylacetone with copper catalysis to give the diketone **2.14** in 44% yield. From there, hydrazine condensation followed by hydrolysis gave the product, **HL2.6** in 21% yield over 4 steps, as outlined in Scheme 2.6.

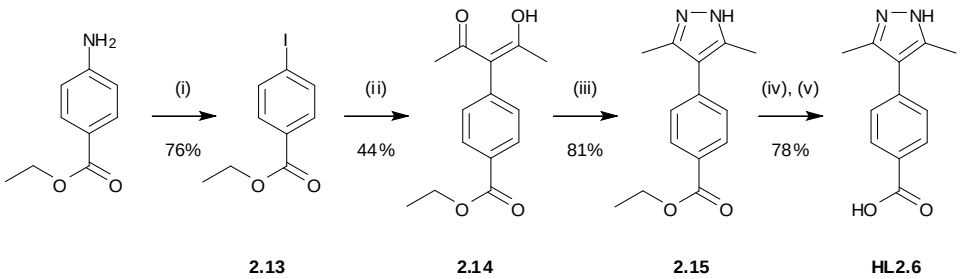

*Scheme 2.6: Synthesis of **HL2.6**. Reagents and conditions: (i) TsOH, $NaNO_2$, KI, MeCN/H_2O, 3 hr, RT;[269] (ii) acetylacetone, CuI, L-proline, K_2CO_3, N_2, DMSO, 90 °C, 8 hr;[268] (iii) $H_2NNH_2{\cdot}H_2O$, EtOH, reflux 24 hr; (iv) LiOH, THF/H_2O, reflux 48 hr; (v) HCl/H_2O, RT.*

Pleasingly, the diketone precursor to **HL2.6**, 3-(ethyl *p*-carboxyphenyl)-pentane-2,4-dione **2.13** was found to exist entirely in the enol form in solution, and as such purification by flash chromatography was greatly simplified compared to the other diketones discussed in this chapter. A sample of **2.13** was crystallised from the eluent (DCM/hexanes) and subjected to single crystal X-ray diffraction, and the data obtained were solved and the structure model refined in the monoclinic space group $P2_1/c$ (R-factor 3.49%). The structure model thus obtained shows the expected structure of compound **2.13** as shown in Figure 2.7, confirming the enol configuration of the diketone as observed in solution. This determination was made on the basis of the sp^2 geometry at the α-position of the diketone, and the position of the proton located exactly mid-way between O(14) and O(17) was determined manually from the residual electron density. No evidence of the other tautomer was found.

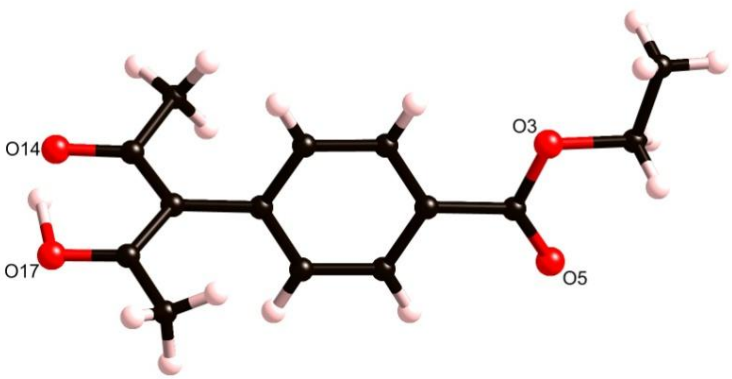

*Figure 2.7: X-ray structure of compound **2.13** showing heteroatom labelling scheme. The diketone proton is shown arbitrarily bonded to O(17).*

Of particular interest is the torsion angle between the planar phenyl and diketo moieties of 72.94(16) ° indicating a high degree of steric repulsion between the methyl groups of the diketone and the phenyl ring. This torsion results in disruption of the intermolecular interactions expected in a solid-state structure of this type, where the majority of the phenyl ring is unable to take part in any π-π stacking interactions due to the steric impedance orthogonal to the plane. However, the conjugated diketone groups from adjacent molecules are positioned parallel, with 3.3497(15) Å between adjacent diketone mean planes, as are the adjacent carbonyl groups, with 3.5353(12) Å separation, as shown in Figure 2.7. No other significant intermolecular interactions are observed in the solid-state structure of **2.13**, nor were any solvent or guest molecules located within the lattice.

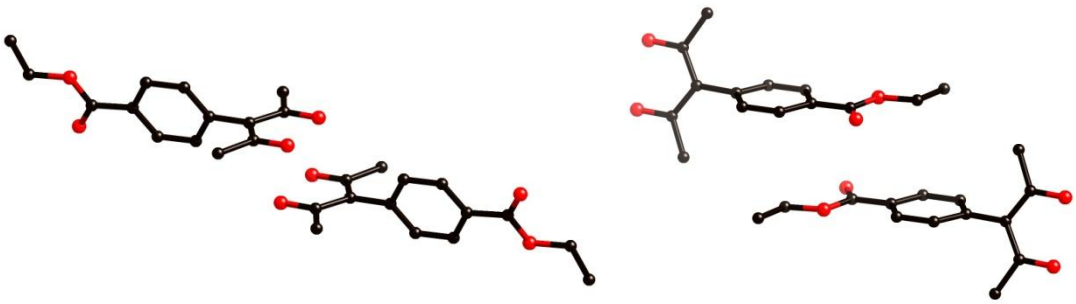

*Figure 2.7: Modes of intermolecular interaction in the structure of **2.13**, hydrogen atoms omitted for clarity.*

To determine the physical dimensions of **HL2.6**, and to compare with the intermolecular interactions observed in **2.13**, ligand **HL2.6** was crystallised solvothermally as the nitrate salt **HL2.6**·HNO_3, by heating a sample of the powdered material in water with trace nitric acid under solvothermal conditions, followed by slow cooling. The pale yellow crystals produced were subjected to single crystal X-ray diffraction, and the diffraction data were solved and the structure model refined in the triclinic space group *P*-1 (R-factor 4.41%). The asymmetric unit of **HL2.6**·HNO_3 shows one molecule of the ligand protonated on the pyrazole nitrogen, and one nitrate anion, as shown in Figure 2.8. Immediately obvious is the reduction in torsion angle between the two rings, at only 36.6(4)°, approximately half that seen for monocyclic precursor compound **2.13**. The difference in torsion is expected to be largely due to the formation of the nitrogen-nitrogen bond which directs the methyl groups further from the *ortho* hydrogen atoms on the phenyl ring, allowing a reduction in torsion angle. Furthermore, the transition from a conjugated acyclic π-system present in **2.13** to an aromatic system in **HL2.6** is likely to increase the drive to achieve conjugation between the two systems, possibly contributing towards overcoming the energetic barrier to rotation from the orthogonal form seen in **2.13**.

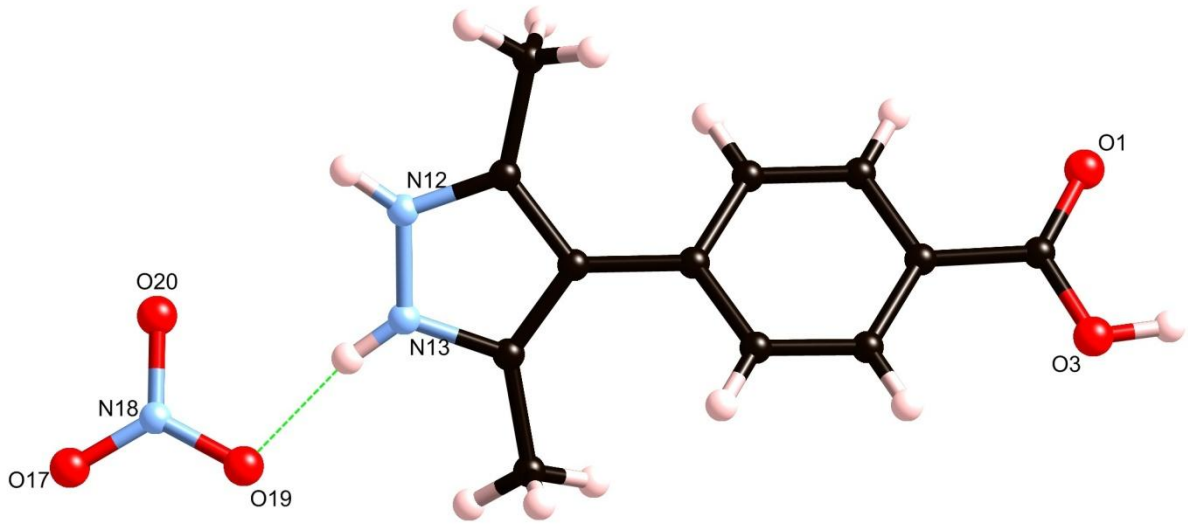

*Figure 2.8: Structure of **HL2.6**·HNO_3 with heteroatom numbering scheme.*

Hydrogen bonding interactions permeate the structure of **HL2.6**·HNO_3, and occur in two distinct groups of self recognition-type interactions. The pyrazolium moiety associates with the nitrate anion *via* N-H···O hydrogen bonding, and this interaction is reciprocated by another equivalent unit of the ion pair, such that two units of the pyrazolium are bridged by two nitrate anions, as shown in Figure 2.9. At the other end of the molecule, the carboxylic acid group associates *via* hydrogen bonding to the equivalent site on another molecule to form an 8-membered hydrogen bonding ring. The net result of these interactions is the formation of a 1-dimensional hydrogen bonded polymer, propagating parallel to the [2,1,1] vector within the lattice.

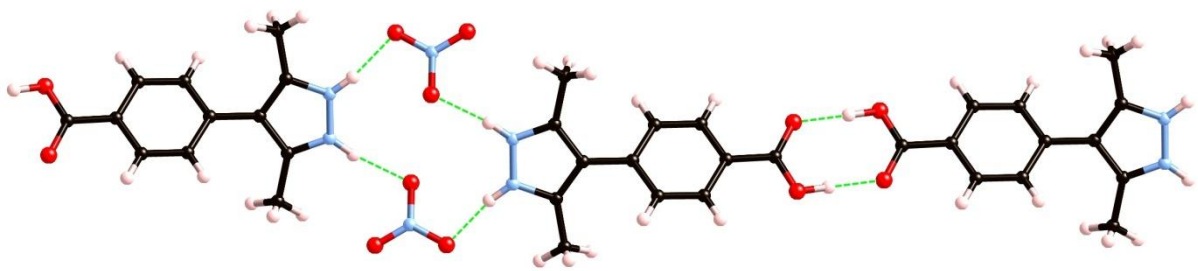

*Figure 2.9: The hydrogen bonding chain formed in **HL2.6**·HNO_3*

In addition to the hydrogen bonding present in **HL2.6**·HNO_3, a number of intermolecular π-π interactions are observed. The individual polymeric strands are bound above and below by equivalent units in a staggered formation, resulting in a sheet-like structure where no substantial inter-strand

interactions are seen parallel to the plane, but π-π interactions between parallel pyrazole rings, at an average interplanar distance of 3.302(2) Å, maintain a densely packed structure.

The crystal structure of **HL2.6** was also collected as the free base, using the colourless crystals obtained as a side product in the hydrothermal reaction of **HL2.6** with cobalt(II) sulfate. The colourless blocks were analysed by single crystal X-ray diffraction, and the data solved and the structure model refined in the monoclinic space group *P*-1 (R-factor 4.81%). Surprisingly, the asymmetric unit of **HL2.6** was found to contain four unique molecules of the ligand, each with a statistically significant difference in the pyrazole-phenyl torsion angle, all of which fall in the range 28.86(9) – 38.29(9)°, comparing well to that seen in the structure of **HL2.6**·HNO_3. The asymmetric unit of **HL2.6** is shown in Figure 2.10 below.

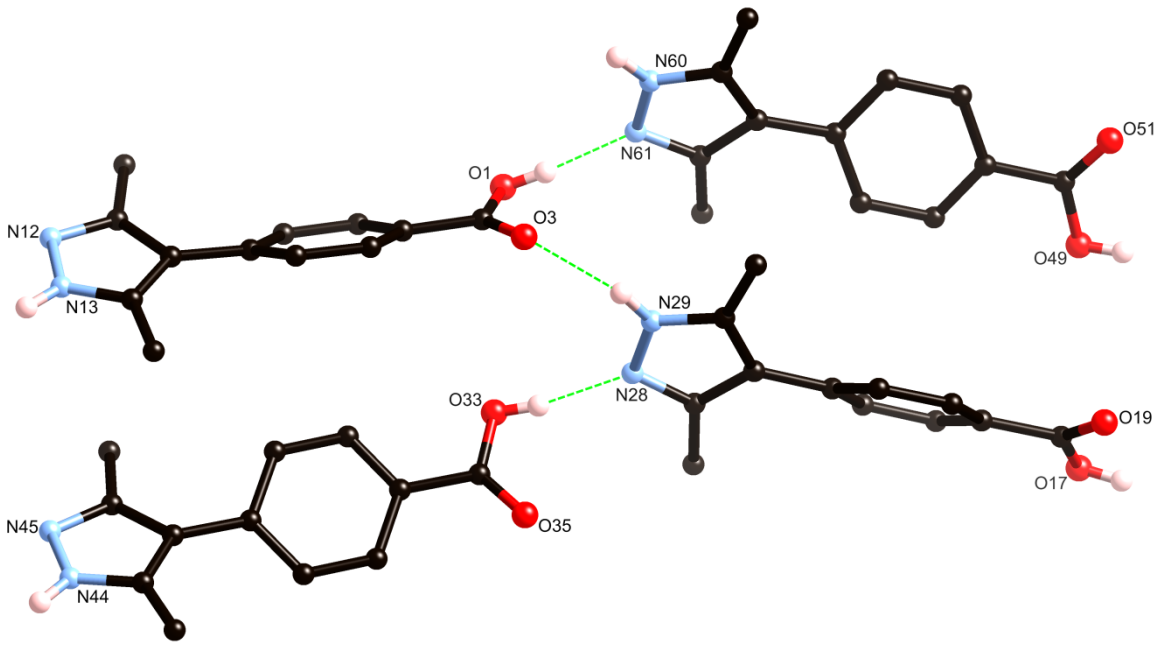

*Figure 2.10: Asymmetric unit of **HL2.6** with heteroatom labelling scheme. Hydrogen atoms not involved in hydrogen bonding omitted for clarity.*

The structure of **HL2.6** is rich in hydrogen bond donor and acceptor sites, and as a result each molecule is involved in a number of hydrogen bonding interactions, of the form O-H···N and N-H···O contacts between pyrazoles and carboxylates, as shown in Figure 2.10 above. The net result of these interactions is the formation of a 2-dimensional, (4,4) sheet parallel to the *ac* plane, shown in Figure 2.11. The chains formed parallel to the *a* edge are helical in nature, and alternate handedness when linked along *c* by the ligand backbone. The torsion between the phenyl and pyrazole rings gives rise to a number of edge-to-face π-π interactions between phenyl groups on adjacent units in the

hydrogen bonding plane, with representative C···π(mean plane) distance 3.540(3) Å. No significant intermolecular interactions were observed between sheets, most likely due to the alternating torsions of the phenyl rings preventing inter-sheet π-π stacking interactions

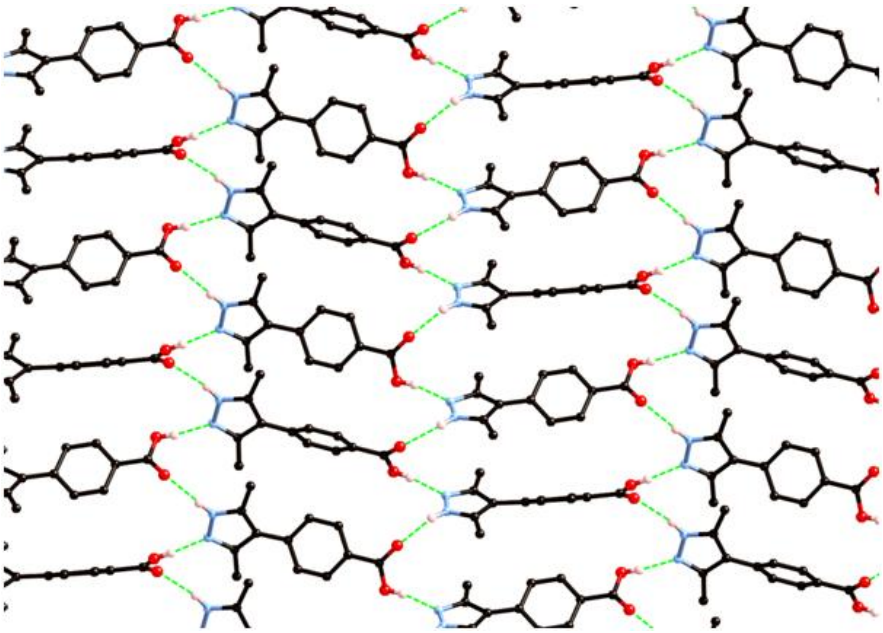

*Figure 2.11: 2-dimensional hydrogen bonding sheet formed by **HL2.6** molecules in the ac crystallographic plane. Hydrogen atoms not involved in hydrogen bonding omitted for clarity.*

*2.2.4 Synthesis of α-(3,5-dimethyl-1H-pyrazol-4-yl)-p-toluic acid **HL2.7***

Finally, ligand α-(3,5-dimethyl-*1H*-pyrazol-4-yl)-*p*-toluic acid **HL2.7** was prepared, in order to examine the effect of internal flexibility on a heteroditopic pyrazole-benzoate compound when forming coordination polymers. Synthesis of **HL2.7** was achieved *via* the key step of appending the diketone moiety to the protected toluic acid residue in a radical process between anhydrous cobalt(II) bis-acetylacetonate and ethyl α-bromotoluate,[259] adapted from the method described above for the synthesis of compound **2.9**, shown in Scheme 2.7. The synthesis was completed by the standard cyclocondensation and ester hydrolysis steps to give the novel pyrazole product in reasonable yield.

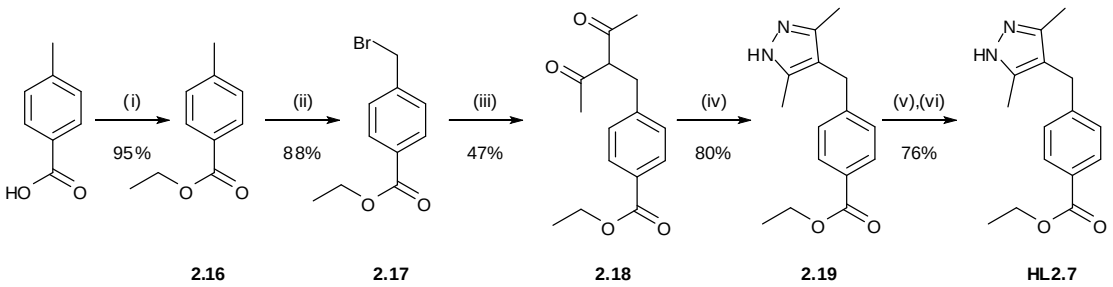

*Scheme 2.7: Synthesis of **HL2.7**. Reagents and conditions: (i) $SOCl_2$, EtOH, reflux 6 hr; (ii) NBS, $(PhCO_2)_2$, $CHCl_3$, reflux 24 hr; (iii) $Co(acac)_2$, 120 °C; (iv) H_2NNH_2, EtOH, reflux 24 hr; (v) LiOH, THF/H_2O, reflux 24hr; (vi) HCl/H_2O, RT*

Single crystals of **HL2.7** were prepared by hydrothermal recrystallisation, and the diffraction data were solved and the structure model refined in the orthorhombic space group *Pbca* (R-factor 3.25%). The asymmetric unit was found to contain one molecule of **HL2.7** in its entirety, and confirmed the expected structure, defined by two aromatic rings joined by a flexible sp^3 methylene linker, with methylene bridge angle 114.68(2)° and a mean pyrazole-phenyl interplanar angle of 68.92(5)°, as shown in Figure 2.12.

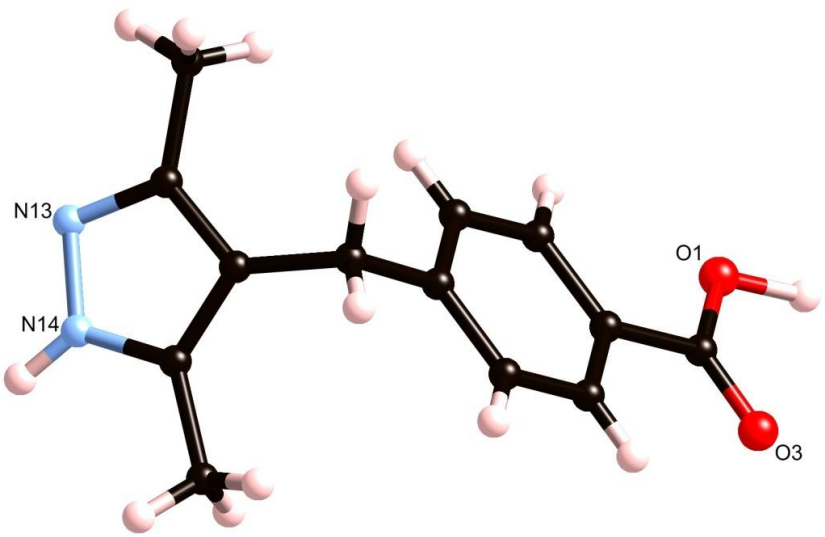

*Figure 2.12: Asymmetric unit of **HL2.7** with heteroatom labelling scheme.*

As was the case with **HL2.6** above, **HL2.7** is rich in hydrogen bond donor and acceptor sites. The modes of hydrogen bonding adopted in the structure are N-H···O and O-H···N interactions between the neutral pyrazole and carboxylic acid moieties. It should be noted that the H(1) proton, represented as bonded to O(1), was manually located from residual electron density and appeared to reside at an

intermediate position significantly closer to O(1) than N(13), and as such any zwitterionic contribution to the structure was ignored for simplicity, although on the basis of relative pKa values, the pyrazole ring was expected to remain fully protonated.[197] Each molecule of **HL2.7** hydrogen bonds to four others through these interactions, as shown in Figure 2.13, resulting in a standard (4,4) hydrogen bonding network, propagating an undulating 2-dimensional sheet along the *bc* plane. Although topologically identical to the network observed in the structure of **HL2.6**, the helical character of the hydrogen bonds is absent in **HL2.7**, where instead a figure-of-8-type zig-zag motif is observed when following hydrogen bonding chains parallel to the *b* edge.

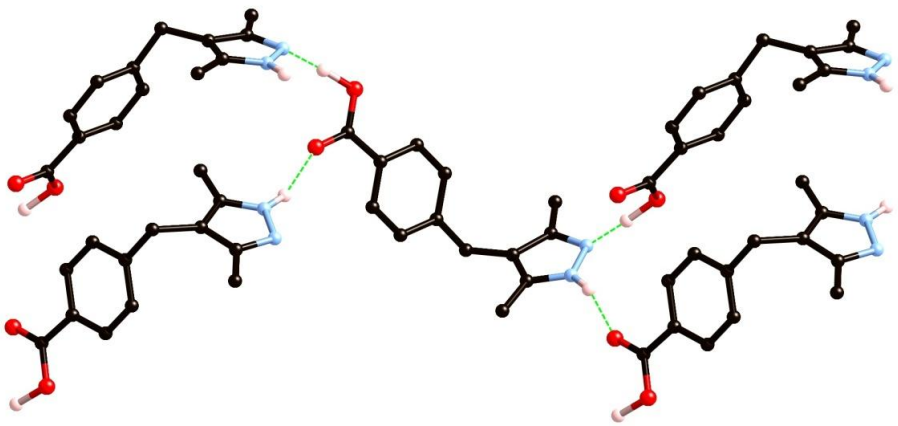

*Figure 2.13: Hydrogen bonding interactions in the structure of **HL2.7**, uninvolved hydrogen atoms omitted for clarity.*

2.3 Synthesis of Pyrazole-Carboxylate coordination polymers

With ligands **L2.1**-**HL2.7** in hand, attention was turned to preparing coordination polymers featuring the pyrazole-carboxylate secondary building unit discussed above. Synthetically, a hydrothermal approach was taken for each of the complexes prepared, with dwell temperature varied where necessary for ligand solubility and stability reasons. In general, equimolar amounts of the pyrazole and carboxylate ligands were combined with a molar excess of either cobalt(II) chloride or cobalt(II) sulfate in water, and allowed to heat under pressure and cool slowly. The complexes formed as purple crystals, and were generally formed as a mixture alongside other solid materials, which analysed for the unreacted ligands. Despite attempts to manipulate the stoichiometry or reaction conditions, insoluble unreacted material was almost always present at the completion of the synthesis. This material was generally removed by soaking the solids in a suitable solvent, such as N,N-

dimethylformamide, until all non-polymeric material had dissolved, then filtering the remaining product and washing with water. As such, any exchangeable solvent present within the compounds may have been compromised, and any reported solvation quantities carry some degree of uncertainty. All crystallographic refinement data, metal-ligand bond lengths and angles, and complete descriptions of hydrogen bonding for crystal structures reported in this chapter can be found in Tables A1-A4, A20 and A25.

*2.3.1 Synthesis of complex poly-[Co(**L2.1**)(**L2.4**)] **2.20***

Ligand **L2.1** was reacted with excess $CoCl_2 \cdot 6H_2O$ in the presence of an equimolar amount of **H_2L2.4** in water at 160 °C under hydrothermal conditions. The resulting purple crystals, formed in 10% yield, were isolated from the solid mixture as described above, and found to be stable to drying in air, as well as heating to 300 °C under a nitrogen stream. No loss of crystallinity was observed during the washing process. The crystals were subjected to single crystal X-ray diffraction, and the data were solved and the structure model refined in the hexagonal space group $P6_522$ (R-factor 3.96%). As expected, the basis of the structure is a tetrahedrally-coordinated Co(II) ion, to which two equivalent units of each **L2.4** and **L2.1** are coordinated in monodentate fashion, and two hydrogen bonds can be seen between the pyrazole and carboxylate moieties, as shown in Figure 2.14. Each ligand contains internal crystallographic symmetry, and as such the asymmetric unit contains only one pyrazole and one phenyl ring.

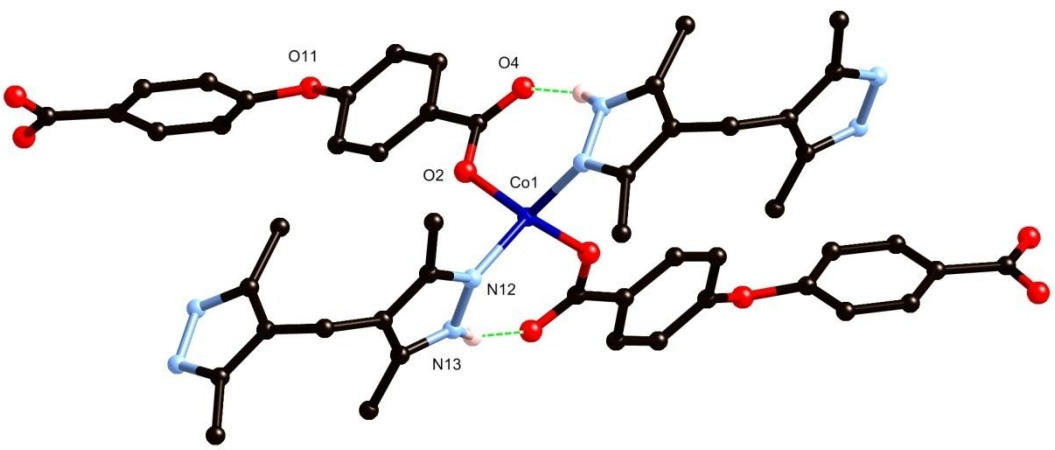

*Figure 2.14: Metal environment of **2.20** showing hydrogen bonding, with heteroatom labelling scheme. Hydrogen atoms not involved in hydrogen bonding omitted for clarity.*

The bifunctional ligands extend the structure into a 3-dimensional polymer, which can be topologically identified with the chiral quartz-dual network ($7^5{\cdot}9$) (**qzd**), a schematic of which can be seen in Figure 2.15. Several interesting features of the structure are not immediately obvious from the topological analysis, such as the overall chirality, an indicator of which can be seen by growing the structure only through **L2.4** linkages, revealing a densely interwoven network of helices of pitch distance *ca.* 48 Å, sharing the same helical axis and all of the same handedness, shown in Figure 2.15. Although the structure described displayed spontaneous resolution into the 6_5 enantiomer, it can be assumed that the bulk sample of **2.20** is racemic, containing an exactly equal quantity of the 6_1 enantiomorph.

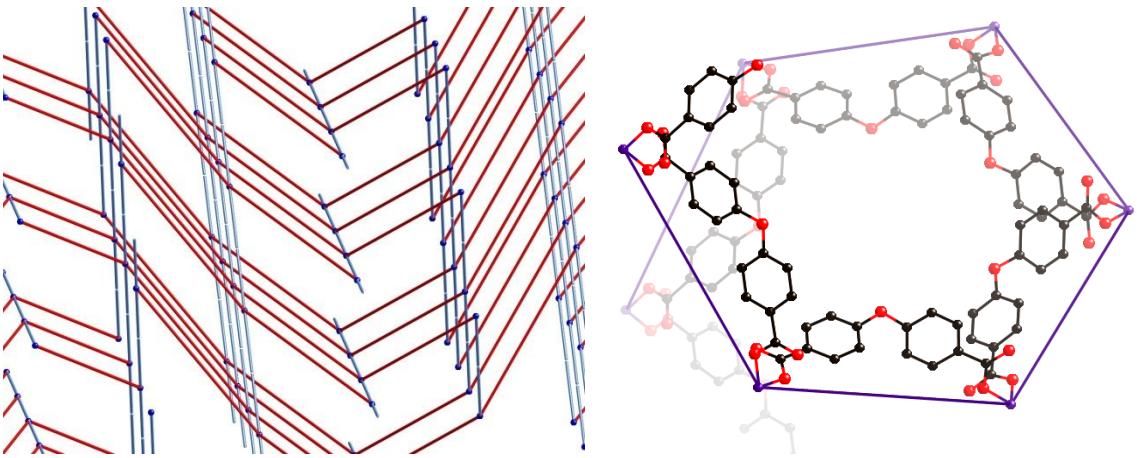

*Figure 2.15: (Left) Schematic representation of the ($7^5.9$) framework of **2.20.** Red links represent connections via **L2.4**, while blue links show connection via **L2.1**. (Right) Representation of a single chain of **L2.4**-linked helices in the structure of **2.20**, showing a single revolution.*

The absolute configuration of the diffracted crystal was determined crystallographically, facilitated by the presence of heavy atoms and confirmed by the Flack parameter calculated as 0.00(3).[270] Of particular interest is the mode of helicity adopted by the **L2.4** ligand. In practice, both ligands **L2.1** and **L2.4** are often seen to adopt a helical character in the solid state,[271-274] governed by the flexible sp^3 linkers between the coordination sites which typically results in helices containing two ligands per rotation. The helices within the structure of **2.20** require six **L2.4** units for a complete rotation, with the result that the pitch is much longer than expected. Unexpectedly, the **L2.1** units, also often found to form helical polymeric chains in such structures, adopt a zig-zag motif in their coordination behaviour.

Although the structure of **2.20** shows small channels along the helical axis, no solvent or residual electron density was crystallographically located within, and the channels with an interatomic

diameter of *ca.* 2 Å were deemed too small to be capable of accommodating a significant quantity of guest molecules. This observation was confirmed by thermogravimetric and micro-analyses, which suggested only trace amounts of water, most likely present on the surfaces. Also observable in the structure of **2.20** are a number of π-π stacking interactions, consistent with a densely packed polymeric species with significant aromatic character on the backbone. As expected by electronic considerations, these interactions occur between the π-rich pyrazole rings and the comparatively electron deficient phenyl rings with a minimum carbon – mean plane distance of 3.436(4) Å for C(8) to the pyrazole mean plane, and an interplanar angle of 6.62(12)°.

*2.3.2 Synthesis of complex poly-[Co(**L2.1**)(**L2.5**)]·2.5H_2O **2.21***

In a similar method to that reported for complex **2.20**, equimolar quantities of **L2.1** and **H_2L2.5** were reacted with excess $CoCl_2 \cdot 6H_2O$ in water, in a pressure vessel at 120 °C, to give purple crystals of complex **2.21** in 22% yield. In this case, the lower temperature was required in order to prevent the decomposition of **H_2L2.5**, which was observed at higher temperatures. An added complication to the synthesis was the sensitivity of the purple crystals to changes in solvation on removal from the mother liquor, or on contact with other solvents. This made isolation of a pure single crystalline sample for bulk phase analysis impossible, as the usual protocol of soaking in dimethylformamide to dissolve unreacted material caused a visible loss of single crystallinity, as did drying to separate the crystals manually. As such, single crystals for X-ray diffraction were mounted directly from the mother liquor, and bulk phase measurements were carried out on the amorphous material resulting from soaking the solid mixture in dimethylformamide. All observations on the amorphous material, including thermal analysis, infrared spectroscopy, microanalysis and solubility tests were consistent with the crystallographically determined model

The structure was obtained by solving and refining the diffraction data in the monoclinic space group *C*2/*c* (R-factor 6.23%). The asymmetric unit of **2.21** consists of a single cobalt(II) ion coordinated to two equivalent molecules of **L2.1** and two equivalent molecules of **L2.5** in a tetrahedral fashion, as shown in Figure 2.16. Substantial electron density was located outside of this coordination sphere, and from void considerations as well as comparison to bulk phase data this density was assigned to 3 water molecules disordered over seven crystallographically distinct sites. As was seen in the structure of **2.20** and those previously observed, hydrogen bonding interactions are obvious between the pyrazole N-H group and the carboxylate oxygen atoms around the coordination sphere. It should be noted that the handedness of the **L2.5** moieties alternates such that one of each

enantiomer is coordinated to each metal centre; these molecules are related by crystallographic symmetry elements and are geometrically identical.

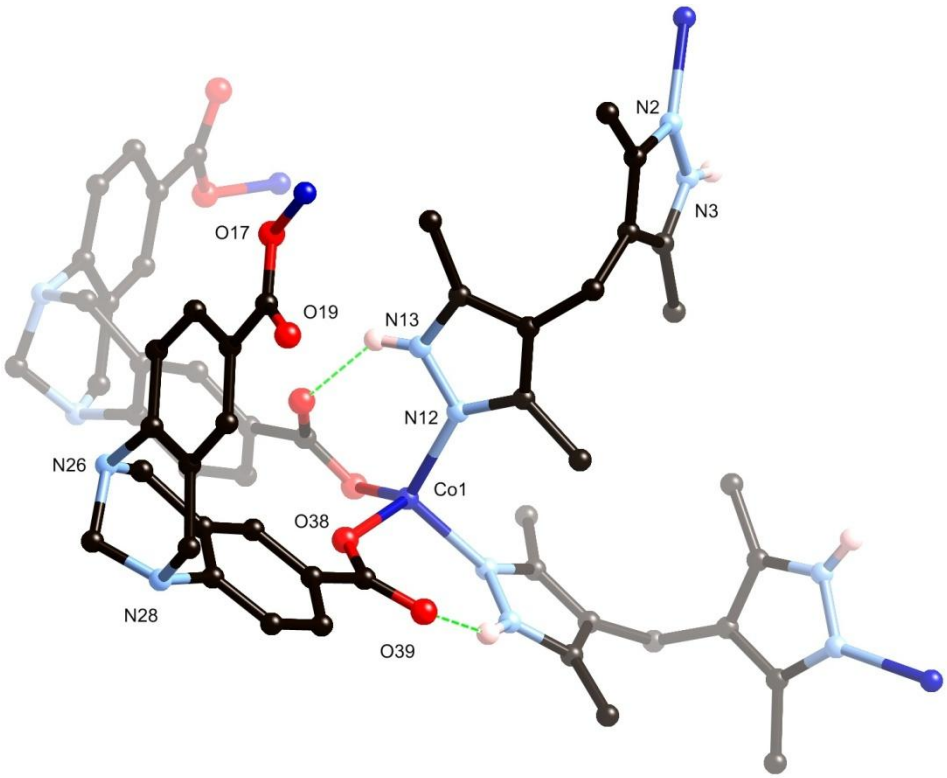

*Figure 2.16: Coordination sphere of **2.21** with unique heteroatom numbering scheme. Disordered water molecules and hydrogen atoms not engaged in hydrogen bonding omitted for clarity.*

The extended structure of **2.21** resembles, in the first instance, a 2-dimensional polymer. Following the links created by **L2.1** gives one-dimensional helical chains parallel to the crystallographic *b* edge, which are linked together by units of **L2.5** into the *a* direction, giving a sheet of (4,4) topology. Within a single sheet, the helices formed by chains of **L2.1** are all of a single handedness, where two **L2.1** units are required for a single revolution giving a pitch of 12.8114(12) Å. A schematic of the connectivity within a single sheet is shown in Figure 2.17. Viewed schematically, these sheets appear to contain large channels proceeding parallel to the *b* edge, contained within walls formed by **L2.1** helices to the left and right, and **L2.5** units above and below. In fact these channels are occupied by disordered water molecules, the large size (*ca.* 6 × 12 Å interatomic distances) and lack of hydrogen bonding donors or acceptors oriented to the inside contributing to the level of disorder of the solvent

molecules, and ease of desolvation. Indeed, thermogravimetric analysis shows onset of solvent loss at room temperature and complete loss of lattice solvent by 100 °C.

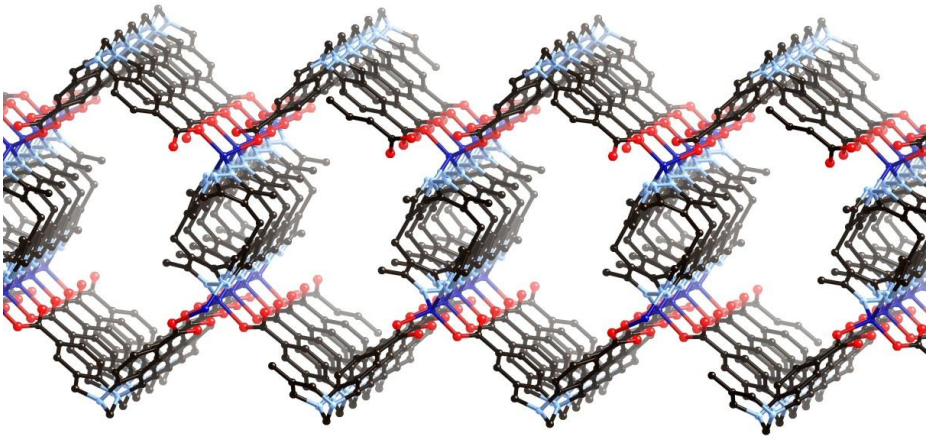

*Figure 2.17: A single sheet of **2.21**, viewed parallel to the b edge. Adjacent interpenetrating sheets and solvent molecules occupying the central cavity omitted for clarity.*

Closer inspection of these cavities also reveals the interpenetration between adjacent sheets parallel to the *c* edge. This uncommon 2D → 3D parallel interpenetration mode occurs by linking the clefts of the Tröger's Base moiety comprising **L2.5** in the opposite fashion to that exhibited in the crystal structure of the free ligand - that is, two opposite-facing clefts interlocking, as shown in Figure 2.18.

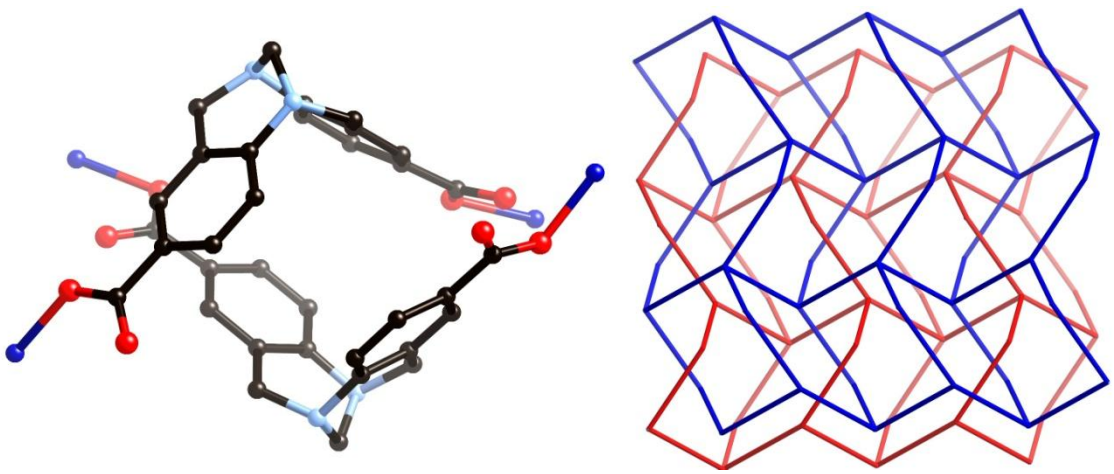

*Figure 2.18: (Left) Interactions at the points of interpenetration between adjacent networks in **2.21**. Hydrogen atoms omitted for clarity. (Right) Schematic of the 2D → 3D parallel interpenetration in **2.21**, independent networks coloured separately. Links through **L2.5** are represented as slightly bent linkers to show the interpenetration mode.*

The point-to-point distances involved in this interaction are all too long (> 4 Å) to be considered strong π-π interactions, though it could be expected that the cooperation of four aromatic systems may result in some attractive interactions. Nonetheless, the ordered separation of the networks seems to be primarily supported by the contents of the channels, namely the continuum of water molecules. Considering the columns of water molecules as structural features of the overall network may explain the rapid loss of crystallinity when the solvation is disturbed; when these molecules are displaced the weak forces between the clefts of **L2.5** units are insufficient to prevent framework collapse.

*2.3.3 Synthesis of poly-[Co(**L2.2**)(**L2.4**)] **2.22***

Complex **2.22** was prepared hydrothermally in a similar manner to **2.20** and **2.21**. The low solubility of **L2.2** in water necessitated a higher reaction temperature of 200 °C, giving a small quantity of purple crystals of **2.22**, which were isolated in 6% yield and found to be air stable. Analysis by single crystal X-ray diffraction in the monoclinic space group $P2_1/c$ (R-factor 3.31%) revealed a structure containing a tetrahedrally coordinated cobalt(II) ion, with two equivalent molecules of **L2.2** and **L2.4**, each bridging metal centres in a bis-monodentate fashion, as shown in Figure 2.19. As expected, two N-H···O hydrogen bonding interactions are evident around the periphery of the Co(II) coordination sphere. No solvent or guest molecules were located within the asymmetric unit, nor was any evidence of significant solvation found by thermal or microanalyses. Demonstrating the level of flexibility brought about by two sp^3 linkers, the mean planes of the pyrazole rings in **L2.2** exhibit angular offsets of between 85 and 86° with the central phenyl ring.

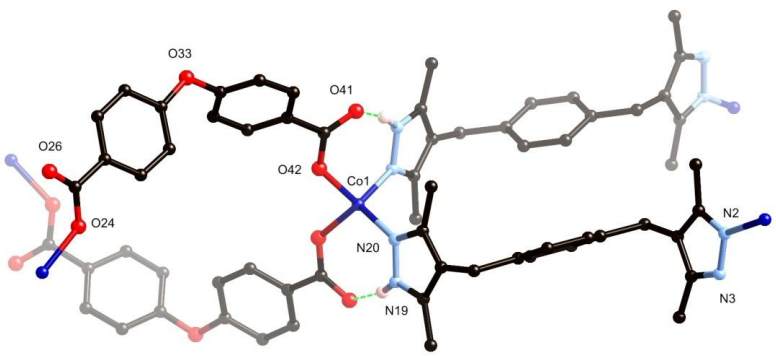

*Figure 2.19: Coordination environment of **2.22** with heteroatom labelling scheme and hydrogen bonding. Hydrogen atoms not involved in hydrogen bonding omitted for clarity.*

Extension of the structure of **2.22** gives a two-dimensional (4,4) network propagating parallel to the *ab* plane, with edge lengths 14.4576(5) Å for links *via* **L2.2** and 12.7765(5) Å for links through **L2.4**. Unsurprisingly, given the large size of these windows, the network of **2.22** is twofold interpenetrated in a parallel 2D → 2D mode, as shown in Figure 2.20. Interestingly, despite the flexibility of the ligands and the number of aromatic systems available, only one mode of π-π stacking is encountered between the interpenetrating networks, occurring between pyrazole rings in a head-to-tail type fashion visible in Figure 2.20, with minimum interatomic distance of 3.692(3) Å for N(20)-C(5) and a mean plane offset of 1.92(9)°. Although some alignment of the **L2.4** π systems is seen between pairs of interpenetrating sheets, the interplanar distances involved are too long (*ca.* 4.3 Å) to contribute significantly to the overall structure. Despite the lack of significant intermolecular interactions, no substantial void space was located within the structure.

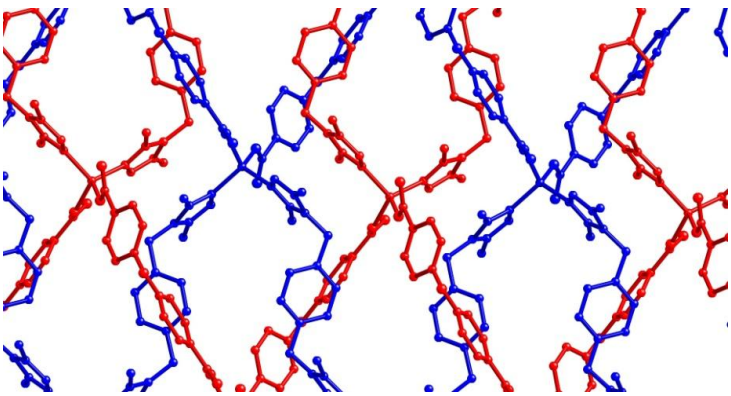

*Figure 2.20: Representation of the interpenetration in **2.22**, independent networks coloured separately.*

Of further interest in the structure of **2.22** is the helical character adopted by chains of both **L2.2** and **L2.4**. Following chains of either ligand down the *b* edge reveals polymeric helices, the likes of which are also observed in the structure of **2.21**, and others involving flexible spacer groups. A single revolution of these helices is shown in Figure 2.21. The handedness of the chains alternates between **L2.2** and **L2.4**, and between interpenetrating sheets, with a pitch of 14.1270 (4) Å, the same for both chains, and a distance equivalent to the length of the crystallographic *b* edge. Compared to the helices formed by **L2.4** in complex **2.20**, the chains in **2.22** adopt the more common mode of two units per revolution.

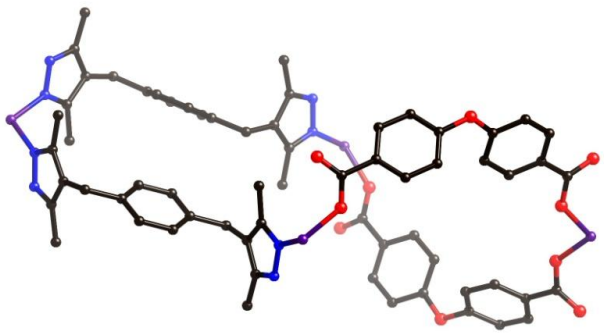

Figure 2.21: A single revolution of two helical chains sharing common nodes, viewed along the b unit cell axis.

*2.3.4 Synthesis of poly-[Co(**L2.3**)(**L2.4**)]·2.5H_2O **2.23***

As with the previous structures, complex **2.23** was prepared by the hydrothermal reaction of ligands **L2.3** and **H_2L2.4** with cobalt(II) sulfate at 160 °C. Although, at 5%, the yield of **2.23** was surprisingly low, probably due to the low aqueous solubility of **L2.3**, sufficient quantity of sample was able to be obtained to carry out structural studies. A structure model was obtained by solving and refining single crystal diffraction data in the monoclinic space group $P2_1/c$ (R-factor 5.51%). Once again, the structure was based around the pyrazole-carboxylate secondary building unit, where two equivalent units of **L2.3** and **L2.4** were seen to coordinate to a cobalt(II) ion, with the expected hydrogen bonding interactions, as shown in Figure 2.22. Disordered water molecules were seen within the asymmetric unit, and to this density was assigned 2.5 water molecules per cobalt, disordered across 5 sites.

When extended through the bridging ligands, several interesting structural features are notable in complex **2.23**. As would be expected, ligand **L2.3** adopts a significant twist of 57.8(5)° between aromatic rings, brought about by the sterically congested neighbourhood of the methyl groups. This twist follows a zig-zag motif when the structure is grown along the **L2.3** linkages. Despite the earlier observations of the tendancy for helicate formation with flexible ligands of this type, ligand **L2.4** also adopts a zig-zag character when extended, with no helical features observed in the entirety of the structure.

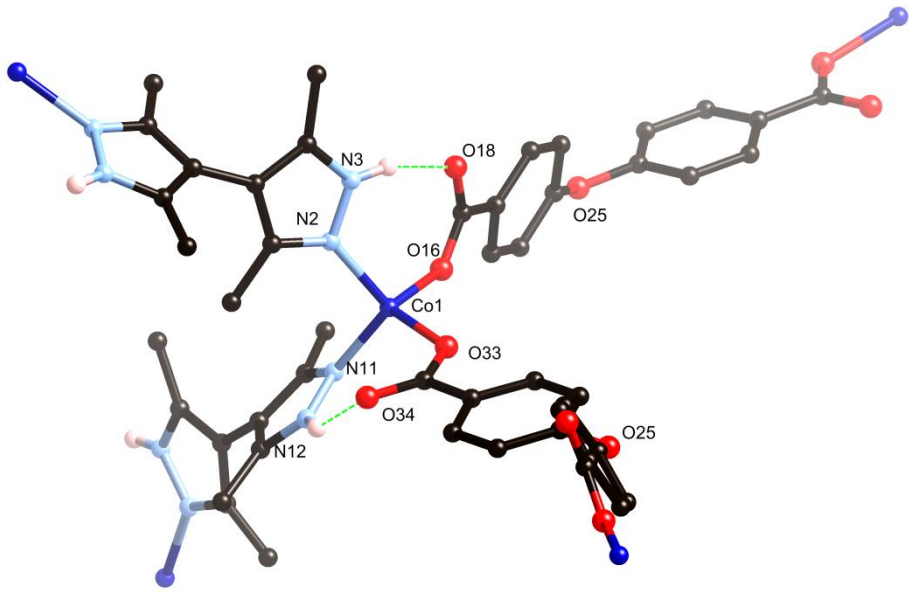

*Figure 2.22: Coordination environment of **2.23** showing heteroatom numbering scheme and hydrogen bonding, hydrogen atoms not involved in hydrogen bonding and disordered solvent molecules omitted for clarity.*

Further extension of the structure of **2.23** into three dimensions reveals a distorted (6,4) diamondoid-type network, where the difference in size of the two bridging ligands gives rise to edge lengths of 9.6247(6) Å and 15.5785(6) Å. The resulting framework contains cavities accessible by windows of *ca.* 25 Å, which inevitably are filled by interpenetrating networks. In this instance, 4-fold interpenetration is observed, as shown in Figure 2.23. The choice of ligands to generate compound **2.23** can be compared to a similar pairing made by Mondal with Zn(II),[255] and the isostructural cobalt(II) compound prepared in our group,[256] namely the **L2.1**/terephthalic acid complex which presented as a triply interpenetrated diamondoid net. As such, the formation of a network of diamondoid topology should not be unexpected, as the functionality and overall flexibility of the ligand system is the same as before, with the most significant difference being the increased length of ligand **L2.4** compared to **L2.1**, likely providing space for interpenetration of one additional network. From these results, it seems reasonable to infer that replacing a flexible bispyrazole and rigid dicarboxylate with a rigid bispyrazole and flexible dicarboxylate of comparable dimensions will give a similar network under these conditions.

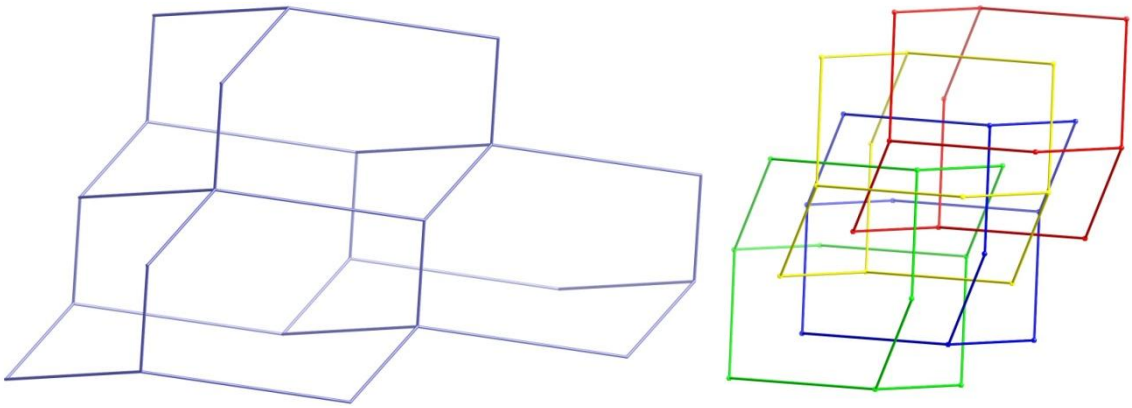

*Figure 2.23: (Left) Schematic representation of a single network of **2.23**; (Right) Interpenetration in **2.23.** independent networks coloured separately.*

The water molecules located in the asymmetric unit fall in regular pockets within the overall structure, and as such no large scale channel structures are observed, nor is any significant void space seen in the unit cell of **2.23**. The water content of these pockets was found to be variable depending on drying conditions; thermogravimetric analysis showed *ca.* 10% mass loss with immediate onset, consistent with 3.5 water molecules per metal, while elemental analysis of a freshly isolated sample was consistent with 7 water molecules per metal. This discrepancy is likely due to the loss of additional solvent molecules under the purge gas stream on the thermogravimetric analysis instrument before the scan was initiated; however the surface water contribution to the elemental analysis value cannot be ignored, and as such the water content of the voids in **2.23** can only be estimated as falling between these two values. Though most π-π stacking interactions are disrupted either by the torsion and steric hinderance of **L2.3** or presence of water molecules in the vicinity of one of the aromatic rings of **L2.4**, one π-π interaction is observed between phenyl rings of **L2.4** on adjacent networks; however, with a comparatively long parallel interplanar distance of 3.720(4) Å the interaction is expected to be relatively weak.

*2.3.5 Synthesis of poly-[Co(**L2.6**)$_2$] **2.24***

Complex **2.24** was prepared by combining excess $CoSO_4 \cdot 7H_2O$ with ligand **HL2.6** hydrothermally with a dwell temperature of 180 °C, giving the product in 24% yield. The purple crystals obtained were subjected to single crystal X-ray diffraction, and the data solved and the structure model refined in the tetragonal space group *I*-42*d* (R-factor 4.17%). The structure model obtained revealed two

crystallographically unique Co(II) ions and two unique molecules of **L2.6**, such that each Co(II) ion was coordinated to four equivalent ligand molecules in a tetrahedral fashion, as shown in Figure 2.24. Both units underwent the expected N-H···O hydrogen bonding interactions, and while the two metal ions displayed minor differences in the angles between coordinating atoms and the ligand pyrazole-phenyl torsion angles, the metal-metal distances for the two unique networks were identical, as was the nodal geometry.

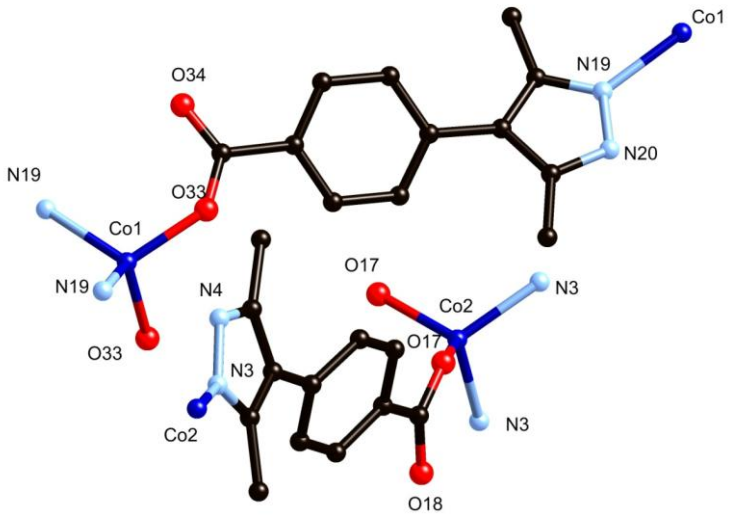

*Figure 2.24: Coordination environment of **2.24** with heteroatom labelling scheme. Hydrogen atoms and phenyl ring disorder omitted for clarity.*

As both unique ligands display the same bridging distance, and the nodal geometries are precisely conserved between the unique networks, the resulting framework displayed a high degree of symmetry. When extending the structure three dimensionally, the standard (6,4) diamondoid network is observed for each crystallographically unique subunit, with edge lengths of 12.3997(2) Å. However, the network itself remains geometrically distorted due to the angles imposed on the nodes by the mode of coordination of **L2.6**, which are measured to be two angles of 73.611(2)° and 4 angles of 129.872(2)° per node, far removed from the ideal 109° tetrahedral angle. The distorted regular diamondoid network formed is shown in Figure 2.25. As expected for a diamondoid network with windows of *ca.* 20×30 Å, interpenetration is observed, in the case of **2.24** an overall quadruply interpenetrated network is the result, with two sets of two crystallographically equivalent frameworks resulting.

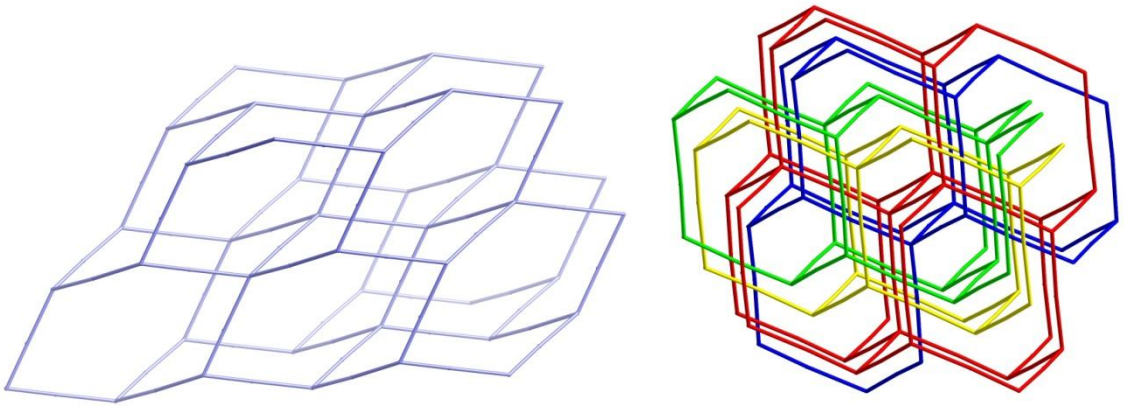

*Figure 2.25 (Left) Schematic representation of the distorted regular diamondoid network of **2.24**; (right) Fourfold interpenetration in the structure of **2.24**, where red and blue networks are crystallographically equivalent, as are green and yellow.*

Interestingly, the two distinct sets of networks associate in an AABB arrangement when viewed along the unique axis, rather than the possible ABAB arrangement, of the type shown by **H_2L2.5**; however, the crystallographically equivalent networks in **2.24** are not enantiomeric as was the case in **H_2L2.5**, evidenced by the presence of both pyrazole-phenyl atropisomers in each framework. The π-π stacking observed in **2.24** is limited, although an interaction does exist between coplanar pyrazole rings on adjacent non-equivalent networks, with a minimum interatomic distance of 3.461(4) Å for C(5)-N(19). Despite being located directly adjacent, no intermolecular interactions are observed between crystallographically equivalent networks. The dense packing of **2.24** leaves no significant void space, and no solvent molecules were located within the lattice. This observation was supported by elemental and thermogravimetric analyses, with only negligible mass loss detected up to 300 °C under nitrogen flow, at which point a slow, single step decomposition process initiates, centred at 415°C.

*2.3.6 Synthesis of poly-[Co(**L2.7**)$_2$]·H_2O **2.25***

Complex **2.25** was prepared by a modification to the standard procedure, in which one drop of 2,4,6-collidine was added to the mixture of cobalt sulfate and **HL2.7** in water, and following a modified hydrothermal protocol in which the dwell period was replaced by a slow heating period, followed by rapid cooling, giving the product in 35% yield. Addition of a weak base and modification of the heating cycle proved invaluable in generating diffraction quality crystals, as despite numerous efforts using the standard conditions, only microcrystalline material was obtained. It is expected that the organic base facilitated deprotonation of the carboxylate group, encouraging coordination, while

allowing the slow growth of better quality crystals. Presence of an organic conjugate acid also likely had an influence on the aqueous solubility of the ligand compared to the other alternative, the bisulfate salt formed by partial deprotonation of the ligand by the sulfate anion. Once obtained, the crystals of **2.25** were subjected to single crystal X-ray diffraction analysis, and the data obtained were solved and the structure model refined in the monoclinic space group *C*2/*c* (R-factor 4.14%). The asymmetric unit of **2.25** was found to contain one Co(II) ion, two non-equivalent molecules of **L2.7** and one water molecule. Interestingly, while the coordination around the metal ion was the tetrahedral N_2-O_2 motif seen previously, only one hydrogen bond between the pyrazole N-H hydrogens and deprotonated carboxylate groups was observed. Protonated pyrazole nitrogen N(15) instead acts as a hydrogen bond donor to the lattice water molecule, which itself acts as a hydrogen bond donor to non-coordinating oxygen atoms O(4) and O(34), the latter of which also accepts a hydrogen bond from pyrazole nitrogen N(20). Possibly due to this discrepancy in the hydrogen bonding environment, the tetrahedral coordination sphere of the Co(II) ion in **2.25** displays the greatest degree of angular distortion of any of the structures discussed (Table A25). The coordination environment of **2.25** is shown in Figure 2.26.

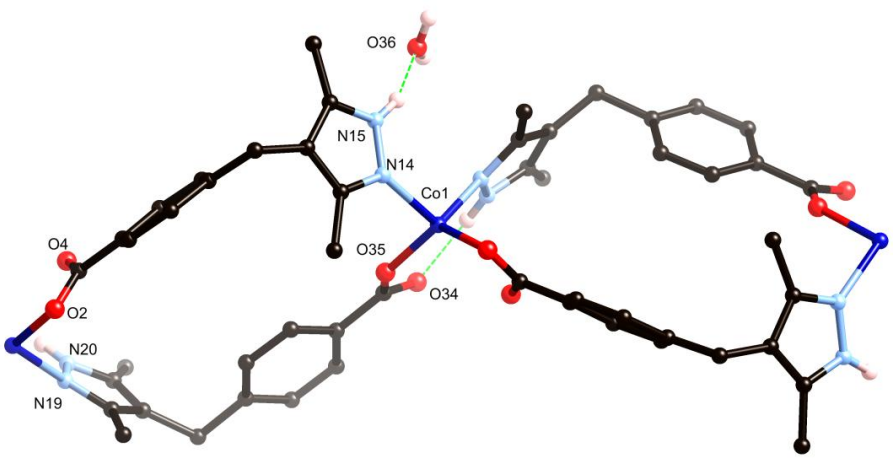

*Figure 2.26: Coordination environment of **2.25** with unique heteroatom labelling scheme. Hydrogen atoms not involved in hydrogen bonding omitted for clarity.*

Topologically, **2.25** resembles a one-dimensional polymeric chain in the first instance, with Co(II) atoms linked by zig-zag chains of **L2.7** parallel to the *c* edge, as shown in Figure 2.27. However, when including hydrogen bonding connections, the network must be considered binodal 3,5-connected, where water molecules are 3-connected nodes, and cobalt ions become 5-connected nodes, owing to their connectivity to two other cobalt sites and three water molecules. The resulting network

adopts a $(4^2 \cdot 6^7 \cdot 8)(4^2 \cdot 6)$ topology, forming a double-layered two-dimensional sheet parallel to the *bc* plane. A schematic diagram is shown in Figure 2.27 below. Aside from these hydrogen bonding interactions, the structure of **2.25** contains few significant intermolecular interactions, with only very weak partial π-π overlap between sheets, and no other significant interactions within each sheet. Thermogravimetric analysis of **2.25** showed a two-step mass loss of 4% up to 150 °C, consistent with the loss of the lattice water (calculated 3.5% mass).

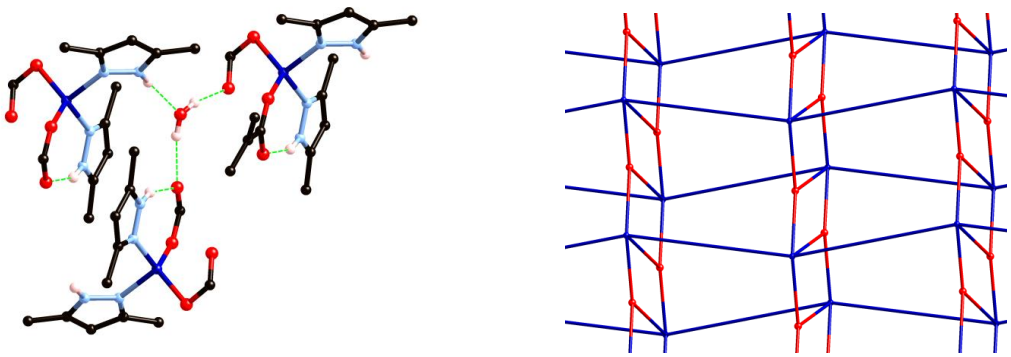

*Figure 2.27 (Left): Representation of the hydrogen bonding interactions in the structure of **2.25**, linking three cobalt ions not connected by coordination bonds. Ligand structure simplified and additional hydrogen atoms omitted for clarity. (Right) Topological representation of the 2-dimensional network formed when accounting for hydrogen bonding linkages in **2.25**. Cobalt ions shown in blue, water molecules displayed as red nodes, where blue linkages represent **L2.7** links and red/blue links represent hydrogen bonds.*

2.4 Discussion

Pleasingly, structures **2.20**-**2.24** all displayed the desired secondary building unit in its entirety, confirming that for the mixed ligand systems studied under these conditions the formation of the SBU is reproducible. In the absence of other limiting factors, such as the network instability in **2.21**, structures containing the $[M(HPz)_2(COO)_2]$ node showed excellent thermal and chemical stability, attributes vital for any functional materials. The incomplete version of the SBU formed in structure **2.25**, notably equivalent to that seen in Mondal's **L2.1**/isophthalic acid system, can be attributed to a number of factors. Most importantly, the **L2.7** ligand system was the only environment studied where the formation of a one-dimensional polymer was possible, due to the flexibility of the ligand and the length complementarity achievable by the use of a single ligand in the reaction mixture. The lower dimensionality species in itself might be expected to enjoy a degree of entropic favourability over a 2- or 3-dimensional species, owing to the increased degrees of conformational freedom possible in a

one-dimensional structure. The structure of **2.25** seems incommensurate with the formation of a second hydrogen bond, which would require reorganisation of both ends of one molecule of **L2.7**, with the immediate effect of a methyl group being reoriented into the interstitial space between layers, presumably resulting in a structure of lower density. Any enthalpic cost associated with the loss of an N-H···O hydrogen bond is more than offset by the inclusion of a water molecule to occupy all remaining hydrogen bond donors and acceptors.

A number of conclusions can be drawn from these data regarding the relationship of rigidity to network topology. Although ligands **L2.3** and **L2.6** possess a certain degree of rotational flexibility, for the purposes of this discussion they will be considered as fully rigid ligands, and likewise ligand **L2.5** will be considered a rigid ligand despite the saturated backbone allowing a slight tweezer-type motion at the coordination sites. Ligands **L2.1**, **L2.4** and **L2.7** contain a single site of conformational flexibility each, whereas ligand **L2.2** contains two flexible sites. A summary of network parameters is given in Table 2.1 below. In the case of compound **2.25**, only the network parameters defined by coordination bonds are reported.

Compound	Flexibility	Topology	Dimensionality	Node Geometry	τ_4(node)	τ_4(metal)	Spacer Elongation (%)
2.20	2	(7^5.9) qzd	3	Sawhorse	0.32	0.90	47.9
2.21	1	(4,4)	2 → 3	Twisted Sawhorse	0.89	0.91	27.8
2.22	3	(4,4)	2	Square Planar	0.08	0.94	13.1
2.23	1	(6,4) dia	3	Tetrahedral	0.82	0.94	61.9
2.24	0	(6,4) dia	3	Tetrahedral	0.71	0.90. 0.97	0
2.25	2	1D chain	1	Linear	n/a	0.88	0

*Table 2.1: Network parameters of structures **2.20-2.25**. Flexibility refers to the number of flexible spacers per [ML_2] repeat unit. τ_4 is defined as ([360-(α+β)]/141), where α and β are the two largest angles within the four-coordinate sphere, with a value of 1 representing a perfect tetrahedron and a value of 0 representing square planar geometry.[275] Spacer elongation is defined as (100[A – B])/B, where A and B are the spacer lengths, A being the longer of the two.*

In this instance, the use of the τ_4 tetrahedral distortion parameter introduced by Houser *et al.*[275] provides a useful quantification of the geometric parameters of each complex, showing, in the first instance, that the geometries of each of the Co(II) ions were comparatively regular with only minor distortion. The greatest deviation to the metal coordination sphere was seen in complex **2.25**, where the loss of one hydrogen bond allowed a slightly larger distortion from ideal geometry, although the effect was minor.

Given tetrahedral geometry for each of the metal ions, Table 2.1 shows that, as would be expected, the topology was dominated by the physical geometry of the metal centre when the linkers were comparatively linear and contained only 1 or 0 sites of flexibility per ML_2 unit, providing the smallest distortions from tetrahedral geometry to the node itself. This point may seem intuitive; however, rigid linkers still require shape complementarity with the SBU, which may be assisted by the one flexible site in **L2.1** or the torsional freedom in **L2.6**. At the other end of the scale, where flexibility was 3 sites per ML_2 in complex **2.22**, the extended network was reduced to a two dimensional sheet, giving a (4,4) network where the nodes resembled square planar geometry, highly distorted from the tetrahedral character of the metal site itself. The formation of a lower dimensionality network was also most likely favoured by the size complementarity of the ligands, where networks with higher degrees of spacer elongation would be expected to find formation of a similar network much more energetically costly. This result mirrors the work of Mondal, where highly flexible ligand backbones typically led to lower dimensionality networks.[254] In the case of **2.20**, where the total flexibility was at an intermediate level, and the spacer elongation prevented the formation of a low dimensionality polymer as was the case in complexes **2.22** and **2.25**, the result was a network in which the node geometry did not resemble that of the SBU, yet sufficient rigidity was present to support a 3-dimensional network. In the case of compound **2.21**, the tetrahedral distortion parameter τ_4 does not provide an accurate representation of the distortion of the nodes from ideal tetrahedral geometry, in that the twisted sawhorse geometry contains no large angles, and does not resemble any common molecular geometries. In this case, the geometry between nodes is a result of the rigid right-angle geometry imposed by the **L2.5** units, enforcing the formation of an entropically favoured 2-dimensional sheet which then undergoes 2D → 3D interpenetration.

Based on these data, and the previous reports of Mondal *et al.*[254, 255], it can be concluded that under hydrothermal conditions, cobalt(II) or zinc(II) complexes with bispyrazole-dicarboxylate mixed ligand systems in which the bifunctional linkers are rigid and linear, or contain a low degree of flexibility, can be expected to reproducibly generate robust 3-dimensional diamondoid-type networks containing the $[M(Hpz)_2(COO)_2]$ secondary building unit at the vertices. Furthermore, where the total

degree of flexibility within the ligand system is too great, it can be expected that the network formed will be of lower dimensionality, either a 1-dimensional polymeric chain or 2-dimensional sheet with the same SBU at the vertices, especially in the instances where the ligands are of complementary length. Finally, where an intermediate degree of flexibility is present, and low dimensionality structures are prohibited by spacer length mis-matching, the resulting network topology will be controlled by the nature of the ligand backbones, where the geometry of the SBU is not represented by the geometry of the network node.

Chapter 3

Complexes of Flexible Pyridyl-Pyrazole Ligands

3.1 Introduction

3.1.1 Helical Structures In Metallosupramolecular Chemistry

Helical structures, most simply visualised as a discrete or one-dimensional winding motif, are relatively common in metallosupramolecular chemistry.[49, 50, 276] In nature, helices are crucial structural elements in proteins, as well as the ubiquitous double-helical structure of DNA.[277, 278] Formation of a helix is usually governed by a number of factors; principal among these is generally flexibility of a molecular strand, allowing axial compression from a straight one-dimensional line, concurrent with expansion into the orthogonal directions, akin to winding a narrow wire into a spring. For a flexible, linear strand, arrangement into a helix, or co-operation with one or more additional strands into a polystranded helix, represents a high density packing arrangement which is especially favourable when hydrogen bonding or other inter- or intra-strand interactions are present. The term *helicate* was first coined by Lehn in 1987,[279] to refer to a metal-containing helical structure in which the metal ion is coordinated by one, two, three or more ligand strands which assemble in a helical fashion. In these cases the metal ions act as templates or anchors, around which the ligand strands wind. A substantial volume of literature describes the synthesis and characterisation of polymetallic helical architectures,[280-288] and the preparation and study of such compounds remains an active area of research.[289-295]

Several terms of nomenclature are required to describe helicate structures.[50] The metal content of a helicate is referred to in terms of nuclearity, *i.e.* mononuclear, dinuclear, trinuclear, polynuclear *etc.*, while the composition of the ligand can be expressed by the terms homotopic or heterotopic, in which the binding sites contain the same or different coordinating groups, respectively. A heterotopic helicate can be further divided into classes depending on the orientation of the coordinating groups; where equivalent binding sites are grouped at the same ends of the helical strand, the term head-to-head can be applied, or head-to-tail in the opposite case. Helices and helicates are chiral entities;[296] in general, helicates formed from achiral ligands will exist as a mixture of the right and left handed enantiomers (Δ and Λ), forming an overall racemic mixture in solution and, typically, in the solid state, although spontaneous resolution of racemic helicates in the solid state has been observed.[297-299] When chiral groups are incorporated on the ligand backbone it is possible to generate helicates as their single enantiomers.[17, 300, 301] It should be noted that by definition, polynuclear helicates must exhibit the same handedness at each metal centre within the same molecule; *i.e.*, in order to be considered a helicate a dinuclear complex must be of the form $\Delta\Delta$ or $\Lambda\Lambda$. The other possible stereoisomer, $\Delta\Lambda$, is referred to as a *meso-helicate* or *mesocate*,[302] in that it contains the same

building blocks as a possible helical structure; however, the twist of the ligands is not conserved between the two ends, and as such the overall structure is not referred to as helical.

3.1.2 The Coordination Chemistry of Heteroleptic Pyrazole Ligands

Heteroleptic pyrazole-containing ligands are well-known in coordination chemistry, where ligand architectures of mixed functionality can have a number of advantages over homoleptic systems.[303-307] Pyrazole derivatives can be coupled with many other heteroaryl functional groups in order to influence the geometric or electronic nature of the resulting complex. For example, replacing one of the pyridine rings in 2,2′-bipyridine with the 3,5-dimethyl-pyrazol-1-yl unit generates a pyridyl-pyrazole ligand which, when incorporated into an Fe(II) complex, facilitates access to both the high and low spin states of the metal ion *via* a broad spin crossover transition,[308] while the corresponding homoleptic species $[Fe(bipy)_3]^{2+}$ exists in the low spin state over all temperatures. Where the substitution pattern allows for a *1H*-pyrazole, such a functional group can be deprotonated to provide anionic character to the ligand, or reacted further to generate more complex ligand assemblies. In the preparation of supramolecular assemblies, pyrazole functionality is often combined with pyridine functional groups, with ligands such as 4-(4′-pyridyl)-3,5-dimethyl-*1H*-pyrazole[309-311] and 3,5-bis(2-pyridyl)-*1H*-pyrazole[312-318] having been recently employed in the synthesis of discrete and polymeric supramolecular assemblies (Scheme 3.1). The synthetic utility of the 3-(2-pyridyl)-pyrazole system has been demonstrated on several occasions by Ward and co-workers,[319] who have prepared a number of discrete supramolecular assemblies and molecular polyhedra from 3-(2-pyridyl) pyrazoles bridged through the pyrazole 1-position to generate ditopic ligands, usually coordinating through N,N chelates.[320-326]

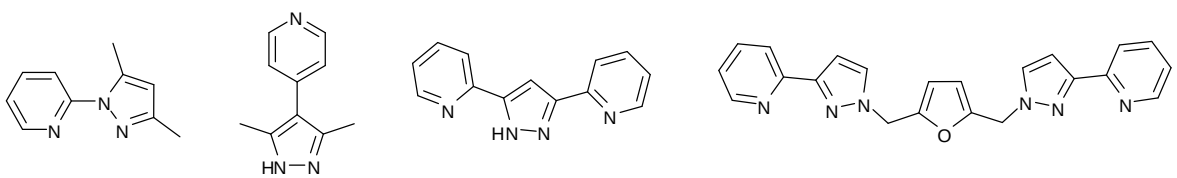

Scheme 3.1: Examples of pyridyl-pyrazole ligands employed within coordination chemistry.

3.2 Ligand Synthesis

The synthesis of 1-heteroaryl pyrazoles is often achieved using one of two methods, differing in the order of formation of the C-N biaryl bond. Using 1-(2-pyridyl)-3,5-dimethylpyrazole as an example, two approaches to its synthesis are shown in Scheme 3.2 below.

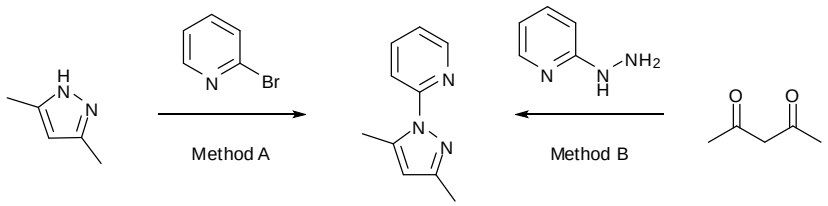

Scheme 3.2: Two possible approaches to the synthesis of 1-(2-pyridyl)-3,5-dimethylpyrazole

Method A involves the reaction of a pre-formed pyrazole ring with a halopyridine, typically in the presence of a strong base such as sodium hydride or potassium metal in a polar solvent with high boiling point to form the biaryl linkage by nucleophilic aromatic substitution.[327, 328] Metal-catalysed versions are also available, allowing similar reactions to take place with the use of less aggressive bases such as potassium or caesium carbonate.[329] Method B employs the condensation reaction between a β-diketone and a suitable aryl hydrazine, which can itself often be generated from the aryl halide. Compared to method A, method B takes place in mild conditions, typically heating in alcohol with or without an acid catalyst. Method A is the more general of the two methods, with no requirement for a stable dicarbonyl precursor; however, method B typically produces higher yields with shorter reaction times and milder conditions.

3.2.1 Synthesis of 4,4′-methylenebis(1-(2-pyridyl)-pyrazole) ***L3.1***

Ligand **L3.1**, 4,4′-methylenebis(1-(2-pyridyl)-pyrazole), was prepared in three steps from commercially available *1H*-pyrazole, as shown in Scheme 3.3. A nucleophilic aromatic substitution method was used to append the pyridine moieties, due to the lack of a suitable dicarbonyl precursor for the 3,5-unsubstituted pyrazole rings. In a method first described by Trofimenko,[330] and subsequently elaborated by Broomhead and Day,[331] pyrazole was first converted to 1,1′-methylenebispyrazole **3.3** by reaction with dichloromethane under phase transfer conditions,[332] and subsequently converted to the dihydrobromide salt. This salt was heated to 200 °C in order to induce the thermal rearrangement to the key precursor 4,4′-methylenebis(1H-pyrazole) **3.4**, which was

converted to the target compound **L3.1** in moderate yield by a double nucleophilic aromatic substitution.

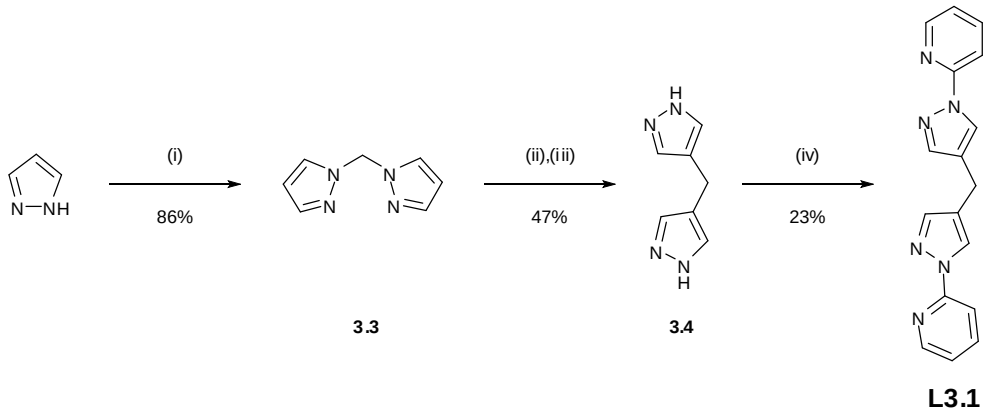

*Scheme 3.3: Synthesis of ligand **L3.1**. Reagents and conditions: (i) CH_2Cl_2, NEt_4Br, KOH, K_2CO_3, reflux 24hr;[332] (ii) HBr, rt; (iii) 200 °C (melt), 90 min;[331] (iv) 2-bromopyridine, NaH, DMF, 110°C, 48 hr.*

*3.2.2 Synthesis of 4,4′-methylenebis(1-(2-pyridyl)-3,5-dimethylpyrazole) **L3.2***

Ligand 4,4′-methylenebis(1-(2-pyridyl)-3,5-dimethylpyrazole), **L3.2** was envisaged as a sterically encumbered version of **L3.1**, providing not only a steric hinderance to the formation of coordinatively saturated species, but also protection from nucleophilic attack and subsequent ring-opening for the 3- and 5- positions of the pyrazole ring, allowing for the use of harsher conditions in its coordination chemistry. Synthetically, **L3.2** was prepared by a double cyclocondensation reaction between 2-hydrazinopyridine and 3,5-diacetyl heptane-2,6-dione **2.8**, the synthesis of which was discussed in Chapter 2.

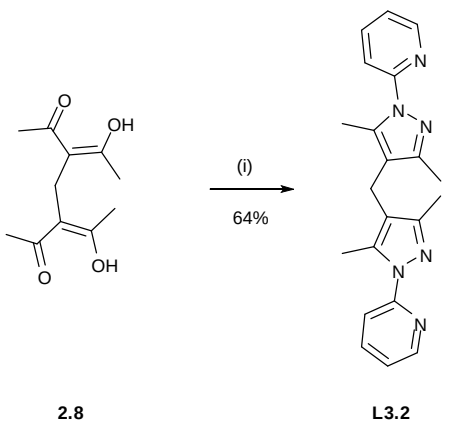

*Scheme 3.4: Synthesis of **L3.2**. Reagents and conditions: (i) 2-hydrazinopyridine, MeOH, reflux 24hr.*

The coordination chemistry of **L3.1** and **L3.2** was expected to vary mainly due to the difference in steric profile. Due to the flexible nature of the linking methylene group between the two binding domains, and the directionality of the binding sites, both ligands were expected to form helical structures when reacted with first row transition metals. Although significantly more compact in terms of potential metal-metal separation than most examples seen in the literature, ligand **L3.1** would be expected to form dinuclear triple helical structures on reaction with octahedral metal ions, whereas the steric bulk of the 3- and 5-methyl groups on the pyrazole rings of **L3.2** would be expected to prevent the formation of coordinatively-saturated helicates, and restrict the coordination mode to perhaps double helicates or polymeric species, in which vacant coordination sites were occupied by solvent or anion molecules.

In order to fully convey the structural properties of metal complexes of **L3.1** and **L3.2**, a number of geometrical parameters must be expressed. Each ligand has four rotatable bonds; two between pyridine and pyrazole rings, with constrained rotation when coordinated to a metal, and two bonds defining the orientation of the sp^3 methylene carbon between the two pyrazole rings. The combination of rotations in these bonds leads to a large number of possible configurations for the ligand. For the expected case of **L3.1** or **L3.2** bridging two metals, several values will be calculated; the metal-metal separation, pyridine-pyrazole interplanar angles, pyrazole-pyrazole interplanar angles, and the two torsion angles describing the twist about the central methylene group φ_1 and φ_2 as shown in Scheme 3.4. The combination of these angles describes all possible degrees of freedom of these ligands within their metal complexes.

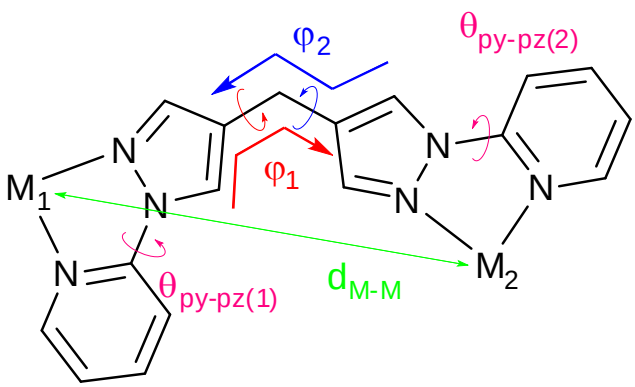

*Scheme 3.4: Representation of the key geometric parameters to be discussed in dinuclear complexes of **L3.1** and **L3.2**, using a dinuclear complex of **L3.1** with $\varphi_1 = 0°$ and $\varphi_2 = 180°$ as an example. Pyrazole-pyrazole interplanar angle not shown.*

3.3 Synthesis of Dinuclear Helicates from L3.1 and L3.2

*3.3.1 Fe(II) Triple Helicates of **L3.1***

Reaction of **L3.1** with $Fe(BF_4)_2 \cdot 6H_2O$ in a 3:2 ratio in acetonitrile gave a dark orange solution containing the soluble complex $[Fe_2(\mathbf{L3.1})_3](BF_4)_4$ **3.5**. A UV/visible spectroscopic titration of iron(II) tetrafluoroborate against the free ligand in acetonitrile confirmed the expected empirical formula with a broad absorption centred at 413 nm (ε = 5700 ± 100 L mol^{-1} cm^{-1}) appearing at maximum absorbance at the 3L:2M stoichiometry, as displayed in Figure 3.1. By plotting the absorbance at representative wavelengths *versus* the number of metal equivalents added (inset, Figure 3.1) it is clear that no further change takes place after this stoichiometry has been reached. The presence of well-defined isosbestic points at 248 and 280 nm suggests a direct transition from the free ligand to the $[M_2L_3]$ complex. The peaks due to the complex at 230, 260, 290 and 413 nm are all in agreement with the literature data for the Fe(II) tris-(1-(2-pyridyl)-pyrazole) complexes reported by Goodwin, although the MLCT $t_2 \rightarrow \pi^*$ band at 413 nm appears at a slightly shorter wavelength in this case (*cf.* 420 nm for $[Fe(py\text{-}pz)_3]$),[306] consistent with the reduced π-acceptor nature of **L3.1**. The exact mass of the complex was determined by high-resolution electrospray mass spectrometry (Figure 3.2), which clearly showed the $[M^{4+}]$ molecular ion at *m/z* 254.5636 (Calculated *m/z* for $C_{51}H_{42}N_{18}Fe_2$ 254.5630)

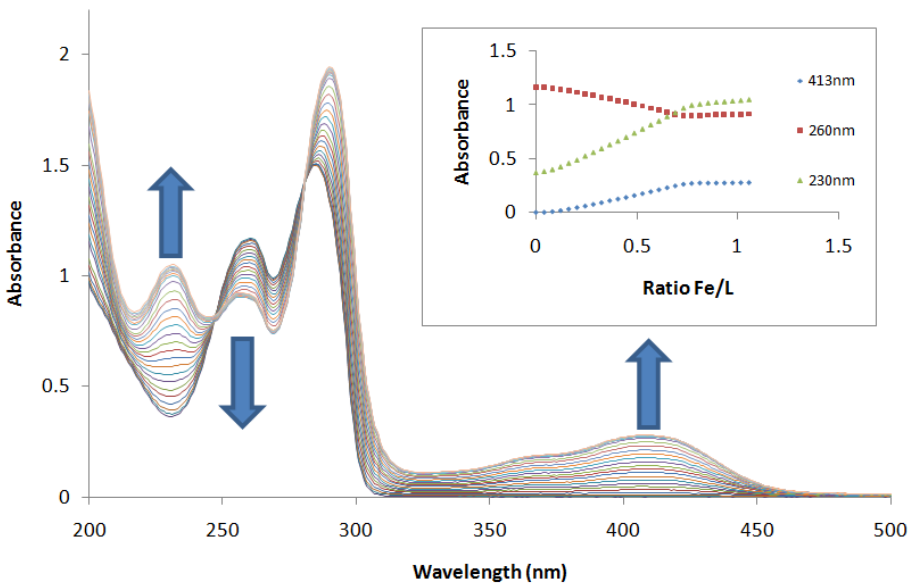

*Figure 3.1 UV-Vis. spectroscopic titration plot of $Fe(BF_4)_2 \cdot 6H_2O$ (2.22×10^{-3} M) against ligand **L3.1** (4.9×10^{-5} M) in acetonitrile. Inset: Absorbance versus equivalents Fe at representative wavelengths.*

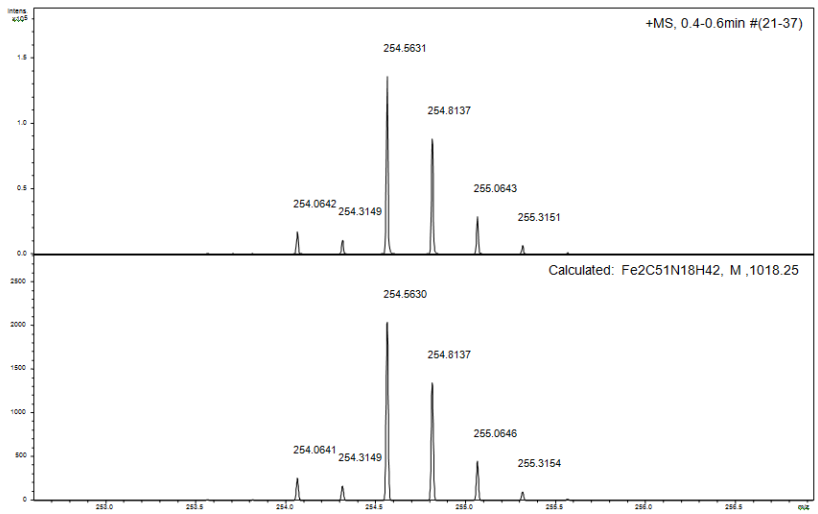

*Figure 3.2: Found (top) and calculated (bottom) electrospray ionization isotope distribution patterns for complex **3.5** in acetonitrile solution.*

The deep orange colour and substantial MLCT transition in the UV/Visible spectrum of **3.5** suggested a low spin electron configuration, and as such a ^{1}H NMR spectroscopic titration was carried out in order to further probe the complex formation in solution. A sample of **L3.1** (7.8×10^{-3} M) in 1.0 mL d_3-acetonitrile was titrated with successive 10 µL aliquots of 3.6×10^{-2} M $Fe(BF_4)_2 \cdot 6H_2O$ solution in the same solvent, and a series of ^{1}H NMR spectra were recorded. The spectral series displayed in Figure 3.3 shows the disappearance of the ligand peaks concurrent with the appearance of peaks due to the formation of **3.5**. The peak multiplicity was obscured by a broadening of each peak once a significant amount of complex was present, likely due to traces of high spin Fe(II) or fluxional processes in solution; however, the broad peaks relating to the complex were assigned on the basis of COSY and nOe correlations.

Of note is the presence of only two sets of signals on initial formation of the complex, and no deviation in the chemical shift of the free ligand signals, suggesting both a lack of meaningful interaction of the free ligand and the complex in solution, and the formation of only one coordinated species, an observation supported by the UV/Visible spectroscopic titration data. The majority of the proton signals experienced only relatively minor and expected downfield shifts on complexation; however, pyrazole proton H^2 and pyridine proton H^7 showed significant upfield shifts of 0.9 and 0.4ppm, respectively, suggesting these protons are forced into edge-to-face interactions with the π systems of adjacent strands by the conformation of the complex, as would be expected in a helical arrangement.

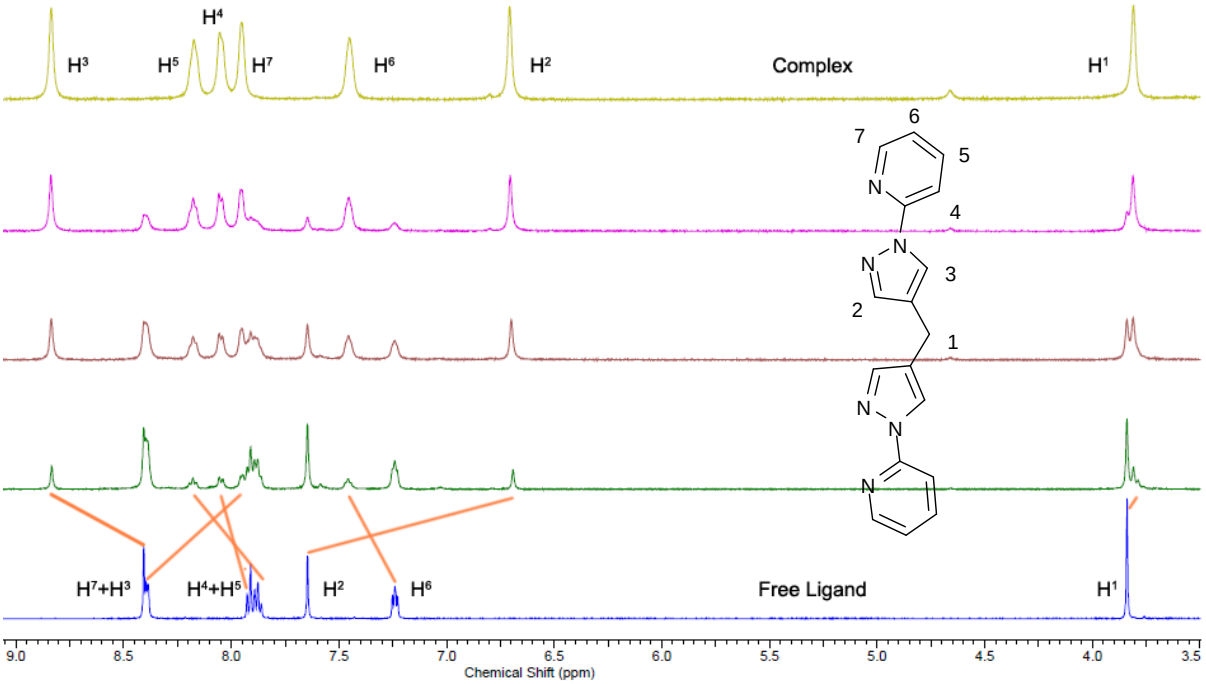

*Figure 3.3: NMR titration of iron(II) tetrafluoroborate against ligand **L3.1** in d_3-acetonitrile. Hydrogen atoms were assigned using COSY and nOe techniques. Equivalents M:L (bottom to top): 0, 0.14, 0.28, 0.42, 0.63, representing 0, 21, 42, 63 and 95 % completeness, respectively.*

In order to fully elucidate the structure of the complex, single crystals were prepared by slow diffusion of toluene into an acetonitrile solution of the complex. Red crystals formed within two weeks, which consisted of a mixture of two compounds: hexagonal blocks of the space group *P*-3*c*1, and parallelogram blocks of the space group $P2_1/n$. In order to generate pure samples of each compound for bulk-phase analysis, a large number of crystallisation solvent/antisolvent combinations were screened. It was found that the hexagonal plates which formed as a single phase from a mixture of acetonitrile and mesitylene in 14% yield were isostructural to the original hexagonal crystals, denoted **3.5A**, and a mixture of nitromethane and benzene generated phase-pure crystals **3.5B**, which, despite containing different solvent molecules, possessed identical packing properties to the other original phase, in 47% yield, as confirmed by single crystal X-ray crystallography (R-factors 6.54 and 10.60%, respectively). As both batches lost crystallinity on drying, phase purity could not be established by powder diffraction, and was instead established by collecting unit cell data from a representative sample of crystals from each batch. As a result of several large areas of diffuse electron density caused by the structural features described below, both structures suffered from weak diffraction, and although the structure of the complex and associated anions themselves can be unambiguously assigned from

the crystallographic model, the position and location of the disordered solvent molecules were unable to be fully determined. A combination of thermal and elemental analyses were used to estimate molecular formulae for the air-dried species, with results best fitting the formulae $[Fe_2(\mathbf{L3.1})_3]\cdot 4(BF_4)\cdot 1.3H_2O$ for **3.5A**, and $[Fe_2(\mathbf{L3.1})_3]\cdot 4(BF_4)\cdot 6CH_3NO_2\cdot 2C_6H_6\cdot 4H_2O$ for **3.5B.** Clearly these values are expected to vary greatly with the degree and duration of drying employed. For the purposes of these studies, samples were isolated by vacuum filtration and allowed to air dry briefly before being placed in sealed vials, where subsequent bulk phase characterisation was carried out immediately where possible, and not more than one week later in the case of elemental analysis.

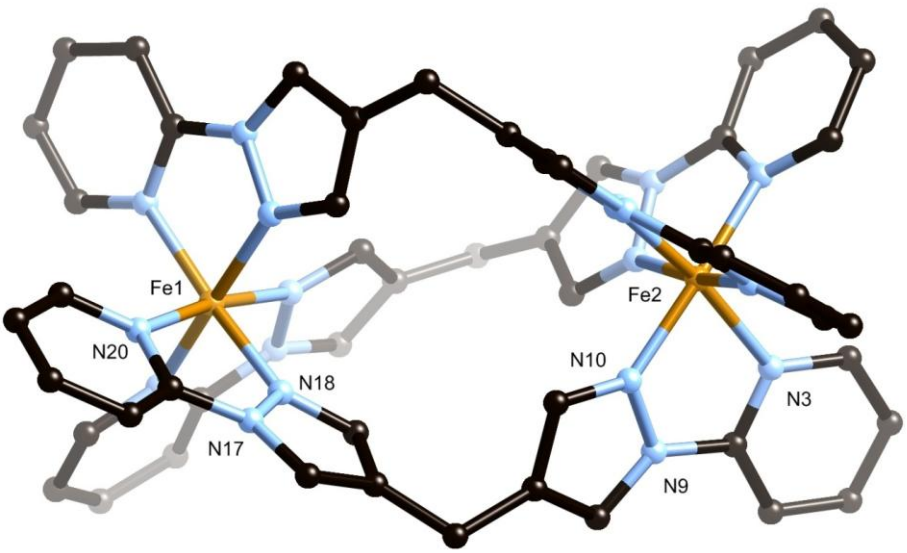

*Figure 3.4: Structure of **3.5A** with heteroatom labelling scheme. Hydrogen atoms and anions omitted for clarity.*

The structure of **3.5A**, as shown in Figure 3.4, consists of two non-equivalent Fe(II) ions, linked by three identical units of **L3.1**, with a threefold symmetry through both metal ions. The structure can be described as a dinuclear triple helicate, with Fe-Fe distance of 7.6133(18) Å. The comparatively compact nature of the complex prohibits any significant void space in the central helical cavity, and as such no guest inclusion is seen to take place. All Fe-N bond distances fall within the range 1.937(4)-1.995(4) Å, indicating both iron centres are in the low spin electron configuration at 113 K, an observation consistent with the room temperature solution data. The asymmetric unit contains two non-equivalent tetrafluoroborate anions, one residing within the aromatic pocket formed at the terminal ends of the helicates (Figure 3.5), with the other slightly disordered anion site being found close to each of the three equivalent helical grooves. The angle representing the flexure at the methylene 'belt' of the helicate was found to be 111.4(4)° on each

strand, suggesting a minimal distortion of the ligand is required in order to conform to the triple helicate shape, while the pyridyl-pyrazole torsion angles are near planar, at 4.8(2) and 6.0(2)°, and the mean interplanar angle between pyrazole rings on the same strand was found to be 69.0(2). The methylene torsion angles φ_1 and φ_2 were measured as 139.2(5) and 128.7(6)°, respectively.

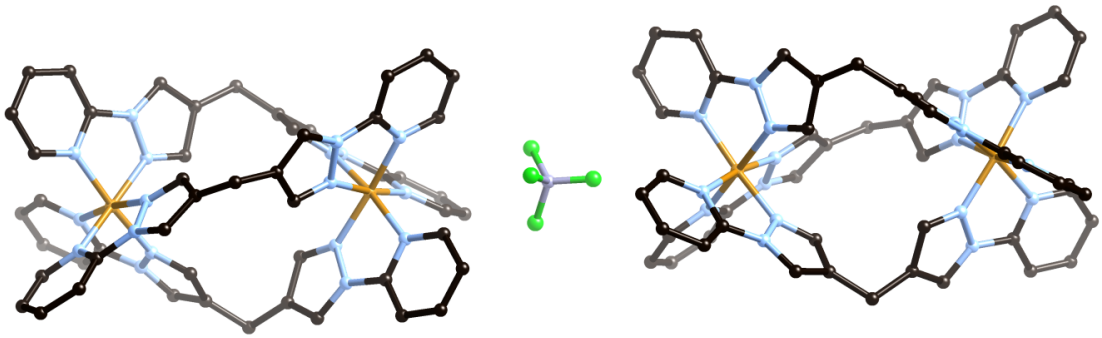

*Figure 3.5: Associations between **3.5A** helicates of alternating handedness along the helical axis, linked through a tetrafluoroborate anion. Additional anions and hydrogen atoms omitted for clarity.*

When the structure is packed in three dimensions, a series of one-dimensional channels is revealed. The helicates associate in linear chains, linked by van der Waals interactions with anions at their termini, and alternating their handedness. Transverse associations are by way of P4AE-type π-π stacking perpendicular to the helical axis between the convex faces of pyridylpyrazole subunits of adjacent molecules, with mean interplanar distance of 3.413(5) Å, shown in Figure 3.6. Interestingly, this interaction is only observed between helicates of alternate handedness, with no significant intermolecular interactions being observed between helicates of the same handedness, either parallel or perpendicular to the helical axis.

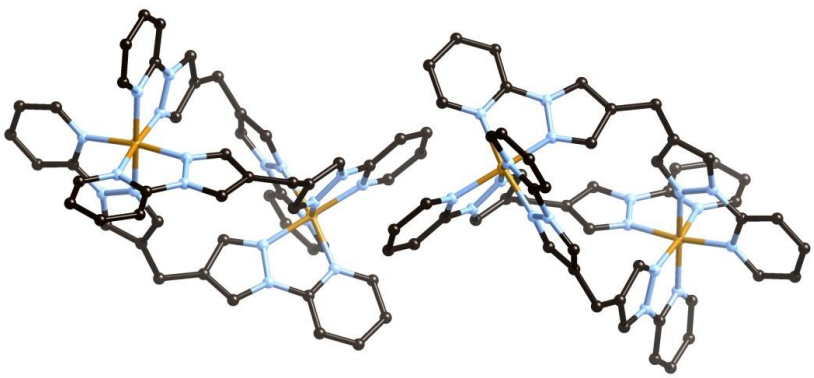

Figure 3.6: P4AE π-π interactions between adjacent helicates of alternate handedness, bridging perpendicular to the helical axis. Anions and hydrogen atoms omitted for clarity.

The central solvent channels have dimensions of approximately 5 × 5 Å and are co-incident with a crystallographic threefold axis. Ill-defined electron density was detected within these channels, most likely due to included acetonitrile or water molecules; however, this density was not able to be modelled satisfactorily due to the highly diffuse nature of the residual electron density peaks and further complicated by the presence of the threefold axis, and as such the SQUEEZE routine within PLATON was applied to the structure model before the final refinement, in order to achieve the best possible geometric precision for the helicate species.[246] Solid samples of **3.5A** appeared to lose crystallinity very rapidly upon exposure to air, and thermal analysis showed very little solvent remained within a sample dried under ambient conditions, with only a slow 1.7 % mass loss up to 200 °C. On the basis of elemental analysis data, this volatile material was assigned as water.

The asymmetric unit of complex **3.5B** contains the entire $[M_2L_3]\cdot 4(BF_4)$ complex, with both iron centres and all three ligands being crystallographically distinct, as shown in Figure 3.7. The structure of the helicate itself is closely related to that found in **3.5A**. As was the case with **3.5A**, the structure of **3.6B** is racemic, and contains both helical enantiomers. The Fe-Fe distance of 7.6339(16) Å compares well to that reported above, and the Fe-N distances again lie within the range 1.93-1.99 Å, indicative of low spin Fe(II). The tetrafluoroborate anions in **3.5B** appeared moderately disordered, with some association in the helicate grooves; however, none was observed at the termini. The methylene bridge angles in **3.5B** range from 111.4(7) to 113.2(6)°, comparing well to **3.5A**, while the pyridine-pyrazole torsion angles, six in total, exhibit a wider range, falling between 3.2(3) and 9.7(3)°. The intra-strand pyrazole-pyrazole interplanar angles lie in the range 65.0(3) – 67.7(3)°, again highly consistent with that observed in **3.5A**, as are the φ_1 and φ_2 angles, which fall between -132.1(8) and -142.3(9)° for each of the three strands. Negative values for φ_1 and φ_2 simply denote the asymmetric unit of **3.5B** being (arbitrarily) modelled as the opposite enantiomer to that of **3.5A**. A comparison of the helicate structures of **3.5A** and **3.5B** can be seen in Figure 3.8 below.

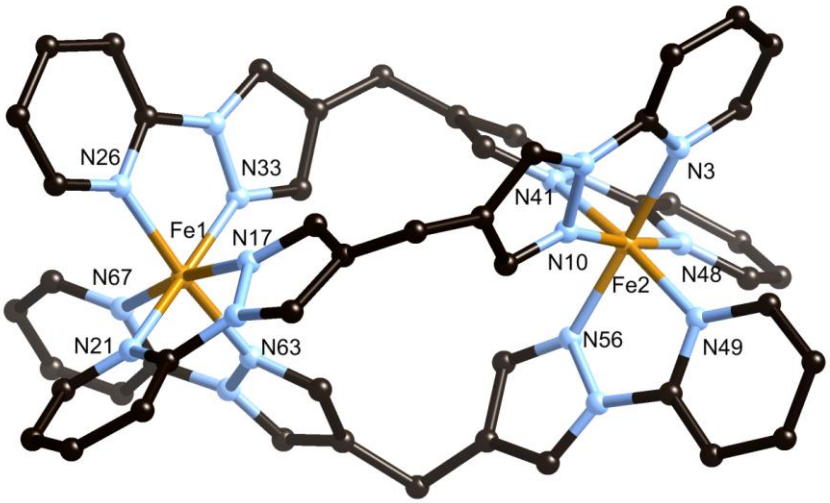

*Figure 3.7: Structure of **3.5B** with labelling scheme for coordinating atoms. Hydrogen atoms, anions and solvent molecules omitted for clarity.*

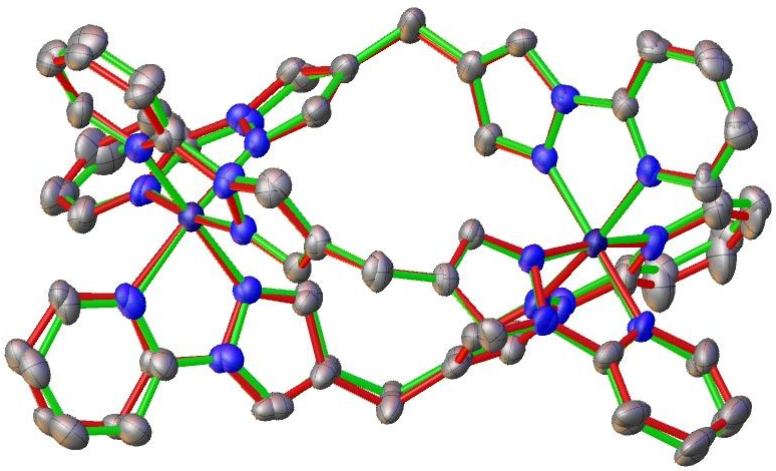

*Figure 3.8: Overlaid structure of like enantiomers of **3.5A** (green) and **3.5B** (red), using both iron sites and a single methylene bridge as anchor points.*

A number of solvent sites were able to be located within the structure, and their location hints at the differences in packing behaviour of **3.5A** and **3.5B**. Aside from weak C-H···O bonding between nitromethane and the ligand backbone, the $MeNO_2$ units do not participate in any significant interactions with the helical species; however, two benzene molecules are observed participating in π-π stacking interactions on both faces, with the closest interatomic distances of the four interactions ranging from 3.358(19) – 3.585(19) Å. The two benzene molecules occupy

four of the six conjugated head groups in these interactions, leaving the remaining two to associate via a direct P4AE interaction, with mean interplanar angle of 3.8(3)° and closest interatomic distance (parallel) of 3.298(12) Å for C(7) - C(23), and closest interatomic distance (perpendicular) of 3.600(11) Å for C(24) - C(42). Unlike the similar interaction observed in **3.5A**, this interaction occurs between concave faces of the ligand strands. The two modes of π-π interactions are shown in Figure 3.9.

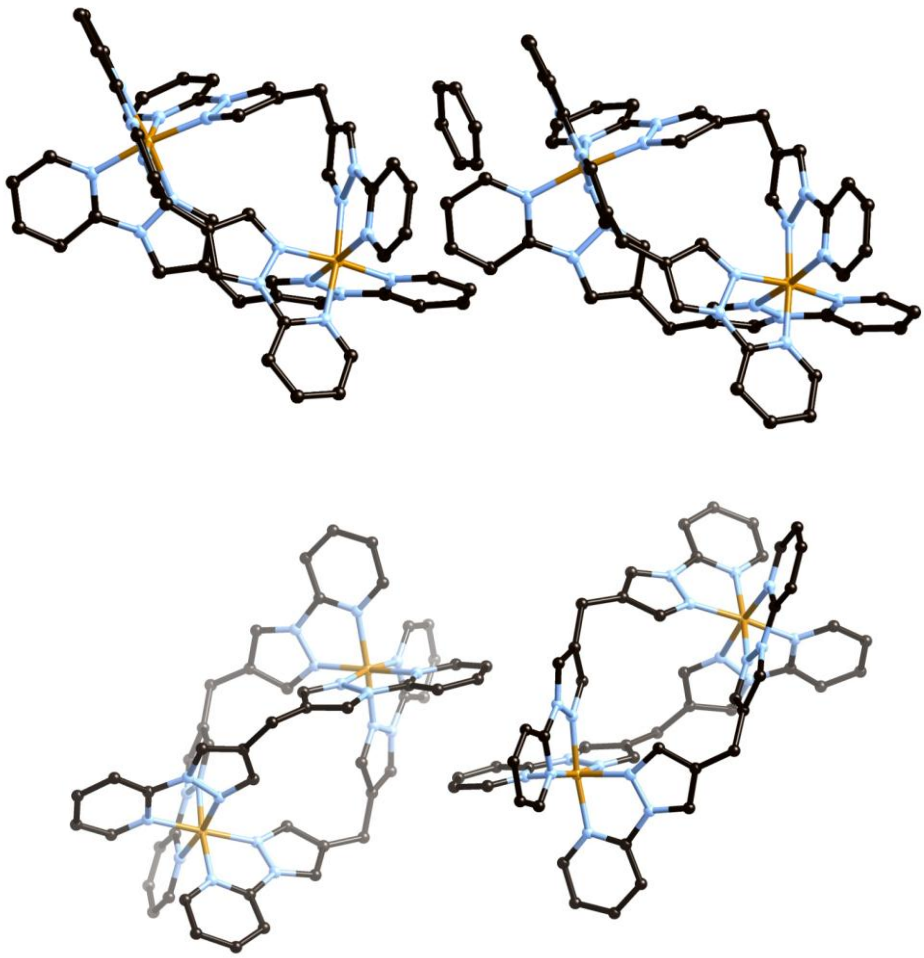

*Figure 3.9: (Top) π-π interactions between **3.5B** helicates and benzene molecules within the lattice. (Bottom) Direct P4AE interactions between concave faces of **L3.1** strands in the structure of **3.5B**.*

The net result of these effects is that the packing of the overall structure is forced into a less efficient, ABCABC-type staggered packing arrangement when viewed down the helical axis, where the cavities above and below each helicate contain the disordered anions and solvent molecules. Despite exhaustive efforts, not all of the solvent was able to be accounted for

crystallographically, and no significant improvement in the accuracy of the model was achieved by applying the SQUEEZE algorithm. As such, the reflection data was not modified by SQUEEZE, and no further refinement was carried out. As was the case with **3.5A,** complex **3.5B** immediately lost crystallinity on drying in air. Thermal analysis of **3.5B** suggested the presence of a considerable amount of volatile material, with a rapid onset of mass loss with a –dM/dT maxima at 54 °C and complete desolvation by 100 °C. The volatile material comprised 24% of the mass of **3.5B**, suggesting considerable retention of solvent molecules within the cavities on removal from solution. Given the stronger interactions of the solvent molecules in **3.5B**, as well as the reduced volatility of nitromethane compared to acetonitrile, it would be expected that at least the crystallographically defined solvent molecules would be retained in a dry sample, in addition to those moieties not able to be located within the lattice, and atmospheric water likely to associate with the solids on exposure to air.

The structures of **3.5A** and **3.5B** are both examples of inefficient crystal packing motifs. The overall shape of the helicates can be roughly approximated to a cylinder, for which a number of possible packing modes can be envisaged. One such mode involves stacking cylinders directly atop one another, which neccesarily leads to one-dimensional channels parallel to the primary axis. This packing mode is represented by **3.5A**, where the helicates are linked along the helical axis by weak interactions with the anions at the termini, leading to one-dimensional channels with six helicates comprising the circumference of each channel. Another possibility would be to pack the cylinders in offset layers, where the cavities in each layer were capped by the layers above and below, leading to zero-dimensional voids, reminiscent of the FCC and HCP motifs of sphere packing. This packing arrangement is represented in the structure of **3.5B**, leading to large pockets of partially localised solvent molecules, but no well-defined channel structures.

*3.3.2 Synthesis of [Co_2(**L3.2**)$_2$(OH_2)$_2$$Cl_2$]·$CoCl_4$·2MeCN **3.6***

Complex **3.6** was prepared by combining ligand **L3.2** with excess $CoCl_2 \cdot 6H_2O$ in warm acetonitrile, giving a gradual colour change from deep blue to dark blue/green. After concentrating the solution by slow evaporation, green crystals of the product deposited, which were isolated by filtration in 14% yield. The crystals were subjected to analysis by single crystal X-ray diffraction, and the data were refined in the monoclinic space group *C*2/*c* (R-factor 4.52%). The structure model revealed a dinuclear double helicate species, where two equivalent cobalt ions are each coordinated in a bidentate fashion by two **L3.2** molecules, and the octahedral coordination sphere of each metal is

completed by one chloride ion and one water molecule in a *cis* arrangement, as shown in Figure 3.10. No significant Jahn-Teller effect was observed in the structure, suggesting the high spin electron configuration for the octahedral cobalt(II) centre. The overall 2+ charge of the helicate species is balanced by the presence of a crystallographically disordered tetrachlorocobalt dianion. An acetonitrile molecule is also included in the asymmetric unit, with no significant interaction to the cationic or anionic species.

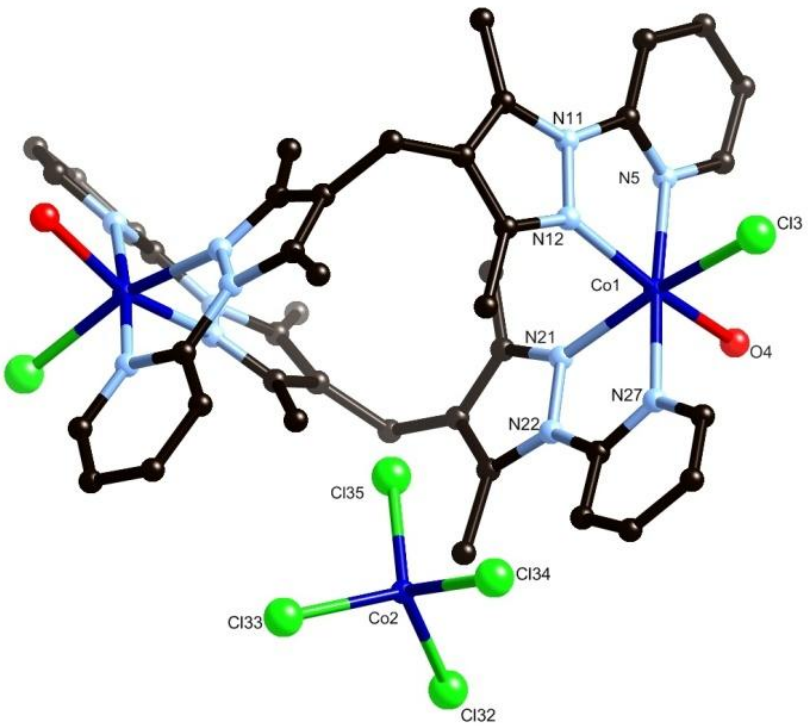

*Figure 3.10: Structure of complex **3.6** with labelling scheme for unique heteroatoms. Hydrogen atoms, acetonitrile molecules and anion disorder omitted for clarity.*

Structurally, the formation of the double helicate requires a degree of flexibility from the ligand backbone. Significant deviations from planarity are observed in each of the two unique pyridylpyrazole conjugated systems, with pyridyl-pyrazole mean interplanar angles of 13.66(15) and 16.48(16)°. Both helical strands are identical and related by a twofold axis passing orthogonal to the helical axis, and parallel to the *b* edge. The angle representing the flexure of the methylene spacer of 115.4(4)° is slightly larger than that observed in the structures of **3.5A** and **3.5B**, while the angle between mean planes of pyrazole rings on the same strand of 99.31(16)° is significantly larger than that observed for the two structures of **3.5**. The metal-metal distance of 9.0171(10) Å is also considerably larger than that observed for the triple helicate species; this observation can be

rationalised by examining the twisting of each pyrazolylpyridine subunit relative to the other. In comparison to the **3.5** helicates, the two binding sites of each **L3.2** molecule in **3.6** are oriented further towards a *trans*-type orientation than that seen in **3.5**, as shown by the smaller φ_1 and φ_2 angles of 125.9(5) and 112.8(5)°. This rotation seems most likely due to steric hinderance from the pyrazole methyl groups, forcing the metal sites further apart. The structural differences between single strands of **3.5** and **3.6** can be seen in Figure 3.11 below.

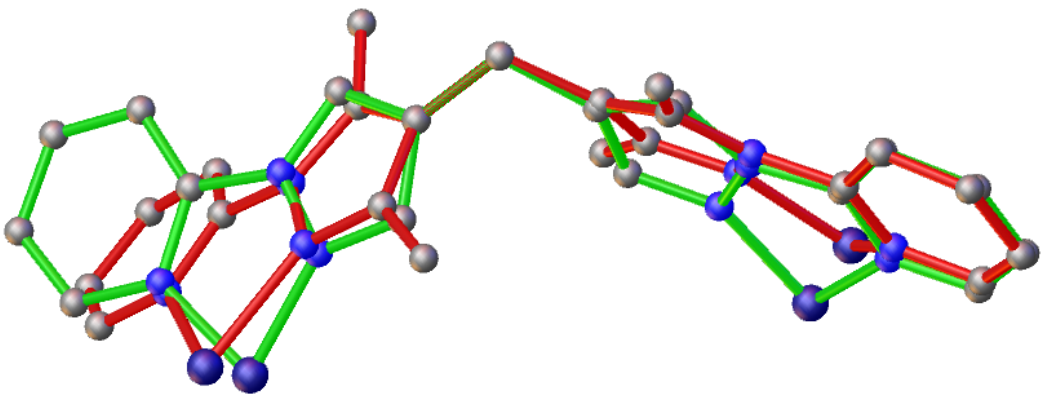

*Figure 3.11: Single helicate strands of **3.5B** (Green) and **3.6** (Red), using the methylene bridge and adjacent atoms as anchor points. The displacement of the metal sites into and out of the page is greater for **3.6**, causing an increased metal-metal separation.*

As shown in Figure 3.12, complex **3.6** exhibits two hydrogen bonding interactions involving the hydrogen atoms of the coordinating water molecule. Adjacent molecules are linked by the 8-membered hydrogen bonding ring, linked by O-H···Cl interactions at the ends of each helicate (D···A distance 3.168(3) Å), which propagates a 1-dimensional chain. The disordered chlorine atoms of the tetrachlorocobalt anion also engage in hydrogen bonding to the other hydrogen atom of the coordinated water; however, due to the nature of the anion disorder it should be stressed that the 1-dimensional chains are not physically linked in this manner. As a result of these interactions, the structure as a whole is relatively well-ordered. Despite a moderate degree of conjugation at the head groups, complex **3.6** exhibits only very minor π-π stacking interactions in the solid state, where full overlap is prohibited by the steric bulk of the chloride ions protruding from the nearby metal binding sites.

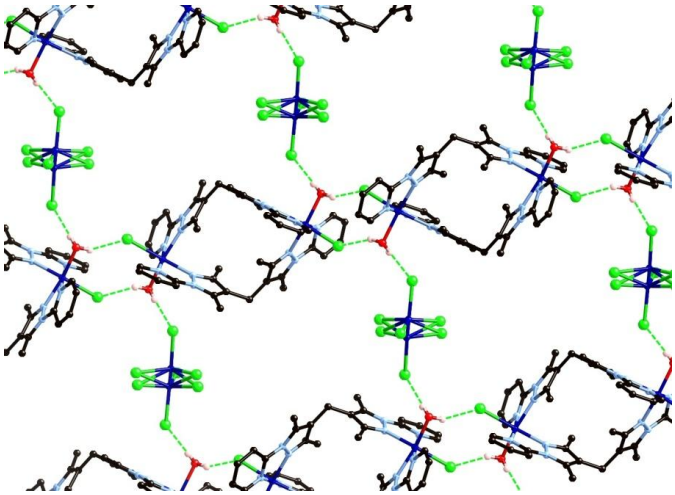

*Figure 3.12: Extended structure of **3.6** viewed parallel to the b unit cell axis. Hydrogen atoms not involved in hydrogen bonding, and acetonitrile molecules omitted for clarity. Tetrachlorocobalt anion shown disordered across two equivalent orientations.*

Thermal analysis of **3.6** shows a broad mass loss of *ca.* 11% initating close to room temperature and centred at approximately 120 °C, consistent with the loss of both acetonitrile molecules and both coordinating water molecules. The high temperature of the transition is likely due to the requirement for a structural rearrangement to allow loss of the acetonitrile molecules, due to the relatively dense packing of the low temperature structure. This transition is followed by a two step decomposition process, with *-dM/dT* maxima at 290 °C and 400 °C. Elemental analysis on a dry sample suggested some loss of lattice acetonitrile on drying in air, being consistent with a formula of $[Co_2(\mathbf{L3.2})_2(OH_2)_2Cl_2]\cdot CoCl_4\cdot 1.5MeCN$.

*3.3.3 Synthesis of $[Ni_2(\mathbf{L3.2})_2Cl_2]\cdot x(MeCN)\cdot x(H_2O)$ **3.7***

Following the successful preparation of **3.6** above, ligand **L3.2** was reacted with $NiCl_2\cdot 6H_2O$ in an attempt to generate an analogous complex. Immediate precipitation was observed when directly mixing the metal and ligand in methanol or acetonitrile and heating at atmospheric pressure, and as such the two components were combined under solvothermal conditions in acetonitrile solution. Large green crystals of the product were formed in 40 % yield; however, these crystals were observed to lose single crystallinity almost instantly on removal from the mother liquor, even when immersed in oil, to give a blue powder which was found to be entirely amorphous by powder diffraction. As such, a single crystal for diffraction was mounted on a glass fibre under oil as quickly as possible and

immediately transferred to the cold gas stream of the diffractometer, where the crystal was sufficiently stable to allow collection of a full data set. Notably, **3.7** also crystallised in the space group *C*2/*c* (R-factor 3.52%), and with a very similar cell volume as **3.6**, although with some difference in length of each unit cell edge. The asymmetric unit of **3.7** was found to contain one Ni(II) ion, coordinated in an octahedral environment to two chloride ions in a *cis* arrangement, and two bidentate pyridylpyrazole groups from **L3.2**. When viewing the extended structure of **3.7**, a structurally similar dinuclear double helicate to **3.6** is observed, with additional chloride ions in the place of the previously observed water molecules, giving an overall neutral species.

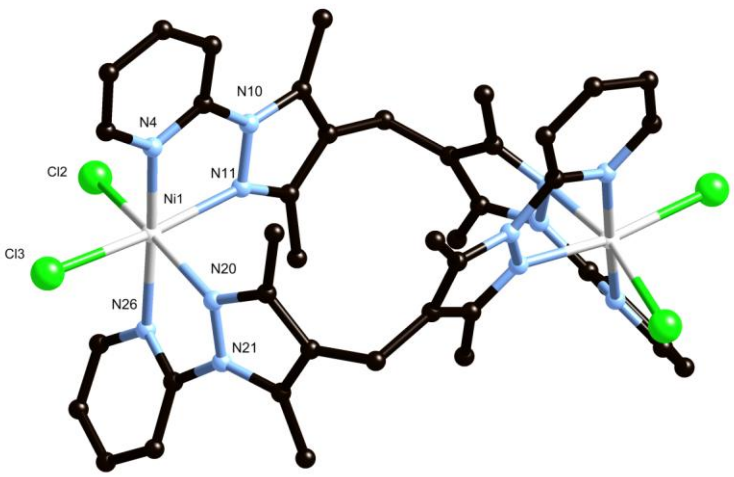

*Figure 3.13: Structure of **3.7** with unique heteroatom labelling scheme. Hydrogen atoms omitted for clarity.*

The two crystallographically equivalent **L3.2** molecules within the complex display varied geometrical parameters to that seen in **3.6**; a slightly longer metal-metal separation of 9.0815(10) Å is observed, caused by smaller φ_1 and φ_2 angles of 114.9(7) and 109.0(8)°, while the pyridyl-pyrazole mean interplanar angles of 10.17(10) and 34.65(9)° are significantly deviated from that previously observed, as is the pyrazole-pyrazole interplanar angle of 107.28(9)°. These deviations can be seen when the helicate structures are overlaid (Figure 3.13), suggesting the main source of the discrepancy to be the twisting of the pyridine head groups in **3.7**, possibly in order to accommodate the more sterically congested coordination sphere caused by incorporation of the second chloride ion.

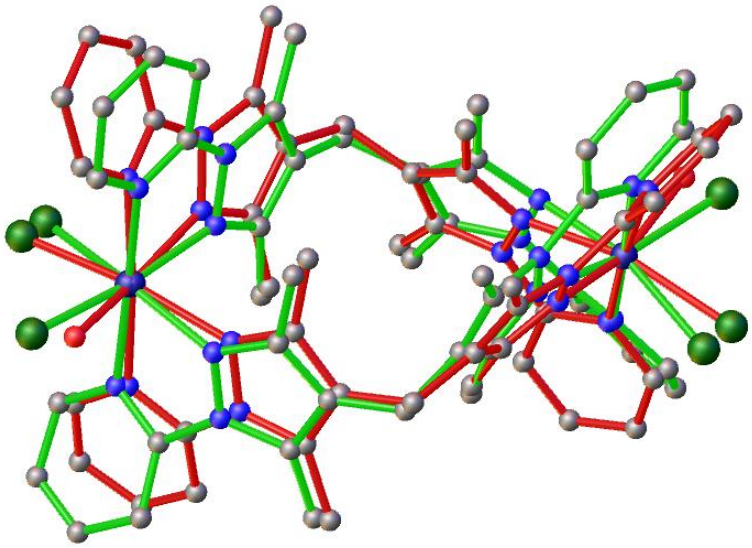

*Figure 3.13: Overlaid structures of **3.6** (Red) and **3.7** (Green), using metal ion positions as anchor points. Hydrogen atoms omitted for clarity.*

While the structure of complex **3.7** itself could be well established from the crystallographic model, a large amount of disordered solvent was also present within the lattice. In order to provide the best precision for the complex itself, the SQUEEZE routine was once again applied to the model,[246] which suggested occupancy of 396 electrons per unit cell, or approximately 5 acetonitrile molecules per helicate. This data was consistent with the thermal analysis of a freshly isolated sample, which showed approximately 17 % loss of mass on heating with onset at room temperature, also consistent with 5 acetonitrile molecules per helicate. Close examination of the position of these areas of diffuse electron density provided insight into the extreme instability of the crystals on drying. All of the located solvent molecules reside within a series of one-dimensional channels running parallel to the *c* edge, showing no significant interaction with the complex. As such, the solvent molecules would be expected to rapidly escape from the crystal when exposed to air, causing a loss of crystallinity. Indeed, the structure of **3.7** contains little to no significant intermolecular interactions, with a broadly similar mode of crystal packing to **3.6**, though without the stabilising interaction of intermolecular hydrogen bonding, nor the hydrogen bond-anchored tetrachlorometallate to prevent solvent channel formation. As shown in Figure 3.14, comparison of **3.6** viewed along the [1,0,1] vector and **3.7** viewed parallel to the *c* edge shows a clear similarity between the 'filled' channel structure of **3.6** and the open channel structure of **3.7**. The colour change from green to blue on drying is likely due to some change in the coordination sphere of the nickel following framework collapse; elemental analysis data of the dry sample, collected approximately one week after isolation, suggests a formula

of $[Ni_2(\mathbf{L3.2})_2Cl_4]\cdot 7H_2O$, implying a substantial amount of water associated with the solids on drying in air. Under these circumstances, the colour change following framework collapse is most likely due to hydrolysis of one or both of the coordinating chloride ions by atmospheric water molecules.

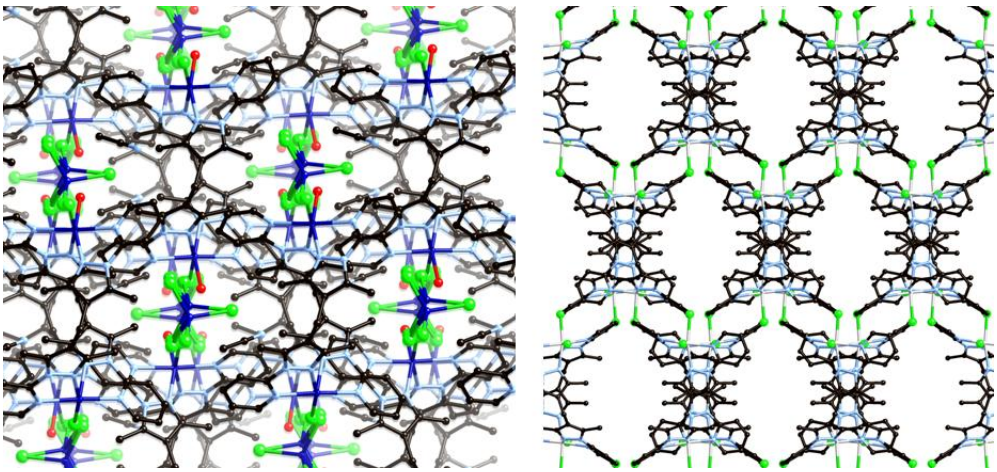

*Figure 3.14: Comparison of the large-scale crystal packing of complexes **3.6** (left) and **3.7** (right), showing the equivalent channel network filled with tetrachlorocobalt anions in **3.6** and empty in **3.7**.*

3.4 Synthesis of Dinuclear L3.2 Copper Complexes

*3.4.1 Synthesis of [(**L3.2**)Cu_2Cl_4] **3.8***

Due to the presence of methyl groups in the 3- and 5-positions of each pyrazole ring on **L3.2**, which can otherwise display susceptibility to nucleophilic attack and ring opening decomposition under harsh conditions, additional coordination chemistry was able to be explored under solvothermal conditions, compared with **L3.1** which displayed poor stability under these conditions. Attempts to generate crystalline samples of a copper(II) chloride complex of **L3.2** at room temperature had failed, due to the insolubility of the complex in common solvents, and rapid precipitation when recrystallised by vigorous heating. Ligand **L3.2** was then reacted with $CuCl_2\cdot 2H_2O$ in acetonitrile under solvothermal conditions. The dark green crystals, obtained in 75 % yield, were analysed by single crystal X-ray diffraction, and the data solved and the structure model refined in the monoclinic space group $P2_1/c$ (R-factor 3.38%). As shown in Figure 3.15, the asymmetric unit of **3.8** contains one molecule of **L3.2** coordinating to two Cu(II) ions in a bis-bidentate fashion, with the copper coordination spheres being completed by two coordinating chloride ions each.

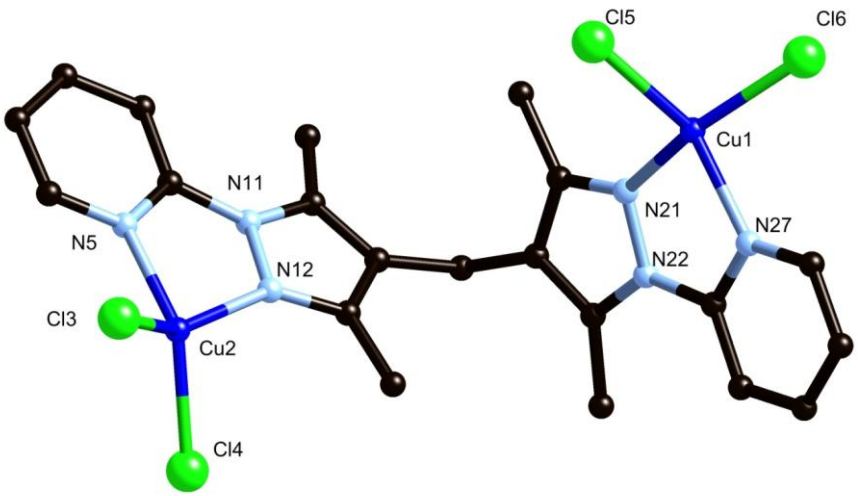

*Figure 3.15: Structure of **3.8** with heteroatom labelling scheme. Hydrogen atoms omitted for clarity.*

The geometry of each copper ion can be characterised as intermediate between square planar and tetrahedral; the *cis* angles within the coordination sphere range from approximately 80 to 100°, although the deviation from square planar geometry can be shown by examining the angular offset of the N-Cu-N and Cl-Cu-Cl mean planes, which reveal values of 38.37(8)° and 47.40(9)° for Cu(1) and Cu(2), respectively, while the τ_4 values of 0.40 and 0.49 also agree with this assessment.[275] This degree of distortion from planarity can be explained in part by the steric clash of the chloride ions with the nearby pyrazole methyl groups, which prohibit strictly square planar geometry, while a purely tetrahedral geometry is likely disfavoured by the comparatively small N-Cu-N bite angles of 80.25(11)° and 79.75(11)° for Cu(1) and Cu(2), respectively. Variations in the coordination geometry between the two copper ions may be due to slightly differing degrees of C-H···Cl hydrogen bonding between the two chloride pairs, as discussed below. The metal-metal separation of 8.7327(6) Å is slightly shorter than that observed for the double helical species **3.7** above, while the methylene bridge angle of 113.0(3)° is slightly smaller, as are the pyridine-pyrazole interplanar angles of 4.92(12) and 8.27(12)°, as well as the pyrazole-pyrazole interplanar angle of 98.11(12)°. The torsion angles φ_1 and φ_2 of 109.5(4) and 120.8(4)° are also comparable with those observed in the double helical species **3.6** and **3.7**.

As the structure of complex **3.8** contains no classically defined hydrogen bond donors, and no solvent molecules or significant void space, the crystal packing seems defined by minor π-π interactions and numerous C-H···Cl interactions throughout the structure, *i.e.* C(24)-H(24A)···Cl(3) with d(D-A) 3.636(4) Å. Although a very weak P4AE-type interaction exists between the internal

faces of adjacent molecules, the mean interplanar distance of 4.026(3) Å for the parallel π-systems and minimum C···C edge-to-face distance of 4.291(5) Å are too long to be considered significant attractive interactions. Instead, a π-π interaction between the convex faces of two angled planes, with minimum C···C distance 3.326(5) Å for C(15)-C(29), and mean interplanar angle of 18.65(10)°, provides the most significant source of attractive intermolecular interactions, as shown in Figure 3.16. This lack of strong intermolecular interactions can be ascribed to the out-of-plane steric bulk of the chloride atoms bonded to each copper, preventing the nearby conjugated aromatic systems from engaging in more efficient overlap with adjacent systems.

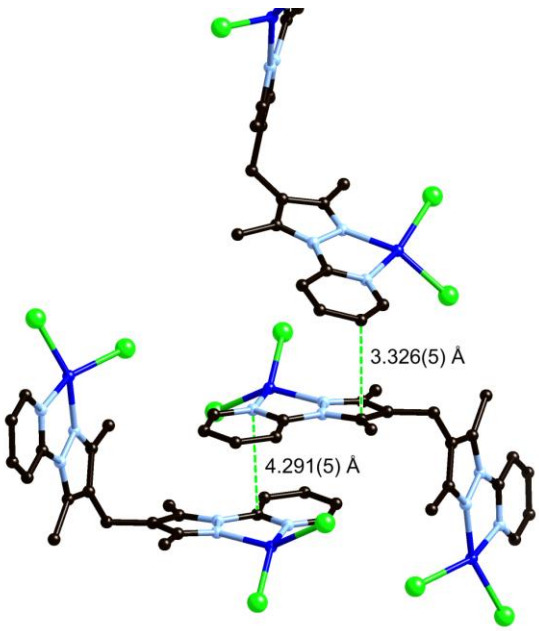

*Figure 3.16: Comparison of possible π-π interaction modes in the structure of **3.8***

*3.4.2 Synthesis of [Cu_2(**L3.2**)($CH_3COO)_4(OH_2)_2$]·$6H_2O$] **3.9***

The title compound was prepared by combining the ligand with two equivalents of $Cu(CH_3COO)_2 \cdot H_2O$ in acetonitrile, and concentrating the solution by slow evaporation, forming blue crystals in 33 % yield. The crystals were analysed by single crystal X-ray diffraction, and the data solved and the structure model refined in the monoclinic space group *C*2/*c* (R-factor 2.67%), to provide a structure model revealing one molecule of **L3.2** coordinating to two equivalent copper ions, the coordination spheres of which were completed by two monodentate acetate ions and a water molecule as shown in Figure 3.17. The metal coordination geometry can be described as square

pyramidal, with the axial coordination site occupied by the water molecule displaying an elongated bond length of 2.2732(15) Å. The metal-metal separation of 9.6209(5) Å is significantly longer than that observed in the previously described structures, caused by an almost entirely *trans* orientation of the two binding sites, with pyrazole-pyrazole interplanar angle 109.21(11)° and equivalent torsion angles φ_1 and φ_2 of -107.1(2)°. The relatively large pyridine-pyrazole interplanar angle of 19.55(8)° suggests a moderate degree of distortion from ideal geometry.

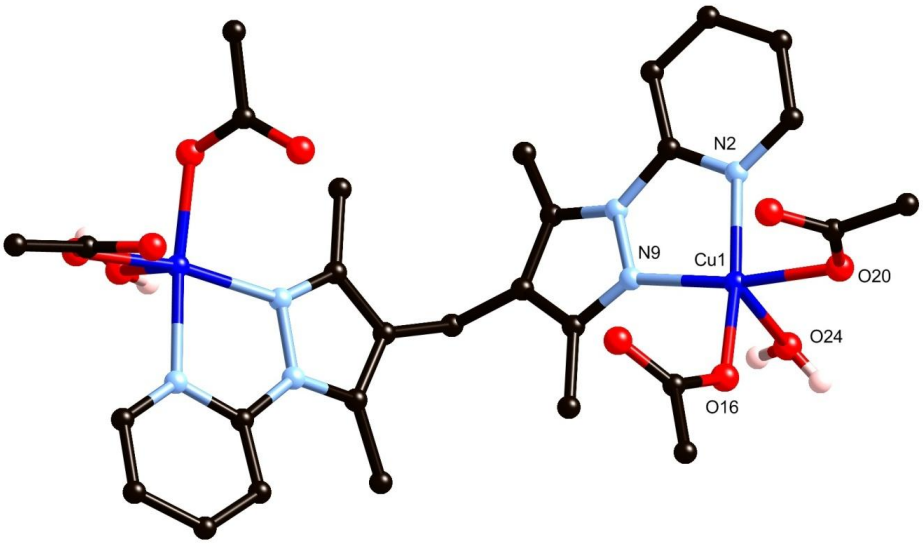

*Figure 3.17: Structure of **3.9** with coordinating atom numbering scheme. Non-coordinating water molecules and hydrogen atoms omitted for clarity with the exceptions of H24A and H24B as shown.*

The extended structure of **3.9** is dominated by the presence of three non-coordinating water molecules per asymmetric unit, which participate in significant hydrogen bonding interactions with the coordinating water and acetate moieties. When all physical linkages and hydrogen bonding interactions are considered, the complete structure is revealed as a complex 3-dimensional network. In order to form a sensible topological description of the complex, nodes were placed at each copper site and allowed to incorporate the connectivity of the coordinating water molecules. The resulting node is 7-connected, with one connection to another copper site *via* **L3.2**, and six connections to other nodes *via* hydrogen bonds donated or accepted by the coordinated water or acetate molecules. Each of the three non-coordinating water molecules in the asymmetric unit links together three other nodes, so each must also be considered a node. With this simplification, the network can be considered a 3,3,3,7-connected tetranodal network. A schematic of the full network can be seen in Figure 3.18

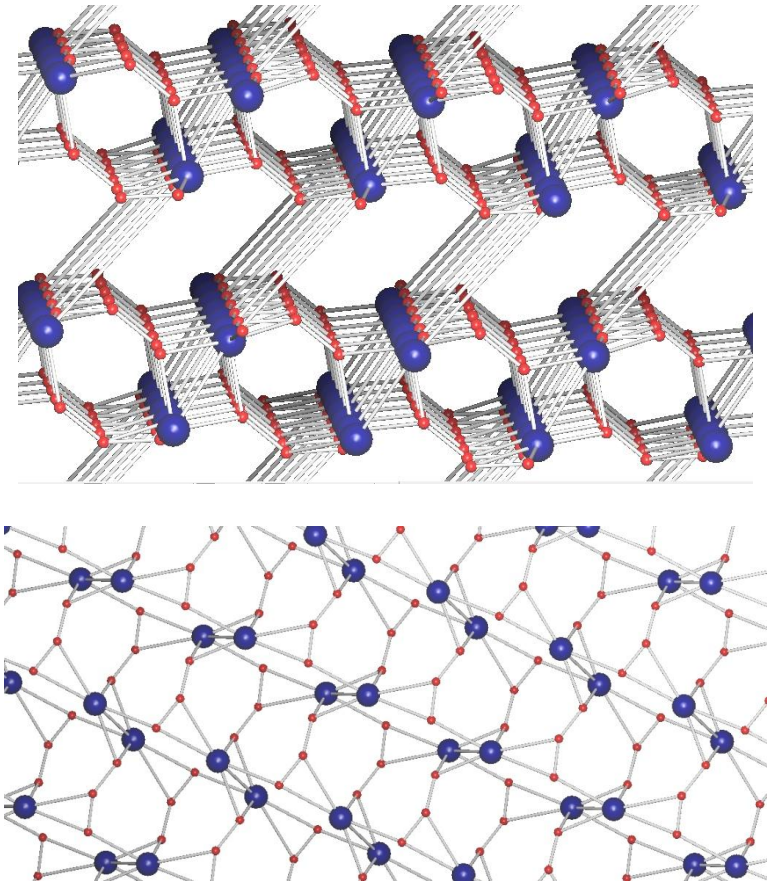

*Figure 3.18 (Top): Topological representation of the hydrogen bonding network of **3.9**, where blue spheres represent the copper coordination sphere and red spheres represent each of the three non-coordinating water molecules. The long linkages represent links via **L3.2**. (Bottom) Schematic of the two-dimensional layers formed by disregarding copper linkages via **L3.2**, viewed from the plane normal.*

In a physical sense, the network of **3.9** can be easier visualised by considering separate 2-dimensional hydrogen bonding sheets, which are then linked into the third dimension by copper-copper linkages *via* **L3.2**. As shown in Figure 3.15 above, this sheet consists of tightly bound hydrogen bonded metal-site dimers linked into sheets by linear trimers of non-coordinating water molecules, the physical basis of which is shown in Figure 3.19. In the cases of such densely interconnected networks, a point symbol is sufficiently cumbersome to be of little practical value; however, a nominal point symbol, as calculated by the ADS routine within TOPOS,[333] of (3.6.7)(3.7.8)(3.7^2)(3^3.4.6^4.7^7.8^3.9^2.10) can be assigned to the full network, where the 2-dimensional sheets generated by ignoring the **L3.2** linkages is described by the point symbol (3.6.7)(3.7.8)(3.7^2)(3^3.4.6^2.7^6.8.9.10). Some apparant π-π interactions are also observed between complexes in **3.9**; however, the long interplanar distance of 3.9957(17) Å between concave faces of **L3.2** units suggests this arrangement is merely the maximisation of

crystallographic density rather than a significant attractive interaction, and provides minimal structural impact compared with the influence of the hydrogen bonding.

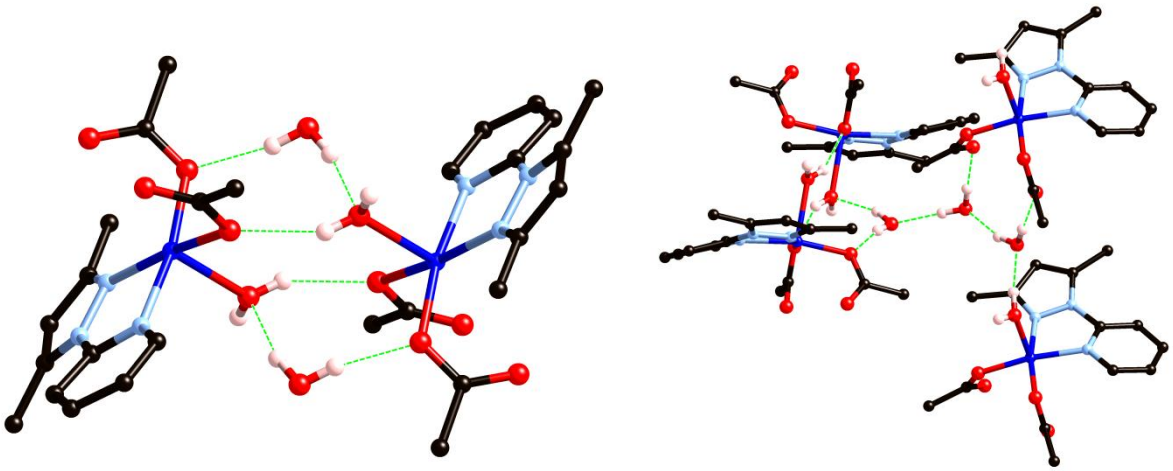

*Figure 3.19: Structures of representative hydrogen bonding synthons in the structure of **3.9**; (left) the hydrogen bonded dimer of copper sites formed by direct interactions and supported by crystallographically equivalent non-coordinating water molecules, and (right) the structure of the linear trimer of non-coordinating water molecules with representative hydrogen bonding. For simplicity, non-hydrogen bonding hydrogen atoms and half of each **L3.2** molecule not shown.*

When a sample of **3.9** was heated to 110 °C for 5 minutes, the loss of solvent resulted in the formation of a green amorphous solid. The solid was analysed by infrared spectroscopy, which showed the loss of the very broad hydrogen bonding O-H stretches at 3062 and 2262 cm^{-1} and substantial diminishing of the non-coordinating carbonyl stretch at 1696 cm^{-1}, while the spectrum from 1600-450 cm^{-1} remained largely unchanged. From this data it seems likely that the green material has lost both the coordinating and lattice water molecules, with the result that the copper coordination sphere has been altered to potentially include one or more bidentate carboxylates.[334] However, due to the amorphous nature of the material produced, no further structural characterisation could be undertaken. Thermogravimetric analysis of **3.9** showed a mass loss of *ca.* 17% by 80 °C, consistent with loss of all lattice and coordinated water molecules (four molecules of H_2O per metal ion), an observation in agreement with the infrared data of the dehydrated product. The comparatively low temperature of water loss in this case is likely due to the slow heating (1 °C/min) and N_2 flow conditions of the TGA apparatus, combined with the columnar nature of the included guest molecules which likely facilitates rapid loss of water under such conditions.

3.5 Solvothermal Synthesis of Polynuclear Copper Complexes of L3.2

*3.5.1 Synthesis of poly-[Cu_2(**L3.2**)$(NO_3)_4$] **3.10***

When reacted with $Cu(NO_3)_2 \cdot 3H_2O$ in acetonitrile under solvothermal conditions, **L3.2** formed several different crystalline compounds, depending on the reaction conditions. A gentle heating mode, in which the pressure vessel was subjected to a three-stage ramping cycle, produced green block crystals, while more vigorous reaction conditions incorporating a 36 hour dwell period produced large blue blocks, along with a small quantity of green needles and yellow plates. The blue blocks could also be produced by adding small quantities of aqueous nitric acid to the lower temperature reaction mixture, or by using Teflon liners which had not been subjected to a rinse cycle after washing with nitric acid as the reaction vessel. A fourth phase of blue/green blocks appeared in very small yield when the nitric acid concentration was increased even further.

Crystals of complex poly-[Cu_2(**L3.2**)$(NO_3)_4$] **3.10** formed in 63 % yield under mild solvothermal conditions in acetonitrile, in which the pressure vessel was heated to 90 °C, then slowly ramped to 120 °C and then cooled with no dwell period. The asymmetric unit of **3.10**, which crystallised in the orthorhombic space group *Pbca* (R-factor 2.62%), contains one molecule of **L3.2** in its entirety, coordinating to two non-equivalent Cu(II) ions in the expected bis-bidentate mode. Each metal ion is bound in a five coordinate square pyramidal fashion, with two binding sites occupied by **L3.2** and three sites occupied by nitrate anions, two of which bridge to adjacent metals. The axial Cu-O bond is lengthened at both sites, with d(Cu-O) = 2.2907 Å for Cu(1)-O(37) and 2.3714(15) Å for Cu(2)-O(41). Geometrically, ligand **L3.2** behaves in a similar manner to previously described structures, with a metal-metal separation of 9.0782(5) Å and pyrazole-pyridine interplanar angles of 16.62(8) and 10.73(8)°, although the binding sites in **3.10** exist in a *cis*-type arrangement, as evidenced by opposing φ_1 and φ_2 angles of -126.3(2) and 61.6(3)°, and a pyrazole-pyrazole interplanar angle of 86.26(8)°. The structure of **3.10** is shown in Figure 3.20.

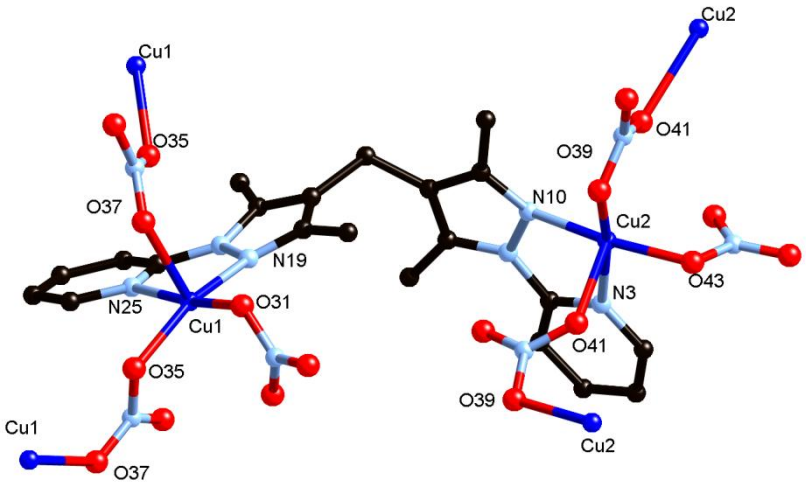

*Figure 3.20: Structure of **3.10** with heteroatom labelling scheme. Hydrogen atoms omitted for clarity.*

When extended through the bridging nitrate anions, **3.10** displays an undulating 2-dimensional (6,3) network shown in Figure 3.21, in which short links *via* nitrate bridges propagate one-dimensional chains parallel to the *b* edge, which are linked in the *a* direction by **L3.2** units. The undulation in the *c* direction encompasses two **L3.2** links, for a total peak-to-trough amplitude of 17.5148(7) Å, calculated as the mean interplanar distance for planes of equivalent copper ions at the peaks and troughs of the sheet. While no significant intermolecular interactions are present within each sheet, adjacent sheets interact with each other *via* convex-face offset face-to-face π-π stacking interactions, at mean interplanar distance 3.6457(16) Å. The packing of each sheet is such that these interactions only occur at the Cu(2) ends of the **L3.2** molecules, those at the peaks and troughs of the undulating sheet; the Cu(1) ends of the **L3.2** are shielded further within each network, and do not experience any significant intermolecular interactions.

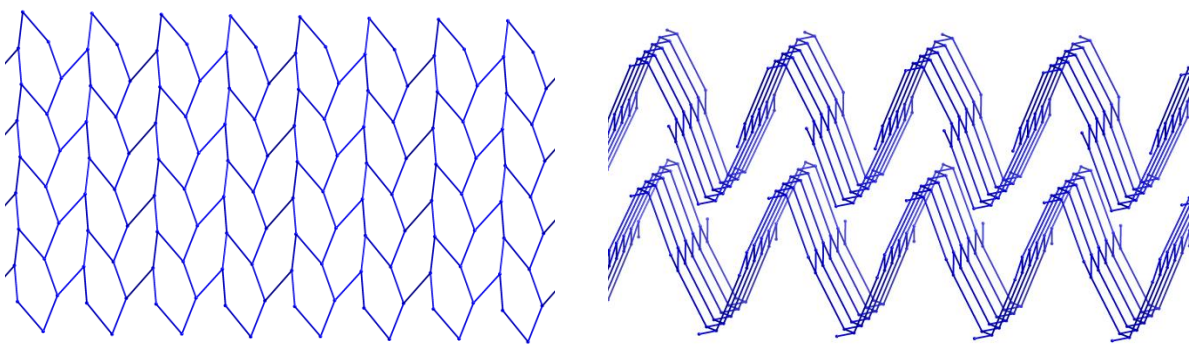

*Figure 3.21: Schematic representations of the two-dimensional network of **3.10**, viewed perpendicular to the plane (left) and view of two independent coplanar networks (right). Metal ions chosen as nodes.*

*3.5.2 Synthesis of [$Cu_2(NO_3)_2$(μ-CH_3CONH)(μ-OH)(**L3.2**)]$_2$·x(H_2O) **3.11***

Complex [$Cu_2(NO_3)_2$(μ-CH_3CONH)(μ-OH)(**L3.2**)]$_2$ **3.11** was first prepared by combining ligand **L3.2** with an excess (4 equivalents) of $Cu(NO_3)_2·3H_2O$ in acetonitrile and heating under solvothermal conditions with 24 hour dwell period at 120 °C, providing blue crystals of **3.11**, as well as small amounts of **3.12** and **3.13**, in approximately 80:10:10 proportions. It was found that compound **3.11** could be produced as a pure phase in 61% yield by increasing the quantity of metal salt in the reaction mixture to 5 equivalents, which simultaneously suppressed the formation of **3.12** and **3.13**. The dark blue block crystals of complex **3.11** were subjected to single crystal X-ray diffraction, and the data were solved and the structure model refined in the monoclinic space group *C*2/*m* (R-factor 4.66%). The asymmetric unit was found to contain a single 5-coordinate square pyramidal copper ion coordinated by one disordered nitrate anion, one hydroxide anion, one half unit of **L3.2** in a bidentate fashion, and one additional donor species. The identity of the unknown ligand species, four atoms in an elongated trigonal planar arrangement, was not immediately obvious, but was assigned from a number of observations. The bridging oxygen species was assigned as hydroxide rather than oxide or water, based on the Cu-O bond length of 1.9056(17) Å, as well as crystallographic localisation of the attached hydrogen atom, which engaged in hydrogen bonding with the nearby nitrate ligand, and the observation of an O-H stretching mode in the infrared spectrum (2931 cm^{-1}). Charge balance considerations therefore required a monoanionic species for the bridging trigonal ligand. The longest bond from the central atom, 1.493(7) Å, was assigned to a C-CH_3 bond, being too long for an N-O (nitrate) bond, an assignment supported by the best matching of the electron density from the terminal atom to carbon, based on evaluating U_{eq} and R-factor values for C, N or O. Chemically sensible species of the appropriate size and coordination capability include the acetate anion or singly-deprotonated acetamide, disordered over two orientations about the central mirror plane. Both options were tested and displayed approximately equal crystallographic fit. The relevant areas of the infrared spectrum were generally complicated by the other functional groups present in the molecule; however, elemental analysis was consistent only with a coordinated acetamide anion, although this assignment remains somewhat tentative, due to the uncertainty in the level of solvation present, as discussed below. The origin of the bridging species can be ascribed to solvothermal hydration of acetonitrile in the presence of free metal ions (or, indeed, in the presence of a [Cu(**L3.2**)] complex), a process known on the industrial scale.[335]

Examining the bulk structure reveals a cyclic Cu_4 tetramer, formed from the asymmetric unit containing one copper ion by a twofold axis and orthogonal mirror plane, in which two **L3.2** molecules coordinate two copper ions each, which are themselves connected by the μ_2-hydroxido

species and the bridging acetamide. The geometry of the **L3.2** ligand is similar to that described above; the pyridyl-pyrazole interplanar angle (10.76(12)°), intra-ligand metal-metal separation (8.3302(12) Å), pyrazole-pyrazole interplanar angle (98.57(18)°) and equivalent φ_1 and φ_2 torsion angles (-118.9(9)°) all agree well with those described above, although the metal-metal distance is somewhat shorter due to the confined environment of the ligand imposed by the metallomacrocyclic enclosure formed by the additional bridging ligands. The metal-metal separation across the hydroxido/acetamido bridge is 3.1718(8) Å. The structure of the tetramer is shown in Figure 3.22.

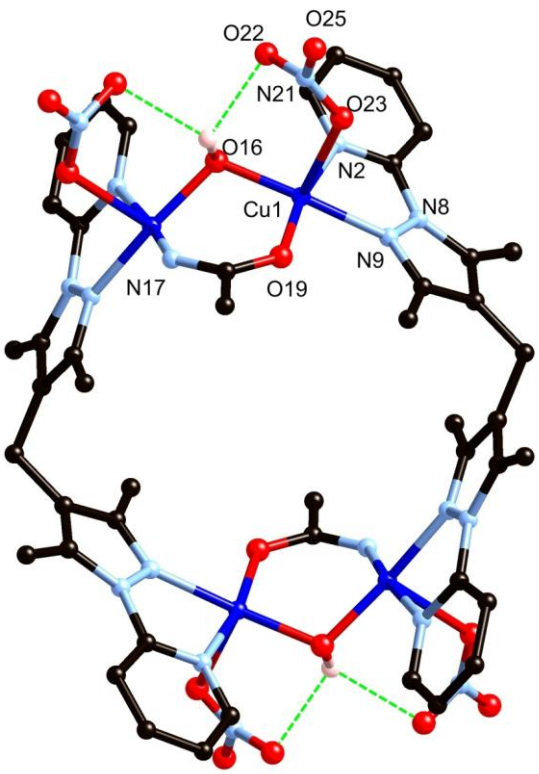

*Figure 3.22: Structure of complex **3.11** with unique heteroatom labelling scheme. Non-hydrogen bonding hydrogen atoms and nitrate disorder omitted for clarity. Acetamide ligand shown in one possible orientation.*

The intermolecular interactions in **3.11** are largely dominated by π-π stacking between pyridylpyrazole moieties on adjacent complexes. The π-π stacking interaction, repeated on each of the four external faces of the molecule, occurs between parallel head groups at an average interplanar distance of 3.504(17) Å. This interaction, combined with the lack of significant interactions parallel to the central cavity, results in large scale alignment of individual units of **3.11** around one-dimensional channels, shown in Figure 3.23. Two types of channels are present – the largest, with void dimensions

ca. 8 × 8 Å interatomic distance, running through the central cavity of the molecule, and the other, *ca.* 9 × 4 Å interatomic distance, resulting from the repulsion of outward facing nitrate moieties on the corners of each complex. Unsurprisingly, these solvent channels contained significant numbers of guest molecules, which despite exhaustive efforts were not able to be modelled crystallographically. As such, the SQUEEZE routine in PLATON was applied in order to generate a satisfactory structural model for the complex itself.[246] Thermal analysis of the compound suggested a slow mass loss of 4.5% up to 150 °C, followed by a multi-step decomposition process. Elemental analysis suggested the volatile material was most likely water, either retained from the synthesis or taken up following loss of crystallinity on drying in air, with 3.5 water molecules per tetramer providing the best match of elemental and thermogravimetric analyses.

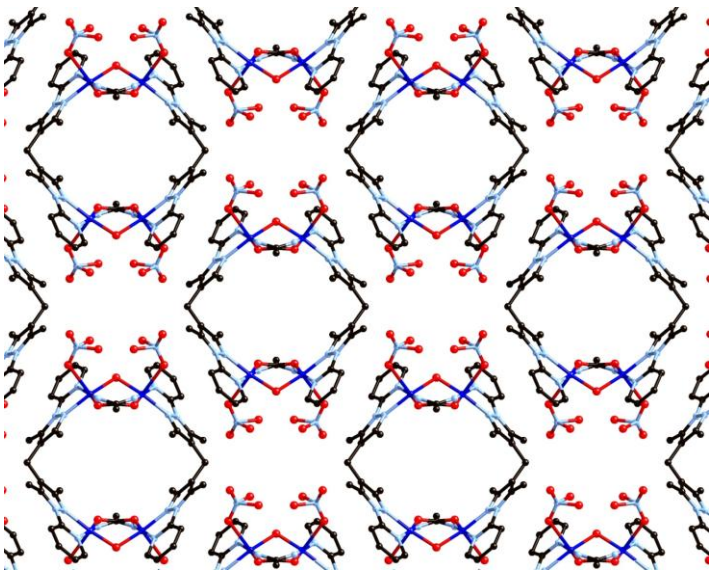

*Figure 3.23: Packing diagram of complex **3.11** viewed parallel to the c unit cell axis. Hydrogen atoms omitted for clarity.*

*3.5.3 Synthesis of poly-[(**L3.2**)Cu(C_2O_4)(NO_3)]·x(H_2O)·x(MeCN) **3.12***

Several crystals of complex poly-[(**L3.2**)Cu(C_2O_4)(NO_3)] **3.12** were initially prepared as a minor product in the same reaction mixture as **3.11**, by combining four equivalents of copper nitrate with the **L3.2** ligand in acetonitrile and heating in a sealed vessel, providing a mixture from which single crystals of **3.12** were manually isolated and subjected to X-ray diffraction, where the data obtained were solved and the structure model refined in the monoclinic space group *P*2/*n* (R-factor 5.05%). The asymmetric unit contains one half of an **L3.2** ligand coordinating in a bidentate fashion to a Cu(II) ion, which is coordinated in a square pyramidal geometry with a nitrate ligand in the axial site

and an unexpected chelating moiety occupying the other two coordination sites. Close inspection of the electron density peaks and the subsequent bond lengths, combined with a prominent infrared absorbance at 1655 cm^{-1} and charge balance considerations, suggested the extra ligand was the oxalate dianion, coordinating in a bis-bidentate bridging mode, as shown in Figure 3.24. Once the identity of the bridging ligand was determined, the complex could be prepared as a pure phase in 52 % yield by adding one drop of diethyl oxalate to the reaction mixture. The **L3.2** ligand is arranged in the standard fashion, with a shallow pyridyl-pyrazole interplanar angle of 4.72(16)°, intermediate pyrazole-pyrazole interplanar angle of 89.0(2)°, equivalent torsion angles φ_1 and φ_2 of 120.9(4)° and metal-metal distance of 8.3663(13) Å.

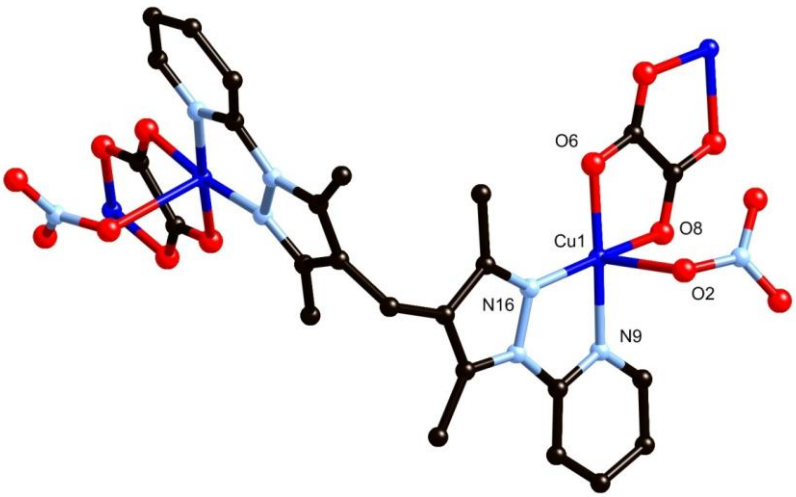

*Figure 3.24: Repeat unit of complex **3.12** with coordinating atom labelling scheme. Hydrogen atoms omitted for clarity.*

The extended structure of **3.12** reveals a one-dimensional zig-zag coordination polymer where the shape is largely dominated by the methylene bridge in the centre of the **L3.2** ligand. These strands interact primarily by π-π stacking interactions, where the conjugated pyridylpyrazole systems partially overlap in parallel at an average distance of 3.264(5) Å between convex faces. The presence of the nitrate anions alternating above and below the equatorial planes of the Cu-ox-Cu region prohibit the oxalate moiety from participating in any π-π stacking interactions. This steric effect also results in the unoccupied axial coordination site of the metal ion remaining comparatively accessible. When the structure is grown in three dimensions, the result is a network of one-dimensional polymers containing solvent channels with corners defined by the **L3.2** central cleft, giving walls with largely aromatic character. Each channel contains nitrate ions and unsaturated metal centres at opposing corners, as displayed in Figure 3.25.

The channel contents were able to be approximated crystallographically, with a best fit of 0.75 acetonitrile molecules per copper, disordered over three orientations and entirely filling the channels. The contents of the voids on a freshly isolated sample were shown to be approximately 12 % by mass from thermogravimetric analysis data; however, due to the rapid onset of mass loss on the instrument, this value is expected to vary substantially depending on the drying conditions. The solids were seen to lose crystallinity on prolonged exposure to air, and thermal decomposition occurred with onset at 175 °C. Elemental analysis of a dry sample suggested 1.5 acetonitrile molecules and 1.5 water molecules per two copper ions, matching the volatile contents suggested by thermogravimetric analysis data.

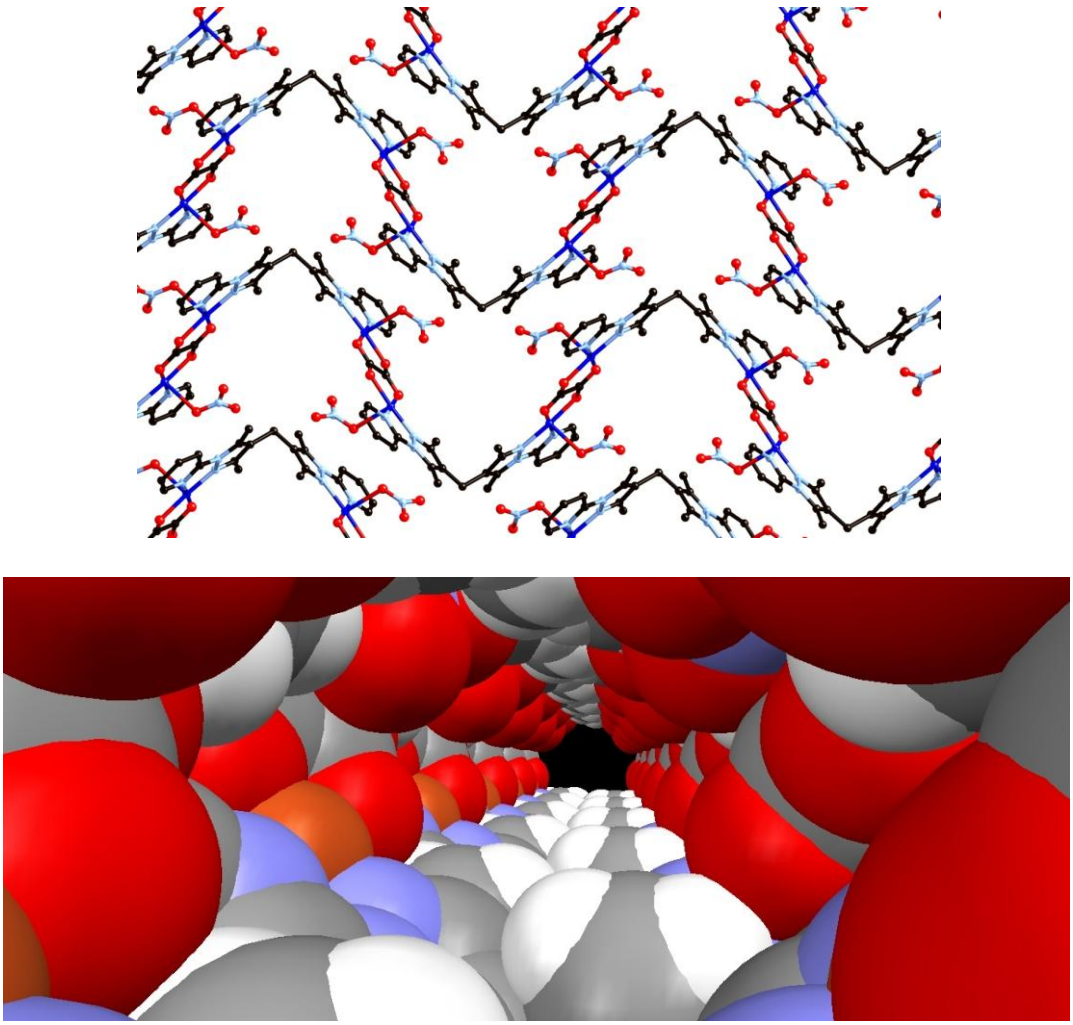

*Figure 3.25: (Top) Representation of the extended structure of **3.12** showing π-π interactions between adjacent chains; (Bottom) Internal surface of a single channel of **3.12**, copper ions coloured orange. Disordered acetonitrile present within pores not shown.*

*3.5.4 Synthesis of poly-[Cu_2(**L3.2**)(μ-CN)$_2$] **3.13***

Complex poly-[Cu_2(**L3.2**)(μ-CN)$_2$] **3.13**, initially formed as a minor component of the crude mixture containing **3.11** and **3.12**, was prepared as a pure phase in 14 % yield by the reaction of ligand **L3.2** with 1.4 equivalents of copper nitrate in acetonitrile under solvothermal conditions with a dwell temperature of 120 °C. The yellow crystals formed were filtered and subjected to single crystal X-ray diffraction, where the data obtained were solved and the structure model refined in the orthorhombic space group *Pccn* (R-factor 3.59%). The structure model suggested the **L3.2** ligand was coordinating in a bis-bidentate fashion to two crystallographically identical copper centres, as shown in Figure 3.26. The tetrahedral coordination sphere of the copper site was completed by an two crystallographically equivalent diatomic bridging ligands. From electron density considerations in the structure model, as well as a prominent infrared absorbance at 2170 cm^{-1} consistent with bridging CN^-, the ligand was identified as the cyanide anion. By the coordination geometry of the metal centres and charge balance considerations, as well as the pale yellow colour of the crystals, it was clear that the metal had been reduced to the cuprous form. The geometry of the **L3.2** ligand showed some discrepancy from that seen in the previous structures, with metal-metal distance 10.4216(7) Å the longest observed for any complexes of **L3.1** or **L3.2**. The pyrazole-pyrazole interplanar angle of 109.7(16)° approaches the maximum possible value, dictated by equivalent φ_1 and φ_2 values of -82.9(3)°, indicating *trans* geometry, leading to a particularly long metal-metal separation. A substantial distortion to the coordination sites were required to accommodate the tetrahedral geometry, with pyridyl-pyrazole interplanar angle of 23.62(10)°.

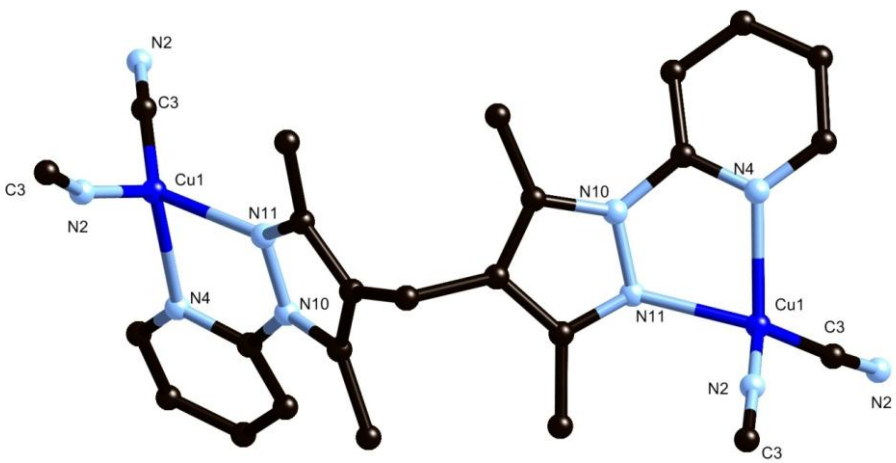

*Figure 3.26: Structure of **3.13** with partial atom labelling scheme, hydrogen atoms omitted for clarity.*

The extended structure of **3.13** can be described as a two-dimensional coordination polymer, where the bridging ligands extend the metal sites into a (6,3) sheet, shown in Figure 3.27. The significant differences in size of the bridging ligands result in severe distortion to the edge lengths of the basic network (10.4216(18) *vs* 4.9537(4) Å). The size of the central cavities of each network (*ca.* 13 Å) necessitates interpenetration of another network, giving a twofold 2D→2D parallel interpenetrated network to maximise density, shown in Figure 3.27. A π-π interaction is observed between pyridylpyrazole units on adjacent interpenetrated sheets, with closest interatomic distance 3.225(4) Å for C(7)-N(4) and average interplanar angle 16.39(11)°, although no significant intermolecular interactions are observed between adjacent pairs of sheets. Due to the high density of the interpenetrated sheets, no significant void space was located, nor were any solvent molecules detected within the lattice.

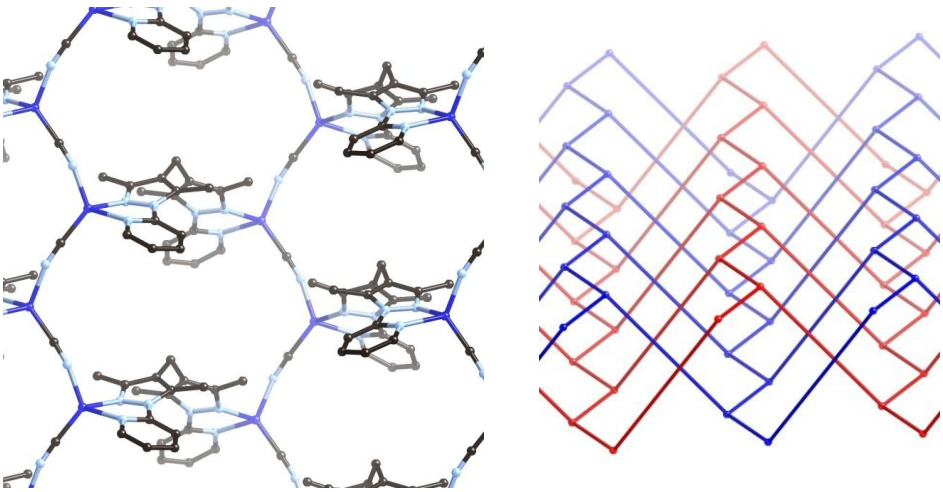

*Figure 3.27 (Left): Single (6,3) sheet of **3.13** showing atom connectivity, hydrogen atoms omitted for clarity. (Right): Interpenetration in **3.13,** independent networks coloured separately.*

3.6 In-Situ Ligand Formation in species 3.10 – 3.13

The origin of the additional ligand species formed *in-situ* was an obvious point of interest in the synthesis of the complexes of **L3.2** prepared solvothermally. In order to determine the specific conditions required to form each species as a pure phase, a number of experiments were carried out in which the metal source, stoichiometry, concentration, heating conditions and presence of additives were varied. In the first instance, complex **3.10** was found to only form under mild heating conditions, where the vessel was rapidly heated to 90 °C, followed by ramping to 120 °C at a rate of 1 °C/hr,

followed by cooling to room temperature at 5 °C/hr. Complex **3.10** could also be formed in heating cycles with a dwell temperature of 100 °C while maintaining the same heating and cooling rates. Despite being comprised of the components used to form the other phases, pure samples of **3.10** could not be used as feedstock to prepare the other complexes, returning no solid material when re-subjected to reaction under solvothermal conditions. Solid samples of **3.10** were observed to decompose energetically on heating in air at 260 °C, presumably due to the densely packed nitrate anions in the vicinity of readily oxidised organic material; whether this decomposition plays a role in the solvothermal system is unknown.

The formation of complex **3.11** was assumed to require a hydrolysis step, in order to prepare sufficient quantities of acetamide to form the required bridging species. With this in mind, it was found that small quantities of **3.11** could be formed under the same mild heating regime as **3.10** when the solution was spiked with small quantities (60 µL or less) of 20 % aqueous nitric acid solution. Addition of excess acid (100 µL of the above mixture) to the reaction mixture formed trace quantities of a crystalline mineral-like structure as the only solid product, which was found by single crystal X-ray diffraction to have the formula $[Cu_4O_3(NO_3)_2]$, suggesting no participation of the ligand at this acid loading, possibly due to decomposition. Complex **3.11** could be prepared as a pure phase by the addition of a greater excess (5 equivalents) of $Cu(NO_3)\cdot 3H_2O$, and by turning to a heating cycle in which the vessel was ramped rapidly to 120 °C and allowed to dwell for 24 – 36 hours, followed by slow cooling to room temperature. This method provided a pure sample of **3.11**, with no visible traces of **3.10** or the other high temperature phases. It is expected that the combination of higher average temperature and higher concentration of free Cu(II) allows the slow formation and complexation of acetamide to remove sufficient quantities of **L3.2** from solution to hinder the formation of **3.10**. Perhaps unsurprisingly, addition of stoichiometric acetamide to the reaction mixture at the start of the reaction failed to increase the yield of **3.11**, instead leading to deposition of brown amorphous material and no isolable products; the effect of larger quantities of acetamide on the solution pH and the potential for the formation of other coordinated species in solution are likely to out-compete the formation of the desired complex.

The formation of **3.12** as a byproduct in the original reaction mixture was unexpected, as a simple reaction pathway from any component of the mixture to the oxalate anion is not obvious. Three plausible sources of oxalate in the solution were considered; a hydrolysis/oxidation of the solvent to form oxalate (by one of several possible pathways), highly oxidative decomposition of the ligand, or fixation of atmospheric carbon dioxide followed by reductive dimerisation. Each of these three mechanistic pathways has been implicated in cases of oxalate formation under solvothermal

conditions, as recently reviewed by Cahill.[336] The possibility of atmospheric carbon dioxide fixation to form oxalate was the simplest to qualitatively test; first, flushing the reaction mixture with nitrogen to remove carbon dioxide, and secondly, by saturating the solution with carbon dioxide. Neither approach was seen to cause a noticable change in the quantity of **3.12** formed by the reaction. Secondly, the oxidation/hydrolysis of acetonitrile was considered. As shown in Scheme 3.4, a number of different pathways for oxalate formation from acetonitrile can be imagined when consideration is given to the highly forcing solvothermal conditions of the reaction, where a movement to the right indicates hydrolysis and movement downwards represents oxidation.

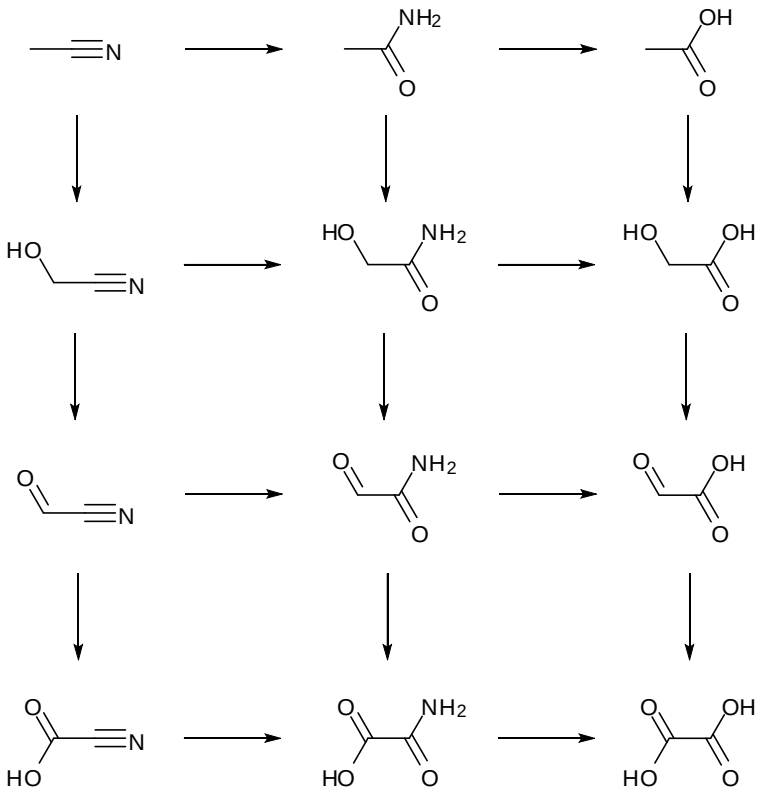

Scheme 3.4: Potential reaction pathways in the conversion of acetonitrile to oxalate. Movement down represents oxidation, and movement to the right represents hydrolysis.

From these considerations it is clear that the formation of oxalate from acetonitrile requires two hydrolysis steps and three oxidation steps, with the most challenging step likely being the first oxidation to the alcohol. With this in mind, a number of possible oxalate precursors were added to the original reaction mixture; acetamide and acetate, the partially and fully hydrolysed species where no oxidation has been undertaken, 2-hydroxyacetic acid, where the nitrile has been fully hydrolysed and the first methyl group oxidation has taken place (incidentally also a key intermediate in the ligand-

based oxalate formation reported by Cahill), and oxamic acid, where the oxidation steps are complete and only one more hydrolysis step is required to form the ligand species. In addition, oxalic acid itself was trialled, as was the use of copper(II) oxalate as the copper species. None of these instances lead to a positive effect on the amount of **3.12** generated, instead giving either no crystalline products or the original mixture of phases, most likely due to causes similar to those suggested for **3.11** above; changes to the solution pH and the formation of other complexes are likely to interfere with the desired process. Finally, diethyl oxalate was used as a slow-release oxalate source, which provided the desired product as a pure phase. From these observations, it seems intuitive that the required co-ligands must be formed slowly *in-situ* such that their presence does not interfere with the formation of any intermediates which may be neccesary for the overall reaction pathway. As a final consideration, pure samples of **3.11** and **3.12** were added to the reaction mixture, to qualitatively test for autocatalytic activity; however, neither compound appeared to influence the outcome of the reaction, suggesting that if a catalytic process involving a [Cu(**L3.2**)] species is involved, the active species is most likely itself an intermediate in the overall reaction. A ligand decomposition pathway cannot be ignored; due to the complex nature of the system studied, this variable was difficult to test, especially with the competing formation of **3.13** when excess ligand was present, and the efficient synthesis of **3.11** in the presence of a larger metal excess. Unfortunately, the paramagnetic nature of the Cu(II) ions in solution precluded further analysis by NMR spectroscopy, and the precise source of oxalate in the reaction mixture remains uncertain.

Finally, the formation of the cyanido ligand in the structure of **3.13** was considered. While a solvent decomposition pathway was thought to be a viable possibility, this was ruled out by the observation that small quantities of **3.13** could be formed in methanol as well as acetonitrile with no external cyanide source, leaving a ligand decomposition pathway as the only sensible option. Under the conditions of formation it is difficult to suggest a specific origin for the cyanide species; a cyano species containing either the pyridine nitrogen or one of the pyrazole nitrogens would require the cleavage of multiple carbon-carbon bonds. In this instance, especially due to the particularly low yield of complex formation under all tested conditions, the most likely conclusion is that formation of **3.13** is a case of trapping of a small quantity of cyanide anions by a particularly stable crystalline assembly. Reduction of the copper ion to the cuprous form could be considered to occur either before or after coordination of the cyanide anion. Complex **3.13** was formed as a pure phase in 14 % yield by simply reducing the amount of $Cu(NO_3)_2$ in the solution to 1.4 equivalents, both providing excess ligand as a low-yielding cyanide source and reducing the concentration of oxidising nitrate in the solution. Complex **3.13** could also be formed as an impure phase with the use of CuCN as a source of

both Cu(I) and the cyanide anion. A summary of the routes to pure phases of **3.10** – **3.13** is shown in Scheme 3.5 below.

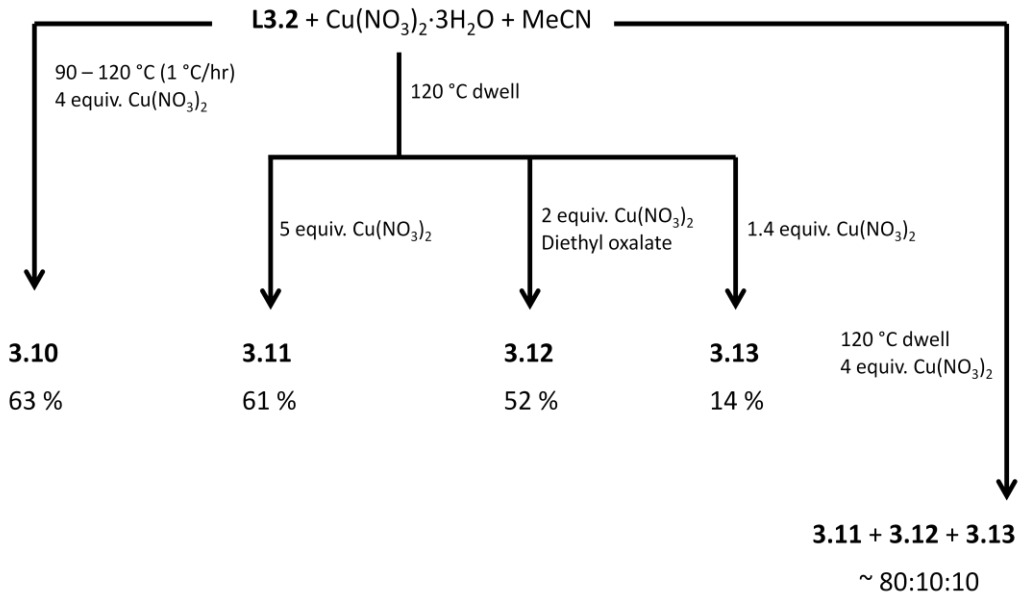

*Scheme 3.5: Summary of synthetic pathways to compounds **3.10** – **3.13** in their mixed phase and pure forms.*

3.7 Geometrical Considerations for Complexes Formed From Ligands L3.1 and L3.2

The key geometric parameters for complexes containing ligands **L3.1** and **L3.2** are summarised in Table 3.1 below. Immediately obvious from Table 3.1 is the discrepancy in metal-metal distance, ranging from 7.6 – 10.4 Å for very similar ligands **L3.1** and **L3.2**, with even a 2.1 Å range within complexes of the same ligand **L3.2**. These ranges are explained with the use of the φ_1 and φ_2 torsion angles, which in a hypothetical system would be free to range from 180° to -180°, with combinations of 180 (equivalent to -180) or 0 for both values representing arrangements where the pyrazole rings are coplanar; clearly this situation is not achievable in these circumstances due to the steric restraints of either the helical framework for the **L3.1** complexes, or the pyrazole methyl groups in **L3.2**. The pyrazole-pyrazole interplanar angle, although coupled to the φ_1 and φ_2 torsion angles, is also reported as an easily visualisable counterpart to φ_1 and φ_2, albeit containing less information.

Compound	Metal Coord. Number	Metal Geometry	Overall Structure	Metal-Metal Distance (Å)	Py-Pz Interplanar Angle (°)	Pz-Pz Interplanar Angle (°)	Torsions φ_1, φ_2 (°)
3.5A	6	Octahedral	Triple helicate	7.6133(18)	4.8(2) - 6.0(2)	69.0(2)	139.2(5), 128.7(6)
3.5B	6	Octahedral	Triple helicate	7.6339(16)	3.2(3) - 9.7(3)	65.0(3) - 67.7(3)	-138.4(8), -132.1(8)*
3.6	6	Octahedral	Double helicate	9.0171(10)	13.66(15) - 16.48(16)	99.31(16)	125.9(5), 112.8(5)
3.7	6	Octahedral	Double helicate	9.0815(10)	10.17(10) - 34.65(9)	107.28(9)	114.9(7), 109.0(8)
3.8	4	Sq. Planar	Linear dinuclear	8.7327(6)	4.92(12) - 8.27(12)	98.11(12)	109.5(4), 120.8(4)
3.9	5	Sq. Pyr.	Hydrogen bonded linear dinuclear	9.6209(5)	19.55(8)	109.21(11)	-107.1(2), -107.1(2)
3.10	5	Sq. Pyr.	(6,3) polymer	9.0782(5)	16.62(8) - 10.73(8)	86.26(8)	-126.3(2), 61.6(3)
3.11	5	Sq. Pyr.	Cyclic tetramer	8.3302(12)	10.76(12)	98.57(18)	-118.9(9), -118.9(9)
3.12	5	Sq. Pyr.	1-D polymer	8.3663(13)	4.72(16)	89.0(2)	120.9(4), 120.9(4)
3.13	4	Tetrahedral	(6,3) polymer	10.4216(7)	23.62(10)	109.7(16)	-82.9(3), -82.9(3)

*Table 3.1: Summary of key structural parameters for complexes **3.5A** – **3.13**. *Denotes the use of a representative value of φ_1 , φ_2 where several values exist.*

The most obvious effect on metal-metal distance is the *cis*- or *trans*- type binding modes of the ligands; where the values of φ_1 and φ_2 have the same sign, this can be envisaged as each bond rotating in opposite directions from the 0,0 (*cis* – coplanar) position, giving a *trans* orientation, while values of φ_1 and φ_2 with opposing signs represent a rotation in the same direction, giving close to a *cis* conformation. Only one complex described above adopts the *cis* configuration, complex **3.10**, resulting in a shorter metal-metal distance than in, for example, complex **3.13**. However, a more general effect on the metal-metal distance is the magnitude of the φ_1 and φ_2 torsion angles rather than their sign. When considering the maximum possible metal-metal distance achievable, the largest value can be visualised to occur near 90, 90 (or, equivalently, -90, -90), where the angle between pyrazole rings is equal to the tetrahedral angle of the methylene spacer. As the trends in Table 3.1 suggest, metal-metal distance is largest when the angles φ_1 and φ_2 are at their closest to 90 or -90°, where the pyrazole-pyrazole interplanar distance is greatest.

Table 3.1 also shows the steric effect of restraining the ligand into a tightly bound environment, such as within a helicate. The pyridyl-pyrazole mean plane angles are clearly influenced by the addition of methyl groups to the pyrazole ring, as seen by the large increase in interplanar angle between the complexes of **L3.1** and **L3.2**. The variability of interplanar angles within just the complexes of **L3.2** can also be explained; complexes **3.8** and **3.12**, where the metal sites contain co-ligands which have some degree of flexibility around the coordination sphere and are comparatively small, exhibit the lowest strain on the pyridine-pyrazole system, allowing better access to the more energetically favourable coplanar conformation. Complexes where the co-ligands are bound either in bridging coordination modes or hydrogen bonding, such as **3.9**, **3.10** and **3.13** exhibit less freedom around the coordination sphere, and as a result display much greater deviations from planarity. The complexes in which the ligands are more tightly bound in a cyclic or helical arrangement, **3.6**, **3.7** and **3.11**, also match these observations, with larger co-ligands and lower degrees of flexibility around the coordination sphere leading to larger interplanar angles.

Chapter 4

Complexes of Pyrazolyl-Benzimidazole Ligands

4.1 Introduction

The combination of versatile synthesis and functionalisation and the presence of both pyridine-like and pyrrole-like nitrogen donor sites has resulted in benzimidazole-based ligands becoming increasingly common in inorganic chemistry, often as an extension to the use of the related and much more prevalent heterocycle, imidazole. As well as in biological systems, such as in the structure of vitamin B-12,[337-339] benzimidazole-derived ligands are also frequently used to form N-heterocyclic carbenes.[340-343] As a supramolecular synthon, benzimidazole itself is limited to, at most, a bent, two-connecting anionic linear bridging ligand; however, the synthetic flexibility of the benzodiazole framework results in the existence of a large number of possible ligands relevant to metallosupramolecular chemistry containing the benzimidazole fragment. One such example is the class of compounds in which two or more benzimidazole moieties are linked together *via* substitution through the N-H group, to generate a bridging ligand of variable length and geometry. This approach has been recently used by Barbour,[344-347] among others,[348-353] to form a range of cyclic dimers using both imidazole and benzimidazole as the coordinating species. Perhaps the most well-known and influential use of benzimidazole-based ligands in supramolecular chemistry is the work pioneered by Williams and Piguet,[285, 354] where ligands based on 5,5′-methylenebis-(2-(2′-pyridyl)benzimidazole) have been used to generate a wide range of helical structures, including luminescent lanthanide helicates.[355, 356] In these instances, the synthetic approach often employed is the reaction of a 1,2-diamine with a heterocyclic carboxylic acid or synthetic equivalent under highly forcing conditions, to close the five-membered ring with two sequential condensation reactions. Benzimidazole ligands have also been employed in the synthesis of coordination polymers and metal-organic frameworks, with several notable examples published in recent years,[357-359] including compounds grouped in the 'zeolitic imidazolate framework' (ZIF) class of materials, which have shown great promise in CO_2 capture.[360-364]

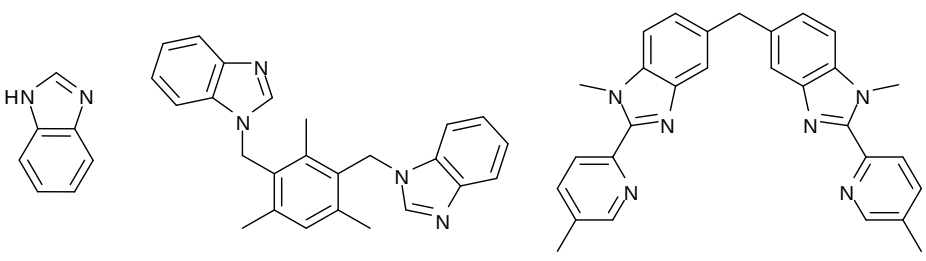

Scheme 4.1: Selected examples of benzimidazole ligands used in metallosupramolecular chemistry. From left to right: 1H-benzimidazole, 1,3-bis(benzimidazol-1-ylmethyl)-2,4,6-trimethylbenzene,[344] 5,5′-methylenebis(l-methyl-2-(5′-methyl-2′-pyridyl)benzimidazole[285]

4.2 Ligand Synthesis

Initially, a class of ligands based on 2-(pyrazol-1-yl)-*1H*-benzimidazole was envisaged, in order to take advantage of the greater degree of synthetic flexibility of the benzimidazole backbone, while also allowing for functionality to be added to the pyrazole ring. Similar to the case described in Chapter 3, synthesis of a generic 2-(pyrazol-1-yl)-benzimidazole was achieved by one of two general methods; formation of the C-N bond between rings, or a cyclocondensation reaction between a 2-hydrazinobenzimidazole and a diketone or synthetic equivalent. In the majority of the cases described below, the latter method was preferred, owing to the ready synthesis of 2-hydrazinobenzimidazole *via* oxidation and nucleophilic substitution of commercially available 2-mercaptobenzimidazole.

*4.2.1 Synthesis of 2-(pyrazolyl)-1H-benzimidazole **L4.1**, 2-(3,5-dimethylpyrazol-1-yl)-1H-benzimidazole **L4.2** and 1-methyl-2-(pyrazolyl)-benzimidazole **L4.3***

Although known to some extent for their toxicological properties,[365-367] where **L4.2** is known under the trade name Rabenzazole, the coordination chemistry of the simple bidentate ligands 2-(pyrazolyl)-*1H*-benzimidazole **L4.1** and 2-(3,5-dimethylpyrazol-1-yl)-*1H*-benzimidazole **L4.2** has not been reported, therefore they were prepared in order to gauge the coordination preferences of the metal binding site, to allow for rational design of more complex ligand scaffolds. Both ligands were prepared by reaction of a dicarbonyl, in this case 1,1,3,3-tetramethoxypropane or acetylacetone, respectively, with 2-hydrazinobenzimidazole, prepared *via* known methods from 2-mercaptobenzimidazole,[368, 369] as shown in Scheme 4.2 below.

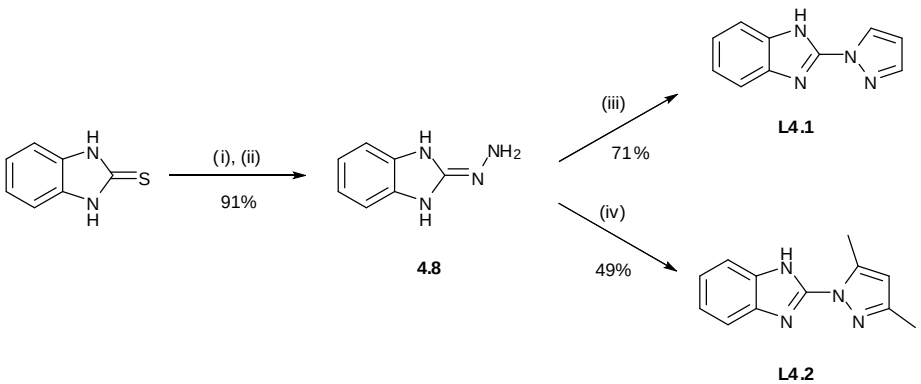

*Scheme 4.2: Synthesis of ligands **L4.1** and **L4.2**. Reagents and conditions: (i) H_2O_2, $NaOH_{(aq)}$, RT; (ii) H_2NNH_2, reflux 4hr;[368] (iii) 1,1,3,3-tetramethoxypropane, $HCl_{(aq)}$, reflux 5 hr; (iv) acetylacetone, MeOH, reflux 16 hr.*

A sample of **L4.2** was crystallised by slow evaporation of a dilute methanol/water solution. The colourless plates obtained were subjected to single crystal X-ray diffraction and the data were solved and the structure model refined in the non-centrosymmetric orthorhombic space group $Pca2_1$ (R-factor 4.37%). The asymmetric unit contains two molecules of the ligand, in the absence of any solvent or other guest molecules, as shown in Figure 4.1. The two molecules of **L4.2** exhibit significant geometrical differences, mainly based on the benzimidazole-pyrazole torsion angle. One unit of **L4.2** exhibits a mean interplanar angle between benzimidazole and pyrazole rings of 31.44(7)°, while the other is effectively co-planar, with interplanar torsion of only 3.73(8)°. Structural justification for the existence of two unique molecules within the asymmetric unit is provided by examining the hydrogen bonding, as displayed in Figure 4.1 below; units of **L4.2** assemble in a dimeric fashion where the imidazole NH and unsubstituted pyrazole nitrogen form two intermolecular hydrogen bonds. This interaction is hindered by the presence of the pyrazole methyl groups, and the two conjugated rings on one molecule are forced out of alignment, likely in order to retain the thermodynamically stable coplanar arrangement on the other moiety.

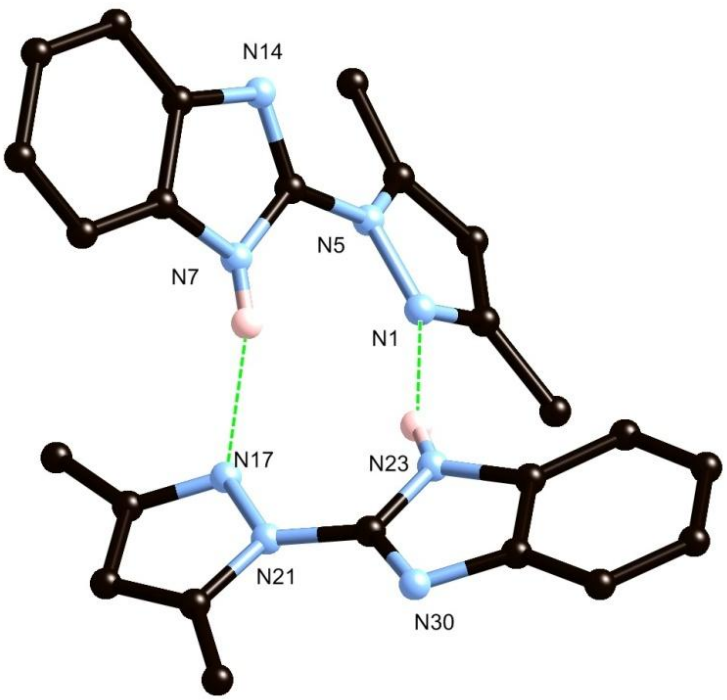

*Figure 4.1: Structure of the asymmetric unit of **L.4.2** showing intermolecular hydrogen bonding interactions. Hydrogen atoms not participating in hydrogen bonding omitted for clarity.*

The dimeric hydrogen bonding interaction in **L4.2** exhausts the hydrogen bond donor capabilities of the ligand, and as a result the only interactions between dimers are π-π stacking and C-H···π interactions. Unsurprisingly, the unit of **L4.2** with smaller torsion angle undergoes more efficient π-π stacking, with 3.5519(12) Å separation between adjacent, equivalent units, with this interaction taking place across the entire molecule. The pyrazole rings of the twisted unit of **L4.2** undergo π-π stacking between equivalent units with 3.491(2) Å interplanar separation, while the benzimidazole moieties engage in weak C-H···π interactions in the same direction, as shown in Figure 4.2, with C···π (mean plane) distance of 3.466(9) Å and a C-H···C angle of 175.96(18)°. Unexpectedly, both interactions occur in a head-to-head type fashion, emphasising both the low degree of π polarisation along the molecule, and the requirement for a non-centrosymmetric space group in this instance.

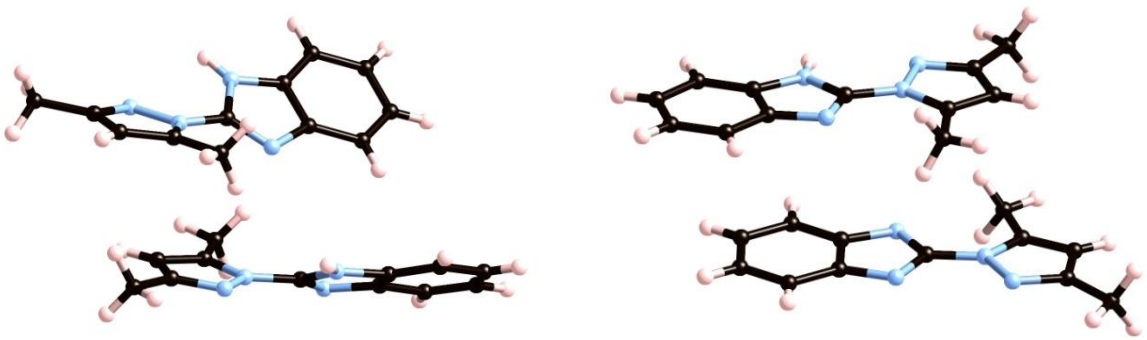

*Figure 4.2: Modes of intermolecular interaction in **L4.2**; (Left) π-π and C-H···π interactions between twisted units of **L4.3**. (Right) Parallel π-π interactions between planar units of **L4.3**.*

It was expected that the benzimidazole N-H group would also act as a hydrogen bond donor in metal complexes containing ligands **L4.1** and **L4.2**, and to probe the influence of this group on the solid state structure of such complexes, the benzimidazole ring of **L4.1** was methylated using dimethyl sulfate in aqueous solution, to afford 1-methyl-2-(pyrazolyl)-benzimidazole **L4.3** (Scheme 4.3). Methylation of the benzimidazole nitrogen was expected to improve solubility by reducing the intermolecular interactions between complexes. While ligand **L4.2** could also be methylated using this method, the resulting compound proved unable to chelate, due to the steric clash between adjacent methyl groups, forcing the two rings out of plane. As such, the coordination chemistry of this compound was not explored.

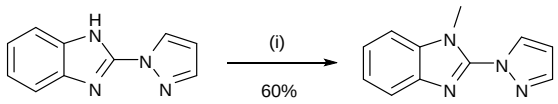

L4.1 **L4.3**

*Scheme 4.3: Synthesis of ligand **L4.3**. Reagents and conditions: (i) Me_2SO_4, NaOH, H_2O, RT.*

*4.2.2 Synthesis of bridged bis-(pyrazolylbenzimidazole) ligands **L4.4**, **L4.5** and **L4.6***

Once the synthesis of **L4.1** was successfully scaled to prepare multi-gram quantities, the ligand itself was used as a precursor towards several more elaborate ligands, all utilising the reactive benzimidazole N-H group to link together two binding sites on a flexible scaffold, starting with α,α′-bis-(2-(1-pyrazolyl)-benzimidazol-1-yl)-*p*-xylene **L4.4**. It was found that the most efficient method of preparing this ligand was the reaction of α,α′-dibromo-*p*-xylene with **L4.1** in acetone in the presence of excess potassium carbonate and a catalytic quantity of potassium iodide, accelerating the rate *via* a Finkelstein process, known for similar compounds.[370] In these reactions, small quantities of the alkyl bromide are converted to the alkyl iodide, which is immediately reacted to the product with regeneration of the iodide catalyst. This process is promoted by the precipitation of potassium bromide, driving the otherwise unfavourable equilibrium towards formation of a modest quantity of the aryl iodide, which is then reacted irreversibly. As shown in Scheme 4.4, a similar process, employing either bromo- or chloro- substituted starting materials, was then employed to prepare similar ligands in which the bridging *para*-xylene group was replaced with *para*-biphenylene and *meta*-xylene to give ligands α,α′-bis-(2-(1-pyrazolyl)-benzimidazol-1-yl)-4,4′-dimethylbiphenylene **L4.5** and α,α′-bis-(2-(1-pyrazolyl)-benzimidazol-1-yl)-*m*-xylene **L4.6**, respectively.

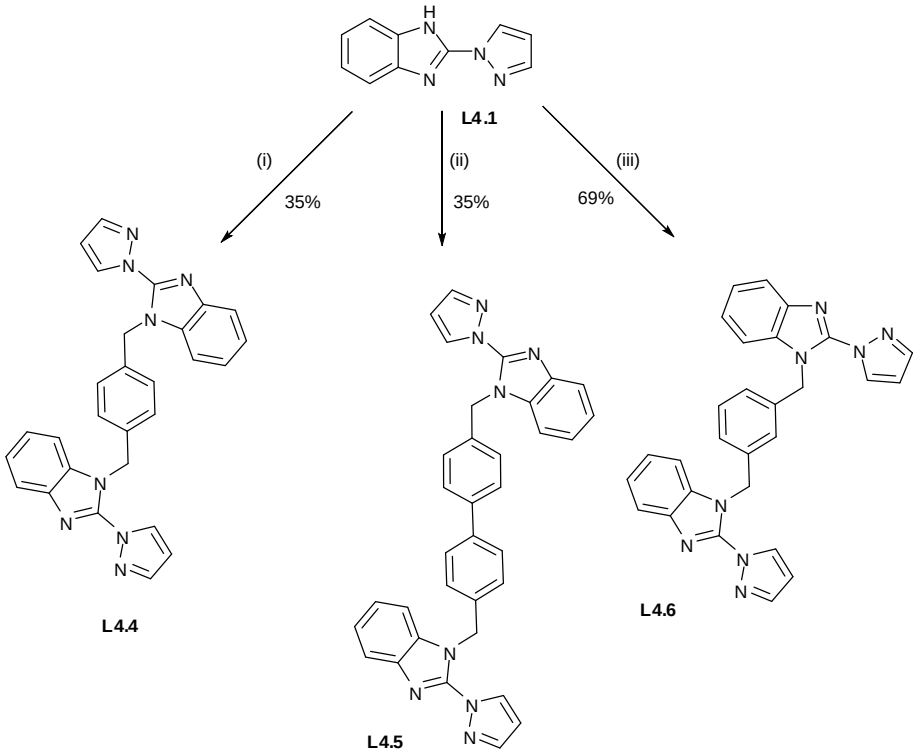

*Scheme 4.4: Synthesis of ligands **L4.4**, **L4.5** and **L4.6**. Reagents and conditions: (i) α,α'-dibromo-p-xylene, acetone, KI, K_2CO_3, reflux; (ii) α,α'-dichloro-4,4'-dimethylbiphenylene, acetone, KI, K_2CO_3, reflux; (iii) α,α'-dibromo-m-xylene, acetone, KI, K_2CO_3, reflux.*

Single crystals of both **L4.5** and **L4.6** were grown by slow evaporation of acetonitrile solutions. The structure of **L4.5** was refined in the monoclinic space group *C*2/*c* (R-factor 5.47%), where the asymmetric unit contained one half of the ligand molecule, with the remainder of the molecule generated by a crystallographic twofold axis passing perpendicular to the biphenyl link. The pyrazole-benzimidazole system was found to exist in a *trans* conformation due to repulsion between the nitrogen lone pair electrons,[371] with interplanar angle of 34.63(10)°. As is expected within a biphenyl moiety, the central phenyl rings display a torsion angle of 48.46(12)°, offering partial conjugation while avoiding the steric clash of the *ortho* hydrogen atoms. The structure of **L4.5** is shown in Figure 4.3 below.

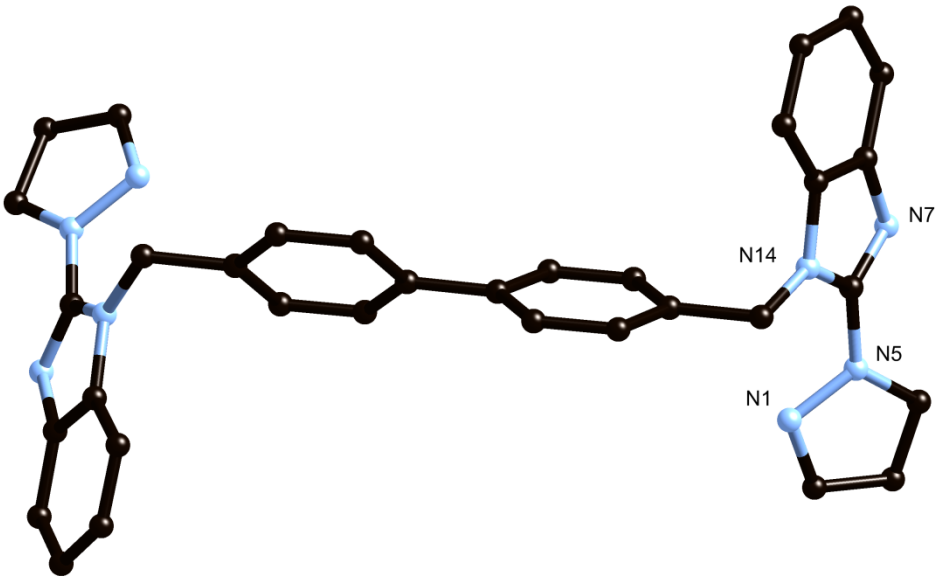

*Figure 4.3: Structure of ligand **L4.5** with heteroatom labelling scheme, hydrogen atoms omitted for clarity.*

The three-dimensional structure of **L4.5** is dominated by two main sets of weak intermolecular interactions. The pyrazolylbenzimidazole moieties interact with equivalent units by way of parallel π-π stacking interactions at mean interplanar distance of 3.863(3) Å, while a weak C-H···π interaction exists between the methylene groups and the pyrazole ring of an adjacent unit, with C···π (mean plane) distance of 3.396(5) Å and <(C-H···N) = 150.32(16)° for C(15)-H(15A)···N(5). Adjacent pyrazolylbenzimidazole units lying in the same plane also undergo a weak dimeric hydrogen bonding-type interaction in which the hydrogen atom of pyrazole carbon C(4) interacts with the lone pair of unsubstituted benzimidazole nitrogen N(7), with d(D-A) = 3.540(4) Å and <(D-H···A) = 144.5(2)° for C(4)-H(4)···N(7).

The structure of ligand **L4.6** was also solved and refined in the monoclinic space group *C*2/*c* (R-factor 4.10%), following crystallisation by slow evaporation from acetonitrile, where the asymmetric unit contained one half equivalent of the ligand due to the twofold axis passing parallel to the plane of the central phenyl ring. As was observed with **L4.5**, the unsubstituted nitrogen atoms of the pyrazole and benzimidazole rings adopt a *trans* conformation, while the pyrazole-benzimidazole interplanar angle of 13.85(7) ° is consistent with the conjugation between both rings in the absence of significant steric constraints. The structure of **L4.6** is shown in Figure 4.4 below.

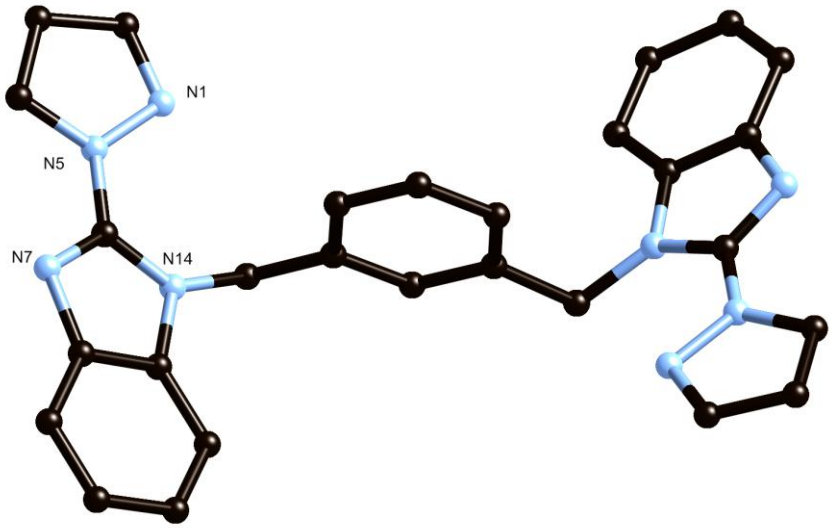

*Figure 4.4: Structure of ligand **L4.6** with heteroatom labelling scheme, hydrogen atoms omitted for clarity.*

Intermolecular interactions in **L4.6** are limited to one example of π-π interaction between parallel pyrazole rings, with a mean interplanar distance of 3.3433(19) Å, and a number of weak edge-to-face C–H···π interactions, also mainly involving the pyrazole rings. The most notable of such interactions is the equivalent pair of C-H···π interactions from the hydrogens at the pyrazole 3-position to each face of the phenylene ring, where the C···π (mean plane) distance of 3.394(3) Å and C-H···C angle of 144.57(14)° suggests an attractive interaction. It is expected that the irregular shape of **L4.6** prevents any more significant π-π stacking interactions, and prevents the engagement of the benzimidazole moiety in any significant interactions whatsoever.

*4.2.3 Synthesis of 4,4′-methylenebis(1-(1-methylbenzimidazol-2-yl)pyrazole) **L4.7***

In order to draw comparisons with the complexes prepared from helicating ligand **L3.1**, a related benzimidazole-substituted version, 4,4′-methylenebis(1-(1-methylbenzimidazol-2-yl)pyrazole) **L4.7** was prepared. Following a similar synthetic strategy to that described in Chapter 3, the benzimidazole functionality was appended to the pre-formed pyrazole by nucleophilic aromatic substitution of the bromobenzimidazole by the pyrazole in the presence of strong base, as shown in Scheme 4.5. The 1-bromo-2-methylbenzimidazole precursor **4.10** was prepared by bromination of 2-mercaptobenzimidazole, followed by methylation with dimethyl sulfate. The substitution reaction did not proceed cleanly with the N-H unsubstituted benzimidazole compound, most likely due to a

combination of solubility reasons and the competitive reactivity of the benzimidazole N-H group under strongly basic conditions. Furthermore, the low solubility of the N-methyl benzimidazole ligand suggested the N-H compound would display very poor solubility, and as such, its synthesis was not pursued further.

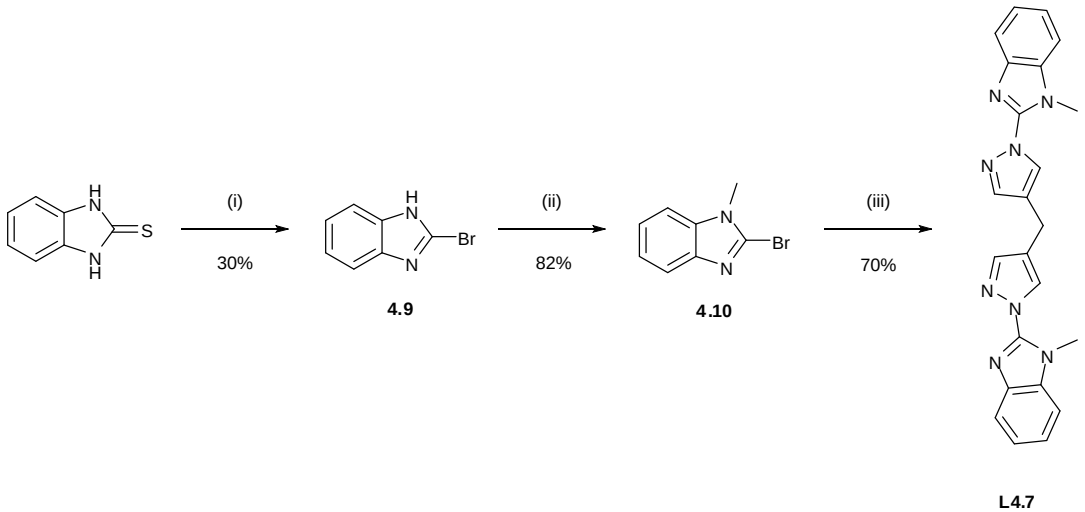

*Scheme 4.5: Synthesis of ligand **L4.7**. Reagents and conditions: (i) HBr/HOAc, Br_2, RT;[372] (ii) Me_2SO_4, NaOH, H_2O, RT;[372] (iii) **3.5**, NaH, DMF, 110 °C, 48 hr.*

4.3 Synthesis of Mononuclear Pyrazolyl-benzimidazole complexes

In order to gauge the coordination capabilities and the effect of pyrazole or benzimidazole methylation on the resulting solid-state structures, several metal complexes were prepared and structurally characterised based on bidentate ligands **L4.1**, **L4.2** and **L4.3**. From examining the structures of these ligands, several inferences can be drawn initially;

- Owing to the extended aromatic nature of the ligand structures, π-π stacking would be expected to play a dominant role, especially where hydrogen bonding interactions are removed by N-H methylation. Notably, although the π system is larger than that of pyrazolylpyridine, the π-excessive nature of the two heterocycles and smaller degree of π polarisation within the conjugated system will likely result in larger interplanar distances and smaller stabilisation energies.

- The steric bulk of the benzimidazole group would be expected to prevent the formation of planar configurations, such as square planar coordination geometry or the formation of a square pyramidal or octahedral complex in which pyrazolylbenzimidazole ligands occupy all binding sites on the equatorial plane, especially when further substitution is present on either ring.
- Owing to the ring geometry, the bite angle of two linked chelating 5-membered rings would be expected to be somewhat smaller than for linked 6-membered rings, or for linked 5- and 6-membered rings. This may have consequences on the ability of the ligands to adhere to metal geometries requiring large bite angles, *i.e.* tetrahedral, or chelation around the equatorial plane of a trigonal bipyramid.

With these expectations in mind, ligands **L4.1** – **L4.3** were reacted with a number of metal ions, and the resulting complexes analysed by single crystal X-ray diffraction. Three representative structures are presented below.

*4.3.1 Synthesis of [Zn(**L4.1**)$_2$(NO$_3$)]·NO$_3$ **4.11***

Two equivalents of ligand **L4.1** were reacted with $Zn(NO_3)_2 \cdot 6H_2O$ in acetonitrile, and single crystals of complex $[Zn(\mathbf{L4.1})_2(NO_3)]\cdot NO_3$ **4.11** were formed by allowing the mixture to stand overnight. Analysis of the mother liquor by electrospray mass spectrometry showed the presence of a $[Zn(\mathbf{L4.1})_2]^{2+}$ species at *m/z* 216.0385 (Calculated for $C_{20}H_{16}N_8Zn$ 216.0389); however, the complex proved insoluble at higher concentrations, preventing analysis by NMR. The crystal structure was solved and refined in the orthorhombic space group *Pnna* (R-factor 3.54%), where the asymmetric unit was revealed to contain one zinc ion coordinating to two equivalent molecules of **L4.1** and one chelating nitrate anion, in which the two coordinating oxygen atoms are crystallographically equivalent. Although six-coordinate in nature, the geometry of the zinc ion is best described as trigonal bipyramidal, in which the nitrate chelate occupies one position on the equatorial plane, and the axial positions are occupied by the crystallographically equivalent benzimidazole nitrogens of each ligand, at a contracted distance of 2.070(2) Å, compared to the pyrazole – zinc bond distance of 2.156(2) Å. The bite angle N(2)-Zn(1)-N(8) of 77.69(7)° corresponds well to the expected value, while the pyrazole-benzimidazole interplanar angle of 5.73(8)° shows the two rings to be close to planarity. The mean interplanar angle between the two equivalent ligands of 38.02(5)° relates to the

N(2)-Zn(1)-N(2) equatorial planar angle between the two coordinating pyrazoles of 130.83(11)°, allowing for twisting within the ligand plane. The structure of complex **4.11** is shown in Figure 4.5

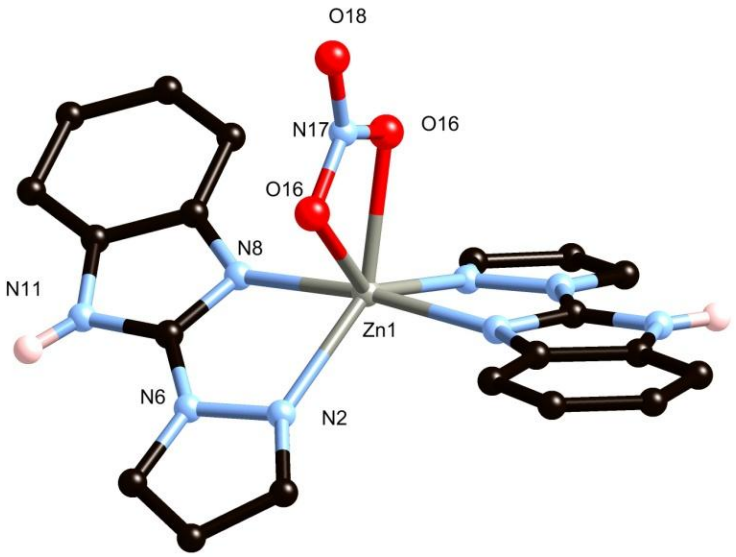

*Figure 4.5: Structure of complex **4.11** with unique heteroatom labelling scheme. Non-coordinating anion omitted for clarity.*

The intermolecular interactions in the structure of **4.11** are dominated in the first instance by hydrogen bonding linkages between the benzimidazole N-H groups and the non-coordinating nitrate anions, which are disordered over two equivalent positions. The nitrate anion bridges two complexes in this manner, which extends the structure into a one-dimensional hydrogen bonded polymer. Additional weak C-H···O interactions occur between the pyrazole C-H closest to the benzimidazole N-H group and one of the two possible orientations of the disordered nitrate, with minimum C···O distance of 3.104(5) Å and C-H···O angle 134.9(2)°. Although the pyrazole ring has some hydrogen bond donor character at the 3- and 5- positions, it seems likely that this interaction is more due to geometric convenience than a significant enthalpic driving force. The hydrogen bonding chain within complex **4.11** is shown in Figure 4.6.

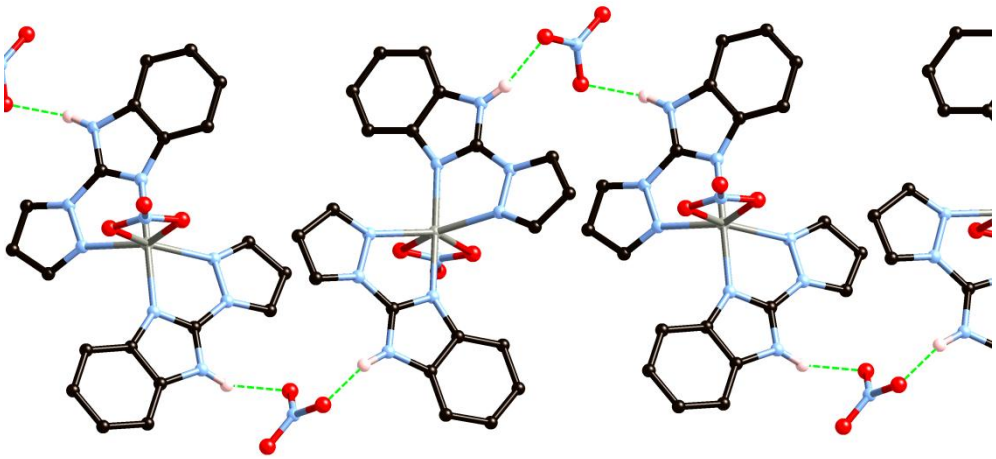

*Figure 4.6: Hydrogen bonded polymeric chain in the structure of **4.11**, hydrogen atoms not involved in hydrogen bonding omitted for clarity. Anion disorder and weak C-H···O hydrogen bonding not shown.*

In addition to these interactions, the structure of **4.11** also exhibits strong π-π interactions, both within the hydrogen bonding chain and to adjacent chains. The interactions within each chain are limited to partial overlap of the pyrazole rings on adjacent complexes, as can be seen in Figure 4.6 above, where the mean interplanar angle of 10.43(15)° and closest interatomic distance of 3.331(5) Å for C(5)-C(5') provide an additional level of stability for the chain structure, although with a small overlap. The primary mode of π-π interactions between two adjacent hydrogen bonding chains involves the overlap of benzimidazole π systems from ligands on adjacent complexes, where one benzimidazole ring interacts with two parallel planes above and below, with interplanar distances of 3.506(2) and 3.246(2) Å. The benzimidazole rings overlap in a head-to-tail fashion, as would be expected on the grounds of π-system polarisation. These interactions form columns parallel to the *a* unit cell axis. Most likely as a result of these significant intermolecular interactions, crystals of complex **4.11** were stable on heating in air above 300 °C.

*4.3.2 Synthesis of [Mn(**L4.2**)$_2$(OH$_2$)(MeCN)]·2(ClO$_4$) **4.12***

Complex [Mn(**L4.2**)$_2$(OH$_2$)(MeCN)]·2(ClO$_4$) **4.12** was prepared by the reaction of ligand **L4.2** with Mn(ClO$_4$)$_2$·6H$_2$O in acetonitrile, followed by slow diffusion of toluene to generate single crystals. Unlike complex **4.11** above, complex **4.12** could not be detected in solution by mass spectrometry. The crystals obtained were analysed by single crystal X-ray diffraction, and the data solved in the triclinic space group *P*-1 (R-factor 4.92%). The asymmetric unit of **4.12** reveals a 6-coordinate

octahedral Mn(II) centre coordinated to two molecules of **L4.2** in a bis-bidentate fashion, as well as one molecule of acetonitrile and one molecule of water, as shown in Figure 4.7. Two perchlorate anions are also present in the asymmetric unit in non-coordinating positions. Geometrically, the octahedral environment of the metal centre is comparably regular for the majority of the *cis* angles, with no deviation from 90 ° greater than *ca.* 7°, except for the two N-Mn-N angles for the chelating **L4.2** moieties, which give bite angles of 72.12(11)° (N26-Mn1-N18) and 72.18(11)° (N13-Mn1-N2), smaller than that observed for complex **4.11**. Complex **4.12** exhibits slightly larger pyrazole-benzimidazole interplanar torsion than was observed in **4.11**, with interplanar angles of 7.68(14)° and 11.39(15)°. As a result of the octahedral coordination observed in **4.12**, the two units of **L4.2** exhibit a mean interplanar angle of 80.05(7)°, much greater than that seen in **4.11**.

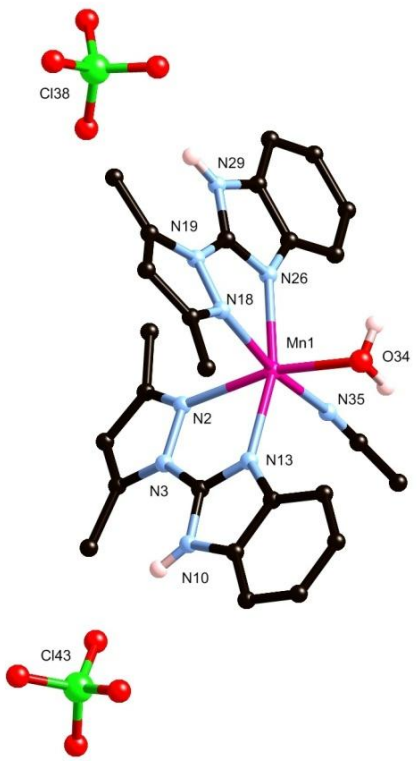

*Figure 4.7: Structure of complex **4.12** showing partial atom labelling scheme. C-H hydrogen atoms omitted for clarity.*

The intermolecular interactions present in **4.12** are dominated by hydrogen bonding, with four distinct hydrogen bond donor sites per complex, namely the N(10) and N(29) imidazole donors, and the two hydrogen atoms attached to coordinating water molecule. As shown in Figure 4.8, two types of arrangements are observed; in the first instance, the discrete complexes are dimerised by a reciprocating pair of N(29)-H(29)···O(40)···H(34B)-O(34) interactions, in which a perchlorate

oxygen bridges the hydrogen bond donors of two adjacent molecules. This strength of the dimerisation is magnified by a weak π-π interaction between the same **L4.2** residues, at a mean interplanar distance of 3.9385(19) Å with zero angular offset. The second type of hydrogen bonding interaction in **4.12** comes about from the O(34)-H(34A)···O(44) and N(10)-H(10)···O(46) pair, in which a perchlorate moiety bridges two complexes through separate oxygen atoms. The greater distance between donor sites in this case prohibits any direct π-π stacking between molecules connected in this way. This interaction alone propagates a one-dimensional hydrogen bonding polymer along the *b* axis, and when combined with the perpendicular dimerisation, the overall network resembles a one-dimensional ladder-type polymer. Interactions between adjacent polymeric strands are limited to small partial overlap π-π stacking and edge-to-face C-H···π interactions. When compared to complex **4.11**, it is clear that the increase in dimensionality of the hydrogen bonding structure in **4.12** is due to the inclusion of a second donor pair belonging to the coordinated water molecule allowing a similar dimerisation interaction to occur while leaving additional sites available for further connectivity. Although the one-dimensional nature of the connectivity in **4.12** leaves a perpendicular aromatic system available for π-π interactions in a second dimension, only very minor overlap was detected between adjacent chains. As was the case with compound **4.11**, no void space or isolated solvent was located within the structure.

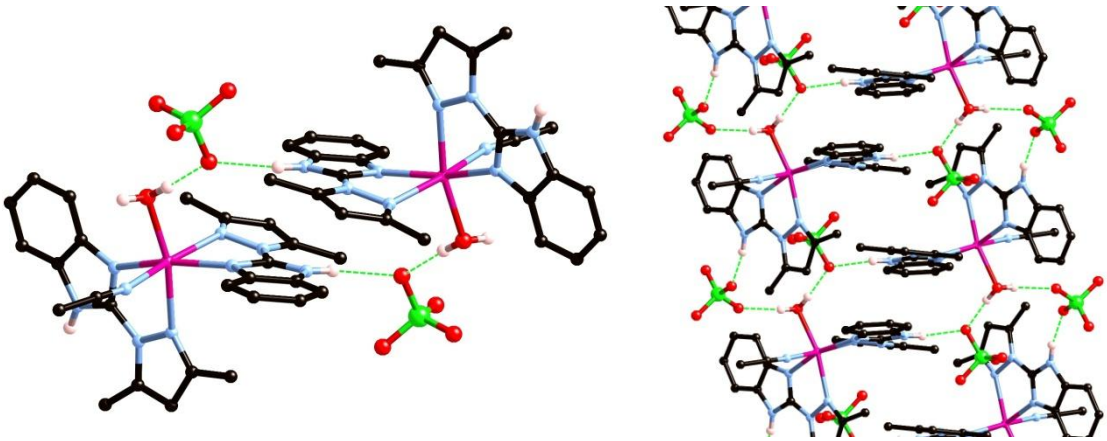

*Figure 4.8: (Left) Structure of the hydrogen bonding dimer in **4.12**, hydrogen atoms not participating in hydrogen bonding omitted for clarity. (Right) Full hydrogen bonding structure of **4.12**.*

*4.3.3 Synthesis of [Cu(**L4.3**)$_2$(NO$_3$)]·(NO$_3$) **4.13***

Complex [Cu(**L4.3**)$_2$(NO$_3$)]·(NO$_3$) **4.13** was prepared in a similar fashion to **4.12** above, by combining the ligand with Cu(NO$_3$)$_2$·3H$_2$O in acetonitrile, followed by diffusion of diethyl ether to generate single crystals of the product in 25 % yield. Electrospray mass spectrometry confirmed the presence of a ligand-containing copper species, with *m/z* 521.0979, consistent with a [Cu(**L4.3**)$_2$(NO$_3$)]$^+$ species in solution. Diffraction of the green crystals obtained revealed a structure in the chiral space group $P2_1$ (R-factor 2.39%), containing in the asymmetric unit one copper ion coordinating to two molecules of **L4.3** and one nitrate ion in a monodentate mode, with one non-coordination nitrate anion also present in the unit cell. Although crystallised in a chiral space group, the structure of **4.13** was found to be racemically twinned with the opposite enantiomer in approximately a 44:56 ratio. The origin of this chirality is likely to be related to crystal packing effects rather than any particular distinguishing feature in the structure, shown in Figure 4.9. The coordination geometry of the copper ion is best described as distorted square pyramidal, displaying an elongated axial bond length of 2.2201(19) for Cu(1)-N(17), *cf.* 2.0371(19) for Cu(1)-N(2), and angle N(2)-Cu(1)-O(32) of 156.37(7)°. The ligands themselves display little distortion from planarity, with pyrazole-benzimidazole interplanar angles of 16.45(8) and 3.46(9)°, leading to bite angles of 77.74(7) and 79.69(7)°, respectively. The angle between the mean planes of the two **L4.3** ligands of 114.40(4)° is markedly smaller than that observed in **4.11**, due to the change in geometry from trigonal bipyramidal to distorted square pyramidal.

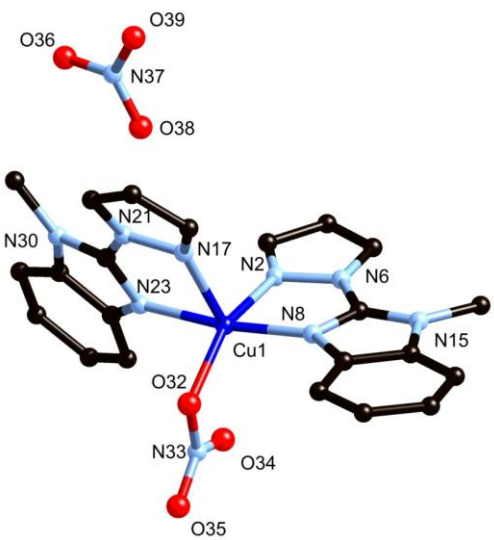

*Figure 4.9: Structure of complex **4.13** with heteroatom labelling scheme. Hydrogen atoms omitted for clarity.*

With the removal of the hydrogen bonding capabilities of ligand **L4.3** by methylation of the benzimidazole nitrogens, the possibilities for intermolecular associations are largely limited to π-π interactions. In this instance, only weak π-π interactions are observed, with each complex interacting with two adjacent complexes by way of two weak parallel π-π interactions each, displaying mean interplanar distances of 3.5326(18) and 3.4426(18) Å, propagating a chain parallel to the *a* axis, shown in Figure 4.10 below. Judging by the long interplanar distance and small degree of overlap, this interaction is unlikely to provide a significant stabilisation to the structure; however, no other significant intermolecular interactions exist in the structure, with the exception of very weak edge-to-face π-π interactions. No substantial void space was observed within the structure, which also exhibited substantially poorer thermal stability than complex **4.11**, decomposing at 230 °C by thermogravimetric analysis.

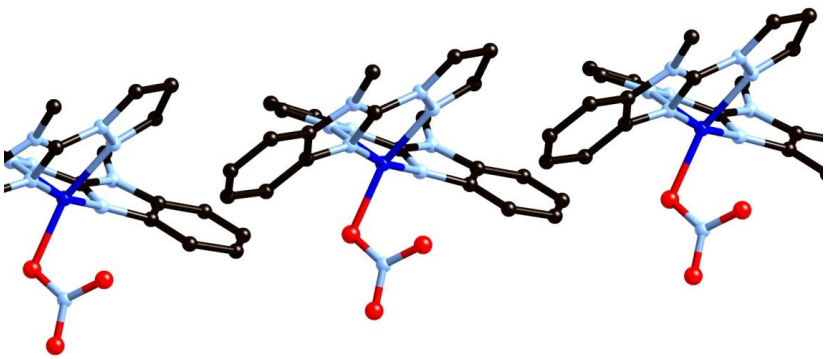

*Figure 4.10: π-π interactions between complexes **4.13**. Hydrogen atoms and non-coordinating nitrate anion omitted for clarity.*

4.4 Copper(II) complexes of bis-(pyrazolylbenzimidazole) ligands L4.4, L4.5 and L4.6

Based on the observations of the coordination capabilities of the simple ligands **L4.1** – **L4.3**, ligands **L4.4** – **L4.6** were employed with emphasis on the formation of Cu(II) complexes, with the aim of forming 5-coordinate species in which the ligands occupy four binding sites, with either an anion or solvent molecule occupying the last coordination site. This particular coordination geometry, seemingly being well matched to the geometry of the individual binding sites, could be expected to generate either discrete or polymeric compounds in conjunction with ambivergent[373] ligands **L4.4** – **L4.6**, depending on the chosen orientation of the flexible methylene spacers.

*4.4.1 Synthesis of poly-[Cu_2(**L4.4**)Cl_4] **4.14***

Complex poly-[Cu_2(**L4.4**)Cl_4] **4.14** was prepared by the reaction of **L4.4** with $CuCl_2 \cdot 2H_2O$ in acetonitrile under solvothermal conditions with dwell temperature 120 °C. The resulting orange block crystals, formed in 30 % yield, were subjected to single crystal X-ray diffraction, and the data solved and the structure model refined in the orthorhombic space group *Pbca* (R-factor 6.25%). The asymmetric unit was found to contain a 5-coordinate Cu(II) ion coordinating to three chloride ions, two of which being crystallographically equivalent, and one ligand of **L4.4** in a bidentate fashion. The metal ion adopts a trigonal bipyramidal geometry with very little angular distortion, and slight contraction of the axial bonds (N(10)-Cu(1) 1.965(6) Å, *cf.* N(4)-Cu(1) 2.118(6) Å). The pyrazole-benzimidazole interplanar angle of 7.7(2)° is within expected limits, as is the bite angle of 78.0(2)°. When the structure is grown, a one-dimensional polymeric structure is revealed, in which two equivalent Cl(3) ions bridge between Cu(1) ions, which are connected by the bis-bidentate **L4.4** linker. The polymer proceeds in a zig-zag fashion parallel to the *c* axis with pyrazolylbenzimidazole groups forming parallel mean planes, as shown in Figure 4.11.

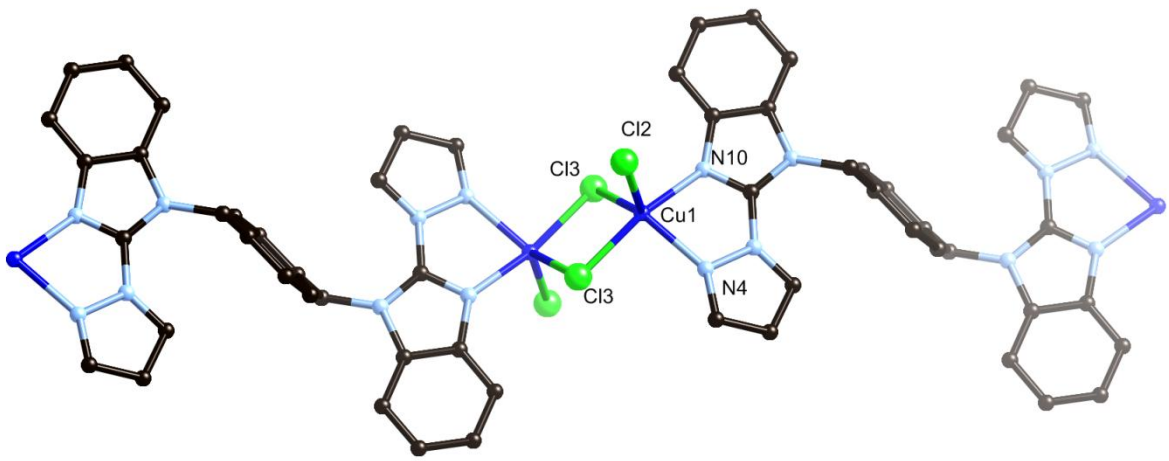

*Figure 4.11: Structure of **4.14** with partial heteroatom labelling scheme, hydrogen atoms omitted for clarity.*

The primary modes of intermolecular interaction in **4.14** are face-to-face and edge-to-face π-π stacking, an example of which is shown in Figure 4.12. Benzimidazole and pyrazole moieties from adjacent strands undergo a partial overlap at a mean interplanar angle of 11.2(3)° and minimum interatomic distance of 3.351(5) Å for C(5)-C(15), linking chains together in the *a* direction, as shown in Figure 4.14, and weak C-H···π interations from the hydrogen atoms at the 5- and 6- positions of the benzimidazoles to the pyrazole ring of the adjacent chain occur with C···π (mean plane) distance

of 3.701(9) Å and C-H···C angle of 151.5(5)° for C(13)-H(13)···C(5), linking chains in the *b* direction. The net result of these interactions is the formation of a densely packed three-dimensional structure, in which no voids or solvent channels are observed, and the crystals retain crystallinity on drying in air, with thermal analysis showed negligible loss of mass below 200 °C.

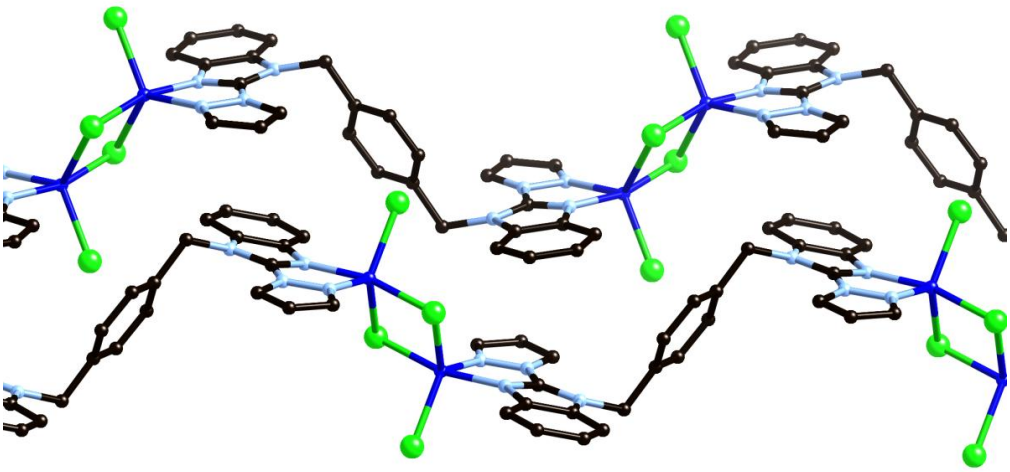

Figure 4.12: Two adjacent chains in the structure of ***4.14*** *showing π-π stacking interactions. Hydrogen atoms omitted for clarity.*

*4.4.2 Synthesis of [Cu_2(**L4.4**)$_2$(OH_2)$_2$]·4ClO_4·PhMe·1.5(MeCN)·2(H_2O)* ***4.15***

Reaction of ligand **L4.4** with either $Cu(ClO_4)_2·6H_2O$ or $Cu(BF_4)_2·6H_2O$ in acetonitrile gave a green solution, which was analysed by both mass spectrometry and a UV/Visible spectroscopic titration, showing a poorly resolved mixture of several metal-containing species, which were not able to be fully identified. Diffusion of toluene vapour into both mixtures yielded green single crystals after several days. Both sets of crystals were analysed by single-crystal X-ray diffraction, and were found to be isostructural. For the purposes of this discussion, the more strongly diffracting perchlorate complex will be analysed; however, it should be noted that for safety reasons all thermal studies were carried out on the structurally identical tetrafluoroborate complex. The structure of complex **4.15** was solved and refined in the monoclinic space group *C*2/*m* (R-factor 7.22%), and was found to contain two unique Cu(II) ions in the unit cell, both coordinating to two bidentate **L4.4** units and one water molecule. Interestingly, each copper site experiences different crystallographic symmetry elements, with Cu(1) coordinating to two non-equivalent halves of **L4.4** units, the remainder of which are generated by a mirror plane running through the phenyl spacer, while Cu(2) lies on a twofold axis,

requiring only one unique half-unit of **L4.4** from which the remaining binding sites are generated by a rotation, and the other half of which are also generated by the mirror plane through the phenyl spacer. In this way, the symmetry of at least the Cu(2) complex is reminiscent of that seen in compound **3.12**, which also crystallised in the relatively unusual space group *C*2/*m*. Furthermore, owing to this inequality in the crystallographic symmetry of the two sites, there exist two Cu(1) dimers for every one Cu(2) dimer.

The ligand geometries do not appear significantly different between the two copper sites; the two pyrazole-benzimidazole interplanar angles of 3.6(3) and 8.4(2)° and bite angles of 77.6(2) and 79.6(2)° for the Cu(1) environment compare well to those for Cu(2) of 4.5(3) and 79.7(2)°. However, each copper site does exhibit slightly different coordination geometries; Cu(1) could be described as either a square pyramidal geometry or trigonal bipyramidal, with the N(35)-Cu(1)-O(39) angle of 145.0(2)° lying near the middle of the expected angle of 120° for equatorial trigonal bipyramidal and 180° for *trans* – square pyramidal. However, the elongated axial Cu(1)-N(3) distance of 2.172(6) Å (*cf.* Cu(1)-N(35) distance of 2.008(5) Å) suggests assignment of a square pyramidal geometry is more appropriate. Cu(2) exhibits similar angular dimensions to Cu(1), with N(41)-Cu(2)-N(41′) angle of 139.1°; however, the lack of significant bond lengthening of the pseudo-axial Cu(2)-O(40) bond (2.090(7) Å, *cf.* 2.063(5) Å for Cu(1)-O(39)) suggests a trigonal bipyramidal assignment is more appropriate. The τ_5 parameter introduced by Reedijk[374] can also be used in this instance, defined as $(\beta-\alpha)/60°$, where β is the angle through the metal ion between donor atoms considered in the axial positions of the trigonal bipyramid (or a *trans* angle through the basal plane of a square pyramid), and α is the largest equatorial angle of the trigonal bipyramid (or the remaining *trans* angle in the basal plane), where a value of zero indicates a perfect square pyramidal geometry and a value of 1 represents trigonal bipyramidal geometry. In this instance, τ_5(Cu1) = 0.46 and τ_5(Cu2) = 0.57, consistent with the above assignments of slight tendency towards square pyramidal for Cu(1) and trigonal bipyramidal for Cu(2).

The noticeable effect of the two coordination geometries is a change in orientation of the water molecule with relation to the mean planes of the coordinating ligands; the Cu(1)-O(39) bond is approximately orthogonal to one ligand mean plane and nearly parallel to the other, while the Cu(2)-O(40) bond overlaps a twofold axis, requiring it to lie exactly between the two ligand mean planes. The action of the crystallographic symmetry elements expands the metal regions into two non-equivalent cyclic dimers, each containing a crystallographically disordered toluene molecule within the central cavity, as shown in Figure 4.13. Also located in the unit cell were 1.5 acetonitrile

molecules, two water molecules and four perchlorate anions per dimer, with poorly resolved residual electron density suggesting the presence of further solvation which was not able to be modelled.

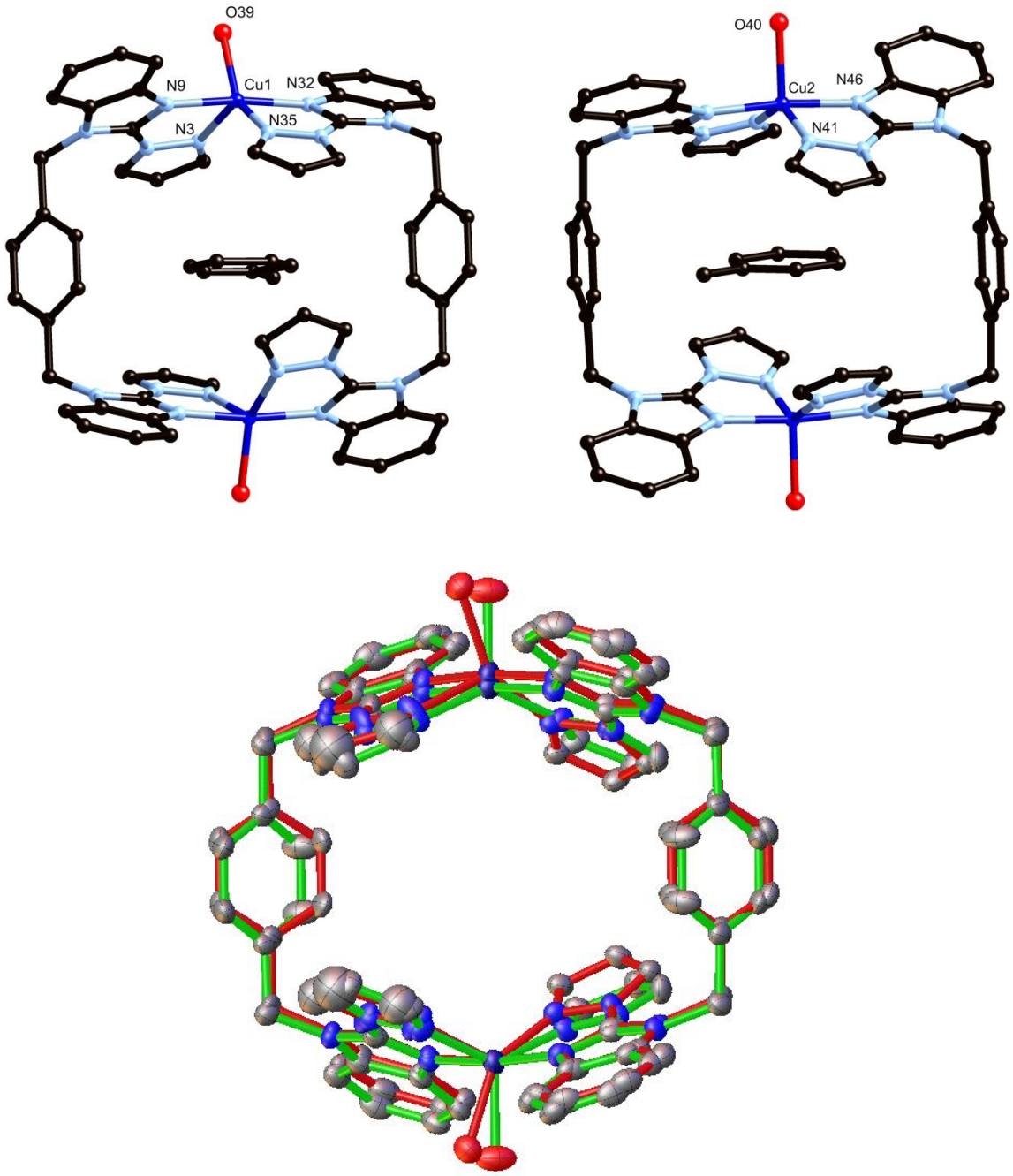

*Figure 4.13: (Top)Structure of complex **4.15** showing dimers of Cu(1) (Left) and Cu(2) (Right) with unique coordinating heteroatom labelling scheme. Hydrogen atoms, anions and additional solvent molecules omitted for clarity. (Bottom) Two non-equivalent units of **4.15** overlaid showing the difference in orientation of the coordinating water molecules, with the Cu(1) dimer coloured red and Cu(2) dimer coloured green.*

Immediately noticeable in the structure of **4.15** is the seemingly strong interaction with the aromatic guest molecule within the cavity of each dimer. Each toluene molecule experiences π-π interactions from four related pyrazolylbenzimidazole moieties, with closest inter-atomic distances of 3.399(8) Å (N(3)-C(92)) within the Cu(1) dimer, and 3.400(6) Å (N(41)-C(87)) within the Cu(2) framework. Each toluene molecule also experiences edge-to-face interactions with the phenylene walls, with minimum C···π (mean plane) distances of 3.515(5) Å and 3.684(5) Å for the Cu(1) and Cu(2) units, respectively. The remaining solvent molecules in the unit cell do not show significant interactions with the complexes. Thermal analysis, carried out on the isostructural tetrafluoroborate analogue, showed a broad single step mass loss of 11% before 100 °C, consistent with loss of the modelled non-coordinating solvents (calculated for 1 PhMe, 1.5 MeCN, $2H_2O$ per dimer 11.6%). Removing these modelled solvents from the crystallographic model showed 18 % solvent accessible area within the unit cell by PLATON calculation.[375] Unsurprisingly, the crystals were seen to instantly lose crystallinity on drying in air.

Intermolecular interactions in **4.15** are a combination of hydrogen bonding and π-π stacking. Complexes engage in hydrogen bonding to selected anions *via* the coordinated water molecules. These interactions are strictly zero-dimensional in nature, and complexes are not linked to each other in this manner; however, these interactions serve to retain reasonable crystallographic order for those anions involved. The primary interactions between complexes are π-π stacking between conjugated pyrazolyl-benzimidazole moieties. Two unique interactions of this type exist; Cu(2) dimers interact only with Cu(1) units, at 10.05(9)° interplanar angle and minimum C-C distance 3.356(8) Å for C(28) - C(47), while Cu(1) units also interact with each other at mean interplanar distance 3.323(4) Å for parallel mean planes. The bent arrangement of the two chelating ligands around each metal results in the propagation of this interaction into a two dimensional sheet perpendicular to the [1,0,1] vector, along which the internal cavity of each complex aligns to form a series of one-dimensional channels containing the encapsulated toluene molecules and non-hydrogen bonded perchlorate anions. These channels seem to be formed more from the shape complementarity of the front and back faces of the complex and the perpendicular π-π interactions than from any particular interaction parallel to the channels; as shown in Figure 4.14, no substantial π-π interactions exist parallel to the channels, but adjacent complexes adopt a clip-like shape in order to pack together efficiently in this manner.

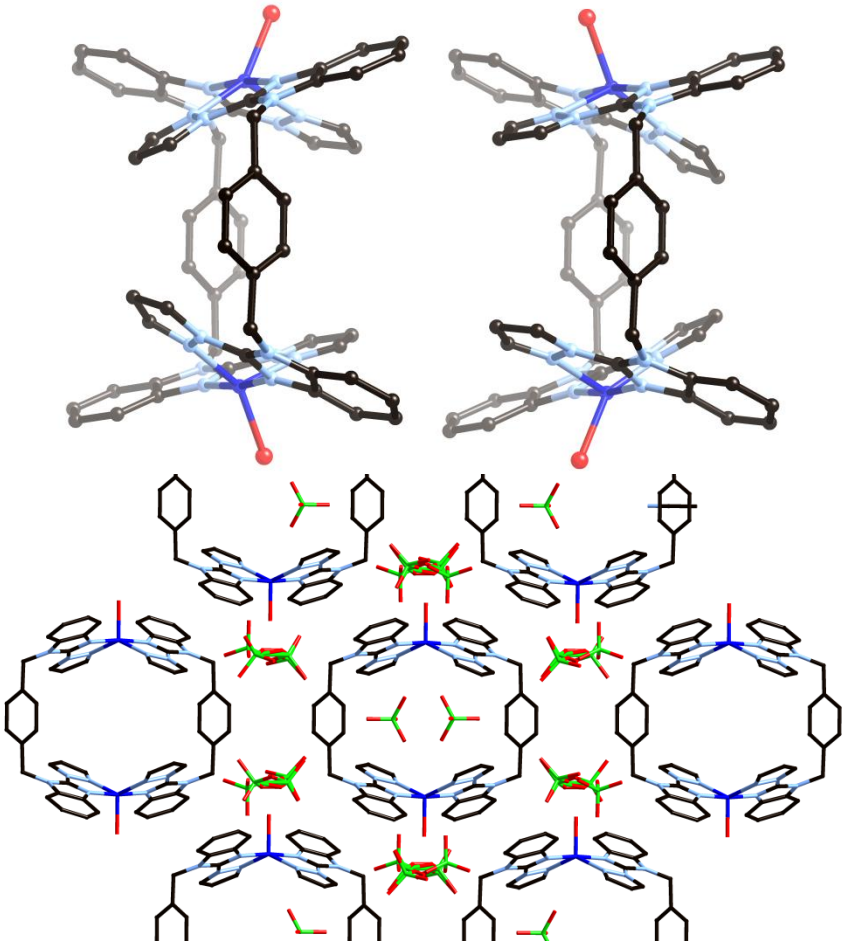

*Figure 4.14: (Top) Interaction between complexes parallel to the central channel in **4.15**. Hydrogen atoms omitted for clarity. (Bottom) Representation of the packing motif in **4.15**, showing a single layer of dimeric complexes and several layers of anions. Central toluene molecules, hydrogen atoms and other solvent molecules omitted for clarity.*

*4.4.3 Synthesis of $[Cu_2(\mathbf{L4.5})_2(OH_2)_2]\cdot 4BF_4\cdot x$(mesitylene) **4.16***

Reaction of ligand **L4.5** with either $Cu(ClO_4)_2\cdot 6H_2O$ or $Cu(BF_4)_2\cdot 6H_2O$ in nitromethane gave immediate formation of a green soluble species **4.16**. Several attempts were made to characterise this compound with UV/Visible spectroscopic titrations; however, the significant insolubility of **L4.5** at the required concentrations hindered progress in this area, while analysis by electrospray mass spectrometry showed a mixture of [ML] and $[M_2L_2]$ species, with the copper ions in either the 1+ or 2+ oxidation state. In order to elucidate the structure of the complex, single crystals were prepared by diffusion of mesitylene into a nitromethane solution of the complex. Unfortunately, any crystalline material generated by a variety of solvent combinations decomposed in a matter of seconds when

removed from the mother liquor, even when coated in inert oil, and as such single crystals for X-ray diffraction were taken directly from the mother liquor and immersed in the cold gas stream of the instrument as quickly as possible. The perchlorate complex was found to adopt a low symmetry setting, and provided poor quality diffraction data, although a low resolution structure model was obtained, which showed the structure possess very similar crystal packing to the tetrafluoroborate analogue, with coordination of the perchlorate anion in place of the coordination water molecule across half of the metal sites. Fortuitously, the tetrafluoroborate analogue provided significantly better diffraction data and higher symmetry, and as such only this structure will be discussed in depth, although the perchlorate analogue showed very similar crystal packing behaviour.

On single crystal X-ray diffraction analysis, the structure of complex **4.16** was solved and refined in the monoclinic space group $P2_1/n$ (R-factor 7.14%). The asymmetric unit was found to contain one molecule of **L4.5** and one copper(II) unit and associated non-coordinating tetrafluoroborate anions. The coordination geometry of the copper ion is best described as trigonal bipyramidal (τ_5 = 0.68), in which two molecules of **L4.5** coordinate in bidentate fashion, with the remaining equatorial coordination site filled by a water molecule. In accordance with this coordination geometry, bond contraction occurs at the axial sites, with benzimidazole-copper bonds N(8)-Cu(1) = 1.954(3) and N(37)-Cu(1) = 1.983(3) Å notably shorter than pyrazole – copper bonds N(40)-Cu(1) = 2.083(4) and N(2)-Cu(1) = 2.036(3) Å. As expected, when the structure is grown, an $[M_2L_2]^{4+}$ dimeric structure is revealed, with an inversion centre located at the mid-point between the two copper ions within the central cavity. The ligand geometry of **4.16** also compares well to those seen in **4.15**, with pyrazole-benzimidazole torsion angles of 2.43(17)° and 2.63(17)° leading to bite angles of 79.64(14) and 80.27(14)°, respectively. As would be expected, the torsion between the two rings of the biphenyl unit of 32.2(2)° indicates steric repulsion between the two rings; small amounts of residual electron density symbolising the other equivalent torsion were deemed too small to warrant explicit modelling. The structure of **4.16** is shown in Figure 4.15.

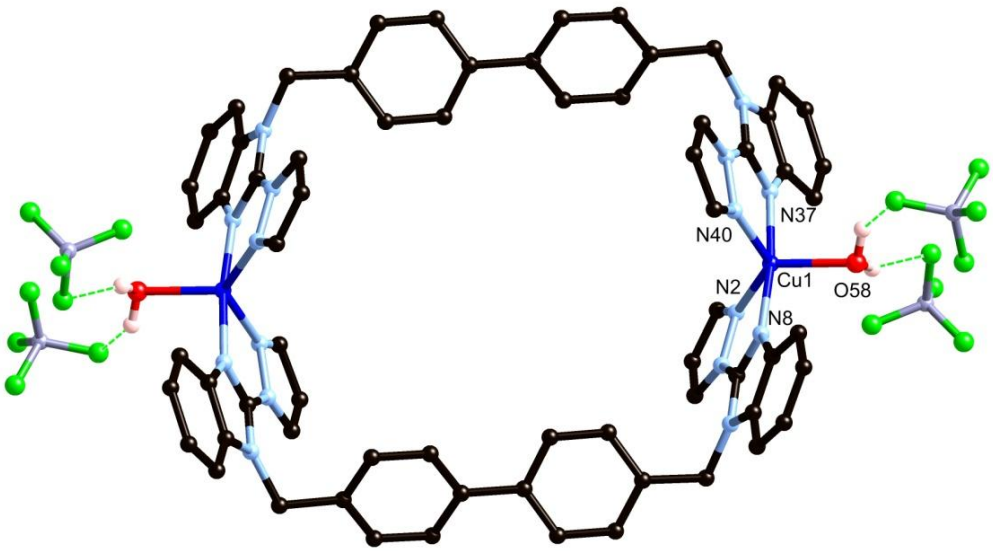

*Figure 4.15: Structure of complex **4.16** with partial heteroatom labelling scheme showing hydrogen bonding between coordinated water molecules and tetrafluoroborate anions. Hydrogen atoms not involved in hydrogen bonding omitted for clarity.*

The structure of **4.16** closely resembles that observed in **4.15**, with the 2 dimensional sheet structures formed by the π-π interactions along the *bc* plane aligning such that the internal cavities of the molecules combine to form polymeric channels along *a*. Due to the high degree of symmetry in the structure of **4.16**, only one type of pyrazolylbenzimidazole-based π-π stacking interaction is required to propagate the two-dimensional sheet, with mean interplanar angle 3.93(8)° and minimum C-C distance 3.424(5) Å for C(7)-C(33). As well as the primary channels within dimers, of interatomic dimensions *ca.*1.0 × 1.3 nm displayed in Figure 4.16 below, a number of other channel-like structures are observed; smaller parallel channels walled by the biphenylene moieties exist between molecules, while inefficient packing between the dimeric species along *a* leads to two-dimensional cavity space parallel to the *bc* plane, where the steric bulk of the pyrazolylbenzimidazole moieties forces the two-dimensional sheets apart, and a similar series of channels along the [1,0,1] vector. Notably, all of the tetrafluoroborate anions were located in positions hydrogen bonding to the coordinated water molecules, substantially reducing the amount of crystallographic disorder within the structure and creating more free space within the primary channels.

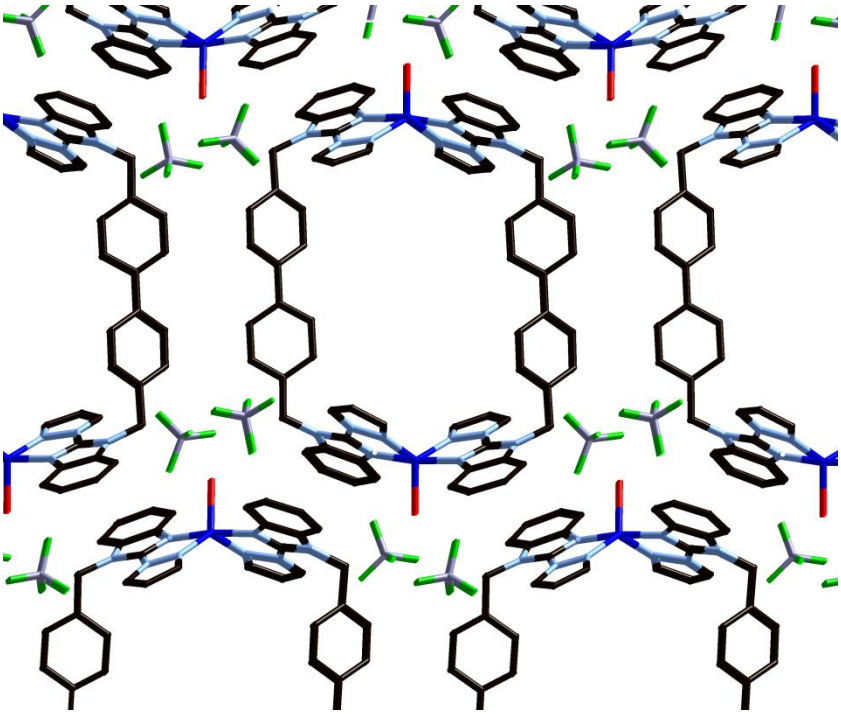

Figure 4.16: Extended structure of ***4.16*** *viewed parallel to the major solvent channels and showing π-π interactions from each complex to four adjacent dimers. Hydrogen atoms omitted for clarity.*

Due to the large size of the cavities within the dimers, no meaningful information could be extracted as to the solvent content of the complex, and as such the SQUEEZE routine was employed to improve the precision of the remaining atoms.[246] This calculation revealed a solvent accessible volume of approximately 30 % of the unit cell, occupied by approximately 600 electrons. This value is consistent with solvation on the order of 5 nitromethane or 3 mesitylene molecules per dimer for the solvated complex. Thermal and elemental analyses were carried out on the dry amorphous sample, in an attempt to determine the solvent content of the framework collapsed material. The thermogravimetric analysis of a freshly isolated sample suggests a mass loss of *ca.* 19% with immediate onset and brief plateau at 180 °C, followed by a two step decomposition process. This value is in approximate agreement with the electron count proposed by SQUEEZE. Elemental analysis, taking place several days after isolation, was consistent with a largely dry sample, showing the retention of only one half of a mesitylene molecule per dimer. This level of desolvation over time is consistent with the immediate onset of mass loss observed in the thermogravimetric analysis.

*4.4.4 Synthesis of [Cu_2(**L4.6**)$_2$(NO_3)$_2$]·2(NO_3)·MeCN **4.17***

Reaction of ligand **L4.6** with $Cu(NO_3)_2 \cdot 3H_2O$ in acetonitrile with gentle heating gave a pale blue/green solution which, on concentrating by slow evaporation over several days, deposited small green rod crystals of complex **4.17**. These crystals were analysed by single crystal X-ray diffraction, and the data obtained were solved and the structure model refined in the monoclinic space group $P2_1/c$ (R-factor 7.37%). The asymmetric unit of **4.17** contains one molecule of **L4.6** in its entirety, coordinating to two crystallographically equivalent Cu(II) ions. One acetonitrile molecule was also located within the asymmetric unit. The metal centre is coordinated in a square pyramidal geometry, with four binding sites occupied by chelating **L4.6** nitrogens, and one coordination site occupied by a monodentate nitrate anion. Benzimidazole nitrogen N(31) occupies the axial coordination site, with a lengthened Cu(1)-N(31) bond of 2.237(6) Å (*cf.* Cu(1)-N(8) 1.973(6) Å). The geometry of the copper site shows very little distortion towards the trigonal bipyramidal geometry, with equatorial *trans* angles N(2)-Cu(1)-N(37) and O(38)-Cu(1)-N(8) of 171.7(2) and 165.8(2)°, respectively. Charge balance is achieved by the presence of a non-coordinating nitrate anion. When the structure is extended by the internal symmetry elements, an $[M_2L_2]^{4+}$ dimer is revealed, as would be expected based on the high solubility, and on comparison to complexes **4.15** and **4.16**. The structure of **4.17** is shown in Figure 4.17.

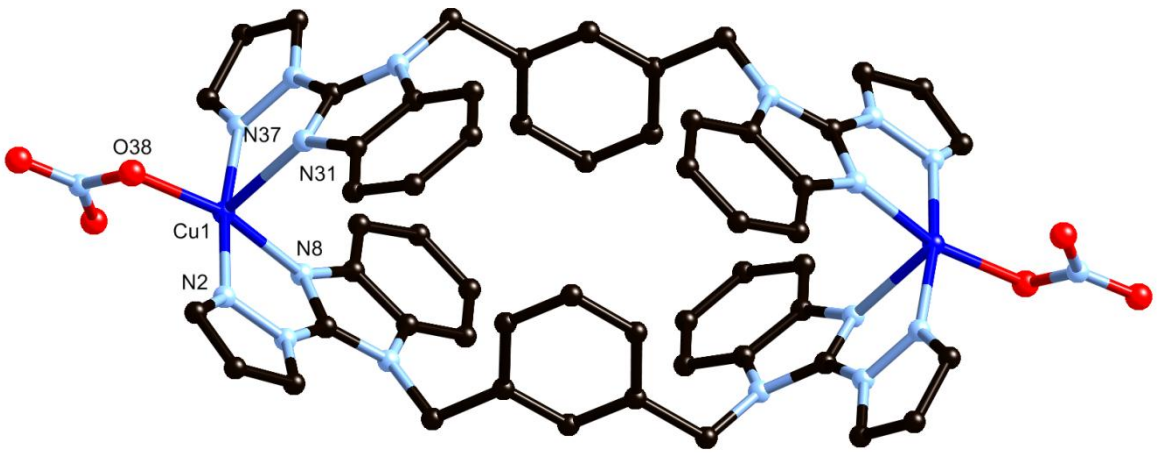

*Figure 4.17: Structure of compound **4.17** showing partial heteroatom labelling scheme. Hydrogen atoms, unbound nitrate anions and solvent molecules omitted for clarity.*

In comparison to complexes **4.15** and **4.16**, compound **4.17** contains no appreciable internal cavity within which to encapsulate solvent molecules or guests. Indeed, the structure of the complex seems

enforced by the ligand geometry to preclude any cavity formation. Although the two *m*-phenylene rings within **4.17** are parallel, the interplanar distance of 4.093(10) Å, as well as the lack of substantial overlap, suggest this arrangement is merely a result of the ligand geometry rather than any attractive interaction. However, several hydrogen atoms from the phenylene ring appear to fall within the range of weak intramolecular C-H···π interactions with the benzimidazole rings, *e.g.* C(20)-H(20)···C(10), with C(20)-π (mean plane) distance of 3.759(7) Å and C-H···C angle of 165.0(5)°, again most likely a result of the ligand geometry rather than significant attractive forces. The primary weak interactions in the structure of **4.17** are intermolecular in nature, and are aided by the regular hexagonal prism-type profile of the discrete complex itself. These interactions are most significant in the *bc* plane, where each conjugated pyrazolyl-benzimidazole unit engages in a π-π stacking interaction with the opposite moiety, at a minimum interatomic distance of 3.253(7) Å for N(31)-N(15) and a slight angular offset of 3.41(10)°. This interaction propagates a 2-dimensional sheet in the *bc* plane, as shown in Figure 4.18, while in the perpendicular *a* direction, no strong interactions are observed.

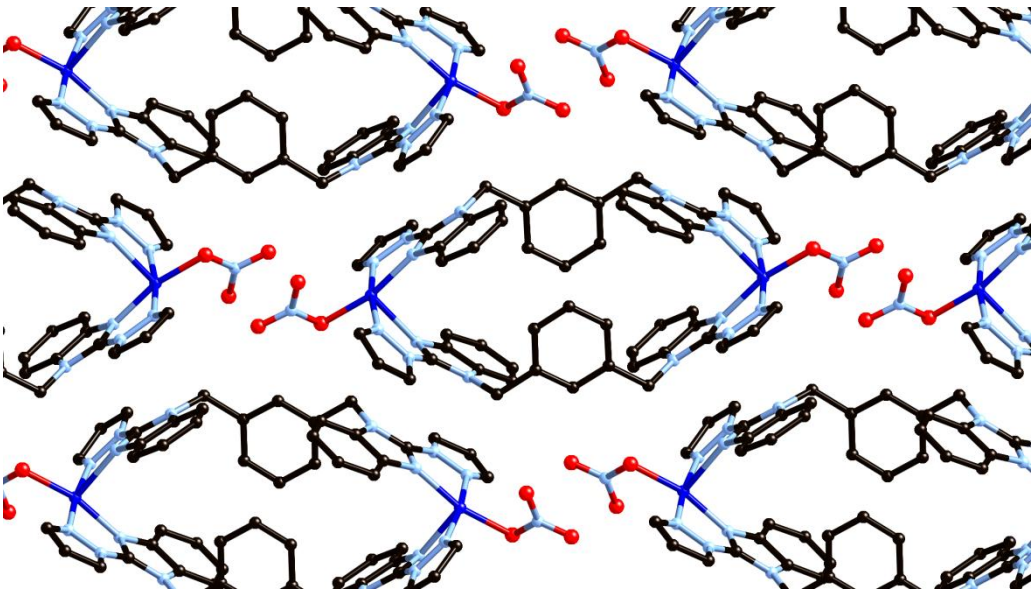

*Figure 4.18: Intermolecular interactions in the extended structure of **4.17**, showing four intermolecular π-π interactions per discrete unit. Hydrogen atoms, unbound nitrate anions and solvent molecules omitted for clarity.*

The lack of interaction parallel to the *a* edge, due to the inwardly bent phenylene rings being prevented from external π-π interaction by the steric bulk of the benzimidazole groups, gives rise to small solvent channels parallel to the *b* unit cell axis, which in the crystallographic model are occupied by acetonitrile moieties. Removal of the modelled solvent from the structure model, followed by the CALC-SOLV routine in PLATON,[375] suggested a 14% solvent accessible volume

within the desolvated structure; however, the crystals were observed to lose solvent immediately on drying in air. Thermogravimetric analysis was carried out on a sample of **4.17**, showing slow loss of *ca.* 3 % mass up to 150 °C with immediate onset, consistent with only one acetonitrile molecule per complex. However, it is expected that significant quantities of solvent are lost immediately following removal of the crystals from the mother liquor. On heating under nitrogen flow, a thermal decomposition was observed at the comparatively low temperature of 180 °C, which may be consistent with an oxidative process involving the densely packed nitrate anions lining the solvent channels.

*4.4.5 Synthesis of [Cu_4(**L4.6**)$_2Cl_8$]·MeCN **4.18***

Ligand **L4.6** gave an amorphous insoluble material on reaction with $CuCl_2 \cdot 2H_2O$ in acetonitrile under mild conditions, and as such the reaction was repeated solvothermally, where a pressure vessel containing **L4.6** with one equivalent of $CuCl_2 \cdot 2H_2O$ in 10 ml acetonitrile was heated to 120 °C and allowed to dwell for 24 hours, followed by slow cooling to room temperature at 6 °C/hr, giving the product **4.18** as small green crystals. The diffraction data were solved and the structure model refined in the triclinic space group *P*-1 (R-factor 4.72%), in which the asymmetric unit contained one molecule of **L4.6** coordinating to two unique copper ions. Immediately obvious is the presence of two different coordination geometries for the copper ions; Cu(1) coordinates in a Jahn-Teller tetragonally distorted octahedral fashion to two nitrogen atoms from ligand **L4.6** and four chloride ions, two of which being crystallographically equivalent, while Cu(2) coordinates in a highly distorted square pyramidal fashion to three unique chloride ions as well as the bidentate ligand **L4.6.** The tetragonal distortion of the Cu(1) ion is displayed as lengthening of the Cu(1)-Cl(3) bond (2.9129(13) Å) and the Cu(1)-Cl(5) bond (2.9486(15) Å), with simultaneous contraction of the equatorial bonds (*e.g.* Cu(1)-N(7) 2.018(4) Å *vs* Cu(2)-N(39) 2.066(4) Å). The geometry of Cu(2), although best described as square pyramidal, is in reality an intermediate between trigonal bipyramidal and square pyramidal (τ_5 = 0.46); the three pseudo-equatorial angles fall in the range 100.65(11) – 141.63(12)° (*cf.* expected values; 120° for trigonal bipyramidal, 90° and 180° for square pyramidal); however, only a moderate bond contraction is observed for the pseudo-axial Cu(2)-N(36) bond (2.010(5) Å *vs* 2.025(4) Å for Cu(1)-N(13)), while a significant bond lengthening is observed for the Cu(2)-Cl(3) bond (2.5835(12) Å *vs* Cu(2)-Cl(6) 2.2668(15) Å), which would be expected from a square pyramidal complex, although this effect is likely enhanced due to the μ^3 nature of chloride Cl(3). When the structure of

4.18 is extended by the action of crystallographic symmetry elements, a centrosymmetric tetranuclear complex of the molecular formula $[Cu_4(\mathbf{L4.6})_2Cl_8]$ is revealed, as shown in Figure 4.19.

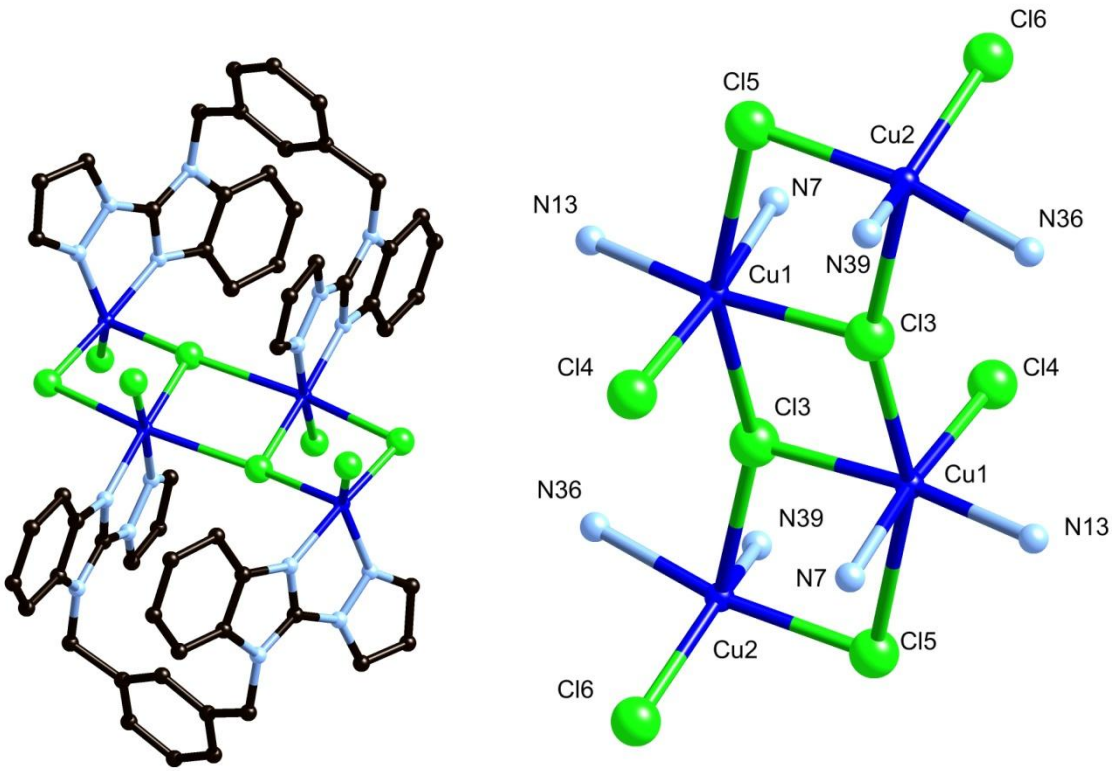

*Figure 4.19: (Left) Structure of complex **4.18**. Hydrogen atoms and solvent molecules omitted for clarity. (Right) Structure of the metal sites of complex **4.18** with labelling scheme for coordinating atoms.*

Notable in the structure of **4.18** is the tapering parallel to the *a* edge from the pyrazolylbenzimidazole units of each ligand, with mean interplanar angle of 26.65(4)°. When considering the three-dimensional structure, it appears this distortion aids the formation of π-π stacking-type interactions between complexes, where the open ends of two **L4.6** ligands are able to interlock with partial overlap of parallel pyrazole rings, at a mean interplanar distance of 3.257(5) Å, as shown in Figure 4.20. This interaction, however, is less significant than the primary mode of intermolecular interaction, being the π-π overlap of the entire pyrazolyl benzimidazole system of adjacent species along the [0,1,1] vector at a mean interplanar distance of 3.233(3) Å and zero angular offset. A third type of π-π stacking is also observed, in the interaction of equivalent parallel phenylene rings at a slightly longer mean interplanar distance of 3.522(4) Å, continuation of which links the complexes along the [1,1,1] vector. The result of all three of these interactions is the formation of a densely packed network with no visible void space. One acetonitrile molecule per tetramer is present in the structure, disordered over

two equivalent orientations; however, no significant interaction is observed with the main residue, and no channel structures were observed. Thermal analysis shows that compound **4.18** is completely desolvated by 100 °C, and a corresponding loss of single crystallinity is observed.

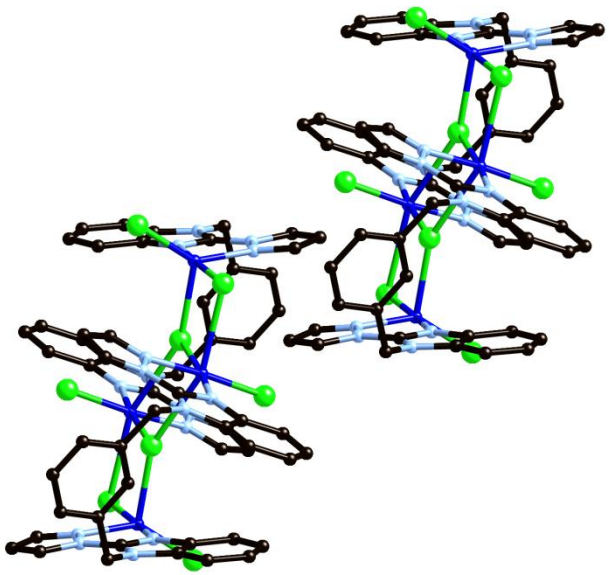

*Figure 4.20: Intermolecular interactions between two units of **4.18** showing π-π interactions between the tapered internal faces of the pyrazolylbenzimidazole systems.*

4.5 Synthesis of $[Zn_2(L4.7)_3]\cdot 4(CF_3SO_3)\cdot 5(MeNO_2)$ 4.19

Ligand **L4.7** was expected to form triple helicate complexes with octahedral transition metals akin to those seen with ligand **L3.1**, and as such, attempts were made to react **L4.7** with Zn(II), Ni(II) and Fe(II) salts. Of the reactions tested, the best and most reproducible results were achieved with Zn(II), where reaction with $Zn(ClO_4)_2\cdot 6H_2O$ in acetonitrile gave colourless crystals by slow evaporation. However, these crystals proved extremely unstable, losing single crystallinity immediately on contact with air and on rapid cooling in the cold stream of the diffractometer, and although a low resolution structure was obtained, efforts were directed to finding a more stable analogue by varying the anions and crystallisation solvents. Solution studies of the complex proved fruitless, with an NMR titration experiment showing substantial broadening of the ligand peaks on addition to metal consistent with rapid fluxional behaviour in solution, while no peaks due to the complex could be detected *via* mass spectrometry. It was found that the reaction of **L4.7** with $Zn(CF_3SO_3)_2$ in nitromethane, followed by slow diffusion of diisopropyl ether, generated single crystals in 20 % yield, which, although slowly

losing crystallinity on removal from the mother liquor, were sufficiently stable to obtain a high resolution crystallographic model. The diffraction data were solved and the structure model refined in the monoclinic space group $P2_1/n$ (R-factor 5.93%), where the asymmetric unit was found to contain two Zn(II) ions coordinating in an octahedral fashion to three molecules of **L4.7** to form a dinuclear triple helicate. The asymmetric unit contained this complex in its entirety, and the charge was balanced by four crystallographically localised trifluoromethanesulfonate anions. Five nitromethane molecules were located in the asymmetric unit, each modelled at full occupancy. The remaining electron density peaks suggested the presence of additional disordered solvent within the unit cell; however, these sites were too diffuse to model suitably, and comprised a sufficiently small fraction of the total volume as to be disregarded. The structure of **4.19** is shown in Figure 4.21.

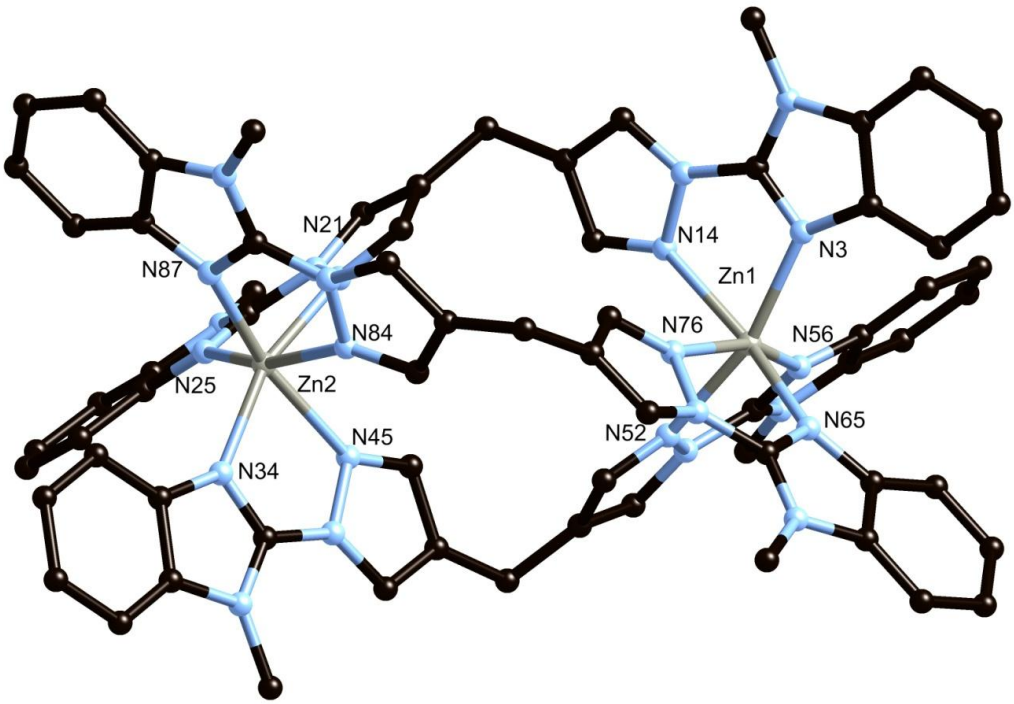

*Figure 4.21: Structure of complex **4.19** with partial heteroatom labelling scheme. Hydrogen atoms, anions and solvent molecules omitted for clarity.*

The structural parameters in **4.19** can be compared to those discussed in Chapter 3, particularly for complexes **3.6A** and **3.6B**. The metal-metal distance of 8.0538(6) Å is longer than those for the triple helicate complexes previously, while the φ_1 and φ_2 values, falling between 131.4(4) – 140.2(4)°, are comparable, and the pyrazole-pyrazole interplanar angles, ranging from 61.93(14) – 69.50(14)°, are in general slightly smaller. The average pyrazole-benzimidazole interplanar angles, which range

between 0.49(14) and 11.77(14)°, indicate a strong degree of conjugation between the ring systems. The small bite angles imposed by the chelating five-membered rings, which fall in the range 74.30(11) – 76.12(11)°, are consistent with the data observed for the other pyrazolylbenzimidazole ligands described above; however, when constrained to an octahedral geometry, these angles force significant distortion to the ideal coordination sphere. This observation is supported by the octahedral distortion parameter Σ, defined as the sum of the absolute value of the deviation of each of the 12 *cis* angles from 90°,[376] which for Zn(1) and Zn(2) are 107.7 and 106.1°, respectively. These data suggest that, as expected, the small bite angle provided by the five-membered rings in **L4.1 – L4.7** provides a highly distorted octahedral coordination sphere, where formation of the octahedral complex only appears to be favoured when other influences, such as the observed tendency for ligands of this type to form triple helicates, are active. For this reason, **4.19** remains the only example of a reproducible octahedral coordination sphere saturated with pyrazolylbenzimidazole ligands that was structurally characterised in the course of this study.

As was the case with complexes **3.6A** and **3.6B**, complex **4.19** possesses no hydrogen bond donor or acceptor sites, and as such the intermolecular interactions were expected to be limited to π-π stacking interactions. Interestingly, unlike complexes **3.6A** and **3.6B** and despite the presence of large conjugated panels facing outwards from the helicate, the only mode of interaction directly between helicates was a "sixfold aryl embrace" type interaction, shown in Figure 4.22, in which the helicates align parallel to the helical axis with six edge-to-face π-π interactions between the terminal benzimidazole rings of each helicate. These interactions all possess minimum carbon – centroid distances in the range of 3.514(4) – 3.714(4) Å. Such interactions have been observed in the structure of metal tris-bipyridine complexes, or complexes containing triphenylphosphine or other closely spaced aromatic systems, as reviewed by Dance.[377] The result of these interactions is a loosely packed assembly of one-dimensional chains of **4.19** molecules running parallel to the [1,0,1] vector, shown in Figure 4.24. The interstitial spaces are occupied by trifluoromethanesulfonate anions and nitromethane molecules, the latter of which also engage in interactions with the π-system of the benzimidazole rings, with minimum interatomic distance 3.352(6) Å and 9.2(2)° interplanar angle for a representative example.

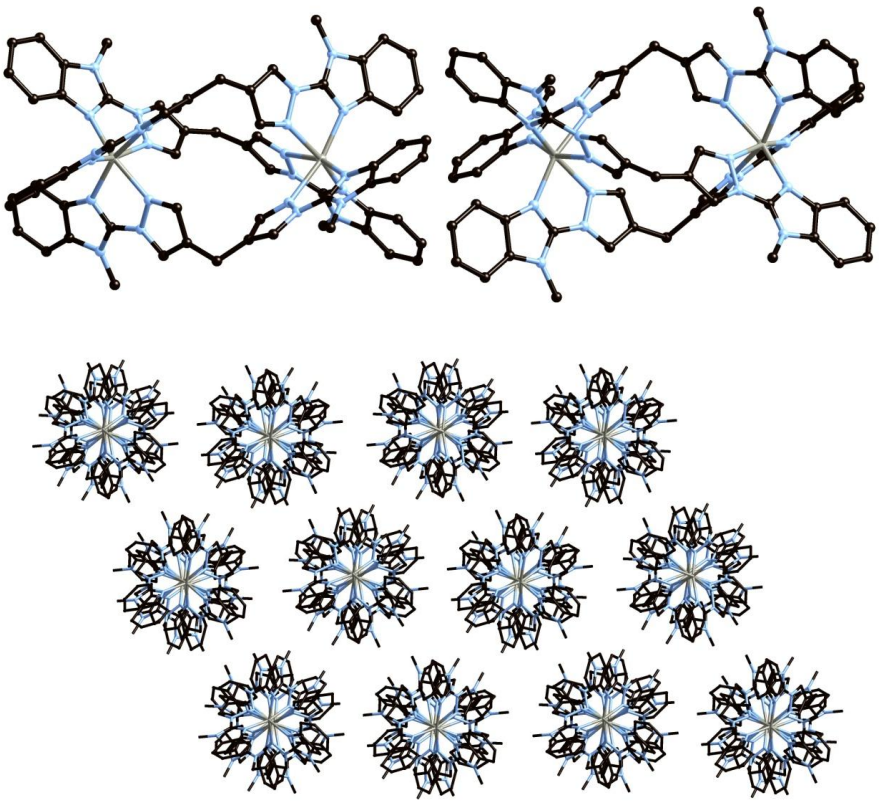

*Figure 4.22: (Top) Sixfold aryl embrace interactions between two adjacent **4.19** helicates; (Bottom) Representation of the packing arrangement in **4.19** viewed parallel to the helical axis. Hydrogen atoms, and interstitial anions and solvent molecules omitted for clarity.*

Although sufficiently stable under inert oil at low temperature to collect a full crystallographic data set, the crystals of **4.19** were observed to lose crystallinity quickly on drying in air. Thermal analysis showed the loss of 18 % mass by 100 °C, indicating the presence of additional solvent molecules beyond the crystallographically determined 5 nitromethane molecules per complex, which account for 14 % of the mass of the complex. Elemental analysis indicated water molecules were also present within the structure, suggesting the formula $[Zn_2(\mathbf{L4.7})_3]\cdot 5MeNO_2\cdot 2H_2O$ for the air-dried sample. As was observed in the structure **3.6B**, the exact degree of solvation is expected to vary with time after removal from the mother liquor, as evidenced by the immediate onset of desolvation on the thermogravimetric analysis instrument.

4.6 Discussion

From the analysis of complexes **4.11** – **4.19** above, several conclusions can be drawn regarding the utility of the 1-(2-benzimidazolyl)-pyrazole ligand system with regard to the construction of metallosupramolecular assemblies. Initially, some level of comparison can be drawn with the 1-(2-pyridyl)-pyrazole complexes discussed in Chapter 3. Replacement of pyridine for benzimidazole would be expected to lower the effective binding strength of the ligand, both by reducing the π-acceptor character and by the geometric constraints imposed by the addition of a second five-membered ring. This effect was readily observed in solution, where despite exhibiting good solubility, complexes **4.15** – **4.17** displayed a mixture of products by mass spectrometry, and UV/Visible spectroscopic titrations failed to show the formation of any dominant species, while complex **4.19** was also not convincingly observed in solution. While weak and reversible binding is generally desirable in the formation of metallosupramolecular architectures, such ligands can also be susceptible to displacement by competitive solvents or anions, as was seen in complex **4.12**, where even in the presence of excess ligand, the [Mn(**L4.2**)$_2$(MeCN)(OH$_2$)] species was formed predominantly.

It was found that by employing Cu(II) salts in reactions with these ligands, products were formed containing relatively predictable coordination geometries, in which four of the five available coordination sites were occupied by two chelating pyrazolylbenzimidazole moieties, in an arrangement suited to the narrow bite angle of the ligands. By maintaining this geometry, the effect of substitution on the benzimidazole backbone was able to be explored. As expected, where hydrogen bonding was present the influence of N-H···(anion) hydrogen bonding dominated the intermolecular interactions; however, substitution of the benzimidazole N-H provided functionality to form the polymetallic architectures **4.14 – 4.18**. Although polymeric structure **4.14** was observed in the presence of coordinating anions, compounds **4.15** – **4.18** dominated in the solid state, with no polymeric material observed under such conditions, presumably due to entropic effects favouring the formation of discrete species, particularly the Cu_2L_2 cyclic dimers. Substitution of the hydrogen bonding N-H group also had drastic effects on solubility, undoubtedly aiding the ability of such complexes to form and controllably crystallise in a range of solvents.

The inclusion of the benzimidazole framework also impacted on the intermolecular interactions by way of an extended π-π stacking synthon. Every structure containing **L4.1 – L4.7** displayed some degree of intermolecular π-π interactions, often encompassing the entire tricyclic conjugated system, as well as partial overlaps and edge-to-face interactions. It is clear that the inclusion of a larger conjugated system impacted on the degree of intermolecular interaction in this way, especially in the structure of **4.19**, where the extended structure was dominated by sixfold aryl

embrace interactions, not seen in related structures **3.6A** and **3.6B** due to the smaller aromatic systems and their close proximity to the sterically encumbered metal sites.

In summary, while the 1-(2-benzimidazolyl)-pyrazole system seemingly exhibited poorer binding properties than the related pyridylpyrazole systems, this deficiency was somewhat offset by a greater potential for functionalisation through the benzimidazole N-H group, and a greater propensity to form π-π stacking arrangements due to the presence of a larger π-system. These observations are of relevance to metallosupramolecular architectures containing the related heterocyclic species indazole, discussed in the following chapter.

Chapter 5

Hetero-Substituted Indazole Ligands

5.1 Introduction

Although well-known in medicinal chemistry,[239, 378, 379] indazole (benzo[d]pyrazole) is not commonly encountered in coordination chemistry, despite being expected to possess similar coordination properties to pyrazole, as well as a greater potential for functionalisation akin to structural isomer benzimidazole.[197] Instances of structurally characterised transition metal complexes containing indazoles are rare, with the most common usage of indazole being the tris-indazolylborate chelating ligands, akin to the well-known tris-pyrazolylborate ligands prevalent throughout coordination chemistry. These compounds have been thoroughly investigated, primarily for their coordination to second and third row transition metals,[380-383] although Janiak, Trofimenko and others have employed such ligands in several studies involving first row transition metals.[384-388] Aside from these, only a handful of studies have reported structural characterisation of complexes containing indazoles coordinated to first-row transition metals, most notable of these being the Fe(II) complex of a bis-indazolylpyridine reported by Halcrow,[243] a Zn(II) biindazole complex described by Foces-Foces,[389] reports by Vinuelos-Zahinos and Rojas in which chelating imine-type functionalities were appended to indazole skeletons,[390, 391] and studies by Lippard,[392] Ng[393] and Scheidt[394] in which unsubstituted indazole was employed as a co-ligand. At the time of writing, only two structurally characterised examples of coordination polymers containing indazoles were known; a Ru(III) species reported by Keppler,[395] and a Cd(II) species reported by Machura.[396] In both instances, other ligands provided the bridging functionality, leading to one-dimensional chains, where a *1H*-indazole was coordinated to the metal ion in a monodentate fashion. Several examples of indazolines and other partially saturated isomers of the indazole skeleton are also known; however, the coordination chemistry of such species is similarly sparse. Furthermore, despite having been reported in the medicinal chemistry literature for some time, there has been only one report to date of the structural characterisation of any indazole carboxylic acid in coordination chemistry, in which Machura and Kruszynski describe the use of indazole-3-carboxyate as a ligand in several rhenium complexes.[397] Some examples of known indazole ligands are shown in Scheme 5.1.

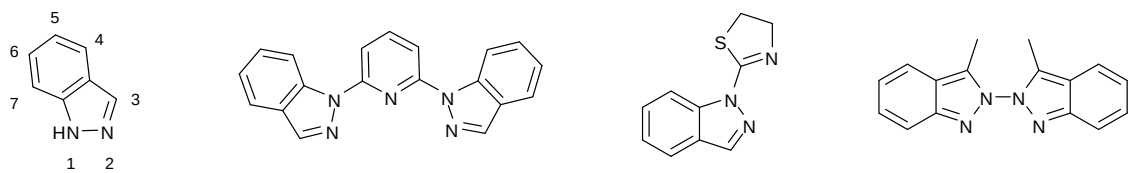

Scheme 5.1: Notable examples of indazole compounds used as ligands with first-row transition metals. Left to right: 1H-indazole with numbering scheme, 2,6-bis(indazol-1-yl)pyridine;[243] 2-(indazol-1-yl)-2-thiazoline;[390] 3,3'-dimethyl-2-2'-biindazole.[389]

5.2 Ligand Synthesis

With the aim of appending additional coordinating groups at each of the seven possible positions around the indazole skeleton, a number of synthetic strategies must be utilised. Firstly, substitution at the 1- and 2- positions was undertaken by reaction of indazole, which was itself prepared by the oxidative cyclisation of 2-aminomethyl aniline,[398] with 2-bromopyridine, under similar reaction conditions to those used in the synthesis of **L3.1**, shown in Scheme 5.2. From literature precedence[243] it was expected that such a reaction would yield a mixture of the two isomers, 1-(2-pyridyl)-indazole **L5.1** and 2-(2-pyridyl)-indazole **L5.2**. The two isomeric compounds were separated chromatographically, and although the final yields of each pure compound were disappointingly low, sufficient quantities were recovered for use in preliminary coordination studies.

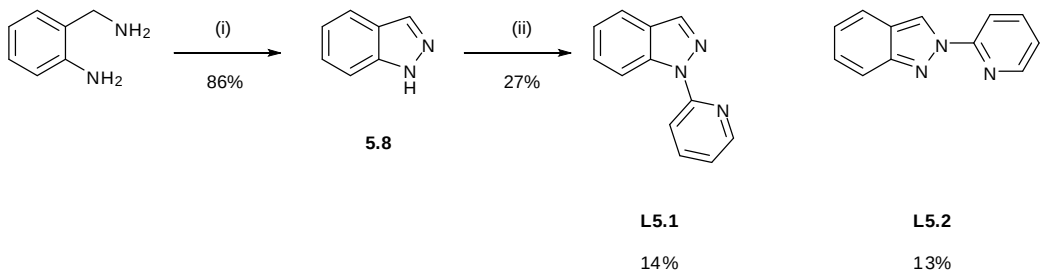

*Scheme 5.2: Synthesis of **L5.1** and **L5.2**. Reagents and conditions: (i) Na_2WO_4, H_2O_2, MeOH, RT;[398] (ii) 2-bromopyridine, NaH, DMF, 110 °C, 48 hours.*

Both **L5.1** and **L5.2** were crystallised by slow evaporation of the 50% toluene/petroleum ether eluent solution from the separation procedure, and both crystal structures were collected, solved and refined in the orthorhombic space group $P2_12_12_1$ (R-factors 3.16 and 3.82%, respectively). The structures themselves, shown in Figure 5.1, are largely unremarkable, both displaying the expected[371] *trans* – coplanar orientations of the pyridine-indazole system and offset face-to-face mode of π-π interactions (mean interplanar distances 3.3595(7) and 3.3505(9) Å for **L5.1** and **L5.2**, respectively). Of interest, however, is the degree of bond localisation present in each of the structures. Unsubstituted indazole compounds are known to favour the *1H* electron configuration,[241] allowing a greater degree of electron delocalisation on the phenyl ring, compared to the *2H* electron configuration, in which the phenyl ring adopts an *ortho*-quinone-type electron configuration. However, *1H* and *2H*-indazole themselves differ in energy by only 15 kJ mol^{-1} in the gas phase,[242] and both 1-methyl and 2-methylindazole possess similar NMR and UV spectra.[197] The positions of the double bonds indicated

in Scheme 5.2, particularly in the five membered ring, would be expected to lead to differing bond lengths as a result of the changes in electronic configurations, although the presence of the conjugated electron withdrawing pyridine group is likely to complicate such an assignment. If partial bond localisation is to be observed, it would be expected to be most visible, and separate from electronegativity considerations due to proximity of the pyridine ring, in the bond between the indazole 3-position (crystallographically labelled C(3)) and the adjacent ring junction carbon labelled C(4), which would be expected to contain more single bond character in **L5.1** and double bond character in **L5.2**, as well as in the ring junction bond, which would be expected to be longer in **L5.2** than the more delocalised case of **L5.1**. This is indeed the case, with C(3)-C(4) distance 1.421(3) Å for **L5.1** and 1.389(3) Å for **L5.2**, and differences in the C(4)-C(9) ring junction bond (1.407(2) *vs* 1.436(3) Å for **L5.1** and **L5.2**, respectively), with the effect reducing in magnitude with greater distance from the five-membered ring.

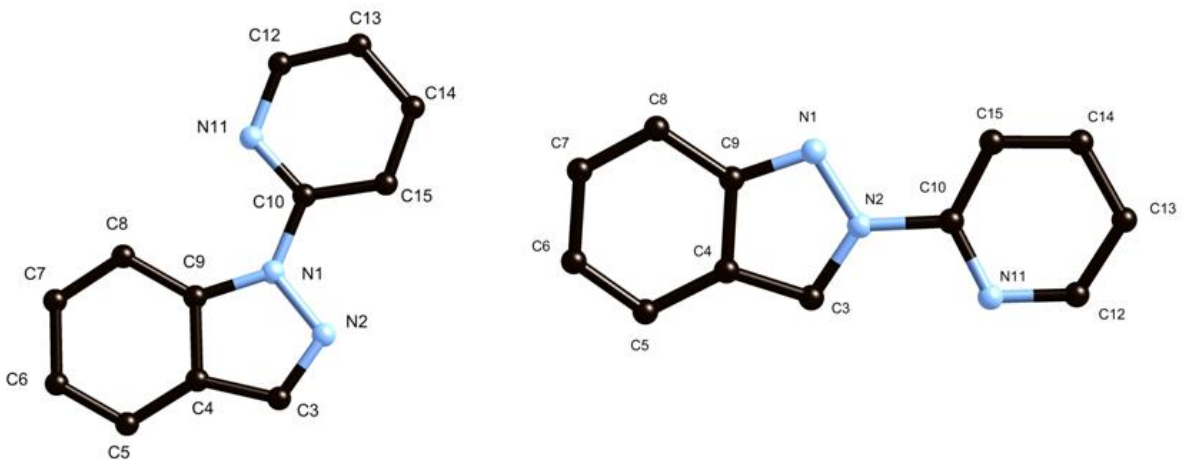

*Figure 5.1: Structure of **L5.1** (left) and **L5.2** (right) with atom labelling scheme. Hydrogen atoms omitted for clarity.*

With ligands **L5.1** and **L5.2** in hand, attention was turned to functionalisation at the remaining five possible carbon atoms of indazole. Carboxylic acid functionality was chosen as the functional group to be appended for the remaining ligands, to lend both anionic character and to provide potential for hydrogen bonding interactions, akin to those seen in the pyrazole-carboxylate systems in Chapter 2. Indazole-3-carboxylic acid **H_2L3** was prepared in three steps from phenylhydrazine according to a modified Stolle-Becker synthetic procedure,[399, 400] in which the hydrazine is first protected as the benzyl hydrazone **5.9**, followed by reaction with oxalyl chloride to form first the semicarbohydrazone intermediate **5.10**, which undergoes a Friedel-Crafts cyclisation on addition of aluminium chloride to

give the N-iminophenyl isatin **5.11**. A one-pot deprotection of the imine followed by hydrolysis/cyclisation then gives the product in good yield, as shown in Scheme 5.3.

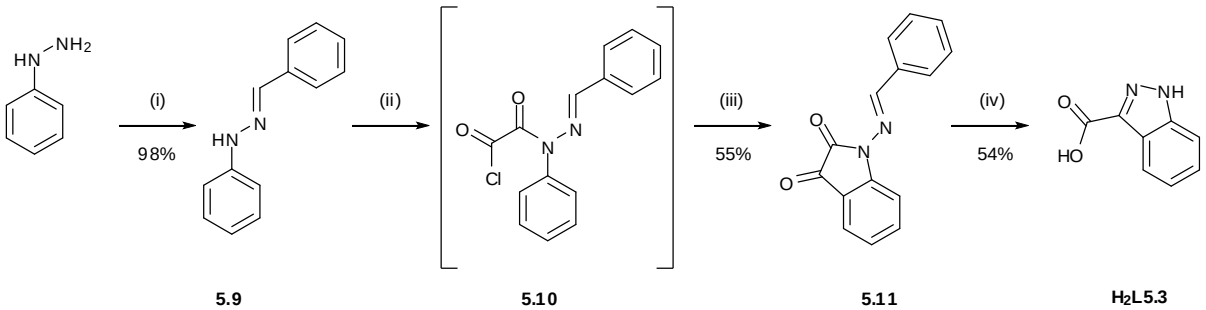

*Scheme 5.3: Synthesis of **H_2L5.3**. Reagents and conditions: (i) PhCHO, HOAc, RT; (ii) oxalyl chloride, DCM, reflux 2 hr; (iii) $AlCl_3$, DCM, reflux 14 hr; (iv) $HCl_{(aq)}$, reflux 1 hr, then HOAc, 115 °C, 1 hr.*[399, 400]

For the remaining ligands, in which the carboxylic acid moiety is appended to positions 4 – 7, a modification to the Jacobson indazole synthesis[245] was adopted, in which the key step is the one-pot diazotisation and ring closing of the acetylated *ortho*-methyl aniline.[401] To this end, the relevant precursors were prepared by reduction of the appropriate isomers of methyl nitrotoluate, in which the carboxylate was protected as the methyl ester throughout the synthesis to aid solubility. In the case of indazole-6-carboxylic acid **H_2L5.6**, *p*-toluic acid was used as the starting material, which is readily mono-nitrated in the *meta*-position, while the other nitro compounds were purchased, owing to the difficulty in selective nitration for the other isomers of toluic acid. The synthesis of ligands **H_2L5.4** – **H_2L5.7** is shown in Scheme 5.4, using the synthesis of **H_2L5.4** as an example. For **H_2L5.4** – **H_2L5.6**, the product of the cyclisation step is the N-acetyl ester, which can be fully deprotected under basic conditions. In the case of **H_2L5.7**, the N-acetyl group was cleaved during the cyclisation step, most likely due to the steric interference of the adjacent methyl ester, although the yield was not negatively affected. The acetyl esters were generally recovered in approximately 90% purity and were not further purified, but were subjected to the deprotection step directly, where the low solubility of the indazole product allowed easy separation from any impurities, with the exception of *1H*-indazole-6-carboxylic acid, where the acetyl ester precursor **5.15** was recovered in analytical purity.

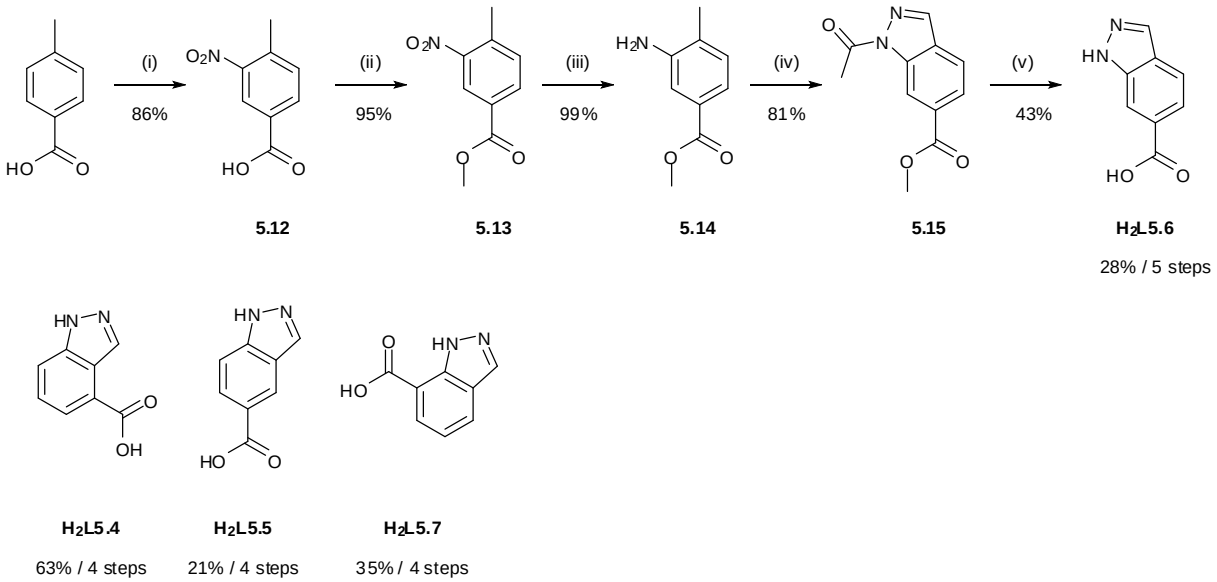

Scheme 5.4: Synthesis of ***H₂L5.4 – H₂L5.7****, using* ***H₂L5.6*** *as an example. Reagents and conditions: (i) HNO_3, H_2SO_4, 2 hr, RT[402] (ii) H_2SO_4, MeOH, reflux 16 hr; (iii) NH_4HCO_2, Pd/C, MeOH, RT 3 hr; (iv) Ac_2O, KOAc, isoamyl nitrite, PhMe, reflux 16 hr; (v) LiOH, THF/H_2O, reflux 48 hr, then $HCl_{(aq)}$.*

Ligand **H_2L5.7** was crystallised by slow evaporation from a methanol solution, and the diffraction data were solved and the structure model refined in the monoclinic space group *P*-1 (R-factor 4.05%). The asymmetric unit was found to contain two molecules of **H_2L5.7** and one water molecule. Structurally, the two units of **H_2L5.7** are largely identical, both existing in the favoured *1H*-configuration. As would be expected, with two hydrogen bond donors and two hydrogen bond acceptors per molecule, hydrogen bonding interactions dominate the solid state structure of **H_2L5.7**, where the lattice water molecule participates in four such interactions, receiving two hydrogen bonds from the two non-equivalent carboxylate O-H groups, and donating two hydrogen bonds to the non-equivalent indazole nitrogen atoms. The **H_2L5.7** units are held rigid by reciprocating hydrogen bonding interactions between the indazole N-H groups and carboxylate oxygen atoms of coplanar, crystallographically equivalent molecules. The result of these interactions is a zig-zag one-dimensional hydrogen bonded polymer, in which water molecules dictate the twist between planes of homo-dimerised **H_2L5.7** units, with a mean interplanar angle 85.080(17)°. The structure of a single hydrogen bonding chain of **H_2L5.7** is shown in Figure 5.2.

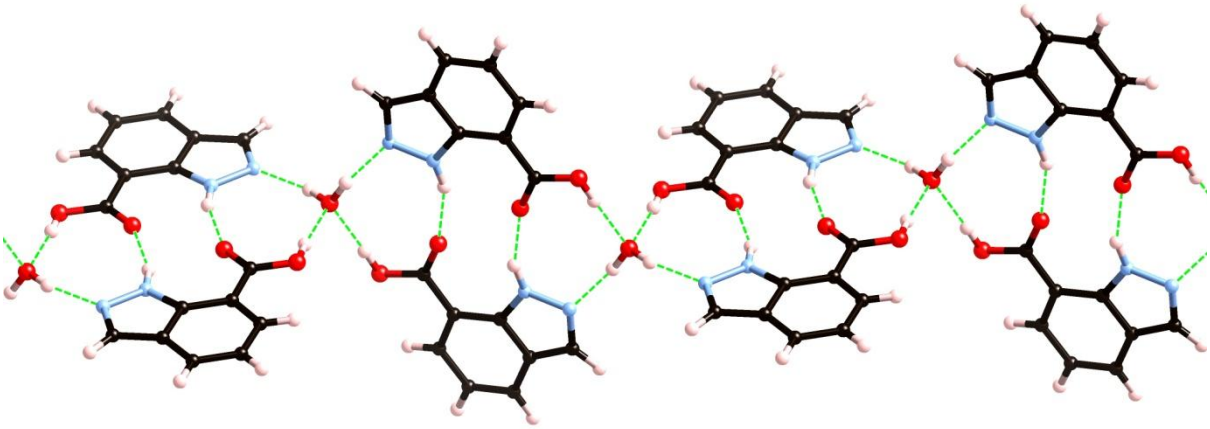

Figure 5.2: Structure of ***(H$_2$L5.7)$_2$***·H_2O *showing hydrogen bonding network.*

The coplanar **H$_2$L5.7** dimers that make up the one-dimensional chain also participate in significant π-π interactions, with homo-dimers interacting with equivalent parallel units at mean interplanar distances of 3.2772(16) and 3.1777(16) Å, indicating a strong interaction, although the units are offset such that the bulk of each **H$_2$L5.7** molecule overlaps the central hydrogen bonding region of the dimers on the adjacent layers. These interactions form one-dimensional stacks in two perpendicular directions orthogonal to the hydrogen bonding chains, propagating a densely packed 3-dimensional network.

5.3 Structures of [Cu(L5.1)$_2$(NO$_3$)]·(NO$_3$)·1.5(H$_2$O) 5.16 and [Cu(L5.1)$_2$(NO$_3$)]·(NO$_3$) 5.17

Ligands **L5.1** and **L5.2** were prepared to test the feasibility of N-pyridyl indazoles and bis-indazoles forming helicates and other discrete complexes akin to those seen in Chapter 3 and 4. Unfortunately the most direct route to an N-pyridyl indazole, namely the reaction of *1H*-indazole with 2-bromopyridine, proceeded unselectively and with poor yield, an observation that has been also made in similar systems, including by Halcrow during the synthesis of the isomeric forms of 2,6-bis(indazolyl)pyridine.[243] Nonetheless, ligands **L5.1** and **L5.2** were each reacted with Cu(NO$_3$)$_2$·3H$_2$O in nitromethane, each giving a green solution. These solutions were analysed by UV/visible spectroscopy in nitromethane, and were found to display broadly similar spectra, with broad MLCT bands centred at 720 nm ([Cu(**L5.1**)$_2$]$^{2+}$) and 750 nm ([Cu(**L5.2**)$_2$]$^{2+}$), relating to a comparatively small energy difference between the MLCT transitions of the two systems of 560 cm^{-1}. The complexes were also detected by mass spectrometry in acetonitrile solution, with a doubly charged peak at *m/z* 226.5438 for both compounds, indicating the presence of a [Cu(**L**)$_2$]$^{2+}$ species. The two

compounds were crystallised by vapour diffusion of benzene for the **L5.1** complex and toluene for the **L5.2** complex.

The crystal structure of [Cu(**L5.1**)$_2$(NO_3)]·(NO_3)·1.5(H_2O) **5.16** was solved and refined in the monoclinic space group $P2_1/n$ (R-factor 5.35%), where the asymmetric unit was found to contain one Cu(II) ion coordinating in a trigonal bipyramidal geometry to two bidentate molecules of **L5.1**, with pyridine nitrogens in the axial positions, and the equatorial binding sites completed by a weakly chelating nitrate anion, with Cu-O bond lengths 2.310(3) and 2.546(4) Å. The Cu-$N_{(pyridine)}$ bond lengths are shorter than those corresponding to the indazole nitrogens, with Cu-N distances 1.977(3) and 1.975(3) Å for N(12) and N(27), respectively, compared with 2.002(3) and 2.030(3) Å for N(2) and N(17), respectively. One additional nitrate anion was located in a crystallographically disordered position, along with 1.5 water molecules per complex, disordered over three sites. Both ligands are approximately planar, with pyridine-indazole interplanar angles 4.6(1) and 5.7(1) °. The structure of **5.16** is shown in Figure 5.3.

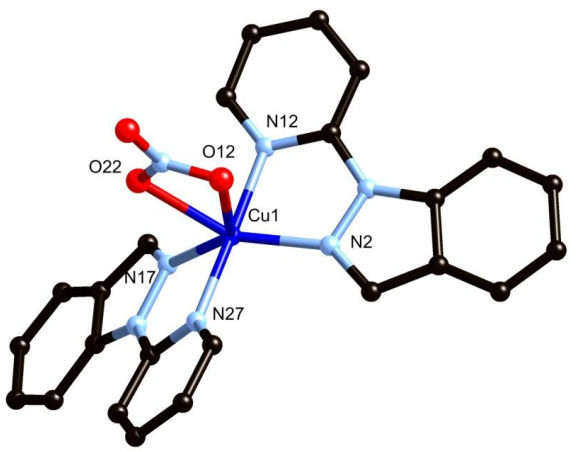

*Figure 5.3: Structure of complex **5.16** with partial atom labelling scheme. Hydrogen atoms and disordered anions and solvents omitted for clarity.*

The intermolecular interactions in **5.16** are, as expected, dominated by π-π stacking. Adjacent complexes align with the non-coordinating oxygen of the coordinating nitrate anion directed towards the metal ion of an adjacent complex, with O(4)-Cu(1) distance 3.245(3) Å, an interaction which forms a one-dimensional chain parallel to the *a* unit cell axis, while adjacent chains interdigitate **L5.1** units, at mean interplanar distances 3.352(2) and 3.420(2) Å for the two unique types of interactions. The disordered nitrate anions and water molecules occupy columnar structures, also parallel to the *a* edge, preventing any significant interaction between complexes parallel to the *c* edge. Thermogravimetric analysis shows a slow loss of 6% mass up to 120 °C, suggesting the presence of

additional lattice water molecules in addition to those modelled (calculated 4.5% mass). A two step decomposition process was seen to initate, with steps centred at 195 and 244 °C, the second step corresponding with the decomposition temperature of 233 °C in air.

The structure of [Cu(**L5.2**)$_2$(NO_3)]·(NO_3) **5.17** was determined in the monoclinic space group $P2_1/c$ (R-factor 4.82%), where the asymmetric unit was found to contain a similar coordination sphere to **5.16**, in which two bidentate molecules of **L5.2** coordinate to a five-coordinate copper, with one coordination site occupied by a nitrate anion; however, the geometry of the Cu(II) ion is best described as square pyramidal, with an elongated axial bond distance of 2.216(3) Å to pyridine nitrogen atom N(2), compared with Cu(1)-N(17) distance 2.032(3) Å, and Cu-N distances for indazole nitrogens N(9) and N(24) of 1.992(3) and 1.970(3) Å, respectively. The ligand molecules also displayed a slightly larger twist between pyridine and indazole rings, with interplanar angles 12.76(10) and 11.66(9)°. One non-coordinating nitrate anion was also located within the unit cell and was well ordered, while no solvent molecules were observed. The structure of **5.17** is shown in Figure 5.4. As was the case in **5.16**, π-π interactions permeate the extended structure of **5.17**. Two types of interactions are present; a chain formed by partial overlap between **L5.2** units on adjacent molecules with mean interplanar distance 3.631(2) Å runs parallel to the *b* edge, while these chains are linked parallel to the *a* edge by a dimeric interaction between the entire conjugated plane of two equivalent **L5.2** units, with interplanar distance 3.538(2) Å. No significant interactions are observed running parallel to the *c* edge, nor were any solvent molecules or channels located within the unit cell.

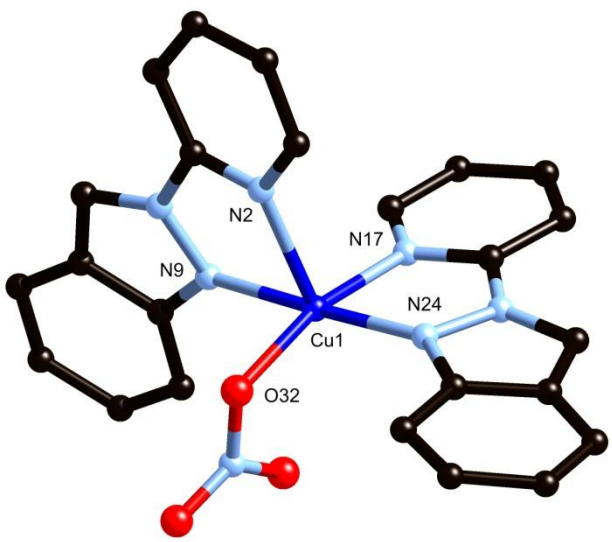

*Figure 5.4: Structure of complex **5.17** with partial atom labelling scheme. Hydrogen atoms and non-coordinating anion omitted for clarity.*

The discrepancy in bond lengths due to the different electronic configurations of **L5.1** and **L5.2** appears lessened on coordination to metal ions, evidenced by the near-equivalent lengths of the ring junction bond of 1.411(5) and 1.420(4) Å for **5.16** and **5.17**, respectively, although the bond from the indazole 3-position to the adjacent ring junction carbon remains substantially longer in **5.16** (1.432(6) Å) compared with **5.17** (1.393(5) Å, representative values). The metal-ligand bond lengths are not directly comparable between complexes, due to the difference in coordination geometry, although the similar MLCT bands in the solution UV/Visible spectra showed reasonable agreement with each other. These figures suggest that while the two isomers still display differences in their electronic structure when coordinated, these differences will likely play a significantly smaller role in their metallosupramolecular chemistry than that of the differences in steric profile between the two, which are most likely the driving forces behind the differences in both the coordination geometry and crystal packing of complexes **5.16** and **5.17**.

5.4 Structure of poly-[Cu(L5.3)(CH_3CONH_2)] 5.18

Ligand *1H*-indazole-3-carboxylic acid **H_2L5.3** was expected to behave in the first instance as a monoanionic N,O-chelating ligand, with potential for further coordination through the second indazole nitrogen and/or carboxylate oxygen. Reactions with transition metals by heating at atmospheric pressure primarily led to insoluble materials, and as such a solvothermal approach was adopted in order to generate crystalline complexes.

Ligand **H_2L5.3** was reacted with one equivalent of $Cu(NO_3)_2 \cdot 3H_2O$ in acetonitrile under solvothermal conditions, where the pressure vessel was held at 120 °C for 36 hours, followed by cooling to room temperature at 5 °C/hr, to give green octahedral crystals of the product **5.18**, which were analysed by single crystal X-ray diffraction. The data obtained were solved and the structure model refined in the tetragonal space group $I4_1/a$ (R-factor 4.61%). The asymmetric unit of **5.18** was found to contain a single Cu(II) ion coordinated in a 5-coordinate, distorted square pyramidal arrangement (τ_5 = 0.43). One unique molecule of **L5.3** was located within the asymmetric unit, coordinating through all four heteroatoms to the equatorial planes of symmetry equivalent metal sites, while the axial coordination site was occupied by the terminal atom of a four-atom trigonal species. Charge balance considerations require a neutral species, and on electron density grounds the coordinating species was assigned as acetamide, coordinating through the oxygen atom. This assignment was supported a prominent infrared absorption at 1667 cm^{-1}, consistent with a weakly coordinating (d(Cu(1)-O(14)) = 2.268(3) Å) neutral C=O stretch, although this region of the spectrum

is somewhat obscured by the presence of **L5.3**. Microanalysis was carried out on a dry sample which confirmed the identity of the ligand, and ruled out other possible identities for the coordinating species, such as acetic acid. This assignment was aided by the lack of void space within the crystal lattice, allowing all other species to be precisely accounted for, unlike in the structure of compound **3.12**, where the exact molecular formula was not known. It is expected that, as was the suspected case in **3.12**, the acetamide moiety arises from the *in-situ* solvothermal hydrolysis of acetonitrile, possibly mediated by the strongly Lewis-acidic copper ion activating the electron-poor quaternary carbon to attack by water. Unlike complex **3.12**, however, **5.18** could be prepared in similar yield by adding acetamide to the reaction mixture; however, the crystals obtained were smaller than those formed in the absence of acetamide, consistent with the slow formation of acetamide providing a rate-limiting step towards crystallisation of the product. The metal region of **5.18** is shown in Figure 5.5.

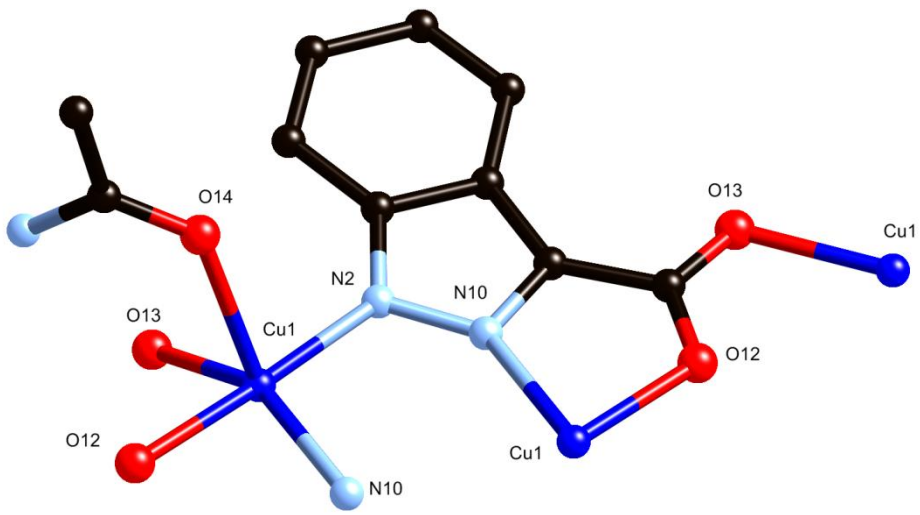

*Figure 5.5: Structure of the repeat unit of complex **5.18** with partial heteroatom labelling scheme. Hydrogen atoms omitted for clarity.*

The extended structure of **5.18** constitutes a three-dimensional polymer, where the copper dimers bridged by the indazole nitrogens are further linked by coordination through the non-chelating oxygen of the carboxylic acid moiety. Topologically, several approaches can be taken to describe the overall network. If each copper ion is considered to be a node, then each ligand must also be a node, as each ligand coordinates to 3 copper ions. With these considerations, the network reduces to the 3-connected **lvt-a** network, with point symbol (4·8·10). However, a more intuitive description of the network can be arrived at by considering a single node to encompass the $[Cu_2(\mathbf{L5.3})_2]$ dimer, which is linked to four adjacent dimers by bonds through the non-chelating carboxylate oxygen atoms. When

the network is considered in this manner, the description simplifies to ($4^2 \cdot 8^4$) and is described by the **lvt** network. In topological terms, the **lvt-a** network is known as a 'decorated' version of the **lvt** network, in which the nodes are replaced by a cluster of nodes with different connectivities. Both terms provide a topological description of the structure; however, for this discussion the **lvt** network provides a more useful description. A schematic of the nodes and full network of **5.18** is shown in Figure 5.6.

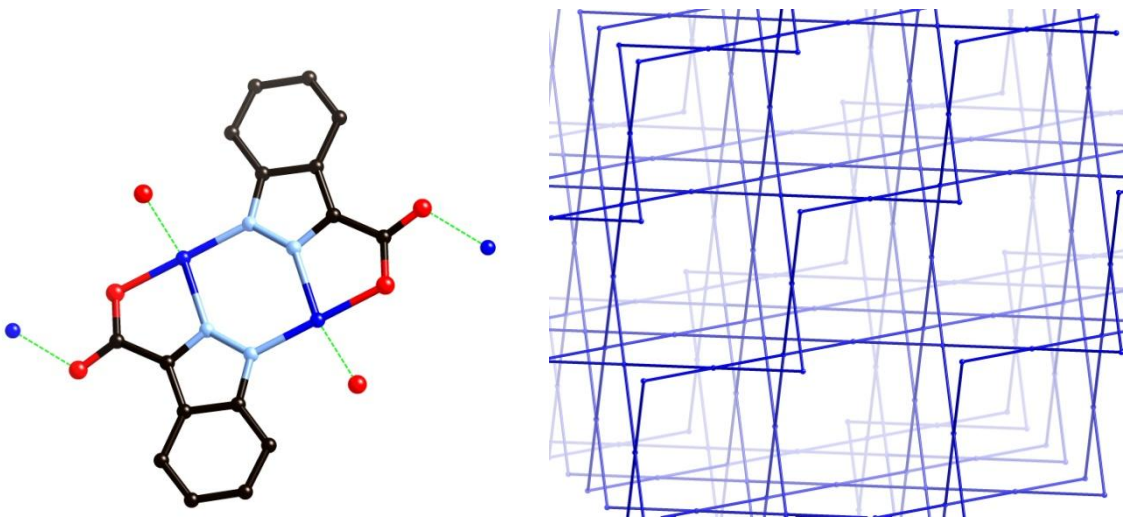

*Figure 5.6: (Left) Structure of the nodes within the **lvt** visualisation of the **5.18** network, with dashed lines representing links to adjacent nodes. Hydrogen atoms and acetamide ligands omitted for clarity. (Right) Schematic representation of the **lvt** network of **5.18**.*

Despite the apparent presence of channels within the network schematic, no significant void space is observed in the structure of **5.18**. In reality, these channels are filled by both the steric bulk of the indazole rings, and the coordinating acetamide molecules. The acetamide molecule within the asymmetric unit forms two hydrogen bonds, as shown in Figure 5.7, both originating from the -NH_2 group; one hydrogen atom points towards the nearby coordinating carboxylate oxygen, to form a six-membered hydrogen bonding ring, while the other interacts with the coordinating acetamide oxygen on an adjacent dimer, to propagate a hydrogen bonding chain parallel to the *c* unit cell axis.

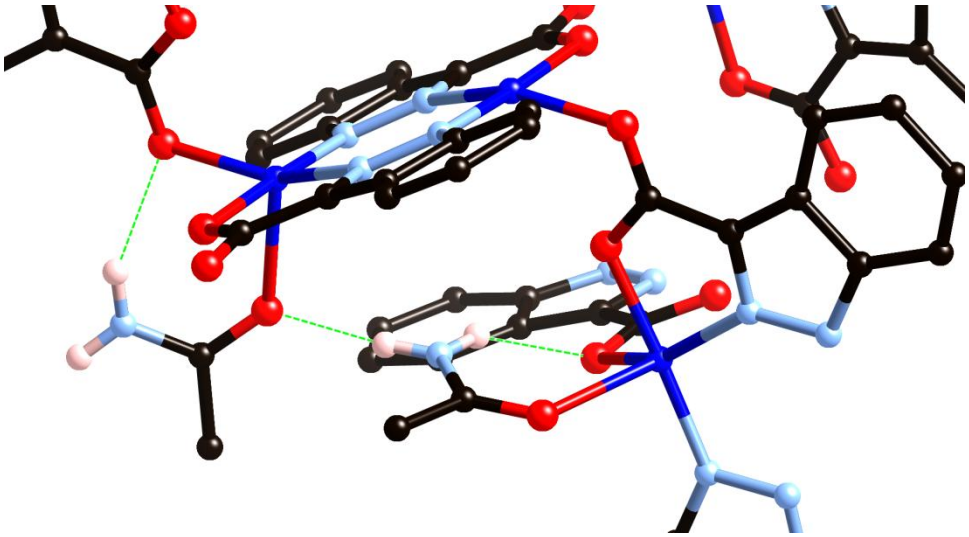

*Figure 5.7: Hydrogen bonding interactions involving acetamide molecules in the structure of **5.18**. Hydrogen atoms not participating in hydrogen bonding omitted for clarity.*

Thermogravimetric analysis of **5.18** shows 20% mass loss with onset at 180 °C and centred at 250 °C, consistent with the loss of acetamide (calculated 20.8 %). This mass loss initiation temperature is somewhat below the boiling point of bulk acetamide (222 °C), which can be rationalised by the strictly linear associations of acetamide molecules within the structure, the relatively accessible channels and the nitrogen purge conditions of the instrument. A small plateau is observed in the TGA trace from *ca.* 250 – 280 °C; however, on heating crystals of **5.18** to this temperature a loss of single crystallinity was observed, suggesting a desolvated single crystalline phase is not accessible from this starting material.

5.5 Structure of poly-[Cd(HL5.4)$_2$(MeOH)$_2$]·2MeOH 5.19

Ligand *1H*-indazole-4-carboxylic acid **H$_2$L5.4** was expected to behave as a bent two-connecting ligand, where chelation is impossible due to the distance between the coordination sites. With this expectation, **H$_2$L5.4** was reacted with Cd(NO$_3$)$_2$·4H$_2$O in methanol under solvothermal conditions at 130 °C. On cooling to room temperature, a colourless solution was recovered, which deposited colourless single crystals of complex **5.19** on standing overnight. Interestingly, single crystals were not observed to deposit when the experiment was repeated outside of the pressure vessel, or when a solvothermal dwell temperature of 100 °C was employed, with only amorphous material forming when the solution was evaporated to near dryness. The crystals obtained were subjected to single

crystal X-ray diffraction, and the data solved and the structure model refined in the polar orthorhombic space group $Pca2_1$ (R-factor 5.17%). The asymmetric unit was found to contain one Cd(II) ion, coordinating in an octahedral geometry to two non-equivalent molecules of **HL5.4** through both the indazole nitrogen atoms and deprotonated carboxylate oxygen atoms in the equatorial plane, with the axial positions occupied by two non-equivalent methanol molecules, with each pair of donor types in a *trans* orientation. Two hydrogen bonding interactions between indazole N-H groups and non-coordinating carboxylate oxygen atoms provide additional stability to the coordination site by way of two seven-membered hydrogen bonding rings, somewhat reminiscent of the pyrazole-carboxylate secondary building unit described in Chapter 2, albeit with a different coordination geometry. Two additional methanol molecules were also found to be present within the asymmetric unit, hydrogen bonding to the coordinated methanol molecules. The structure of complex **5.19** is shown in Figure 5.8.

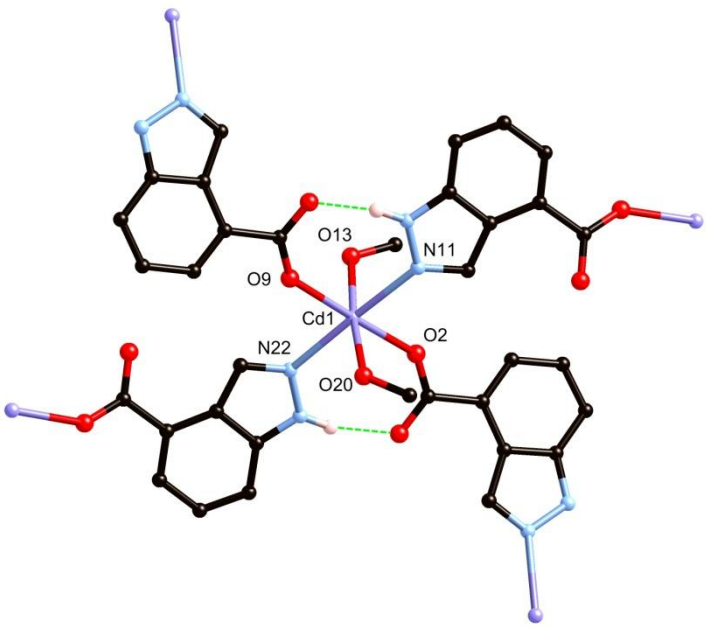

*Figure 5.8: Structure of complex **5.19** with partial heteroatom labelling scheme. Selected hydrogen atoms omitted for clarity.*

The structure of **5.19** extends into a two-dimensional network parallel to the *ab* plane *via* bridging through the **HL5.4** units, with each metal ion being connected to four others, resulting in the well-known (4,4) topology. Due to the bent geometry of the ligand, no significant void space is observed in the windows defined by the four-membered circuits. Adjacent sheets are linked by hydrogen bonding interactions originating from the coordinating methanol molecules *via* the non-coordinating methanol

molecules, and terminating with the non-coordinating carboxylate on an adjacent sheet. The distances involved in these interactions, as well as the high degree of planarity within each sheet, precludes any significant π-π interactions, with the closest interatomic distance between aromatic carbon atoms on adjacent planes 3.749(12) Å for C(19)-C(26). As a result of the weak and flexible inter-sheet interactions, the crystals proved unstable to drying, with complete loss of single crystallinity within seconds after removal from their mother liquor. Thermogravimetric analysis showed a loss of 14.5% mass by 100 °C with immediate onset; this value was consistent with the loss of one of the two non-coordinating methanol molecules prior to mounting on the instrument, an observation not unexpected given the rapid collapse of the framework. Elemental analysis sugested a formula of [Cd(**HL5.4**)$_2$]·MeOH·H_2O, consistent with loss of most of the lattice methanol molecules and some association of water with the dry solid on standing in air for several days.

5.6 Complexes of *1H*-indazole-5-carboxylic acid H_2L5.5

*5.6.1 Structure of poly-[Zn(**H_2L5.5**)$_4$(SiF_6)]·x(PhMe)* ***5.20***

Due to the favourable orientation of the coordination sites with respect to a linear bridging coordination mode, *1H*-indazole-5-carboxylic acid **H_2L5.5** was expected to show the most potential for the formation of robust three-dimensional coordination frameworks, and as such, many trials were carried out in coordination with transition metal ions. On reaction with $Cu(BF_4)_2·6H_2O$ in methanol in a glass vial, followed by diffusion of toluene over several weeks, one crystal was obtained of a coordination compound which revealed, by single crystal X-ray diffraction, the presence of a hexafluorosilicate anion bridging [Cu(**H_2L5.5**)$_4$] units into a series of one-dimensional polymers, where the anions presumably originated from the attack of fluoride ions on the borosilicate glassware. Several attempts were made to repeat this synthesis on a useful scale, but a pure phase was never able to be obtained. A similar structure was expected to be achievable with other first row transition metals, and it was found that the reaction of **H_2L5.5** with $ZnSiF_6·6H_2O$ in methanol, followed by slow diffusion of toluene, formed an isostructural complex **5.20** as a pure phase in 33% yield. The only structural difference between the two compounds was a Jahn-Teller tetragonal elongation of the Cu-F bonds in the Cu(II) species (Cu-F distances 2.276(3) and 2.207(3) Å, *cf.* Cu-N distance 2.00(6) Å) which was not present in the Zn(II) analogue (Zn-F distances 2.071(2) and 2.129(2) Å for F(14) and F(17), respectively, *cf.* Zn-N distance 2.1037(11) Å).

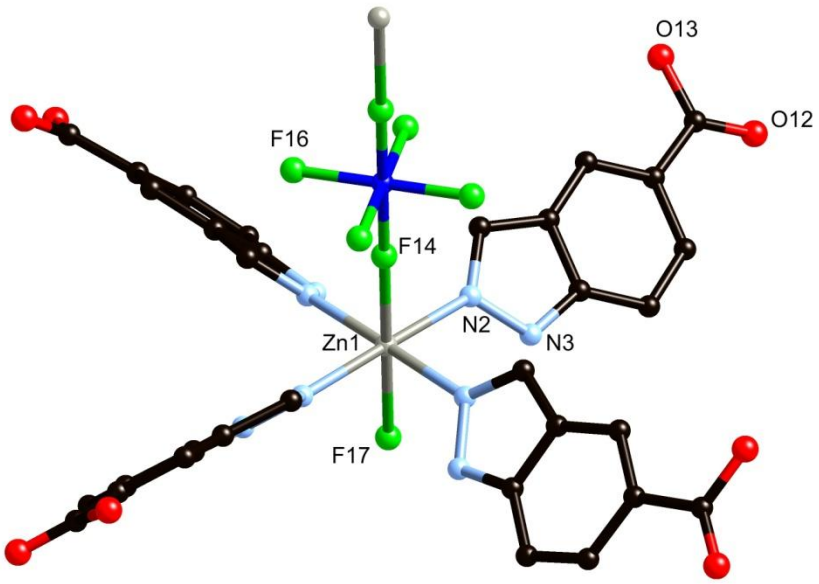

*Figure 5.9: Structure of complex **5.20** with unique heteroatom labelling scheme. Hydrogen atoms omitted for clarity.*

The diffraction data for the Zn(II) compound were solved and the structure model refined in the tetragonal space group *P*4/*ncc* (R-factor 2.88%), where the asymmetric unit was found to contain one Zn(II) ion coordinating in an octahedral arrangement to the indazole nitrogen of four equivalent **H_2L5.5** units in a square planar arrangement, while the axial coordination sites were occupied by a bridging hexafluorosilicate anion, resulting in the formation of a one-dimensional polymer running parallel to the *c* edge. The structure of **5.20** is shown in Figure 5.9. Individual strands of **5.20** linked through the hexafluorosilicate anions extrude protonated carboxylic acid groups outwards, which subsequently link to adjacent strands through several hydrogen bonding interactions. In the first instance, the O-H group of each carboxylic acid acts as a hydrogen bond donor to the equatorial fluoride atom of an adjacent strand, with a particularly short D-A distance of 2.6145(13) Å for O(13)-F(16) indicating an unusually strong bond, aided by the negative charge of the anion and the favourable sterics of the system. This interaction is further strengthened by a second hydrogen bond, from protonated indazole nitrogen atom N(3) to carboxylate oxygen atom O(12), with N-O distance 2.7246(15) Å, effectively forming a 12-membered ring containing two strong hydrogen bonds. Each protruding indazole group also participates in a dimeric π-π stacking with the equivalent unit from an adjacent strand, with parallel mean planes separated by 3.4823(14) Å. The summation of these strong intermolecular interactions, shown in Figure 5.10, was expected to lend a significant stability to the overall framework.

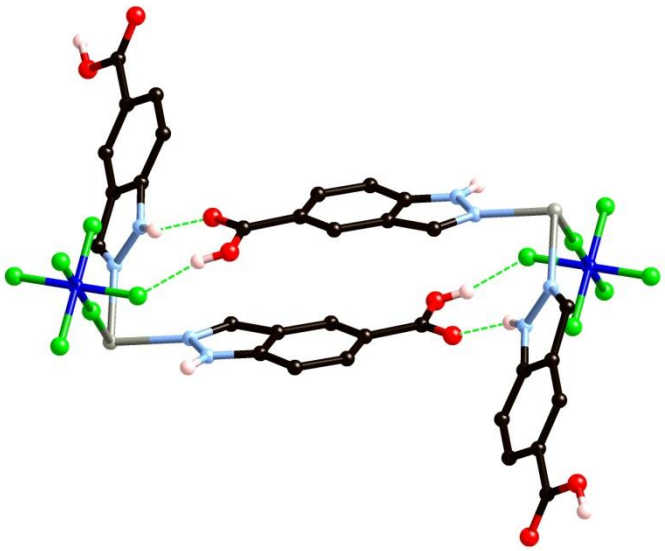

Figure 5.10: Primary modes of intermolecular interaction in the structure of ***5.20****, showing π-π stacking and two modes of hydrogen bonding interactions. Selected hydrogen atoms and full coordination sphere omitted for clarity.*

When these modes of intermolecular interaction are considered in the extended structure, a one-dimensional channel structure becomes apparent passing parallel to the *c* unit cell axis. The square channels, shown in Figure 5.11 below, are defined by approximate interatomic dimensions of 8 × 8 Å. The structure draws obvious comparisons to the work of Zaworotko[119] and subsequently Kitagawa,[403] who investigated the properties of axially hexafluorosilicate-bridged sheets of Cu(II) and Zn(II) square-grid complexes of 4,4-bipyridine. The channel contents of **5.20** were not able to be appropriately modelled crystallographically, and as such the SQUEEZE routine was applied,[246] which suggested a void content of *ca.* 400 electrons per unit cell, equivalent to 8 toluene molecules per unit cell, or 2 toluene molecules per Zn(II) ion. This solvation formula was precisely matched by elemental analysis. The crystals retained their single crystallinity on standing in air for extended periods, and were subjected to thermogravimetric analysis under nitrogen flow, which showed loss of only 4% mass by 80 °C, consistent with approximately 20% of the encapsulated solvent, followed by a slow decomposition process with onset of 80 °C, presumably concurrent with the loss of remaining solvent. A sample of **5.20** was heated to 80 °C in air, and although the onset of decomposition was clear, single crystal X-ray diffraction was able to be carried out, where the SQUEEZE analysis suggested a void content of 335 electrons, further consistent with the loss of approximately 20% of the encapsulated solvent. These data suggest that the channels in **5.20** are likely too small to efficiently allow removal of the toluene molecules by heating, as at 8 Å minimum interatomic distance, a structural rearrangement would be required by the framework in order to allow complete

evacuation of the pores. The toluene molecules may also play a templating role in the synthesis of the complex; the synthesis of **5.20** was unable to be repeated using any antisolvent besides toluene, including benzene or *p*-xylene, suggesting some shape or size dependence as well as the usual dependence on diffusion rate, dielectric constant *etc.* In the case of the related compounds prepared by Kitagawa and Zaworotko, the Cu(II) compound was found to be considerably more stable than the Zn(II) analogue; future work may focus on the large scale preparation of the structurally identical Cu(II) phase of **5.20** in order to test this hypothesis.

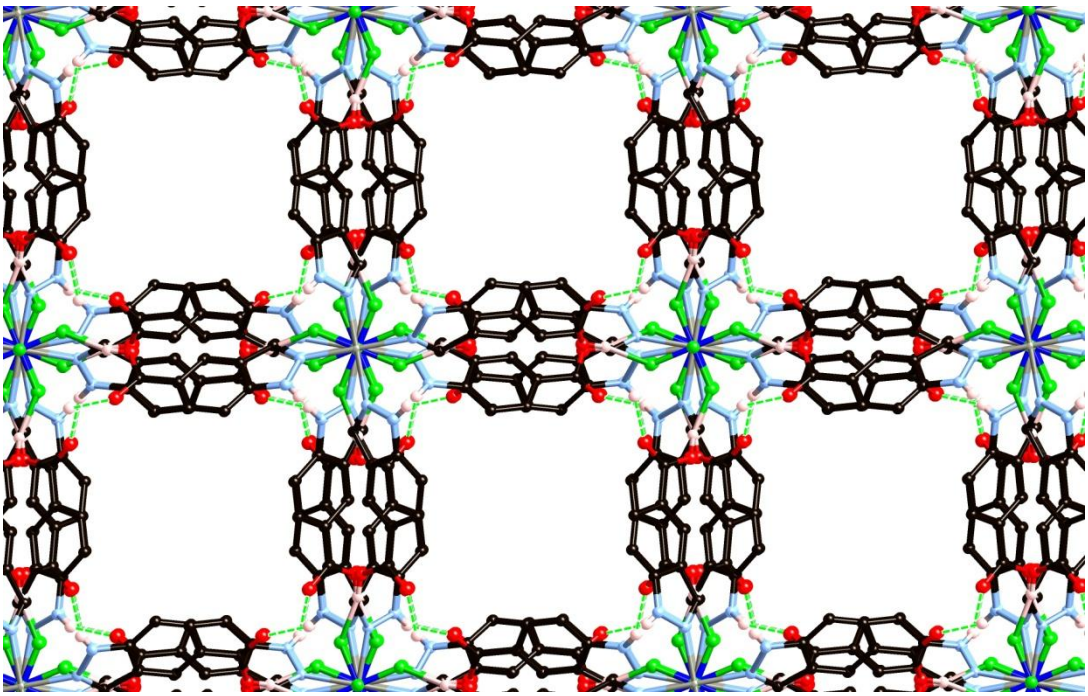

*Figure 5.11: Channel structure of complex **5.20** viewed along the c unit cell axis. Selected hydrogen atoms omitted for clarity.*

*5.6.2 Synthesis of poly-[Cu(**HL5.5**)$_2$]·x(H$_2$O) **5.21***

While attempting to prepare a larger scale sample of the Cu(II) analogue to **5.20**, ligand **H$_2$L5.5** was combined with copper nitrate and ammonium hexafluorosilicate in a methanol/water mixture and heated under solvothermal conditions, producing a small quantity of purple/pale yellow dichroic crystals of complex **5.21**, along with amorphous decomposition products. It was found that this material could be prepared as a pure phase by combining a molar excess of both **H$_2$L5.5** and NH_4SiF_6 with $Cu(NO_3)_2 \cdot 3H_2O$ in 2 ml of a 50% methanol/water mixture, and heating in a pressure vessel to

100 °C with 24 hour dwell period, followed by cooling at 4 °C per hour. The crystals obtained were subjected to single crystal X-ray diffraction, where the data were solved and the structure model refined in the rhombohedral space group R-3 (R-factor 3.79%). The asymmetric unit was found to contain one molecule of **HL5.5** coordinating to a Cu(II) ion *via* the deprotonated carboxylate group and indazole nitrogen atom, leading to a square planar coordination geometry. Despite containing no hexafluorosilicate species within the unit cell, complex **5.21** only formed in the presence of either ammonium hexafluorosilicate or ammonium hexafluorozirconate. Interestingly, complex **5.21** was not observed to form in the presence of ammonium chloride or sodium hexafluorosilicate. The exact nature of this apparant templation is currently unknown, and is currently the subject of further investigation. The structure of **5.21** is shown in Figure 5.12.

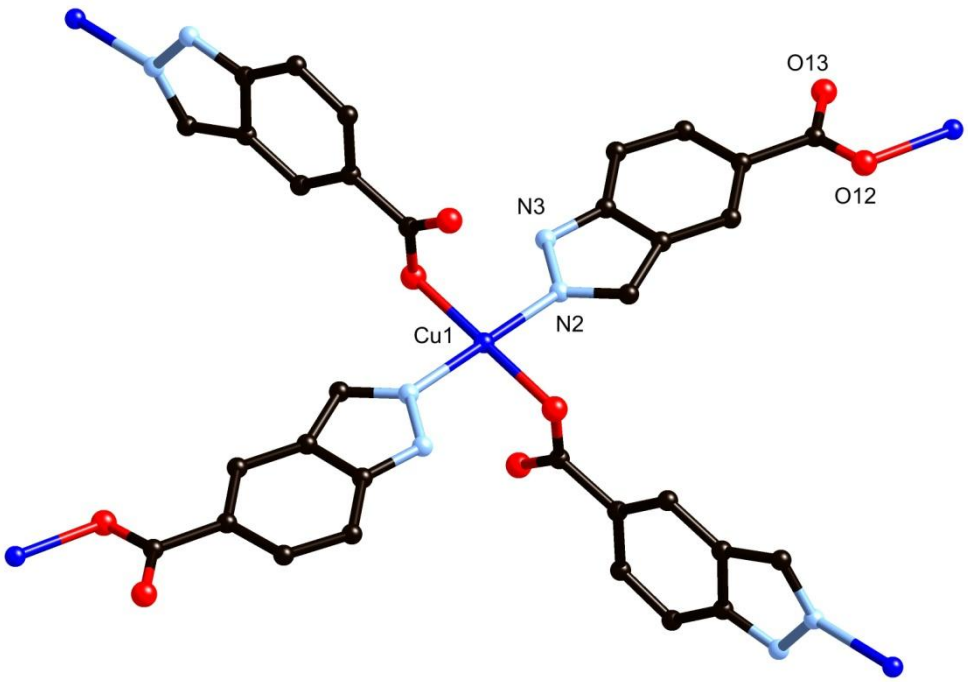

*Figure 5.12: Structure of complex **5.21** with unique heteroatom labelling scheme. Hydrogen atoms omitted for clarity.*

Each Cu(II) ion in **5.21** is linked to four others *via* the bridging **HL5.5** groups, propagating a three-dimensional polymer. Assigning nodes to the metal ions, the network is described by the 4 connected ($6^4 \cdot 8^2$) **nbo** network. Close examination of the crystal structure revealed the presence of twofold interpenetration within the structure; however, due to the presence of hydrogen bonding interactions between the indazole N-H groups and carboxylate oxygen atoms on the adjacent framework, the two

networks are tightly bound together. The hydrogen bonding interactions in **5.21** and topological representation are shown in Figure 5.13.

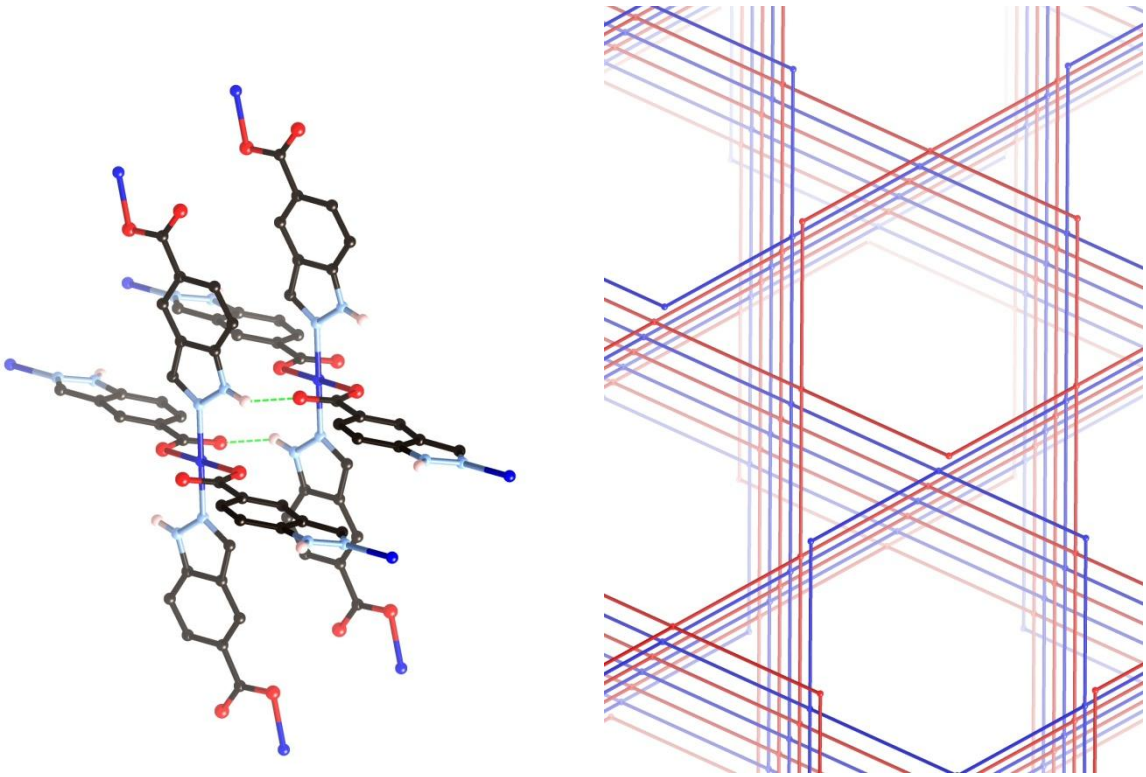

*Figure 5.13: (Left) Hydrogen bonding interactions between frameworks in the structure of **5.21**, hydrogen atoms not participating in hydrogen bonding interactions omitted for clarity. (Right) Topological representation of the structure of **5.21**, independent networks coloured separately.*

The primary channels in **5.21**, hexagonal in shape and running parallel to the *c* unit cell axis and with interatomic diameter of *ca*. 12 Å, are left unobstructed by the interpenetration, and were found to contain no crystallographically ordered guests. The electron density present in these channels was so diffuse as to prevent explicit modelling of the solvent guests, and the use of the SQUEEZE routine was not required due to the already high degree of accuracy evident in the unmodified data. However, SQUEEZE was used to estimate the void contents on electron density grounds,[246] and suggested a void content of 427 electrons per unit cell, equivalent to approximately 47 electrons per copper, consistent the equivalent of 2.5 methanol molecules, 4.5 water molecules, or a combination of the two solvents, occupying 36% of the unit cell volume, or 184 $Å^3$ per metal ion. This value was larger than that suggested by thermal analysis (9% mass loss, consistent with two water molecules or one methanol molecule per metal site) or elemental analysis (two methanol molecules and one water molecule per three Cu(II) ions); however, the open nature of the channels would be expected to

facilitate rapid guest exchange, causing these values to vary with the degree of drying and length of air exposure. Thermal analysis showed complete desolvation by 150 °C, followed by a plateau until 250 °C, when a slow decomposition process initiated. On heating to 150 °C for 2 hours, a single crystalline sample of **5.21** showed no visible signs of loss of crystallinity, and both an X-ray powder diffraction pattern and single crystal data collection showed the structure was maintained. The crystal structure of **5.21** after heating was structurally identical to the original collection; however, the void contents calculated by SQUEEZE were reduced to 37 electrons per unit cell, while the refinement statistics improved markedly (R-factor 2.65%) with no explicit modelling of the void contents or removal of structure factors corresponding to the void volume, suggesting significant desolvation of the channels while maintaining the network structure. A comparison of the powder diffraction data for the fresh and desolvated **5.21** is shown in Figure 5.14.

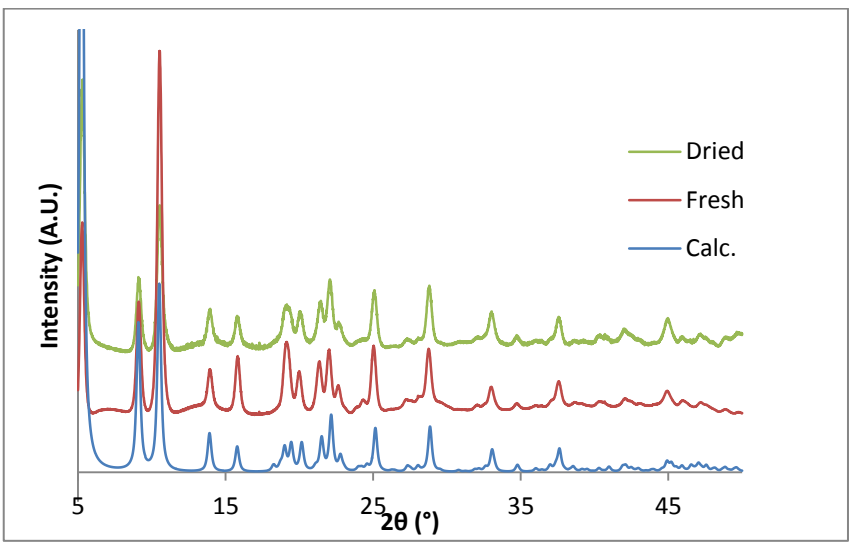

*Figure 5.14: Comparison of the X-ray powder diffraction patterns for freshly isolated **5.21** (red) against a sample dried at 150 °C for 2 hours (green), and the simulated pattern calculated from the single crystal data (blue).*

The presence of large pores, and exceptional thermal stability of complex **5.21** allowed gas sorption experiments to be carried out by Assoc. Prof. Brendan Abrahams and Keith White at The University of Melbourne. Desolvation of **5.21** was achieved by maintaining the compound at a temperature of 150 °C overnight under dynamic vacuum. While no significant sorption of H_2 was observed at low temperature, CO_2 isotherms measured at 258 and 273 K show uptake of CO_2 by the desolvated compound. Figure 5.15 shows that the 273 K isotherm does not follow a typical Type 1 isotherm path, with a point of inflection apparent in the isotherm curve at a pressure of approximately 280 kPa. This shape is suggestive of a cooperative effect in the CO_2 sorption process. As the pressure is increased

beyond this point the isotherm begins to flatten, consistent with Type 1 behaviour. At the maximum pressure measured, 124 cm^3 of CO_2 (at STP) is sorbed per gram of compound, corresponding to an uptake of ~24% ($m(CO_2)/m$(host network)). The desorption curve indicates significant hysteresis with over 100 cm^3 of CO_2 (at STP) retained per gram of the compound at 507 kPa. The sorption and desorption isotherms recorded at 258 K exhibit a similar shape and indicate slightly greater sorption at a given pressure compared with the 273 K measurement. Hysteresis is again observed upon in the desorption isotherm at the lower temperature.

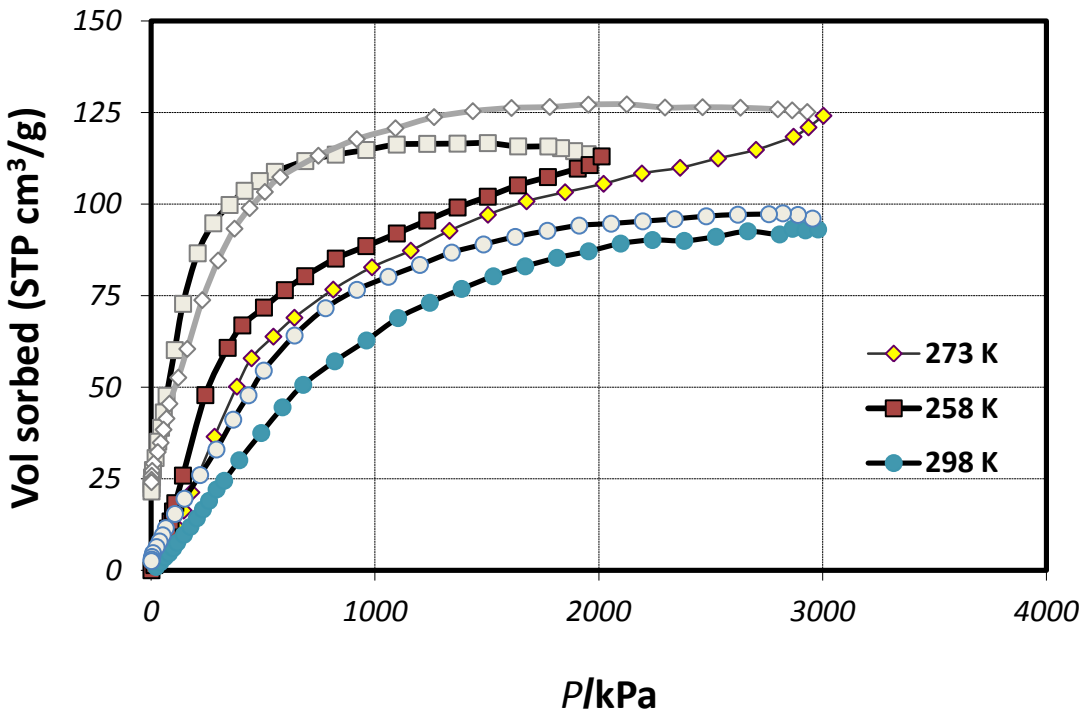

*Figure 5.15: CO_2 sorption isotherms for compound **5.21** collected at 258, 273 and 298 K. Coloured points show the sorption behaviour with increasing pressure, while grey points show the corresponding desorption process.*

Figure 5.16 shows the isosteric heat of sorption Q_{SP} as a function of amount of CO_2 sorbed, calculated using a virial-type thermal adsorption equation based on the 258 K and 173 K isotherms. The zero-loading value of -11.1 kJ mol^{-1} is unremarkable compared to other non-functionalised coordination polymer materials,[159] however the increase in magnitude to -12.5 kJ mol^{-1} is further indicative of a cooperative sorption process, indicating that the process of CO_2 binding becomes more energetically favoured for a period following the initial sorption. Prompted by the quantity of CO_2 sorbed by **5.21**, a CH_4 sorption experiment was also carried out at 273 K; however, as was the case with the H_2 experiments, negligible sorption was detected, up to a pressure of 25 atm. These results suggest a

degree of selectivity of sorption in **5.21**, which could potentially lead to applications in gas purification processes, such as natural gas sweetening.[160]

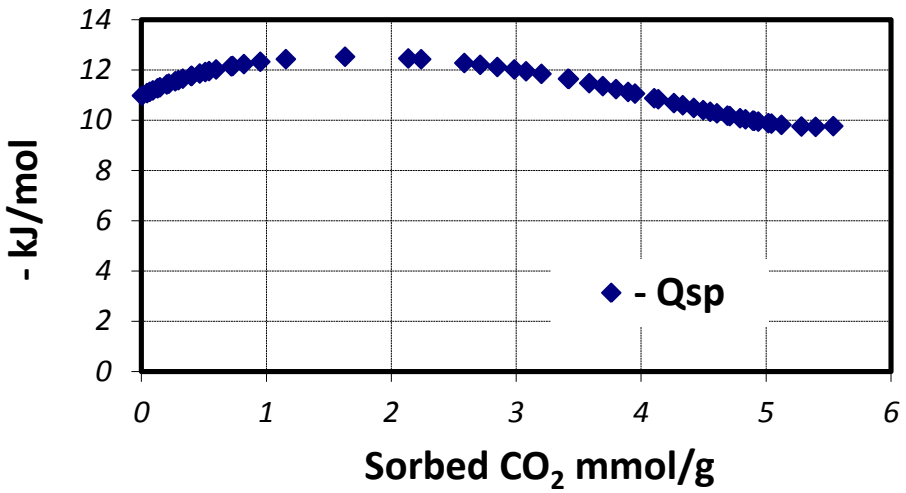

Figure 5.16: Plot of isosteric heat of sorption Q_{SP} against quantity of CO_2 sorbed.

5.7 Synthesis of $[Cu_3(HL5.6)_4(NO_3)_2(EtOH)_2]\cdot 3(C_6H_6)\cdot 2(H_2O)$ 5.22

Despite numerous attempts, complexes analogous to **5.20** and **5.21** were not formed when utilising *1H*-indazole-6-carboxylic acid **H_2L5.6** in place of **H_2L5.5**. Although the geometric differences between the two molecules are slight, propagation of the different bridging angle presumably does not allow the formation of the extended networks **5.20** and **5.21**. Nonetheless, ligand **H_2L5.6** was reacted with $Cu(NO_3)_2\cdot 3H_2O$ in a 3:4 ratio in ethanol, and subjected to a slow diffusion of benzene vapour, producing blue/green crystals of complex **5.22** within one month. It should be noted that equivalent structures, varying only in the degree of solvation, were produced using methanol as the solvent and either benzene or toluene as the antisolvent; however, the ethanol/benzene mixture produced the most pure and reproducible crystalline batches. The crystals were subjected to single crystal X-ray diffraction, and the data were solved and the structure model refined in the triclinic space group *P*-1 (R-factor 5.35%). The asymmetric unit contained two non-equivalent Cu(II) sites, both located on crystallographic special positions. Cu(1) is coordinated by four unique carboxylate oxygen atoms from two non-equivalent units of **HL5.6**, and one ethanol molecule in a square pyramidal arrangement, with the ethanol molecule occupying the axial position at an elongated bond length of 2.161(3) Å. Applying the crystallographic symmetry operations in this region reveals the well-known

copper paddlewheel structural motif,[404] in which two equivalent Cu(1) units are coordinated by four exo-bidentate carboxylate ligands with axial solvent molecules, and Cu-Cu distance 2.6324(9) Å, resulting in an overall square planar-type arrangement for the coordinating ligands. The Cu(2) ion coordinates in a Jahn-Teller distorted octahedral arrangement, with four monodentate indazole nitrogen atoms from two crystallographically unique **HL5.6** units occupying the equatorial plane, and disordered nitrate anions coordinating in the axial positions with Cu(2)-O(30) distance 2.372(3) Å. Also present in the structure are two water molecules per three Cu(II) ions, hydrogen bonding to half of the protonated indazole nitrogen atoms (where the other half of the protonated indazole nitrogen atoms donate hydrogen bonds to one contributor of the disordered nitrate ligands), and one benzene molecule per Cu(II) ion. The basic structure of **5.22** is shown in Figure 5.17.

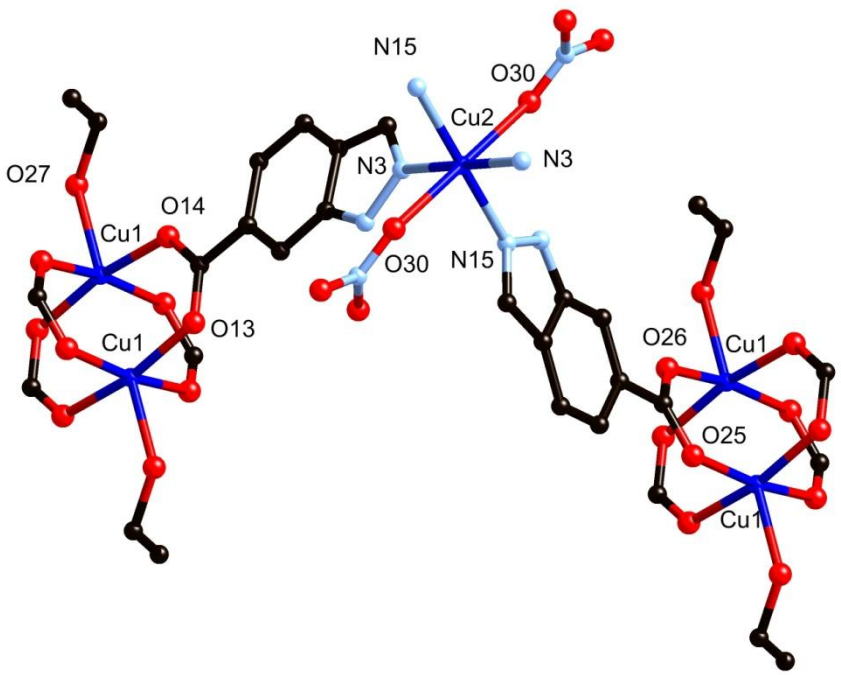

*Figure 5.17: Structure of complex **5.22** with partial heteroatom labelling scheme. Hydrogen atoms, nitrate anion disorder and solvent molecules omitted for clarity.*

With ligand **HL5.6** acting as a 2-connected linear bridge, and considering the entire paddlewheel cluster as a node, the network of **5.22** can be described as a (4,4) 2-dimensional sheet, shown in Figure 5.18. Adjacent sheets are stacked in such a way as to form square-walled one-dimensional channels passing through the windows parallel to the [0,1,1] vector, which are occupied by the benzene molecules within the unit cell. The aromatic rings of **HL5.6** are oriented orthogonal to the mean plane of the sheet, while hydrogen bonding is only observed within sheets, limiting interactions

between sheets to weak hydrogen bonding between the coordinating ethanol molecule and one orientation of the disordered nitrate molecule of the adjacent sheet. As such, when the crystals of **5.22** were removed from the mother liquor, a loss of single crystallinity was observed. Thermal analysis shows three sequential mass losses totalling *ca.* 30 % before 250 °C, with immediate onset, consistent with the loss of all of the coordinating and non-coordinating solvent molecules. These transitions lead directly into decomposition, with no appreciable plateau regions. Elemental analysis data were consistent with the rapid loss of benzene molecules on standing in air, with retention of water and ethanol molecules, suggesting a formula of $[Cu_3(\mathbf{HL5.6})_4(NO_3)_2(EtOH)_2]\cdot 3(H_2O)$ for the air-dried sample.

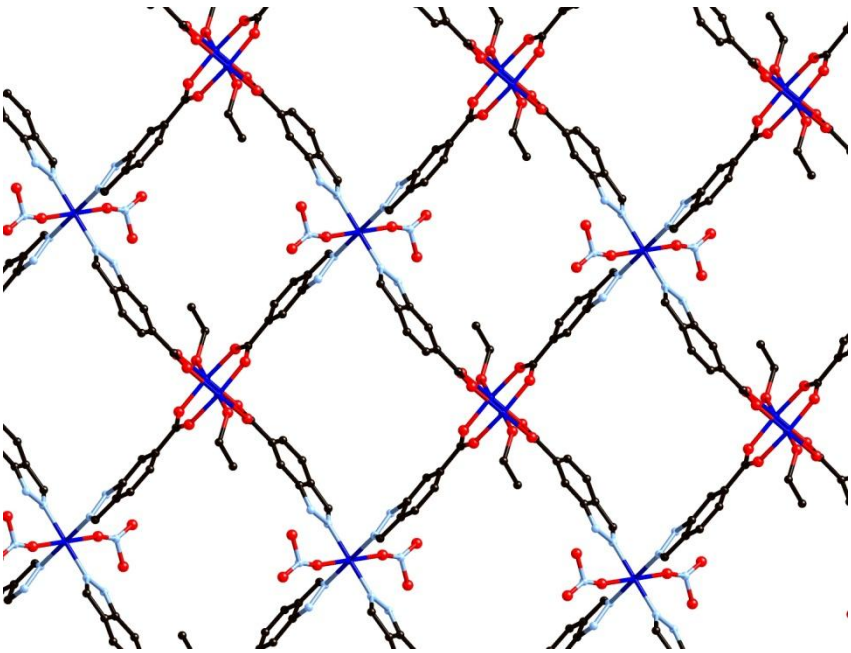

*Figure 5.18: (4,4)-sheet structure of complex **5.22**. Hydrogen atoms, solvent molecules and coordinating anion disorder omitted for clarity.*

5.8 Synthesis of $[Cu(HL5.7)_2]\cdot H_2O\cdot MeOH$ 5.23

Ligand $\mathbf{H_2L5.7}$ was reacted with $Cu(NO_3)_2\cdot 3H_2O$ in methanol, and the solution was allowed to stand for several days, during which time purple rod crystals deposited, which were isolated by filtration and found to be stable to drying. Analysis of the material by single crystal X-ray diffraction in the monoclinic space group *C*2/*c* (R-factor 4.21%) revealed one Cu(II) ion, coordinating to two equivalent chelating molecules of **HL5.7** in a *trans*- square planar arrangement, where the ligand

mean planes are parallel. Although it seems that such a coordination mode would require the *2H*-electron configuration for the indazole rings, as was the case for ligand **L5.2**, the distortions to the relevant bond lengths are small enough to be considered inconsequential; in this instance, the effect of coordination through the 1-position and protonation of the 2-position cannot be accurately represented by a single resonance contributor. Also present within the unit cell was one molecule of water per Cu(II) ion, and one methanol molecule, disordered over two equivalent orientations. The structure of **5.23** is shown in Figure 5.19.

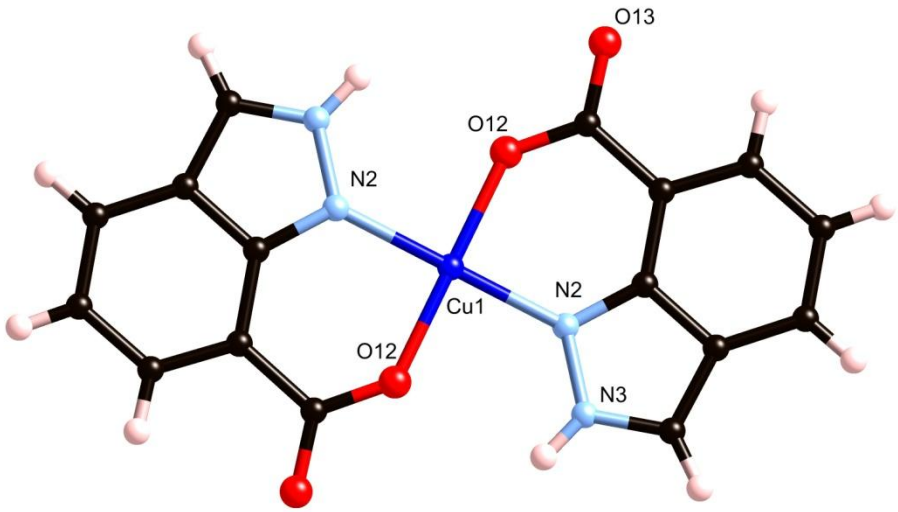

*Figure 5.19: Structure of complex **5.23** with unique heteroatom labelling scheme. Solvent molecules omitted for clarity.*

The intermolecular interactions in **5.23** are dominated by hydrogen bonding, where indazole nitrogen atom N(3) donates a hydrogen bond to the lattice water molecule, which itself donates a hydrogen bond to carboxylate oxygen atom O(13). These two interactions are duplicated by crystallographic symmetry, with the result that the lattice water molecule acts as a hydrogen bonded bridge between [Cu(**HL5.7**)] moieties, taking part in four hydrogen bonds, two as a donor and two as a receptor. The mode of hydrogen bonding is in fact equivalent to that seen in the structure of the free ligand hydrate above, where *in lieu* of the reciprocating N-H···O hydrogen bonds holding two units of the free ligand together, the square planar Cu(II) ion achieves the same result, with N(2)-O(12) distance of 2.686(3) Å slightly shorter than the equivalent distances in the free ligand structure of 2.816(2) and 2.826(2) Å. As was the case in the free ligand structure, these interactions propagate a one-dimensional chain, parallel to the *a* unit cell axis. Adjacent chains interact by way of parallel π-π stacking interactions on each face of the complex, at mean interplanar distance 3.315(3) Å, although

again, similar to the case in the free ligand structure, the aromatic ring planes are directly above the metal ions of adjacent chains, providing little overlap with the aromatic systems of the ligands, but a very weak overlap with the axially oriented d-orbitals of the metal. The disordered methanol molecules also donate hydrogen bonds to carboxylate oxygen atom O(13), but do not contribute to the topological description of the complex. The structure of one chain of **5.23** units is shown in Figure 5.20.

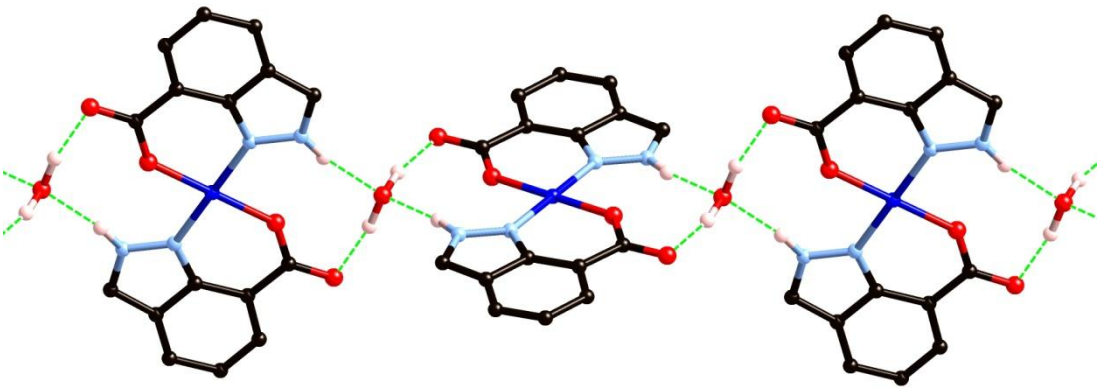

*Figure 5.20: Hydrogen bonding chain in the structure of complex **5.23.** Hydrogen atoms not participating in hydrogen bonding and methanol molecules omitted for clarity.*

5.9 Discussion

From the results presented above, it is clear that the synthetic versatility of the indazole skeleton is likely to lead to very promising outcomes in the synthesis of metallosupramolecular assemblies. The systematic substitution of the seven available positions around the indazole rings leads to the formation of 0-, 1-, 2- and 3-dimensional architectures. While the attachment of pyridine groups to the 1- and 2-positions gave new chelating ligands **L5.1** and **L5.2**, a large drawback exists in the synthesis of such systems, in the low yield and poor selectivity when a standard nucleophilic aromatic substitution strategy is employed. The modest difference in electronic properties of the two ligands was eclipsed by the differences in steric profile between the L-shaped **L5.1** and linear **L5.2**, and it would be expected that, in related systems, the directionality of the phenyl ring would play a role in the steric accessibility around the metal site, as well as presenting a useful handle for intermolecular interactions. Nonetheless, the synthesis of complexes **5.16** and **5.17** has shown that N-(2-pyridyl)-indazoles can be employed as bidentate chelating ligands and, with the use of improved synthetic

techniques, may be a route to 1-(2-pyridyl)-pyrazole analogues for more complex and functionalisable metallosupramolecular assemblies.

Carboxylic acid-functionalised indazoles **H_2L5.3 – H_2L5.7** have further demonstrated the versatility of the 1,2-diazole-carboxylic acid mixed ligand system, with the formation of a range of polymeric materials. Where the carboxylic acid groups are in positions capable of chelation with the diazole nitrogens, as was the case in **H_2L5.3** and **H_2L5.7**, the clear preference is for N,O-chelation in which the remaining heteroatoms can act either as directed hydrogen bond donors (**5.23**) or coordinate further (**5.18**), taking advantage of increased N-H acidity brought about a combination of the inherently greater acidity of indazole compared to pyrazole, the presence of an electron withdrawing carboxylate functional group, and the electron donation to the chelated metal ion.

Where chelation was not possible, due to the distance and orientation of the coordinating groups, the formation of coordination polymers was observed for ligands **H_2L5.4 – H_2L5.6**. Carboxylic acid substitution at the 4-position gave a ligand **H_2L5.4** in which the binding sites were oriented at approximately right angles, though with a relatively small linear separation. The combination of these effects led to the formation of a low dimensionality (4,4) polymer, both by the convergent angles of the coordinating atoms and planarity of the two binding sites. However, when the carboxylic acid group was appended to the adjacent 5-position, the coordinating groups adopted a divergent geometry, giving rise to 3-dimensional coordination polymer **5.21** and 3-dimensional hydrogen bonded metallopolymer **5.20**. The presence of encapsulated toluene molecules within **5.20** hindered any prospects for sorption applications, owing to the structural collapse accompanying desolvation; however, the exceptional thermal stability displayed by **5.21** allowed a gas sorption study to be carried out, which revealed a tendency for cooperative CO_2 sorption with broad hysteresis, and negligible sorption of methane or hydrogen. Despite a similar shape to **H_2L5.5**, ligand **H_2L5.6** was only found to form a two-dimensional (4,4) network on reaction with Cu(II), and was not capable of generating analogous networks to **5.20** or **5.21** under the tested conditions. Nonetheless, the structure of **5.22** displays the well-known Cu(II) ‘paddlewheel’ secondary building unit, which dictates that the remainder of the structure must adopt a planar arrangement, aided by the pseudo-square planar coordination mode adopted by the remaining Cu(II) ions. Hydrogen bonding interactions from the indazole N-H groups to interstitial solvent molecules were insufficient to prevent framework collapse on drying, most likely by shearing between 2-dimensional layers. The paddlewheel motif itself is known to be capable of leading to highly robust 3-dimensional frameworks, and may be of greater use where the ligand geometry lends itself to the formation of a 3-dimensional network, or where additional perpendicular interactions can be engineered.

The role of the ammonium hexafluorosilicate additive in the synthesis of **5.21** remains unclear; although the complex could be formed in small amounts by changing the Cu(II) source to the chloride or sulfate salts, changing the solvent mixture in a relatively broad range, or changing the dwell temperature, no product could be formed under any of the tested conditions without the presence of either ammonium hexafluorosilicate or hexafluorozirconate. Possible templation effects of the hexafluorosilicate dianion include steric templation of the hexagonal pores by the octahedral anion, or the formation of a reactive $Cu(SiF_6)$ species which can be coordinated selectively by four molecules of **HL5.5** a square planar fashion, similar to that observed in compound **5.20**. Also necessary to the product formation is the ammonium ion, which may act by lending solubility to the hexafluorosilicate anion as the soluble ion pair, and likely solubilises the **H_2L5.5** species by partial protonation.

Chapter 6

Substituted Pyrazole-Carboxylate Ligands

6.1 Introduction

Although pyrazole ligands are frequently employed with 3,5-unsubstituted- or 3,5-dimethyl-substitution patterns, many other possibilities exist for substitution of additional coordinating groups in these positions. Since pyrazole itself is relatively difficult to directly substitute in the 3- and 5-positions, two common synthetic methodologies are often adopted in order to achieve 3- or 5-substitution. Either an appropriately substituted precursor, usually a 1,3-diketone, can be prepared, often by a Claisen condensation route; or a readily available disubstituted pyrazole such as 3,5-dimethyl-*1H*-pyrazole can be derivitised, *i.e.* by oxidation of the methyl groups to carboxylic acids. Shown in Scheme 6.1 are two common ligands that have prepared by such methods; 3,5-bis(2-pyridyl)-*1H*-pyrazole **bpypz**, which can be prepared in two steps starting with the Claisen condensation of 2-acetylpyridine and ethyl pyridine-2-carboxylate,[405] and *1H*-pyrazole-3,5-dicarboxylic acid **pzdc**, prepared by oxidation of 3,5-dimethyl-*1H*-pyrazole by potassium permanganate.[406]

Ligand **bpypz** has been used mainly in the synthesis of multimetallic complexes for magnetism studies, either for the formation of $[M_2L_2]^{n+}$ dimers in which the binding sites in the equatorial planes of each metal are occupied by pyridylpyrazole chelates,[407-412] with axial sites available for the coordination of solvent molecules or anions, or the formation of larger clusters or circular helicates comprising $[M_4L_4]^{n+}$ or $[M_5L_6]^{n+}$ structures.[413-417] Several co-ligands have also been employed in metal-**bpypz** structures, taking advantage of the electronic properties of the pyridyl-pyrazole chelating system and close proximity of the two binding sites in ruthenium-based water oxidation catalysts.[418-420] The **pzdc** ligand has seen use both in the formation of materials for magnetism studies and in the preparation of coordination polymers, discussed in a key paper by Powell and co-workers,[225] as well as being used in a wide range of transition metal, lanthanide and mixed-metal compounds, both discrete and polymeric.[224, 226, 421-424] In these instances, the large variety of possible coordination modes of the pyrazole-carboxylate system become evident, with a wide range of chelating and bridging coordination modes being observed; common amongst these is the $[M_2L_2]$ dimer similar to that observed in transition metal-**bpypz** complexes, where the second oxygen of the carboxylic acid functional group is free to coordinate further.

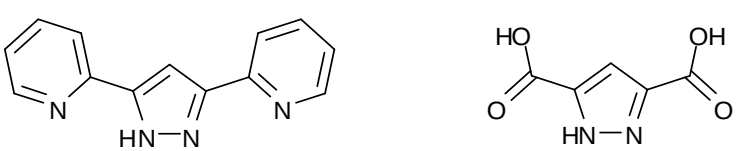

*Scheme 6.1: Structures of known symmetric 3,5-disubstituted pyrazoles **bpypz** (left) and **pzdc** (right).*

Despite the existence of over 100 structurally characterised metal complexes of each **bpypz** and **pzdc**, and the obvious usefulness of the chelating pyrazole-3-carboxylate or 3-(2-pyridyl)-pyrazole motifs, very few structurally characterised examples of pyrazole-based ligands containing both N,O- and N,N-chelating sites had been reported at the time of writing (CSD version 5.33, February 2012 update), most involving the use of oxime,[425] hydrazide,[426] or amide functionality,[427] while no examples of *1H*-pyrazole-3-heteroaryl-5-carboxylic acid compounds coordinating to metal ions have been reported to date. The closely related ligand *1H*-pyrazole-3-carboxylic acid, although widely used as a precursor in medicinal chemistry,[428, 429] appears in only three reported instances of structurally characterised transition metal complexes; a report by Halcrow and co-workers in which two such ligands chelated to two Cu(II) ions to form a discrete species,[430] a report by Li in which the solvothermal reaction of **pzdc** gave a similar species with imidazole and aqua ligands capping the Cu(II) dimer, where the ligand was formed by *in-situ* monodecarboxylation of **pzdc**,[431] and one instance of an Ir(III) complex of *1H*-pyrazole-3-carboxylate containing two cyclometallated 2-phenylpyridine ligands.[432] Slightly greater interest has been directed towards the more sterically encumbered ligand 5-methyl-*1H*-pyrazole-3-carboxylic acid, with the synthesis of several discrete and one-dimensional transition metal complexes reported in recent years,[433-435] however this ligand is similarly underrepresented in the coordination polymer literature.

6.2 Ligand Synthesis

With a view to generating a range of pyrazole-carboxylate ligands containing additional coordinating functionality, several approaches relating to different isomeric substitution patterns can be considered. Firstly, a combination of the synthetic strategies discussed in Chapters 2 and 3 can be employed to generate a ligand containing a chelating pyridylpyrazole group combined with a carboxyphenyl moiety appended at the pyrazole 4-position. To this end compound **2.14**, previously used as the esterified diketone precursor to ligand **HL2.6**, was reacted with 2-hydrazinopyridine to give the ester **L6.1**, which was subjected to base hydrolysis to generate ligand **HL6.2**, as shown in Scheme 6.2.

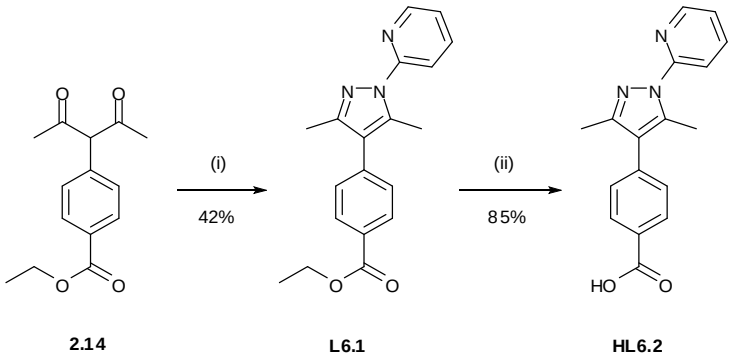

*Scheme 6.2: Synthesis of ligands **L6.1** and **HL6.2**. Reagents and conditions: (i) 2-hydrazinopyridine, EtOH, reflux; (ii) KOH, THF/H_2O, reflux 48 hr, then $HCl_{(aq)}$*

Another possible form of the pyridyl-pyrazole-carboxylate heteroleptic ligand system is 5-pyridyl-*1H*-pyrazole-3-carboxylic acid **H_2L6.3**, in which two bidentate coordination sites are present, with potential for both a pyridylpyrazole N,N and pyrazole-carboxylate N,O chelation. Ligand **H_2L6.3**, a known compound from the medicinal chemistry patent literature,[436] was prepared following literature procedures for the related 5-methyl-*1H*-pyrazole-3-carboxylic acid,[437] employing a Claisen condensation between 2-acetylpyridine and diethyl oxalate to form the diketone ester **6.6**, which was reacted with hydrazine hydrate to form the pyrazole ester **6.7**, from which ligand **H_2L6.3** was available *via* base hydrolysis. An analogous procedure was used to generate the novel pyrazine equivalent **H_2L6.4**, starting from 2-acetylpyrazine.

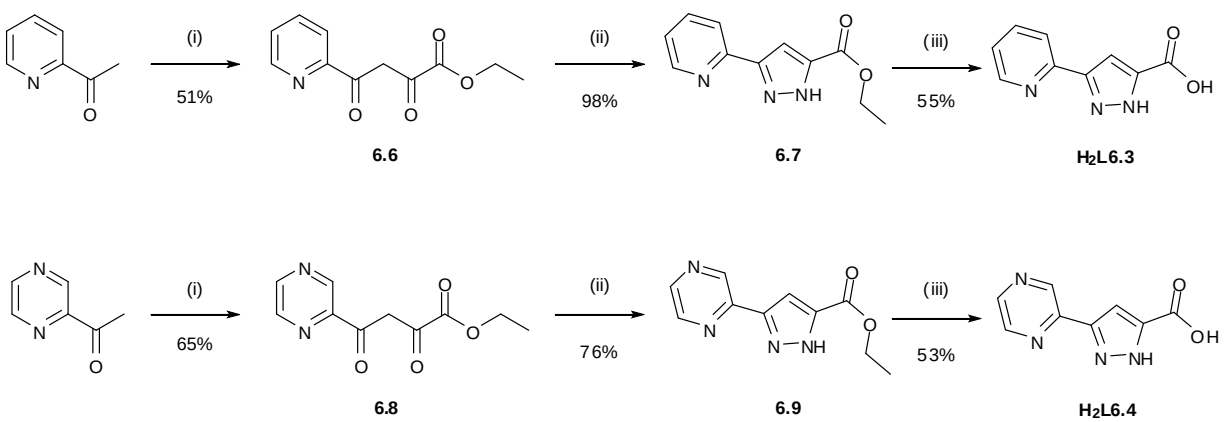

*Scheme 6.3: Synthesis of **H_2L6.3** and **H_2L6.4**. Reagents and conditions: (i) Diethyl oxalate, NaOEt, PhMe, N_2, 0°C → RT, 14 hr; (ii) H_2NNH_2, EtOH, reflux 8 hr; (iii) LiOH, H_2O/THF, reflux 48hr, then $HCl_{(aq)}$.*

Finally, *1H*-pyrazole-3-carboxylic acid **H_2L6.5** was prepared as a 5-unsubstituted comparison to the well-known **pzdc** ligand, and to contrast with *1H*-indazole-3-carboxylic acid **H_2L5.3**. Several synthetic routes are known to 3-methylpyrazole, from which the acid is available *via* permanganate oxidation,[438] and due to the commercial availability of the starting material, the cyclocondensation of 2-acetylacetaldehyde dimethyl acetal was chosen as the desired method.[208] From the methyl precursor **6.10**, oxidation gave **H_2L6.5** in a low but sufficient yield, as shown in Scheme 6.4.

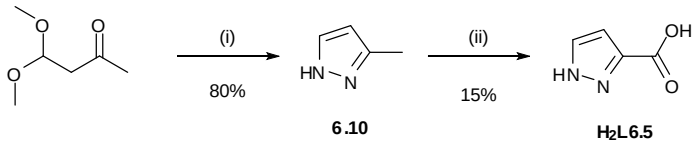

*Scheme 6.4: Synthesis of **H_2L6.5**. Reagents and conditions: (i) H_2NNH_2, 10% $HCl_{(aq)}$;[208] (ii) $KMnO_4$, H_2O, 60 °C → reflux, 6 hours, then $HCl_{(aq)}$[438]*

6.3 Complexes of L6.1 and HL6.2

*6.3.1 Synthesis of [Cu(**L6.1**)$_2$MeCN]·2(ClO_4) **6.11***

Prior to hydrolysis to form ligand **HL6.2**, ligand **L6.1** was reacted with $Cu(ClO_4)_2·6H_2O$ in acetonitrile, and the mixture analysed by electrospray mass spectrometry to show the presence of a $[Cu(\mathbf{L6.1})_2]^{2+}$ species at *m/z* 352.6141. Single crystals of complex **6.11** were prepared in 19% yield from the diffusion of diisopropyl ether into the acetonitrile solution, and the small green rod crystals obtained were subjected to analysis by single crystal X-ray diffraction, where the data were solved and the structure model refined in the orthorhombic space group $P2_12_12$ (R-factor 4.46%). The structure model reveals a 5-coordinate Cu(II) centre coordinated by two crystallographically equivalent molecules of **L6.1** in a bidentate fashion, with the coordination sphere completed by a single acetonitrile molecule, Figure 6.1. The coordination geometry of the Cu(II) ion is trigonal bipyramidal in nature, with contracted Cu(1)-N(9) distance 1.956(4) Å, compared to the Cu(1)-N(2) distance of 2.073(4) Å, and equatorial N-Cu-N angles of 122.88(11) and 114.2(2)° for N(26)-Cu(1)-N(2) and N(2)-Cu(1)-N(2′), respectively. The pyridylpyrazole unit subtends a bite angle of 79.82(17)°, seemingly well suited to such a geometry. Two crystallographically equivalent disordered perchlorate anions are present per metal site, and no significant interactions were seen between the anion and complex. Although the pyridylpyrazole moiety is held relatively planar by coordinating to the metal, with interplanar angle 8.6(8)°, the torsion between the pyrazole and phenyl ring of 40.9(8)°

likely prohibits any substantial π-π interactions, with the result that no significant intermolecular interactions are observed within the structure.

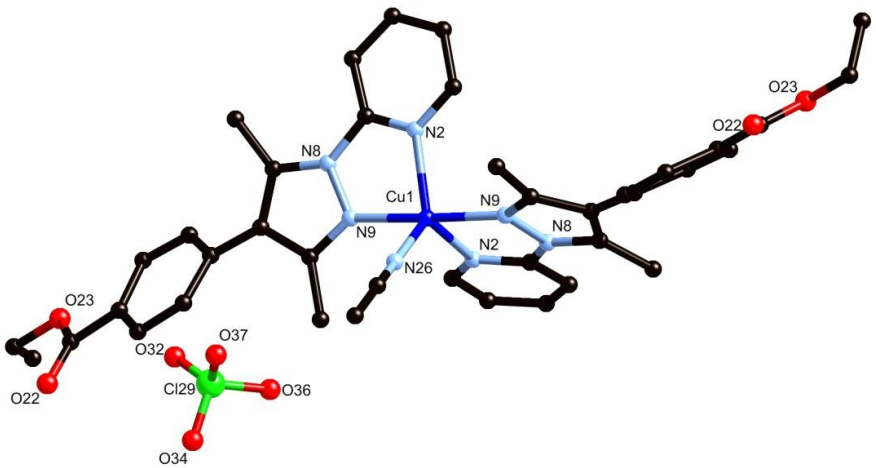

*Figure 6.1: Structure of complex **6.11** with heteroatom labelling scheme. Hydrogen atoms and anion disorder omitted for clarity.*

*6.3.2 Synthesis of poly-[Cu(**L6.2**)(MeOH)(NO_3)] **6.12***

Following the hydrolysis of **L6.1** to form **HL6.2**, the first attempt to generate a polymeric complex was undertaken by reacting **HL6.2** with one equivalent of $Cu(NO_3)_2 \cdot 3H_2O$ in methanol under solvothermal conditions with 24 hour dwell time at 120 °C and 5 °C/hr cooling rate. The resulting small green rod crystals, obtained in 28% yield, were found to be weakly diffracting and displayed severe non-merohedral twinning, and as a result only a poor quality structure solution could be obtained (final R-factor 9.93%), despite several collections. The asymmetric unit of complex **6.12**, solved and refined in the triclinic space group *P*-1, shows one deprotonated molecule of **L6.2** coordinating to two equivalent Cu(II) ions, with two coordination sites provided by the N,N chelate of the pyridylpyrazole system, and one occupied by the deprotonated carboxylate of **L6.2**. The remaining two coordination sites are occupied by a nitrate anion and a methanol molecule, to give a square pyramidal coordination sphere in which the axial site is occupied by the methanol molecule with Cu(1)-O(28) distance 2.206(6) Å and O(24)-Cu(1)-N(2) angle of 154.9(3). A second oxygen atom from the coordinating nitrate also makes a weak contribution to the electron density around the

metal site, with Cu(1)-O(26) distance 2.571(7) Å. As was the case with complex **6.11**, the pyridyl-pyrazole system is relatively coplanar, with interplanar angle 7.2(3)°, while the pyrazole-phenyl interplanar angle of 47.6(3)° remains consistent with that expected due to the steric clash between pyrazole methyl groups and phenyl *ortho* hydrogen atoms. An intramolecular hydrogen bond exists in the vicinity of the metal site, between the protonated methanol ligand and the non-coordinating oxygen atom of the adjacent carboxylate, forming a favourable 6-membered hydrogen bonding ring. The structure of complex **6.12** is shown in Figure 6.2.

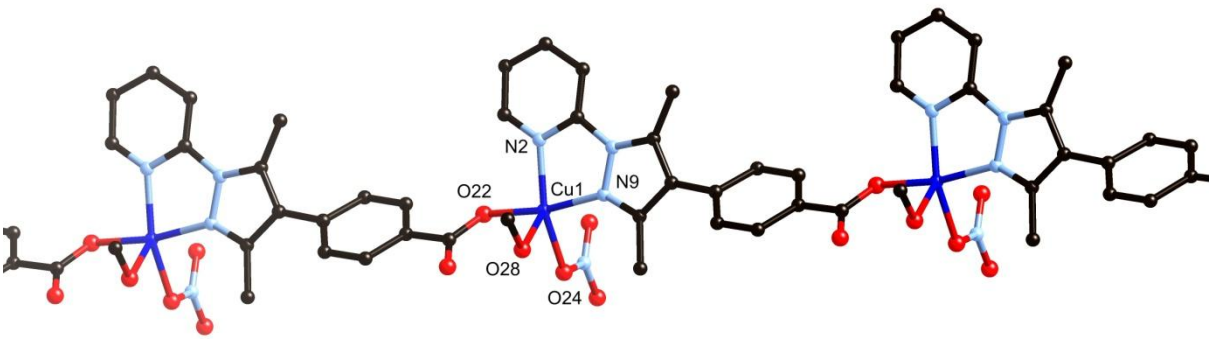

*Figure 6.2: Structure of compound **6.12** with partial heteroatom labelling scheme. Hydrogen atoms omitted for clarity.*

As can be seen in Figure 6.2, the coordination through the pyridylpyrazole and carboxylate groups of **L6.2** gives rise to a one-dimensional coordination polymer, proceeding along the [1,0,1] vector. Due to the lack of significant conjugation between the pyrazole and phenyl ring, and the degree of steric encumberance caused by both the twist angle between the coordinating groups and the pyrazole methyl groups, no significant intermolecular interactions exist between parallel strands. Small amounts of residual electron density were detected at several locations throughout the lattice; however, their identity could not be confirmed crystallographically. Thermogravimetric analysis of a dry sample of **6.12** showed clean loss of 6.5% mass centred at 120 °C, consistent with loss of the coordinating methanol molecule (calculated mass 7%), while elemental analysis of a freshly isolated sample showed some retention of a further 0.5 methanol molecules per copper. Due to the poorly resolved structural model provided by the X-ray diffraction data, the precise degree of solvation cannot be definitively assigned.

*6.3.3 Structure of $[Cu_2(SO_4)_2(H_2O)_2(\mathbf{HL6.2})_2]\cdot H_2O\cdot MeOH$ **6.13***

Ligand **HL6.2** was reacted with $Cu(SO_4)_2\cdot 5H_2O$ in an ethanol/water mixture under solvothermal conditions with 24 hour dwell period at 100 °C, followed by cooling at 4 °C/hr, to generate green single crystals of complex **6.13** in 50% yield. The X-ray diffraction data were solved and the structure model refined in the non-centrosymmetric monoclinic space group *Cc* (R-factor 4.38%), where the structure was found to exhibit racemic twinning. The asymmetric unit was found to contain two molecules of **HL6.2** coordinating to two Cu(II) ions, which were bridged by two sulfate anions. The coordination sphere of each copper is completed by one water molecule, giving a square pyramidal geometry in which the axial site is occupied by a sulfate oxygen with Cu-O distances 2.238(3) Å and 2.217(3) Å for Cu(1) and Cu(2), respectively. Both water molecules undergo intramolecular hydrogen bonding interactions to the adjacent sulfate anions, forming six-membered hydrogen bonding rings. The geometry of the **HL6.2** ligand is closely related to that observed for structure **6.12**, with pyridyl-pyrazole interplanar angles of 8.90(14) and 5.02(13)°, pyrazole-phenyl interplanar angles of 43.84(14) and 50.70(14)°, and N-Cu-N bite angles of 80.15(14) and 80.18(14)° for Cu(1) and Cu(2), respectively. Also included in the asymmetric unit are one water molecule and one ethanol molecule, where the ethanol molecule acts as a hydrogen bond donor to the water molecule, which itself bridges two units of **6.13**,, as discussed below. The structure of **6.13** is shown in Figure 6.3.

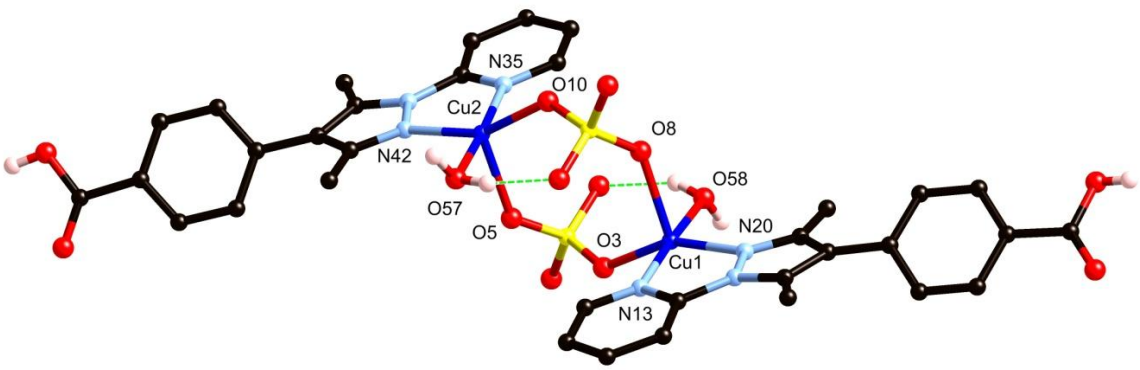

*Figure 6.3: Structure of **6.13** showing partial heteroatom labelling scheme. Selected hydrogen atoms and solvent molecules omitted for clarity.*

The extended structure of **6.13** is dominated by hydrogen bonding interactions, where each molecule possesses four hydrogen bond donor sites, in the two carboxylic acids and two outward-facing hydrogen atoms from the coordinating water molecules. The most significant hydrogen bonding interaction is that in the region of the metal dimer, where a one-dimensional ladder is propagated by a

series of reciprocating hydrogen bonds between the water hydrogen atoms H(57A) and H(58B) and sulfate oxygen atoms O(7) and O(12), respectively, where two hydrogen bonds exist between each pair of molecules. The benzoic acid groups which extrude from the central ladder are interdigitated with those from adjacent chains, supported by hydrogen bonds between the carboxylate O-H groups and sulfate oxygens from the central ladders. One set of these interactions is further supported by two hydrogen bonds donated by the non-coordinating water molecule to carboxylate oxygen atom O(33) and oxygen atom O(57) belonging to a coordinating water molecule. Since this interaction links two centres which were already linked by a carboxylic acid – sulfate hydrogen bond, the non-coordinating water molecule has no impact on the overall topology; however, the presence of this water molecule hydrogen bonding to only one of the two carboxylic acids disrupts the symmetry of the complex, which appears otherwise centrosymmetric. The extended structure of **6.13** is shown in Figure 6.4.

When considering the hydrogen bonding interactions from a topological standpoint, with the copper-copper centroid as a node, the network consists of a (3,6) two-dimensional sheet. Adjacent sheets interact by way of π-π interactions between pyridylpyrazole groups, at interplanar angle 0.79(13)° and minimum interatomic distance 3.228(5) Å for N(20)-C(38). Thermal analysis of **6.13** showed loss of 10% mass by 100 °C, consistent with loss of both the non-coordinating solvent molecules and the coordinating water molecules, followed by a broad plateau up to 250 °C leading to decomposition. Heating the crystals to 100 °C in air revealed that this desolvation was accompanied by a loss of single crystallinity. Identical structural properties and thermal behaviour were observed when preparing the complex using methanol in place of ethanol.

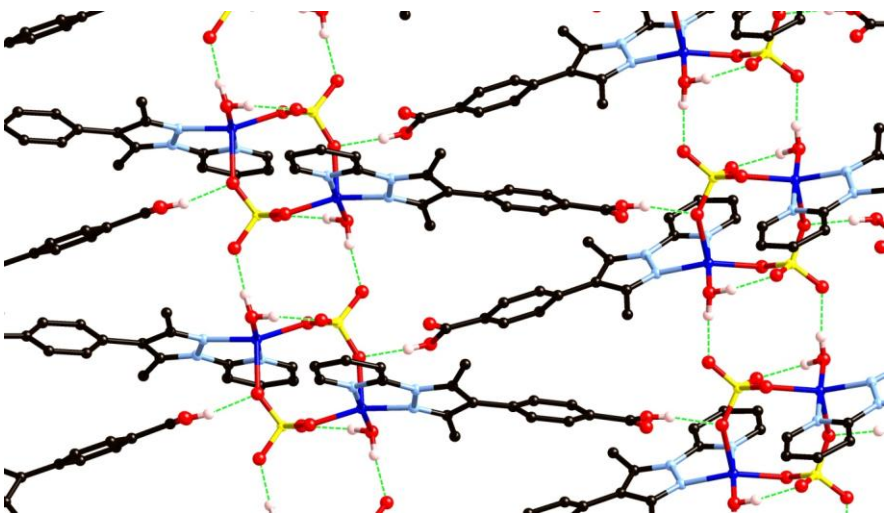

*Figure 6.4: Hydrogen bonded network of **6.13**. Non coordination solvent molecules and hydrogen atoms not participating in hydrogen bonding omitted for clarity.*

6.4 Complexes of H_2L6.3 and H_2L6.4

Examining the structure of ligands **H_2L6.3** and **H_2L6.4**, and comparing with the known symmetric 3,5-bis(2-pyridyl)-*1H*-pyrazole **bpypz** and *1H*-pyrazole-3,5-dicarboxylic acid **pzdc** ligands, the coordination mode would be expected, in the first instance, to resemble a neutral $[M_2L_2]$ dimer when reacted with metals in the +2 oxidation state with the potential to coordinate in square planar, square pyramidal or octahedral coordination modes. However, the inclusion of further coordination sites, namely the non-chelating carboxylate oxygen or the second nitrogen atom in the pyrazine ring may provide the capabilities to link such dimeric complexes into polymeric assemblies, adopting the "metalloligand" approach. Both ligands were found to form insoluble metal complexes on reaction under mild conditions, and as such, solvothermal routes were employed to generate single crystalline samples of all complexes.

6.4.1 Structure of $[Cu_2(\mathbf{L6.3})_2(MeOH)_2]$ ***6.14***

Ligand **H_2L6.3** was combined with an excess of $CuCl_2 \cdot 2H_2O$ in 5 ml of methanol in a pressure vessel and heated to 130 °C, allowed to dwell for 24 hours, and cooled to room temperature at 5 °C/hr. The purple rod crystals obtained in 21% yield were subjected to single crystal X-ray diffraction, where the data were solved and the structure model refined in the triclinic space group *P*-1 (R-factor 2.65%). The structure was found to consist of two equivalent Cu(II) ions coordinated by two doubly deprotonated ligand molecules, forming a neutral centrosymmetric $[Cu_2(\mathbf{L6.3})_2]$ species, in which the axial coordination sites of the copper ions are occupied by methanol molecules on opposing faces of the dimer, leading to an overall square pyramidal coordination sphere for the metal ions. The two Cu(II) ions are separated by a distance of 3.9582(7) Å. The bite angles subtended by the two chelating domains, 79.95(9) and 80.47(8)° for N(1)-Cu(1)-N(5) and N(6)-Cu(1)-O(3), respectively, impart a relatively regular coordination geometry, while the angles from the coordinating methanol to each atom in the basal plane *via* the Cu(II) centre all lie in the range 90.04(7)-96.73(8)°. The pyridine – pyrazole system was found to be effectively coplanar, with interplanar angle 0.58(10)°, while the torsion angle of the pyrazole-carboxylate system of 0.6(3)° also symbolises planarity, and the metal ions were found to lie within the ligand mean plane within crystallographic error. The structure of complex **6.14** is shown in Figure 6.5.

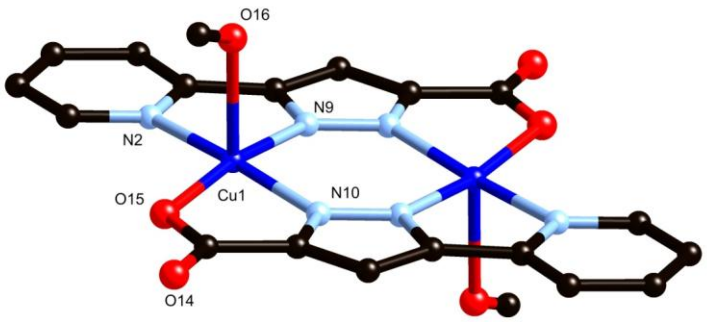

*Figure 6.5: Structure of complex **6.14** with unique heteroatom labelling scheme. Hydrogen atoms omitted for clarity.*

Molecules of **6.14** interact by way of hydrogen bonding between the methanol ligands and coordinating carboxylate oxygens of the adjacent complexes. Each pair of dimers is held together by two such interactions, and further supported by a strong offset face-to-face π-π interaction with mean interplanar distance 3.2843(19) Å, in which the metal ions themselves are separated by a distance of 3.7710(7) Å. Propagation of these interactions leads to the formation of a one-dimensional polymeric structure running parallel to the *a* unit cell axis. A representation of the intermolecular interactions in **6.14** is shown in Figure 6.6. The crystals themselves remain stable on drying in air, and thermogravimetric analysis showed good thermal stability until approximately 75 °C, when a rapid one-step loss of mass occurs consistent with loss of both coordinating methanol molecules. After desolvation the remaining material loses no further mass until the decomposition process with onset slightly above 300 °C. On heating in air, a loss of single crystallinity was observed in conjunction with the loss of the coordinating methanol molecules.

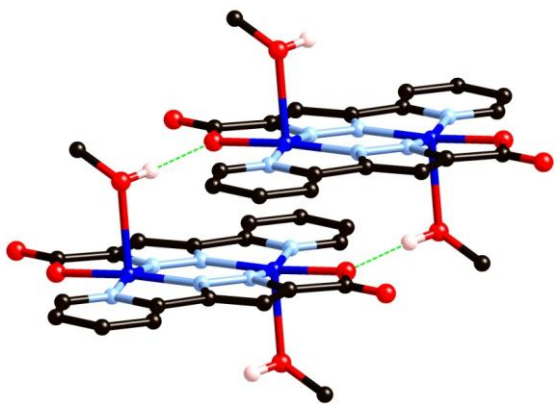

*Figure 6.6: Intermolecular interactions between units of complex **6.14**. Hydrogen atoms not participating in hydrogen bonding omitted for clarity.*

*6.4.2 Structure of poly-[Cu_2(**L6.3**)$_2$] **6.15***

In a similar method to that discussed for complex **6.14**, complex **6.15** was prepared by the solvothermal reaction of **H_2L6.4** with excess $Cu(NO_3)_2 \cdot 3H_2O$ in 2 ml of methanol, employing the same heating cycle described above. The dark-blue block crystals obtained in 62% yield were analysed by single crystal X-ray diffraction, revealing a structure in the monoclinic space group $P2_1/c$ (R-factor 3.20%). The structure was found to consist of an equivalent [Cu_2(**L6.3**)$_2$] dimer to that seen in **6.14**; however, instead of methanol molecules coordinating in the axial sites, the non-chelating carboxylate oxygen atoms of adjacent complexes act as ligands, forming a polymeric assembly. The axial Cu(1)-O(14) distance of 2.278(2) Å is shorter than the axial bond in **6.14** of 2.341(2) Å, while the remaining structural parameters for the dimer itself are closely related to those of **6.14**, although the Cu(II) ions are pushed out of the ligand plane by 0.101(2) Å towards the axial ligands in **6.15**, leading to a longer Cu-Cu distance of 3.9789(5) Å. The pyridine – pyrazole interplanar angle of 5.75(9)° is notably larger than that observed in **6.14**, as is the carboxylate-pyrazole torsion of 3.7(3) °, suggesting a slight conformational change is required to adopt the new binding mode. The structure of **6.15** is shown in Figure 6.7.

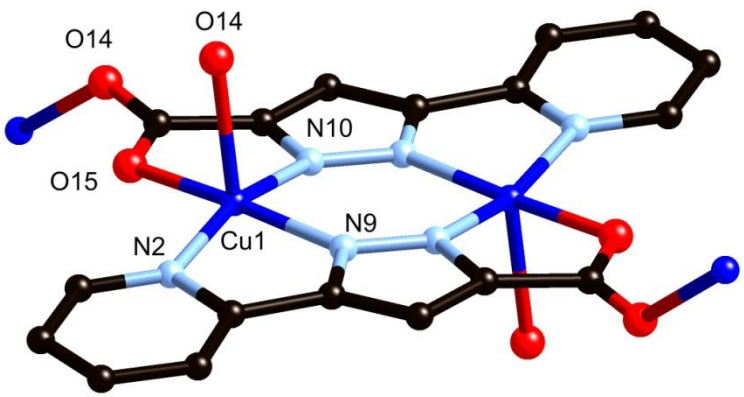

*Figure 6.7: Structure of **6.15** with unique heteroatom labelling scheme. Hydrogen atoms omitted for clarity.*

The [Cu_2(**L6.3**)$_2$] dimer extends into a two-dimensional sheet by the linkages between copper atoms and carboxylate oxygens, propagating a (4,4) 2-dimensional sheet parallel to the *bc* plane, as shown in Figure 6.8. The network resembles a herringbone-type motif dictated by the C(13)-O(14)-Cu(1) angle of 133.50(16)° imparting an interplanar angle of 42.19(8)° between mean planes of adjacent dimers. The windows of each circuit are interdigitated by the two adjacent sheets, taking advantage of a strong offset face-to-face π-π stacking arrangement, with mean interplanar distance of 3.272(2) Å where the

maximum overlap is between pyridine rings. Unlike in structure **6.14**, however, these interactions do not bring adjacent Cu(II) centres into close proximity. While elemental analysis suggested some association of atmospheric water molecules with the solids on prolonged standing in air, thermal analysis of a freshly isolated sample of **6.15** showed no significant mass loss below 300 °C, when, similar to **6.14**, a single step decomposition process is initiated.

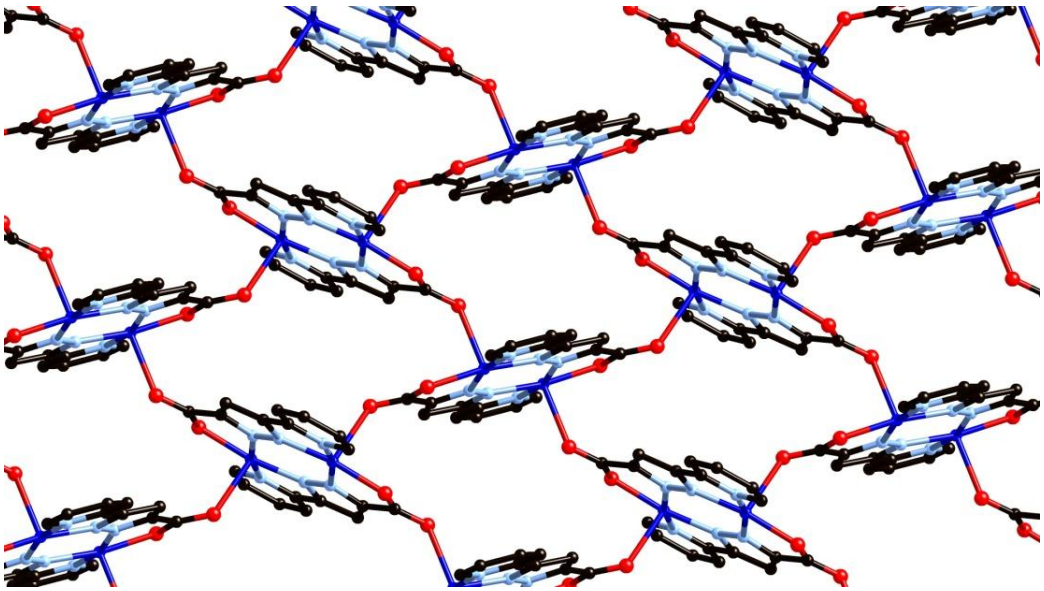

*Figure 6.8: A single 2-dimensional sheet in the structure of **6.15** viewed perpendicular to the bc plane. Hydrogen atoms and interdigitating sheets omitted for clarity.*

*6.4.3 Structure of [Co(**HL6.4**)$_2$(OH$_2$)$_2$] **6.16***

Ligand **H$_2$L6.4** was expected to form complexes in which the second nitrogen from the pyrazine ring would engage in further coordination beyond the formation of an [M$_2$L$_2$] dimer, either to extend the dimers into a polymeric network akin to the behaviour of the carboxylate oxygen in **6.15**, or perhaps coordinate to a second metal ion to form a binodal network. While several Cu(II) complexes of **L6.4** were obtained, in low yield and impure and poorly reproducible phases, no evidence was observed of coordination through the second pyrazine nitrogen atom, where either discrete or carboxylate bridged dimers, equivalent to **6.14** and **6.15**, were formed instead. When reacted with CoSO$_4$·7H$_2$O under hydrothermal conditions, two phases could be reproducibly obtained in good yields, depending on the dwell temperature and presence of base. After testing several stoichiometries, [Co(**HL6.4**)$_2$(OH$_2$)$_2$] **6.16** was prepared as a pure phase by combining the ligand **H$_2$L6.4** with 0.66 equivalents of

$CoSO_4 \cdot 7H_2O$ in water, and heating to 130 °C under hydrothermal conditions, allowing to dwell for 24 hours, and cooling to room temperature at 5 °C/hr. The orange crystals, obtained in 40% yield, were analysed in the monoclinic space group $P2_1/c$ (R-factor 2.76%), where the structure consisted of an octahedral Co(II) ion coordinating to two equivalent molecules of **HL6.4** *via* pyrazole-carboxylate N,O-chelates in the equatorial plane, with the axial coordination sites occupied by two crystallographically equivalent water molecules. The structure of **6.16** is shown in Figure 6.9.

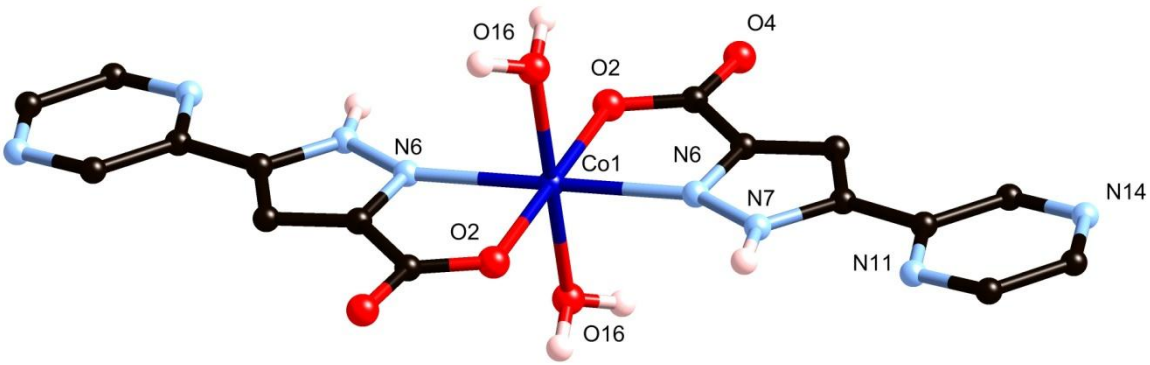

*Figure 6.9: Structure of complex **6.16** with unique heteroatom labelling scheme. Selected hydrogen atoms omitted for clarity.*

By charge balance considerations as well as the comparatively long metal-ligand bond lengths (2.030(1)-2.214(1) Å), the oxidation state of the cobalt ion was assigned as +2. The octahedral geometry is comparatively regular, dictated by the bite angle of the N,O chelate of 79.26(5)°, while the O(2)-C(3)-C(5)-N(6) torsion of 2.1(2)° compares well to those observed in **6.14** and **6.15**. The pyrazole and pyrazine rings exist in a *cis* conformation, with interplanar angle of 3.58(7)°, providing a weak interaction between the protonated pyrazole N-H group and the lone pair of the pyrazine nitrogen atom, indicated by the N(11)-H(7) distance of 2.646(2) Å. The structure of complex **6.16** encloses six classically defined hydrogen bond donors and up to 12 possible acceptor sites, and as such, the extended network is dominated by hydrogen bonding interactions. Two distinct types of hydrogen bonding interactions are observed; the coordinating water molecules each donate two hydrogen bonds to non-coordinating carboxylate oxygen atoms on adjacent complexes, each of which receives two such interactions. Four complexes are bridged by each of these interactions, giving rise to an 8-membered ring comprised of four hydrogen bonds, as shown in Figure 6.10. The second mode of hydrogen bonding involves donation of a hydrogen bond from the pyrazole N-H group to the 4-nitrogen atom of the pyrazine ring on an adjacent complex. This interaction is reciprocated by a weak

C-H···N hydrogen bond (C(13)-O(2) distance 3.232(2) Å) from the pyrazine 5-position to the coordinating carboxylate oxygen atom, as shown in Figure 6.10. The close proximity of adjacent aromatic systems encourages strong π-π stacking interactions, where adjacent ligand mean planes overlap with interplanar angle 3.41(7)° and minimum interatomic distance 3.355(2) Å for C(15)-C(8).

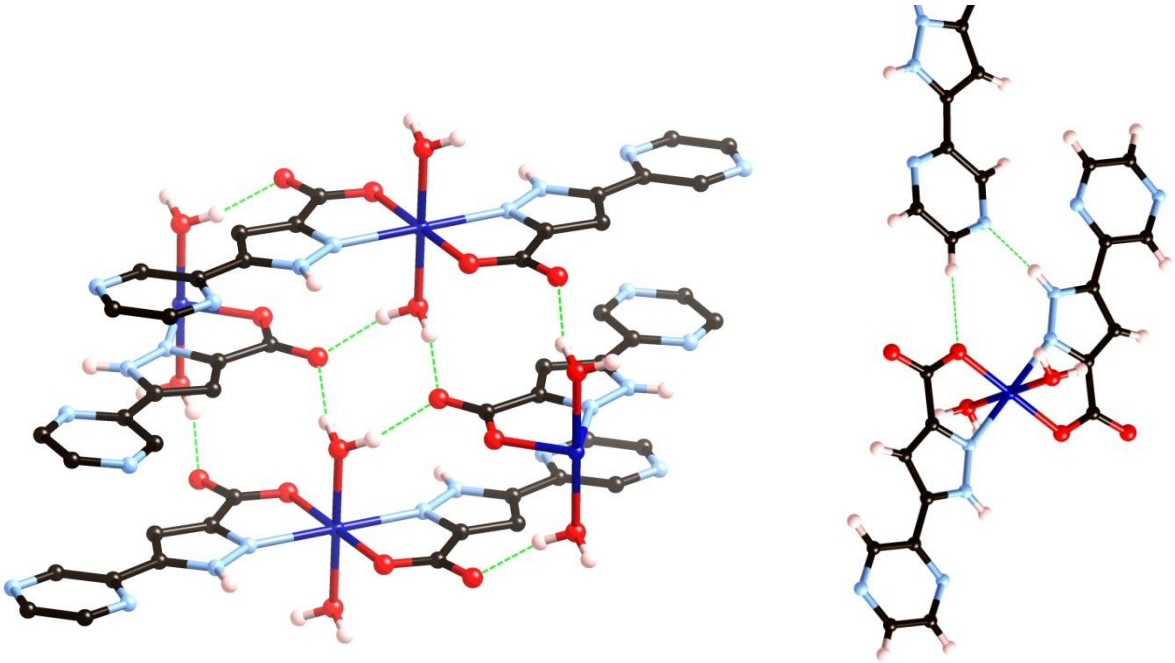

*Figure 6.10: Modes of hydrogen bonding interactions in **6.16**, showing the 8 membered ring between four adjacent complexes (left) and N-H···N and reciprocating C-H···O interactions (right).*

When the hydrogen bonding in **6.16** is considered from a topological standpoint, an 8-connected node can be assigned to each cobalt centre. Analysis of the resulting network reveals a ($4^{24}\cdot6^{4}$) **bcu** body-centred cubic topology associated with the structure, a schematic of which is shown in Figure 6.11. Although the **bcu** topology itself can potentially define channels, in the case of **6.16** the dense packing of the bulky ligands and relatively small inter-nodal distances preclude the formation of any physical void space. Thermal analysis showed the loss of the coordinating water molecules as a single step transition centred at 190 °C, with a mass loss of 7.4% (calculated mass 7.6%), followed by a single step decomposition process centred at 265 °C.

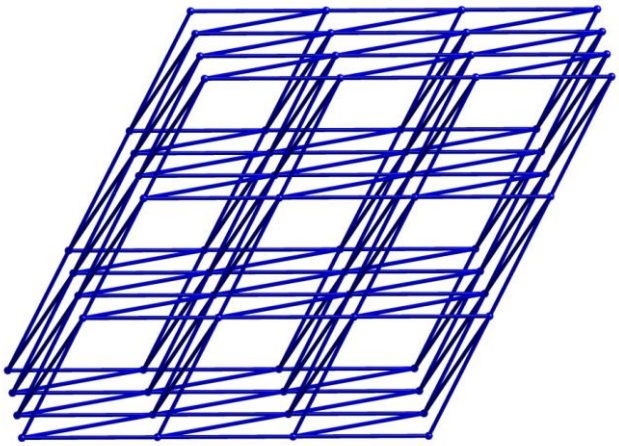

*Figure 6.11: Schematic representation of the **bcu** topology of the hydrogen bonding network within compound **6.16**, with metal ions selected as nodes.*

*6.4.4 Structure of poly-[Co_2(**L6.4**)$_2$(OH_2)$_3$]·5(H_2O) **6.17***

When **H_2L6.4** was combined with 0.66 equivalents of $CoSO_4 \cdot 7H_2O$, the same ratio employed for complex **6.16**, in water in the presence of a small quantity of 2,4,6-trimethylpyridine and heated to 180 °C, allowed to dwell for 72 hours and cooled to room temperature at 10 °C/hr, small, poorly crystalline orange rods of complex **6.17** were formed as a pure phase in 83% yield, and were isolated by filtration and subjected to single crystal X-ray diffraction. The structure model, solved and refined in the monoclinic space group $P2_1/c$ (R-factor 7.45%), revealed three unique Co(II) environments, each occupying crystallographic special positions and with total occupancy of 2, and two doubly deprotonated molecules of **L6.4**. Each cobalt(II) ion coordinates in an octahedral fashion to a different ligand set; in a coordination mode reminiscent of that seen in complex **6.16**, Co(1) is coordinated to two equivalent pyrazole-carboxylate N,O-chelates and two equivalent water molecules in a *trans* orientation, where the non-coordinating carboxylate oxygen atom displays slight crystallographic disorder, while Co(2) is also coordinated by two equivalent N,O-chelates, with monodentate pyrazine nitrogen atoms completing the coordination sphere in a *trans* orientation. Co(3) is coordinated by two non-equivalent pyrazine-pyrazole N,N-chelates, while the remaining coordination sites are occupied by two non-equivalent water molecules in a *cis* orientation. Each coordination sphere is relatively regular in its coordination geometry, with minimum *cis* angle of 76.9(2)° for N(23)-Co(3)-N(27), and all metal-ligand bond lengths fall in the range 2.060(6)-2.191(5) Å, with no elongation or contraction along a particular axis, suggesting the high spin Co(II) electronic configuration for all three metal

ions. Two hydrogen bonding interactions are observed within the asymmetric unit, further linking metal sites across each pyrazole bridge, originating from the *cis* oriented coordinating water molecules of Co(3) to the coordinating carboxylate oxygens of Co(1) and Co(2). The structure of complex **6.17** is shown in Figure 6.12.

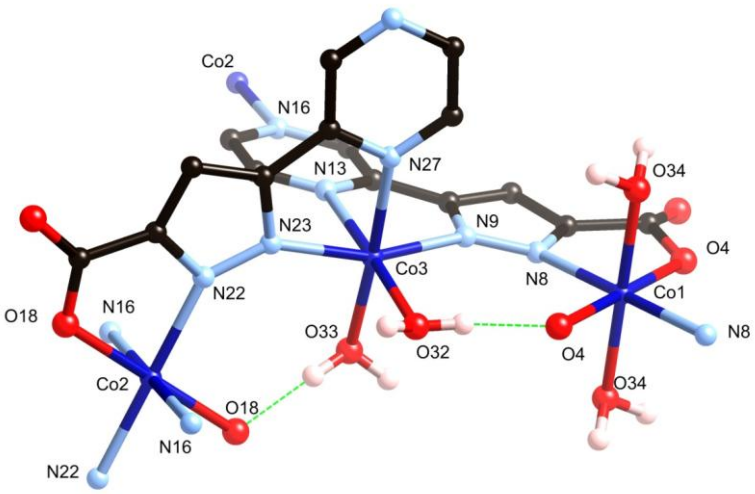

*Figure 6.12: Structure of **6.17** with labelling scheme for coordinating atoms. Selected hydrogen atoms omitted for clarity.*

When the complete structure of **6.17** is considered, a two-dimensional sheet is evident, in which one-dimensional chains running parallel to the [1,0,1] vector are bridged into two dimensions by the pyrazine bridge between Co(2) and Co(3), to form a sheet parallel to the *ac* plane. Interestingly, a topological description of this sheet requires only two nodes; since Co(1) only links together two ligands, it can be considered a link; likewise, the molecule of **L6.4** in which the second pyrazine nitrogen atom does not coordinate only links two metal ions, and must also be a link. The remaining molecule of **L6.4** connects all three metal ions, and is linked to itself *via* the Co(1) link, and linked to Co(2) directly and *via* the Co(3)-**L4.6** link. As such, the only nodes required to describe the network are the 3-connected molecule of **L4.6**, assigned arbitrarily to pyrazole carbon C(11), and the four-connected Co(2). The network itself can be assigned the point symbol $(4\cdot6^2)_2(4^2\cdot6^2\cdot8^2)$, and is displayed in Figure 6.13.

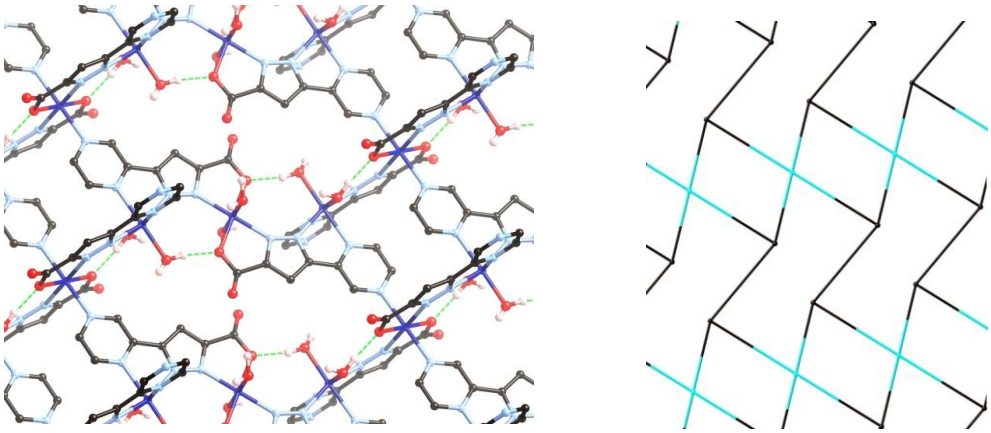

*Figure 6.13: 2-dimensional sheet structure of **6.17** (left), showing one dimensional strands progressing left to right linked in the perpendicular direction by pyrazine bridges, and (right) topological representation of the two-dimensional network of **6.17**, with cobalt ions coloured light blue and ligand nodes coloured black. Notable is the equivalent one-dimensional progression of closely bridged metal sites left-to-right, and linking in the perpendicular direction by pyrazine bridges.*

The two-dimensional sheets in **6.17** are linked into a three-dimensional structure by hydrogen bonding from coordinating water molecule O(32) to the non-coordinating pyrazine nitrogen atom of an adjacent sheet. These pyrazine rings also engage in an interdigitating mode of π-π stacking, with interplanar angle 20.4(3)° and minimum interatomic distance 3.448(8) Å for C(31)-C(24). These interdigitating columns of **L6.4** moieties define a series of one-dimensional channels passing parallel to the *c* unit cell axis, with interatomic dimensions of *ca.* 5 × 10 Å, shown in Figure 6.14. Despite the presence of potential hydrogen bond donors in the coordinating water molecules of Co(1) and Co(3), and a number of carboxylate oxygen atoms lining the pore walls, the contents of the channels were not able to be determined crystallographically, due to the poor diffraction characteristics of the crystals, and as such the SQUEEZE routine was carried out,[246] which suggested a void volume of 24% of the unit cell, occupied by 20 water molecules per unit cell, or 2.5 water molecules per cobalt ion, further to the 1.5 coordinating water molecules per cobalt. Thermogravimetric analysis showed a total mass loss of 21%, occurring in three discrete steps before 180 °C. This value is also consistent with a total of four water molecules per cobalt ion. Although a broad plateau is present in the thermogravimetric analysis trace from *ca.* 180-320 °C, heating the crystals in air to afford desolvation led to a loss of crystallinity. Elemental analysis displayed a slightly reduced solvation formula of 2 non-coordinating water molecules per cobalt ion, as expected after prolonged standing in air.

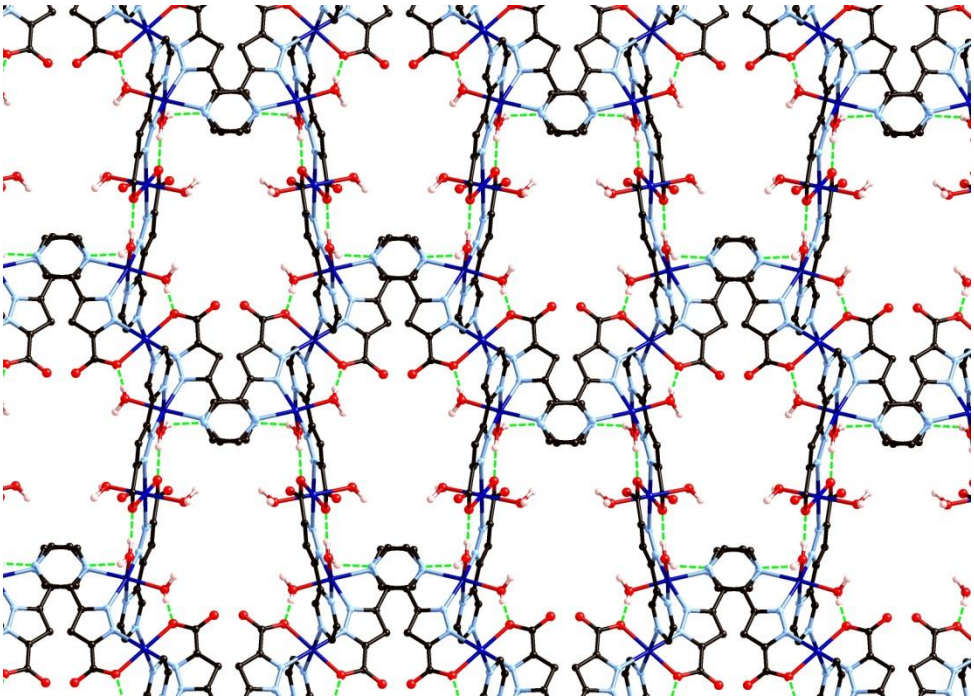

*Figure 6.14: Channel structure of **6.17**, viewed parallel to the c unit cell axis. Selected hydrogen atoms omitted for clarity.*

6.5 Structure of poly-[Cu(L6.5)(NMP)]·xNMP 6.18

Ligand **H_2L6.5** was synthesised primarily to act as an analogue to *1H*-indazole-3-carboxylic acid **H_2L5.3**, in which the coordinating groups are largely unchanged, while the aromatic backbone of the molecule is removed. Subjecting **H_2L6.5** to the exact conditions used to generate complex **5.18** failed to yield any identifiable products, most likely due to the low stability of 5-unsubstituted pyrazoles under solvothermal conditions. Instead, **H_2L6.5** was combined with $Cu(NO_3)_2{\cdot}3H_2O$ in a variety of solvents under more mild conditions. It was found that carrying out the reaction in N-methyl pyrrolidone (NMP) produced a blue microcrystalline solid on standing. Furthermore, addition of water to the mixture caused the solids to redissolve. As such, the reaction was carried out in a 9:1 mixture of NMP and water, and the product poly-[Cu(**L6.5**)$_2$(NMP)]·xNMP **6.18** was crystallised slowly in 13% yield by allowing the solution to stand in a $CaCl_2$ dessicator for several weeks. Smaller crystals could also be obtained by using a 20:1 NMP:H_2O mixture and allowing the mixture to stand in a sealed vial. The blue crystals obtained were subjected to single crystal X-ray diffraction, and the data obtained were solved and the structure model refined in the tetragonal space group $I4_1/a$ (R-factor 6.51%). Notably, the crystal structure was solved in the same space group as **5.18,** although

with a considerably larger unit cell, of volume 5981.2(5) Å^3 (compared with 4531.2(8) Å^3 for **5.18**). The structure model revealed an equivalent coordination mode for the **L6.5** ligand as was the case for **L5.3**, in which each heteroatom coordinates to a Cu(II) ion, firstly with the formation of a [Cu_2(**L6.5**)$_2$] dimer, which is then linked into a three-dimensional network by bridging through the second carboxylate oxygen atom. Although the structure of the dimer itself is superimposable with that observed in **5.18**, the geometry of the coordination to the second carboxylate oxygen exhibits a slight deviation; while the metal site in **5.18** exhibited some distortion towards the trigonal bipyramidal geometry, with N(10)-Cu(1)-O(13) angle 150.85(15)° falling half way between the expected value for square planar and trigonal bipyramidal, the equivalent N(6)-Cu(1)-O(9) angle in **6.18** of 169.84(16) shows a much greater tendency towards the square pyramidal geometry. This assignment is supported by the τ_5 values of 0.43 and 0.09 for **5.18** and **6.18**, respectively. The coordination sphere of the Cu(II) ion is completed by an NMP molecule in the axial position, with Cu(1)-O(10) distance 2.337(4), significantly longer than the equivalent Cu(1)-O(14) bond in **5.18** of 2.268(3). These data are consistent with the weaker nature of NMP as an oxygen donor ligand when compared to acetamide, due to a combination of reduction in available delocalised electron density by methylation of the amine and cyclisation, loss of the hydrogen bonding chelate-type interactions, and increased steric bulk of the backbone. The structure of **6.18** is shown in Figure 6.15.

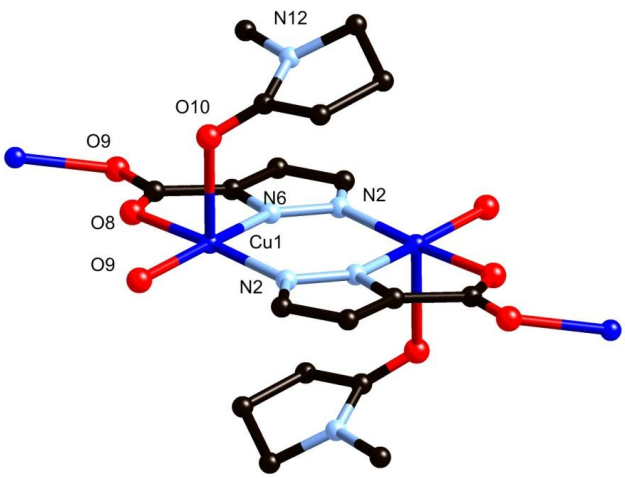

*Figure 6.15: Structure of compound **6.18** with heteroatom labelling scheme. Hydrogen atoms omitted for clarity.*

As would be expected due to the structural similarities with compound **5.18**, the extended network of **6.18** can be described by the **lvt** topology by making the same assignment of nodes to the centroid of the pyrazole-bridged copper dimer. Interestingly, while the topologies are identical, the physical

structures of **5.18** and **6.18** are substantially different. While **5.18** comprised a densely packed network with no appreciable void space, **6.18** defines a more open structure, where channels are observed running parallel to the *a* and equivalent *b* unit cell axes, with interatomic dimensions *ca.* 9 Å, while no void space is observed parallel to the unique axis. When the structures of **5.18** and **6.18** are directly compared, this discrepancy becomes intuitive; as shown in Figure 6.16, when the additional carbon atoms comprising the indazole ring are considered separately, the same channel structure can be observed in **5.18**, where the void space in **6.18** is filled by the sterically bulky indazole phenyl rings.

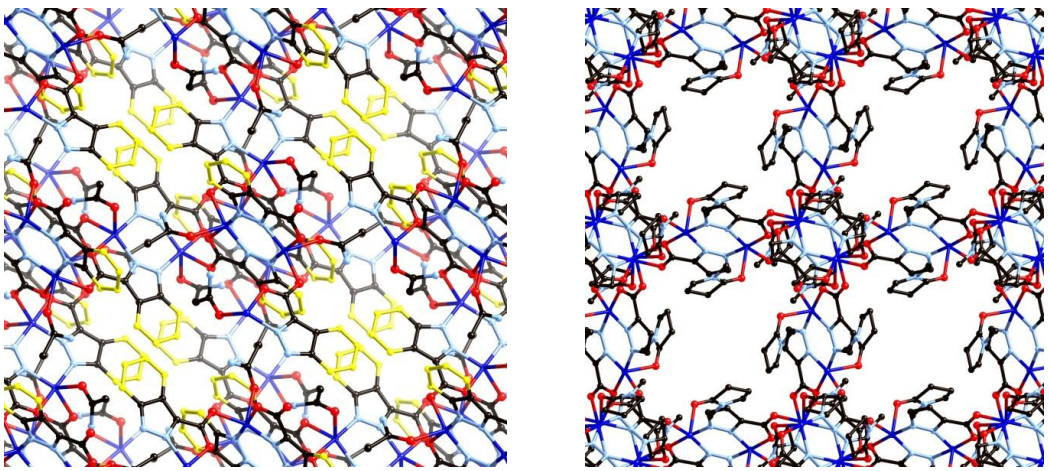

*Figure 6.16: Comparison of the structures of **5.18** (left) and **6.18** (right), viewed perpendicular to the unique axis, in which the additional carbons present to comprise the indazole phenyl rings in **5.18** have been coloured yellow. Hydrogen atoms omitted for clarity.*

Unfortunately, the diffuse electron density within the channels in the crystallographic model of **6.18** was unable to be satisfactorily modelled, and as such the SQUEEZE routine was applied to the crystallographic data,[246] which suggested a void content of 1230 electrons per unit cell, equivalent to 153 electrons per $[Cu_2L_2]$ unit. These data are consistent with a void occupancy of approximately 3 non-coordinating molecules of NMP per dimer, suggesting a total volatile mass percentage of 59%, including the coordinating solvent molecules. Thermogravimetric analysis is in approximate agreement with this value, showing a total of 52% mass loss by 150 °C, with onset at room temperature, followed by a brief plateau, a further 6% mass loss centred at 210 °C, and a rapid decomposition centred at 310 °C. Elemental analysis confirmed the loss of lattice solvent on prolonged standing in air, suggesting a molecular formula for a dry sample of poly-[Cu(**L6.5**)(NMP)]·0.5(NMP)·0.5(H_2O). Compound **6.18** was observed to retain single crystallinity on soaking in diethyl ether, chloroform or acetonitrile; however, the crystals disintegrated instantly on

removal from any of these more volatile solvents, preventing the collection of a guest-exchanged crystal structure. Hydrogen gas sorption experiments were carried out using a sample of **6.18** which had been soaked in acetonitrile and baked under dynamic vacuum at 125 °C; however, no significant uptake was observed at 77K, most likely due to framework collapse accompanying the desolvation procedure.

6.6 Discussion

Examining the structures **6.11**-**6.18**, several points of interest are apparent in the nature of the coordination modes and dimensionality of the metal complexes formed by ligands **L6.1**-**H_2L6.5**. Ligands **L6.1** and **HL6.2** displayed largely the expected coordination behaviour; the simple chelating coordination mode available to **L6.1** in complex **6.11** was repeated following hydrolysis of the ester, where metal ions were bridged into a one-dimensional polymer by coordination of the carboxylate in complex **6.12**, or where hydrogen bonding interactions were dominant in combination with a bridging anionic co-ligand, forming a 2-dimensional sheet in **6.13**. The utility of the combination of chelating pyridylpyrazole and carboxylate functionality in **HL6.2** was somewhat hindered by the presence of the methyl groups at the pyrazole 3- and 5-positions, preventing the formation of a coordination polymer of higher dimensionality by sterically restricting the number of chelating groups able to coordinate to the metal centre, as was observed in Chapter 3. Removal of these steric constraints might be expected to provide a route to a more useful family of heteroleptic pyridylpyrazole-carboxylate ligands.

The preference for the formation of a discrete $[M_2L_2]$ dimer, in which the pyrazole moiety bridges two metals through the deprotonated N,N- bridge and is augmented by an N,O or N,N-chelate, was preserved for 3,5-unsymmetric pyrazole ligands **H_2L6.3**-**H_2L6.5,** aided by the electron deficient subtituents on the pyrazole 3- and 5-positions increasing the N-H acidity of the pyrazole ring, allowing for deprotonation under mild conditions. The presence of the second carboxylate oxygen atom in **H_2L6.3** and **H_2L6.5** allows these dimers to act as metalloligands, linked into polymeric assemblies by coordination through the second carboxylate oxygen atom to vacant metal sites on adjacent dimers. Such complexes also present ideal geometry for strong π-π interactions, with highly π-polarised character and large conjugated surfaces, as well as potential interactions to unsaturated metal sites, providing an additional structural facet such as the interdigitating mode of inter-sheet interaction in **6.15**. In the case of complexes **6.16** and **6.17**, the preferential coordination of the N,O-chelating site compared to the comparatively electron poor pyrazine group allowed the formation of a

discrete monometallic compound **6.16** or, under more forcing conditions, the related polymeric compound **6.17**, where similar coordination environments were linked by further coordination through the pyrazine bridges.

Unfortunately, although polymeric compounds **6.17** and **6.18** both displayed sizable solvent channels, neither proved sufficiently stable to drying to show usefulness for sorption applications. In the case of **6.17**, instability on drying was expected, due to the low dimensionality of the network and reliance on hydrogen bonding to support the desolvated framework. Complex **6.18**, although defined by a 3-dimensional network of coordination bonds, most likely displayed poor stability on desolvation due to the nature of the bridging between $[Cu_2(\mathbf{L6.5})_2(NMP)_2]$ dimers, which was effectively monodentate in nature and contained significant degrees of rotational freedom, likely causing collapse of the framework following removal of the bulky guest molecules or under thermal stress. Nonetheless, it is expected that complexes containing 3,5-unsymmetric pyrazole-chelated metallodimers such as were those described above may provide a route to useful metalloligand-type nodes in coordination polymer materials when more robust bridging functionalities can be incorporated.

Chapter 7

Conclusions and Future Work

7.1 Conclusions

The results discussed in the preceding chapters have further reinforced the versatility of the 1,2-diazole tecton in metallosupramolecular chemistry, leading to the synthesis of a number of new discrete and polymeric assemblies. In Chapter 2, several bis-*1H*-pyrazoles were employed to generate a series of Co(II) coordination polymers with bis-carboxylate co-ligands. These results showed the usefulness of hydrogen bond donor sites in the direct vicinity of the metal centre in generating robust and reproducible coordination architectures, as well as the impact of ligand geometry and flexibility on the dimensionality of the network when the metal ion geometry was held constant.

Chapter 3 further explored the metallosupramolecular chemistry of flexible bis-pyrazoles, where the hydrogen bond donor functionality was removed and replaced with pyridine groups allowing for chelation, giving rise to more varied coordination motifs and leading to several helicate structures as well as low dimensionality coordination polymers, including new cases of unexpected *in-situ* solvothermal ligand formation.

Chapter 4 extended this work to include benzimidazole functionality extending from the 1-position of several pyrazole ligands, where binding sites were connected by flexible linkers appended through either benzimidazole or pyrazole groups, leading to the formation of a series of related Cu(II) metallocycles and a helicate closely related to those reported in Chapter 3.

Chapter 5 introduced the indazole ring system as a previously unexplored metallosupramolecular tecton, employing all seven possible modes of mono-substitution to generate a family of discrete and polymeric assemblies. Substitution of a 2-pyridyl moiety at the 1- or 2- position gave simple chelating ligands, while carboxylic acid functionality at positions 3-7 gave ligands capable of forming coordination polymers of varying dimensionality, including compound **5.21**, which displayed hysteretic CO_2 uptake.

Finally, Chapter 6 explored other possible substitution patterns for the pyrazole ring system with the synthesis of several pyrazole-carboxylate ligands with additional heterocyclic functionality, leading to the synthesis of three-dimensional coordination polymers displaying considerable solvent-accessible volumes, as well as discrete materials in which hydrogen bonding again plays a key structure-directing role.

By examining these results, the key findings can be summarised;

- The presence of an N-H group directly adjacent to a strongly coordinating donor atom, a property exclusive to 1,2-diazoles and a very small group of other heterocycles, is key to their versatility as ligands in metallosupramolecular assemblies, allowing for either structure-directing hydrogen bonding interactions, deprotonation leading to an anionic ligand species, or the straightfoward synthesis of chelating ligands.
- Matching the carboxylate functionality with pyrazole or indazole coordinating groups gives a useful blend of steric and electronic factors, providing anionic character, hydrogen bond acceptors and polarised π-systems to generate stable, neutral coordination assemblies.
- Benzodiazole ring systems, particularly indazole, possess unique potential as ligands in metallosupramolecular chemistry owing to their comparatively straightforward synthesis and functionalisation, as well as possessing many of the desirable properties of pyrazole-based ligands. Access to more diverse ligand geometries allows the formation of new coordination assemblies that utilise mixed diazole-carboxylate functional groups, which may prove invaluable in the ongoing search for new robust coordination materials.

7.2 Future Work

The results presented in Chapters 2-6 represent progress in the synthesis of metallosupramolecular assemblies based on 1,2-diazoles, and it is expected that these discoveries will lead to further work in this field. To this end, several promising areas of further study were identified, and preliminary screening was carried out to establish the viability of further investigations. The compounds described below were prepared on trial scales, mostly in the final weeks of this research, and as such, full characterisation was not carried out due to time constraints. Instead, these compounds are presented as starting points for future work in this area.

7.2.1 Mixed Pyrazole-Carboxylate Ligands

The structures of metal complexes containing both diazole and carboxylic acid ligands in Chapters 2, 5 and 6 have shown the versatility of the pyrazole-carboxylate mixed ligand system, both in terms of synthetic availability of the functional groups and compatibility of the two groups as ligands, especially in coordination modes capable of hydrogen bonding interactions. Ligand **HL2.6**, used in

the synthesis of complex **2.24**, still contains great potential for the synthesis of porous coordination frameworks, due to its rigid nature, distance between binding sites and potential for hydrogen bonding. Substantial efforts were made to prepare a 'MOF-5 analogue' structure containing **L2.6** units as linkers, akin to recent work employing 3,5-dimethyl-*1H*-pyrazole-4-carboxylic acid as a ligand.[439] Although cubic crystalline material was obtained on reaction of **HL2.6** with $Zn(NO_3)_2 \cdot 6H_2O$ in DMF, structural characterisation was never achieved, due to extremely poor crystallinity and slow decomposition in air. Interestingly, when subjected to the solvothermal ammonium hexafluorosilicate-templated reaction with $Cu(NO_3)_2 \cdot 3H_2O$ which was developed for the synthesis of complex **5.21**, ligand **HL2.6** also produced a robust and porous coordination polymer, identified as a threefold-interpenetrated **lvt** network, containing inter-framework hydrogen bonding and considerable pore volume of 39%, while the metal coordination geometry was very similar to that observed in **5.21**. An optimisation study and sorption measurements are expected to be carried out in the near future, while the role of the hexafluorosilicate anion, and applicability of the method to other, similar structures, represents another avenue requiring further exploration. The structure of poly-[Cu(**L2.6**)$_2$] is shown in Figure 7.1.

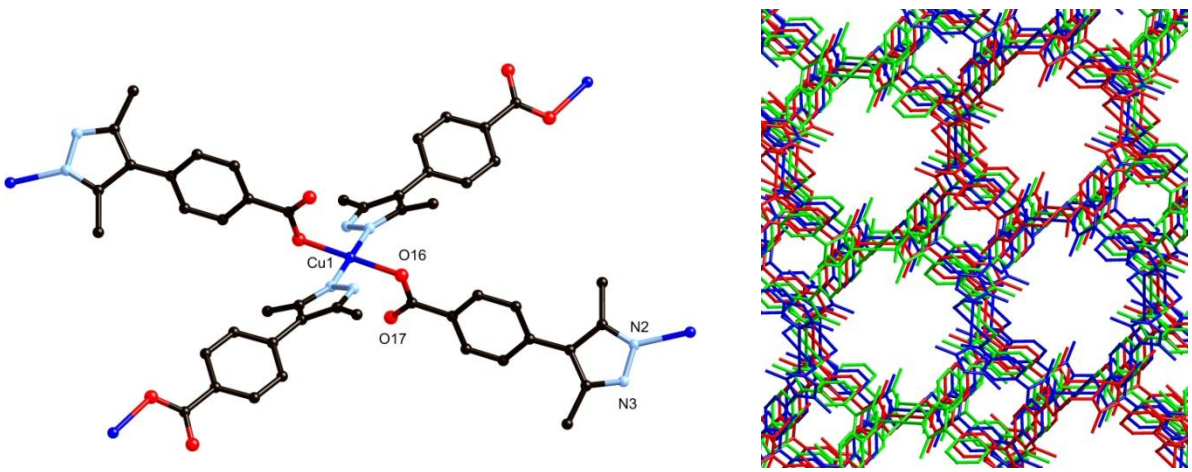

*Figure 7.1: (Left) Structure of poly-[Cu(**L2.6**)$_2$] wth unique heteroatom labelling scheme. Hydrogen atoms omitted for clarity. (Right) Extended structure of poly-[Cu(**L2.6**)$_2$] viewed slightly offset to the unique axis. Independent networks coloured separately.*

As well as its further use as a ligand, the synthetic route developed to prepare **HL2.6** can be applied to other systems, in order to generate related compounds with different functionality. Ligand 1-(3,5-dimethyl-*1H*-pyrazol-4-yl)-benzene-3,5-dicarboxylic acid **H_2L7.1** was prepared on a trial scale by the same method, using 5-aminoisophthalic acid as a starting material, and coordination polymers poly-[Zn(**L7.1**)] and poly-[Co(**L7.1**)] were prepared by combining **H_2L7.1** with either $ZnSO_4 \cdot 7H_2O$

or $CoSO_4 \cdot 7H_2O$ and 2,4,6-trimethylpyridine in water and heating to 160 °C. These materials, obtained as impure phases in a mixture with amorphous material, possessed no void space or encapsulated solvent molecules; however, both show the great potential for ligands such as **H_2L7.1** in the formation of further coordination polymer materials. The structures of poly-[Zn(**L7.1**)] and poly-[Co(**L7.1**)] are shown in Figure 7.2. The extended structure of poly-[Zn(**L7.1**)] is that of the 4-connected **unc** network, with both metal and ligand acting as equivalent 4-connected nodes, while poly-[Co(**L7.1**)] adopts the zeolitic **crb** topology, again with both ligand and metal acting as equivalent 4-connecting nodes.

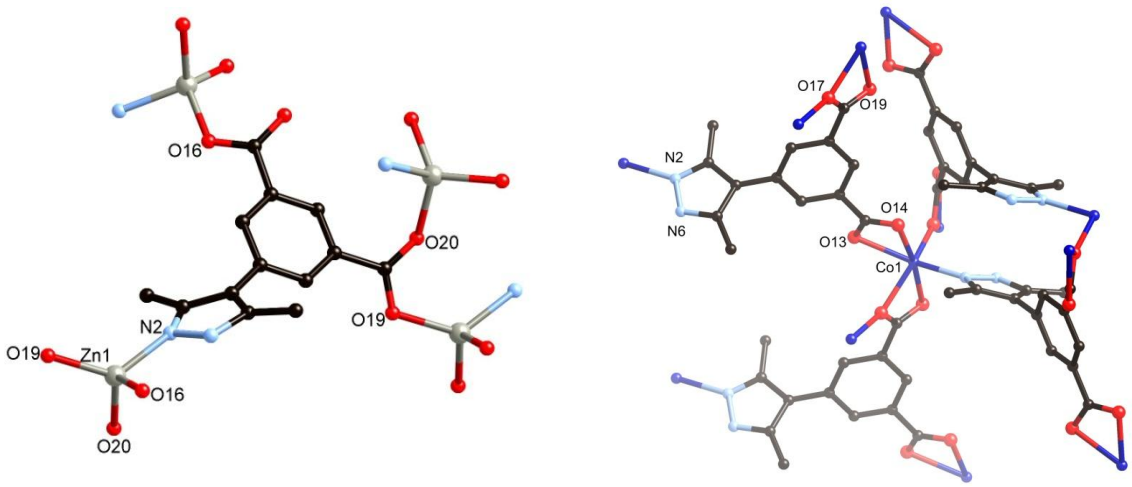

*Figure 7.2: (Left) Structure of poly-[Zn(**L7.1**)] with unique heteroatom labelling scheme. Hydrogen atoms omitted for clarity. (Right) Structure of poly-[Co(**L7.1**)] with unique heteroatom labelling scheme. Hydrogen atoms omitted for clarity.*

7.2.2 Application of the Jacobson Indazole Synthesis to Other Fused Heterocycles

The modified Jacobson synthesis proved an efficient method for the synthesis of ligands **H_2L5.4** – **H_2L5.7**, proving tolerant to both electronic and steric changes within the substrate. This synthetic method, requiring only an unsubstituted aromatic amine located *ortho* to a methyl group, was employed in the synthesis of several other fused ring systems. Using 3-methyl-4-amino-*1H*-pyrazole (prepared by the nitration and reduction of 3-methyl-*1H*-pyrazole **6.10**) as a starting material provided the fused system N,N′-diacetyl-pyrazolo-(4,5)[d]-pyrazole **7.2**, while the same reaction starting with 3,5-dimethyl-4-amino-*1H*-pyrazole provided a methyl substituted version **7.3**. Unfortunately, neither compound could be isolated as the neutral deprotected compound, and were only reliably handled as either the N,N′-diacetyl compounds or as the hydrobromide salts. As such, no structurally

characterised metal complexes could be isolated from either compound; however, it is expected that if the difficulties in deprotection can be addressed, compounds **7.2** and **7.3** could represent a new class of compact, rigid bis-pyrazole ligands for use in coordination polymer synthesis. The structures of **7.2** and **7.3**·HBr are shown in Figure 7.3.

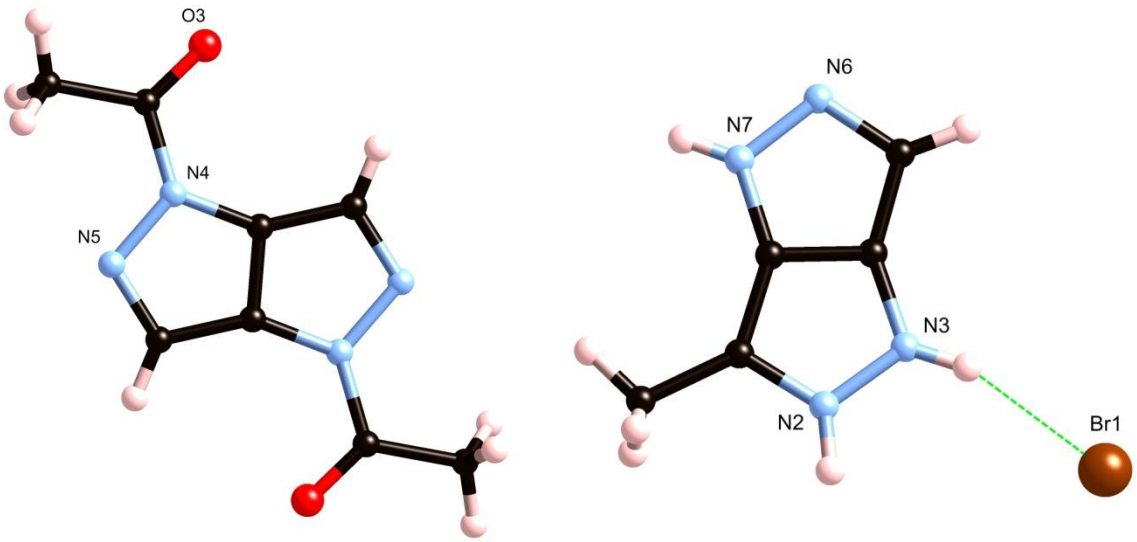

*Figure 7.3: (Left) Structure of **7.2** with unique heteroatom labelling scheme. (Right) Structure of **7.3**·HBr with heteroatom labelling scheme.*

An equivalent method was also applied to 7-methyl-8-aminoquinoline, prepared by nitration and reduction of 7-methylquinoline, to generate the chelating ligand *1H*-pyrazolo-(3,4)[h]-quinoline **HL7.4**, which can be considered a diazole analogue to common chelating ligand 1,10-phenanthroline, in which one of the pyridine rings is replaced with a pyrazole ring fused at the 3,4-position. Several discrete complexes were prepared containing **HL7.4**, including an $[M_4L_6]^{2+}$ complex with Cu(II), which was notably similar to an equivalent complex reported by Ward with related bicyclic ligand 3-(2-pyridyl)-*1H*-pyrazole.[440] Despite the presence of a second nitrogen atom on the five membered ring lending the possibility of a polymeric coordination mode, no polymeric complexes have been prepared to date incorporating **HL7.4**, while studies into the potentially interesting photochemical properties of metal complexes of **HL7.4** are expected to be carried out in the future through a collaboration with Prof. Luisa De Cola. The structure of **HL7.4**·HNO_3, and a representative structure of a $[Cu_4(\mathbf{L7.4})_6]^{2+}$ complex are shown in Figure 7.4.

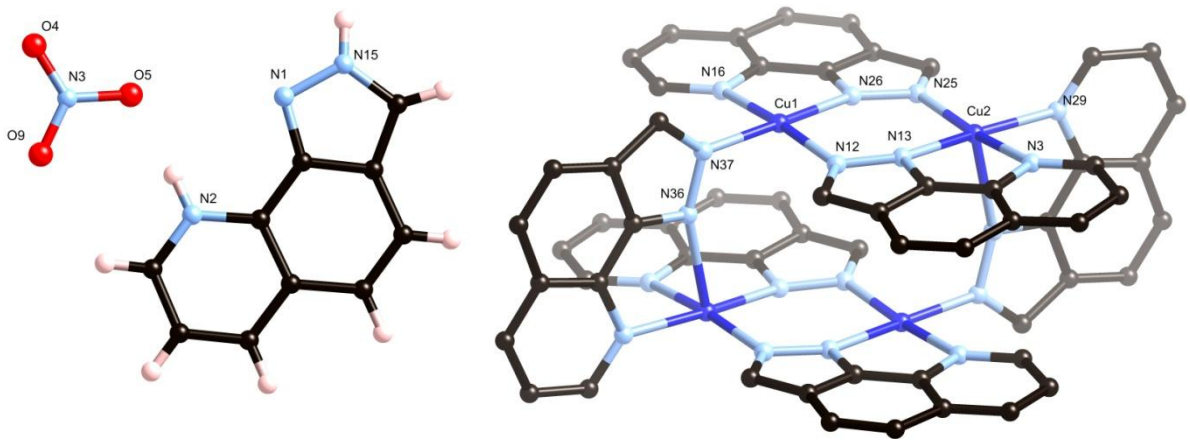

*Figure 7.4: (Left) Structure of **L7.4**·HNO_3 with heteroatom labelling scheme; (Right) Representative structure of $[Cu_4(\mathbf{L7.4})_6]^{2+}$ with unique heteroatom labelling scheme. Hydrogen atoms, coordinating and non-coordinating anions and solvent molecules omitted for clarity.*

7.2.3 Indazoles as Ligands in Metallosupramolecular Assemblies

In addition to the pyridine and carboxylic acid substitution appended to the indazole skeleton in Chapter 5, a number of other substitution modes were envisaged. Flexible bis-indazole compound 5,5'-methylenebis(7-methyl-*1H*-indazole) **7.5,** shown in Figure 7.5, was prepared in 3 steps from 2,6-dimethylaniline, and was expected to act as an indazole analogue to bis-pyrazole ligand **L2.1**; however, the combination of low solubility and poor hydrolytic stability under solvothermal conditions hampered efforts to generate metal complexes containing compound **7.5** as a ligand. Nonetheless, it is expected that flexible bis-indazole ligands such as **7.5** could act as useful supramolecular tectons, especially given the possibilities for functionalisation of the aromatic backbone, or, if a suitable synthetic methodology were developed, more synthetically versatile analogues to flexible pyridylpyrazole ligands **L3.1** and **L3.2**. The synthesis of indazole-dicarboxylic acid ligands was also briefly investigated, with *1H*-indazole-3,6-dicarboxylic acid expected to display potentially interesting coordination modes and conceivably being available from 4-(carboxymethyl)-phenylhydrazine, although somewhat unsurprisingly, the intramolecular Friedel-Crafts cyclisation was found to proceed poorly in the presence of electron withdrawing substituents. Nonetheless, with the use of modified synthetic methods it is expected that indazoles containing additional coordinating groups represent a novel route to new coordination polymers of high connectivity which may be unavailable from more traditional ligand sets.

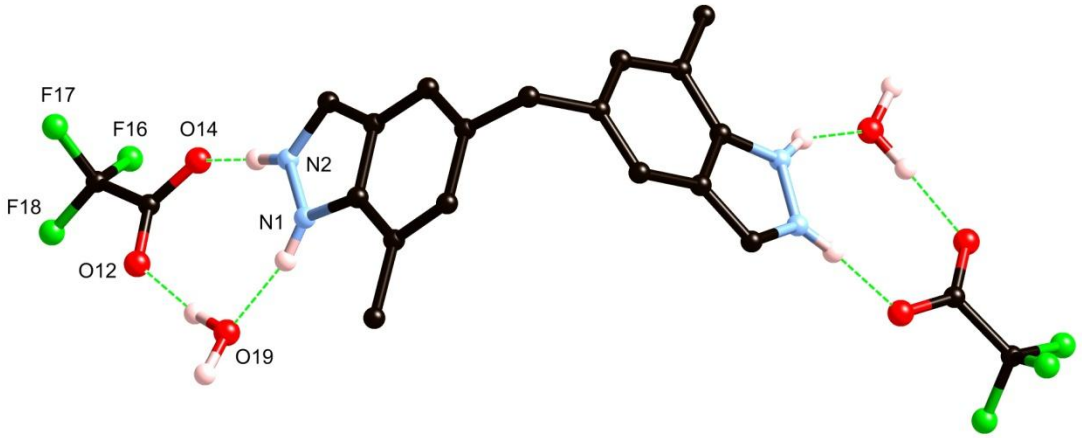

Figure 7.5: Structure of **7.5**·*2(CF_3CO_2)*·*2(H_2O) with unique heteroatom labelling scheme. Hydrogen atoms not participating in hydrogen bonding omitted for clarity.*

Chapter 8

Experimental Data

8.1 Materials and Methods

General Information

Unless otherwise specified, all reagents and starting materials were reagent grade, purchased from standard suppliers and used as received. Water was purified by reverse osmosis *in-house*. Where anhydrous solvents were required, the HPLC-grade solvent was either distilled from standard drying agents or dried by passing over a sealed column of activated alumina. Melting points were recorded on an Electrothermal melting point apparatus and are uncorrected. Elemental analysis was carried out by Campbell Microanalytical Laboratory, University of Otago. Except where otherwise specified, all reactions were carried out in air.

Infrared Spectroscopy

All infrared spectra were recorded on a Perkin-Elmer Spectrum One FTIR instrument operating in diffuse reflectance mode with samples prepared as KBr mulls (KBr), or in transmittance mode with liquid samples pressed between KBr discs (neat). The following abbreviations are used: s: strong, m: medium, w: weak, sh: sharp, br: broad.

Thermogravimetric Analysis

Thermogravimetric analyses were carried out on an Alphatech SDT Q600 TGA/DSC apparatus. All samples were heated on alumina crucibles under nitrogen flow of 100 mL/min. Unless otherwise specified, all heating cycles consist of heating at 1 °C/min to 500 °C.

Solvothermal Syntheses

All solvothermal reactions were carried out within Parr Instruments Teflon lined stainless steel acid digestion bombs, models 4744 (23 mL capacity) and 4749 (45 mL capacity), which were heated using the specified parameters in two Carbolite PF60 programmable ovens with Eurotherm 3508 temperature controllers. Unless otherwise specified, initial heating rates for each cycle were 200 °C/hr. Prior to each use, the vessels were cleaned by heating 10 mL of 10% nitric acid solution to 180 °C, allowing to dwell at this temperature for 12 hours, and cooling to room temperature, following which the Teflon inserts were rinsed several times, refilled with water and subjected to the same heating cycle. Vessels cleaned by this method were not found to impart any detectable pH change to a further loading of water on heating.

Nuclear Magnetic Resonance

All spectra were recorded on a Varian INOVA 500 or Varian Unity 300 instrument, operating at 500 and 300 MHz, respectively, for ^{1}H, and 125 and 75 MHz, respectively, for ^{13}C. All samples were dissolved in commercially available deuterated solvents d_6-DSMO, $CDCl_3$, CD_3CN, CD_3OD or D_2O. Spectra were referenced to the residual solvent peaks and/or TMS. 1D-nOesy, COSY, HSQC and HMBC experiments were employed where required, using standard Varian pulse sequences. NMR titration experiments were carried out by dissolving the free ligand in 1 ml d_3-MeCN at the concentration specified, and recording ^{1}H spectra following each subsequent 10 µL addition of metal solution in the same solvent at room temperature.

UV/Visible Spectroscopy

UV/Visible spectra were recorded on a Varian CARY UV/Visible spectrometer in the range 200 – 800 nm for acetonitrile or 400-800 nm for nitromethane. Samples were measured in quartz curvettes of path length 1 cm and approximate capacity 3 ml. UV/Visible complexiметric titrations were carried out by dissolving the free ligand in 10 ml spectroscopic grade acetonitrile at the concentration specified, and recording spectra of the free ligand and following each addition of 10 µL of metal solution in the same solvent. All concentrations were chosen such that the total change in volume of the solvent did not exceed 5%.

Mass Spectrometry

Mass spectra were recorded by Dr Marie Squire and Dr Meike Holzenkaempfer on either a DIONEX Ultimate 3000 or Bruker MaXis 4G spectrometer, both of which were operated in high resolution positive ion electrospray mode. Samples were dissolved and diluted to the required concentration in HPLC grade acetonitrile or methanol.

Gas sorption

Sorption measurements were carried out by Keith White and Assoc. Prof. Brendan Abrahams at The University of Melbourne, Australia. A sample of **5.21** was baked at 150 °C under dynamic vacuum overnight. The dried sample on which the gas sorption studies were undertaken had a mass of 103.6 mg. Between isotherm measurements the sample was re-baked at 150 °C for 2 hours. Gas sorption data were measured using a Sieverts-type BELsorp-HP automatic gas sorption apparatus (BEL Japan Inc.). Ultra-high purity CH_4, CO_2, and He were used for the sorption studies.

Corrections were made for non-ideal gas behaviour at high pressures of each gas at each measurement and reference temperature. Source data were obtained from the NIST fluid properties website.[441]

Sample compartment temperatures between 258 K and 298 K were controlled by a Julabo F25-ME chiller/heater. A calibrated external Pt100 temperature probe monitored the flask temperature. Samples were kept at the measurement temperature for a minimum of 1 hr after the desired temperature had been achieved to allow thermal equilibrium to be attained before data measurement commenced.

Isosteric heats of sorption were calculated using least-squares fitting of a virial-type thermal adsorption equation that modelled lnP as a function of amount of surface excess of gas sorbed over all measurement temperatures.[442] Only data up to and including the maximum surface excess were modelled. The optimised virial coefficients and R^2 values are given in Table 8.1.

Table 8.1. Optimised virial coefficients for modelling excess CO_2 sorption on **5.21**.

Gas	**CO_2**
Temp /K	258, 273
a0	-1318.52
a1	-304.524
a2	186.9174
a3	-59.6777
a4	11.49733
a5	-0.87919
b	10.58333
R^2	0.9975281

X-Ray Crystallography

Refinement data and hydrogen bond parameters are presented in Appendix 1. X-ray crystallographic data collection and refinement was carried out with either a Bruker APEXII instrument, using graphite-monochromated Mo Kα (λ = 0.71073 Å) radiation, or an Oxford-Agilent SuperNova instrument with focused microsource Cu Kα (λ = 1.5418 Å) radiation and ATLAS CCD area detector. All structures were solved using direct methods with SHELXS[443] and refined on F^2 using all data by full matrix least-squares procedures with SHELXL-97[444] within OLEX-2.[445] Non-hydrogen atoms were refined with anisotropic displacement parameters. Hydrogen atoms were included in calculated positions, or were manually assigned from residual electron density where appropriate, with isotropic displacement parameters 1.2 times the isotropic equivalent of their carrier atoms. The functions minimized were $\Sigma w(F^2_o - F^2_c)$, with $w=[\sigma^2(F^2_o)+aP_2+bP]^{-1}$, where $P=[\max(F_o)^2+2F^2_c]/3$. Graphical representations of crystallographic data were prepared using the CrystalMaker, OLEX-2[445] and TOPOS[333] packages. Crystallographic data for all compounds is included in .cif format as electronic supplementary information. As discused in the text, where voids containing highly disordered solvent molecules were present, the SQUEEZE routine[246] was carried out; this technique was employed only when sensible explicit modelling of the electron density due to solvent molecules was not possible, and where a considerable benefit to the refinement was gained.

X-Ray Powder Diffraction

X-Ray Powder Diffraction data were collected using an Oxford-Agilent SuperNova instrument using Cu Kα (λ = 1.5418 Å) radiation and an ATLAS CCD area detector. Samples were prepared by grinding *ca.* 5 mg of analyte with a minimum quantity of Paratone-N oil and applying a sample of approximately 0.5 mm diameter to a thin glass fibre mounted on a goniometer head, which was mounted directly in the beam path. Diffraction data was recorded using four averaged 360° scans in Φ with 150 second exposure time per rotation frame. The diffraction data were integrated radially and a background correction manually applied, using a 6th order polynomial to approximate the absorbance due to the fibre and oil. The results of X-ray powder diffraction experiments are presented as electronic supporting information.

8.2 Ligand Synthesis

Chapter 2

The following compounds were prepared according to literature methods, and all characterisation data were found to be consistent with that provided; 3,5-diacetyl-heptane-2,6-dione **2.8**;[258] 4,4′-methylenebis-(3,5-dimethyl-*1H*-pyrazole) **L2.1**;[446] 1,1,2,2-tetraacetylethane **2.10**;[260] 3,3′,5,5′-tetramethyl-4,4′-bipyrazole **L2.3**;[447] 4,4′-oxybis-benzonitrile **2.11**;[448] 2,8-dicarboxyethyl-6H,12H-5,11-methanodibenzo[b,f][1,5]diazocine **2.12**;[263] ethyl *p*-iodobenzoate **2.13**;[269] ethyl *p*-toluate **2.16**;[449] ethyl α-bromo-*p*-toluate **2.17**.[450]

Synthesis of α,α′-*p*-xylylenebis(3,5-dimethyl-1H-pyrazol-4-yl) **L2.2**

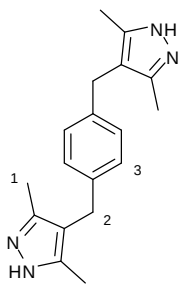

α,α′-dibromo-*p*-xylene (1.6 g; 6.1 mmol) was combined with anhydrous [Co(acac)$_2$] (1.55 g; 6.0 mmol) in 20 mL chloroform, and the mixture was stirred until homogeneous. The solution was then immersed in an oil bath at 120°C and the solvent allowed to evaporate with stirring, at which point a thick purple oil remained. The temperature was maintained for *ca.* 30 minutes, until the reaction mixture was dark green in colour. The mixture was cooled and partitioned several times between water and diethyl ether, and the organic layers combined, washed with dilute hydrochloric acid solution, dried and evaporated under reduced pressure to give 1.30 g of α,α′-*p*-xylylenebis-(2,4-pentanedion-3-yl) **2.9** as a thick yellow oil, which was used directly in the next step without purification.

Crude **2.9** (1.30 g; 3.9 mmol) prepared as above was dissolved in 40 mL methanol. To this solution was added, dropwise with stirring, hydrazine hydrate (0.52 mL; 10 mmol, 2.5 equiv.) in 10 mL methanol. The resulting solution was refluxed for 6 hours and cooled, at which point the product precipitated as a fine white powder. The solid was filtered and dried *in vacuo*. Yield 435 mg (1.5 mmol, 28%). m.p. 308-312 °C; δ_H(300 MHz, d_6-DMSO) 2.01 (s, 12H, H^1), 3.57 (s, 4H, H^2), 6.97 (s, 4H, H^3); δ_C (75 MHz, d_6-DMSO) 11.32, 28.70, 114.14, 128.55, 139.27, 141-142 (broad); *m/z* (ESMS) 317.1732 ([M+H$^+$], calculated for $C_{18}H_{23}N_4$ 317.1742); υ_{max}(KBr)/cm^{-1} 3181s, 2927s, 1903m, 1694m, 1586s, 1509s, 1466s, 1438m, 1300s, 1206s, 1141s, 1050s, 1001m, 838s, 739s.

Synthesis of 4,4′-oxybisbenzoic acid **H_2L2.4**

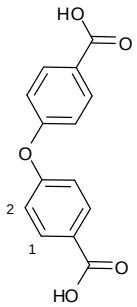

4-cyanophenol (4.72 g; 40 mmol), anhydrous potassium carbonate (14 g; 100 mmol) and 4-nitrobenzonitrile (5.92 g; 40 mmol) were added to a dried 100 mL flask equipped with a condenser and septum, and the apparatus was degassed with argon. 75 mL dry dimethylformamide was added, and the mixture as heated to 120 °C with stirring for 7 hours, following which the mixture was allowed to cool and was stirred under Ar at room temperature for 72 hours. The mixture was then poured onto 200 mL of water, giving a white precipitate, which was extracted with two 100 mL portons of dichloromethane and 100 mL diethyl ether. The organic phases were combined, washed with water, dried over $MgSO_4$ and evaporated to dryness to give a white solid, which was recrystallised from acetone to give 4,4′-oxybisbenzonitrile **2.11**, which was used directly. Yield 5.5 g (63 %)

Compound **2.11** (2.7 g; 11 mmol) prepared above was added to 150 mL of 50% ethanol/water and stirred. Freshly ground potassium hydroxide (37.5 g; 670 mmol) was added to the mixture, which was then refluxed for 48 hours. On completion of heating, the excess ethanol was evaporated under reduced pressure, and the mixture was acidified to pH 2.5 with 30% hydrochloric acid solution. The resulting white precipitate was filtered, slurried with acetone several times and evaporated, and the off-white powder obtained was dried *in vacuo* to give 2.4 g of the diacid. Yield 85%. m.p. >300 °C; δ_H(300 MHz, d_6-DMSO) 7.15 (d, 4H, J = 8.2 Hz, H^2), 7.99 (d, 4H, J = 8.3 Hz, H^1); δ_c(75 MHz, d_6-DMSO) 118.82, 126.54, 131.92, 159.59, 166.76; *m/z* (ESMS) 334.9713 ([M-H^++2K^+], calculated for $C_{14}H_9O_5K_2$ 334.9724); υ_{max}(KBr)/cm^{-1} 2998m br, 1685s, 1597s, 1505s, 1427s, 1254m, 1161m, 941m br, 883m, 690w, 653m, 622m.

Synthesis of 2,8-dicarboxy-6H,12H-5,11-methano-dibenzo[b,f][1,5]diazocine **L2.5**

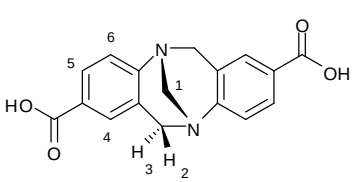

2,8-bis(ethoxycarbonyl)-6H,12H-5,11-methanodibenzo[b,f]-[1,5] diazocine (1.0 g; 2.7 mmol) was suspended in 150 mL THF with stirring. To this mixture was added an aqueous solution of LiOH (420 mg; 10 mmol) in 50mL H_2O and the mixture refluxed for 8 hours, cooled and stirred overnight. The resultant pale yellow solution was filtered and concentrated under vacuum. To the remaining aqueous residue was added 150 mL water, and the solution was filtered and acidified to pH 2.5 with aqueous HCl. The resulting white suspension was stirred for 30 mins and filtered to give a white solid, which was dried *in vacuo* to give an off-

white powder. Yield 850 mg (2.7 mmol, 100%). Crystals suitable for a single crystal X-ray diffraction study were obtained by recrystallisation from acetonitrile in a Parr Instruments acid digestion bomb. These crystals were found to rapidly lose solvent on drying. m.p. >300 °C; (Found: C, 65.1; H, 4.4; N, 11.3%. $C_{17}H_{14}N_2O_4 \cdot 0.8MeCN$ requires C, 65.1; H, 4.8; N, 11.3%); δ_H (500 MHz, d_6-DMSO) 4.26-4.28 (4H, m, H^1+H^3), 4.70 (2H, d, J = 16.9 Hz, H^2), 7.20 (2H, d, J = 8.3 Hz, H^6), 7.57 (2H, s, H^4), 7.69 (2H, d, J = 8.3 Hz, H^5); δ_C (126 MHz, d_6-DMSO) 58.13, 65.88, 124.91, 125.75, 128.13, 128.25, 128.68, 152.49, 167.03; *m/z* (ESMS) 311.1046. ([M+H^+], calculated for $C_{17}H_{15}N_2O_4^+$ 311.1032); υ_{max}(KBr)/cm^{-1} 2903m br, 1685s sh, 1610m, 1569w, 1426m, 1297s, 1210m, 956m, 850w, 771w.

Synthesis of ethyl 4-(2,4-pentanedion-3-yl)-benzoate **2.14**

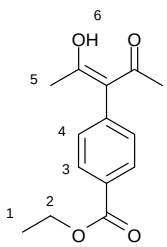

In a 100 mL round bottomed flask equipped with a magnetic stirrer and septum, L-proline (380 mg; 3.3 mmol, 20 mol %), recrystallised cuprous iodide (310 mg; 1.6 mmol, 10 mol %) and anhydrous potassium carbonate (9 g; 65 mmol) were added and flushed with N_2. In a separate flask, freshly distilled 2,4-pentanedione (5.0 mL; 49 mmol), ethyl 4-iodobenzoate (4.52 g, 16 mmol) and 25 mL of anhydrous dimethyl sulfoxide were combined and flushed with a stream of N_2 before being added via syringe to the solid mixture, which was heated to 90 °C with vigorous stirring under N_2 for 8 hours. On completion, the mixture was poured onto 250 mL of 10% HCl solution and extracted with ethyl acetate, which was washed, dried and evaporated under reduced pressure to give a dark brown residue. The crude material was purified by flash chromatography (silica gel, 5:1 CH_2Cl_2/hexanes) to yield the product as pale yellow crystals. Yield 1.7 g (44%). m.p. 55-58 °C; δ_H (300 MHz, $CDCl_3$) 1.33 (t, 3H, J = 7.3 Hz, H^1), 1.86 (s, 6H, H^5), 4.33 (q, 2H, J = 7.3 Hz, H^2), 7.44 (d, 2H, J = 8.1 Hz, H^4), 7.98 (d, 2H, J = 8.1 Hz, H^3), 16.87 (s, 1H, H^6); δ_C (125 MHz, $CDCl_3$) 14.21, 23.99, 60.84, 114.28, 129.06, 129.51, 131.59, 141.50, 165.56, 190.62; *m/z* (ESMS) 249.1121 ([M+H^+], calculated for $C_{14}H_{17}O_4$ 249.1127); υ_{max}(KBr)cm^{-1} 2983m sh, 1712s, 1607m br, 1284s, 1176m, 1110s, 1024m, 916m.

Synthesis of ethyl 4-(3,5-dimethyl-1H-pyrazol-4-yl)-benzoate **2.15**

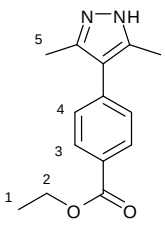

To a solution of **2.14** (1.30 g; 5.2 mmol) in 40 mL methanol was added dropwise a solution of hydrazine hydrate (310 µL; 6.4 mmol, 1.2 equiv.) in 5 mL methanol. The resulting solution was refluxed for 8 hours, followed by cooling to room temperature and stirring overnight. On completion, the solution was evaporated to dryness to give the product as a pale yellow solid. Yield 1.04 g (81 %). m.p. 79-84 °C; δ_H(500 MHz, $CDCl_3$) 1.32 (t, 3H, *J* = 7.1 Hz, H^1), 2.29 (s, 6H, H^5), 4.31 (q, 2H, *J* = 7.1 Hz, H^2), 7.34 (d, 2H, *J* = 8.3 Hz, H^4), 8.08 (d, 2H, *J* = 8.3 Hz, H^3); δ_c(125 MHz, $CDCl_3$) 11.96, 14.76, 61.36, 118.19, 128.72, 129.35, 130.16, 142.41, 166.94; *m/z* (ESMS) 267.1103 ([M+Na^+], calculated for $C_{14}H_{16}N_2O_2Na$ 267.1104); υ_{max}(KBr)cm^{-1} 2980br, 1711s, 1609m, 1273s, 1180s sh, 1104m, 1007m, 865m, 712m.

Synthesis of 4-(3,5-dimethyl-1H-pyrazol-4-yl)-benzoic acid **HL2.6**

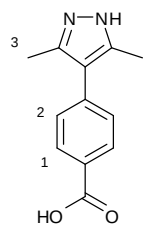

Compound **2.15** (800 mg; 3.3 mmol) was dissolved in 40 mL tetrahydrofuran and stirred. To this solution was added a solution of lithium hydroxide (4.0 g; 170 mmol) in 20 mL water, and the resulting slurry was refluxed for 72 hours. Upon completion, the mixture was reduced to approximately 1/3 volume under reduced pressure, 100 mL water was added and the solution was filtered. The filtrate was taken to pH 3.0 with dilute hydrochloric acid, and the resulting white precipitate was filtered and dried in air at 70 °C. Yield 550 mg (78%). m.p. 278-281 °C (decomp); δ_H(300 MHz, d_6-DMSO) 2.22 (s, 6H, H^3), 7.40 (d, 2H, *J* = 8.1 Hz, H^2), 7.95 (d, 2H, *J* = 8.1 Hz, H^1); δ_C(125 MHz, d_6-DMSO) 12.29, 116.72, 128.43, 129.12, 130.19, 139.56, 167.94; *m/z* (ESMS) 217.0974 ([M+H^+], calculated for $C_{12}H_{13}N_2O_2$ 217.0977); υ_{max}(KBr)cm^{-1} 3284s sh, 2467w br, 1942w br, 1680s, 1609s, 1528m, 1266s, 1177m, 1010s, 865m, 804m. Single crystals of **HL2.6** were prepared as the nitrate salt or as the free base by hydrothermal recrystallisation.

Synthesis of Ethyl-α-(2,4-pentanedion-3-yl)-toluate **2.18**

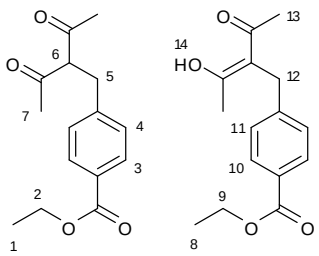

Ethyl-α-bromotoluate (4.86 g; 20 mmol) was combined with anhydrous [$Co(acac)_2$] (2.4 g; 10 mmol) in 25 mL chloroform, and the mixture stirred until homogeneous. The solution was immersed in an oil bath at 120 °C and the chloroform allowed to evaporate with stirring. The remaining mixture was allowed to stir while maintaining the temperature until a dark green colour was observed (*ca.* 30 minutes), at which time the mixture was cooled and exhaustively extracted with a water/diethyl ether mixture. The organic layers were combined, washed with dilute hydrochloric acid solution, dried and evaporated to dryness to give a dark brown oil. The oil was purified by flash chromatography (5:1 DCM/hexanes) to give a yellow liquid which was found by comparing the relative peak integrals in the ^{1}H NMR spectra to comprise both the diketo and keto-enol tautomers in approximately an 8:7 ratio. Yield 2.45 g (47 %) δ_H(500 MHz, $CDCl_3$) 1.35-1.39 (overlapping triplets, 6H, $J^1 = J^2 = 7.1$ Hz, $H^1 + H^8$), 2.03 (s, 6H, H^{13}), 2.12 (s, 6H, H^7), 3.17 (d, 2H, $J = 7.7$ Hz, H^5), 3.69 (s, 2H, H^{12}), 4.03 (t, 1H, $J = 7.7$ Hz, H^6), 4.32-4.38 (overlapping quartets, 4H, $J^1 = J^2 = 7.1$ Hz, $H^2 + H^9$), 7.20-7.22 (overlapping doublets, 4H, $J^1 = J^2 = 8.3$ Hz, $H^4 + H^{11}$), 7.95 (overlapping doublets, 4H, $J^1 = J^2 = 8.3$ Hz, $H^3 + H^{10}$), 16.83 (s, 1H, H^{14}); δ_C(500 MHz, $CDCl_3$) 14.53, 23.47, 29.99, 33.22, 34.20, 61.08, 61.12, 69.55, 107.94, 127.63, 128.92, 129.00, 129.29, 130.15, 130.18, 143.65, 145.35, 166.45, 166.55, 192.15, 203.22; *m/z* (ESMS) 263.1292 ([$M+H^+$], calculated for $C_{15}H_{19}O_4$ 263.1283); υ_{max}(neat)cm^{-1} 2982m sh, 1718s, 1610m, 1278m, 1106s, 1021s, 943m, 736s.

Synthesis of Ethyl-α-(3,5-dimethyl-1H-pyrazol-4-yl)-toluate **2.19**

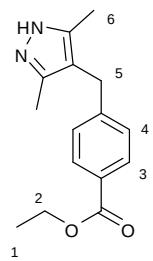

Compound **2.18** (1.80 g; 6.9 mmol) was dissolved in 40 mL methanol with stirring. To this mixture was added dropwise a solution of hydrazine hydrate (450 µL, 9 mmol) in 5 mL methanol. The resulting solution was refluxed for 24 hours, before cooling and evaporating under reduced pressure, to give the title compound as a pale yellow solid. Yield 1.43 g (80%). m.p. 104-109 °C; δ_H(500 MHz, $CDCl_3$) 1.36 (t, 3H, $J = 7.1$ Hz, H^1), 2.13 (s, 6H, H^6), 3.77 (s, 2H, H^5), 4.34 (q, 2H, $J = 7.1$ Hz, H^2), 7.15 (d, 2H, $J = 8.3$ Hz, H^4), 7.92 (d, 2H, $J = 8.3$ Hz, H^3); δ_C(500 MHz, $CDCl_3$) 11.03, 14.50, 29.19, 61.04, 113.55, 128.24, 128.45, 129.89, 142.71, 146.27, 166.82; *m/z* (ESMS) 259.1443 ([$M+H^+$], calculated for

$C_{15}H_{19}N_2O_2$ 259.1447); υ_{max}(KBr)cm^{-1} 2986s, 1930m, 1720s, 1611m, 1414m, 1277s, 1177s, 1105s, 1023m, 854m, 736s

Synthesis of α-(3,5-dimethyl-1H-pyrazol-4-yl)-toluic acid **HL2.7**

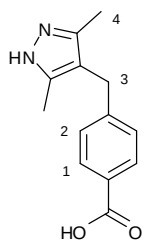

Compound **2.19** (1.0 g; 3.8 mmol) was dissolved in 40 mL tetrahydrofuran with stirring. To this mixture was added a solution of lithium hydroxide (5 g; 210 mmol) dissolved in 20 mL water. The resulting suspension was refluxed for 24 hours, cooled and concentrated under reduced pressure. The residue was added to 100 mL water and filtered, and the filtrate acidified to pH 3.0 with dilute hydrochloric acid solution, at which point the product precipitated as a white solid, which was filtered and dried in air at 70 °C. Yield 670 mg (76 %). m.p. 242-244 °C; δ_H(500 MHz, d_6-DMSO) 2.04 (s, 6H, H^4), 3.72 (s, 2H, H^3), 7.21 (d, 2H, *J* = 8.3 Hz, H^2), 7.84 (d, 2H, *J* = 8.3 Hz, H^1); δ_C(125 MHz, d_6-DMSO) 10.64, 28.48, 112.61, 128.17, 128.27, 129.42, 140.99, 146.80, 167.27; *m/z* (ESMS) 307.0260 ([M – H^+ + $2K^+$], calculated for $C_{13}H_{13}N_2O_2K_2$ 307.0251); υ_{max}(KBr)cm^{-1} 3287s, 1682s, 1313m, 1291s, 743s, 515s.

Chapter 3

The following compounds were prepared according to literature methods, and all characterisation data were consistent with that reported;1,1′-methylenebis-pyrazole **3.3**;[451] 4,4′-methylenebis-*1H*-pyrazole **3.4**.[331]

Synthesis of 4,4′-methylenebis(1-(2-pyridyl)pyrazole) **L3.1**

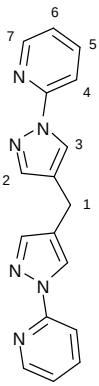

To sodium hydride (650 mg; 13.6 mmol, 50% suspension in mineral oil) in 10 mL anhydrous dimethylformamide was added **3.4** (1 g; 6.8 mmol) under nitrogen atmosphere at 0 °C. The resulting slurry was stirred for 1 hour, at which time 2-bromopyridine (2.9 g, 17 mmol, 1.8 mL) was added dropwise. The mixture was heated to 110 °C and stirred for 48 hours. On completion, 100 mL of saturated potassium carbonate solution was added and the mixture extracted with several portions of dichloromethane. The organic residues were dried and evaporated, and the residue taken up in 6 M HCl solution, washed with hexane, neutralised and extracted into dichloromethane, which was dried and evaporated to give a small volume of residual

dimethylformamide containing the product. The residue was recrystallised from ethanol/water to give the product as a white polycrystalline material. Yield 510 mg (23%). m.p. 81-83 °C; δ_H(500 MHz, $CDCl_3$) 3.82 (s, 2H, H^1), 7.13 (ddd, 2H, J^1 = 7.3 Hz, J^2 = 5.0 Hz, J^3 = 0.9 Hz, H^6), 7.62 (s, 2H, H^3), 7.78 (ddd, 2H, J^1 = 8.3 Hz, J^2 = 7.3 Hz, J^3 = 1.8 Hz, H^5), 7.93 (d, 2H, J = 8.3 Hz, H^4), 8.36 (dd, 2H, J^1 = 5.0 Hz, J^2 = 1.0 Hz, H^7), 8.38 (s, 2H, H^2); δ_C (125 MHz, $CDCl_3$) 19.85, 112.36, 121.41, 122.72, 125.73, 138.88, 142.27, 148.20, 151.53; *m/z* (ESMS) 325.1175 ([M+Na^+], calculated for $C_{17}H_{14}N_6Na$ 325.1172); υ_{max}(KBr)/cm^{-1} 3069w, 1596s, 1577s, 1472s, 1454s, 1392s, 1286m, 1250m, 1139m, 1057m, 955s, 779s, 648m, 606m.

Synthesis of 4,4′-methylenebis(1-(2-pyridyl)-3,5-dimethylpyrazole) **L3.2**

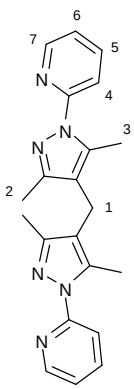

To **2.8** (720 mg; 3.4 mmol) in 20 mL methanol was added 2-hydrazinopyridine (1.0 g; 8.5 mmol), and the mixture was refluxed for 24 hours. On completion, the dark red solution was evaporated to dryness to give a deep red paste. The paste was recrystallised from a methanol/water mixture to give an off-white solid, which was filtered and dried to give 780 mg of the product. Yield 64%. m.p. 126-128 °C δ_H(500 MHz, $CDCl_3$) 2.15 (s, 6H, H^2), 2.56 (s, 6H, H^3), 3.55 (s, 2H, H^1), 7.12 (ddd, 2H, J^1 = 7.0 Hz, J^2 = 5.0 Hz, J^3 = 1.3 Hz, H^6), 7.75-7.80 (m, 4H, H^4 + H^5), 8.40 (ddd, 2H, J^1 = 4.0 Hz, J^2 = 1.8 Hz, J^3 = 0.7 Hz, H^7); δ_C (125 MHz, $CDCl_3$) 12.77, 12.84, 18.25, 116.41, 117.37, 120.91, 138.09, 138.42, 147.72, 149.48, 153.89; *m/z* (ESMS) 381.1802 ([M+Na^+], calculated for $C_{21}H_{22}N_6Na$ 381.1798); υ_{max}(KBr)/cm^{-1} 3071w, 2925m, 1580s, 1443s, 1377m, 1361s, 1064m, 896m, 778s.

Chapter 4

The following compounds were prepared according to literature procedures, and all characterisation data were consistent with that reported: 2-hydrazino-*1H*-benzimidazole **4.8**;[368] 2-bromo-*1H*-benzimidazole **4.9**;[372] 1-methyl-2-bromobenzimidazole **4.10**.[372]

Synthesis of 2-(pyrazol-1-yl)-*1H*-benzimidazole **L4.1**

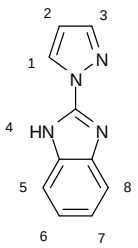

To a solution of 2-hydrazinobenzimidazole (750 mg; 5 mmol) in a mixture of 10 mL water and 0.75 mL HCl was added 1,1,3,3-tetramethoxypropane (820 µL; 5 mmol) dropwise. The resulting mixture was heated to reflux for 2 hours, allowed to cool and filtered. The filtrate was neutralised with solid potassium carbonate, causing the product to precipitate as a pale tan solid, which was filtered and dried *in vacuo*. Yield 650 mg (71%). m.p. 233-235 °C; δ_H(500 MHz, d_6-DMSO) 6.66 (s, 1H, H^2), 7.19-7.21 (m, 2H, H^6 + H^7), 7.46 (d, 1H, *J* = 6.1 Hz, H^5), 7.58 (d, 1H, *J* = 7.7 Hz, H^8), 7.94 (s, 1H, H^3), 8.59 (s, 1H, H^1), 13.10 (s, br, 1H, H^4); δ_C(125 MHz, d_6-DMSO) 109.16, 111.65, 118.38, 122.16, 122.49, 129.06, 133.66, 141.72, 142.98, 146.12; *m/z* (ESMS) 185.0821 ([M+H^+], calculated for $C_{10}H_9N_4$ 185.0822); υ_{max}(KBr)/cm^{-1} 2943m br, 1628m, 1574s, 1479m, 1460s, 1387m, 1324m, 1273m, 1226m, 1076s, 927s, 740s.

Synthesis of 2-(3,5-dimethyl-pyrazol-1-yl)-benzimidazole **L4.2**

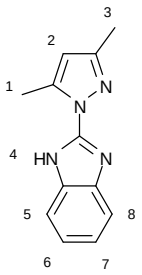

To a solution of 2-hydrazinobenzimidazole (420 mg; 3.1 mmol) in 10 mL ethanol was added acetylacetone (320 µL; 3.2 mmol) in a dropwise fashion. The resulting mixture was refluxed overnight, and the solvent was removed under vacuum to give a brown residue. This material was recrystallised from a methanol/water mixture to give the product as a pale brown solid. Yield 320 mg (49%). m.p. 124-126 °C; δ_H (500 MHz, $CDCl_3$) 2.31 (s, 1H, H^3), 2.82 (s, 1H, H^1), 6.05 (s, 1H, H^2), 7.22-7.27 (m, 2H, H^7 + H^6), 7.37 (d, 1H, *J* = 7.3 Hz, H^5), 7.71 (d, 1H, *J* = 7.6 Hz, H^8), 10.07 (s, 1H, H^4); δ_C(75 MHz, $CDCl_3$) 13.70, 13.97, 109.59, 110.56, 119.30, 122.45, 122.84, 132.25, 142.70, 142.97, 146.96, 151.6; *m/z* (ESMS) 235.0956 ([M+Na^+], calculated for $C_{12}H_{12}N_4Na$ 235.0954); υ_{max}(KBr)/cm^{-1} 2927m br, 1626m, 1555s, 1459s, 1339m, 1297w, 1273s, 1246m, 1097m, 800w, 738s.

Synthesis of 1-methyl-2-(1-pyrazolyl)-benzimidazole **L4.3**

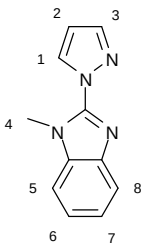

To a stirred solution of **L4.1** (580 mg; 3.2 mmol) in 10 mL of 1M NaOH solution was added dimethyl sulfate (400 µL; 4.2 mmol, 1.3 equiv.). The resulting mixture was stirred at room temperature for 2 hours. On completion, the solution was extracted with dichloromethane, and the organic residues combined, dried over $MgSO_4$ and evaporated to dryness to give the product **L4.3** as an off-white solid. Yield 380 mg (60%). m.p. 81-83 °C; δ_H(500 MHz, $CDCl_3$) 4.09 (s, 3H, H^4), 6.51 (d, 1H, *J* = 2.3 Hz, H^2), 7.30-7.38 (m, 3H, H^5-H^7), 7.71 (d, 1H, *J* = 8.7 Hz, H^8), 7.81 (s, 1H, H^3), 8.39 (d, 1H, *J* = 2.4 Hz, H^1); δ_C(125 MHz, $CDCl_3$) 32.35, 108.04, 109.81, 119.57, 123.11, 131.42, 136.02, 140.76, 142.90; *m/z* (ESMS) 199.0978 ([M+H^+], $C_{11}H_{11}N_4$ requires 199.0978); υ_{max}(KBr)/cm^{-1} 3117s, 2948m, 1617m, 1548s, 1493s, 1459s, 1375m, 1287s, 1219m, 1205m, 1114s, 1052s, 939s, 760s, 731s.

Synthesis of α,α′-bis (2-(1-pyrazolyl)-benzimidazol-1-yl)-*p*-xylene **L4.4**

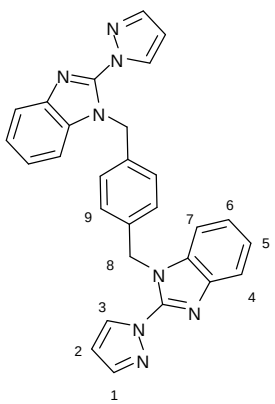

L4.1 (1 g; 5.2 mmol) was combined with potassium carbonate (1.6 g; 12mmol) and potassium iodide (60 mg; 0.4mmol) in a two-necked flask and degassed with N_2. To the solid mixture was added 40 mL of dry acetone, and the resulting slurry was stirred for 30 minutes at room temperature. α,α′-dichloro-*p*-xylene (470 mg; 2.6 mmol) was added, and the mixture was heated to reflux for 24 hours under a positive pressure of nitrogen. On completion, the mixture was filtered, and the solids were washed several times with acetone. The acetone washings were combined and evaporated to dryness to give an off-white solid, which was slurried in ethanol, filtered, and washed with several portions of cold ethanol. Yield 430 mg (35%). m.p. 200-202 °C; δ_H (500 MHz, d_6-DMSO) 5.80 (s, 4H, H^8), 6.62 (t, 2H, J^1 = 2.6 Hz, J^2 = 1.0 Hz, H^2), 7.03 (s, 4H, H^8), 7.24 (m, 4H, H^5 + H^6), 7.50 (d, 2H, *J* = 6.5 Hz, H^7), 7.64 (d, 2H, H^4, *J* = 7.3 Hz), 7.91 (d, 2H, *J* = 1.0 Hz, H^1), 8.50 (d, 2H, *J* = 2.1 Hz, H^3); δ_C (125 MHz, $CDCl_3$) 48.40, 108.16, 110.59, 119.69, 123.30, 123.33, 127.60, 131.55, 135.39, 136.13, 140.88, 143.04, 145.49; *m/z* (ESMS) 493.1866 ([M+Na^+], calculated for $C_{28}N_{22}N_8Na$ 493.1860); υ_{max}(KBr)/cm^{-1} 3099m, 2945m, 1713m, 1542s, 1516s, 1485s, 1460s, 1404m, 1374m, 1294m, 1166m, 1043s, 935s, 742s.

Synthesis of α,α′-bis (2-(1-pyrazolyl)-benzimidazol-1-yl)-4,4′-dimethylbiphenylene **L4.5**

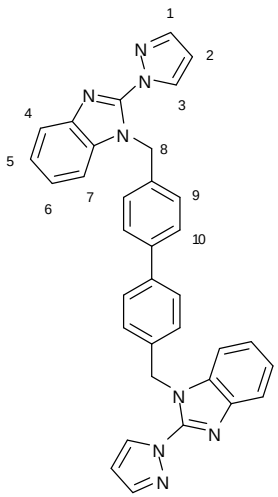

L4.1 (1.3 g; 7.1 mmol) was combined with anhydrous potassium carbonate (2.1 g; 16 mmol) and potassium iodide (80 mg; 0.5 mmol) in 50 mL of dry acetone under a nitrogen atmosphere. To this mixture was added α,α′-dichloro-4,4′-dimethylbiphenylene (850 mg; 3.4 mmol), and the mixture was heated to reflux overnight, during which time a fine powder precipitated. On completion, the mixture was cooled and filtered, and the solids were exhaustively extracted into hot chloroform, which was filtered and evaporated to dryness. The solids obtained were filtered and washed with methanol. Yield 650 mg (35 %). m.p. 254-257 °C; δ_H (500 MHz, $CDCl_3$) 5.91 (s, 4H, H^8), 6.49 (dd, 2H, H^2, J^1 = 1.8 Hz, J^2 = 2.4 Hz), 7.20 (d, 4H, H^{10}, J = 8.1 Hz), 7.23 – 7.32 (m, 6H, H^5 – H^7), 7.40 (d, 4H, H^9, J = 8.2 Hz), 7.74 (d, 2H, H^4, J = 8.0 Hz), 7.78 (d, 2H, H^1, J = 1.5 Hz), 8.38 (d, 2H, H^3, J = 2.5 Hz); δ_c (125 MHz, $CDCl_3$) 48.51, 108.19, 110.67, 119.72, 123.32, 123.37, 127.56, 127.60, 131.58, 135.49, 135.72, 140.19, 140.95, 143.08, 145.61; *m/z* (ESMS) 547.2346 ([M+H^+], $C_{34}H_{27}N_8$ requires 547.2353; υ_{max}(KBr)/cm^{-1} 3463w, 1617w, 1546s, 1489m, 1456m, 1425w, 1402w, 1285w, 1051w, 1007w, 932m, 763s, 737s.

Synthesis of α,α′-bis (2-(1-pyrazolyl)-benzimidazol-1-yl)-*m*-xylene **L4.6**

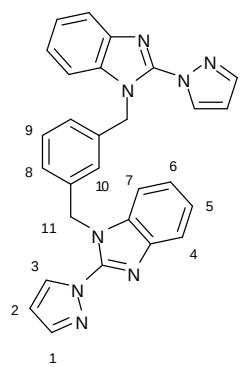

L4.1 (1.3 g; 7.1 mmol) was combined with anhydrous potassium carbonate (2.1 g; 16 mmol) and potassium iodide (80 mg; 0.5mmol) in 50 mL of dry acetone under a nitrogen atmosphere. To the stirred mixture was added α,α′-dibromo-*m*-xylene (890 mg; 3.4 mmol), and the resulting mixture was heated to reflux overnight. On completion, the mixture was cooled and filtered, and the solids washed several times with cold acetone. The filtrates were combined and evaporated to dryness, and the remaining solids were washed with methanol to afford **L4.6** as an off-white powder. Yield 1.1 g (69%). m.p. 197-201 °C; δ_H(500 MHz, $CDCl_3$) 5.76 (s, 4H, H^{11}), 6.41 (dd, 2H, J^1 = 1.7 Hz, J^2 = 0.9 Hz, H^2), 6.94 (s, 1H, H^{10}), 7.05 (d, 2H, J = 7.5 Hz, H^8), 7.13-7.21 (m, 5H, H^6, H^7, H^9), 7.30 (t, 2H, J = 7.1 Hz, H^5), 7.62 (d, 2H, J = 1.1 Hz, H^1), 7.73 (d, 2H, J = 7.9 Hz, H^4), 8.25 (d, 2H, J = 2.0 Hz, H^3); δ_C (125 MHz, $CDCl_3$) 48.48, 108.07, 110.47, 119.66, 123.24, 123.30, 125.94, 126.68, 129.33, 131.38, 135.33, 137.12, 140.85, 142.88, 145.41; *m/z* (ESMS) 493.1856 ([M+Na^+], $C_{28}H_{22}N_8Na$ requires 493.1860);

υ_{max}(KBr)/cm^{-1} 3132m, 3055m, 1884m, 1781m, 1710m, 1592s, 1544s, 1485s, 1363w, 1249m, 1177m, 1036s, 940s, 742s.

Synthesis of 4,4′-methylenebis(1-(1-methyl-2-benzimidazolyl)-pyrazole) **L4.7**

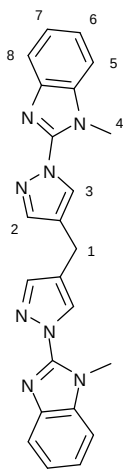

3.4 (300 mg; 2.1 mmol) was dissolved in 15 mL of dry N,N-dimethylformamide under a nitrogen atmosphere at 0 °C. To this solution was added sodium hydride (210 mg; 4.3 mmol) as a 50% dispersion in mineral oil, and the mixture was stirred for 1 hour. To the resulting mixture was added 1-methyl-2-bromobenzimidazole (900 mg; 4.3 mmol), and the mixture was heated to 110 °C under nitrogen and maintained at this temperature for 48 hours. On completion, the mixture was added to 100 mL of ice water, causing the product to precipitate as an off-white powder. This solid was collected by filtration and recrystallised from ethanol/water to give the product as a white solid. Yield 580 mg (70 %). m.p. 181 – 183 °C; δ_H(500 MHz, d_6-DMSO) 3.88 (s, 2H, H^1), 4.02 (s, 6H, H^4), 7.25-7.32 (m, 4H, H^6 + H^7), 7.61 (d, overlapping, 4H, J = 8.0 Hz, H^5 + H^8), 7.94 (s, 2H, H^2), 8.40 (s, 2H, H^3); δ_C (125 MHz, d_6-DMSO) 18.32, 31.99, 110.65, 118.72, 122.53, 122.64, 122.69, 129.99, 135.73, 140.13, 143.09, 145.42; *m/z* (ESMS) 409.1880 ([M+H$^+$], calculated for $C_{23}H_{21}N_8$ 409.1884); υ_{max}(KBr)/cm^{-1} 2923m, 1616w, 1592m, 1544s, 1497s, 1460m, 1402m, 1234m, 1007m, 960s, 744s.

Chapter 5

The following compounds were prepared according to literature procedures, and all characterisation data were consistent with that reported: *1H*-indazole **5.8**;[398] benzaldehyde phenylhydrazone **5.9**;[400] N-benzilidineamino isatin **5.11**;[400] 3-nitro-4-methyl benzoic acid **5.12**;[452]methyl 3-nitro-4-methyl benzoate **5.13**;[453] methyl 3-amino-4-methyl benzoate **5.14**.[453]

Synthesis of 1-(2-pyridyl)-indazole **L5.1** and 2-(2-pyridyl)-indazole **L5.2**

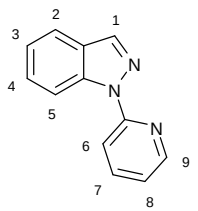

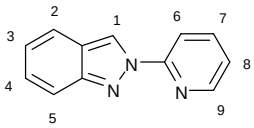

indazole (1 g; 8.5 mmol) was dissolved in 10 mL anhydrous dimethylformamide at 0 °C under nitrogen atmosphere. To the stirred mixture was added portionwise sodium hydride (490 mg; 10.2 mmol, 50% dispersion in oil), and the resulting mixture left to stir at 0 °C for 30 minutes. At this time, 2-bromopyridine (900 µL; 9.4 mmol) was added, and the mixture was heated to 110 °C and stirred under nitrogen for 48 hours. On completion, the mixture was poured onto 100 mL water, and extracted into dichloromethane. The organic layers were dried and evaporated to give a brown residue, which was taken up in 10 mL 50% aqueous HCl, and washed with several portions of petroleum ether, filtered, and neutralised with potassium carbonate. The resulting suspension was extracted with dichloromethane, and the organic phase was dried and evaporated to dryness to yield an orange oil, containing both **L5.1** and **L5.2**, as well as starting materials. The oil was subjected to flash chromatography, eluting with 50% ethyl acetate/petroleum ether on silica gel, and the fraction containing the two isomers of the product was evaporated to dryness and chromatographed with 50% toluene/petroleum ether on alumina to yield the two separate isomers of the product. Combined yield 450 mg (27 %).

1-(2-pyridyl)-indazole **L5.1:** Yield 230 mg (14 %). m.p. 71-74 °C; δ_H (500 MHz, $CDCl_3$) 7.16 (ddd, 1H, J^1 = 7.2 Hz, J^2 = 4.9 Hz, J^3 = 0.9 Hz, H^4), 7.29 (t, 1H, J = 7.9 Hz, H^7), 7.53 (ddd, 1H, J^1 = 8.3 Hz, J^2 = 7.2 Hz, J^3 = 1.1 Hz, H^8), 7.78 (d, 2H, J = 7.9 Hz, H^6), 7.84 (ddd, 1H, J^1 = 8.3 Hz, J^2 = 7.3 Hz, J^3 = 1.8 Hz, H^3), 8.06 (d, 1H, J = 8.4 Hz, H^2), 8.21 (s, 1H, H^1), 8.54 (d, 1H, J = 3.6 Hz, H^5), 8.86 (d, 1H, J = 8.6 Hz, H^9); δ_c (125 MHz, $CDCl_3$) 113.71, 115.51, 120.15, 120.96, 122.73, 126.22, 128.16, 137.01, 138.50, 139.07, 147.93, 154.55; *m/z* (ESMS) 196.0872 ([M+H^+], $C_{12}H_{10}N_3$ requires 196.0869); υ_{max}(KBr)/cm^{-1} 3550m, 3410m, 1616s, 1587s, 1500s, 1479s, 1451s, 1353m, 1199s, 1145m, 1078m, 1010s, 978s, 778s, 627s.

2-(2-pyridyl)-indazole **L5.2**: Yield 220 mg (13 %). m.p. 87-93 °C; δ_H (500 MHz, $CDCl_3$) 7.09 (t, 1H, J = 7.0 Hz, H^3), 7.28-7.33 (m, 2H, H^5+H^8), 7.71-7.75 (m, 2H, H^2+H^4), 7.89 (dt, 1H, J^1 = 7.9 Hz, J^2 = 1.8 Hz, H^7), 8.28 (d, 1H, J = 8.0 Hz, H^6), 8.50 (d, 1H, J = 3.9 Hz, H^9), 9.10 (s, 1H, H^1); δ_c (125 MHz, $CDCl_3$) 114.34, 118.28, 120.85, 121.46, 122.64, 122.94, 123.03, 127.84, 139.12, 148.58, 150.55, 152.12; *m/z* (ESMS) 196.0877 ([M+H^+], $C_{12}H_{10}N_3$ requires 196.0869); υ_{max}(KBr)/cm^{-1} 3058m, 1911m, 1790m, 1592s, 1517s, 1474s, 1434s, 1374m, 1350m, 1313m, 1199s, 1146s, 1056s, 956m, 907m, 758s.

Synthesis of *1H*-indazole 4-carboxylic Acid **H_2L5.4**

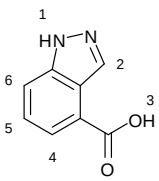

To 50 mL dry toluene under a nitrogen atmosphere was added methyl 2-methyl 3-aminobenzoate (1.4 g, 8.5 mmol) and potassium acetate (430 mg, 4.4 mmol), and the mixture was heated to reflux, at which time acetic anhydride (2.6 mL, 28 mmol) was added, and the mixture was stirred at reflux for 10 minutes. Isoamyl nitrite (1.7 mL, 13 mmol) was added over 30 minutes, and the mixture was refluxed overnight. On cooling, the mixture was filtered and evaporated to dryness, to give 1.4 g of an orange solid which analysed for methyl 1-acetyl-indazole-4-carboxylate. This solid was dissolved in 50 mL tetrahydrofuran, which was added to a solution of lithium hydroxide (7 g, 290 mmol) in 50 mL water, and the resulting mixture was refluxed for 48 hours. On cooling, the mixture was concentrated on a rotary evaporator, and the resulting aqueous phase was filtered and taken to pH 4 with dilute HCl. The product was then filtered, washed with water and dried *in vacuo*. Yield 950 mg (69 %). m.p. 272-275 °C; δ_H(500 MHz, d_6-DMSO) 7.46 (dd, 1H, J^1 = 8.0 Hz, J^2 = 7.2 Hz, H^5), 7.79 (d, 1H, J = 7.0 Hz, H^6), 7.82 (d, 1H, J = 8.0 Hz, H^4), 8.40 (s, 1H, H^2), 13.2 (br s, 2H, H^1+H^3); δ_c(125 MHz, d_6-DMSO) 115.46, 121.34, 123.09, 123.83, 125.59, 133.88, 140.62, 167.48; *m/z* (ESMS) 163.0503 ([M+H^+], calculated for $C_8H_7N_2O_2$ 163.0502; υ_{max}(KBr)/cm^{-1} 3254s br, 1679s, 1617m, 1444w, 1365w, 1302s, 1199s, 1089w, 951s, 753s

Synthesis of *1H*-indazole 5-carboxylic acid **H_2L5.5**

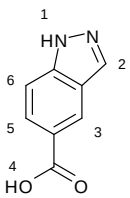

To 40 mL dry toluene under a nitrogen atmosphere was added methyl 3-methyl 4-aminobenzoate (1.3 g, 7.9 mmol) and potassium acetate (400 mg, 4.1 mmol), and the mixture was heated to reflux, at which time acetic anhydride (2.3 mL, 25 mmol) was added, and the mixture was stirred at temperature for 10 minutes. Isoamyl nitrite (1.7 mL, 13 mmol) was added over 30 minutes, and the mixture was refluxed overnight. On cooling, the mixture was filtered and evaporated to dryness, to give an orange solid, which was filtered and washed with petroleum ether, giving 1.44 g of methyl 1-acetyl-indazole-5-carboxylate. This material was taken up in 50 mL tetrahydrofuran and added to a solution of lithium hydroxide (7 g, 290 mmol) in 50 mL water, and the resulting mixture was refluxed for 48 hours. On cooling, the mixture was concentrated on a rotary evaporator to remove tetrahydrofuran, and the aqueous phase was filtered and taken to pH 4 with dilute hydrochloric acid, causing precipitation of the product, which was filtered, washed with water and dried *in vacuo*. Yield 600 mg (47%). m.p. 297-301 °C (decomp.); δ_H(500 MHz, d_6-DMSO) 7.60 (d, 1H, J = 8.8 Hz, H^6), 7.91 (dd, 1H, J^1 = 8.8 Hz, J^2 = 1.6 Hz, H^5), 8.24

(d, 1H, J = 0.8 Hz, H^2), 8.45 (dd, 1H, J^1 = 1.3 Hz, J^2 = 0.8 Hz, H^3), 13.2 (br s, 2H, H^4 + H^1); δ_c(125 MHz, d_6-DMSO) 110.22, 122.71, 123.17, 123.95, 126.73, 135.35, 141.78, 167.84; *m/z* (ESMS) 163.0504 ([M+H^+], calculated for $C_8H_7N_2O_2$ 163.0502); υ_{max}(KBr)/cm^{-1} 3297s br, 2504m br, 1686s, 1622m, 1469w, 1357m, 1319s, 1269s, 1203m, 1134m, 1080m, 948s, 768s.

Synthesis of methyl 1-acetyl-indazole-6-carboxylate **5.15**

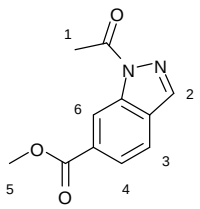

Methyl 3-amino-4-methylbenzoate **5.14** (1.5 g; 9.1 mmol) was added to potassium acetate (460 mg; 4.7 mmol) in 50 mL anhydrous toluene; the mixture was heated to reflux under a nitrogen atmosphere, and acetic anhydride (2.8 mL; 30 µmol) was added in one portion. To the refluxing mixture was added isoamyl nitrite (1.86 mL; 14 mmol) dropwise over 30 minutes. The mixture was then allowed to reflux overnight, followed by cooling to room temperature and filtration. The precipitate was washed several times with toluene, and the combined filtrates were evaporated to dryness to give a brown solid, which was washed with several portions of petroleum ether and a small quantity of cold water, and dried *in vacuo*, to give the acetyl ester precursor **5.15** as a white microcrystalline solid. Yield 1.2 g (5.6 mmol, 61 %). m.p. 162-164 °C; δ_H (500 MHz, $CDCl_3$) 2.81 (d, 1H, J = 1.3 Hz, H^1), 3.97 (d, 1H, J = 1.6 Hz, H^5), 7.78 (dd, 1H, J^1 = 8.6 Hz, J^2 = 0.8 Hz, H^4), 8.04 (dd, 1H, J^1 = 8.3 Hz, J^2 = 1.3 Hz, H^3), 8.17 (s, 1H, H^6), 9.11 (s, 1H, H^2); δ_C (125 MHz, $CDCl_3$) 23.29, 52.74, 117.53, 120.98, 125.65, 129.21, 131.34, 138.90, 139.54, 167.03, 171.19; *m/z* (ESMS) 219.0761 ([M+H^+], calculated for $C_{11}H_{11}N_2O_3$ 219.0764); υ_{max}(KBr)/cm^{-1} 2960m, 1709s br, 1587m, 1416m, 1294m, 1246s, 1201m, 1139m, 1093w, 1034w, 969m, 942s, 899m, 741m.

Synthesis of *1H*-Indazole 6-carboxylic acid **H_2L5.6**

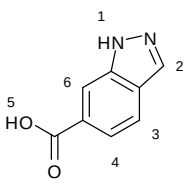

Compound **5.15** (1 g; 4.6 mmol) was dissolved in 40 mL tetrahydrofuran, and this solution was added to a 40 mL aqueous solution of lithium hydroxide (5 g; 208 mmol). The resulting suspension was heated to reflux with vigorous stirring overnight, at which time the solution was concentrated under vacuum to remove the organic phase. The resulting solution was filtered and taken to pH 3 with concentrated hydrochloric acid, causing precipitation of the product as a pale brown solid, which was filtered and dried under vacuum. Yield 315 mg (2.0 mmol, 43 %). m.p. 292-296 °C (decomp); δ_H (500 MHz, d_6-DMSO) 7.67 (dd, 1H, J^1 = 8.3 Hz, J^2 = 1.0 Hz, H^4), 7.85 (dd, 1H, J^1 = 8.3 Hz, J^2 = 0.8 Hz, H^3), 8.15 (s, 1H, H^6), 8.18 (d, 1H, J = 0.8 Hz, H^2), 13.24 (br s, 2H, H^1 + H^5); δ_C (125 MHz, CD_3OD) 114.06, 121.99,

122.65, 127.14, 130.56, 135.18, 141.43, 170.36; *m/z* (ESMS) 163.0503 ([M+H$^+$], calculated for $C_8H_7N_2O_2$ 163.0502); υ_{max}(KBr)/cm^{-1} 3258br, 2864br, 2582br, 1679s, 1579m, 1518m, 1425m, 1230s, 1087m, 954s, 857m, 762m, 693m.

Synthesis of *1H*-Indazole 7-Carboxylic Acid **H_2L5.7**

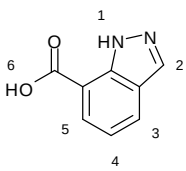

To 60 mL dry toluene under a nitrogen atmosphere was added methyl 2-amino 3-methylbenzoate (1.8 g, 11 mmol) and potassium acetate (560 mg, 5.7 mmol), and the mixture was heated to reflux, at which time acetic anhydride (3.2 mL, 34 mmol) was added, and the mixture was stirred at temperature for 10 minutes. Isoamyl nitrite (2.3 mL, 18 mmol) was added over 30 minutes, and the mixture was refluxed overnight. On cooling, the mixture was filtered and evaporated to dryness, to give 1.6 g of a pale brown solid, which analysed for methyl *1H*-indazole-7-carboxylate. This material was taken up in 40 mL tetrahydrofuran, which was added to a solution of lithium hydroxide (5 g, 210 mmol) in 40 mL water, and the mixture was refluxed for 48 hours. On cooling, the mixture was concentrated on a rotary evaporator, and the resulting aqueous phase was filtered and taken to pH 4 with dilute HCl, and the product was filtered, washed with water and dried *in vacuo*. Yield 810 mg (5 mmol, 45 %). m.p. 218 – 222 °C (decomp); δ_H(500 MHz, d_6-DMSO) 7.23 (t, 1H, J = 7.5 Hz, H^4), 7.97 (dd, 1H, J^1 = 7.5 Hz, J^2 = 1.0 Hz, H^3), 8.06 (dd, 1H, J^1 = 7.8 Hz, J^2 = 0.8 Hz, H^5), 8.206 (s, 1H, H^2), 13.1 (br s, 2H, H^1+H^6); δ_c(125 MHz, d_6-DMSO) 113.75, 120.09, 124.59, 126.46, 128.95, 134.28, 138.02, 166.99; *m/z* (ESMS) 163.0503 ([M+H$^+$], calculated for $C_8H_7N_2O_2$ 163.0502); υ_{max}(KBr)/cm^{-1} 3316s br, 1700s, 1619m, 1592m, 1509m, 1285s, 1201m, 1145m, 1078m, 1056w, 943m, 858s, 745s, 638m, 601m.

Chapter 6

The following compounds were prepared according to literature procedures, and all characterisation data were consistent with that reported: Ethyl 1-(2-pyridyl)-1,3-dioxobutanoate **6.6**;[454] Ethyl 3-(2-pyridyl)-*1H*-pyrazole-5-carboxylate **6.7**;[455] 3-(2-pyridyl)-*1H*-pyrazole-5-carboxylic acid **H_2L6.3**;[436] 3-methyl-*1H*-pyrazole **6.10**;[208] *1H*-pyrazole-3-carboxylic acid **H_2L6.5**.[438]

Synthesis of 1-(2-pyridyl)-3,5-dimethyl-4-(ethyl 4-carboxyphenyl)-pyrazole **L6.1**

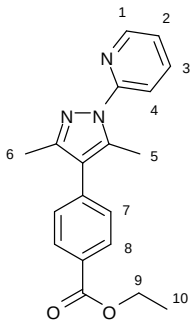

To ethyl 4-(2,4-pentanedion-3-yl) benzoate **2.14** (680 mg; 2.7mmol) in 20 mL ethanol was added 2-hydrazinopyridine (350 mg; 3.2 mmol). The resulting mixture was heated to reflux overnight. On cooling, the solution was evaporated to dryness to give a dark yellow oil, which was purified by flash chromatography (silica gel, 2:1 DCM/EtOAc), and recrystallised from MeOH/H_2O to give the product as a colourless crystalline material. Yield 370 mg (42%). m.p. 86-87 °C; δ_H (300 MHz, $CDCl_3$) 1.40 (t, 3H, J = 7.2 Hz, H^{10}), 2.32 (s, 3H, H^6), 2.60 (s, 3H, H^5), 4.39 (q, 2H, J = 7.2 Hz, H^9), 7.19 (ddt, 1H, J^1 = 6.6 Hz, J^2 = 4.8 Hz, J^3 = 1.8 Hz, H^2), 7.38 (dd, 2H, J^1 = 8.0 Hz, J^2 = 0.4 Hz, H^7), 7.80-7.86 (m, 2H, overlapping, H^3 + H^4), 8.10 (dd, 2H, J^1 = 8.0 Hz, J^2 = 0.4 Hz, H^8), 8.44 (ddd, 1H, J^1 = 4.8 Hz, J^2 = 1.8 Hz, J^3 = 0.8 Hz, H^1); δ_C (125 MHz, $CDCl_3$) 13.03, 13.49, 14.59, 61.17, 116.82, 121.49, 121.93, 128.83, 129.81, 129.93, 138.53, 138.59, 147.88, 148.35, 153.88, 166.77; *m/z* (ESMS) 322.1559 ([M+H^+], calculated for $C_{19}H_{20}N_3O_2$ 322.1550); υ_{max}(KBr)/cm^{-1} 2980w, 1710s, 1581m, 1520w, 1480m, 1435m, 1367m, 1280s, 1180m, 1109s, 1010m, 779s.

Synthesis of 1-(2-pyridyl)-3,5-dimethyl-4-(4-carboxyphenyl)-pyrazole **HL6.2**

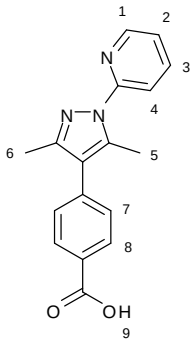

To 1-(2-pyridyl)-3,5-dimethyl-4-(ethyl 4-carboxyphenyl)-pyrazole **L6.1** (300 mg; 810 µmol) in 20 mL THF was added a solution of potassium hydroxide (2 g; 36 mmol) in 20 mL water. The resulting mixture was refluxed for 48 hours. On cooling, the mixture was concentrated under reduced pressure, filtered, and the solids were washed several times with water. The combined filtrate was taken to pH 4 with dilute hydrochloric acid, causing precipitation of the product as a white solid, which was filtered, washed with water and dried *in vacuo.* Yield 220 mg (85 %). m.p. 170-172 °C; δ_H (500 MHz, d_6-DMSO) 2.27 (s, 3H, H^6), 2.59 (s, 3H, H^5), 7.37 (dd, 1H, H^2, J^1 = 6.4 Hz, J^2 = 5.1 Hz), 7.48 (d, 2H, H^7, J = 8.1 Hz), 7.86 (d, 1H, H^4, J = 8.3 Hz); 7.98 – 8.04 (m, 3H, H^3 + H^8), 8.51 (d, 1H, H^1, J = 3.7 Hz); δ_C (125 MHz, d_6-DMSO) 12.79, 13.28, 116.37, 121.26, 121.85, 129.45, 129.64, 130.35, 136.92, 137.76, 139.23, 147.46, 147.83, 152.97, 167.56; *m/z* (ESMS) 316.1058 ([M+Na^+], calculated for $C_{17}H_{15}N_3O_2Na$ 316.1056); υ_{max}(KBr)/cm^{-1} 2925m br, 1694s, 1611m, 1481s, 1429s, 1315m, 1183s, 1008m, 855m, 782m.

Synthesis of Ethyl 1-(2-pyrazinyl)-1,3-dioxobutanoate **6.8**

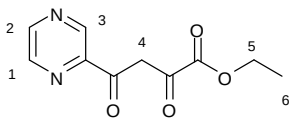

To a slurry of sodium ethoxide (2.72 g; 40 mmol) in 40 mL dry toluene at 0 °C under a nitrogen atmosphere was added diethyl oxalate (5.4 mL; 40 mmol) in one portion. 2-acetylpyrazine (4.92 g; 40 mmol) was added portionwise over 30 minutes, following which the mixture was allowed to warm to room temperature and was stirred overnight. On completion, the mixture was poured into 40 mL of 10% aqueous acetic acid, causing the precipitation of a pale yellow solid, which was filtered, washed with water and dried *in vacuo*. Yield 5.8 g (65%). m.p. 131-133 °C; δ_H (500 MHz, d_6-DMSO) 1.29 (t, 3H, H^6, J = 6.9 Hz), 4.28 (q, 2H, H^5, J = 6.9 Hz), 7.21 (broad s, 1H, H^4), 8.80 (s, 1H, H^1), 8.88 (s, 1H, H^2), 9.21 (s, 1H, H^3); δ_C (125 MHz, d_6-DMSO) 14.02, 61.86, 97.12, 143.41, 144.30, 148.07; *m/z* (ESMS) 223.0719 ([M+H^+], calculated for $C_{10}H_{11}N_2O_4$ 223.0713); υ_{max}(KBr)/cm^{-1} 2982m, 1731s, 1634s, 1471w, 1438m, 1372m, 1328s, 1246s, 1170m, 1070s, 1017s, 830s, 784s.

Synthesis of Ethyl 3-(2-pyrazinyl)-*1H*-pyrazole-5-carboxylate **6.9**

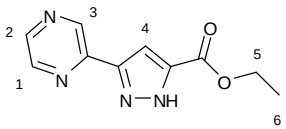

To a solution of **6.8** (4.5 g; 20 mmol) in 50 mL ethanol was added hydrazine hydrate (1.2 mL; 24 mmol) dropwise with stirring at room temperature. The resulting solution was refluxed for 4 hours, then cooled to room temperature and filtered. The filtrate was evaporated under reduced pressure to give **6.9** as a brown solid, which was slurried in a small volume of diethyl ether, filtered and dried *in vacuo*. Yield 3.38 g (76 %); m.p. 249-253 °C (decomp.); δ_H (500 MHz, d_6-DMSO) 1.31 (t, 3H, H^6, J = 7.2 Hz), 4.31 (q, 2H, H^5, J = 7.2 Hz), 7.42 (s, 1H, H^4), 8.59 (d, 1H, H^3, J = 2.4 Hz), 8.67 (dd, 1H, H^2, J^1 = 2.4 Hz, J^2 = 1.5 Hz), 9.23 (d, 1H, H^1, J = 1.2 Hz); δ_C (125 MHz, d_6-DMSO) 14.31, 60.70, 107.22, 141.75, 143.95, 144.40, 145.26, 160.65; *m/z* (ESMS) 219.0884 ([M+H^+], calculated for $C_{10}H_{11}N_4O_2$ 219.0877); υ_{max}(KBr)/cm^{-1} 3349m, 3299m, 3119s, 2856m br, 1666s, 1621m, 1513s, 1444m, 1329m, 1275m, 1145m, 1021s, 969s, 864s, 556m.

Synthesis of 3-(2-pyrazinyl)-*1H*-pyrazole-5-carboxylic acid **H_2L6.4**

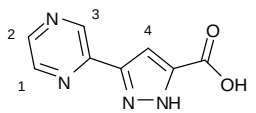

Compound **6.9** (930 mg; 4.3mmol) was dissolved in 20 mL tetrahydrofuran, to which was added a solution of lithium hydroxide (3 g; 125 mmol) in 20 mL water. The resulting mixture was refluxed for 24 hours, followed by cooling to room temperature and concentrating under reduced pressure. A further 20 mL water was added and the mixture was filtered, and the filtrate was acidified with dilute hydrochloric acid, causing precipitation of the product as a fine white powder, which was isolated by filtration and dried *in vacuo*. Yield 430 mg (53 %). m.p. 289-290 °C (decomp.); δ_H (500 MHz, d_6-DMSO) 7.37 (s, 1H, H^4), 8.60 (d, 1H, H^3, J = 2.3 Hz), 8.67 (dd, 1H, H^2, J^1 = 2.3 Hz, J^2 = 1.5 Hz), 9.22 (d, 1H, H^1, J = 1.1 Hz); δ_C (125 MHz, d_6-DMSO) 107.21, 141.62, 143.96, 144.43; *m/z* (ESMS) 191.0563 ([M+H^+], calculated for $C_8H_7N_4O_2$ 191.0564); υ_{max}(KBr)/cm^{-1} 3125s br, 1716s, 1524m, 1428m, 1307w, 1284w, 1240s, 1168s, 1022s, 960m, 851m.

8.3 Synthesis of the Complexes

Chapter 2

Synthesis of poly-[Co(**L1**)(**L4**)] **2.20**

To $CoCl_2 \cdot 6H_2O$ (117 mg; 0.49 mmol) in 10 mL water was added **L2.1** (50 mg; 0.25 mmol) and **H_2L4** (62 mg; 0.25 mmol). The mixture was stirred briefly and placed in a digestion bomb which was heated at 160 °C for 23 hours and then cooled to room temperature at 6 °C/hr. The product was isolated as purple crystals, together with clear needles, which were removed by washing with DMF and then water. Yield 13 mg (10 %). m.p. >300 °C; (Found: C, 57.6; H, 4.7; N, 10.9%. $C_{25}H_{24}N_4O_5Co$ requires: C, 57.8; H, 4.7; N, 10.8%); υ_{max}(KBr)/cm^{-1} 2850m br, 1609m, 1594m, 1555m, 1498m, 1371s, 1241s, 1162s sh, 881m, 780m, 660m.

Synthesis of poly-[Co(**L2.1**)(**L2.5**)] **2.21**

To a solution of $CoCl_2 \cdot 6H_2O$ (117 mg; 0.49 mmol) in 10 mL of water was added **L2.1** (50 mg; 0.25 mmol) and **H_2L2.5** (75 mg; 0.25 mmol). The mixture was stirred briefly and placed in a

digestion bomb which was heated at 120 °C for 24 hours and then cooled to room temperature at 6 °C/hr. The product was isolated as purple crystals, together with amorphous white solids, which were removed by washing with DMF and then with water. Single crystals suitable for an X-ray diffraction study were isolated directly. Yield 34 mg (22%). m.p. >300 °C; (Found: C, 54.7; H, 5.3; N, 13.7%. $C_{28}H_{28}N_6O_4Co{\cdot}2.5H_2O$ requires C, 54.5; H, 5.4; N, 13.6%); υ_{max}(KBr)/cm^{-1} 3601w br, 3228m br, 2902m, 1614m, 1588s, 1529s, 1376s, 1211m, 794s, 617m.

Synthesis of poly-[Co(**L2.2**)(**L2.4**)] **2.22**

To a solution of $CoSO_4{\cdot}7H_2O$ (70 mg; 0.25 mmol) in 10 mL water was added **H_2L2.4** (36 mg; 0.12 mmol) and **L2.2** (31 mg; 0.12 mmol). The mixture was stirred briefly and placed in a digestion bomb which was heated at 200 °C for 36 hours and then cooled to room temperature at 10 °C/hr. The product was isolated as purple crystals, together with colourless needles, which were removed by first washing with DMF, then with boiling EtOH:$CHCl_3$ solution, and finally with water and then air dried. Single crystals suitable for an X-ray diffraction study were isolated directly. Yield 4 mg (6%). m.p. >300 °C; (Found: C, 62.6; H, 5.0; N, 9.1%. $C_{32}H_{30}N_4O_5Co$ requires: C, 62.8; H, 5.3; N, 9.2%); υ_{max}(KBr)/cm^{-1} 2842m br, 1595s, 1558s, 1494m, 1377s, 1299m, 1241s, 1159m, 1062m, 1012m, 877m, 782m.

Synthesis of poly-[Co(**L2.3**)(**L2.4**)] **2.23**

To a solution of $CoSO_4{\cdot}7H_2O$ (53 mg; 0.19 mmol) in 2 mL water was added **L2.3** (20 mg, 0.10 mmol) and **H_2L2.4** (25 mg, 0.08 mmol). The mixture was added to a digestion bomb and heated to 180 °C for 48 hours and cooled to room temperature at 5 °C/hr, to give a mixture of purple plate crystals, colourless crystals and white amorphous solids. The purple crystals were isolated and purified by hand under magnification to give a yield of *ca.* 2.0 mg (5 %) per batch. m.p. >300 °C; (Found: C, 45.7; H, 4.47; N, 8.79; $C_{24}H_{18}N_4O_5Co{\cdot}7H_2O$ requires C, 45.9; H, 5.14; N, 8.93 %); υ_{max}(KBr)/cm^{-1} 2926m br, 1594s, 1540m, 1497m, 1366s, 1289w, 1248s, 1158m, 1054m, 881m, 823w, 781w, 663m.

Synthesis of poly-[Co(**L2.6**)$_2$] **2.24**

HL2.6 (10 mg; 46 µmol) and $CoSO_4.7H_2O$ (20 mg; 71 µmol) were added to 0.5 mL water in a digestion bomb, which was sealed and heated to 180 °C. Following a 72 hour dwell at this temperature, the vessel was cooled at a rate of 10 °C/hr, and was opened to reveal a mixture of purple and colourless crystals, each of which were manually isolated from the mixture for single crystal structure determination. The colourless crystals analysed for the free ligand. A bulk sample of complex **2.24** was obtained by soaking the solid mixture in two 5 mL portions of dimethylformamide, filtering the remaining purple solids, and washing several times with water. The crystals were found to retain crystallinity throughout this process. Yield 2.7 mg (24 %). m.p. >300 °C (decomp); (Found C, 58.5; H, 4.55; N, 11.3; $C_{24}H_{22}N_4O_4Co$ requires C, 58.9; H, 4.51; N, 11.5); υ_{max}(KBr)cm^{-1} 3047w, 1610s, 1587s, 1484m, 1406s, 1324m, 1286m, 1187w, 1011m, 866m, 777s, 699s, 511m.

Synthesis of poly-[Co(**L2.7**)$_2$]·H_2O **2.25**

HL2.7 (10 mg; 44 µmol) and $CoSO_4.7H_2O$ (20 mg; 71 µmol) were added to 2 mL of water in a digestion bomb, to which was added one drop of 2,4,6-collidine. The bomb was sealed and heated to 80 °C, and then slowly heated to 120 °C at a rate of 1.5 °C/hr, followed by cooling to room temperature at 8 °C/hr. The purple crystalline product was isolated as a pure phase by vacuum filtration. Yield 4.1 mg (35 %). m.p. >300 °C; (Found C, 58.3; H, 5.33; N, 10.3; $C_{26}H_{28}N_4O_5Co$ requires C, 58.3; H, 5.27; N, 10.5 %; υ_{max}(KBr)cm^{-1} 3450 w br, 2926s br, 1657w, 1595s, 1544s, 1412m, 1388m, 1371s, 1300m, 1176m, 1059m, 1018m, 856s, 792w, 747s.

Chapter 3

Synthesis of [Fe_2(**L3.1**)$_3$]·4(BF_4)·1.3(H_2O), **3.5A**

To **L3.1** (20 mg, 66 µmol) in 10 mL acetonitrile was added $Fe(BF_4)_2.6H_2O$ (15 mg; 44 µmol, 0.66 equiv). The resulting red solution was heated at 50 °C for 1 hr, followed by cooling to room temperature and filtration. The product was crystallised by slow diffusion of mesitylene into the acetonitrile filtrate. The crystals immediately began losing crystallinity following removal from their mother liquor. The molecular formula of the amorphous solid obtained was estimated as

$[Fe_2(\mathbf{L3.1})_3]\cdot 4(BF_4)\cdot 1.3(H_2O)$ by elemental and thermogravimetric analyses. Yield 4.2 mg (14 %); m.p. >300 °C; (Found: C, 43.9; H, 3.2; N, 18.3; $C_{51}H_{42}B_4N_{18}F_{16}Fe_2\cdot 1.3H_2O$ requires: C, 44.1; H, 3.2; N, 18.1 %; υ_{max}(KBr)/cm^{-1}: 3081 m br, 1611 m, 1563 w, 1490 s, 1453 m, 1374 m, 1330 w, 1054 s, 976 m, 777 s.

Synthesis of $[Fe_2(\mathbf{L3.1})_3]\cdot 4(BF_4)\cdot 6MeNO_2\cdot 2C_6H_6\cdot 4H_2O$, **3.5B**

The title compound was prepared in a method analogous to that of **3.5A**, except the primary solvent was nitromethane, and single crystals were generated by diffusion of benzene vapour. After filtration, the solvated molecular formula of **3.5B** was best estimated at $[Fe_2(\mathbf{L3.1})_3]\cdot 4(BF_4)\cdot 6MeNO2\cdot 2C_6H_6\cdot 4H_2O$ by a combination of elemental and thermogravimetric analyses. Yield 18.6 mg (47 %); m.p. >300 °C; Found: C, 42.1; H, 3.3; N, 17.0; $C_{51}H_{42}B_4N_{18}F_{16}Fe_2\cdot 6MeNO_2\cdot 2C_6H_6\cdot 4H_2O$ requires: C, 42.3; H, 4.1; N, 17.1 %); υ_{max}(KBr)/cm^{-1}: 3414 s, 3125 m, 1616 s, 1565 w, 1490 s, 1455 m, 1415 m, 1375 m, 1331 m, 1056 s br, 978 m, 774 m, 601 m.

Synthesis of $[Co(\mathbf{L3.2})Cl(OH_2)]_2^{2+}[CoCl4]^{2-}.2MeCN$ **3.6**

To $CoCl_2.6H_2O$ (13 mg; 55 µmol) in 10 mL acetonitrile was added **L3.2** (10 mg; 30 µmol), and the resulting mixture was heated to 50 °C with stirring. Gradually the colour changed from blue to dark blue/green, at which point the solution was filtered and left to concentrate by evaporation. Dark green crystals formed within 1 week, when single crystals for X-ray diffraction were isolated directly. The crystals proved unstable in concentrated solution and on slow drying in air, and as such the solution was not allowed to evaporate to dryness. Material for bulk phase analysis was isolated 2 days after the crystals began to form. Crystals obtained by this method were found to be air stable and retained their crystallographically defined acetonitrile and water molecules, as well as a small quantity of residual water which was not removed for fear of disturbing the included solvent. Yield 4.5mg (14%). m.p. >300 °C (decomp.); (Found C, 44.6; H, 4.62; N, 16.0; $C_{44}H_{54}N_{14}O_2Cl_6Co_3.0.5H_2O$ requires C, 44.8; H, 4.49; N, 15.9%); υ_{max}(KBr)/cm^{-1} 3330m br, 2243m sh, 1605s, 1569m, 1489s, 1447s, 1361m, 1310m, 1155w, 1076w, 1010m, 902m, 780s.

Synthesis of **[**Ni_2(**L3.2**)$_2Cl_4$] **3.7**

To $NiCl_2 \cdot 6H_2O$ (6 mg; 25 µmol) in 10 mL acetonitrile was added **L3.2** (10 mg; 30 µmol), and the mixture was added to a 23 mL Parr instruments Teflon lined acid digestion bomb, which was heated to 90 °C, followed by heating at a rate of 1 °C/hr to 120 °C, and then cooled to room temperature at 6 °C/hr. The green crystals of the product formed were isolated by filtration. Yield 6.1 mg (40 %). m.p. >300 °C; (Found C, 45.5; H, 5.70; N, 15.1; $C_{42}H_{44}N_{12}Cl_4Ni_2 \cdot 7H_20$ requires C, 45.8; H, 5.30; N, 15.3 %); υ_{max}(KBr)/cm^{-1} 3355 br, 1643m, 1606s, 1569m, 1486s, 1449s, 1466m, 1310m, 1277w, 1196w, 1153m, 1077m, 1017m, 895m, 785s.

Synthesis of [Cu_2(**L3.2**)Cl_4] **3.8**

Compound **L3.2** (10 mg; 30 µmol) and $CuCl_2.2H_2O$ (10 mg; 56 µmol) were added to 10 mL acetonitrile in a 23 mL Parr Instruments Teflon lined acid digestion bomb, and the mixture was heated to 110 °C for 24 hours, followed by cooling at 5 °C/hr to room temperature. On cooling, the resulting dark green block crystals were filtered and dried. Yield 13 mg (75 %) m.p. >300°C; (Found C, 40.6; H, 3.56; N, 13.5; $C_{21}H_{22}N_6Cl_4Cu_2$ requires C, 40.2; H, 3.54; N, 13.4%); υ_{max}(KBr)/cm^{-1} 2967w, 1609s, 1566m, 1486s, 1455s, 1368m, 1312m, 1275m, 1155s, 1066m, 1028m, 904s, 778s.

Synthesis of [Cu_2(**L3.2**)$(CH_3COO)_4(OH_2)_2$] **3.9**

Compound **L3.2** (10 mg; 30 µmol) was added to a solution of $Cu(CH_3COO)_2 \cdot H_2O$ (12 mg; 60 µmol) in 10 mL acetonitrile, and the resulting dark blue solution was stirred with gentle heating for 1 hour. After this period, the mixture was filtered and allowed to concentrate by evaporation, at which point blue needle crystals deposited once the solution was concentrated to approximately 1/3 volume. The solids were isolated by filtration. Yield 7.2 mg (33%). m.p. 105-110 °C (decomp); %). (Found C, 40.5; H, 6.00; N, 9.78; $C_{29}H_{49}N_6O_{16}Cu_2$ requires C, 40.3; H, 5.71; N, 9.71%); υ_{max}(KBr)/cm^{-1} 3062 m br, 2262 w br, 1696w, 1597s, 1572s, 1492s, 1344m, 1275m, 1157m, 1022m.

Synthesis of $[Cu_2(\mathbf{L3.2})(NO_3)_2]$ **3.10**

Compound **L3.2** (10 mg; 30 µmol) was added to $Cu(NO_3)_2 \cdot 3H_2O$ (28 mg; 120 µmol) in 5 mL acetonitrile, which was added to a 23 mL acid digestion bomb. The mixture was heated to 90 °C, followed by slow heating at 1 °C/hr to 120 °C, and cooled to room temperature at 6 °C/hr. The green crystals of the product were isolated by filtration. Yield 13.9 mg (63%). m.p. 259-260 °C (decomp); (Found C, 34.7; H, 2.93; N, 19.1; $C_{21}H_{22}N_{10}O_{12}$ requires C, 34.4; H, 3.02; N, 19.1%); υ_{max}(KBr)/cm^{-1} 3102m, 2934w, 2489w, 2295m, 2013w, 1744w, 1611s, 1569m, 1486s, 1456m, 1369m, 1283s, 1158s, 1015s, 877w, 768s.

Synthesis of $[Cu_2(NO_3)_2(\mu\text{-}CH_3CONH)(\mu\text{-}OH)(\mathbf{L3.2})]_2$ **3.11**

Compound **L3.2** (10 mg; 30 µmol) was added to $Cu(NO_3)_2 \cdot 3H_2O$ (40 mg; 170 µmol) in 10 mL acetonitrile, and the mixture was placed in a 23 mL acid digestion bomb, which was heated to 120 °C, allowed to dwell for 24 hours, and cooled to room temperature at 5 °C/hr, giving large blue block crystals as a pure phase which were isolated by filtration. Yield 14.7 mg (61 %). m.p. >300 °C. (Found C, 38.8; H, 4.16; N, 17.4; $C_{46}H_{54}N_{18}O_{16}Cu_4 \cdot 3.5H_2O$ requires C, 38.6; H, 4.29; N, 17.6 %); υ_{max}(KBr)/cm^{-1} 2931m br, 2245w, 1752w, 1662m, 1606m, 1572s, 1367s br, 1155m, 901m, 781m, 672w.

Synthesis of poly-$[(\mathbf{L3.2})Cu(C_2O_4)(NO_3)]$ **3.12**

Compound **L3.2** (10 mg; 30 µmol), $Cu(NO_3)_2 \cdot 3H_2O$ (14 mg; 60 µmol) and 1 drop of diethyl oxalate were added to 10 mL acetonitrile in a 23 mL acid digestion bomb, and heated to 120 °C for 24 hours, followed by cooling to room temperature at 5 °C/hr. The product formed as green rod crystals which were isolated by filtration. Single crystals of **3.12** were also formed as a minor product when the same reaction was carried out in the absence of diethyl oxalate, and the identity of both sets of crystals was confirmed by performing unit cell checks on representative samples. Yield 8.9 mg (52%). m.p. >300 °C (decomp); (Found C, 40.0; H, 3.41; N, 17.0; $C_{23}H_{22}Cu_2N_8O_{10} \cdot 1.5H_2O \cdot 1.5MeCN$ requires C, 39.7; H, 3.78; N, 16.9%); υ_{max}(KBr)/cm^{-1} 3603m br, 2249m, 1655s, 1608m, 1570m, 1494s, 1458s, 1361s, 1165m, 1034m, 793s.

Synthesis of poly-[Cu_2(**L3.2**)$(CN)_2$] **3.13**

Compound **L3.2** (10 mg; 30 µmol), $CuNO_3.3H_2O$ (10 mg; 43 µmol) and 5 mL acetonitrile were combined in a 23 mL acid digestion bomb, which was sealed and heated to 100 °C for 24 hours followed by cooling to room temperature at 5 °C/hr. The product formed as pale yellow needle crystals, which were isolated by filtration and found to be air stable. Yield 2.0 mg (13 %); m.p. >300 °C; (Found C, 51.6; H, 4.49; N, 20.8; $C_{23}H_{21}N_8Cu_2$ requires C, 51.5; H, 3.95; N, 20.9 %); υ_{max}(KBr)/cm^{-1} 3078m, 2928m, 2106s sh, 1666m, 1594s, 1478s, 1447s, 1382m, 1367m, 1155w, 1076w, 787s, 758m.

Chapter 4

Synthesis of [Zn(**L4.1**)$_2$$(NO_3)$]·$NO_3$ **4.11**

To **L4.1** (10 mg; 54 µmol) in 10 mL acetonitrile was added $ZnNO_3 \cdot 6H_2O$ (8 mg; 27 µmol), and the resulting mixture was stirred with gentle heating and filtered. Pale orange single crystals of the product deposited on standing for several days and were isolated by filtration. Yield 5.7 mg (38 %). m.p. >300 °C; (Found C, 43.4; H, 2.96; N, 25.1; $C_{20}H_{16}N_{10}O_6Zn$ requires C, 43.1; H, 2.89; N, 25.1 %); *m/z* (ESMS) 216.0385 ([M-2(NO_3^-)], calc for $C_{20}H_{16}N_8Zn$ 216.0389); υ_{max}(KBr)/cm^{-1} 3130m, 2765m br, 1933w, 1749w, 1628m, 1584s, 1541m, 1509m, 1459s, 1291s, 1061m, 1011m, 948m, 761s.

Synthesis of [Mn(**L4.2**)$_2$$(OH_2)$$(MeCN)$]·$2ClO_4$ **4.12**

To **L4.2 (**10 mg; 47 µmol) in 10 mL acetonitrile was added $Mn(ClO_4)_2 \cdot 6H_2O$ (9 mg; 24 µmol), and the mixture was stirred with heating and filtered. Single crystals of **4.12** were generated by slow diffusion of toluene into the acetonitrile solution. Yield 6.4 mg (36%); (Found C, 42.0; H, 3.93; N, 16.7; $C_{26}H_{29}N_9O_9Cl_2Mn$ requires C, 42.3; H, 3.96; N, 17.1%); υ_{max}(KBr)/cm^{-1} 3388m br, 2939m, 2281m, 1623w, 1578m, 1559s, 1462s, 1279s, 1122s br, 980m, 916w, 813m, 747s, 625m.

Synthesis of $[Cu(\mathbf{L4.3})_2(NO_3)]\cdot NO_3$ **4.13**

To **L4.3** (10 mg; 51 µmol) in 10 mL acetonitrile was added $CuNO_3\cdot 3H_2O$ (6 mg; 26 µmol) and the mixture was stirred with heating and filtered. The filtrate was subjected to diffusion of diethyl ether vapour which generated the product as green crystals after several days. Yield 3.7 mg (25 %). m.p. 230-233 °C (decomp.); (Found C, 45.4; H, 3.57; N, 24.0; $C_{22}H_{40}N_{10}O_6Cu$ requires C, 45.3; H, 3.45; N, 24.0 %); *m/z* (ESMS) 521.0979 ($[M\text{-}NO_3^+]$, calc for $C_{22}H_{20}N_9O_3Cu$ 521.0980); υ_{max}(KBr)/cm^{-1} 3109m, 2384m, 2290m, 1914m, 1742w, 1569s, 1540s, 1462s, 1344s, 1300m, 1237m, 1212m, 1133w, 1064s, 1010s, 972s, 749s.

Synthesis of poly-$[Cu_2(\mathbf{L4.4})Cl_4]$ **4.14**

L4.4 (10 mg; 21 µmol) and $CuCl_2.2H_2O$ (4 mg; 21 µmol) were combined in 2 mL acetonitrile and sealed in a 23 mL acid digestion bomb, which was heated to 120 °C for 36 hours, followed by cooling to room temperature at 3 °C per hour. On completion, the orange crystals were filtered, washed with acetonitrile and air dried. Yield 4.1 mg (30%). m.p. 294-299 °C (decomp.); (Found C, 45.3; H, 3.17; N, 15.3; $C_{28}H_{22}N_8Cl_4Cu_2$ requires C, 45.5; H, 3.00; N, 15.2 %); υ_{max}(KBr)/cm^{-1} 3128m, 2337m, 1909m, 1711m, 1552s, 1505m, 1479m, 1459s, 1415m, 1344m, 1296m, 1205m, 1052s, 949s, 754s, 539m.

Synthesis of $[Cu_2(\mathbf{L4.4})_2(OH_2)_2]\cdot 4ClO_4\cdot PhMe\cdot 2MeCN\cdot 2H_2O$ **4.15**

To **L4.4** (10 mg; 21 µmol) in 10 mL acetonitrile was added $Cu(ClO_4)_2\cdot 6H_2O$ (8 mg; 21 µmol). The resulting green solution was stirred with gentle heating for 10 minutes, followed by filtration. Single crystals were obtained by diffusion of toluene into the filtrate, giving green blocks within 4 days. Yield 8.1 mg (24 %). (Found C, 46.8; H, 3.58; N, 14.9. $C_{67}H_{66}N_{18}O_{20}Cl_4Cu_2$ requires C, 47.0; H, 3.89; N, 14.7%; *m/z* (ESMS) 533.1257 ($C_{56}H_{44}N_{16}Cu_2^{2+}$ requires 533.1257); υ_{max}(KBr)/cm^{-1} 3120m, 2973m, 2870m, 2251w, 1892w, 1804w, 1584s, 1484s, 1460s, 1344m, 1296m, 1195m, 1116m, 1066m, 933s, 757s, 614m. An equivalent procedure was used to generate the tetrafluoroborate analogue.

Synthesis of $[Cu_2(\mathbf{L4.5})_2(OH_2)_2]^{4+}\cdot 4(BF_4^-)\cdot 0.5(C_9H_{12})$ **4.16**

L4.5 (10 mg; 18 μmol) was slurried in 5 mL nitromethane, to which was added $Cu(BF_4)_2\cdot 6H_2O$ (6 mg; 18 μmol), and the mixture was stirred with heating until the ligand had fully dissolved, giving a green solution. This mixture was filtered, and the filtrate was subjected to vapour diffusion from mesitylene, which yielded large single crystals of the product after 3 weeks. The crystals proved extremely unstable to removal from the mother liquor. Yield 4.9 mg (17%); m.p. >300 (decomp); (found C, 53.7; H, 4.18; N, 14.0; $C_{68}H_{52}N_{16}B_4F_{16}Cu_2\cdot 0.5(C_9H_{12})$ requires C, 53.5; H, 3.59; N, 13.8 %); *m/z* (ESMS) 609.1582 ($[M]^{2+}$, calculated for $C_{68}H_{52}N_{16}Cu_2$ 609.1571); υ_{max}(KBr)/cm^{-1} 3472m, 3157m, 1609w, 1556s, 1512m, 1464s, 1413m, 1300m, 1212w, 1067s, 958m, 814m, 752s, 588w.

Synthesis of $[Cu_2(\mathbf{L4.6})_2(NO_3)_2]\cdot 2(NO_3)\cdot$MeCN **4.17**

L4.6 (10 mg; 21 μmol) and $Cu(NO_3)_2\cdot 3H_2O$ (5 mg; 22 μmol) were combined in 10 mL acetonitrile and heated gently with stirring for 15 minutes. The resulting green solution was filtered and allowed to slowly concentrate by evaporation, where green crystals of the product deposited within 5 days. Yield 7.1 mg (48%). m.p. 200-207 °C (decomp.); (Found C, 51.3; H, 3.61; N, 22.1; $C_{60}H_{50}N_{22}O_{12}Cu_2$ requires C, 51.5; H, 3.60; N, 22.0 %); υ_{max}(KBr)/cm^{-1} 3465w br, 3095w, 2245w, 1608w, 1557s, 1533s, 1500s, 1462m, 1342s, 1292s, 1223w, 1180w, 1063m, 1015m, 748s.

Synthesis of $[Cu_4Cl_8(\mathbf{L4.6})_2]\cdot$MeCN **4.18**

L4.6 (10 mg; 21 μmol) and $CuCl_2\cdot 2H_2O$ (4 mg; 24 μmol) were combined in 10 mL acetonitrile and added to a 23 mL acid digestion bomb, which was sealed and heated to 120 °C and allowed to dwell for 36 hours, followed by cooling to room temperature at 3 °C/hr, at which time the product was isolated by filtration. Yield 3.4 mg (24 %). m.p. 283 – 286 °C (decomp.); (Found C, 45.9; H, 3.10; N, 15.5; $C_{56}H_{44}N_{16}Cl_8Cu_4\cdot$MeCN requires C, 45.8; H, 3.12; N, 15.7 %); υ_{max}(KBr)/cm^{-1} 3140w, 2262w, 1613m, 1561s, 1535m, 1509m, 1477m, 1456s, 1293m, 1214m, 1064m, 1051m, 955s, 922m, 740s.

Synthesis of $[Zn_2(\mathbf{L4.7})_3]\cdot 4(CF_3SO_3)\cdot 5(MeNO_2)$ **4.19**

L4.7 (10 mg; 25 µmol) was added to 5 mL nitromethane, to which was added $Zn(CF_3SO_3)_2\cdot 6H_2O$ (6 mg; 17 µmol). The mixture was heated gently for 5 minutes and filtered, and the filtrate was subjected to diffusion of diisopropyl ether vapour. Colourless single crystals of the product formed within one week. Yield 3.8 mg (20 %). m.p. >300 °C; (Found C, 40.8; H, 3.52; N, 17.5; $C_{73}H_{60}N_{24}O_{12}F_{12}S_4Zn_2\cdot 5MeNO_2\cdot 2H_2O$ requires C, 40.8; H, 3.47; N, 17.7 %); υ_{max}(KBr)/cm^{-1} 3518m, 2967m, 1548s, 1461s, 1409m, 1256s, 1157s, 1030s, 976s, 923m, 817w, 746s, 637s, 517w.

Chapter 5

Synthesis of $[Cu(\mathbf{L5.1})_2(NO_3)]\cdot(NO_3)\cdot 1.5(H_2O)$ **5.16**

L5.1 (10 mg; 51 µmol) and $CuNO_3\cdot 3H_2O$ (6 mg; 25 µmol) were combined in 5 mL nitromethane, which was stirred with gentle heating for 5 minutes and filtered. The filtrate was subjected to diffusion of benzene vapour, which deposited green crystals of the product within one week. Yield 4.2 mg (28%). m.p. 233-235 °C (decomp); (Found C, 47.5; H, 3.27; N, 18.4; $C_{24}H_{18}N_8O_6Cu\cdot 1.5H2O$ requires C, 47.6; H, 3.50; N, 18.5%); *m/z* (ESMS, MeCN) 226.5438 ([M^{2+}], calculated for $C_{24}H_{18}N_6Cu$ 226.5439); υ_{max}(KBr)/cm^{-1} 3514m, 1617m, 1476s, 1437m, 1349s, 1298s, 1214m, 1155m, 1091w, 1055w, 913w, 773s, 746s, 615m.

Synthesis of $[Cu(\mathbf{L5.2})_2(NO_3)]\cdot(NO_3)$ **5.17**

L5.2 (10 mg; 51 µmol) and $CuNO_3\cdot H_2O$ (6 mg; 25 µmol) were combined in 5 mL nitromethane, which was stirred with gentle heating for 5 minutes and filtered. The filtrate was subjected to diffusion of toluene vapour, which deposited green crystals within several days. Yield 6 mg (42%). m.p. 254-255 °C (decomp); (Found C, 49.9; H, 3.07; N, 19.4; $C_{24}H_{18}N_8O_6Cu$ requires C, 49.9; H, 3.14; N, 19.4%); *m/z* (ESMS, MeCN) 226.5438 ([M^{2+}], calculated for $C_{24}H_{18}N_6Cu$ 226.5439); υ_{max}(KBr)/cm^{-1} 3073m, 1630m, 1575m, 1521s, 1450s, 1327s, 1300s, 1278m, 1231w, 1150w, 1025m, 814m, 764s.

Synthesis of poly-[Cu(**L5.3**)(CH_3CONH_2)] **5.18**

H_2L5.3 (10 mg; 62 µmol) was added to $CuNO_3 \cdot 3H_2O$ (15 mg; 62 µmol) in 5 mL of acetonitrile within a 23 mL acid digestion bomb, which was sealed and heated to 120 °C, allowed to dwell for 36 hours, and cooled at 5 °C/hr to room temperature. The product was isolated as a pure crystalline phase consisting of green octahedral blocks. Yield 12.1 mg (43 µmol, 69 %). m.p. >300 °C (decomp); (Found C, 42.4; H, 3.16; N, 14.9; $C_{10}H_8N_3O_3Cu$ requires C, 42.5; H, 3.21; N, 14.9 %); υ_{max}(KBr)/cm^{-1} 3397s, 3153m, 1667s, 1580s, 1470m, 1343m, 1195m, 1149w, 1091w, 1003w, 958w, 846s, 799m, 734m, 650m, 562m.

Synthesis of poly-[Cd(**HL5.4**)$_2$(MeOH)$_2$]·2MeOH **5.19**

H_2L5.4 (10 mg; 61 µmol) was combined with $Cd(NO_3)_2 \cdot 4H_2O$ (8 mg; 26 µmol) in 5 mL methanol, and added to a 23 mL acid digestion bomb, which was heated to 130 °C, allowed to dwell for 24 hours, and cooled to room temperature at 5 °C/hr. The solution obtained was filtered and allowed to stand for 2 days, at which point colourless crystals of the product deposited and were isolated by filtration. Yield 3.2 mg (22%). m.p. >300 °C; (Found C, 41.8; H, 2.89; N, 11.9; $C_{16}H_{10}N_4O_4Cd \cdot MeOH \cdot H_2O$ requires C, 42.1; H, 3.33; N, 11.6%); υ_{max}(KBr)/cm^{-1} 3096s br, 1541s, 1410m, 1360s, 1300s, 1205s, 1091s, 959s, 876m, 796m, 761s.

Synthesis of poly-[Zn(**H_2L5.5**)$_4$(SiF_6)] **5.20**

H_2L5.5 (25mg; 153 µmol) was dissolved in 10 mL methanol, to which was added $ZnSiF_6$ (12 mg; 47 µmol). The mixture was stirred with heating for 10 minutes, at which point 2 mL of toluene was added, and the solution was filtered. The filtrate was subjected to diffusion of toluene vapour, which deposited colourless crystals of the product after 1 month. Yield 10.7 mg (27%); m.p. >300 °C (decomp.); (Found C, 53.0; H, 3.78; N, 10.7; $C_{32}H_{24}N_8O_8F_6ZnSi \cdot 2PhMe$ requires C, 53.1; H, 3.88; N, 10.8%); υ_{max}(KBr)/cm^{-1} 3277m, 1939m, 1709s, 1633m, 1585m, 1515m, 1414m, 1361w, 1303m, 1239w, 1192w, 1081m, 966s, 729w.

Synthesis of poly-[Cu(**HL5.5**)$_2$] **5.21**

H$_2$L5.5 (10 mg; 61 µmol) was combined with Cu(NO$_3$)$_2$·3H$_2$O (4 mg; 16 µmol) and NH$_4$SiF$_6$ (5 mg; 28 µmol) in a 1:1 MeOH/H$_2$O mixture (2 mL), and added to a 23 mL acid digestion bomb, which was heated to 100 °C, allowed to dwell for 24 hours, and cooled to room temperature at 4 °C/hr. The purple crystals obtained were filtered and washed sequentially with methanol, water, and a further portion of methanol, and were air dried. Yield 3.6 mg (59%); m.p. >300 °C; (Found C, 48.6; H, 2.86; N, 13.5; C$_{48}$H$_{30}$N$_{12}$O$_{12}$Cu$_3$·2MeOH·H$_2$O requires C, 48.4; H, 3.30; N, 13.6%); υ_{max}(KBr)/cm^{-1} 3250m; 1817w, 1633m, 1599s, 1570s, 1513m, 1458m, 1380s, 1273m, 1133m, 1083s, 971s, 857s, 793s, 781s, 597m.

Synthesis of [Cu$_3$(**HL5.6**)$_4$(NO$_3$)$_2$(EtOH)$_2$]·3(C$_6$H$_6$)·2(H$_2$O) **5.22**

To a solution of **H$_2$L5.6** (10 mg; 62 µmol) in 5 mL ethanol was added CuNO$_3$·3H$_2$O (11 mg; 44 µmol), and the mixture was stirred with gentle heating for 10 minutes. The mixture was filtered and the filtrate was subjected to diffusion of benzene vapour, which deposited blue/green crystals of the product within one month. Yield 3.6 mg (18%). m.p. >300 °C; (Found C, 39.3, H, 2.95, N, 12.4; C$_{36}$H$_{32}$N$_{10}$O$_{16}$Cu$_3$·3H$_2$O requires C, 39.1; H, 3.46; N, 12.7%); υ_{max}(KBr)/cm^{-1} 3285m br, 2921m br, 1679w 1610w, 1577m, 1514m, 1410s, 1360s, 1223m, 1094w, 968s, 675m.

Synthesis of [Cu(**HL5.7**)$_2$]·H$_2$O·MeOH **5.23**

H$_2$L5.7 (10 mg; 61 µmol) was dissolved in 10 mL methanol, to which was added CuNO$_3$·3H$_2$O (7 mg; 28 µmol). The resulting mixture was stirred with gentle heating for 10 minutes and filtered. Purple rod crystals formed in the filtrate within 3 days, and were isolated by filtration. Yield 5.1 mg (43 %). m.p. >300 °C; (Found C, 47.2; H, 3.26; N, 13.2; C$_{17}$H$_{13}$N$_4$O$_6$Cu requires C, 47.2; H, 3.03; N, 12.9 %); υ_{max}(KBr)/cm^{-1} 2929m br, 1633s, 1596s, 1517w, 1448m, 1357s, 1326m, 1190m, 1153w, 1122w, 1035m, 989m, 876m, 852s, 765s, 515m.

Synthesis of [Cu(**L6.1**)$_2$MeCN]·2(ClO_4) **6.11**

To $Cu(ClO_4)_2.6H_2O$ (6 mg; 16 µmol) in 10 mL acetonitrile was added **L6.1** (10 mg; 32 µmol). The mixture was heated briefly with stirring and filtered. Single crystals of the product were formed by slow diffusion of diisopropyl ether into the filtrate, which gave dark green crystals over several weeks. Yield 2.5 mg (19%). (Found C, 51.0; H, 4.36; N, 10.5; $C_{40}H_{41}N_7O_{12}Cl_2Cu$ requires C, 50.8; H, 4.37; N, 10.4%); *m/z* (ESMS) 352.6141 ([M^{2+}-MeCN], $C_{38}H_{38}N_6O_4Cu^{2+}$ requires 352.6120), 705.2275 ([M^+-MeCN], $C_{38}H_{38}N_6O_4Cu^+$ requires 705.2245); υ_{max}(KBr)/cm^{-1} 3413s, 2931m, 2281m, 1717s, 1615s, 1469m, 1273s, 1090s br, 868m, 773m, 623m

Synthesis of poly-[Cu(**L6.2**)(MeOH)(NO_3)] **6.12**

To **HL6.2** (10 mg; 34 µmol) in 5 mL methanol was added $CuNO_3·3H_2O$ (4 mg; 16 µmol), and the mixture was added to a 23 mL acid digestion bomb which was heated to 120 °C, allowed to dwell for 24 hours, then cooled to room temperature at 5 °C/hr. The green crystals formed were isolated by filtration. Yield 2.0 mg (28 %); m.p. 289-293 (decomp.); (Found C, 48.5; H, 4.04; N, 12.1; $C_{18}H_{18}N_4O_5Cu$ requires C, 48.1; H, 4.03; N, 12.4 %); υ_{max}(KBr)/cm^{-1} 2771m, 1610s, 1451s, 1370m, 1304m, 1163w, 1018s, 868w, 813m, 776m, 701m, 523w.

Synthesis of [$Cu_2(SO_4)_2(H_2O)_2$(**HL6.2**)$_2$]·H_2O·MeOH **6.13**

To **HL6.2** (10 mg; 34 µmol) in 2 mL of a 50 % ethanol/water mixture was added $CuSO_4·5H_2O$ (9 mg; 36 µmol), and the mixture was added to a 23 mL acid digestion bomb, which was heated to 100 °C, allowed to dwell for 24 hours, and cooled at a rate of 4 °C/hr to room temperature. Green crystals of the product were isolated by filtration. Yield 8.4 mg (50 %); m.p. >300 °C; (Found C, 43.2; H, 3.97; N, 8.44; $C_{36}H_{42}N_6O_{16}S_2Cu_2$ requires C, 43.0; H, 4.21; N, 8.35 %); υ_{max}(KBr)/cm^{-1} 2938m br, 1714s, 1610s, 1489m, 1451m, 1251m, 1176s, 1100s, 1061s, 984m, 864w, 783m, 637m.

Synthesis of $[Cu_2(\mathbf{L6.3})_2(MeOH)_2]$ **6.14**

To **H_2L6.3** (10 mg; 53 µmol) in 5 mL MeOH was added $CuCl_2 \cdot 2H_2O$ (20 mg; 120 mmol), and the mixture was heated in a 23 mL acid digestion bomb to 100 °C, allowed to dwell for 24 hours, and cooled to room temperature at 4 °C/hr. The purple rod crystals were isolated by filtration, washed with methanol and air dried. Yield 6.2 mg (21%); m.p. >300 °C; (Found C, 42.8; H, 3.37; N, 14.9; $C_{10}H_9N_3O_3Cu$ requires C, 42.5; H, 3.21; N, 14.9%); υ_{max}(KBr)/cm^{-1} 2821s br, 1663m, 1519w, 1451s, 1317m, 1254m, 1028m, 986m, 780s.

Synthesis of poly-$[Cu_2(\mathbf{L6.3})_2]$ **6.15**

To **H_2L6.3** (10 mg; 53 µmol) in 5 mL MeOH was added $CuNO_3 \cdot 3H_2O$ (15 mg; 60 mmol), and the mixture was heated in a 23 mL acid digestion bomb to 130 °C, allowed to dwell for 24 hours, and cooled to room temperature at 5 °C/hr. The blue block crystals of the product were isolated by filtration and air dried. Yield 8.3 mg (62%). m.p. >300 °C; (Found C, 42.3; H, 2.10; N, 16.3; $C_{18}H_{10}N_6O_4Cu_2 \cdot 0.5H_2O$ requires C, 42.4; H, 2.17; N, 16.5%); υ_{max}(KBr)/cm^{-1} 3061m, 2331m, 1609s, 1583m, 1518m, 1446m, 1286s, 1075m, 1045m, 1021w, 992m, 814m, 797m, 777s, 647w.

Synthesis of $[Co(\mathbf{HL6.4})_2(OH_2)_2]$ **6.16**

To **H_2L6.3** (10 mg; 53 µmol) in 3 mL H_2O was added $CoSO_4 \cdot 7H_2O$ (10 mg; 36 µmol), and the mixture was added to a 23 mL acid digestion bomb, which was heated to 130 °C, allowed to dwell for 24 hours, and cooled to room temperature at 5 °C/hr. The orange crystals of the product were collected by filtration and dried in air. Yield 4.9 mg (40%). m.p. >300 °C (decomp.); (Found C, 40.8; H, 2.83; N, 23.7; $C_{16}H_{14}N_8O_6Co$ requires C, 40.6; H, 2.98; N, 23.7%); υ_{max}(KBr)/cm^{-1} 3068s br, 1606s, 1506m, 1478m, 1397w, 1360s, 1318m, 1207w, 1141w, 1020s, 839s, 514s.

Synthesis of poly-$[Co_2(\mathbf{L6.4})_2(OH_2)_3] \cdot 5(H_2O)$ **6.17**

To **H_2L6.3** (10 mg; 53 µmol) in 2 mL H_2O was added $CoSO_4 \cdot 7H_2O$ (10 mg; 36 µmol) and one drop of 2,4,6-trimethylpyridine, and the mixture was added to a 23 mL acid digestion bomb, which was heated to 180 °C, allowed to dwell for 72 hours, and cooled to room temperature at 10 °C/hr. The

orange rod crystals of the product were isolated by filtration and washed with water. Yield 8.4 mg (83%). m.p. >300 °C; (Found C, 30.9, H, 3.39; N, 18.1; $C_{16}H_{14}N_8O_7Co_2 \cdot 4H_2O$ requires C, 31.0; H, 3.58; N, 18.1%); υ_{max}(KBr)/cm^{-1} 3324m br, 2928m br, 2340w, 1601m, 1536w, 1497m, 1425m, 1316s, 1226m, 1190m, 1149m, 1039s, 985m, 824m, 779m.

Synthesis of poly-[Cu(**L6.5**)(NMP)]·0.5(NMP) **6.18**

H_2L6.5 (200 mg; 1.8 mmol) was added to $CuNO_3 \cdot 3H_2O$ (220 mg; 0.9 mmol) in 20 mL of N-methyl pyrrolidone containing 2 mL of water. The mixture was stirred with heating and then filtered, and the filtrate was left to stand in a calcium chloride dessicator for a period of several weeks, giving the product as large blue blocks which were isolated by filtration. Yield 125 mg (13 %). m.p. >300 °C; (Found C, 41.9; H, 4.87; N, 14.6; $C_9H_{11}N_3O_3Cu \cdot 0.5(H_2O) \cdot 0.5(C_5H_9NO)$ requires C, 41.7; H, 5.02; N, 14.8 %); υ_{max}(KBr)/cm^{-1} 3519m, 2873s, 1668s, 1582m, 1524m, 1385m, 1302s, 1145s, 1114m, 1073w, 986w, 823s, 773s, 632m.

Appendix 1

Crystallographic Refinement Data

Chapter 2

Table A1 Crystallographic Data for Compounds **H_2L2.5, 2.13** and **HL2.6.HNO_3**

Compound reference	**H_2L2.5**	**2.13**	**HL2.6.HNO_3**
Chemical formula	$C_{17}H_{13}N_2O_4$•C_2H_3N	$C_{14}H_{16}O_4$	$C_{12}H_{13}N_2O_2$•NO_3
Formula Mass	351.36	248.27	279.25
Crystal System	Tetragonal	Monoclinic	Triclinic
a/Å	16.8305(5)	12.9044(4)	7.4272(4)
b/Å	16.8305(5)	7.4504(2)	8.9566(6)
c/Å	23.0344(7)	14.8804(5)	10.4607(6)
α/°	90.00	90.00	72.810(4)
β/°	90.00	112.887(2)	70.221(4)
γ/°	90.00	90.00	78.066(4)
Unit cell volume/Å^3	6524.9(3)	1318.02(7)	621.14(6)
Temperature/K	113(2)	114(2)	114(2)
Space group	$I4_1cd$	$P2_1/c$	$P\bar{1}$
No. of formula units per unit cell, *Z*	16	4	2
Radiation type	MoKα	MoKα	MoKα
No. of reflections measured	77264	24410	11815
No. of independent reflections	2224	2327	2209
R_{int}	0.0633	0.0424	0.0652
Final R_1 values ($I > 2\sigma(I)$)	0.0416	0.0349	0.0441
Final $wR(F^2)$ values ($I > 2\sigma(I)$)	0.1026	0.0955	0.1064
Final R_1 values (all data)	0.0447	0.0418	0.0786
Final $wR(F^2)$ values (all data)	0.1048	0.1006	0.1177
Flack Parameter	-0.2(13)		

Table A2 Crystallographic Data for compounds **H_2L2.6, H_2L2.7** and **2.20**

Compound reference	**H_2L2.6**	**H_2L2.7**	**2.20**
Chemical formula	$C_{12}H_{12}N_2O_2$	$C_{13}H_{14}N_2O_2$	$C_{25}H_{24}CoN_4O_5$
Formula Mass	216.24	230.26	519.41
Crystal System	Triclinic	Orthorhombic	Hexagonal
a/Å	9.6538(5)	16.9424(5)	9.6004(5)
b/Å	10.4193(6)	7.4436(2)	9.6004(5)
c/Å	21.9388(14)	18.1452(6)	48.307(2)
α/°	91.284(4)	90.00	90.00
β/°	101.971(4)	90.00	90.00
γ/°	102.808(4)	90.00	120.00
Unit cell volume/Å^3	2099.6(2)	2288.34(12)	3855.8(3)
Temperature/K	113(2)	112(2)	134(2)
Space group	$P\bar{1}$	*Pbca*	$P6_522$
No. of formula units per unit cell, *Z*	8	8	6
Radiation type	MoKα	MoKα	MoKα
No. of reflections measured	16213	39230	72632
No. of independent reflections	7393	2023	2289
R_{int}	0.0757	0.0540	0.1220
Final R_1 values ($I > 2\sigma(I)$)	0.0481	0.0325	0.0396
Final $wR(F^2)$ values ($I > 2\sigma(I)$)	0.0669	0.0866	0.0868
Final R_1 values (all data)	0.1136	0.0476	0.0494
Final $wR(F^2)$ values (all data)	0.0806	0.0929	0.0913
Flack Parameter			0.01(3)

Table A3 Crystallographic Data for compounds **2.21**, **2.22** and **2.23**

Compound reference	**2.21**	**2.22**	**2.23**
Chemical formula	$C_{28}H_{28}CoN_6O_7$	$C_{32}H_{30}CoN_4O_5$	$C_{24}H_{22}CoN_4O_7$
Formula Mass	619.51	609.53	537.39
Crystal System	Monoclinic	Monoclinic	Monoclinic
a/Å	28.891(3)	11.6235(3)	13.2180(4)
b/Å	12.8115(12)	14.1270(4)	14.5433(4)
c/Å	20.640(3)	19.4587(6)	14.2067(5)
α/°	90.00	90.00	90.00
β/°	128.629(4)	94.770(2)	104.579(2)
γ/°	90.00	90.00	90.00
Unit cell volume/Å^3	5968.0(12)	3184.15(16)	2643.07(14)
Temperature/K	111(2)	113(2)	113(2)
Space group	*C*2/*c*	$P2_1/c$	$P2_1/c$
No. of formula units per unit cell, *Z*	8	4	4
Radiation type	MoKα	MoKα	MoKα
No. of reflections measured	57801	59577	44598
No. of independent reflections	5550	5633	4675
R_{int}	0.2178	0.0670	0.0479
Final R_1 values ($I > 2\sigma(I)$)	0.0623	0.0331	0.0551
Final $wR(F^2)$ values ($I > 2\sigma(I)$)	0.1198	0.0931	0.1622
Final R_1 values (all data)	0.1507	0.0474	0.0603
Final $wR(F^2)$ values (all data)	0.1538	0.0995	0.1694

Table A4 Crystallographic Data for compounds **2.24** and **2.25**

Compound reference	**2.24**	**2.25**
Chemical formula	$C_{24}H_{22}CoN_4O_4$	$C_{26}H_{26}CoN_4O_4{\bullet}H_2O$
Formula Mass	489.39	535.45
Crystal System	Tetragonal	Monoclinic
a/Å	14.85742(19)	33.0036(8)
b/Å	14.85742(19)	8.55033(11)
c/Å	39.7127(9)	21.3589(4)
α/°	90.00	90.00
β/°	90.00	124.052(3)
γ/°	90.00	90.00
Unit cell volume/Å^3	8766.3(2)	4993.8(2)
Temperature/K	120.0(1)	120.0(1)
Space group	$I\bar{4}\,2d$	*C*2/*c*
No. of formula units per unit cell, *Z*	16	8
Radiation type	CuKα	CuKα
No. of reflections measured	13461	24880
No. of independent reflections	3736	4294
R_{int}	0.0299	0.0360
Final R_1 values ($I > 2\sigma(I)$)	0.0417	0.0414
Final $wR(F^2)$ values ($I > 2\sigma(I)$)	0.1168	0.0968
Final R_1 values (all data)	0.0486	0.0497
Final $wR(F^2)$ values (all data)	0.1227	0.1026
Flack Parameter	0.0(4)	

Chapter 3

Table A5 Crystallographic Data for compounds **3.5A, 3.5B** and **3.6**

Compound reference	**3.5A**	**3.5B**	**3.6**
Chemical formula	$C_{51}H_{42}B_4F_{16}Fe_2N_{18}$	$2(C_{51}H_{42}Fe_2N_{18})\bullet 8(BF_4)\bullet 5(CH_3NO_2)\bullet 4(C_6H_6)$	$C_{42}H_{48}Cl_2Co_2N_{12}O_2\bullet Cl_4Co\bullet 2(C_2H_3N)$
Formula Mass	1365.96	3346.56	1224.52
Crystal System	Trigonal	Monoclinic	Monoclinic
a/Å	13.5577(4)	21.1374(8)	18.2456(5)
b/Å	13.5577(4)	17.2342(6)	12.3133(3)
c/Å	36.9200(13)	23.8071(8)	23.6387(7)
α/°	90.00	90.00	90.00
β/°	90.00	112.774(2)	90.591(2)
γ/°	120.00	90.00	90.00
Unit cell volume/Å^3	5877.1(3)	7996.5(5)	5310.5(3)
Temperature/K	113(2)	113(2)	113(2)
Space group	$P\bar{3}\,c1$	$P2_1/n$	$C2/c$
No. of formula units per unit cell, *Z*	4	2	4
Radiation type	MoKα	MoKα	MoKα
No. of reflections measured	102779	155637	46990
No. of independent reflections	3479	18369	4703
R_{int}	0.1278	0.1774	0.0713
Final R_1 values ($I > 2\sigma(I)$)	0.0654	0.1060	0.0452
Final $wR(F^2)$ values ($I > 2\sigma(I)$)	0.1977	0.3080	0.1318
Final R_1 values (all data)	0.1123	0.2318	0.0717
Final $wR(F^2)$ values (all data)	0.2377	0.3614	0.1442

Table A6 Crystallographic Data for compounds **3.7**, **3.8** and **3.9**

Compound reference	**3.7**	**3.8**	**3.9**
Chemical formula	$C_{42}H_{44}Cl_4N_{12}Ni_2$	$C_{21}H_{22}Cl_4Cu_2N_6$	$2(C_{15}H_{19}CuN_3O_5)\bullet 6(H_2O)$
Formula Mass	976.11	627.33	865.83
Crystal System	Monoclinic	Monoclinic	Monoclinic
a/Å	28.6333(9)	9.9054(3)	23.6250(6)
b/Å	11.9722(4)	18.7950(5)	9.0426(2)
c/Å	18.4977(6)	13.3344(3)	17.2200(4)
α/°	90.00	90.00	90.00
β/°	122.416(2)	97.0170(10)	91.108(2)
γ/°	90.00	90.00	90.00
Unit cell volume/Å^3	5353.0(3)	2463.90(11)	3678.05(15)
Temperature/K	113(2)	113(2)	121(2)
Space group	$C2/c$	$P2_1/c$	$C2/c$
No. of formula units per unit cell, *Z*	4	4	4
Radiation type	MoKα	MoKα	MoKα
No. of reflections measured	42434	42782	31178
No. of independent reflections	4741	4365	3266
R_{int}	0.0789	0.0396	0.0511
Final R_1 values ($I > 2\sigma(I)$)	0.0352	0.0338	0.0267
Final $wR(F^2)$ values ($I > 2\sigma(I)$)	0.0953	0.0871	0.0707
Final R_1 values (all data)	0.0521	0.0369	0.0326
Final $wR(F^2)$ values (all data)	0.0996	0.0898	0.0729

Table A7 Crystallographic Data for compounds **3.10**, **3.11** and **3.12**

Compound reference	**3.10**	**3.11**	**3.12**
Chemical formula	$C_{21}H_{22}Cu_2N_{10}O_{12}$	$C_{46}H_{52}Cu_4N_{14}O_4$•4($NO_3$)	$C_{54}H_{44}Cu_4N_{19}O_{20}$
Formula Mass	733.57	1367.45	1533.24
Crystal System	Orthorhombic	Monoclinic	Monoclinic
a/Å	17.6399(3)	20.7889(7)	8.5679(3)
b/Å	9.21560(13)	19.4936(4)	9.3862(3)
c/Å	33.6259(5)	8.6159(3)	20.5910(8)
α/°	90.00	90.00	90.00
β/°	90.00	113.996(4)	101.038(2)
γ/°	90.00	90.00	90.00
Unit cell volume/Å^3	5466.29(14)	3189.82(16)	1625.29(10)
Temperature/K	120.0(1)	120.0(1)	113(2)
Space group	*Pbca*	*C*2/*m*	*P*2/*n*
No. of formula units per unit cell, *Z*	8	2	1
Radiation type	CuKα	CuKα	MoKα
No. of reflections measured	12073	8264	26978
No. of independent reflections	4704	2834	2882
R_{int}	0.0233	0.0197	0.0608
Final R_1 values ($I > 2\sigma(I)$)	0.0262	0.0466	0.0505
Final $wR(F^2)$ values ($I > 2\sigma(I)$)	0.0635	0.1340	0.1419
Final R_1 values (all data)	0.0334	0.0511	0.0669
Final $wR(F^2)$ values (all data)	0.0671	0.1383	0.1538

Table A8 Crystallographic Data for compound **3.13**

Compound reference	**3.13**
Chemical formula	$C_{23}H_{22}Cu_2N_8$
Formula Mass	537.57
Crystal System	Orthorhombic
a/Å	9.0732(3)
b/Å	28.1429(9)
c/Å	8.6165(2)
α/°	90.00
β/°	90.00
γ/°	90.00
Unit cell volume/Å^3	2200.19(11)
Temperature/K	113(2)
Space group	*Pccn*
No. of formula units per unit cell, *Z*	4
Radiation type	MoKα
No. of reflections measured	28507
No. of independent reflections	1946
R_{int}	0.0591
Final R_1 values ($I > 2\sigma(I)$)	0.0359
Final $wR(F^2)$ values ($I > 2\sigma(I)$)	0.0857
Final R_1 values (all data)	0.0423
Final $wR(F^2)$ values (all data)	0.0893

Table A9 Crystallographic Data for compounds **L4.2**, **L4.5** and **L4.6**

Compound reference	**L4.2**	**L4.5**	**L4.6**
Chemical formula	$C_{12}H_{12}N_4$	$C_{34}H_{26}N_8$	$C_{28}H_{22}N_8$
Formula Mass	212.26	546.63	470.54
Crystal System	Orthorhombic	Monoclinic	Monoclinic
a/Å	7.9751(7)	22.8850(13)	15.2080(8)
b/Å	12.8730(13)	5.8864(4)	9.8349(5)
c/Å	20.639(2)	20.0948(12)	15.8712(9)
α/°	90.00	90.00	90.00
β/°	90.00	100.118(4)	103.713(4)
γ/°	90.00	90.00	90.00
Unit cell volume/Å^3	2118.9(4)	2664.9(3)	2306.2(2)
Temperature/K	113(2)	112(2)	113(2)
Space group	*Pca*21	*C*2/*c*	*C*2/*c*
No. of formula units per unit cell, *Z*	8	4	4
Radiation type	MoKα	MoKα	MoKα
No. of reflections measured	33238	13617	12822
No. of independent reflections	3755	2342	2047
R_{int}	0.0974	0.0482	0.0406
Final R_1 values ($I > 2\sigma(I)$)	0.0437	0.0547	0.0410
Final $wR(F^2)$ values ($I > 2\sigma(I)$)	0.0875	0.1389	0.0971
Final R_1 values (all data)	0.0686	0.0829	0.0608
Final $wR(F^2)$ values (all data)	0.0986	0.1570	0.1083
Flack Parameter	0(2)		

Table A10 Crystallographic Data for compounds **4.11**, **4.12** and **4.13**

Compound reference	**4.11**	**4.12**	**4.13**
Chemical formula	$C_{20}H_{16}N_9O_3Zn{\bullet}NO_3$	$C_{26}H_{29}MnN_9O{\bullet}2(ClO_4)$	$C_{22}H_{20}CuN_9O_3{\bullet}NO_3$
Formula Mass	557.80	737.42	584.02
Crystal System	Orthorhombic	Triclinic	Monoclinic
a/Å	17.9967(6)	9.2388(4)	8.38106(12)
b/Å	17.0731(5)	10.5983(5)	9.70111(12)
c/Å	7.1411(2)	17.1164(8)	14.61186(19)
α/°	90.00	78.849(3)	90.00
β/°	90.00	75.370(3)	93.7418(12)
γ/°	90.00	76.372(3)	90.00
Unit cell volume/Å^3	2194.17(12)	1559.91(12)	1185.49(3)
Temperature/K	110(2)	114(2)	120.0(1)
Space group	*Pnna*	$P\bar{1}$	$P2_1$
No. of formula units per unit cell, *Z*	4	2	2
Radiation type	MoKα	MoKα	CuKα
No. of reflections measured	40038	29508	14560
No. of independent reflections	2530	5514	4083
R_{int}	0.0576	0.0990	0.0195
Final R_1 values ($I > 2\sigma(I)$)	0.0354	0.0492	0.0239
Final $wR(F^2)$ values ($I > 2\sigma(I)$)	0.1001	0.1080	0.0627
Final R_1 values (all data)	0.0551	0.0889	0.0241
Final $wR(F^2)$ values (all data)	0.1081	0.1189	0.0628
Flack Parameter			0.00(15)

Table A11 Crystallographic Data for compounds **4.14**, **4.15** and **4.16**

Compound reference	**4.14**	**4.15**	**4.16**
Chemical formula	$C_{14}H_{11}Cl_2CuN_4$	$3(C_{56}H_{48}Cu_2N_{16}O_2)\bullet12(ClO_4)\bullet4(C_2H_3N)\bullet(C_7H_7)\bullet(C_7H_5)\bullet6(O)$	$C_{68}H_{56}Cu_2N_{16}O_2\bullet4(BF_4)$
Formula Mass	369.71	4946.40	1603.61
Crystal System	Orthorhombic	Monoclinic	Monoclinic
a/Å	13.1443(15)	32.0348(12)	9.9837(4)
b/Å	12.9478(9)	22.4812(9)	31.5048(13)
c/Å	16.2550(18)	16.2814(7)	15.4944(6)
α/°	90.00	90.00	90.00
β/°	90.00	113.141(2)	94.777(2)
γ/°	90.00	90.00	90.00
Unit cell volume/Å^3	2766.4(5)	10782.1(8)	4856.6(3)
Temperature/K	113(2)	113(2)	113(2)
Space group	*Pbca*	*C*2/*m*	$P2_1/n$
No. of formula units per unit cell, *Z*	8	2	2
Radiation type	MoKα	MoKα	MoKα
No. of reflections measured	12857	65850	89185
No. of independent reflections	2431	10310	8591
R_{int}	0.0781	0.1097	0.0611
Final R_1 values ($I > 2\sigma(I)$)	0.0625	0.0722	0.0714
Final $wR(F^2)$ values ($I > 2\sigma(I)$)	0.1617	0.1875	0.2146
Final R_1 values (all data)	0.1113	0.1418	0.0899
Final $wR(F^2)$ values (all data)	0.1921	0.2285	0.2272

Table A12 Crystallographic Data for compounds **4.17**, **4.18** and **4.19**

Compound reference	**4.17**	**4.18**	**4.19**
Chemical formula	$C_{56}H_{44}Cu_2N_{18}O_6\bullet2(C_2H_3N)\bullet2(NO_3)$	$2(C_{28}H_{22}Cl_4Cu_2N_8)\bullet2(CN_{0.5})$	$C_{69}H_{60}N_{24}Zn_2\bullet5(CH_3NO_2)\bullet4(CF_3O_3S)$
Formula Mass	1398.30	1516.86	2257.65
Crystal System	Monoclinic	Triclinic	Monoclinic
a/Å	11.7585(6)	11.4487(6)	19.2654(3)
b/Å	20.1001(11)	11.5507(6)	21.8353(2)
c/Å	14.1309(8)	12.1914(6)	23.4402(3)
α/°	90.00	81.823(3)	90.00
β/°	114.922(4)	67.556(3)	105.8548(13)
γ/°	90.00	79.806(3)	90.00
Unit cell volume/Å^3	3028.8(3)	1461.61(13)	9485.36(19)
Temperature/K	113(2)	113(2)	120.0(1)
Space group	$P2_1/c$	$P\bar{1}$	$P2_1/n$
No. of formula units per unit cell, *Z*	2	1	4
Radiation type	MoKα	MoKα	CuKα
No. of reflections measured	35120	28059	33067
No. of independent reflections	5350	5193	16328
R_{int}	0.1194	0.0628	0.0291
Final R_1 values ($I > 2\sigma(I)$)	0.0737	0.0472	0.0593
Final $wR(F^2)$ values ($I > 2\sigma(I)$)	0.1688	0.1099	0.1599
Final R_1 values (all data)	0.1519	0.0757	0.0736
Final $wR(F^2)$ values (all data)	0.2044	0.1237	0.1737

Table A13 Crystallographic Data for compounds **L5.1**, **L5.2** and **H_2L5.7**

Compound reference	**L5.1**	**L5.2**	**H_2L5.7**
Chemical formula	$C_{12}H_9N_3$	$C_{12}H_9N_3$	$2(C_8H_6N_2O_2)\bullet H_2O$
Formula Mass	195.22	195.22	342.31
Crystal System	Orthorhombic	Orthorhombic	Triclinic
a/Å	5.0093(4)	5.6717(6)	4.9524(7)
b/Å	13.0798(9)	11.2569(11)	10.9756(9)
c/Å	14.2500(10)	14.8452(16)	14.6313(15)
α/°	90.00	90.00	81.698(8)
β/°	90.00	90.00	83.854(10)
γ/°	90.00	90.00	78.805(9)
Unit cell volume/Å^3	933.67(12)	947.80(17)	769.43(15)
Temperature/K	120.0(1)	120.0(1)	120.0(1)
Space group	$P2_12_12_1$	$P2_12_12_1$	$P\bar{1}$
No. of formula units per unit cell, *Z*	4	4	2
Radiation type	CuKα	CuKα	CuKα
No. of reflections measured	3408	4430	4382
No. of independent reflections	1603	1609	2637
R_{int}	0.0167	0.0255	0.0259
Final R_1 values ($I > 2\sigma(I)$)	0.0316	0.0382	0.0405
Final $wR(F^2)$ values ($I > 2\sigma(I)$)	0.0844	0.0921	0.1017
Final R_1 values (all data)	0.0338	0.0467	0.0497
Final $wR(F^2)$ values (all data)	0.0861	0.0997	0.1095
Flack Parameter	-0.5(6)	0.1(6)	

Table A14 Crystallographic Data for compounds **5.16**, **5.17** and **5.18**

Compound reference	**5.16**	**5.17**	**5.18**
Chemical formula	$C_{24}H_{18}CuN_7O_3$ $\bullet NO_3\bullet 1.5(H_2O)$	$C_{24}H_{18}CuN_7O_3\bullet NO_3$	$C_{10}H_9CuN_3O_3$
Formula Mass	605.03	578.00	282.74
Crystal System	Monoclinic	Monoclinic	Tetragonal
a/Å	7.2872(2)	18.0728(19)	16.6545(16)
b/Å	15.9102(5)	7.5078(6)	16.6545(16)
c/Å	21.2623(6)	18.9452(19)	16.3362(18)
α/°	90.00	90.00	90.00
β/°	99.328(3)	115.277(13)	90.00
γ/°	90.00	90.00	90.00
Unit cell volume/Å^3	2432.58(13)	2324.5(4)	4531.2(8)
Temperature/K	120.0(1)	120.0(1)	112(2)
Space group	$P2_1/n$	$P2_1/c$	$I41/a$
No. of formula units per unit cell, *Z*	4	4	16
Radiation type	CuKα	CuKα	MoKα
No. of reflections measured	8346	8353	9990
No. of independent reflections	4196	3992	1998
R_{int}	0.0284	0.0382	0.0853
Final R_1 values ($I > 2\sigma(I)$)	0.0535	0.0482	0.0461
Final $wR(F^2)$ values ($I > 2\sigma(I)$)	0.1339	0.1239	0.0962
Final R_1 values (all data)	0.0707	0.0602	0.0882
Final $wR(F^2)$ values (all data)	0.1471	0.1327	0.1129

Table A15 Crystallographic Data for compounds **5.19**, **5.20** and **5.21**

Compound reference	**5.19**	**5.20**	**5.21**
Chemical formula	$C_{18}H_{18}CdN_4O_6$•2(CH_4O)	$C_{32}H_{24}F_6N_8O_8SiZn$	$C_{16}H_{10}CuN_4O_4$
Formula Mass	562.85	856.05	385.82
Crystal System	Orthorhombic	Tetragonal	Trigonal
a/Å	15.1574(4)	17.4234(3)	33.6525(6)
b/Å	11.3084(3)	17.4234(3)	33.6525(6)
c/Å	13.5468(5)	15.1625(4)	4.80132(11)
α/°	90.00	90.00	90.00
β/°	90.00	90.00	90.00
γ/°	90.00	90.00	120.00
Unit cell volume/Å^3	2321.99(13)	4602.97(17)	4708.98(16)
Temperature/K	120.0(1)	120.0(1)	120.0(1)
Space group	*Pca*21	*P4/ncc*	$R\bar{3}$
No. of formula units per unit cell, *Z*	4	4	9
Radiation type	CuKα	CuKα	CuKα
No. of reflections measured	8852	9088	26227
No. of independent reflections	3484	2322	1883
R_{int}	0.0344	0.0222	0.0274
Final R_1 values ($I > 2\sigma(I)$)	0.0517	0.0288	0.0379
Final $wR(F^2)$ values ($I > 2\sigma(I)$)	0.1324	0.0728	0.1331
Final R_1 values (all data)	0.0567	0.0317	0.0396
Final $wR(F^2)$ values (all data)	0.1391	0.0745	0.1348
Flack Parameter	-0.013(17)		

Table A16 Crystallographic Data for compounds **5.22** and **5.23**

Compound reference	**5.22**	**5.23**
Chemical formula	$C_{36}H_{32}Cu_3N_{10}O_{16}$ •$_1$.5($C_{12}H_{12}$)•2(H_2O)	$C_{16}H_{10}CuN_4O_4$ •CHO•H_2O
Formula Mass	1321.69	432.85
Crystal System	Triclinic	Monoclinic
a/Å	10.2213(6)	25.730(2)
b/Å	11.4215(5)	4.5836(2)
c/Å	14.0872(7)	17.8406(13)
α/°	105.934(4)	90.00
β/°	101.559(4)	124.140(11)
γ/°	104.354(4)	90.00
Unit cell volume/Å^3	1467.04(13)	1741.5(3)
Temperature/K	120.0(1)	120.0(1)
Space group	$P\bar{1}$	*C2/c*
No. of formula units per unit cell, *Z*	1	4
Radiation type	CuKα	CuKα
No. of reflections measured	20765	4941
No. of independent reflections	5002	1509
R_{int}	0.0333	0.0262
Final R_1 values ($I > 2\sigma(I)$)	0.0535	0.0421
Final $wR(F^2)$ values ($I > 2\sigma(I)$)	0.1518	0.1163
Final R_1 values (all data)	0.0599	0.0438
Final $wR(F^2)$ values (all data)	0.1597	0.1177

Chapter 6

Table A17 Crystallographic Data for compounds **6.11**, **6.12** and **6.13**

Compound reference	**6.11**	**6.12**	**6.13**
Chemical formula	$C_{40}H_{41}CuN_7O_4$ •2(ClO_4)	$C_{18}H_{18}CuN_4O_6$	$C_{34}H_{34}Cu_2N_6O_{14}S_2$ •H_2O•C_2H_6O
Formula Mass	946.24	449.90	1005.96
Crystal System	Orthorhombic	Triclinic	Monoclinic
a/Å	11.3951(7)	8.9455(18)	18.9584(6)
b/Å	18.8074(14)	8.9661(12)	7.7343(2)
c/Å	9.5857(6)	12.325(2)	27.5712(8)
α/°	90.00	85.304(12)	90.00
β/°	90.00	70.334(17)	90.203(2)
γ/°	90.00	87.355(13)	90.00
Unit cell volume/Å^3	2054.3(2)	927.6(3)	4042.7(2)
Temperature/K	113(2)	120.0(1)	113(2)
Space group	$P2_12_12$	$P\bar{1}$	*Cc*
No. of formula units per unit cell, *Z*	2	2	4
Radiation type	MoKα	CuKα	MoKα
No. of reflections measured	31082	5934	43496
No. of independent reflections	3642	3197	9274
R_{int}	0.1463	0.0758	0.0742
Final R_1 values ($I > 2\sigma(I)$)	0.0446	0.0993	0.0438
Final $wR(F^2)$ values ($I > 2\sigma(I)$)	0.0565	0.2630	0.0933
Final R_1 values (all data)	0.1077	0.1297	0.0577
Final $wR(F^2)$ values (all data)	0.0654	0.2888	0.0995
Flack Parameter	0.026(18)		0.530(11)

Table A18 Crystallographic Data for compounds **6.14**, **6.15** and **6.16**

Compound reference	**6.14**	**6.15**	**6.16**
Chemical formula	$C_{20}H_{18}Cu_2N_6O_6$	$C_9H_5CuN_3O_2$	$C_{16}H_{14}CoN_8O_6$
Formula Mass	565.48	250.70	473.28
Crystal System	Triclinic	Monoclinic	Monoclinic
a/Å	5.0428(3)	7.9539(4)	10.5213(3)
b/Å	9.7974(5)	13.8622(7)	11.7161(3)
c/Å	10.9673(6)	7.4109(4)	7.3655(2)
α/°	111.019(3)	90.00	90.00
β/°	90.989(4)	93.976(3)	98.150(3)
γ/°	93.939(4)	90.00	90.00
Unit cell volume/Å^3	504.09(5)	815.15(7)	898.77(5)
Temperature/K	112(2)	113(2)	120.0(1)
Space group	$P\bar{1}$	$P2_1/c$	$P2_1/c$
No. of formula units per unit cell, *Z*	1	4	2
Radiation type	MoKα	MoKα	CuKα
No. of reflections measured	7947	21587	2703
No. of independent reflections	1771	2504	1554
R_{int}	0.0399	0.0650	0.0169
Final R_1 values ($I > 2\sigma(I)$)	0.0265	0.0320	0.0276
Final $wR(F^2)$ values ($I > 2\sigma(I)$)	0.0552	0.0970	0.0730
Final R_1 values (all data)	0.0346	0.0485	0.0296
Final $wR(F^2)$ values (all data)	0.0582	0.1119	0.0744

Table A19 Crystallographic Data for compounds **6.17** and **6.18**

Compound reference	**6.17**	**6.18**
Chemical formula	$C_{16}H_{14}Co_2N_8O_7$	$C_9H_{11}CuN_3O_3$
Formula Mass	548.21	272.75
Crystal System	Monoclinic	Tetragonal
a/Å	16.4804(11)	18.0584(8)
b/Å	17.6769(15)	18.0584(8)
c/Å	8.5148(5)	18.3413(11)
α/°	90.00	90.00
β/°	99.192(6)	90.00
γ/°	90.00	90.00
Unit cell volume/Å^3	2448.7(3)	5981.2(5)
Temperature/K	120.0(1)	113(2)
Space group	$P2_1/c$	$I4_1/a$
No. of formula units per unit cell, *Z*	4	16
Radiation type	CuKα	MoKα
No. of reflections measured	8332	36629
No. of independent reflections	4796	2647
R_{int}	0.0526	0.0626
Final R_1 values ($I > 2\sigma(I)$)	0.0745	0.0651
Final $wR(F^2)$ values ($I > 2\sigma(I)$)	0.1920	0.1589
Final R_1 values (all data)	0.0993	0.0702
Final $wR(F^2)$ values (all data)	0.2094	0.1620

Appendix 2

Hydrogen Bonding Parameters

Table A20: Hydrogen bonding parameters for structures in Chapter 2

Compound	D	H	A	$d_{(D-H)}$ (Å)	$d_{(H\cdots A)}$ (Å)	$d_{(D\cdots A)}$ (Å)	$<_{(DHA)}$ (°)	Symmetry Code used to generate acceptor atom
H_2L2.5	O1	H1	N10	0.84	1.89	2.729(2)	171.7	1-y,-1/2+x,1/4+z
	O13	H13	N22	0.84	1.96	2.798(3)	174.9	1-y,-1/2+x,1/4+z
HL2.6·HNO_3	N13	H13	O19	0.86	1.86	2.707(3)	169.5	-1+x,+y,+z
	O3	H3	O1	0.82	1.81	2.629(2)	172	
	N12	H12	O20	0.86	1.92	2.772(3)	170.4	-x,-y,1-z
HL2.6	O51	H51	N12	0.82	1.82	2.636(3)	171.3	1-x,1-y,1-z
	N60	H60	O3	0.86	1.99	2.787(3)	153	1-x,1-y,-z
	O1	H1	N45	0.82	1.82	2.622(3)	166.3	1-x,1-y,-z
	N13	H13	O33	0.86	2.07	2.844(3)	150.3	2-x,1-y,1-z
	O35	H35	N29	0.82	1.83	2.635(3)	168.8	1-x,1-y,1-z
	N44	H44	O17	0.86	2.13	2.910(3)	150.2	1-x,1-y,-z
	O19	H19	N61	0.82	1.84	2.654(3)	172.7	-x,1-y,-z
	N28	H28	O49	0.86	2.06	2.854(3)	152.7	1-x,1-y,1-z
HL2.7	N14	H14	O3	0.915(15)	1.934(15)	2.8008(17)	157.4(17)	1/2-x,1-y,-1/2+z
	O1	H1	N13	0.830(5)	1.829(6)	2.6520(16)	172(2)	+x,1/2-y,1/2+z
2.20	N13	H13	O4	0.88	1.98	2.791(4)	152.1	
2.21	N26	H26	O23	0.86	1.92	2.710(6)	152.4	
	N36	H36	O4	0.86	2.11	2.775(6)	133.9	
2.22	N3	H3	O41	0.857(15)	1.924(16)	2.757(2)	163.7(19)	
	N19	H19	O26	0.839(16)	1.866(17)	2.680(2)	163(2)	
2.23	N12	H12	O34	0.86	2.08	2.833(4)	145.3	
	N3	H3	O18	0.86	2.05	2.800(4)	145.8	
2.24	N4	H4	O18	0.843(19)	1.84(2)	2.667(4)	167(5)	1/2-y,1-x,-1/4+z
	N20	H20	O34	0.85(2)	1.90(3)	2.729(4)	166(6)	1-y,3/2-x,1/4+z
2.25	O36	H36A	O34	0.85	1.97	2.806(3)	168	-1/2+x,1/2-y,-1/2+z
	O36	H36B	O42	0.85	2.04	2.863(3)	162	1-x,1-y,1-z
	N15	H15	O36	0.86	1.95	2.764(3)	156.4	1-x,+y,3/2-z
	N20	H20	O34	0.86	1.95	2.757(3)	154.6	+x,-y,-1/2+z

Table A21: Hydrogen bonding parameters for structures in Chapter 3

Compound	D	H	A	$d_{(D-H)}$ (Å)	$d_{(H\cdots A)}$ (Å)	$d_{(D\cdots A)}$ (Å)	$<_{(DHA)}$ (°)	Symmetry Code used to generate acceptor atom
3.7	O4	H4A	Cl3	0.854(10)	2.37(2)	3.168(3)	156(5)	1/2-x,3/2-y,-z
	O4	H4B	Cl32	0.75(5)	2.30(5)	3.045(4)	177(5)	1/2-x,-1/2+y,1/2-z
3.10	O27	H27A	O18	0.857(10)	1.871(10)	2.726(2)	176(3)	
	O26	H26A	O22	0.844(10)	1.941(10)	2.784(2)	177(3)	
	O26	H26B	O27	0.837(10)	1.958(13)	2.774(2)	165(3)	
	O25	H25A	O16	0.857(10)	1.936(11)	2.781(2)	169(3)	
3.12	O16	H16	O25	0.84(2)	2.29(3)	2.866(6)	126(3)	1/2+x,1/2+y,+z;
	O16	H16	O22	0.84(2)	2.11(2)	2.856(8)	147(2)	1/2+x,1/2+y,+z;

Table A22: Hydrogen bonding parameters for structures in Chapter 4

Compound	D	H	A	$d_{(D-H)}$ (Å)	$d_{(H\cdots A)}$ (Å)	$d_{(D\cdots A)}$ (Å)	$<_{(DHA)}$ (°)	Symmetry Code used to generate acceptor atom
L4.2	N23	H23	N1	0.86	2.19	3.028(3)	163.5	-1/2+x,2-y,+z
	N7	H7	N17	0.86	2.05	2.880(3)	162	1/2+x,2-y,+z
4.11	N11	H11	O21	0.81(3)	1.94(3)	2.741(4)	167(3)	+x,3/2-y,1/2-z
4.12	O34	H34A	O44	0.842(10)	1.95(2)	2.772(5)	163(6)	1-x,2-y,1-z
	O34	H34B	O40	0.850(10)	1.943(11)	2.792(4)	176(4)	+x,1+y,+z
	N29	H29	O40	0.82(4)	2.10(4)	2.861(5)	154(4)	1-x,1-y,1-z
	N10	H10	O46	0.97(5)	1.99(5)	2.918(5)	159(4)	1-x,1-y,1-z
4.15	O39	H39A	O65	0.851(10)	2.01(9)	2.776(7)	149(17)	
	O39	H39B	O75	0.852(10)	1.877(18)	2.721(9)	171(9)	1-x,1-y,1-z
	O39	H39B	O74	0.852(10)	2.43(13)	2.915(14)	117(11)	1-x,1-y,1-z
	O40	H40	O62	0.847(7)	2.20(10)	2.944(7)	146(16)	
	O40	H40	O63	0.847(7)	2.41(18)	2.969(8)	124(18)	
4.16	O58	H1A	F51	0.849(10)	2.56(5)	2.717(4)	92(4)	-1/2+x,3/2-y,-1/2+z
	O58	H1B	F47	0.841(10)	2.67(4)	2.733(5)	86(3)	1/2+x,3/2-y,-1/2+z

Table A23: Hydrogen bonding parameters for structures in Chapter 5

Compound	D	H	A	$d_{(D-H)}$ (Å)	$d_{(H\cdots A)}$ (Å)	$d_{(D\cdots A)}$ (Å)	$<_{(DHA)}$ (°)	Symmetry Code used to generate acceptor atom
H_2L5.7	O11	H11	O25	0.84	1.84	2.670(2)	172.3	
	O23	H23	O25	0.84	1.84	2.676(2)	177.8	-x,-y,1-z
	N1	H1	O12	0.88	1.97	2.816(2)	160.7	1-x,1-y,-z
	N13	H13	O24	0.88	2.01	2.826(2)	152.8	-1-x,-y,1-z
	O25	H25A	N14	0.85	2.00	2.841 (2)	171	1+x,+y,+z
	O25	H25B	N2	0.85	1.97	2.809(2)	168.9	1-x,1-y,-z
5.16	O2	H2B	O3	0.85	2.18	2.836(10)	134.2	
	O10	H10B	O6	0.85	1.52	2.359(17)	166.5	
5.18	N16	H16A	O13	0.86	2.12	2.873(5)	146.2	
	N16	H16B	O14	0.86	1.92	2.781(5)	174	5/4-y,-1/4+x,-1/4+z
5.19	N3	H3	O4	0.88	1.86	2.721(6)	165.5	-1/2+x,-1-y,+
	N7	H7	O5	0.88	1.85	2.718(7)	168.1	1/2+x,-y,+z
	O13	H13	O14	0.847(10)	1.88(3)	2.694(7)	159(8)	
	O14	H14	O5	0.84	1.95	2.747(7)	158.7	-1/2-x,+y,-1/2+z
	O15	H15	O4	0.84	1.93	2.729(8)	157.9	-1/2-x,+y,1/2+z
	O20	H20	O15	0.859(18)	1.867(18)	2.713(7)	168(10)	
5.20	O13	H13	F16	0.84	1.79	2.6145(13)	165.2	1-y,1-x,1/2-z
	N3	H3	O12	0.88	1.93	2.7246(15)	149.4	1/2+y,1-x,1-z
5.21	N3	H3	O13	0.860(18)	1.99(3)	2.721(2)	143(3)	+x,+y,1+z
5.22	O27	H27	O36	0.83(6)	2.02(6)	2.757(7)	148(5)	1+x,+y,+z
	O27	H27	O35	0.83(6)	2.00(6)	2.713(8)	144(5)	1+x,+y,+z
	N16	H16	O35	0.88	1.90	2.759(9)	163.4	1+x,1+y,+z
	N4	H4	O33	0.88	2.05	2.860(7)	152.5	-1-x,1-y,-z
	N4	H4	O37	0.88	1.89	2.760(8)	172.5	-1-x,1-y,-z
	O37	H37A	N31	0.85	1.61	2.360(11)	145.2	
	O37	H37B	O32	0.85	2.26	2.872(8)	129.3	-2-x,1-y,-z
5.23	N3	H3	O14	0.88	1.95	2.819(3)	169.7	+x,-1+y,+z
	O14	H14	O13	0.97	1.88	2.833(3)	168.2	1-x,1-y,1-z

Table A24: Hydrogen bonding parameters for structures in Chapter 6

Compound	D	H	A	$d_{(D-H)}$ (Å)	$d_{(H\cdots A)}$ (Å)	$d_{(D\cdots A)}$ (Å)	$<_{(DHA)}$ (°)	Symmetry Code used to generate acceptor atom
6.12	O28	H28	O23	0.851(10)	1.751(19)	2.595(7)	171(9)	
6.13	O34	H34	O5	0.84	1.93	2.753(4)	166.6	1/2+x,5/2-y,1/2+z
	O55	H55	O8	0.84	1.87	2.706(4)	176.8	-1/2+x,3/2-y,-1/2+z
	O58	H58A	O6	0.861(10)	1.87(2)	2.650(4)	150(4)	
	O58	H58B	O12	0.855(10)	1.810(15)	2.639(4)	163(4)	+x,1+y,+z
	O57	H57A	O7	0.855(10)	1.736(11)	2.587(4)	173(3)	+x,-1+y,+z
	O57	H57B	O11	0.863(10)	1.735(16)	2.569(4)	162(4)	
	O59	H59A	O57	0.846(10)	2.024(11)	2.870(4)	179(5)	1/2+x,5/2-y,1/2+z
	O1	H1	O59	0.84	2.00	2.838(5)	174.8	-1/2+x,-1/2+y,+z
	O59	H59B	O33	0.828(19)	1.98(2)	2.797(4)	170(5)	
6.14	O16	H16	O15	0.845(10)	1.821(11)	2.662(3)	174(3)	-1+x,+y,+z
6.16	N7	H7	N14	0.88	2.24	3.099(2)	167.1	-1-x,1/2+y,1/2-z
	O16	H16A	O4	0.869(17)	1.829(18)	2.6688(18)	162(2)	-x,-1/2+y,1/2-z
	O16	H16B	O4	0.881(17)	1.804(18)	2.6678(18)	166(3)	+x,3/2-y,1/2+z
6.17	O32	H32A	N30	0.86	2.06	2.820(8)	146.7	+x,3/2-y,1/2+z
	O33	H33A	O18	0.87	1.78	2.642(7)	171.5	1-x,1-y,2-z
	O32	H32B	O4	0.85(2)	1.75(3)	2.591(7)	169(10)	-1+x,+y,+z

Appendix 3

Selected Bond Lengths & Angles

Table A25: Selected bond lengths (Å) and angles (°) from structures in Chapter 2

2.20						Symmetry Codes
Co1-O2	1.926(2)	O2-Co1-O2^{1}	108.87(14)	O2^{1}-Co1-N12^{1}	115.00(10)	1: 1-y,1-x,1/6-z
Co1-N12	1.988(3)	O2-Co1-N12^{1}	100.20(10)	N12-Co1-N12^{1}	117.92(10)	
2.21						
Co1-O24	1.936(3)	O24-Co1-O2	111.94(15)	O2-Co1-N25	100.18(16)	
Co1-O2	1.965(3)	O24-Co1-N25	111.17(17)	O2-Co1-N35	119.67(16)	
Co1-N25	2.003(4)	O24-Co1-N35	106.32(16)	N35-Co1-N25	107.32(16)	
Co1-N35	1.992(4)					
2.22						
Co1-O42	1.9424(14)	O42-Co1-O24	98.80(6)	O24-Co1-N2	110.95(7)	
Co1-O24	1.9466(14)	O42-Co1-N2	108.17(6)	O24-Co1-N20	112.52(7)	
Co1-N2	1.9962(17)	O42-Co1-N20	115.37(7)	N2-Co1-N20	110.48(7)	
Co1-N20	1.9989(17)					
2.23						
Co1-O16	1.928(3)	O16-Co1-N2	108.99(13)	N2-Co1-N11	106.93(12)	
Co1-N2	2.000(3)	O16-Co1-O33	106.76(12)	O33-Co1-N2	115.54(12)	
Co1-O33	1.929(3)	O16-Co1-N11	106.24(13)	O33-Co1-N11	111.98(13)	
Co1-N11	2.002(3)					
2.24						
Co1-O33	1.915(2)	O33^{1}-Co1-O33	101.67(17)	O17^{3}-Co2-O17	109.16(15)	1: 1-x,2-y,+z
Co1-N19	2.003(3)	O33-Co1-N19^{2}	116.49(13)	O17-Co2-N3^{4}	111.31(12)	2: -1/2+y,1+x,-1/4+z
Co2-O17	1.938(2)	O33^{1}-Co1-N19^{2}	110.64(12)	O17^{3}-Co2-N3^{4}	111.08(12)	3: 1-x,-y,+z
Co2-N3	2.017(3)	N19^{2}-Co1-N19^{3}	101.58(16)	N3^{5}-Co1-N3^{6}	102.80(16)	4: 1-x,-y,+z
						5: 1-y,1/2-x,1/4+z
						6: +y,-1/2+x,1/4+z
2.25						
Co1-O35^{1}	1.941(2)	O35^{1}-Co1-O2	123.40(9)	O2-Co1-N19	109.35(8)	1: +x,-y,-1/2+z
Co1-O2	2.000(2)	O35^{1}-Co1-N19	112.82(8)	O2-Co1-N14^{1}	104.24(8)	
Co1-N19	2.010(2)	O35^{1}-Co1-N14^{1}	97.03(8)	N19-Co1-N14^{1}	107.80(9)	
Co1-N14^{1}	2.040(2)					

Table A26: Selected bond lengths (Å) and angles (°) from structures in Chapter 3

3.5A						Symmetry Codes
Fe1-N18	1.937(4)	N18-Fe1-N18^{1}	92.11(16)	N10^{1}-Fe2-N10	91.11(17)	1: 1-y,+x-y,+z
Fe1-N20	1.973(4)	N18-Fe1-N20	91.23(15)	N10-Fe2-N3	80.12(17)	
Fe2-N10	1.953(4)	N18^{1}-Fe1-N20	80.64(16)	N10-Fe2-N3^{1}	91.38(17)	
Fe2-N3	1.995(4)	N18^{1}-Fe1-N20	172.12(16)	N10^{1}-Fe2-N3	170.92(17)	
		N20^{1}-Fe1-N20	96.36(15)	N3^{1}-Fe2-N3	97.64(17)	
3.5B						
Fe1-N17	1.928(7)	N49-Fe2-N3	96.1(3)	N17-Fe1-N67	171.1(3)	
Fe1-N67	1.975(7)	N49-Fe2-N48	94.7(3)	N17-Fe1-N26	90.2(3)	
Fe1-N33	1.926(7)	N56-Fe2-N49	81.3(3)	N17-Fe1-N63	91.1(3)	
Fe1-N26	1.967(7)	N56-Fe2-N3	171.4(3)	N17-Fe1-N21	81.8(3)	
Fe1-N63	1.929(7)	N56-Fe2-N48	92.0(3)	N67-Fe1-N21	95.2(3)	
Fe1-N21	1.978(7)	N41-Fe2-N49	172.1(3)	N33-Fe1-N17	91.9(3)	
Fe2-N49	1.971(6)	N41-Fe2-N56	92.1(2)	N33-Fe1-N67	91.7(3)	
Fe2-N56	1.937(6)	N41-Fe2-N10	92.4(3)	N33-Fe1-N26	81.0(3)	
Fe2-N41	1.925(6)	N41-Fe2-N3	91.2(2)	N33-Fe1-N63	91.6(3)	
Fe2-N10	1.936(6)	N41-Fe2-N48	81.2(3)	N33-Fe1-N21	172.6(3)	
Fe2-N3	1.995(6)	N10-Fe2-N49	91.9(3)	N26-Fe1-N67	98.4(3)	
Fe2-N48	1.979(6)	N10-Fe2-N3	81.2(3)	N26-Fe1-N21	95.2(3)	
		N10-Fe2-N48	173.2(3)	N63-Fe1-N67	80.6(3)	
		N48-Fe2-N3	96.4(3)	N63-Fe1-N26	172.5(3)	
		N10-Fe2-N56	90.7(3)	N63-Fe1-N21	92.2(3)	
3.6						
Co1-Cl3	2.4116(12)	O4-Co1-Cl3	95.19(10)	N27-Co1-N5	176.05(13)	
Co1-O4	2.114(3)	O4-Co1-N21	91.23(13)	N12-Co1-Cl3	92.97(10)	
Co1-N21	2.133(4)	O4-Co1-N27	89.15(13)	N12-Co1-O4	160.81(13)	
Co1-N27	2.163(3)	O4-Co1-N5	89.43(13)	N12-Co1-N21	85.23(13)	
Co1-N12	2.083(3)	N21-Co1-Cl3	164.84(10)	N12-Co1-N27	107.86(13)	
Co1-N5	2.187(3)	N21-Co1-N27	73.97(13)	N12-Co1-N5	74.15(12)	
		N21-Co1-N5	109.75(13)	N5-Co1-Cl3	84.08(10)	
		N27-Co1-Cl3	92.38(9)			
3.7						
Ni1-Cl3	2.3920(8)	Cl3-Ni1-Cl2	95.18(3)	N26-Ni1-Cl3	84.32(7)	
Ni1-Cl2	2.4262(8)	N4-Ni1-Cl3	92.36(7)	N26-Ni1-Cl2	91.35(7)	
Ni1-N4	2.099(3)	N4-Ni1-Cl2	92.22(7)	N26-Ni1-N20	76.74(10)	
Ni1-N20	2.143(2)	N4-Ni1-N20	100.27(10)	N11-Ni1-Cl3	168.25(7)	
Ni1-N26	2.120(3)	N4-Ni1-N26	175.32(9)	N11-Ni1-Cl2	88.13(7)	
Ni1-N11	2.113(2)	N4-Ni1-N11	76.22(9)	N11-Ni1-N20	85.55(7)	
		N20-Ni1-Cl3	93.91(7)	N11-Ni1-N26	106.91(10)	
		N20-Ni1-Cl2	164.22(7)			
3.8						
Cu1-Cl6	2.2244(8)	Cl5-Cu1-Cl6	97.67(3)	Cl3-Cu2-Cl4	100.64(4)	
Cu1-Cl5	2.2131(9)	N27-Cu1-Cl6	95.63(8)	N12-Cu2-Cl3	145.19(9)	
Cu1-N27	1.997(3)	N27-Cu1-Cl5	149.67(8)	N12-Cu2-Cl4	102.42(8)	
Cu1-N21	1.972(3)	N21-Cu1-Cl6	154.61(8)	N12-Cu2-N5	79.75(11)	
Cu2-Cl3	2.2052(9)	N21-Cu1-Cl5	98.19(8)	N5-Cu2-Cl3	95.52(9)	
Cu2-Cl4	2.2333(11)	N21-Cu1-N27	80.25(10)	N5-Cu2-Cl4	145.35(9)	
Cu2-N12	1.977(3)					
Cu2-N5	1.999(3)					

Table A26 continued: Selected bond lengths (Å) and angles (°) from structures in Chapter 3

3.9						Symmetry Codes
Cu1-O20	1.9764(14)	O20-Cu1-N9	169.96(6)	O16-Cu1-O20	89.24(6)	
Cu1-N9	2.0015(16)	O20-Cu1-N2	90.79(6)	O16-Cu1-N9	100.30(6)	
Cu1-N2	2.0467(17)	O20-Cu1-O24	90.30(6)	O16-Cu1-N2	168.31(7)	
Cu1-O24	2.2732(15)	N9-Cu1-N2	79.23(7)	O16-Cu1-O24	93.34(6)	
Cu1-O16	1.9563(14)	N2-Cu1-O24	98.34(6)	N9-Cu1-N2	79.23(7)	
3.10						
Cu2-N3	1.9886(18)	N3-Cu2-O39	166.85(7)	O35-Cu1-O37	94.85(6)	
Cu2-N10	1.9803(17)	N3-Cu2-O41	85.98(6)	O31-Cu1-O35	89.86(6)	
Cu2-O43	1.9593(15)	N10-Cu2-N3	80.69(7)	O31-Cu1-O37	82.01(6)	
Cu2-O39	1.9913(15)	N10-Cu2-O39	98.29(7)	O31-Cu1-N25	172.05(7)	
Cu2-41	2.3715(15)	N10-Cu2-O41	106.24(6)	O31-Cu1-N19	100.26(7)	
Cu1-O35	1.9996(15)	O43-Cu2-N3	95.22(7)	N25-Cu1-O35	91.67(7)	
Cu1-O31	1.9566(14)	O43-Cu2-N10	167.56(7)	N25-Cu1-O37	90.08(6)	
Cu1-O37	2.2907(15)	O43-Cu2-O39	88.34(6)	N25-Cu1-N19	80.82(7)	
Cu1-N25	1.9786(17)	O43-Cu2-O41	85.05(6)	N19-Cu1-O35	159.14(7)	
Cu1-N19	1.9878(18)	O39-Cu2-O41	81.71(6)	N19-Cu1-O37	104.53(6)	
3.11						
Cu1-N17	1.937(2)	N17-Cu1-O16	94.57(9)	O16-Cu1-N2	92.79(12)	Note: N17 and O19 constrained to occupy equivalent positions, identical angles not shown
Cu1-O16	1.9055(18)	N17-Cu1-N2	172.17(8)	O16-Cu1-N9	167.41(12)	
Cu1-O19	1.937(2)	N17-Cu1-N9	93.89(8)	N2-Cu1-N9	79.30(11)	
Cu1-N9	2.009(3)					
Cu1-N2	2.008(3)					
3.12						
Cu1-O1	1.973(3)	O1-Cu1-N2	176.99(15)	O4-Cu1-N2	94.80(14)	
Cu1-N2	1.982(4)	O1-Cu1-O17	91.93(14)	O4-Cu1-O17	88.35(14)	
Cu1-N3	1.961(4)	N2-Cu1-O17	90.94(15)	N3-Cu1-O4	173.29(13)	
Cu1-O4	1.970(3)	N3-Cu1-O1	99.6(13)	N3-Cu1-O17	96.84(15)	
Cu1-O17	2.376(4)	N23-Cu1-N2	80.91(15)	O4-Cu1-O1	84.41(12)	
3.13						
Cu1-N2	1.970(3)	N2-Cu1-N4	118.21(10)	$C3^{1}$-Cu1-N2	121.88(12)	1: -5/2-x,+y,-1/2+z
Cu1-N4	2.160(3)	N2-Cu1-N11	98.89(10)	$C3^{1}$-Cu1-N4	106.82(11)	
Cu1-N11	2.094(3)	N11-Cu1-N4	75.68(9)	$C3^{1}$-Cu1-N11	127.56(11)	
$Cu1-C3^{1}$	1.896(3)					

Table A27: Selected bond lengths (Å) and angles (°) from structures in Chapter 4

4.11						Symmetry Codes
Zn1-N8	2.070(2)	N8-Zn1-N8[1]	170.53(11)	O16[1]-Zn1-O16	57.23(9)	1: 1/2-x,1-y,+z
Zn1-O16	2.243(2)	N8-Zn1-O16	94.74(7)	N2-Zn1-O16	86.58(7)	
Zn1-N2	2.156(2)	N8-Zn1-O16[1]	93.57(7)	N2[1]-Zn1-O16	142.22(7)	
		N8-Zn1-N2	77.70(7)	N2-Zn1-N2[1]	130.81(11)	
		N8[1]-Zn1-N2	98.30(7)			
4.12						
Mn1-O34	2.171(3)	O34-Mn1-N18	94.26(11)	N35-Mn1-N2	89.59(11)	
Mn1-N18	2.267(3)	O34-Mn1-N35	84.94(11)	N26-Mn1-N18	72.11(11)	
Mn1-N35	2.221(3)	O34-Mn1-N26	97.26(11)	N26-Mn1-N2	95.55(11)	
Mn1-N26	2.222(3)	O34-Mn1-N2	166.58(10)	N13-Mn1-N18	97.63(11)	
Mn1-N2	2.324(3)	O34-Mn1-N13	95.91(11)	N13-Mn1-N35	93.71(11)	
Mn1-N13	2.194(3)	N18-Mn1-N2	93.49(11)	N13-Mn1-N26	163.85(12)	
		N35-Mn1-N18	168.66(11)	N13-Mn1-N2	72.18(11)	
		N35-Mn1-N26	96.74(11)			
4.13						
Cu1-N23	1.9815(18)	N23-Cu1-N2	93.08(7)	N8-Cu1-N2	79.69(7)	
Cu1-N2	2.0371(19)	N23-Cu1-O32	93.22(7)	N8-Cu1-O32	95.05(7)	
Cu1-N8	1.9570(17)	N23-Cu1-N17	77.74(7)	N8-Cu1-N17	100.38(7)	
Cu1-O32	2.0291(15)	N2-Cu1-N17	107.70(7)	O32-Cu1-N2	156.37(7)	
Cu1-N17	2.2201(19)	N8-Cu1-N23	171.67(8)	O32-Cu1-N17	95.89(6)	
4.14						
Cu1-Cl3[1]	2.258(2)	Cl3[1]-Cu1-Cl3	86.05(7)	N10-Cu1-Cl2	94.63(18)	1: -x,1-y,-z
Cu1-Cl3	2.544(2)	Cl3[1]-Cu1-Cl2	99.81(9)	N10-Cu1-N4	78.0(2)	
Cu1-Cl2	2.336(3)	Cl2-Cu1-Cl3	117.72(9)	N4-Cu1-Cl3[1]	93.45(18)	
Cu1-N10	1.965(6)	N10-Cu1-Cl3	89.18(17)	N4-Cu1-Cl3	125.01(17)	
Cu1-N4	2.118(6)	N10-Cu1-Cl3[1]	165.40(19)	N4-Cu1-Cl2	116.50(17)	
4.15						
Cu1-N9	1.975(5)	N9-Cu1-N3	77.6(2)	N46-Cu1-N46[2]	173.7(3)	1: +x,1-y,+z
Cu1-N3	2.165(6)	N9-Cu1-N32	172.5(2)	N46-Cu2-N41	98.0(2)	2: 1-x,+y,-z
Cu1-N32	1.978(5)	N9-Cu1-N35	94.4(2)	N46[2]-Cu2-N41	79.7(2)	
Cu1-N35	2.011(5)	N9-Cu1-O39	92.8(2)	N46[2]-Cu2-N41[2]	98.0(2)	
Cu1-O39	2.070(4)	N32-Cu1-N3	102.0(2)	N46-Cu2-N41[2]	79.7(2)	
Cu2-N46	1.953(5)	N32-Cu1-N35	79.6(2)	N46-Cu2-O40	93.17(14)	
Cu2-N41	2.059(5)	N32-Cu1-O39	94.7(2)	N46[2]-Cu2-O40	93.17(14)	
Cu2-O40	2.085(6)	N35-Cu1-N3	125.4(2)	N41-Cu2-N41[2]	139.2(3)	
		N35-Cu1-O39	145.02(19)	N41-Cu2-O40	110.41(14)	
		O39-Cu1-N3	89.6(2)	N41[2]-Cu2-O40	110.41(14)	
4.16						
Cu1-N37	1.971(3)	N37-Cu1-N40[1]	79.59(13)	N8-Cu1-N2	80.19(12)	1: 1-x,1-y,-z
Cu1-N8	1.955(3)	N37-Cu1-N2	97.28(13)	N8-Cu1-O58	90.78(12)	
Cu1-N40[1]	2.079(3)	N37-Cu1-O58	96.50(12)	N40[1]-Cu1-O58	104.11(13)	
Cu1-N2	2.041(3)	N8-Cu1-N37	172.45(12)	N2-Cu1- N40[1]	131.65(13)	
Cu1-58	2.087(3)	N8-Cu1- N40[1]	96.71(12)	N2-Cu1-O58	124.07(13)	

Table A27 Continued: Selected bond lengths (Å) and angles (°) from structures in Chapter 4

4.17						Symmetry Codes
Cu1-O38	1.974(4)	O38-Cu1-N2	91.6(2)	N8-Cu1-O38	165.8(2)	
Cu1-N2	2.016(6)	O38-Cu1-N31	98.89(18)	N8-Cu1-N2	79.5(2)	
Cu1-N8	1.973(5)	O38-Cu1-N37	94.22(19)	N8-Cu1-N31	93.1(2)	
Cu1-N31	2.237(5)	N2-Cu1-N31	96.4(2)	N8-Cu1-N37	95.9(2)	
Cu1-N37	2.018(6)	N2-Cu1-N37	171.7(2)	N37-Cu1-N31	76.8(2)	
4.18						
Cu1-Cl3	2.3059(14)	CL4-Cu1-Cl3	95.47(5)	Cl6-Cu2- $Cl3^{1}$	116.11(5)	1: 1-x,-y,1-z
Cu1-Cl4	2.2242(13)	N13-Cu1-Cl3	170.47(11)	N39-Cu2- $Cl3^{1}$	100.65(11)	
Cu1-N13	2.025(4)	N13-Cu1-Cl4	93.99(11)	N39-Cu2-Cl5	93.22(12)	
Cu1-N7	2.018(4)	N7-Cu1-Cl3	91.39(12)	N39-Cu2-Cl6	141.63(12)	
$Cu2-Cl3^{1}$	2.5835(12)	N7-Cu1-Cl4	172.99(12)	N36-Cu2- $Cl3^{1}$	85.83(11)	
Cu2-Cl5	2.2620(16)	N7-Cu1-N13	79.18(15)	N36-Cu2-Cl5	169.22(12)	
Cu2-Cl6	2.2668(15)	$Cl5-Cu2-Cl3^{1}$	89.91(5)	N36-Cu2-Cl6	93.50(12)	
Cu2-N39	2.066(4)	Cl5-Cu2-Cl6	97.26(7)	N36-Cu2-N39	77.87(15)	
Cu2-N36	2.010(5)					
4.19						
Zn1-N56	2.085(3)	N56- Zn1-N3	103.61(11)	N25- Zn2-N21	76.12(11)	
Zn1-N3	2.109(3)	N56- Zn1-N65	102.39(11)	N25- Zn2-N87	102.48(11)	
Zn1-N65	2.094(3)	N56- Zn1-N76	160.74(11)	N25- Zn2-N84	163.14(11)	
Zn1-N76	2.164(3)	N56- Zn1-N52	74.98(11)	N25- Zn2-N45	93.24(11)	
Zn1-N52	2.225(3)	N56- Zn1-N14	94.65(11)	N34- Zn2-N25	104.02(11)	
Zn1-N14	2.234(3)	N3- Zn1-N76	95.30(11)	N34- Zn2-N21	160.38(11)	
Zn2-N25	2.098(3)	N3- Zn1-N52	162.01(11)	N34- Zn2-N87	106.08(11)	
Zn2-N34	2.073(3)	N3- Zn1-N14	74.30(11)	N34- Zn2-N84	92.66(11)	
Zn2-N21	2.183(3)	N65- Zn1-N3	104.08(11)	N34- Zn2-N45	74.96(11)	
Zn2-N87	2.113(3)	N65- Zn1-N76	76.08(11)	N21- Zn2-N84	87.35(11)	
Zn2-N84	2.214(3)	N65- Zn1-N52	93.65(11)	N21- Zn2-N45	85.43(11)	
Zn2-N45	2.215(3)	N65- Zn1-N14	162.70(11)	N87- Zn2-N21	92.85(11)	
		N76- Zn1-N52	85.90(11)	N87- Zn2-N84	74.68(11)	
		N76- Zn1-N14	86.86(11)	N87- Zn2-N45	163.31(11)	
		N52- Zn1-N14	87.86(11)	N84- Zn2-N45	88.65(11)	

Table A28: Selected bond lengths (Å) and angles (°) from structures in Chapter 5

5.16						Symmetry Codes
Cu1-N12	1.977(3)	N12-Cu1-N2	80.25(12)	N27-Cu1-N17	79.91(12)	
Cu1-N27	1.975(3)	N12-Cu1-N17	102.55(12)	N27-Cu1-O22	88.73(11)	
Cu1-N2	2.002(3)	N12-Cu1-O22	89.02(12)	N2-Cu1-N17	137.21(12)	
Cu1-N17	2.030(3)	N27-Cu1-N12	176.55(12)	N2-Cu1-O22	136.54(11)	
Cu1-O22	2.310(3)	N27-Cu1-N2	99.63(12)	N17-Cu1-O22	86.19(11)	
5.17						
Cu1-N17	2.032(3)	N17-Cu1-N2	102.02(10)	N9-Cu1-N2	77.39(10)	
Cu1-O32	2.029(2)	O32-Cu1-N17	166.62(10)	N24-Cu1-N17	80.64(11)	
Cu1-N9	1.992(3)	O32-Cu1-N2	91.19(9)	N24-Cu1-O32	94.33(10)	
Cu1-N24	1.970(3)	N9-Cu1-N17	95.73(11)	N24-Cu1-N9	176.35(11)	
Cu1-N2	2.216(3)	N9-Cu1-O32	89.13(10)	N24-Cu1-N2	103.67(10)	
5.18						
Cu1-O12	1.973(3)	O12-Cu1-O13	86.10(13)	N2-Cu1-O13	94.50(14)	
Cu1-O13	2.012(3)	O12-Cu1-O14	85.67(13)	N2-Cu1-O14	91.30(14)	
Cu1-O14	2.268(3)	O12-Cu1-N10	81.97(14)	N2-Cu1-N10	98.84(15)	
Cu1-N2	1.930(4)	O13-Cu1-O14	90.32(13)	N10-Cu1-O13	150.85(14)	
Cu1-N10	1.999(4)	N2-Cu1-O12	176.91(15)	N10-Cu1-O14	115.03(14)	
5.19						
Cd1-O2	2.260(5)	O2-Cd1-N11	82.77(19)	$O9^{1}$-Cd1-O20	92.7(2)	1: 1/2+x,-y,+z
Cd1-$O9^{1}$	2.255(4)	O2-Cd1-$N22^{2}$	96.03(19)	N11-Cd1-O13	82.38(19)	2: 1/2+x,-1-y,+z
Cd1-N11	2.307(5)	O2-Cd1-O13	86.0(2)	N11-Cd1-O20	92.8(2)	
Cd1-$N22^{2}$	2.304(5)	O2-Cd1-O20	90.3(2)	$N22^{2}$-Cd1-N11	178.2(2)	
Cd1-O13	2.340(5)	$O9^{1}$-Cd1-O2	177.0(2)	$N22^{2}$-Cd1-O13	98.92(19)	
Cd1-O20	2.308(5)	$O9^{1}$-Cd1-N11	96.99(19)	$N22^{2}$-Cd1-O20	85.9(2)	
		$O9^{1}$-Cd1-$N22^{2}$	84.28(18)	O20-Cd1-O13	174.26(19)	
		$O9^{1}$-Cd1-O13	90.94(19)			
5.20						
Zn1-N2	2.1037(11)	N2-Zn1-$N2^{2}$	89.995(1)	F14-Zn1-N2	90.56(3)	1: 3/2-x,+y,1/2+z
Zn1-F14	2.0710(16)	N2-Zn1-$N2^{3}$	178.89(6)	F14-Zn1-$F17^{1}$	180.0	2: +y,3/2-x,+z
Zn1-$F17^{1}$	2.1292(16)	N2-Zn1-$F17^{1}$	89.44(3)			3: 3/2-x,3/2-y,+z
5.21						
Cu1-O12	1.9525(15)	O12-Cu1-N2	91.47(7)	$N2^{1}$-Cu1-N2	179.999(1)	1: 5/3-x,1/3-y,1/3-z
Cu1-N2	1.9781(18)	$O12^{1}$-Cu1-N2	88.54(7)	$O12^{1}$-Cu1-O12	179.996(1)	
5.22						
Cu1-$Cu1^{1}$	2.6323(10)	O13-Cu1-$Cu1^{1}$	86.17(8)	O26-Cu1-O25	168.85(11)	1: 1-x,2-y,1-z
Cu1-O13	1.957(2)	O13-Cu1-O25	88.58(10)	O26-Cu1O27	93.84(11)	2: -x,2-y,-z
Cu1-$O14^{1}$	1.952(2)	O13-Cu1-O26	90.77(11)	O27-Cu1-$Cu1^{1}$	173.59(9)	3: -1-x,1-y,-z
Cu1-O25	1.969(2)	O13-Cu1-O27	98.87(12)	$N3^{3}$-Cu2-N3	180.0	4: -1+x,-1+y,+z
Cu1-O26	1.965(2)	$O14^{1}$-Cu1-$Cu1^{1}$	82.41(8)	N3-Cu2-$N15^{2}$	91.28(11)	
Cu1-O27	2.161(3)	$O14^{1}$-Cu1-O13	168.53(11)	$N3^{3}$-Cu2-$N15^{2}$	88.72(11)	
Cu2-N3	2.012(3)	$O14^{1}$-Cu1-O25	89.67(11)	N3-Cu2-$O30^{3}$	92.79(11)	
Cu2-$N15^{2}$	2.012(3)	$O14^{1}$-Cu1-O26	88.76(11)	N3-Cu2-O30	87.21(11)	
Cu2-O30	2.372(3)	$O14^{1}$-Cu1-O27	92.60(12)	$N15^{2}$-Cu2-$N15^{3}$	180.00(7)	
		O25-Cu1-$Cu1^{1}$	86.77(8)	$N15^{4}$-Cu2-$O30^{3}$	91.80(11)	
		O25-Cu1-O27	97.26(11)	$N15^{4}$-Cu2-O30	88.20(11)	
		O26-Cu1-$Cu1^{1}$	82.08(8)			
5.23						
Cu1-O12	1.916(2)	O12-Cu1-$O12^{1}$	179.998(1)	O12-Cu1-N2	91.31(10)	1: 1-x,-y,1-z
Cu1-N2	1.927(3)	$O12^{1}$-Cu1-N2	88.69(10)	$N2^{1}$-Cu1-N2	180.00(14)	

Table A29: Selected bond lengths (Å) and angles (°) from structures in Chapter 6

6.11						Symmetry Codes
Cu1-N26	2.073(5)	N26-Cu1-N2	122.88(11)	N9-Cu1-N2	98.05(18)	1: -1-x,-y,+z
Cu1-N9	1.956(4)	N9-Cu1-N26	91.94(13)	N9^{1}-Cu1-N2	79.82(17)	
Cu1-N2	2.073(4)	N9-Cu1-N9^{1}	176.1(3)	N2-Cu1-N2^{1}	114.2(2)	
6.12						
Cu1-O22	1.931(5)	O2-Cu1-O28	95.7(2)	N9^{1}-Cu1-O24	96.9(2)	1: 1+x,+y,-1+z
Cu1-O28	2.206(6)	O22-Cu1-N9^{1}	170.1(2)	N9^{1}-Cu1-N2^{1}	79.5(2)	
Cu1-N9^{1}	1.982(6)	O22-Cu1-O24	91.8(2)	O24-Cu1-O28	86.4(3)	
Cu1-O24	2.007(6)	O22-Cu1-N2^{1}	90.7(2)	N24-Cu1-N2^{1}	154.9(3)	
Cu1-N2^{1}	2.022(6)	N9^{1}-Cu1-O28	89.5(2)	N2^{1}-Cu1-O28	118.2(2)	
6.13						
Cu2-O57	1.977(3)	O57-Cu2-N42	98.09(13)	O58-Cu1-O3	91.63(13)	
Cu2-O10	1.959(3)	O57-Cu2-O5	87.53(10)	O58-Cu1-N20	97.83(14)	
Cu2-N42	1.990(4)	O10-Cu2-O57	90.88(12)	O58-Cu1-N13	176.84(13)	
Cu2-N35	1.975(3)	O10-Cu2-N42	154.71(12)	O58-Cu1-O8	82.85(11)	
Cu2-O5	2.217(3)	O10-Cu2-N35	89.50(13)	O3-Cu1-N20	154.99(13)	
Cu1-O58	1.952(3)	O10-Cu2-O5	106.56(11)	O3-Cu1-N13	89.28(13)	
Cu1-O3	1.977(3)	N42-Cu2-O5	97.45(12)	O3-Cu1-O8	101.32(12)	
Cu1-N20	2.017(4)	N35-Cu2-O57	176.49(13)	N20-Cu1-O8	102.80(12)	
Cu1-N13	1.996(3)	N35-Cu2-N42	80.18(14)	N13-Cu1-N20	80.15(14)	
Cu1-O8	2.238(3)	N25-Cu2-O5	95.70(12)	N13-Cu1-O8	99.94(12)	
6.14						
Cu1-N9	1.924(2)	N9-Cu1-O16	96.73(9)	O15-Cu1-N2	104.83(8)	
Cu1-O16	2.341(2)	N9-Cu1-O15	171.57(9)	N2-Cu1-O16	92.71(8)	
Cu1-O15	1.9884(18)	N9-Cu1-N2	79.95(9)	N10-Cu1-O16	96.47(8)	
Cu1-N2	2.039(2)	N9-Cu1-N10	93.73(9)	N10-Cu1-O15	80.47(8)	
Cu1-N10	1.925(2)	O15-Cu1-O16	90.04(7)	N10-Cu1-N2	169.43(9)	
6.15						
Cu1-N10	1.921(2)	N10-Cu1-O14	97.36(8)	N9-Cu1-O15	171.03(8)	
Cu1-O14	2.2778(18)	N10-Cu1-N9	92.96(8)	N9-Cu1-N2	79.46(8)	
Cu1-N9	1.937(2)	N10-Cu1-O15	80.86(8)	O15-Cu1-O14	87.63(7)	
Cu1-O15	2.0257(17)	N10-Cu1-N2	167.09(8)	O15-Cu1-N2	105.36(7)	
Cu1-N2	2.027(2)	N9-Cu1-O14	99.67(8)	N2-Cu1-O14	94.23(7)	
6.16						
Co1-O2	2.0300(12)	O2^{1}-Co1-O2	180.0	O16-Co1-O16^{1}	180.0	1: -x,1-y,-z
Co1-O16	2.0936(14)	O2^{1}-Co1-O16^{1}	89.34(5)	O16-Co1-N6	88.34(5)	
Co1-N6	2.2139(14)	O2-Co1-O16^{1}	90.66(5)	O16-Co1-N6^{1}	91.66(5)	
		O2-Co1-N6	100.74(5)	N6-Co1-N6^{1}	180.0	
		O2-Co1-N6^{1}	79.2695)			

Table A29 Continued: Selected bond lengths (Å) and angles (°) from structures in Chapter 6

6.17						Symmetry Codes
Co1-N8	2.101(5)	N8-Co1-N8[1]	179.999(1)	O18-Co2-N16[2]	91.3(2)	1: 2-x,1-y,1-z
Co1-O34	2.140(7)	N8[1]-Co1-O34	93.0(3)	N16[2]-Co2-N16	179.999(1)	2: 1-x,1-y,2-z
Co1-O4	2.063(5)	N8-Co1-O34	87.0(3)	O32-Co3-O33	89.1(2)	3: 1-x,1-y,1-z
Co2-N22	2.118(6)	O34-Co1-O34[1]	180.0(4)	O32-Co3-N13[3]	176.1(2)	
Co2-O18	2.060(6)	O4-Co1-N8	80.1(2)	O32-Co3-N9[3]	102.43(18)	
Co2-N16	2.182(5)	O4-Co1-N8[1]	99.9(2)	O32-Co3-N23	93.09(18)	
Co3-O32	2.069(4)	O4[1]-Co1-O34[1]	92.0(3)	O32-Co3-N27	94.8(2)	
Co3-O33	2.108(5)	O4-Co1-O34	88.0(3)	O33-Co3-N13[3]	87.0(2)	
Co3-N13[3]	2.191(5)	O4-Co1-O4[1]	180.0(4)	O33-Co3-N23	101.5(2)	
Co3-N9[3]	2.108(5)	N22-Co1-N22[2]	180.0(3)	O33-Co3-N27	175.82(18)	
Co3-N23	2.129(6)	N22-Co2-N16[2]	87.74(19)	N9[3]-Co3-O33	88.2(2)	
Co3-N27	2.159(6)	N22-Co2-N16	92.27(19)	N9[3]-Co3-N13[3]	77.1(2)	
		O18-Co2-N22[2]	100.6(2)	N9[3]-Co3-N23	161.9(2)	
		O18-Co2-N22	79.4(2)	N9[3]-Co3-N27	92.4(2)	
		O18[2]-Co2-O18	180.0(2)	N23-Co3-N13[3]	88.1(2)	
		O18-Co2-N16	88.7(2)	N23-Co3-N27	76.9(2)	
				N27-Co3-N13[3]	89.1(2)	
6.18						
Cu1-O8	2.016(4)	O8-Cu1-O10	93.90(15)	N6-Cu1-O8	82.27(15)	
Cu1-O9	1.947(3)	O9-Cu1-O8	90.11(14)	N6-Cu1-N2	96.40(17)	
Cu1-N6	1.960(4)	O9-Cu1-N6	169.84(16)	N6-Cu1-O10	98.31(16)	
Cu1-N2	1.968(4)	O9-Cu1-N2	90.62(16)	N2-Cu1-O8	175.03(17)	
Cu1-O10	2.337(4)	O9-Cu1-O10	88.87(15)	N2-Cu1-O10	91.03(17)	

References

1. J. M. Lehn, *Supramolecular Chemistry: Concepts and Perspectives*, Wiley-VCH, **1995**.
2. J. W. Steed and J. L. Atwood, *Supramolecular Chemistry*, Wiley, **2009**.
3. J. W. Steed, D. R. Turner and K. J. Wallace, *Core Concepts in Supramolecular Chemistry and Nanochemistry*, Wiley VCH, **2007**.
4. J. M. Lehn, *Angew. Chem., Int. Ed. Engl.*, **1990**, *29*, 1304-1319.
5. F. M. Menger, *Proc. Natl. Acad. Sci. U. S. A.*, **2002**, *99*, 4818-4822.
6. E. N. Lassettre, *Chem. Rev.*, **1937**, *20*, 259-303.
7. W. M. Latimer and W. H. Rodebush, *J. Am. Chem. Soc.*, **1920**, *42*, 1419-1433.
8. C. J. Pedersen, *Angew. Chem., Int. Ed. Engl.*, **1988**, *27*, 1021-1027.
9. D. J. Cram, *Angew. Chem., Int. Ed. Engl.*, **1988**, *27*, 1009-1020.
10. J. M. Lehn, *Angew. Chem., Int. Ed. Engl.*, **1988**, *27*, 89-112.
11. "The Nobel Prize in Chemistry 1987". Nobelprize.org. 12 Jul 2012 http://www.nobelprize.org/nobel_prizes/chemistry/laureates/1987/
12. Image Credit: http://en.wikipedia.org/wiki/Cryptand; accessed 10/7/2012
13. V. Bohmer, *Angew. Chem., Int. Ed. Engl.*, **1995**, *34*, 713-745.
14. K. Kim, N. Selvapalam, Y. H. Ko, K. M. Park, D. Kim and J. Kim, *Chem. Soc. Rev.*, **2007**, *36*, 267-279.
15. G. Wenz, *Angew. Chem., Int. Ed. Engl.*, **1994**, *33*, 803-822.
16. E. C. Constable, *Chem. Ind.*, **1994**, 56-59.
17. P. J. Steel, *Acc. Chem. Res.*, **2005**, *38*, 243-250.
18. G. M. Whitesides and B. Grzybowski, *Science*, **2002**, *295*, 2418-2421.
19. G. R. Desiraju, *Angew. Chem., Int. Ed. Engl.*, **1995**, *34*, 2311-2327.
20. M. Simard, D. Su and J. D. Wuest, *J. Am. Chem. Soc.*, **1991**, *113*, 4696-4698.
21. G. R. Desiraju, *Angew. Chem., Int. Ed. Engl.*, **2007**, *46*, 8342-8356.
22. E. C. Constable, *Chem. Commun.*, **1997**, 1073-1080.
23. B. J. Holliday and C. A. Mirkin, *Angew. Chem., Int. Ed. Engl.*, **2001**, *40*, 2022-2043.
24. T. Steiner, *Angew. Chem., Int. Ed. Engl.*, **2002**, *41*, 48-76.
25. W. S. Horne and S. H. Gellman, *Acc. Chem. Res.*, **2008**, *41*, 1399-1408.
26. A. R. Sanford, K. Yamato, X. W. Yang, L. H. Yuan, Y. H. Han and B. Gong, *Eur. J. Biochem.*, **2004**, *271*, 1416-1425.
27. M. W. Hosseini, *Acc. Chem. Res.*, **2005**, *38*, 313-323.
28. V. A. Russell and M. D. Ward, *Chem. Mater.*, **1996**, *8*, 1654-1666.

29. C. B. Aakeroy and D. J. Salmon, *CrystEngComm*, **2005**, *7*, 439-448.
30. G. R. Desiraju, *Acc. Chem. Res.*, **1996**, *29*, 441-449.
31. C. A. Hunter and J. K. M. Sanders, *J. Am. Chem. Soc.*, **1990**, *112*, 5525-5534.
32. C. A. Hunter, K. R. Lawson, J. Perkins and C. J. Urch, *J. Chem. Soc., Perkin Trans. 2*, **2001**, 651-669.
33. C. Janiak, *J. Chem. Soc., Dalton Trans.*, **2000**, 3885-3896.
34. M. O. Sinnokrot, E. F. Valeev and C. D. Sherrill, *J. Am. Chem. Soc.*, **2002**, *124*, 10887-10893.
35. C. Horn, B. Ali, I. Dance, M. Scudder and D. Craig, *CrystEngComm*, **2000**, 6-15.
36. V. Russell, M. Scudder and I. Dance, *J. Chem. Soc., Dalton Trans.*, **2001**, 789-799.
37. I. Dance and M. Scudder, *Chem. Eur. J.*, **1996**, *2*, 481-486.
38. P. Metrangolo, H. Neukirch, T. Pilati and G. Resnati, *Acc. Chem. Res.*, **2005**, *38*, 386-395.
39. C. M. Che, M. C. Tse, M. C. W. Chan, K. K. Cheung, D. L. Phillips and K. H. Leung, *J. Am. Chem. Soc.*, **2000**, *122*, 2464-2468.
40. Q. L. Chu, D. C. Swenson and L. R. MacGillivray, *Angew. Chem., Int. Ed. Engl.*, **2005**, *44*, 3569-3572.
41. H. Schmidbaur and A. Schier, *Chem. Soc. Rev.*, **2008**, *37*, 1931-1951.
42. J. C. Ma and D. A. Dougherty, *Chem. Rev.*, **1997**, *97*, 1303-1324.
43. A. Ranganathan, V. R. Pedireddi and C. N. R. Rao, *J. Am. Chem. Soc.*, **1999**, *121*, 1752-1753.
44. C. P. Brock and J. D. Dunitz, *Chem. Mater.*, **1994**, *6*, 1118-1127.
45. B. Douglas, D. McDaniel and J. Alexander, *Concepts and Models of Inorganic Chemistry*, *3rd Ed.*, John Wiley & Sons, **2006**.
46. C. E. Housecroft and A. G. Sharpe, *Inorganic Chemistry*, Pearson Prentice Hall, **2008**.
47. M. Nishio, *CrystEngComm*, **2004**, *6*, 130-158.
48. M. Nishio, Y. Umezawa, K. Honda, S. Tsuboyama and H. Suezawa, *CrystEngComm*, **2009**, *11*, 1757-1788.
49. M. Albrecht, *Chem. Rev.*, **2001**, *101*, 3457-3497.
50. C. Piguet, G. Bernardinelli and G. Hopfgartner, *Chem. Rev.*, **1997**, *97*, 2005-2062.
51. M. Fujita, *Acc. Chem. Res.*, **1999**, *32*, 53-61.
52. T. J. Hubin and D. H. Busch, *Coord. Chem. Rev.*, **2000**, *200*, 5-52.
53. M. Weck, B. Mohr, J. P. Sauvage and R. H. Grubbs, *J. Org. Chem.*, **1999**, *64*, 5463-5471.
54. V. Balzani, A. Credi and M. Venturi, *Chem. Soc. Rev.*, **2009**, *38*, 1542-1550.
55. J. P. Collin, C. Dietrich-Buchecker, P. Gavina, M. C. Jimenez-Molero and J. P. Sauvage, *Acc. Chem. Res.*, **2001**, *34*, 477-487.
56. G. A. Breault, C. A. Hunter and P. C. Mayers, *Tetrahedron*, **1999**, *55*, 5265-5293.
57. O. Lukin and F. Vogtle, *Angew. Chem., Int. Ed. Engl.*, **2005**, *44*, 1456-1477.

58. F. Li, J. K. Clegg, L. F. Lindoy, R. B. Macquart and G. V. Meehan, *Nature Comm.*, **2011**, *2*, 205-205.
59. J. Rebek, *Acc. Chem. Res.*, **1984**, *17*, 258-264.
60. Image Credit: http://en.wikipedia.org/wiki/File:Supramolecular_Assembly_Lehn.jpg accessed 10/7/2012
61. B. Hasenknopf, J. M. Lehn, B. O. Kneisel, G. Baum and D. Fenske, *Angew. Chem., Int. Ed. Engl.*, **1996**, *35*, 1838-1840.
62. Image Credit: http://en.wikipedia.org/wiki/File:Molecular_Knot_RecTravChimPays-Bas_427_1993_commons.jpg, Accessed 10/7/2012
63. C. O. Dietrichbuchecker and J. P. Sauvage, *Angew. Chem., Int. Ed. Engl.*, **1989**, *28*, 189-192.
64. G. F. Swiegers and T. J. Malefetse, *Chem. Rev.*, **2000**, *100*, 3483-3537.
65. K. S. Chichak, S. J. Cantrill, A. R. Pease, S. H. Chiu, G. W. V. Cave, J. L. Atwood and J. F. Stoddart, *Science*, **2004**, *304*, 1308-1312.
66. J. F. Ayme, J. E. Beves, D. A. Leigh, R. T. McBurney, K. Rissanen and D. Schultz, *Nature Chem.*, **2012**, *4*, 15-20.
67. F. Hof, S. L. Craig, C. Nuckolls and J. Rebek, *Angew. Chem., Int. Ed. Engl.*, **2002**, *41*, 1488-1508.
68. M. Yoshizawa, J. K. Klosterman and M. Fujita, *Angew. Chem., Int. Ed. Engl.*, **2009**, *48*, 3418-3438.
69. M. Fujita, *Chem. Soc. Rev.*, **1998**, *27*, 417-425.
70. T. Kusukawa and M. Fujita, *J. Am. Chem. Soc.*, **2002**, *124*, 13576-13582.
71. P. D. Beer and P. A. Gale, *Angew. Chem., Int. Ed. Engl.*, **2001**, *40*, 486-516.
72. T. Gunnlaugsson, M. Glynn, G. M. Tocci, P. E. Kruger and F. M. Pfeffer, *Coord. Chem. Rev.*, **2006**, *250*, 3094-3117.
73. B. E. Collins and E. V. Anslyn, *Chem. Eur. J.*, **2007**, *13*, 4700-4708.
74. E. B. Veale, D. O. Frimannsson, M. Lawler and T. Gunnlaugsson, *Org. Lett.*, **2009**, *11*, 4040-4043.
75. D. C. Magri, G. J. Brown, G. D. McClean and A. P. de Silva, *J. Am. Chem. Soc.*, **2006**, *128*, 4950-4951.
76. A. P. de Silva, H. Q. N. Gunaratne, T. Gunnlaugsson, A. J. M. Huxley, C. P. McCoy, J. T. Rademacher and T. E. Rice, *Chem. Rev.*, **1997**, *97*, 1515-1566.
77. Image Credit: http://www.optimedical.com/products/opti/opti_r_over.htm accessed 10/7/2012
78. A. Garcia-Bernabe, M. Kramer, B. Olah and R. Haag, *Chem. Eur. J.*, **2004**, *10*, 2822-2830.
79. A. Denicourt-Nowicki, A. Ponchel, E. Monflier and A. Roucoux, *Dalton Trans.*, **2007**, 5714-5719.
80. S. Angelos, Y. W. Yang, K. Patel, J. F. Stoddart and J. I. Zink, *Angew. Chem., Int. Ed. Engl.*, **2008**, *47*, 2222-2226.

81. M. E. Davis and M. E. Brewster, *Nat. Rev. Drug. Discov.*, **2004**, *3*, 1023-1035.
82. R. A. Rajewski and V. J. Stella, *J. Pharm. Sci.*, **1996**, *85*, 1142-1169.
83. R. A. Smaldone, R. S. Forgan, H. Furukawa, J. J. Gassensmith, A. M. Z. Slawin, O. M. Yaghi and J. F. Stoddart, *Angew. Chem., Int. Ed. Engl.*, **2010**, *49*, 8630-8634.
84. P. Mal, B. Breiner, K. Rissanen and J. R. Nitschke, *Science*, **2009**, *324*, 1697-1699.
85. M. B. Duriska, S. M. Neville, B. Moubaraki, J. A. Cashion, G. J. Halder, K. W. Chapman, C. Balde, J. F. Letard, K. S. Murray, C. J. Kepert and S. R. Batten, *Angew. Chem., Int. Ed. Engl.*, **2009**, *48*, 2549-2552.
86. Image Credit: http://www.ch.cam.ac.uk/group/nitschke/research/cages, accessed 10/7/2012.
87. http://www.chem.monash.edu.au/honours/2011/batten-stuart/project2.html accessed 10/7/2012.
88. T. S. Koblenz, J. Wassenaar and J. N. H. Reek, *Chem. Soc. Rev.*, **2008**, *37*, 247-262.
89. P. W. N. M. van Leeuwen, *Supramolecular Catalysis*, Wiley VCH, **2008**.
90. J. Chen and J. Rebek, *Org. Lett.*, **2002**, *4*, 327-329.
91. M. Yoshizawa, M. Tamura and M. Fujita, *Science*, **2006**, *312*, 251-254.
92. M. D. Pluth, R. G. Bergman and K. N. Raymond, *J. Am. Chem. Soc.*, **2008**, *130*, 11423-11429.
93. M. Yoshizawa, S. Miyagi, M. Kawano, K. Ishiguro and M. Fujita, *J. Am. Chem. Soc.*, **2004**, *126*, 9172-9173.
94. C. J. Brown, R. G. Bergman and K. N. Raymond, *J. Am. Chem. Soc.*, **2009**, *131*, 17530-17531.
95. K. Suzuki, S. Sato and M. Fujita, *Nature Chem.*, **2010**, *2*, 25-29.
96. J. Brown, *Phil. Trans.*, **1724**, *33*, 17-24.
97. K. Itaya, I. Uchida and V. D. Neff, *Acc. Chem. Res.*, **1986**, *19*, 162-168.
98. H. J. Buser, D. Schwarzenbach, W. Petter and A. Ludi, *Inorg. Chem.*, **1977**, *16*, 2704-2710.
99. T. D. Keene, M. J. Murphy, J. R. Price, D. J. Price and C. J. Kepert, *Dalton Trans.*, **2011**, *40*, 11621-11628.
100. G. N. Newton, M. Nihei and H. Oshio, *Eur. J. Inorg. Chem.*, **2011**, 3031-3042.
101. K. R. Dunbar and R. A. Heintz, *Prog. Inorg. Chem.*, **1997**, *45*, 283-391.
102. B. F. Hoskins and R. Robson, *J. Am. Chem. Soc.*, **1990**, *112*, 1546-1554.
103. G. Ferey, *Chem. Soc. Rev.*, **2008**, *37*, 191-214.
104. S. L. James, *Chem. Soc. Rev.*, **2003**, *32*, 276-288.
105. C. Janiak, *Dalton Trans.*, **2003**, 2781-2804.
106. S. Kitagawa, R. Kitaura and S. Noro, *Angew. Chem., Int. Ed. Engl.*, **2004**, *43*, 2334-2375.
107. A. J. Blake, N. R. Champness, P. Hubberstey, W. S. Li, M. A. Withersby and M. Schroder, *Coord. Chem. Rev.*, **1999**, *183*, 117-138.

108. A. K. Cheetham, G. Ferey and T. Loiseau, *Angew. Chem., Int. Ed. Engl.*, **1999**, *38*, 3268-3292.
109. M. E. Davis, *Nature*, **2002**, *417*, 813-821.
110. M. Eddaoudi, J. Kim, N. Rosi, D. Vodak, J. Wachter, M. O'Keeffe and O. M. Yaghi, *Science*, **2002**, *295*, 469-472.
111. M. Eddaoudi, H. L. Li and O. M. Yaghi, *J. Am. Chem. Soc.*, **2000**, *122*, 1391-1397.
112. K. Barthelet, J. Marrot, D. Riou and G. Ferey, *Angew. Chem., Int. Ed. Engl.*, **2001**, *41*, 281-284.
113. C. Serre, F. Millange, C. Thouvenot, M. Nogues, G. Marsolier, D. Louer and G. Ferey, *J. Am. Chem. Soc.*, **2002**, *124*, 13519-13526.
114. R. Kitaura, S. Kitagawa, Y. Kubota, T. C. Kobayashi, K. Kindo, Y. Mita, A. Matsuo, M. Kobayashi, H. C. Chang, T. C. Ozawa, M. Suzuki, M. Sakata and M. Takata, *Science*, **2002**, *298*, 2358-2361.
115. M. Kondo, T. Okubo, A. Asami, S. Noro, T. Yoshitomi, S. Kitagawa, T. Ishii, H. Matsuzaka and K. Seki, *Angew. Chem., Int. Ed. Engl.*, **1999**, *38*, 140-143.
116. M. Kondo, T. Yoshitomi, K. Seki, H. Matsuzaka and S. Kitagawa, *Angew. Chem., Int. Ed. Engl.*, **1997**, *36*, 1725-1727.
117. B. F. Abrahams, B. F. Hoskins, D. M. Michail and R. Robson, *Nature*, **1994**, *369*, 727-729.
118. S. S. Y. Chui, S. M. F. Lo, J. P. H. Charmant, A. G. Orpen and I. D. Williams, *Science*, **1999**, *283*, 1148-1150.
119. S. Subramanian and M. J. Zaworotko, *Angew. Chem., Int. Ed. Engl.*, **1995**, *34*, 2127-2129.
120. Image Credits: MOF-5: http://en.wikipedia.org/wiki/File:IRMOF-1_wiki.png, Accessed 10/7/2012; MIL-53: http://commons.wikimedia.org/wiki/File:MIL-53ht.png, Accessed 10/7/2012; HKUST-1: http://www.netl.doe.gov/newsroom/netlog/june2007/netlog_june07.html; Accessed 10/7/2012
121. M. O'Keeffe, *Chem. Soc. Rev.*, **2009**, *38*, 1215-1217.
122. D. J. Tranchemontagne, J. L. Mendoza-Cortes, M. O'Keeffe and O. M. Yaghi, *Chem. Soc. Rev.*, **2009**, *38*, 1257-1283.
123. S. Kitagawa and R. Matsuda, *Coord. Chem. Rev.*, **2007**, *251*, 2490-2509.
124. G. Ferey and C. Serre, *Chem. Soc. Rev.*, **2009**, *38*, 1380-1399.
125. A. J. Fletcher, K. M. Thomas and M. J. Rosseinsky, *J. Solid State Chem.*, **2005**, *178*, 2491-2510.
126. G. Ferey, C. Mellot-Draznieks, C. Serre and F. Millange, *Acc. Chem. Res.*, **2005**, *38*, 217-225.
127. J. J. Perry, J. A. Perman and M. J. Zaworotko, *Chem. Soc. Rev.*, **2009**, *38*, 1400-1417.
128. C. Janiak and J. K. Vieth, *New. J. Chem.*, **2010**, *34*, 2366-2388.
129. C. J. Kepert, *Chem. Commun.*, **2006**, 695-700.
130. T. D. Keene, D. J. Price and C. J. Kepert, *Dalton Trans.*, **2011**, *40*, 7122-7126.

131. O. K. Farha, K. L. Mulfort, A. M. Thorsness and J. T. Hupp, *J. Am. Chem. Soc.*, **2008**, *130*, 8598-8599.
132. W. Kaneko, M. Ohba and S. Kitagawa, *J. Am. Chem. Soc.*, **2007**, *129*, 13706-13712.
133. A. L. Goodwin and C. J. Kepert, *Phys. Rev. B*, **2005**, *71*.
134. R. Ohtani, K. Yoneda, S. Furukawa, N. Horike, S. Kitagawa, A. B. Gaspar, M. C. Munoz, J. A. Real and M. Ohba, *J. Am. Chem. Soc.*, **2011**, *133*, 8600-8605.
135. V. N. Vukotic and S. J. Loeb, *Chem. Eur. J.*, **2010**, *16*, 13630-13637.
136. H. X. Deng, S. Grunder, K. E. Cordova, C. Valente, H. Furukawa, M. Hmadeh, F. Gandara, A. C. Whalley, Z. Liu, S. Asahina, H. Kazumori, M. O'Keeffe, O. Terasaki, J. F. Stoddart and O. M. Yaghi, *Science*, **2012**, *336*, 1018-1023.
137. P. D. Southon, L. Liu, E. A. Fellows, D. J. Price, G. J. Halder, K. W. Chapman, B. Moubaraki, K. S. Murray, J. F. Letard and C. J. Kepert, *J. Am. Chem. Soc.*, **2009**, *131*, 10998-11009.
138. R. B. Getman, Y. S. Bae, C. E. Wilmer and R. Q. Snurr, *Chem. Rev.*, **2012**, *112*, 703-723.
139. L.-C. Lin, A. H. Berger, R. L. Martin, J. Kim, J. A. Swisher, K. Jariwala, C. H. Rycroft, A. S. Bhown, M. W. Deem, M. Haranczyk and B. Smit, *Nature Mater.*, **2012**, *11*, 633-641.
140. T. Duren, F. Millange, G. Ferey, K. S. Walton and R. Q. Snurr, *J. Phys. Chem. C*, **2007**, *111*, 15350-15356.
141. S. S. Han, J. L. Mendoza-Cortes and W. A. Goddard, *Chem. Soc. Rev.*, **2009**, *38*, 1460-1476.
142. N. Stock and S. Biswas, *Chem. Rev.*, **2012**, *112*, 933-969.
143. M. D. Allendorf, R. J. T. Houk, L. Andruszkiewicz, A. A. Talin, J. Pikarsky, A. Choudhury, K. A. Gall and P. J. Hesketh, *J. Am. Chem. Soc.*, **2008**, *130*, 14404-14405.
144. D. Zacher, O. Shekhah, C. Woll and R. A. Fischer, *Chem. Soc. Rev.*, **2009**, *38*, 1418-1429.
145. K. W. Chapman, G. J. Halder and P. J. Chupas, *J. Am. Chem. Soc.*, **2009**, *131*, 17546-17547.
146. P. Serra-Crespo, E. Stavitski, F. Kapteijn and J. Gascon, *R.S.C. Advances*, **2012**, *2*, 5051-5053.
147. M. Yoon, R. Srirambalaji and K. Kim, *Chem. Rev.*, **2012**, *112*, 1196-1231.
148. J. Lee, O. K. Farha, J. Roberts, K. A. Scheidt, S. T. Nguyen and J. T. Hupp, *Chem. Soc. Rev.*, **2009**, *38*, 1450-1459.
149. D. J. Lun, G. I. N. Waterhouse and S. G. Telfer, *J. Am. Chem. Soc.*, **2011**, *133*, 5806-5809.
150. A. D. Burrows, C. G. Frost, M. F. Mahon and C. Richardson, *Angew. Chem., Int. Ed. Engl.*, **2008**, *47*, 8482-8486.
151. Z. Q. Wang, K. K. Tanabe and S. M. Cohen, *Chem. Eur. J.*, **2010**, *16*, 212-217.
152. S. M. Cohen, *Chem. Rev.*, **2012**, *112*, 970-1000.
153. C. Wang, T. Zhang and W. B. Lin, *Chem. Rev.*, **2012**, *112*, 1084-1104.
154. O. R. Evans and W. B. Lin, *Acc. Chem. Res.*, **2002**, *35*, 511-522.
155. Y. J. Cui, Y. F. Yue, G. D. Qian and B. L. Chen, *Chem. Rev.*, **2012**, *112*, 1126-1162.

156. J. R. Li, R. J. Kuppler and H. C. Zhou, *Chem. Soc. Rev.*, **2009**, *38*, 1477-1504.
157. L. J. Murray, M. Dinca and J. R. Long, *Chem. Soc. Rev.*, **2009**, *38*, 1294-1314.
158. X. B. Zhao, B. Xiao, A. J. Fletcher, K. M. Thomas, D. Bradshaw and M. J. Rosseinsky, *Science*, **2004**, *306*, 1012-1015.
159. K. Sumida, D. L. Rogow, J. A. Mason, T. M. McDonald, E. D. Bloch, Z. R. Herm, T. H. Bae and J. R. Long, *Chem. Rev.*, **2012**, *112*, 724-781.
160. D. M. D'Alessandro, B. Smit and J. R. Long, *Angew. Chem., Int. Ed. Engl.*, **2010**, *49*, 6058-6082.
161. J. L. C. Rowsell and O. M. Yaghi, *Angew. Chem., Int. Ed. Engl.*, **2005**, *44*, 4670-4679.
162. N. Armaroli and V. Balzani, *Energy for a Sustainable World: From the Oil Age to a Sun-Powered Future*, Wiley-VCH, **2011**.
163. R. S. Haszeldine, *Science*, **2009**, *325*, 1647-1652.
164. S. Choi, J. H. Drese and C. W. Jones, *ChemSusChem*, **2009**, *2*, 796-854.
165. Image Credit: http://www.esrl.noaa.gov/gmd/ccgg/trends/, accessed 10/7/2012
166. R. Krishna, *Chem. Soc. Rev.*, **2012**, *41*, 3099-3118.
167. S. Kitagawa and K. Uemura, *Chem. Soc. Rev.*, **2005**, *34*, 109-119.
168. R. Vaidhyanathan, S. S. Iremonger, K. W. Dawson and G. K. H. Shimizu, *Chem. Commun.*, **2009**, 5230-5232.
169. R. Vaidhyanathan, S. S. Iremonger, G. K. H. Shimizu, P. G. Boyd, S. Alavi and T. K. Woo, *Science*, **2010**, *330*, 650-653.
170. M. Dinca and J. R. Long, *Angew. Chem., Int. Ed. Engl.*, **2008**, *47*, 6766-6779.
171. S. Q. Ma, J. M. Simmons, D. F. Sun, D. Q. Yuan and H. C. Zhou, *Inorg. Chem.*, **2009**, *48*, 5263-5268.
172. T. Sagara, J. Klassen, J. Ortony and E. Ganz, *J. Chem. Phys.*, **2005**, *123*, 014701-014704.
173. T. Duren, Y. S. Bae and R. Q. Snurr, *Chem. Soc. Rev.*, **2009**, *38*, 1237-1247.
174. U. Eberle, M. Felderhoff and F. Schuth, *Angew. Chem., Int. Ed. Engl.*, **2009**, *48*, 6608-6630.
175. J. Yang, A. Sudik, C. Wolverton and D. J. Siegel, *Chem. Soc. Rev.*, **2010**, *39*, 656-675.
176. N. Armaroli and V. Balzani, *ChemSusChem*, **2011**, *4*, 21-36.
177. H. Furukawa, N. Ko, Y. B. Go, N. Aratani, S. B. Choi, E. Choi, A. O. Yazaydin, R. Q. Snurr, M. O'Keeffe, J. Kim and O. M. Yaghi, *Science*, **2010**, *329*, 424-428.
178. S. I. Orimo, Y. Nakamori, J. R. Eliseo, A. Zuttel and C. M. Jensen, *Chem. Rev.*, **2007**, *107*, 4111-4132.
179. F. H. Stephens, V. Pons and R. T. Baker, *Dalton Trans.*, **2007**, 2613-2626.
180. Y. W. Li and R. T. Yang, *J. Am. Chem. Soc.*, **2006**, *128*, 726-727.
181. Image Credit: http://www.sciencewatch.com/dr/fbp/2011/11augfbp/11augfbpKim/, accessed 17/7/2012
182. A. B. Rao and E. S. Rubin, *Environ. Sci. Technol.*, **2002**, *36*, 4467-4475.

183. H. Q. Yang, Z. H. Xu, M. H. Fan, R. Gupta, R. B. Slimane, A. E. Bland and I. Wright, *J. Environ. Sci.*, **2008**, *20*, 14-27.
184. T. M. McDonald, W. R. Lee, J. A. Mason, B. M. Wiers, C. S. Hong and J. R. Long, *J. Am. Chem. Soc.*, **2012**, *134*, 7056-7065.
185. A. R. Millward and O. M. Yaghi, *J. Am. Chem. Soc.*, **2005**, *127*, 17998-17999.
186. A. F. Wells, *Structural Inorganic Chemistry*, Clarendon Press, **1984**.
187. M. O'Keeffe and O. M. Yaghi, *Chem. Rev.*, **2012**, *112*, 675-702.
188. S. R. Batten, S. M. Neville and D. R. Turner, *Coordination Polymers: Design, Analysis and Application*, Royal Society of Chemistry, **2009**.
189. N. W. Ockwig, O. Delgado-Friedrichs, M. O'Keeffe and O. M. Yaghi, *Acc. Chem. Res.*, **2005**, *38*, 176-182.
190. (Image Credit: http://yaghi.chem.ucla.edu/gallery/photo?photo_id=10454, accessed 10/7/2012)
191. M. O'Keeffe, M. A. Peskov, S. J. Ramsden and O. M. Yaghi, *Acc. Chem. Res.*, **2008**, *41*, 1782-1789.
192. S. R. Batten and R. Robson, *Angew. Chem., Int. Ed. Engl.*, **1998**, *37*, 1460-1494.
193. L. Carlucci, G. Ciani and D. M. Proserpio, *Coord. Chem. Rev.*, **2003**, *246*, 247-289.
194. H. Wu, J. Yang, Z. M. Su, S. R. Batten and J. F. Ma, *J. Am. Chem. Soc.*, **2011**, *133*, 11406-11409.
195. S. Yang, X. Lin, W. Lewis, M. Suyetin, E. Bichoutskaia, J. E. Parker, C. C. Tang, D. R. Allan, P. J. Rizkallah, P. Hubberstey, N. R. Champness, K. M. Thomas, A. J. Blake and M. Schröder, *Nature Mater.*, **2012**, *advance online publication*.
196. Image Credit: http://yaghi.chem.ucla.edu/gallery/photo?photo_id=1547, Accessed 10/7/2012.
197. T. Eicher, S. Hauptmann and A. Speicher, *The Chemistry of Heterocycles: Structure, Reactions, Syntheses, and Applications*, Wiley-VCH, **2003**.
198. J. Alvarez-Builla, *Modern Heterocyclic Chemistry*, Wiley-VCH Verlag, **2011**.
199. K. Brune, *Acute Pain*, **1997**, *1*, 33-40.
200. T. D. Penning, J. J. Talley, S. R. Bertenshaw, J. S. Carter, P. W. Collins, S. Docter, M. J. Graneto, L. F. Lee, J. W. Malecha, J. M. Miyashiro, R. S. Rogers, D. J. Rogier, S. S. Yu, G. D. Anderson, E. G. Burton, J. N. Cogburn, S. A. Gregory, C. M. Koboldt, W. E. Perkins, K. Seibert, A. W. Veenhuizen, Y. Y. Zhang and P. C. Isakson, *J. Med. Chem.*, **1997**, *40*, 1347-1365.
201. W. Al Jaroudi and A. E. Iskandrian, *J. Am. Coll. Cardiol.*, **2009**, *54*, 1123-1130.
202. J. L. G. dePaz, J. Elguero, C. FocesFoces, A. L. LlamasSaiz, F. AguilarParrilla, O. Klein and H. H. Limbach, *J. Chem. Soc., Perkin Trans. 2*, **1997**, 101-109.

203. J. L. M. Abboud, P. Cabildo, T. Canada, J. Catalan, R. M. Claramunt, J. L. G. Depaz, J. Elguero, H. Homan, R. Notario, C. Toiron and G. I. Yranzo, *J. Org. Chem.*, **1992**, *57*, 3938-3946.
204. J. Elguero, *Comprehensive Heterocyclic Chemistry: Five-membered rings with two heteroatoms and fused carbocyclic derivatives*, Pergamon Press, **1996**.
205. C. N. Foces-Foces, I. Alkorta and J. Elguero, *Acta Crystallogr., Sect. B: Struct. Sci.*, **2000**, *56*, 1018-1028.
206. S. Thomas, C. G. Young, B. Broce and J. L. Templeton, *Inorg. Synth.*, **2002**, *33*, 218-227.
207. G. K. Schweitz and E. W. Benson, *J. Chem. Eng. Data*, **1968**, *13*, 452-453.
208. G. W. Craig, M. Eberle, B. Irminger, A. Schuckenbohmer, Y. Laime and P. Muller, *Heterocycles*, **2007**, *71*, 1967-1974.
209. J. Rimland, A. Dunne, S. S. Hunjan, R. Sasse, I. Uings, D. Montanari, M. Caivano, P. Shah, D. Standing, D. Gray, D. Brown, W. Cairns, R. Trump, P. W. Smith, N. Bertheleme, P. D'Alessandro, S. Gul, M. Vimal, D. N. Smith and S. P. Watson, *Bioorg. Med. Chem. Lett.*, **2010**, *20*, 2340-2343.
210. M. S. Yen and I. J. Wang, *Dyes and Pigments*, **2004**, *63*, 1-9.
211. H. Reimlinger, *Chem. Ber.*, **1959**, *92*, 970-977.
212. N. Kitajima and W. B. Tolman, *Prog. Inorg.Chem.*, **1995**, *43*, 419-531.
213. R. Mukherjee, *Coord. Chem. Rev.*, **2000**, *203*, 151-218.
214. S. Trofimenko, *Chem. Rev.*, **1972**, *72*, 497-509.
215. S. Trofimenko, *Prog. Inorg.Chem.*, **1986**, *34*, 115-210.
216. M. A. Halcrow, *Dalton Trans.*, **2009**, 2059-2073.
217. B. P. Sullivan, D. J. Salmon, T. J. Meyer and J. Peedin, *Inorg. Chem.*, **1979**, *18*, 3369-3374.
218. P. J. Steel, F. Lahousse, D. Lerner and C. Marzin, *Inorg. Chem.*, **1983**, *22*, 1488-1493.
219. H. J. Choi, M. Dinca and J. R. Long, *J. Am. Chem. Soc.*, **2008**, *130*, 7848-7850.
220. N. Marques, A. Sella and J. Takats, *Chem. Rev.*, **2002**, *102*, 2137-2159.
221. A. P. Sadimenko, in *Advances in Heterocyclic Chemistry, Vol 81*, ed. A. R. Katritzky, **2001**, vol. 81, pp. 167-252.
222. S. Trofimenko, *Chem. Rev.*, **1993**, *93*, 943-980.
223. C. Pettinari and R. Pettinari, *Coord. Chem. Rev.*, **2005**, *249*, 525-543.
224. J. C. Bayon, P. Esteban, G. Net, P. G. Rasmussen, K. N. Baker, C. W. Hahn and M. M. Gumz, *Inorg. Chem.*, **1991**, *30*, 2572-2574.
225. P. King, R. Clerac, C. E. Anson and A. K. Powell, *Dalton Trans.*, **2004**, 852-861.
226. Y. Wang, Y. Song, Z. R. Pan, Y. Z. Shen, Z. Hu, Z. J. Guo and H. G. Zheng, *Dalton Trans.*, **2008**, 5588-5592.
227. Y. Mulyana, C. J. Kepert, L. F. Lindoy, A. Parkin and P. Turner, *Dalton Trans.*, **2005**, 1598-1601.

228. G. Yang, R. G. Raptis and P. Safar, *Cryst. Growth Des.*, **2008**, *8*, 981-985.
229. H. J. Choi, M. Dinca and J. R. Long, *J. Am. Chem. Soc.*, **2008**, *130*, 7848-7850.
230. K. V. Domasevitch, I. Boldog, E. B. Rusanov, J. Hunger, S. Blaurock, M. Schroeder and J. Sieler, *Z. Anorg. Allg. Chem.*, **2005**, *631*, 1095-1100.
231. J. He, J.-X. Zhang, G.-P. Tan, Y.-G. Yin, D. Zhang and M.-H. Hu, *Cryst. Growth Des.*, **2007**, *7*, 1508-1513.
232. L. Hou, Y.-Y. Lin and X.-M. Chen, *Inorg. Chem.*, **2008**, *47*, 1346-1351.
233. J. Hunger, H. Krautscheid and J. Sieler, *Cryst. Growth Des.*, **2009**, *9*, 4613-4625.
234. L. Lin, R. Yu, W. Yang, X.-Y. Wu and C.-Z. Lu, *Cryst. Growth Des.*, **2012**, *12*, 3304-3311.
235. V. V. Ponomareva, K. V. Domasevich, V. V. Komarchuk, J. Sieler, H. Krautscheid and V. V. Skopenko, *Zh. Neorg. Khim.*, **2006**, *51*, 1445-1453.
236. J.-P. Zhang, S. Horike and S. Kitagawa, *Angew. Chem., Int. Ed. Engl.*, **2007**, *46*, 889-892.
237. J.-P. Zhang and S. Kitagawa, *J. Am. Chem. Soc.*, **2008**, *130*, 907-917.
238. ISI Web of Science, search string (<heterocycle>) AND (*supramolecular* OR "coordination polymer"* OR "metal-organic framework*"). Results (number of publications, 13/7/2012): *pyrazol* 683; *imidazol* 2385; *pyrazin* 857; *carboxyl* 7295; *pyridin* 7314; (*cyano* OR *nitril* NOT acetonitrile) 1599; *pyrimidin* 740
239. P. K. Moore, R. C. Babbedge, P. Wallace, Z. A. Gaffen and S. L. Hart, *Br. J. Pharmacol.*, **1993**, *108*, 296-297.
240. R. S. Turnbull, *J. Can. Dent. Assoc.*, **1995**, *61*, 127-134.
241. J. Catalan, J. C. Delvalle, R. M. Claramunt, G. Boyer, J. Laynez, J. Gomez, P. Jimenez, F. Tomas and J. Elguero, *J. Phys. Chem.*, **1994**, *98*, 10606-10612.
242. J. Catalan, J. L. G. dePaz and J. Elguero, *J. Chem. Soc., Perkin Trans. 2*, **1996**, 1027-1027.
243. R. Pritchard, C. A. Kilner and M. A. Halcrow, *Tetrahedron Lett.*, **2009**, *50*, 2484-2486.
244. W. Stadlbauer, *Science of Synthesis*, Thieme, **2002**.
245. F. Jacobson and L. Huber, *Chem. Ber.*, **1908**, *41*, 660-671.
246. P. Vandersluis and A. L. Spek, *Acta Crystallogr., Sect. A*, **1990**, *46*, 194-201.
247. B. Moulton and M. J. Zaworotko, *Chem. Rev.*, **2001**, *101*, 1629-1658.
248. G. M. Day, *Crystallogr. Rev.*, **2011**, *17*, 3-52.
249. C. Mellot-Draznieks, J. Dutour and G. R. Ferey, *Angew. Chem., Int. Ed. Engl.*, **2004**, *43*, 6290-6296.
250. C. Mellot-Draznieks, S. Girard, G. Ferey, J. C. Schon, Z. Cancarevic and M. Jansen, *Chem. Eur. J.*, **2002**, *8*, 4103-4113.
251. R. E. Morris, *J. Mater. Chem.*, **2005**, *15*, 931-938.
252. R. Robson, *J. Chem. Soc., Dalton Trans.*, **2000**, 3735-3744.
253. J. Kim, B. L. Chen, T. M. Reineke, H. L. Li, M. Eddaoudi, D. B. Moler, M. O'Keeffe and O. M. Yaghi, *J. Am. Chem. Soc.*, **2001**, *123*, 8239-8247.

254. T. Basu, H. A. Sparkes, M. K. Bhunia and R. Mondal, *Cryst. Growth Des.*, **2009**, *9*, 3488-3496.
255. R. Mondal, M. K. Bhunia and K. Dhara, *CrystEngComm*, **2008**, *10*, 1167-1174.
256. C. S. Hawes, *BSc Honours Research Project, University of Canterbury*, **2008**.
257. A. Goswami, S. Sengupta and R. Mondal, *CrystEngComm*, **2012**, *14*, 561-572.
258. B. D. Wilson, *J. Org. Chem.*, **1963**, *28*, 314-320.
259. J. Marquet, M. Morenomanas, P. Pacheco and A. Vallribera, *Tetrahedron Lett.*, **1988**, *29*, 1465-1468.
260. R. G. Charles, *Org. Synth.*, **1959**, *39*, 61.
261. L. Y. Cho and J. R. Romero, *Tetrahedron Lett.*, **1995**, *36*, 8757-8760.
262. G. Maglio, R. Palumbo, A. Schioppa and D. Tesauro, *Polymer*, **1997**, *38*, 5849-5856.
263. D. Didier, B. Tylleman, N. Lambert, C. Velde, F. Blockhuys, A. Collas and S. Sergeyev, *Tetrahedron*, **2008**, *64*, 6252-6262.
264. B. Dolensky, J. Elguero, V. Kral, C. Pardo and M. Valik, in *Advances in Heterocyclic Chemistry, Vol 93*, **2007**, vol. 93, pp. 1-56.
265. D. A. Lenev, K. A. Lyssenko, D. G. Golovanov, V. Buss and R. G. Kostyanovsky, *Chem. Eur. J.*, **2006**, *12*, 6412-6418.
266. S. Sergeyev, *Helv. Chim. Acta*, **2009**, *92*, 415-444.
267. M. Faroughi, A. C. Try, J. Klepetko and P. Turner, *Tetrahedron Lett.*, **2007**, *48*, 6548-6551.
268. Y. W. Jiang, N. Wu, H. H. Wu and M. Y. He, *Synlett*, **2005**, 2731-2734.
269. E. A. Krasnokutskaya, N. I. Semenischeva, V. D. Filimonov and P. Knochel, *Synthesis*, **2007**, 81-84.
270. H. D. Flack, *Acta Crystallogr., Sect. A*, **1983**, *39*, 876-881.
271. T. Basu and R. Mondal, *CrystEngComm*, **2010**, *12*, 366-369.
272. Y. W. Hu, G. H. Li, X. M. Liu, B. Hu, M. H. Bi, L. Gao, Z. Shi and S. H. Feng, *CrystEngComm*, **2008**, *10*, 888-893.
273. J. Q. Liu, Y. Y. Wang, Y. N. Zhang, P. Liu, Q. Z. Shi and S. R. Batten, *Eur. J. Inorg. Chem.*, **2009**, 147-154.
274. C. Y. Sun, S. Gao and L. P. Jin, *Eur. J. Inorg. Chem.*, **2006**, 2411-2421.
275. L. Yang, D. R. Powell and R. P. Houser, *Dalton Trans.*, **2007**, 955-964.
276. M. J. Hannon and L. J. Childs, *Supramolecular Chem.*, **2004**, *16*, 7-22.
277. P. J. Flory and W. G. Miller, *J. Mol. Biol.*, **1966**, *15*, 284-297.
278. J. D. Watson and F. H. C. Crick, *Nature*, **1953**, *171*, 737-738.
279. J. M. Lehn, A. Rigault, J. Siegel, J. Harrowfield, B. Chevrier and D. Moras, *Proc. Natl. Acad. Sci. U. S. A.* , **1987**, *84*, 2565-2569.
280. R. F. Carina, A. F. Williams and C. Piguet, *Helv. Chim. Acta*, **1998**, *81*, 548-557.
281. B. Conerney, P. Jensen, P. E. Kruger and C. MacGloinn, *Chem. Commun.*, **2003**, 1274-1275.

282. E. C. Constable, E. Figgemeier, I. A. Hougen, C. E. Housecroft, M. Neuburger, S. Schaffner and L. A. Whall, *Dalton Trans.*, **2005**, 1168-1175.
283. S. Goetz and P. E. Kruger, *Dalton Trans.*, **2006**, 1277-1284.
284. D. A. McMorran and P. J. Steel, *Angew. Chem., Int. Ed. Engl.*, **1998**, *37*, 3295-3297.
285. S. G. Telfer, B. Bocquet and A. F. Williams, *Inorg. Chem.*, **2001**, *40*, 4818-4820.
286. C. D. B. Vandevyver, A. S. Chauvin, S. Comby and J. C. G. Bunzli, *Chem. Commun.*, **2007**, 1716-1718.
287. J. D. Xu and K. N. Raymond, *Angew. Chem., Int. Ed. Engl.*, **2006**, *45*, 6480-6485.
288. R. M. Yeh and K. N. Raymond, *Inorg. Chem.*, **2006**, *45*, 1130-1139.
289. E. C. Constable, G. Q. Zhang, C. E. Housecroft, M. Neuburger and J. A. Zampese, *Eur. J. Inorg. Chem.*, **2010**, 2000-2011.
290. C. R. K. Glasson, G. V. Meehan, J. K. Clegg, L. F. Lindoy, J. A. Smith, F. R. Keene and C. Motti, *Chem. Eur. J.*, **2008**, *14*, 10535-10538.
291. C. R. K. Glasson, G. V. Meehan, C. A. Motti, J. K. Clegg, P. Turner, P. Jensen and L. F. Lindoy, *Dalton Trans.*, **2011**, *40*, 12153-12159.
292. D. Pelleteret, R. Clerac, C. Mathoniere, E. Harte, W. Schmitt and P. E. Kruger, *Chem. Commun.*, **2009**, 221-223.
293. F. Stomeo, C. Lincheneau, J. P. Leonard, J. E. O'Brien, R. D. Peacock, C. P. McCoy and T. Gunnlaugsson, *J. Am. Chem. Soc.*, **2009**, *131*, 9636-9637.
294. Z. Zhang, Y. K. Chen and D. Dolphin, *Dalton Trans.*, **2012**, *41*, 4751-4753.
295. Z. Zhang and D. Dolphin, *Inorg. Chem.*, **2010**, *49*, 11550-11555.
296. C. He, Y. G. Zhao, D. Guo, Z. H. Lin and C. Y. Duan, *Eur. J. Inorg. Chem.*, **2007**, 3451-3463.
297. A. M. Garcia-Deibe, J. S. Matalobos, M. Fondo, M. Vazquez and M. R. Bermejo, *Inorg. Chim. Acta*, **2004**, *357*, 2561-2569.
298. S. Khatua, H. Stoeckli-Evans, T. Harada, R. Kuroda and M. Bhattacharjee, *Inorg. Chem.*, **2006**, *45*, 9619-9621.
299. Q. Z. Sun, Y. Bai, G. J. He, C. Y. Duan, Z. H. Lin and Q. J. Meng, *Chem. Commun.*, **2006**, 2777-2779.
300. G. Baum, E. C. Constable, D. Fenske, C. E. Housecroft and T. Kulke, *Chem. Eur. J.*, **1999**, *5*, 1862-1873.
301. W. Zarges, J. Hall, J. M. Lehn and C. Bolm, *Helv. Chim. Acta*, **1991**, *74*, 1843-1852.
302. M. Albrecht and S. Kotila, *Angew. Chem., Int. Ed. Engl.*, **1995**, *34*, 2134-2137.
303. K. Dedeian, J. M. Shi, N. Shepherd, E. Forsythe and D. C. Morton, *Inorg. Chem.*, **2005**, *44*, 4445-4447.
304. M. A. Halcrow, *Coord. Chem. Rev.*, **2005**, *249*, 2880-2908.
305. P. J. Steel and E. C. Constable, *J. Chem. Soc., Dalton Trans.*, **1990**, 1389-1396.

306. K. H. Sugiyarto and H. A. Goodwin, *Aust. J. Chem.*, **1988**, *41*, 1645-1663.
307. C. H. Yang, S. W. Li, Y. Chi, Y. M. Cheng, Y. S. Yeh, P. T. Chou, G. H. Lee, C. H. Wang and C. F. Shu, *Inorg. Chem.*, **2005**, *44*, 7770-7780.
308. A. T. Baker, N. J. Ferguson, H. A. Goodwin and A. D. Rae, *Aust. J. Chem.*, **1989**, *42*, 623-638.
309. Q. Cui, X.-Y. Cao and L.-F. Tang, *Polyhedron*, **2005**, *24*, 209-214.
310. K.-T. Youm, S. Huh, Y. J. Park, S. Park, M.-G. Choi and M.-J. Jun, *Chem. Commun.*, **2004**, 2384-2385.
311. J.-X. Zhang, J. He, Y.-G. Yin, M.-H. Hu, D. Li and X.-C. Huang, *Inorg. Chem.*, **2008**, *47*, 3471-3473.
312. R. Ishikawa, M. Nakano, A. Fuyuhiro, T. Takeuchi, S. Kimura, T. Kashiwagi, M. Hagiwara, K. Kindo, S. Kaizaki and S. Kawata, *Chem. Eur. J.*, **2010**, *16*, 11139-11144.
313. M. Munakata, L. P. Wu, M. Yamamoto, T. Kuroda-Sowa, M. Maekawa, S. Kawata and S. Kitagawa, *J. Chem. Soc., Dalton Trans.*, **1995**, 4099-4106.
314. N. Planas, G. J. Christian, E. Mas-Marza, X. Sala, X. Fontrodona, F. Maseras and A. Llobet, *Chem. Eur. J.*, **2010**, *16*, 7965-7968.
315. S. Romain, J. Rich, C. Sens, T. Stoll, J. Benet-Buchholz, A. Llobet, M. Rodriguez, I. Romero, R. Clerac, C. Mathoniere, C. Duboc, A. Deronzier and M.-N. Collomb, *Inorg. Chem.*, **2011**, *50*, 8427-8436.
316. C. J. Schneider, J. D. Cashion, B. Moubaraki, S. M. Neville, S. R. Batten, D. R. Turner and K. S. Murray, *Polyhedron*, **2007**, *26*, 1764-1772.
317. C. Sens, M. Rodriguez, I. Romero, A. Llobet, T. Parella and J. Benet-Buchholz, *Inorg. Chem.*, **2003**, *42*, 8385-8394.
318. K. Yoneda, K. Adachi, S. Hayami, Y. Maeda, M. Katada, A. Fuyuhiro, S. Kawata and S. Kaizaki, *Chem. Commun.*, **2006**, 45-47.
319. M. D. Ward, J. A. McCleverty and J. C. Jeffery, *Coord. Chem. Rev.*, **2001**, *222*, 251-272.
320. S. P. Argent, H. Adams, T. Riis-Johannessen, J. C. Jeffery, L. P. Harding, O. Mamula and M. D. Ward, *Inorg. Chem.*, **2006**, *45*, 3905-3919.
321. Z. R. Bell, L. P. Harding and M. D. Ward, *Chem. Commun.*, **2003**, 2432-2433.
322. H. Fenton, I. S. Tidmarsh and M. D. Ward, *Dalton Trans.*, **2010**, *39*, 3805-3815.
323. P. L. Jones, K. J. Byrom, J. C. Jeffery, J. A. McCleverty and M. D. Ward, *Chem. Commun.*, **1997**, 1361-1362.
324. A. Stephenson and M. D. Ward, *Dalton Trans.*, **2011**, *40*, 10360-10369.
325. I. S. Tidmarsh, T. B. Faust, H. Adams, L. P. Harding, L. Russo, W. Clegg and M. D. Ward, *J. Am. Chem. Soc.*, **2008**, *130*, 15167-15175.
326. M. D. Ward, *Chem. Commun.*, **2009**, 4487-4499.
327. D. L. Jameson and K. A. Goldsby, *J. Org. Chem.*, **1990**, *55*, 4992-4994.

328. J. M. Stanley, X. Zhu, X. Yang and B. J. Holliday, *Inorg. Chem.*, **2010**, *49*, 2035-2037.
329. H. Zhang, Q. Cai and D. W. Ma, *J. Org. Chem.*, **2005**, *70*, 5164-5173.
330. S. Trofimenko, *J. Am. Chem. Soc.*, **1970**, *92*, 5118-5126.
331. N. J. Wheate, J. A. Broomhead, J. G. Collins and A. I. Day, *Aust. J. Chem.*, **2001**, *54*, 141-144.
332. L. D. Field, B. A. Messerle, M. Rehr, L. P. Soler and T. W. Hambley, *Organometallics*, **2003**, *22*, 2387-2395.
333. V. A. Blatov, *IUCr CompComm Newsletter*, **2006**, *7*, 4-38.
334. G. B. Deacon and R. J. Phillips, *Coord. Chem. Rev.*, **1980**, *33*, 227-250.
335. E. E. Gilbert and E. J. Rumanowski, *United States Pat.*, US3040095, 1962.
336. K. E. Knope, H. Kimura, Y. Yasaka, M. Nakahara, M. B. Andrews and C. L. Cahill, *Inorg. Chem.*, **2012**, *51*, 3883-3890.
337. B. Krautler, R. Konrat, E. Stupperich, G. Farber, K. Gruber and C. Kratky, *Inorg. Chem.*, **1994**, *33*, 4128-4139.
338. P. G. Lenhert and D. C. Hodgkin, *Nature*, **1961**, *192*, 937-938.
339. M. L. Ludwig and R. G. Matthews, *Annu. Rev. Biochem.*, **1997**, *66*, 269-313.
340. T. L. Amyes, S. T. Diver, J. P. Richard, F. M. Rivas and K. Toth, *J. Am. Chem. Soc.*, **2004**, *126*, 4366-4374.
341. F. E. Hahn and M. C. Jahnke, *Angew. Chem., Int. Ed. Engl.*, **2008**, *47*, 3122-3172.
342. I. J. B. Lin and C. S. Vasam, *Coord. Chem. Rev.*, **2007**, *251*, 642-670.
343. M. Poyatos, J. A. Mata and E. Peris, *Chem. Rev.*, **2009**, *109*, 3677-3707.
344. M. du Plessis and L. J. Barbour, *Dalton Trans.*, **2012**, *41*, 3895-3898.
345. L. Dobrzanska, D. J. Kleinhans and L. J. Barbour, *New. J. Chem.*, **2008**, *32*, 813-819.
346. S. V. Potts and L. J. Barbour, *New J. Chem.*, **2010**, *34*, 2451-2457.
347. C. E. Willans, S. French, K. M. Anderson, L. J. Barbour, J. A. Gertenbach, G. O. Lloyd, R. J. Dyer, P. C. Junk and J. W. Steed, *Dalton Trans.*, **2011**, *40*, 573-582.
348. J. Yang, J. F. Ma, S. R. Batten and Z. M. Su, *Chem. Commun.*, **2008**, 2233-2235.
349. J. L. Du, T. L. Hu, S. M. Zhang, Y. F. Zeng and X. H. Bu, *CrystEngComm*, **2008**, *10*, 1866-1874.
350. C. Y. Su, Y. P. Cai, C. L. Chen, H. X. Zhang and B. S. Kang, *J. Chem. Soc., Dalton Trans.*, **2001**, 359-361.
351. Q. A. Zhang, L. S. He, J. M. Liu, W. Wang, J. Y. Zhang and C. Y. Su, *Dalton Trans.*, **2010**, *39*, 11171-11179.
352. Y. Q. Lan, S. L. Li, J. S. Qin, D. Y. Du, X. L. Wang, Z. M. Su and Q. Fu, *Inorg. Chem.*, **2008**, *47*, 10600-10610.
353. C. Y. Su, Y. P. Cai, C. L. Chen, M. D. Smith, W. Kaim and H. C. zur Loye, *J. Am. Chem. Soc.*, **2003**, *125*, 8595-8613.

354. S. Ruttimann, C. Piguet, G. Bernardinelli, B. Bocquet and A. F. Williams, *J. Am. Chem. Soc.*, **1992**, *114*, 4230-4237.

355. C. Piguet, J. C. G. Bunzli, G. Bernardinelli, G. Hopfgartner and A. F. Williams, *J. Am. Chem. Soc.*, **1993**, *115*, 8197-8206.

356. A. S. Chauvin, S. Comby, B. Song, C. D. B. Vandevyver, F. Thomas and J. C. G. Bunzli, *Chem. Eur. J.*, **2007**, *13*, 9515-9526.

357. X. R. Meng, Y. L. Song, H. W. Hou, Y. T. Fan, G. Li and Y. Zhu, *Inorg. Chem.*, **2003**, *42*, 1306-1315.

358. C. Y. Su, Y. P. Cai, C. L. Chen and B. S. Kang, *Inorg. Chem.*, **2001**, *40*, 2210-2211.

359. Y. L. Yao, Y. X. Che and J. M. Zheng, *Cryst. Growth. Des.*, **2008**, *8*, 2299-2306.

360. R. Banerjee, A. Phan, B. Wang, C. Knobler, H. Furukawa, M. O'Keeffe and O. M. Yaghi, *Science*, **2008**, *319*, 939-943.

361. H. Hayashi, A. P. Cote, H. Furukawa, M. O'Keeffe and O. M. Yaghi, *Nature Materials*, **2007**, *6*, 501-506.

362. K. S. Park, Z. Ni, A. P. Cote, J. Y. Choi, R. D. Huang, F. J. Uribe-Romo, H. K. Chae, M. O'Keeffe and O. M. Yaghi, *Proc. Natl. Acad. Sci. U. S. A.*, **2006**, *103*, 10186-10191.

363. A. Phan, C. J. Doonan, F. J. Uribe-Romo, C. B. Knobler, M. O'Keeffe and O. M. Yaghi, *Acc. Chem. Res.*, **2010**, *43*, 58-67.

364. B. Wang, A. P. Cote, H. Furukawa, M. O'Keeffe and O. M. Yaghi, *Nature*, **2008**, *453*, 207-211.

365. F. J. Stutzenberger and J. N. Parle, *J. Gen. Microbiol.*, **1973**, *76*, 197-209.

366. L. Anfossi, C. Baggiani, P. Baravalle, C. Giovannoli, L. Guzzella and F. Pozzoni, *Anal. Lett.*, **2009**, *42*, 807-820.

367. Y.-J. Lian, G.-F. Pang, H.-R. Shu, C.-L. Fan, Y.-M. Liu, J. Feng, Y.-P. Wu and Q.-Y. Chang, *J. Agric. Food Chem.*, **2010**, *58*, 9428-9453.

368. M. Eberle, F. Bachmann, A. Strebel, S. Roy, S. Srivastava and G. Saha, *United States Pat.*, US20070066670A1, 2007.

369. J. H. Chang, K. W. Lee, D. H. Nam, W. S. Kim and K. Shin, *Org. Process. Res. Dev.*, **2002**, *6*, 674-676.

370. H. J. Lu, J. Gao, Y. T. Fan and H. W. Hou, *J. Coord. Chem.*, **2003**, *56*, 1025-1032.

371. C. M. Fitchett, C. Richardson and P. J. Steel, *Org. Biomol. Chem.*, **2005**, *3*, 498-502.

372. J. W. Ellingboe, W. Spinelli, M. W. Winkley, T. T. Nguyen, R. W. Parsons, I. F. Moubarak, J. M. Kitzen, D. Vonengen and J. F. Bagli, *J. Med. Chem.*, **1992**, *35*, 705-716.

373. C. M. Fitchett and P. J. Steel, *Polyhedron*, **2007**, *26*, 400-405.

374. A. W. Addison, T. N. Rao, J. Reedijk, J. Vanrijn and G. C. Verschoor, *J. Chem. Soc., Dalton Trans.*, **1984**, 1349-1356.

375. A. L. Spek, *J. Appl. Crystallogr.*, **2003**, *36*, 7-13.

376. M. G. B. Drew, C. J. Harding, V. McKee, G. G. Morgan and J. Nelson, *J. Chem. Soc., Chem. Commun.*, **1995**, 1035-1038.
377. I. Dance and M. Scudder, *J. Chem. Soc., Dalton Trans.*, **1998**, 1341-1350.
378. P. K. Moore, P. Wallace, Z. Gaffen, S. L. Hart and R. C. Babbedge, *Br. J. Pharmacol.*, **1993**, *110*, 219-224.
379. G. Corsi, G. Palazzo, C. Germani, P. S. Barcellona and B. Silvestrini, *J. Med. Chem.*, **1976**, *19*, 778-783.
380. A. J. Canty, A. Dedieu, H. Jin, A. Milet, B. W. Skelton, S. Trofimenko and A. H. White, *Inorg. Chim. Acta*, **1999**, *287*, 27-36.
381. A. Carella, G. Vives, T. Cox, J. Jaud, G. Rapenne and J. P. Launay, *Eur. J. Inorg. Chem.*, **2006**, 980-987.
382. R. Pettinari, C. Pettinari, F. Marchetti, R. Gobetto, C. Nervi, M. R. Chierotti, E. J. Chan, B. W. Skelton and A. H. White, *Inorg. Chem.*, **2010**, *49*, 11205-11215.
383. P. Oulie, J. Teichert, L. Vendier, C. Dablemont and M. Etienne, *New. J. Chem.*, **2006**, *30*, 679-682.
384. C. Janiak, S. Temizdemir, S. Dechert, W. Deck, F. Girgsdies, J. Heinze, M. J. Kolm, T. G. Scharmann and O. M. Zipffel, *Eur. J. Inorg. Chem.*, **2000**, 1229-1241.
385. Z. G. Gu, W. Liu, Q. F. Yang, X. H. Zhou, J. L. Zuo and X. Z. You, *Inorg. Chem.*, **2007**, *46*, 3236-3244.
386. Z. G. Gu, Y. F. Xu, L. C. Kang, Y. Z. Li, J. L. Zuo and X. Z. You, *Inorg. Chem.*, **2009**, *48*, 5073-5080.
387. A. L. Rheingold, B. S. Haggerty, G. P. A. Yap and S. Trofimenko, *Inorg. Chem.*, **1997**, *36*, 5097-5103.
388. C. Janiak, S. Temizdemir and S. Dechert, *Inorg. Chem. Commun.*, **2000**, *3*, 271-275.
389. J. C. Cuevas, J. Demendoza, P. Prados, F. Hernandezcano and C. Focesfoces, *J. Chem. Soc., Chem. Commun.*, **1986**, 1641-1642.
390. F. J. Barros-Garcia, A. Bernalte-Garcia, F. Luna-Giles, M. A. Maldonado-Rogado and E. Vinuelas-Zahinos, *Polyhedron*, **2006**, *25*, 52-60.
391. R. Caris, B. C. Peoples, M. Valderrama, G. Wu and R. Rojas, *J. Organomet. Chem.*, **2009**, *694*, 1795-1801.
392. E. Reisner, J. Telser and S. J. Lippard, *Inorg. Chem.*, **2007**, *46*, 10754-10770.
393. M. H. Sadr, B. Soltani, S. Gao and S. W. Ng, *Acta Crystallogr., Sect. E: Struct. Rep. Online*, **2008**, *64*, M109-M109.
394. N. J. Silvernail, A. Barabanschikov, J. T. Sage, B. C. Noll and W. R. Scheidt, *J. Am. Chem. Soc.*, **2009**, *131*, 2131-2140.
395. I. N. Stepanenko, A. A. Krokhin, R. O. John, A. Roller, V. B. Arion, M. A. Jakupec and B. K. Keppler, *Inorg. Chem.*, **2008**, *47*, 7338-7347.

396. B. Machura, I. Nawrot and K. Michalik, *Polyhedron*, **2011**, *30*, 2619-2626.
397. B. Machura, A. Swietlicka, M. Wolff and R. Kruszynski, *Polyhedron*, **2010**, *29*, 2061-2069.
398. N. Coskun and M. Cetin, *Tetrahedron*, **2007**, *63*, 2966-2972.
399. R. Stolle and W. Becker, *Chem. Ber.*, **1924**, *57*, 1123-1124.
400. H. S. Lowrie, *J. Med. Chem.*, **1966**, *9*, 664-669.
401. C. Ruchardt and V. Hassmann, *Liebigs Ann. Chem.*, **1980**, 908-927.
402. J. E. Reiner, D. V. Siev, G.-L. Araldi, J. J. Cui, J. Z. Ho, K. M. Reddy, L. Mamedova, P. H. Vu, K.-S. S. Lee, N. K. Minami, T. S. Gibson, S. M. Anderson, A. E. Bradbury, T. G. Nolan and J. E. Semple, *Bioorg. Med. Chem. Lett.*, **2002**, *12*, 1203-1208.
403. S. Noro, S. Kitagawa, M. Kondo and K. Seki, *Angew. Chem., Int. Ed. Engl.*, **2000**, *39*, 2082-2084.
404. C. B. Aakeroy, N. Schultheiss and J. Desper, *Dalton Trans.*, **2006**, 1627-1635.
405. V. Montoya, J. Pons, X. Solans, M. Font-Bardia and J. Ros, *Inorg. Chim. Acta*, **2005**, *358*, 2763-2769.
406. H. H. Lee, B. F. Cain, W. A. Denny, J. S. Buckleton and G. R. Clark, *J. Org. Chem.*, **1989**, *54*, 428-431.
407. K. Nakano, N. Suemura, S. Kawata, A. Fuyuhiro, T. Yagi, S. Nasu, S. Morimoto and S. Kaizaki, *Dalton Trans.*, **2004**, 982-988.
408. J. Casabo, J. Pons, K. S. Siddiqi, F. Teixidor, E. Molins and C. Miravitlles, *J. Chem. Soc., Dalton Trans.*, **1989**, 1401-1403.
409. M. Munakata, L. P. Wu, M. Yamamoto, T. KurodaSowa, M. Maekawa, S. Kawata and S. Kitagawa, *J. Chem. Soc., Dalton Trans.*, **1995**, 4099-4106.
410. M. Du, S. T. Chen, Y. M. Guo, X. H. Bu and J. Ribas, *J. Mol. Struct.*, **2005**, *737*, 17-21.
411. C. J. Schneider, J. D. Cashion, B. Moubaraki, S. M. Neville, S. R. Batten, D. R. Turner and K. S. Murray, *Polyhedron*, **2007**, *26*, 1764-1772.
412. K. Yoneda, K. Nakano, J. Fujioka, K. Yamada, T. Suzuki, A. Fuyuhiro, S. Kawata and S. Kaizaki, *Polyhedron*, **2005**, *24*, 2437-2442.
413. J. Z. Hou, M. Li, Z. Li, S. Z. Zhan, X. C. Huang and D. Li, *Angew. Chem., Int. Ed. Engl.*, **2008**, *47*, 1711-1714.
414. R. Ishikawa, M. Nakano, A. Fuyuhiro, T. Takeuchi, S. Kimura, T. Kashiwagi, M. Hagiwara, K. Kindo, S. Kaizaki and S. Kawata, *Chem. Eur. J.*, **2010**, *16*, 11139-11144.
415. J. Pons, F. J. Sanchez, J. Casabo, A. Alvarez-Larena, J. F. Piniella and J. Ros, *Inorg. Chem. Commun.*, **2003**, *6*, 833-836.
416. K. Yoneda, K. Adachi, K. Nishio, M. Yamasaki, A. Fuyuhiro, M. Katada, S. Kaizaki and S. Kawata, *Angew. Chem., Int. Ed. Engl.*, **2006**, *45*, 5459-5461.

417. S. Romain, J. Rich, C. Sens, T. Stoll, J. Benet-Buchholz, A. Llobet, M. Rodriguez, I. Romero, R. Clerac, C. Mathoniere, C. Duboc, A. Deronzier and M. N. Collomb, *Inorg. Chem.*, **2011**, *50*, 8427-8436.
418. J. Mola, C. Dinoi, X. Sala, M. Rodriguez, I. Romero, T. Parella, X. Fontrodona and A. Llobet, *Dalton Trans.*, **2011**, *40*, 3640-3646.
419. N. Planas, G. J. Christian, E. Mas-Marza, X. Sala, X. Fontrodona, F. Maseras and A. Llobet, *Chem. Eur. J.*, **2010**, *16*, 7965-7968.
420. C. Sens, I. Romero, M. Rodriguez, A. Llobet, T. Parella and J. Benet-Buchholz, *J. Am. Chem. Soc.*, **2004**, *126*, 7798-7799.
421. W. L. Driessen, L. Chang, C. Finazzo, S. Gorter, D. Rehorst, J. Reedijk, M. Lutz and A. L. Spek, *Inorg. Chim. Acta*, **2003**, *350*, 25-31.
422. J. Zhao, L. S. Long, R. B. Huang and L. S. Zheng, *Dalton Trans.*, **2008**, 4714-4716.
423. X. H. Zhou, Y. H. Peng, X. D. Du, C. F. Wang, J. L. Zuo and X. Z. You, *Cryst. Growth. Des.*, **2009**, *9*, 1028-1035.
424. L. Pan, X. Y. Huang, J. Li, Y. G. Wu and N. W. Zheng, *Angew. Chem., Int. Ed. Engl.*, **2000**, *39*, 527-530.
425. L. V. Penkova, A. Maciag, E. V. Rybak-Akimova, M. Haukka, V. A. Pavlenko, T. S. Iskenderov, H. Kozlowski, F. Meyer and I. O. Fritsky, *Inorg. Chem.*, **2009**, *48*, 6960-6971.
426. S. K. Dey, T. S. M. Abedin, L. N. Dawe, S. S. Tandon, J. L. Collins, L. K. Thompson, A. V. Postnikov, M. S. Alam and P. Muller, *Inorg. Chem.*, **2007**, *46*, 7767-7781.
427. J. Klingele, A. I. Prikhod'ko, G. Leibeling, S. Demeshko, S. Dechert and F. Meyer, *Dalton Trans.*, **2007**, 2003-2013.
428. K. Moriyama, T. Suzuki, K. Negishi, J. D. Graci, C. N. Thompson, C. E. Cameron and M. Watanabe, *J. Med. Chem.*, **2008**, *51*, 159-166.
429. E. Abdel-Hafez, G. Abuo-Rahma, M. Abdel-Aziz, M. F. Radwan and H. H. Farag, *Bioorg. Med. Chem.*, **2009**, *17*, 3829-3837.
430. I. Sylvestre, C. A. Kilner and M. A. Halcrow, *Private Communication OJUKOU, Cambridge Structural Database Version 5.33, February 2012*, **2009**.
431. S. Y. Zhang, Y. H. Li and W. Li, *Inorg. Chim. Acta*, **2009**, *362*, 2247-2252.
432. T. Hajra, J. K. Bera and V. Chandrasekhar, *Aust. J. Chem.*, **2011**, *64*, 561-566.
433. F. L. Hu, X. H. Yin, Y. Mi, J. L. Zhang, Y. Zhuang and X. Z. Dai, *Inorg. Chem. Commun.*, **2009**, *12*, 628-631.
434. F. L. Hu, X. H. Yin, Y. Mi, Y. Zhuang, S. S. Zhang and Z. J. Huang, *J. Coord. Chem.*, **2009**, *62*, 3613-3620.
435. C. X. An, Y. C. Lu, Z. F. Shang and Z. H. Zhang, *Inorg. Chim. Acta*, **2008**, *361*, 2721-2730.
436. K. Miura and Y. Nishikimi, *International Pat.*, WO2008153027A1, 2008.

437. A. Riahi, M. Shkoor, O. Fatunsin, R. A. Khera, C. Fischer and P. Langer, *Org. Biomol. Chem.*, **2009**, *7*, 4248-4251.
438. N. Fatin-Rouge, E. Toth, D. Perret, R. H. Backer, A. E. Merbach and J.-C. G. Buenzli, *J. Am. Chem. Soc.*, **2000**, *122*, 10810-10820.
439. C. Montoro, F. Linares, P. E. Quartapelle, I. Senkovska, S. Kaskel, S. Galli, N. Masciocchi, E. Barea and J. A. R. Navarro, *J. Am. Chem. Soc.*, **2011**, *133*, 11888-11891.
440. K. L. V. Mann, E. Psillakis, J. C. Jeffery, L. H. Rees, N. M. Harden, J. A. McCleverty, M. D. Ward, D. Gatteschi, F. Totti, F. E. Mabbs, E. J. L. McInnes, P. C. Riedi and G. M. Smith, *J. Chem. Soc., Dalton Trans.*, **1999**, 339-348.
441. http://webbook.nist.gov/chemistry/fluid/, Accessed 21/6/2012.
442. L. Czepirski and J. Jagiello, *Chem. Eng. Sci.*, **1989**, *44*, 797-801.
443. G. M. Sheldrick, *Acta Crystallogr., Sect. A*, **2008**, *64*, 112-122.
444. G. M. Sheldrick, SHELXL-97, Programs for X-ray Crystal Structure Refinement, **1997**, p. University of Gottingen.
445. O. V. Dolomanov, L. J. Bourhis, R. J. Gildea, J. A. K. Howard and H. Puschmann, *J. Appl. Crystallogr.*, **2009**, *42*, 339-341.
446. P. E. Kruger, G. D. Fallon, B. Moubaraki and K. S. Murray, *J. Chem. Soc., Chem. Commun.*, **1992**, 1726-1729.
447. I. Boldog, E. B. Rusanov, A. N. Chernega, J. Sieler and K. V. Domasevitch, *Polyhedron*, **2001**, *20*, 887-897.
448. J. Doiron, A. H. Soultan, R. Richard, M. M. Toure, N. Picot, R. Richard, M. Cuperlovic-Culf, G. A. Robichaud and M. Touaibia, *Eur. J. Med. Chem.*, **2011**, *46*, 4010-4024.
449. J. McNulty, J. J. Nair, S. Cheekoori, V. Larichev, A. Capretta and A. J. Robertson, *Chem. Eur. J.*, **2006**, *12*, 9314-9322.
450. P. Rajakumar, S. Selvam, V. Shanmugaiah and N. Mathivanan, *Bioorg. Med. Chem. Lett.*, **2007**, *17*, 5270-5273.
451. L. D. Field, B. A. Messerle, M. Rehr, L. P. Soler and T. W. Hambley, *Organometallics*, **2003**, *22*, 2387-2395.
452. B. Weinstein, O. P. Crews, Jr., M. A. Leafier, B. R. Baker and L. Goodman, *J. Org. Chem.*, **1962**, *27*, 1389-1395.
453. D. S. Noyce and L. J. Dolby, *J. Org. Chem.*, **1961**, *26*, 1732-1737.
454. K. Ma, P. Wang, W. Fu, X. Wan, L. Zhou, Y. Chu and D. Ye, *Bioorg. Med. Chem. Lett.*, **2011**, *21*, 6724-6727.
455. S. He, L. Chen, Y.-N. Niu, L.-Y. Wu and Y.-M. Liang, *Tetrahedron Lett.*, **2009**, *50*, 2443-2445.